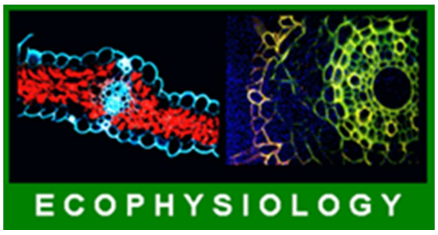

UNIVERSITÄT BONN

Contribution of phenylpropanoids to the suberin barrier in roots of *Arabidopsis thaliana*

Dissertation

Zur

Erlangung des Doktorgrades (Dr. rer. nat.)

der

Mathematisch-Naturwissenschaftlichen Fakultät

der

Rheinischen Friedrich-Wihelms-Universität Bonn

vorgelegt von

Christopher Millán Hidalgo

aus

Frechen

Bonn, Juli 2018

Angefertigt mit der Genehmigung der Mathematisch-Naturwissenschaftlichen Fakultät der Rheinischen Friedrich-Wilhelms-Universität Bonn

1. Gutachter: **PD Dr. Rochus Franke**
2. Gutachter: **Prof. Dr. Peter Dörmann**

Tag der Promotion: 16.10.2018

Erscheinungsjahr: 2019

Affirmation for the Ph.D. Thesis

I herewith declare, that I have written this Ph.D. thesis independently and myself. I have used no other sources than those listed. I have indicated all places where the extract words or analogous text were taken from sources. I assure that this thesis has not been submitted for examination elsewhere.

Bonn,_____ _____

Christopher Millán Hidalgo

Contents

List of Abbreviations

4CL	*4-Hydroxycinnamoyl-coenzyme A Ligase*
µg	microgram
µM	Micro mole
bp	base pair
ABC	ATP Binding Cassette
ABRC	Arabidopsis Biological Resource Centre
ASFT	*Arabidopsis Feruloyl-Coenzyme A Transferse*
BSTFA	N, O-bis(trimethylsilyl)trifluoro acetamide
C3H	*p-Coumaroyl Shikimate 3-Hydroxylase*
C4H	*Cinnamate-4-Hydroxylase*
CAD	*Cinnamyl Alcohol Dehydrogenase*
CASP	*Casparian Strip Protein*
CCoAOMT	*Caffeoyl-CoA O-methyl Transferase*
CCR	*Cinnamoyl-CoA Reductase*
CDEF	*Cuticle Destructing Factor*
cDNA	complementary DNA
CIF	*Casparian Strip Intrinsic Factor*
Col	*Columbia*
COMT	*Caffeic Acid O-Methyl Transferase*
CS	Casparian strips
CSD	*Casparian Strip Membrane Domain*
CW	primary cell wall
Cx	cortex cell
DER 736	diglycidylether of polypropylene glycol
DEX	dexamethasone
DMAE	dimethylaminoethanol
DMSO	dimethyl sulfoxide
DNA	desoxyribonucleic acid
DZ	differentiation zone

EDTA	ethylenediaminetetraacetic acid
En	endodermal cell
Ep	epidermal cell
ER	Endoplasmatic reticulum
ERL-4206	vinylcyclohexene dioxide
ESB	*Enhanced Suberin*
EZ	elongation zone
F5H	*Ferulic Acid/Coniferaldehyde/Coniferyl Alcohol 5-Hydroxylase*
FACT	*A Fatty Alcohol:Caffeoyl-CoA Caffeoyl Transferase*
FHT	*Fatty ω-Hydroxyacid/Fatty Alcohol Hydroxycinnamoyl Transferase*
FID	flame ionisation detector
g	gram
G	guiacyl
GC	gas-chromatograph
h	hour
H	hydroxyphenyl
HCT	*Hydroxycinnamoyl-coenzme A Shikimate/Quinate Hydroxycinnamoyl-transferase*
HM	homozygous
HPLC	high pressure liquid chromatography
HQT	*Hydroxycinnamoyl-Quinate Transferase*
HZ	heterozygous
kbp	kilo base pair
KCS	*Ketoacyl CoA Synthase*
l	litre
LAC	laccase
LB	left border
Ler	*Landsberg erecta*
LP	left genomic primer
M	mole
MeOH	methanol
mg	miligram

min	minute
ml	mililiter
mM	milimol
mm	millimetre
MS	mass-spectroscopy
MYB	*Myeloblastis*
MZ	meristematic zone
NAC	*No apical meristem* (*NAM*), *Arabidopsis transcription activation factor* (*ATAF*), *Cup-shaped cotyledon* (*CUC*)
NaOH	sodium hydroxide
NASC	Nottingham Arabidopsis Stock Centre
NSA	nonenyl succinic anhydride
OD	optical density
OH	Hydroxyl-group
Pc	pericycle cell
PCR	polymerase chain reaction
PI	propidium iodide
PM	plasma membrane
PRX	peroxidase
QC	quiescent centre
RB	right border
REF	*reduced epidermal fluorescence*
RP	right genomic primer
RNA	ribonucleic acid
rpm	revolutions per minute
RT-PCR	reverse transcriptase polymerase chain reaction
s	second
S	syringyl
SAM	S-Adenosyl Methionine
SASSC	Sendai Arabidopsis Seed Stock Centre
SGN	schengen
SL	suberin lamellae

Sm	*Selaginella moellendorffii*
TAE-buffer	TRIS-acetic acid-EDTA-buffer
TEM	transmission electron microscopy
TZ	transition zone
U	enzyme activity (unit)
UV	ultraviolet
Va	vacuole
VAN	*Va*nillin *S*ynthase
v/v	volume per volume
w/v	weight per volume
w/w	weight per weight
WT	wildtype

1. Introduction

1.1. An improved suberin barrier copes with agricultural challenges

Studying suberisation is challenging but worth. Agricultural production of crop plants is threatened by abiotic and biotic stress factors. For example, drought can cause massive crop failure like in the north of Germany during early summer in 2018 (rbb24, 5/7/2018). Increased suberisation improves the drought tolerance of plants (North and Nobel, 1994; Frenger, 2014) and may prevent massive crop failure in the future. Furthermore, an increased suberisation seems to improve the resistance of plants against salinity (Reinhard and Rost, 1995), waterlogged conditions (Watanabe et al., 2013) and pathogen infestation (Biggs and Miles, 1988). Agricultural production of crop plants is not only required for nutrition but also necessary as a resource for industry. Thus, by improving only one barrier plants can become resistant against several abiotic and biotic stress factors.

Suberin consists of a polyaliphatic and a polyaromatic domain (Bernards, 2002). In the past decade suberin research was focused on the polyaliphatic domain, but our knowledge about the function of the polyaromatic domain is limited. Therefore, this study tries to elucidate the role of aromatics to the suberin barrier.

1.2. *Arabidopsis thaliana* as a model organism

My previous work was focused on potato tubers silenced in a phenylpropanoid pathway gene with respect to the suberin formation (Millán Hidalgo, 2015). This work continues the research on aromatics in suberin formation, however due to the difficulties in regards to transforming potato tubers, I started to investigate the influence of phenylpropanoids on the suberin barrier in roots of *Arabidopsis thaliana*.

Arabidopsis thaliana, known as tale cress, was not the first choice of plant biologist to study the herbal organism in general. In the history of plant research several plant species were chosen as model organism for instance *Solanum lycopersicum*, *Oryza sativa*, *Hordeum vulgare*, *Zea mays*, *Pisum sativum* and *Petunia axillaris*. However, in the past plant researchers failed to reach consensus on which species was most suitable for studying

Fig. 1: *Arabidopsis thaliana*
A fully developed plant is presented with inflorescence and young siliques (drawing by K. Sutliff) (Meinke et al al., 1998).

process common to all plants. Therefore, plant biologists began to search for another model organism suitable for the common genetic and molecular approaches in the 1970s. The attention was drawn to *Arabidopsis thaliana* because of the early work of Laibach in Germany in the 1940s and the later studies of Rédei in the United States in the 1970s (Meinke et al., 1998). Friedrich Laibach was a Ph.D. student of Eduard A. Strasburger at the Rheinische Friedrich-Wilhelms-Universität Bonn. In his Ph.D. thesis he studied the number of chromosome sets to find a suitable plant for the genetic cytology (Nover, 2002). Finally, he believed *Arabidopsis thaliana* had the potential to be a model organism to study genetics and developmental physiology similar to *Drosophila melanogaster* in zoology (Laibach, 1943). Due to the release of a genetic map (Koornneef et al., 1983) and several publications outlining the relevance of *Arabidopsis thaliana* as a model organism to study plant physiology, biochemistry and development (Meinke and Sussex, 1979; Koornneef et al., 1980), *Arabidopsis* was further established as a model organism in the early 1980s. From a genetic point of view, *Arabidopsis thaliana* has a small genome in comparison to other species. The genome of *Arabidopsis* is about 125 Mbp and contains 25,498 genes (The Arabidopsis Genome Initiative, 2000). For example, the genome of *Oriza sativa* is 3-fold bigger, of *Zea mays* 20-fold and of *Triticum* L. 120-fold. Gene duplication and transposons are responsible for the increased genome size of these crop plants (Campbell et al., 2011; Kempken and Kempken, 2012). The genome of *Arabidopsis thaliana* was the first completely sequenced plant genome in the year 2000. However, around 30 % of the known genes are not characterised (Kempken and Kempken, 2012).

Other benefits of *Arabidopsis thaliana* are the size of the plant and the short life cycle. The diameter ranges between 2 to 10 cm depending on the growth conditions. The leaves are organised in a rosette. The mature stem with siliques reaches an altitude of 15 to 20 cm. Several inflorescences are developed on one stem (fig. 1). The whole life cycle of *Arabidopsis thaliana* takes place within 6 weeks from the seed germination, developing a rosette and a

stem, flowering to maturing seeds. The plant produces several hundred of siliques with more than 5,000 seeds. Furthermore, cultivation of the plant can take place either in pots filled with soil, hydroponics or on petri dishes filled with growth media.

Among the most important tools for plant research are the seed stock centres. In 1990 the Nottingham Arabidopsis Stock Centre (NASC) was established by public British funding. One year later the US counterpart the Arabidopsis Biological Resource Centre (ABRC) was founded by the National Science Foundation (NSF). In addition, Sendai Arabidopsis Seed Stock Centre (SASSC) in Japan is providing similar resources. These seed stock centres collect, preserve, propagate and distribute seeds which are of use to the current research. They have a large collection of different *Arabidopsis* ecotypes and mutant lines such as T-DNA insertion and transposon lines. These mutations are inserted randomly throughout the genome during the mutation process and the insertion sites are subsequently mapped. Mutant lines with insertions in genes of interest can be obtained which allows the function and characterisation of a certain gene (Scholl et al., 2000; Meinke and Scholl, 2003).

Since the availability of the completely sequenced genome and mutant stock centres of *Arabidopsis thaliana* molecular plant research without *Arabidopsis* became unthinkable.

1.3. Morphology of the *Arabidopsis thaliana* root

A vascular plant body is composed of three organs: shoot, leaves and root (Campbell et al., 2011). The root is a high differentiated multicellular organisation which is only found in vascular plants. The root is the central organ of vascular plants responsible for the absorption of water and dissolved minerals to ensure the development and the growth of the plant. Roots give mechanical stability by anchoring the plant body to its substrate. From the evolutionary aspect, it appears that the root was the vegetative organ evolved the latest. It might be that early land plants grew close or on the water. Therefore, early land plants focused on maximising photosynthesis by development of stem and leaves (Seago Jr. and Fernando, 2013). In the Early Devonian, early land plants showed already developed stems and leaves, but roots were absent. These early land plants only exhibited a structure with considerable similarity to roots, such as those of *Asteroxylan mackiei*. During the Middle Devonian, a fern-like plant *Lorophyton goense* gives the first convincing evidence of a developed root (Seago Jr. and Fernando, 2013).

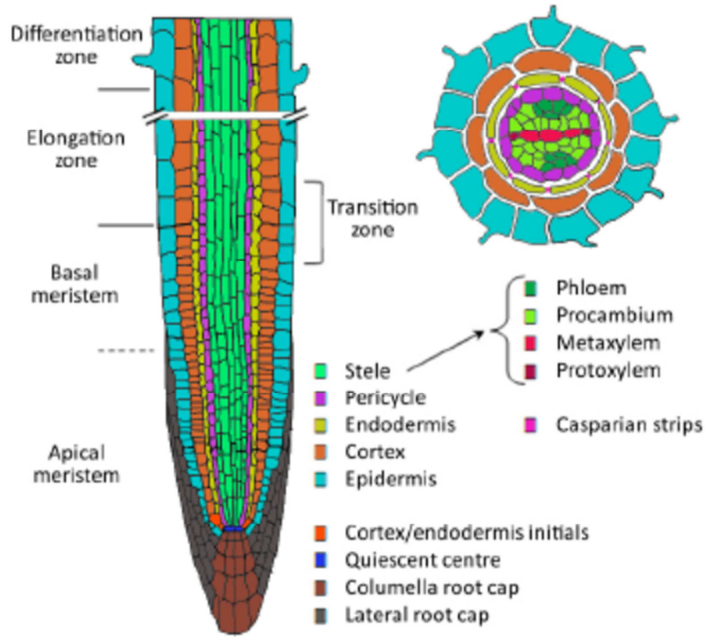

Fig. 2: Cellular organisation of an *Arabidopsis thaliana* root

On the left longitudinal section through the root reveals the apical-basal polarity. The vascular tissue (stele with phloem, cambium and xylem) is surrounded by single-celled layers forming a concentric root shape. Different cell types are each differently coloured. Cell division takes place in the meristematic zone. Stop of cell division and start of elongation becomes visible in the transition zone. After cell elongation in the elongation zone cells start to differentiate in the differentiation zone. On the right cross section through the root reveals the vascular tissue surrounded by the different differentiated cell layers (De Smet et al., 2015).

The root of *Arabidopsis thaliana* shows a basic cellular organisation. It can be described in a radial and an apical-basal polarity (fig 2). Following the radial polarity the root centre contains a vascular bundle with two xylem and phloem strands as conductive elements. The vascular bundle is surrounded by pericycle cells, which are able to develop to lateral root primordia. The pericycle cells are surrounded by endodermal cells, which act as a selective barrier. The cell layer outwards of the endodermis consist of cortical cells, which give mechanical stability and provide protection. Finally, the outer root layer comprises epidermal cells. The epidermis contains trichoblast cell lineage which are able to develop further into root hairs (Dolan et al., 1993; Peret et al., 2009). Apical root growth is promoted by cell division followed by cell elongation. At the root tip a region of undifferentiated and dividing cells is located, which is called the root apical meristem (RAM). These cells are stem cells or initials of certain tissues (e. g. endodermis and cortex initials). The RAM is protected by the root cap consisting of lateral and columella root cap cells. Maintaining of these undifferentiated and dividing cells is the task of the quiescent centre (QC). The QC is a group of non-mitotically active cells, which are surrounded by the stem cells. Removal of the QC results in de-novo formation of QC which demonstrates a high degree of autoregulation of the cellular organisation. Stem cells underneath the QC develop further into cells of the columella root cap, whereas stem cells laterally and above located differentiate into lateral root cap cells, vascular, endodermal, cortical and epidermal cells (Sanz et al., 2012; De Smet et al., 2015). Some of these cell divisions are asymmetrically

(Dolan et al., 1993). With respect to the development of cortical and endodermal cells the stem cells undergo an anticlinal (in transverse orientation) asymmetrical cell division resulting in a daughter and another initial cell. Followed by another asymmetrical and periclinal (in longitudinal orientation) cell division of the daughter cells an inner endodermal and an outer cortical cell is formed. Two transcription factors are responsible for the second asymmetrical and periclinal cell division. Both SCARECROW and SHORT-ROOT are essential for the second cell division but only SHORT-ROOT causes the endodermal specification (Di Laurenzio et al., 1996; Helanriutta et al., 2000). The specified daughter cells of the different tissues start to divide several times. This occurs in the meristematic zone (MZ) and is caused by the polar auxin transport. The phytohormone auxin promotes cell division and inhibits the cell elongation. A threshold distance between daughter cells and the root tip provokes the cell elongation, due to the decreasing concentration of auxin. Still it is not clear whether elongating cells further divide at a large cell size or the cell division is stopped by the initial and increasing elongation rate process. A border between the MZ and the elongation zone (EZ) becomes visible, which is called the transition zone (TZ) (fig. 2). The elongation of the developed daughter cells causes the movement of the root tip deeper into the soil. The root cap protects the meristematic active zone during the forward pushing movement by the elongation of the daughter cells. A fully elongated daughter cell starts to differentiate. This zone is called the differentiation zone (DZ) (fig 2). In this zone, endodermal cells generate a selective barrier by the formation of Casparian strips as well as suberin. Additionally, trichoblast cells in the epidermis develop into root hairs and lateral roots develop (Sanz et al., 2012; De Smet et al., 2015; Barberon, 2017).

1.4. Radial water and nutrient transport and the endodermis as a selective barrier

Three different pathways are described for the radial water and nutrient transport through the root: the apoplastic, symplastic and coupled trans-cellular pathway (fig. 3). Water and nutrients diffuse through the free space between the cell walls and intercellular spaces of epidermis, cortex and endodermis towards the stele. This is the transport through the apoplastic pathway. The driving force of the diffusion is caused by an ion gradient in the free

space of the cell wall and the external solution. The apoplastic diffusion is achieved by the chemical composition of the cell wall. The cell wall is composed of cellulose, hemicellulose, glycoproteins and pectin forming a porous network permeable for water, ions, gases and other solutes (Peterson and Cholewa, 1998; Nobel, 1999; Barberon and Geldner, 2014). Caused by the partially free carboxylic group of homogalacturonan in the pectin structure, cations may accumulate in the root apoplast through a non-metabolic process. However, negatively charged anions are repelled by the free carboxylic groups (Mohnen, 2008; Barberon and Geldner, 2014). This non-metabolic process contributes to the uptake of silicon, iron and aluminium (Lobreaux et al., 1992; Wang et al., 2004).

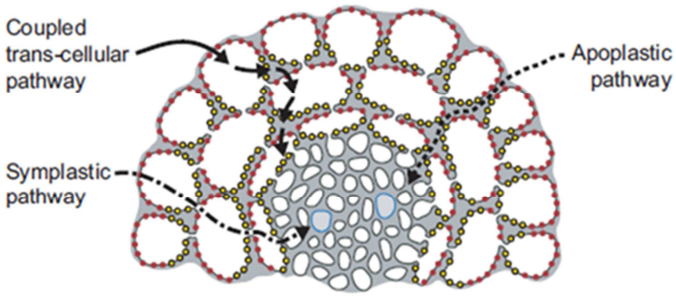

Fig. 3: Radial transport of water and nutrients through the root

Three radial transport pathways are known for the transport of water and nutrients through a root. The apoplastic pathway describes the diffusion of nutrients and water through the intercellular space between the cell walls into the vascular tissue. The symplastic pathway is characterised by the transport of molecules via the cytoplasmic continuum generated by interconnected plasmodesmata. The coupled trans-cellular pathway is carried out by influx and efflux transporters. Red dots are influx, whereas yellow dots indicate efflux transporters. All three pathways are present before endodermal differentiation (Barberon, 2017).

The second pathway is the symplastic pathway mediated by cell-to-cell transport. The symplastic pathway is reasoned by plasmodesmata. Plasmodesmata are channels in the cell wall interconnecting the cytosol of adjacent cells. The transport rate is limited to the number of plasmodesmata and the aperture size. Deposition of callose, a β-1,3-linked homopolymer of glucose, restricts the trafficking of macromolecules through the plasmodesmata (Barberon and Geldner, 2014).

The coupled trans-cellular pathway is carried out by active transport mediated through influx and efflux transporters. Nutrients are transported from one cell to another by crossing the apoplastic space. The transporters are polarly distributed from the epidermis, over cortex to endodermis cells. Nutrients pass the symplast of one cell, are transported by efflux transporters into the apoplast and finally transported into the symplast of the neighbouring cell via influx transporters. This transport resembles the polar auxin transport in the root. The mechanism of this transport is independent by the mass flow of nutrients. It seems to be

an efficient directional long-distance transport (Löfke et al., 2013; Barberon and Geldner, 2014).

1.4.1. State I formation of Casparian strips

Endodermal differentiation is characterised by two developmental stages (fig. 5, differentiated state I and differentiated state II). The first one is the formation of Casparian strips (CS). Casparian strips were discovered by Johann Xaver Robert Caspary (Caspary, 1866). He was the assistant of Ludolph Christian Treviranus the director of the botanical garden in Bonn (Barthlott, 1990). Casparian strips are situated between endodermal cells forming a ring around the endodermal cell. At the early stage of CS formation the ring is patchy, which is called string of pearl stage. Later on, the patches fuse together. This ring is orientated in a periclinal manner around the endodermal cell. Basically, Casparian strips are primary cell wall modifications. They seal intercellular space between the cell wall of two adjacent endodermal cells. Consequently, the apoplastic diffusion of water and nutrients in the vascular tissue is blocked, forcing solutes to enter the symplast of endodermal cells. The plant can control the water and nutrient uptake and can prevent toxic compounds from entering the vascular tissue (Schreiber, 1996; Barberon and Geldner, 2014). In the literature CS are often considered to be similar with tight junctions in animal epithelium (Barberon and Geldner, 2014). However, tight junctions are established by protein-mediated cell-cell interaction, whereas Casparian strip formation is achieved by guided proteins to ensure the localised impregnation of the cell wall (Barberon and Geldner, 2014; Pfister et al., 2014). In past decades, the chemical structure of CS was unclear. In the beginning of the past century it was suggested that CS are made of lignin due to histochemical (Kroemer, 1903; Ziegenspeck, 1921) and electron microscopic analysis (Falk and Sitte, 1963). But further histochemical staining of different species revealed the presence of suberin in the CS (Wilson and Peterson, 1983). Although Lukas Schreiber could demonstrate by histochemical staining, scanning electron microscopy, FTIR spectroscopy, gas chromatography and mass spectroscopy analysis of isolated Casparian strips of *Clivia miniata* roots, that the chemical nature of CS is that of a lignified cell wall similar to the cell walls of xylem vessels (Schreiber et al., 1994). Later on, typical suberin constituents were found in hypodermal and endodermal cell walls of isolated CS of *Clivia miniata* by chemical analysis (Zeier and

Schreiber, 1997). However, Sadaf Naseer and further collaborative researchers prove by genetic, pharmacological and specific chemical analysis that Casparian strips are made of lignin and suberin is not involved in the formation of a functional Casparian strip barrier in *Arabidopsis thaliana*. By promoter GUS-assays they demonstrated the promoter activity of suberin specific genes after the formation of Casparian strips during root development (Naseer et al., 2012). Occurrence of Casparian strips was shown by autofluorescence and functionality proven by the propidium iodide assay, a fluorescent molecule entering the apoplastic pathway and finally blocked by Casparian strips (Alassimone et al., 2010; Naseer et al., 2012; Hosmani et al., 2013; Lee et al., 2013). Phenylpropanoid pathway provides monomers for the lignin synthesis. Treating the roots with the phenylpropanoid pathway inhibitor piperonylic acid (PA) provokes a disruptive Casparian strip barrier without autofluorescence. The Casparian strips were recovered by feeding the plant with G-monolignols, a typical lignin monomer. Finally, the mutant *arabidopsis histidine transfer protein 6* (*ahp6*) was used and treated with cytokinin. This combination leads to strongly delayed formation of xylem vessels but intact CS formation and functionality. The first five mm of the root tip were subjected to thioacidolysis and analysed. Typical lignin monomers were found and based on these results, it is concluded that Casparian strips are made of lignin or a lignin-like polymer in *Arabidopsis thaliana* (Naseer et al., 2012). Still, it is arguable whether Casparian strips in other plant species may contain suberin as well. It cannot be excluded that endodermal cells of different plant species already were suberised which may lead to misinterpretation of the results.

In the past few years the molecular mechanism of CS formation could be clarified in parts and research is still in process. To begin with, there is the receptor-like kinase SCHENGEN3 (SGN3), which is located in a broad band in the plasma membrane of endodermal cells (fig. 4) (Pfister et al., 2014). Another receptor-like cytoplasmic kinase SCHENGEN1 (SGN1) can only be found in the outer plasma membrane facing the cortical cells. SGN3 and SGN1 overlap in a particular transition zone of the endodermal cell, where the CS is formed later (Doblas et al., 2017). The interacting kinases bind two peptides which, upon binding, are expected to cause lignification and suberisation through a signalling cascade. The peptides CASPARIAN STRIP INTRINSIC FACTOR 1 and 2 (CIF1 and CIF2) are expressed in the stele. They diffuse from the stele into the apoplast and bind to SGN3 as well as a complex of SGN1 and SGN3 (Doblas et al., 2017; Nakayama et al., 2017; Matsubayashi, 2018). Four membrane-

spanning proteins, called CASPs, establish a ring-like membrane domain in the endodermis, which is called Casparian strip membrane domain (CSD). By acting as a scaffold the CASPs organise the spatially cell wall biosynthetic enzymes ESB1, PER64 and RBOHF (Hosmani et al., 2013). ENHANCED SUBERIN 1 (ESB1) is a dirigent protein. The protein contains a dirigent-domain, which means ESB1 is a non-enzymatic protein supposed to guide bond formation between two monolignols to define the stereochemistry of the resulting dimeric lignin. Thus, ESB1 may guide the synthesis of lignin by providing a template for a specific order of monolignol subunits during lignin deposition in the cell wall. However, this has to be proved biochemically (Hosmani et al., 2013). Furthermore, the CSD recruits not only ESB1 but also the peroxidase PER64 and RBOHF, a specific NAPDH oxidase to polymerise monolignols by oxidative coupling locally (Roppolo et al., 2011; Lee et al., 2013; Hosmani et al., 2013; Pfister et al., 2014). Though, the mechanism of spanning a fine band between adjacent endodermal cells in their primary cell wall is still unknown. Loss of function of ESB1 or different CASP proteins causes a disrupted CS barrier which is accompanied by enhanced suberisation. Furthermore, the mutants reveal ectopic deposition of lignin (Roppolo et al., 2011; Hosmani et al., 2013; Barberon et al., 2017). However, the *sgn3* mutants show a disrupted CS barrier but normal suberisation (Pfister et al., 2014). The reason of this phenomenon is still unclear but Doblas et al. (2017) give a possible explanation: If the Casparian strip is finally established the CIF-proteins are not able to diffuse to the region, where SGN3 and SGN1 are co-localised and can interact (fig. 4). It is assumed that this diffusion barrier causes a reduction in the signalling which is reported to the endodermal cell that the CS has been established. It seems that the CIF-peptides are a barrier surveillance system which maintains the process of CSD growth and lignification as well as reactivation of lignification or suberisation until an apoplastic barrier has been formed (Doblas et al., 2017).

Control of gene expression of at least *CASP1*, *PER64* and *ESB1* is mediated through the transcription factor *MYB36*. It directly and positively regulates the gene expression of the mentioned proteins (Kamiya et al., 2015).

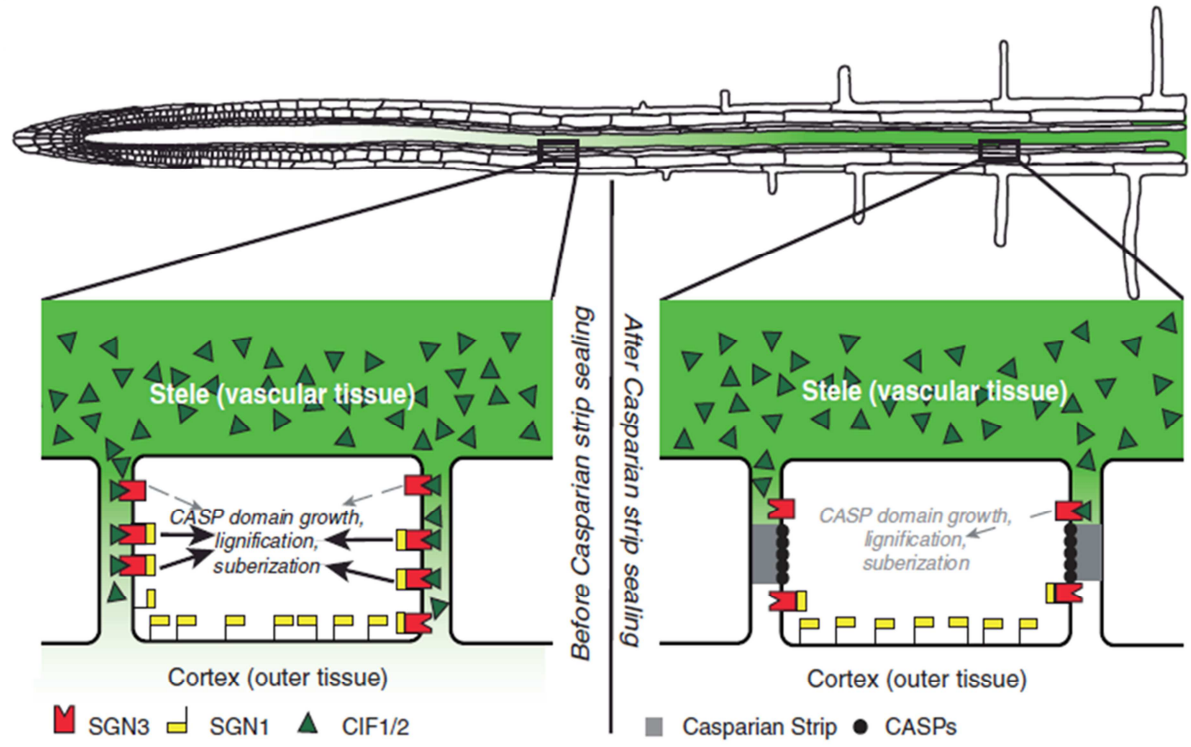

Fig. 4: Proposed action of both receptor-like kinase SGN3 and SGN1 with CIF-peptides

CIF-peptides diffuse from the vascular tissue into apoplast of endodermal cells and bind to the receptor-like kinase SGN3. In the transition zone of the endodermal cell SGN3 and SGN1 are co-localised and can interact. When binding of the CIF-peptide the lignification and suberisation process proceeds (bold arrows). Binding of CIF-peptides only to the SGN3 receptor promotes the growth of the Casparian strip domain (dashed arrow). Establishment of the CS restricts diffusion of CIF-peptides to the side of co-localised SGN3 and SGN1 receptor-like kinase and reduces signalling of lignification and suberisation (Doblas et al., 2017).

A lot of the molecular mechanism of the CS formation could be elucidated in the past few years. However, how the fine CS band is spanned between adjacent endodermal cells is still unknown. Research in this topic will proceed.

1.4.2. State II formation of suberin

The second state of endodermal differentiation is characterised by the formation of suberin (fig. 5, differentiated state II). It is deposited as lamellae (fig. 6) between the primary cell wall and close to the plasma membrane. Basically, it is a secondary cell wall deposition. Suberin covers the entire surface of the endodermal cell. It is a hydrophobic polymer consisting of major aliphatic and minor aromatic compounds (Franke et al., 2005). The chemical composition of suberin is described in the following chapter (1.5.). Suberisation seems to start randomly in the differentiation zone. During early stages of suberisation few

endodermal cells are suberised, which leads to a patchy appearance. This section is called the patchy suberised zone. Proceeding suberisation of the endodermal cells forms a continuous suberised network. This section is called the continuously suberised zone (fig. 5 differentiate state II) (Barberon, 2017). In the past suberin was regarded as an apoplastic barrier since suberisation impairs the root hydraulic conductance value in *Zea mays* (Zimmermann et al., 2010; Franke and Schreiber, 2007). Furthermore, decreased suberin content correlates positively with an increased hydraulic conductance and an accumulation of sodium ions accompanied by sensitivity to salt (Beissons et al., 2007; Ranathunge and Schreiber, 2011). Loss of water either due to drought or osmotic stress induces suberisation process (North and Nobel, 1994; Reinhardt and Rost, 1995). In contrast, reduction of endodermal suberin lamellae facilitates oxygen diffusion into the vascular tissue (Enstone and Peterson, 2005) and radial loss of oxygen is prevented by accumulation of suberin in Amazonian floodplain or wetland species. In contrast, lignified tissue seems unlikely to act as barrier against oxygen molecules (De Simone et al., 2003; Soukup et al., 2007). With respect to the radial water and nutrient transport the role of suberin seems to act as a bidirectional barrier. It separates the plant from the environment and the plant vascular tissue from the plant outer cortical tissue (Franke and Schreiber, 2007). Incubating seedlings with fluorescein di-acetate (FDA) demonstrates that the transport of the fluorescent cellular tracer is restricted by suberisation (Barberon et al., 2016). Incubating cotyledons of *Arabidopsis thaliana* seedlings with carboxyl-FDA allows the observation of the transport of the fluorescent dye into the phloem of leaves and further into pericycle cells of roots. Further transport from pericycle cells into the endodermal cell is blocked as well (Oparka et al., 1994) emphasising the character of suberin as a bidirectional barrier. Suberisation seems not to influence the apoplastic pathway, because PI staining of mutants expressing CUTICLE DESTRUCTING FACTOR 1 (CDEF1) in the endodermis, where it acts as a suberin-degrading enzyme, still demonstrates the apoplastic diffusion blockage of the apoplastic tracer PI. Based on this experiment suberisation seems to influence the coupled trans-cellular pathway (fig. 5, differentiated state II) (Naseer et al., 2012; Barberon et al., 2016). Nonetheless, *Arabidopsis thaliana* mutants expressing *CDEF1* in the endodermis still have suberin monomers (personal communication with PD Dr. Rochus Benni Franke, University of Bonn). Thus, the suberin barrier is not completely degraded. From the ultrastructural view it is not clear how suberin is affected by CDEF1. The suberin barrier might be perforated by

CDEF1. Maybe the holes in the suberin barrier are still smaller than the large PI molecule and nonetheless suberin blocks the apoplastic diffusion of PI into the stele as well. Definitively, suberin cannot be excluded to be an apoplastic barrier as well. Furthermore, the experiments of radial loss of oxygen still give evidence that suberin acts as a barrier in regard to oxygen, but lignified tissue does not (Franke and Schreiber, 2007). It might be possible that suberin influences both coupled trans-cellular and apoplastic pathway with respect to water, nutrients and solutes.

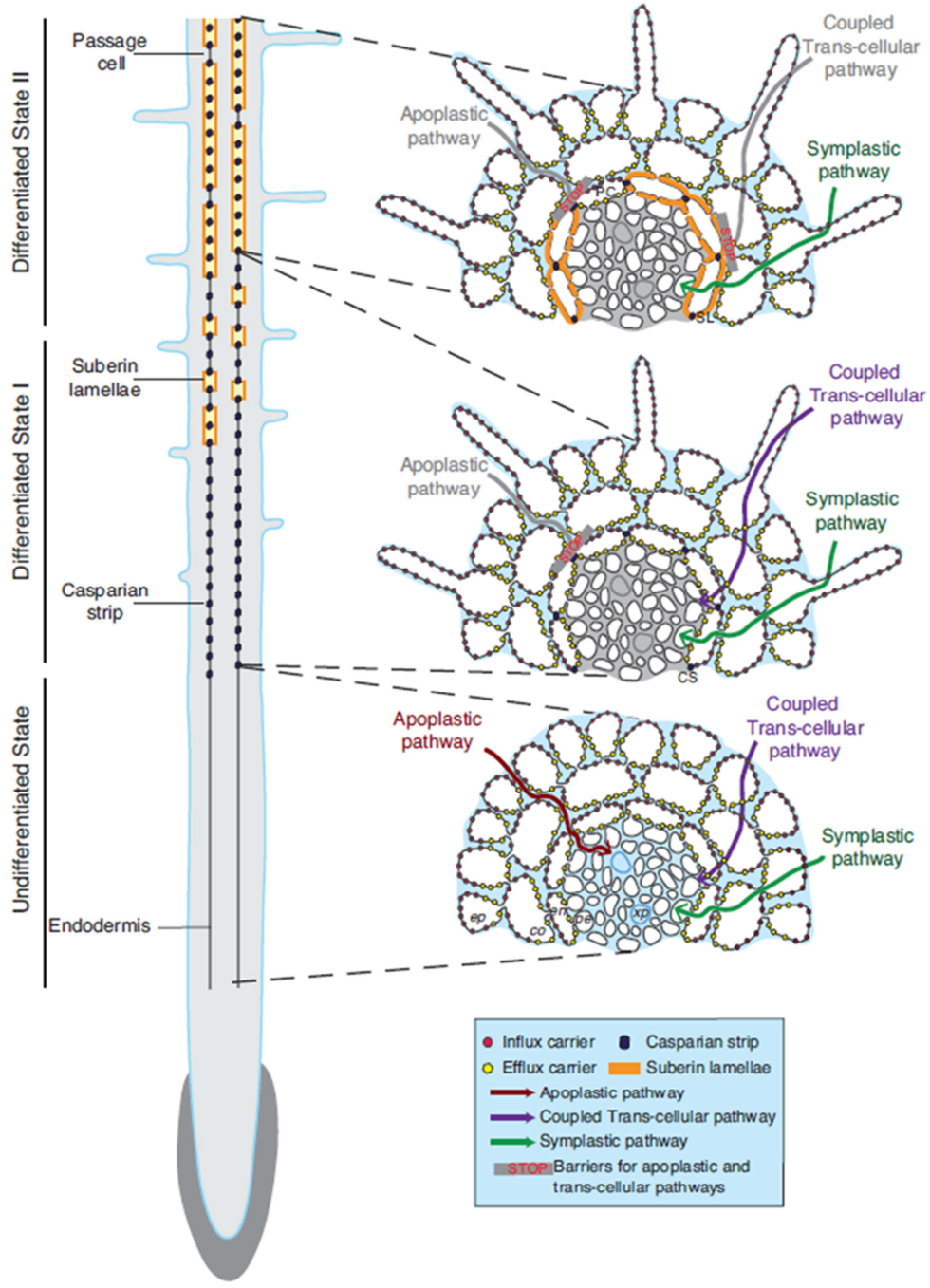

Fig. 5: Schematic view of endodermal differentiation in transversal and longitudinal view of an *Arabdiopsis thaliana* root

On the left side longitudinal view presents the undifferentiated state of the endodermis without CS and suberin, the first differentiated state with CS as dot-like structure and the second differentiate state with patchy and continuously suberised zone. On the right side transversal view of an *Arabidopsis thaliana* root represents the undifferentiated state with all possible radial transport pathways, the first differentiated state with localised CS between endodermal cells blocking the apoplastic pathway and the second differentiated state with impregnations of suberin lamellae on the surface of endodermal cells blocking the coupled trans-cellular pathway (Andersen et al., 2015).

1.5. Ultrastructure and chemical composition of suberin

As already described in chapter 1.4.2., suberin is deposited as lamellae between the primary cell wall and the plasma membrane. The occurrence of suberin is not just restricted to the endodermal root tissue. It is also found in aerial organs of the bark tissue of the cork-oak tree (*Quercus suber*), in suberised bundle sheath cells of grasses separating mesophyll cells from vascular tissue, seed coats and peridermal tissue of storage organs like the potato tuber (Kollatukudy, 1981; Kollatukudy, 2001; Graça and Santos, 2007; Franke and Schreiber, 2007). Suberin is not only present in the cell wall of root endodermal cells, it is also coating the cell wall of hypodermal and rhizodermal cells of primary roots (Perumalla et al., 1990) and the root periderm of angiosperms contains considerable amounts (Franke et al., 2005). Furthermore, suberised cells are also found in all plant tissues upon mechanical or pathogen damage (Biggs and Miles, 1988; Franke et al., 2005; Schreiber et al., 2005). Among species the ultrastructure of suberin appears to be similar (fig. 6). In the transmission electron microscopy suberin appears as alternating electron-translucent and -opaque lamellae. The electron-translucent lamellae show regular diameter, while diameter of electron-opaque lamellae may be irregular (Bernards and Razem, 2001; Franke et al., 2005; Teixeira and Pereira, 2010).

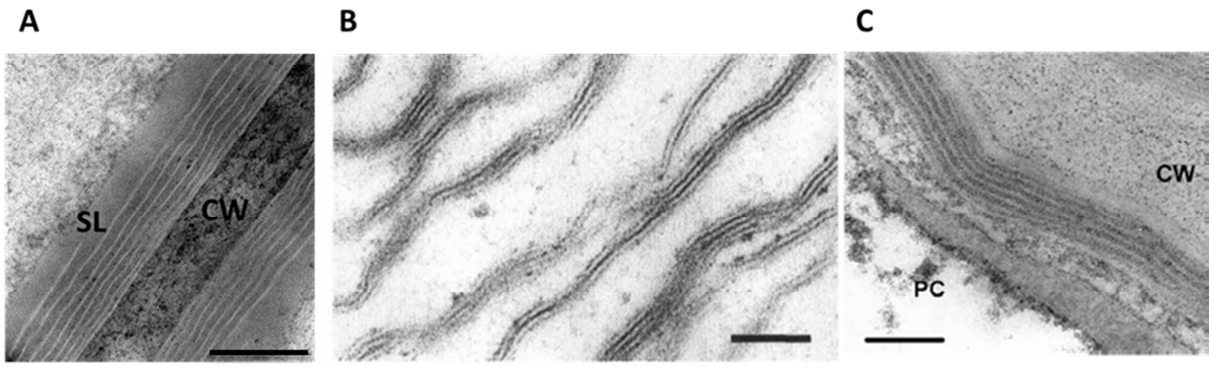

Fig. 6: Ultrastructure of suberin lamellae in different plant species

The ultrastructure of suberin lamellae seems to be similar among the plant species and the different suberised tissues.

A: Suberin lamellae of peridermal tissue of the potato tuber, scale bar: 200 nm. B: Suberin lamellae of green cotton fiber, scale bar: 50 nm (Schmutz et al., 1996). C: Suberin lamellae of *Arabidopsis thaliana* root tissue at the beginning of secondary thickening of the root, scale bar: 100 nm (Franke et al., 2005).

The chemical composition of suberin can differ among species. According to its chemical nature suberin can be divided into two domains: the first one is the polyaliphatic and the second one the polyaromatic domain. However, the term "suberin" is not clearly defined with respect to the chemical composition. Graça considers the polyaliphatic domain to be "suberin", whereas Bernards regards as suberin both polyaliphatic and polyaromatic domain. Both, Bernards and Graça postulate models for the chemical composition of the suberin (Bernards, 2002; Graça and Santos, 2007). The differences between both will be described in the following paragraphs. In addition, this thesis accepts the suberin term of Bernards.

The polyaliphatic domain is characterised by cross-linkages to the polyaromatic domain formed by ester bonds. The polyaliphatic domain consists of glycerol and derived fatty acids, for instance α, ω-dicarboxylic acids, ω-hydroxy acids and primary alcohols ranging usually from carbon chain length 16 to 24 in *Arabidopsis thaliana* (Franke et al., 2005). Partial depolymerisation of peridermal tissue from *S. tuberosum* and *Q. suber* reveal that the backbone of suberin consists of glycerol linked in succession to α, ω-dicarboxylic acid (Graça, 2015). The function of the suberin polymer is mostly determined by the polyaliphatic domain, supposedly due to its hydrophobic character (Zimmermann et al., 2000; Franke and Schreiber, 2007; Graça and Santos, 2007; Serra et al., 2009; Serra et al., 2009b; Serra, 2010). Carbon chain length may differ among species, for instance roots of *Oryza sativa*, *Zea mays* or peridermal tissue of *Solanum tuberosum* suberin contain carbon chain length from 16 to 30 (Schreiber et al., 2005; Serra et al., 2009). Dominant aliphatic compounds are both single unsaturated 18-hydroxyoctadec-9-enoic acid and octadec-9-ene-1,18-dioic acid in *Arabidopsis thaliana* (Franke et al., 2005). In *Quercus suber* the 9-epoxyoctadecane-1,18-dioic acid and 22-hydroxydocosanoic acid can be found as dominant aliphatic molecules. Epoxy derived fatty acids are at the moment only found in *Quercus suber* (Graça and Santos, 2007). Root suberin of soybean seems to be dominated by 18-hydroxyoctadec-9-enoic acid and octadec-9-enoic acid (Thomas et al., 2007). Several genes involved in the suberin aliphatic biosynthesis were identified in the last decade. The first identified suberin mutant was *gpat5* with an impaired GLYCEROL-3PHOSPHATE SN2-ACYLTRANSFERASE 5 (GPAT5),

which is an enzyme with acyl-CoA:glycerol-3-phosphate acyltransferase activity. Knockout mutation results in a 50 % decrease of aliphatic suberin especially in the content of very long chain α, ω-dicarboxylic and ω-hydroxy acids (Beisson et al., 2007). In subsequent studies, the enzymes HYDROXYLASE OF ROOT SUBERIZED TISSUES (HORST) and ROOT ALIPHATIC PLANT HYDROXYLASE (RALPH) were characterised. Both enzymes belong to the subfamily of cytochrome P450 monooxygenases. A Knockout mutation of *HORST* decreases the content of ω-hydroxy and α, ω-dicarboxylic acids with a carbon chain length smaller than 20, whereas a knockout of *RALPH* affects carbon chain lengths longer than 20 (Höfer et al., 2008; Compagnon et al., 2009). Very-long-chain fatty acids are synthesised by condensation of C2 units to an acyl-CoA by 3-ketoacyl CoA synthase (KCS). Two KCS enzymes, KCS20 and KCS2/DAISY are involved in the synthesis of both fatty acids with carbon chain length of 22 and 24. Double knockout of these two genes results in decreased corresponding fatty acids and derivatives in root suberin (Lee et al., 2009). Of particular interest is the experiment of treating green cotton fibers with a specific inhibitor of the endoplasmic reticulum-associated fatty acid elongases. Here, the inhibition provokes discontinuous suberin layers. A small proportion of the electron-translucent suberin lamellae was thinner after treatment with S-ethyl-N,N-dipropylthiocarbamate (EPTC). Chemical analysis of treated green cotton fibers showed a higher proportion of 16 carbon chain lengths, indicating that the usual found chain lengths of 18 carbon atoms were shortened to 16. Missing carbon atoms in the fatty acid chain length corresponds to the decreased diameter of electron-translucent lamellae, indicating that the electron-translucent lamellae may contain the aliphatic domain. In contrast, the electron-opaque lamellae with more flexible diameter would be composed of aromatic substances (Schmutz et al., 1996).

So far only one transcription factor has been described to induce the suberisation in *Arabidopsis thaliana*. Overexpression of *MYB41* in leaves of *Arabidopsis thaliana* and *Nicotiana benthamiana* provokes the suberisation of the cell walls of both epidermal and mesophyll cells. The ectopic suberisation reveals a typical suberin lamellar-like ultrastructure. All known biosynthetic genes are highly expressed due to the ectopic expression of *MYB41*. Interestingly, lignin seems to be induced with corresponding phenylpropanoid biosynthetic genes as well. However, MYB41 is not expressed in the endodermis under non-stress conditions. In contrast, abiotic stresses, such as salt stress, induce the expression of *MYB41*. Thus, the peptide MYB41 is a transcription factor that

induces suberisation under stress conditions (Kosma et al., 2014; Vishwanath et al., 2015). Furthermore, two *Arabidopsis* NAC-transcription factors (ANAC) were characterised by Marc Stefan Frenger and Katharina Markus. Both *ANAC038* and *ANAC058* are involved regulating suberin biosynthesis (Frenger, 2014; Markus, 2018). Research on both transcription factors is still proceeding.

As described above, suberin contains not only a polyaliphatic but also a polyaromatic domain. The polyaromatic is spatially distinct from the polyaliphatic domain (Bernards, 2002). Studying the metabolism of radio labelled ^{13}C phenylalanine in *Solanum tuberosum* by using nuclear magnetic resonance (NMR) showed that a major component of the polyaromatic domain consists of hydroxycinnamic acids, which are covalently cross-linked, but not due to ester bonds (Bernards et al., 1995). In addition, another NMR study showed the presence of guiacyl- and syringyl-phenolic compounds, which seem to be linked to polysaccharide-type glycosides in suberised cell walls (Yan and Stark, 2000). Guiacyl- and syringyl-monomers are typical lignin compounds (Weng et al., 2010). Two lignin-specific analytical procedures, thioacidolytic analysis and "derivatisation followed by reductive cleavage" (DFRC) (Lapierre et al., 1986; Lu and Ralph, 1997) show that suberised potato periderm contains only 5 to 6 % of the amount of monolignols in comparison to lignified tissue (Bernards, 2002). This appears contradictory. Bernards explains this phenomenon by tissue dependant polyaromatic profile. Cell walls in the stele consists of 100 % lignin and thereby only of monolignols. Cell walls close to the epidermis are composed of a mixture of hydroxycinnamates and monolignols. But the amount of monolignols is a relatively small one. Thus, in its subcellular location and assembly the polyaromatic domain resembles lignin, but the precursors are different (Bernards, 2002). Polymerisation of the polyaromatic domain may occur by a hydrogen peroxide mediated process operated presumably by a cell wall anionic peroxidase (Bernards, 2002; Graça, 2010). The involvement of an anionic peroxidase has been implicated since a long time (Kollatukudy 1980; Espelie and Kollatukudy, 1985). However, in tomato suberin biosynthesis cationic peroxidases have been proposed and during wound-stress cationic peroxidases accumulate in potato tubers (Bernards et al., 1999; Quiroga et al., 2000). Thus, the involvement of a peroxidase is assumed but there are still evidences missing. Partial depolymerisation also demonstrated that ferulic acid is exclusively esterified to ω-hydroxy acids which are again linked to glycerol (Graça and Santos, 2007). In *Arabidopsis thaliana* around 5 % of the total suberin consists of

esterified aromatic compounds. The pre-dominant aromatic compound is ferulic acid followed by p-coumaric acid (Franke et al., 2005). The content of aromatic substances may differ among the plant species. Depolymerised suberin of *Quercus suber* bark tissue consists of up to 9 % ferulic acid (García-Vallejo et al., 1997). Between 10 and 15 % ferulic acid can be found in the seed coats of *Arabidopsis thaliana* and *Brassica napus* (Molina et al., 2006). Only one mutant is connected to the aromatic constituents. A feruloyl transferase, which belongs to the BAHD family of acyl-transferases, could be characterised. The knockout mutation leads to decreased amounts of esterified ferulic acid. However, no ultrastructural differences were found (Molina et al., 2009).

Two suberin ultrastructure models were proposed in the last decade, which both consider the chemical composition and the lamellar-like ultrastructure of suberin. The first one from Mark Bernards (fig. 7 A) describes that the polyaromatic domain is covalently attached to the polysaccharides of the primary cell wall. Glycerol acts as a linker molecule and connects the polyaromatic with the polyaliphatic domain. The polyaliphatic domain is a linear stacked glycerol-based polyester with esterified ferulic acid. Electron-translucent lamellae are formed by the predominately aliphatic zones, while the aromatic-rich zone would yield into the electron opaque lamellae. Thickness of an electron-translucent lamella is approximately to 2.5 nm, which corresponds to a C_{22}-hydrocarbon chain esterified to glycerol at each end. The combination of electron-translucent and -opaque lamellae is about 3 to 4 nm (Bernards, 2002).

The proposed model of Graça (fig. 7 B) describes a regularly stacked poly(acylglycerol) macromolecule, which represents the electron-translucent lamellae. The poly(acylglycerol), also defined as polyaliphatic domain, is the core of suberin and thus termed as “suberin” by Graça. In the suberin core unsaturated aliphatic monomers are present and bend the hydrocarbon chain. Rigidity is given to the macromolecular structure by the corresponding stacked 9,10-epoxy and 9,10-hydroxy derived fatty acids. In this way, secondary bonds like hydrogen bridges and cross-linkages are established via functional groups. The polyaliphatic domain is esterified to ferulic acid, which is covalently linked to the lignin-like polyaromatic domain. The polyaromatic domain contributes to the electron-opaque lamellae. Polyaromatic and polyaliphatic domain are alternated connected to each other which results in the lamellar-like structure of the suberin. Polyaromatics, which do not neighbour on both sides the suberin polyester, consists predominately of guiacyl lignin, that together with

polysaccharides implicate the formation of the primary cell wall (Graça and Santos, 2007; Graça, 2015).

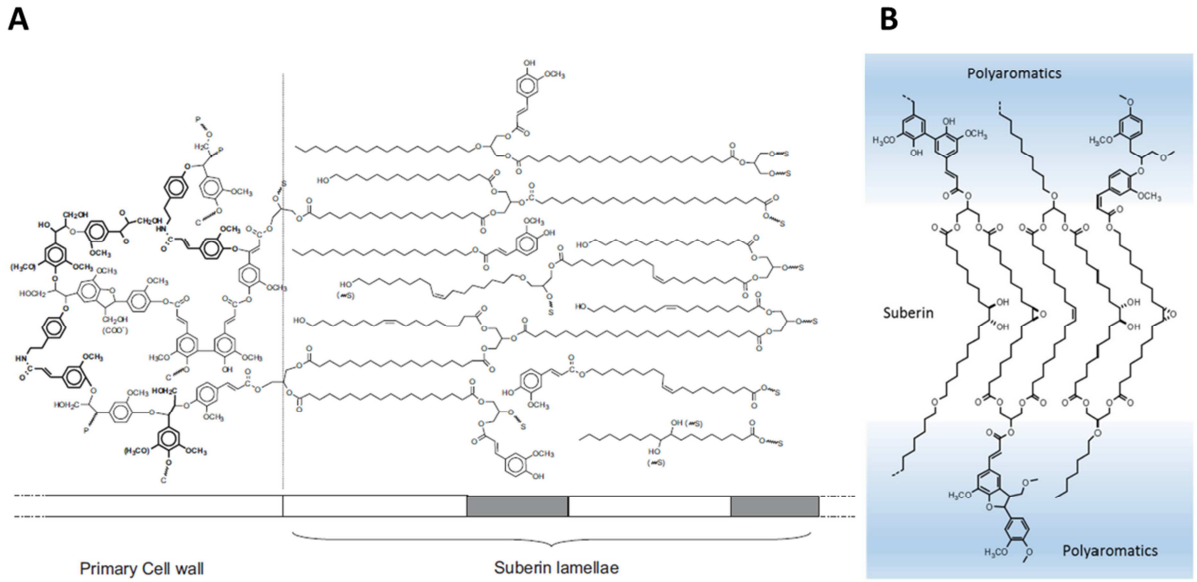

Fig. 7: The current proposed models of suberin chemical composition consistent with lamellar-like ultrastructure

A: The proposed model of Mark Bernards: The polyaromatic domain is covalently bond to the primary cell wall. Bold-faced phenolic compounds could be isolated with analytical techniques, others are assumed. Glycerol links the polyaromatic with the polyaliphatic domain. The aliphatic domain is linear and stacked. Formation of lamellae occurs via alternating aliphatic- and aromatic-rich zones (Bernards, 2002). **B:** José Graça's proposed suberin model: The backbone of the suberin is a poly(acylglycerol) core. The macromolecular structure is bent to the mid-chain unsaturated derived fatty acids. The packed arrangement of the poly(acylglycerol) is reinforced by the presence of 9,10-epoxy and 9,10-hydroxy derived fatty acids establishing hydrogen bridges and cross linkages. The polyaliphatic domain is esterified to ferulic acid which is covalently attached to the lignin-like polyaromatic domain. Alternating polyaromatic and poly(acylglycerol) domains form the lamellar-like ultrastructure. The polyaromatic domain which is not covalently bond at each end to the poly(acylglycerol) domain is covalently anchored in the primary cell wall (Graça, 2015).

Suberin monomers have to be exported to the extracellular space. The transport mechanism is still poorly understood. Monomers have to be either transported actively into the extracellular space, secreted via vesicles or there is an unknown transport mechanism (fig. 8). Three ATP binding cassette (ABC) transporters of the clade G were characterised (ABCG2, ABCG6 and ABCG20). ABC transporters pump different substrates across membranes by using energy from ATP hydrolysis (Higgins and Linton, 2004). Triple knockout of all three ABCG transporters cause a reduction in aliphatic suberin compounds with an incomplete suberin formation (Yadav et al., 2014). Regarding vesicular export, an increased number of vesicles fusing with the plasma membrane were observed in the cytosol of undifferentiated endodermal cells (personal communication with Marie Barberon, University of Geneva). It

might be possible that for instance these ABCG transporters are secreted via vesicles into the plasma membrane and suberin monomers are transported simultaneously the same way. Nonetheless, the way suberin monomers are transported to the extracellular space is poorly described and completely unknown is the manner how suberin monomers are assembled in the extracellular space. Enzymes are assumed to be in the cell wall, which mediate the polymerisation of suberin (fig. 8).

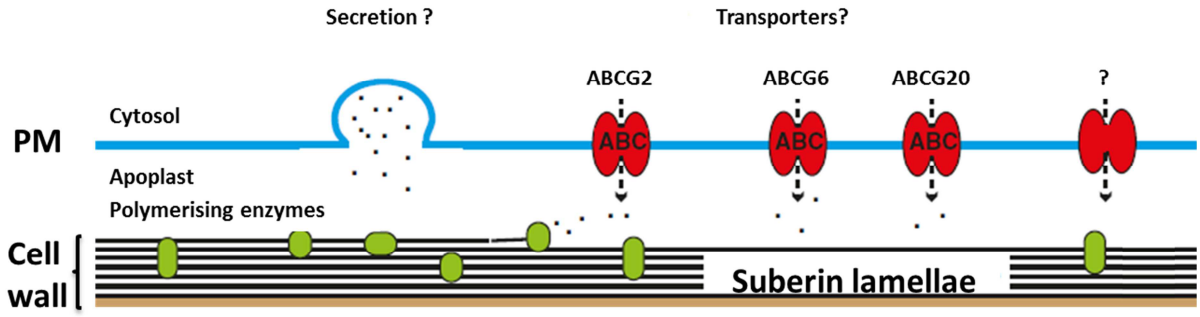

Fig. 8: Possible transport mechanisms of suberin monomers and polymerising enzymes involved in suberin assembly
Suberin monomers are either secreted via vesicles, actively transported mediated by ABC transporters or exported via an unknown transport mechanism. In the extracellular space the suberin monomers have to be polymerised to suberin lamellae by a still unknown mechanism probably processed by polymerising enzymes (altered from Andersen et al., 2015).

1.6. Suberin associated waxes

The suberin polymer is also found in association with non-covalently bonded waxes. These waxes are extracted with chloroform. For example the wax of isolated *Solanum tuberosum* peridermal tissue is composed of alkanes, primary alcohols, fatty acids and alkyl ferulates. Alkyl ferulates are the predominant monomer class of suberin associated waxes in *S. tuberosum* peridermal tissue (Espelie et al., 1980; Schreiber et al., 2005). Roots of *Glycine max*, *Arabidopsis thaliana*, *Iris germanica* and *Camelina sativa* have similar suberin associated wax compounds (Thomas et al., 2007; Li et al., 2007b; Meyer et al., 2011; Razeq et al., 2014). Suberin associated waxes play a major role in sealing properties of the peridermal tissue in potato tubers (Schreiber et al., 2005; Schreiber, 2010). So called “root waxes” were only found in peridermal tissue of the *Arabidopsis thaliana* root. These waxes consist of sn-2 monoacylglycerols, alkyl hydroxycinnamates, fatty acids, primary alcohols, alkanes, sterols. Predominant of alkyl hydroxycinnamates are the alkyl caffeate and alkyl coumarate esters (Li et al., 2007b; Molina et al., 2009; Kosma et al., 2012). As far it is known, A FATTY ALCOHOL:CAFFEOYL-CoA CAFFEOYL TRANSFERASE (FACT), which belongs to the

BAHD family enzymes, is involved in generating alkyl caffeate esters and FATTY ACYL-CoA REDUCTASEs (FARs) are responsible for the synthesis of primary alcohols (Kosma et al., 2012). However, the physiological function of root waxes is unknown. Abiotic stresses, such as salt stress, do not influence the root wax composition significantly. It is further suggested, that alkyl hydroxycinnamates have an antioxidant activity and may protect the plant against oxidative stress or they may function as antimicrobial compounds. Knockout of the *FAR* genes or of *FACT* appears to result in low survival rates against pathogen attack (Domergue and Kosma, 2017). Further research of root waxes could contribute to our understanding of how suberin and these associated waxes may interact and contribute to an effective barrier.

1.7. Chemical composition of lignin

When plants moved during evolution from an aquatic environment to a terrestrial one, they were challenged with several abiotic factors. Water protected the ancestors of terrestrial plants in their aquatic habitat from desiccation, reduced the gravitation by buoyancy and minimised the UV-B radiation. Furthermore, co-evolution of herbivores and pathogens impeded the colonisation of the terrestrial environment as a new ecological niche (Raven, 1984). The development of phenylpropanoids by plants was a crucial step to cope with many stress factors. Deamination of the amino acid phenylalanine enabled plants to tolerate UV-B radiation. Cinnamic acid shows absorbance maxima in the UV-B range (280-320 nm). The survival in a terrestrial environment became possible due to the accumulation of phenylpropanoids as early land plants could protect their haploid spores against UV radiation (Lowry et al., 1980). The move onto land was also hindered by the lack of mechanical reinforcement which additionally limited the growth of the early land plants (Bateman et al., 1998). The development of lignin strengthened the plant and gave it the physical rigidity to stand upright. Furthermore, lignified water-conducting cells enabled the water transport over longer distances. Together the strengthened plant body and the ability to transport water over long-distance by deposition of lignin in the cell wall expanded the size of terrestrial plants. The degradation of the lignin polymer by pathogens or herbivores is difficult due to the randomness of linkages within the lignin polymer. The plants invest in the advantageous process of lignification even if is a major carbon sink in terrestrial plants. It is estimated that about 30 % of the total biomass in the biosphere is caught by lignification.

Only the production of cellulose catches a higher amount of carbon (Boerjan et al., 2003). The colonisation of the terrestrial environment by plants provoked severe alterations. Chemical weathering of rocks caused by the release of organic acids from the roots of early tracheophytes and accumulation of dead plant material accompanied by decay contributed to the formation of soil (Gensel and Edwards, 2001). Lignification of cell walls also led to the technical progress of humanity. The coal, dead plant material in swamps and peat bogs compressed by deposited soil over millions of years, initiated the industrialisation and heralded the industrial revolution (Hayatsu et al., 1979; Allen, 2010).

In *Arabidopsis thaliana* lignin is found in various different tissues. Interfascicular fibers of the stem and cell walls of xylem bundles are lignified. In the root tissue the vascular bundles of the tracheary elements and the Casparian strip in the endodermis are lignified. Lignification of tracheary elements and interfascicular fibers are secondary cell wall modifications, whereas the Casparian strip development is a primary cell wall modification (Dharmawardhana et al., 1992; Jones et al., 2001; Hoffmann et al., 2004; Barberon and Geldner, 2014; Zhao, 2016).

The chemical structure of the lignin polymer is composed of hydroxycinnamyl alcohols. These hydroxycinnamyl alcohols are *p*-coumaryl alcohol, coniferyl alcohol and sinapyl alcohol (Boerjan et al., 2003). Hydroxycinnamyl alcohols are called monolignols (Bernards, 2002). The lignin composition derived from the monolignols is commonly referred to as hydroxyphenyl (H), guiacyl (G) and syringyl (S) lignin. H- and G-monolignols are the lignin fundament of all tracheophytes. Within the lignin polymer small amounts of hydroxycinnamaldehyds, hydroxycinnamic acids, dihydroconiferyl alcohol and ferulate were found as well. Thus, lignin may contain nearly any homopolymer rather than the three fundamental monolignols. Furthermore, there is also a particular variation in the lignin composition among species. Seed coats of vanilla orchids contain catechyl monolignols, so called C-lignin derived from caffeoyl alcohol (Tobimatsu et al., 2013; Zhao, 2016). S-monolignols are specific compounds only found in angiosperms and in the lycophyte *Selaginella* (Weng et al., 2008b; Weng and Chapple, 2010).

The lignin polymer is composed of a certain ratio of the three monolignols through oxidative coupling. Educts of the oxidative coupling reaction are monomers but also oligomers (fig. 9). Several covalently linkages are found in lignin such as β-O-4’, β-5’, 5’-5’, 4-O-5’, β- β’ and β-1. The oxidative coupling of the monomers and oligomers seems to be a combinatorial process

only controlled by the chemical properties and concentrations of the reactants as well as the conditions in the surrounding environment. The monolignols have to be transported into the apoplast, where the polymerisation takes place (Ralph et al., 2004; Weng and Chapple, 2010).

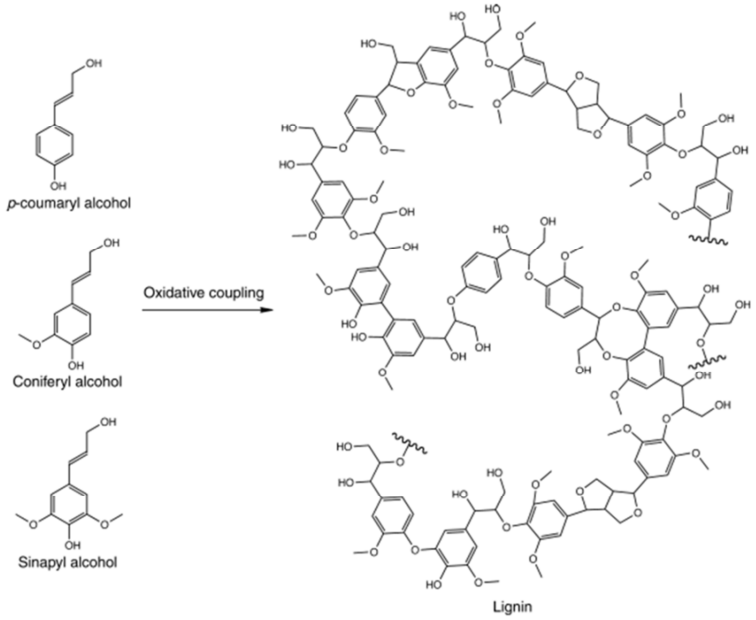

Fig. 9: Chemical structure of the lignin polymer and its monolignols

Oxidative coupling of monolignols leads to the growth of the lignin polymer. Characteristic of the lignin polymer is the high diversity of covalently linkages, which impedes the chemical degradation of the polymer by pathogens and herbivores for instance (Weng and Chapple, 2010).

Polymerisation of the lignin monolignols seems to be tissue-dependent. For example, the peroxidase PER64 is involved in the polymerisation process of CS but knockout mutation of *PER64* does not affect the lignin composition of the stem. In contrast, loss of function mutations in the laccases LAC4, LAC11 and LAC17 and especially the triple knockout mutant *lac4*lac11*lac17* abolish the lignin content in the root. However, CS formation is still present. Thus, this indicates that peroxidase and laccase are not redundant regarding lignin polymerisation and both are specialised in polymerising lignin in different plant tissues (Zhao et al., 2013; Zhao, 2016).

Master regulators of the lignification of xylem vessel cell differentiation and interfascicular fibers could be identified. The VASCULAR-RELATED NAC-DOMAIN (VND) 1-7 and the NAC SECONDARY WALL THICKENING PROMOTING FACTOR (NST) 1-3 play a crucial role in lignification process. Also two MYB transcription factors *MYB58* and *MYB63* promote the lignification (Zhao, 2016). Two mediators, MED5a and MED5b (also known as REF4), act as

lignin repressors in *Arabidopsis thaliana*. Both regulate as a large mediator complex the phenylpropanoid homeostasis in response to metabolic alterations. For instance, they participate in the cross-talk of tryptophan and phenylalanine biosynthesis pathway to regulate the allocation of metabolites to these pathways (Bonawitz et al., 2014; Zhao, 2016).

1.8. Phenylpropanoid pathway

The phenylpropanoid pathway provides metabolites of the secondary metabolism in plants. These metabolites share the same basic molecular structure: an aromatic ring-system. The products of the phenylpropanoid pathway have a positive effect on human health. For instance, it has been reported that phenylpropanoids show antioxidant effects in vitro, are estrogen-like, cause vasodilation activities, exhibit anti-inflammatory, anti-aging effects as well as anticancer chemopreventive action (Othlof et al., 2000; Othlof et al., 2003; Hoffmann et al., 2004; Luo et al., 2008; Pandey and Rizvi, 2009). Still, the question remains to be answered whether aromatic compounds have antioxidant effects in vivo, because aromatic compounds are extensively metabolised in organisms. The metabolised aromatic compounds may reduce the antioxidant effect of the parent aromatic (Manach et al., 1998; Othlof et al., 2003).

As already described, the phenylpropanoid pathway allocates the precursors of the lignin polymer, the phenylpropanoids (Franke et al., 2002b). The compounds have various functions in the plant, as they protect it against harmful UV-B radiation by sinapate esters (Jin et al., 2000), flavonoids provide the pigmentation of flowers (Holton et al., 1993) and may be involved in fungal pathogen defence in *Solanum tuberosum* (Maher et al., 1994; Sonnante et al., 2010).

Precursor of phenylpropanoid derivatives is the amino acids L-phenylalanine (fig. 10) and in some plant species also L-tyrosine. In maize and soybean the use of tyrosine as precursor of the phenylpropanoid pathway could be demonstrated by enzymatic assay (Rösler et al., 1997; Khan et al., 2003). Phenylalanine ammonia lyase (PAL) is the first enzyme of the phenylpropanoid pathway (fig. 10). It is responsible for the deamination of the L-phenylalanine resulting in *trans*-cinnamic acid. *Arabidopsis thaliana* has four isoforms of PAL. The substrate of all PALs is L-phenylalanine, whereas in *Zea mays* PAL activity could be

demonstrated for both L-phenylalanine and L-tyrosine. Deamination of L-tyrosine results in the formation of *p*-coumaric acid (Rösler et al., 1997; Cochrane et al., 2004).

Cinnamate-4-hydroxylase (C4H) is a cytochrome P450 monooxygenase. It hydroxylates the carbon atom at *para* position of the aromatic ring. Product of this hydroxylation step is *p*-coumaric acid. 4-hydroxycinnamoyl-coenzme A ligase (4CL) attaches coenzyme A to *p*-coumaric acid and provides *p*-coumaroyl CoA. It is an important key substrate because it used for the flavonoid, isoflavonoid, anthocyanin, stilbene as well as *p*-hydroxyphenyl lignin synthesis, or it is further used as substrate for the following downstream products. The hydroxycinnamoyl-coenzme A shikimate/quinate hydroxycinnamoyl-transferase (HCT), which belongs to the BAHD acyltransferase superfamily, connects *p*-coumaroyl CoA to either shikimate or quinate. Another cytochrome P450 monooxygenase p-coumaroyl shikimate 3-hydroxylase (C3H) hydroxylates the esterified *p*-coumaroyl quinate or *p*-coumaroyl shikimate at *ortho*-position of the aromatic ring. Afterwards the ester bond is disestablished by HCT resulting in caffeoyl CoA. Caffeoyl-CoA *O*-methyl transferase (CCoAOMT) methylates the hydroxyl-group at the *ortho*-position by using S-adenosyl methionine (SAM) as a methyl donor. As a product of the reaction the important feruloyl-CoA for suberin synthesis is released (fig. 10). The oxidoreductase cinnamoyl-CoA reductase (CCR) uses either *p*-coumaroyl CoA or feruloyl CoA as a substrate and cleaves off the coenzyme A. This catalysed reaction yields into the formation of *p*-coumaraldehyde and coniferaldehyde respectively. Cinnamyl alcohol dehydrogenase (CAD), which is also an oxidoreductase, reduces the functional aldehyde-group to an alcohol-group producing of *p*-coumaryl and coniferyl alcohol. Both enzymes CCR and CAD are established in the core biosynthetic pathway of the monolignols. The synthesis of S-monolignols requires the two enyzmes ferulic acid/coniferaldehyde/coniferyl alcohol 5-hydroxylase (F5H) and caffeic acid *O*-methyl transferase (COMT). COMT, similar to CCoAOMT, is also a SAM-dependent *O*-methyltransferase. The combination of both enzymes leads finally to the addition of a 5-methoxy group to ferulic acid, coniferaldehyde or the coniferyl alcohol resulting in the formation of sinapic acid, sinapaldehyde or sinapyl alcohol (Franke et al., 2002a; Franke et al., 2002b; Hoffmann et al., 2003; Hoffmann et al., 2004).

As mentioned the lycophyte *Selaginella moellendorffii* contains S-lignin. A novel identified P450 enzyme in *Selaginella moellendorffii* (SmF5H) is involved in its synthesis of S-lignin. Studies on enzyme kinetics reveal that SmF5H is able to hydroxylate the *ortho* position of the

aromatic ring of coniferaldehyde and coniferyl alcohol expressed in F5H-deficient *Arabidopsis* mutant (Weng et al., 2008b). Furthermore, expressed in an *Arabidopsis* C3H and F5H double knockout mutant enables the S-lignin synthesis via a new route in the phenylpropanoid pathway not present in angiosperms. The enzyme SmF5H can synthesise S-lignin by using *p*-coumaraldehyde and *p*-coumaroyl alcohol. Caffealdehyde and caffeyl alcohol are the products of this reaction and are again used as substrates by COMT resulting in the corresponding G-units. Thus, the enzyme SmF5H opens an independent pathway of S-lignin synthesis without the participation of HCT, C3H and CCoAOMT (Weng et al., 2010) (fig. 10).

The hydroxycinnamaldehyde dehydrogenase (HCALDH) is responsible for the catalysis of the $NADP^+$-dependent oxidation of coniferaldehyde and sinapaldehyde to produce ferulate and sinapate. Finally, these ferulate and sinapates are involved in the synthesis of sinapate esters in the leaves of *Arabidopsis thaliana*. However, HCALDH only contributes 10 % of the total sinapate esters in leaves (Nair et al., 2004; Fraser and Chapple, 2011). The combination of C3H and COMT by using *p*-coumaric acid as an initial substrate shows another possible route to synthesise sinapate esters without HCALDH (Hoffmann et al., 2004).

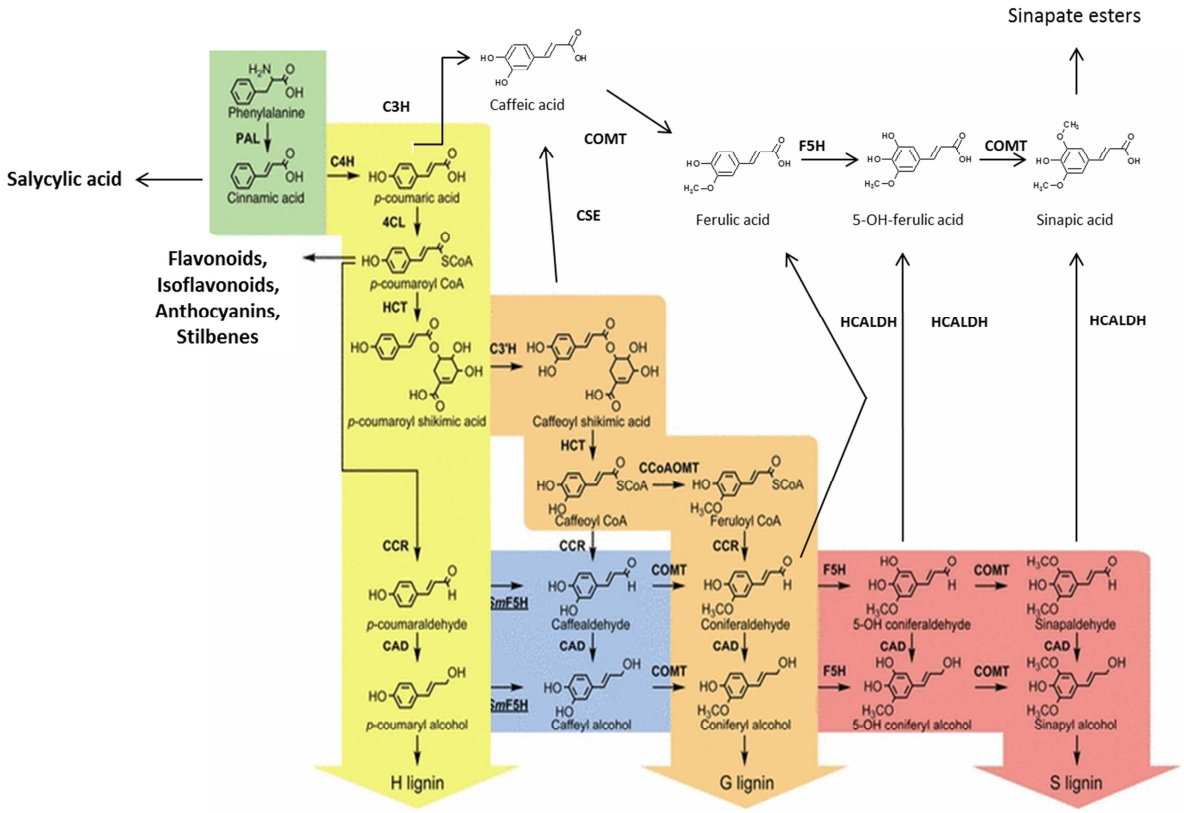

Fig. 10: Phenylpropanoid pathway known in *Arabidopsis thaliana* with additional route employed by SmF5H

The preferred route of the synthesis of the three different monolignols is shown in different colours. H-monolignol synthesis is depicted in yellow, whereas G-monolignols synthesis is presented in orange and S-monolignol synthesis in red. The new route of S-lignin synthesis employed by SmF5H is shown in blue. Schematic view of the phenylpropanoid pathway shows the high flexibility and plasticity of the phenylpropanoid biosynthesis. CAD: cinnamyl-alcohol dehydrogenase, CCoAOMT: caffeoyl-CoA *O*-methyl transferase CCR: cinnamoyl-CoA reductase, C3H: p-coumaryl shikimate 3-hydroxylase, C4H: cinnamate 4-hydroxylase, 4CL: 4-hydroxycinnamoyl-CoA ligase, COMT: caffeic acid *O*-methyl transerase, CSE: caffeoyl shikimate esterase, F5H: ferulic acid/coniferaldehyde/coniferyl alcohol 5-hydroxylase, HCT: hydrocinnamoyl-CoA shikimate/quinate hydroxycinnamoyltransferase, PAL: phenylalanine ammonia-lyase (altered from Hoffmann et al., 2004; Weng and Chapple, 2010; Fraser and Chapple, 2011; Zhao, 2016).

1.9. Aim of this Ph.D. thesis

Crop failures caused by abiotic stress factors such as drought and salinity and biotic stress factors like pathogen infestation may be prevented by an improved suberin barrier. In the last decade suberin research was limited on the polyaliphatic domain, but less is known about the polyaromatic domain. In this thesis I will focus on the contribution of phenylpropanoids to the suberin polymer. Elucidating the role of phenylpropanoids to the suberin barrier may additionally increase our knowledge about suberin development, its ultrastructure and how suberin impairs the diffusion of water, solutes and nutrients into the vascular tissue.

Due to the availability of knockout mutants in the *Arabidopsis* stock centres, the established analytical methods in the laboratory and the easy handling this work will use *Arabidopsis thaliana* as an organism to study the contribution of phenylpropanoids to the suberin barrier. Selection of putative candidate genes will be performed through databank enquiry of co-expression studies by using known suberin, lignin and Casparian strip genes as references. Roots of seedlings will be histochemical analysed and mature roots will be used for the analytical approaches. Depending on the results, further experimental approaches will be performed.

2. Materials and methods

2.1. Materials

2.1.1. Plant material

In this study the plant species *Arabidopsis thaliana* (L.) Heynh ecotype Columbia was used for different experiments. If another ecotype was used it will be explicit described. The used T-DNA insertion mutant lines and the corresponding wildtype plants were obtained from the Nottingham Arabidopsis Stock Centre (NASC, Nottingham, United Kingdom). The mutant lines *esb1* was provided by group members of the ERA-CAPS project, whereas the mutant lines *ref1-4*, *ref3-2*dex::REF3*, *ref8-1*med5a*med5b*, *ref8-2*fah1-2*AtC4H::SmF5H*, *cadc*cadd*, *cadc*cadd*fah1-2* were provided by Dr. Jeong Im-Kim (Horticultural Science Department, University of Florida) and by Prof. Dr. Clint Chapple (Purdue University).

2.1.2. Chemicals and reagents

Unless otherwise notated, chemicals were delivered by the companies Carl Roth (Karlsruhe, Germany), Sigma-Aldrich (München, Germany), Macherey-Nagel (Düren, Germany) and Merck (Darmstadt, Germany). Oligonucleotides were ordered from Thermo Fisher Scientific/Invitrogen (Schwerte, Germany).

2.1.3. Kits

In this study different kits were used:

- Total RNA isolation from plant, NucleoSpin® RNA Plant, Macherey-Nagel (Düren, Germany)
- PEQGOLD PLANT DNA MINI Kit, VWR
- SuperScript™ III One-Step RT-PCR System with Platinum® *Taq*-Polymerase, Invitrogen/Life technologies GmbH (Darmstadt, Germany)

2.2. Methods

2.2.1. Breeding conditions of soil-grown plants

Arabidopsis thaliana plants germinated and grew in the climate chamber at 20-22°C, 100 µE $m^{-2}s^{-1}$ light intensity and day-night rhythm of 16/8 h. The seeds were put on top of wet soil (Goldhumus) and stratified in the dark at 4 °C overnight. A plastic cover prevented the drying out of the soil and the seedlings to ensure a well germination. The plants were watered with tap water. In addition, a systemic insecticide (*Confidor WG70*; Imidacloprid, Bayer CropScience, Langenfeld, Germany) protected the plants against pests and a mineral fertilizer (*Flory 3 verde*, Planta, Regenstauf) provided essential trace elements to the plants.

2.2.2. Breeding conditions of hydroponic cultures

In order to cultivate *Arabidopsis thaliana* plants in hydroponic cultures the plants grew in cultivation containers (Araponics, Liège, Belgium). In total 18 plants could grow in seedling holders in one container. The hydroponic cultures grew in the same climate chamber under the same described breeding conditions like the soil-grown plants (chapter 2.2.1). Cigarette filters from the brand Gizeh were speared with a wooden stick. The covering paper of the cigarette filter was removed and the filters were washed in ethanol and water. The washed cigarette filters were put into the seedling holders. At least two seeds were put onto one cigarette filter (Lenz et al., 2013). Two litres nutrient solution was filled into the container to ensure that cigarette filters with seedling holders are embedded with nutrient solution. The nutrient solution was made from concentrates from General Hydroponics (Fleurance, France). According to the instruction manual two litres distilled water was concentrated with 1 ml of each concentrate solution. To protect the seeds from drying out a plastic cover was put onto the container for five days. The nutrient solution was changed once per week.

2.2.3. Breeding conditions of MS-agar grown seedlings

About 100 mg seed material was sterilised with 70 % ethanol containing 0.05 % triton X-100 for 10 minutes shaking at room temperature. Afterwards the sterilisation solution was removed under the sterile bench and the seeds were washed thrice with 96 % ethanol and the seeds were air-dried. Dried and sterilised seeds were placed in a row on ½ MS-agar plates with an autoclaved toothpick. The lid was fixed with parafilm. The sown seeds were stratified on ½ MS-agar plates at 4 °C in the dark overnight. On the following day the ½ MS-agar plates containing the seeds were put vertical in the climate chamber into a plate holder. The seedlings grew about for seven days when the primary root reached a length about one cm.

2.2.3.1. Feeding experiments and dexamethasone treatment of MS-agar grown seedlings

Coniferylalcohol, *trans* ferulic acid and dexamethasone stock solutions of 10 mM were prepared in either DMSO. Dissolved solutions were sterile filtrated and added to the autoclaved ½ MS-agar media. The final concentration in the ½ MS-agar media was 10 µM. Dried and sterilised seeds were placed in a row on ½ MS-agar plates containing 10 µM of one of the three compounds. Stratification and growing process were performed according to the previous described method (chapter 2.2.3.). The dexamethasone treatment was performed according to the personal communication with Dr. Jeong Im-Kim (Horticultural Science Department, University of Florida).

2.2.3.2. Piperonylic acid treatment

Piperonylic acid (PA) stock solution of 10 mM was prepared in liquid ½ MS-media. Dissolved solution was sterile filtrated and added to either liquid ½ MS-media or ½ MS-agar media. The final concentration was 10 µM. Seedlings incubated in liquid ½ MS-media containing PA for 24 h. Another group was transferred onto ½ MS plates containing 10 µM PA on the last two days before harvesting. The third group germinated and grew on ½ MS plates containing 10 µM PA. As a positive control *esb1* was used. The mutant *esb1* grew only on ½ MS plates without PA.

2.2.4. Hybridisation of *Arabidopsis thaliana*

Arabidopsis thaliana is able to pollinate itself. Therefore, hybridisation of different genotypes is possible. To avoid self-pollination or cross pollination a closed florescence has to be used. The female florescence organ starts to mature earlier than the male florescence organs. The maturation of the female florescence organ starts when the sepals and the petals are still closed. The gynoecium is surrounded by the male florescence organs the anthers. After maturation of the male florescence organs the anthers release pollen grains. The pollen grains are received by the stigma and pollinate the female florescence organs.
In order to hybridise two different genotypes a closed florescence was chosen. By using precise forceps petals, sepals and anthers were removed. From the pollen grain donator plant matured anthers were dissected and put onto the prepared stigma of the receptor plant. If a yellowish covering could be seen with a magnifying glass, the stigma was covered with cling film to avoid cross pollination. A successful pollination led to a silique which was harvested after 2 weeks. According to the Mendelian inheritance the F_1 generation should be heterozygous, which was proofed by genetic approaches. An identified heterozygous plant was pollinated by itself. The F_2 generation should exhibit a segregation pattern of 1:2:1. According to the Mendelian inheritance a double knockout mutant should be possible to identify (Mendel, 1866).

2.2.5. Selection of putative candidate genes involved in the assembling of the aromatic polyester in suberin

Aromatic compounds are synthesised via the phenylpropanoid pathway. Most of the selected genes were used in this work due to the participation in the phenylpropanoid pathway. Studying phenylpropanoid pathway genes ensures to determine influences on the synthesis of *trans* ferulic acid. The gene *ASFT* was chosen due to the reason that knockout mutation causes loss of transesterified ferulic acid (Molina et al., 2009). The two MYB transcription factors MYB4 and MYB7 work antagonistically in the regulation of flavonoid biosynthesis (Fornalé et al., 2014). Possibly, the knockout of each single MYB transcription factor could influence the synthesis of ferulic acid. Based on freely available databanks the selected candidate genes were screened on co-expression of suberin specific genes and

tissue specific expression. Most relevant was the tissue specific expression of the candidate genes. The tissue specific expression of the candidate genes was analysed via the Arabidopsis eFP browser (http://bar.utoronto.ca/efp/cgi-bin/efpweb.cgi; Winter et al., 2007). The co-expression of the candidate genes was investigated by using the ATTED-II databank (http://atted.jp/; Obayashi et al., 2007).

2.2.6. Molecular biological approaches

2.2.6.1. Isolation of genomic DNA

The kit *peqgold Plant DNA Mini Kit* (VWR; Darmstadt, Germany) was used to extract genomic DNA. The extraction of genomic DNA was performed according to the instructions. At first the plant material is lysed. Afterwards the DNA is purified by a silica membrane. A specific buffer system removes all remaining cell fragments, lipids, secondary metabolites and proteins. Finally, the genomic DNA is eluted.

2.2.6.2. Isolation of RNA

In order to isolate RNA the kit *Total RNA isolation from plant, NucleoSpin® RNA Plant* (Macherey-Nagel; Düren, Germany) was used. The RNA extraction was performed according to the instructions manual.

2.2.6.3. Determination of nucleic acid concentration

The validation of nucleic acids quantity was determined by *NANODROP 2000c Spectrophotometer* (PEQLAB; Erlangen, Germany). DNA and RNA respectively have an absorption maximum at an OD value of 260 nm. The calculation of the nucleic acid concentration was made by the formula:

Formula 1: Calculation of the nucleic acid concentration

c: concentration of the nucleic acid, OD260: optical density at 260 nm, V: dilution factor, F: multiplication factor (50 for genomic DNA and 40 for RNA)

$$c\left[\frac{\mu g}{ml}\right] = OD_{260} \times V \times F$$

Afterwards the absorption of 280 nm was measured. The calculation of the ratio of both ODs represents the protein contamination. A ratio between 1.8 and 2.0 of a nucleic acid sample is seen to be sufficient pure. A ratio less than 1.8 shows a contamination of phenol or protein, whereas a higher value than 2.0 exhibits denaturation of nucleic acids.

2.2.6.4. Validation of RNA quality

In order to verify the RNA quality the RNA was loaded into a 1% (w/v) ethidium bromide-stained agarose gel. Exactly 200 ng RNA were used to separate by electrophoresis. Under UV-light three RNA fragments (28S, 18S and 5S) were visualised by the fluorescence signal. In this process it is important to obtain a similar intensity of all RNA fragments to ensure that the RNA is not degraded and can be used beyond doubts.

2.2.6.5. Polymerase chain reaction (PCR)

The polymerase chain reaction (PCR) is a useful tool in the molecular biology to amplify areas of interest in the genomic DNA. The amplification was performed by using the *KAPA2G® FAST 2x ReadyMix with Dye* (Sigma Aldrich, München, Germany) according to the instructions.

The amplification of genomic DNA areas for cloning was made with the *Phusion® High Fidelity DNA Polymerase* (Thermo Fisher Scientific; Schwerte, Germany) according to the protocol of the kit. All PCR samples were heated by *Primus 96 advanced Thermocycler* (PEQLAB; Erlangen, Germany). The composition of the PCR samples and the temperature program are listed below.

Tab. 1: Composition of PCR with *KAPA2G® FAST 2x ReadyMix with Dye*

Reagent	Volume [µl]	Concentration (final)
KAPA2G® FAST 2x Ready Mix with Dye	12.5	1x
Forward primer (50 µM)	1.25	0.5 µM
Reverse primer (50 µM)	1.25	0.5 µM
Template DNA	As required	≤ 250 ng
HPLC deionised water	Fill up to 25	-

Tab. 2: Temperature program of the thermocycler with *KAPA2G® FAST 2x ReadyMix with Dye*

Reaction step		Temperature [°C]	Time
Initial Denaturation		95	2 min
	Denaturation	95	15
PCR amplification	Hybridisation	Primer depending	30
35 cycles	Elongation	72	5 s/kbp
Final elongation		72	5 min

Tab. 3: Composition of *Phusion® High Fidelity DNA Polymerase*

Reagent	Volume [µl]	Concentration (final)
5x Phusion® HF Buffer	4	1x
10 mM dNTPs	1	200 µM
Forward primer (50 µM)	1.25	0.5 µM
Reverse primer (50 µM)	1.25	0.5 µM
Template DNA	As required	≤ 250 ng
Phusion® DNA Polymerase	0.2	0.02 U/µl
HPLC deionised water	Fill up to 20	-

Tab. 4: Temperature program of the thermocycler with *Phusion® High Fidelity DNA Polymerase*

Reaction step		Temperature [°C]	Time
Initial Denaturation		98	30 s
	Denaturation	98	10
PCR amplification	Hybridisation	Primer depending	30
35 cycles	Elongation	72	15 s/kbp
Final elongation		72	5 min

2.2.6.6. Ethidium bromide-stained agarose gel electrophoresis

The PCR samples were provided with an appropriate amount of six-fold loading buffer (0.1% bromine phenol blue (w/v); 40% saccharose (w/v)) to achieve a one-fold loading buffer concentration. Afterwards, the PCR samples were applied on a 1% agarose gel in TAE-buffer. The verification of the PCR fragment size was done by the use of a 100 bp DNA ladder. Ethidium bromide was used to visualise the PCR fragments. The separation by electrophoresis was performed at 120 V. Finally, when the fragments were separated a picture was taken by using UV-light.

2.2.6.7. Genotyping of T-DNA insertion mutants

In order to identify the position of a T-DNA insertion a PCR primer set of three primers was chosen. The gene specific primers flank the presumed position of the T-DNA insertion, whereas the T-DNA insertion primer aligns the left border of the T-DNA insertion. The amplicon size of the product of the gene specific primer and the combination of the T-DNA and a gene specific primer has to be different to differentiate wildtype plants from T-DNA insertion mutants. In one PCR set up with all three primers together three possible results could be obtained from two alleles: wildtype/wildtype, wildtype/mutant and mutant/mutant.

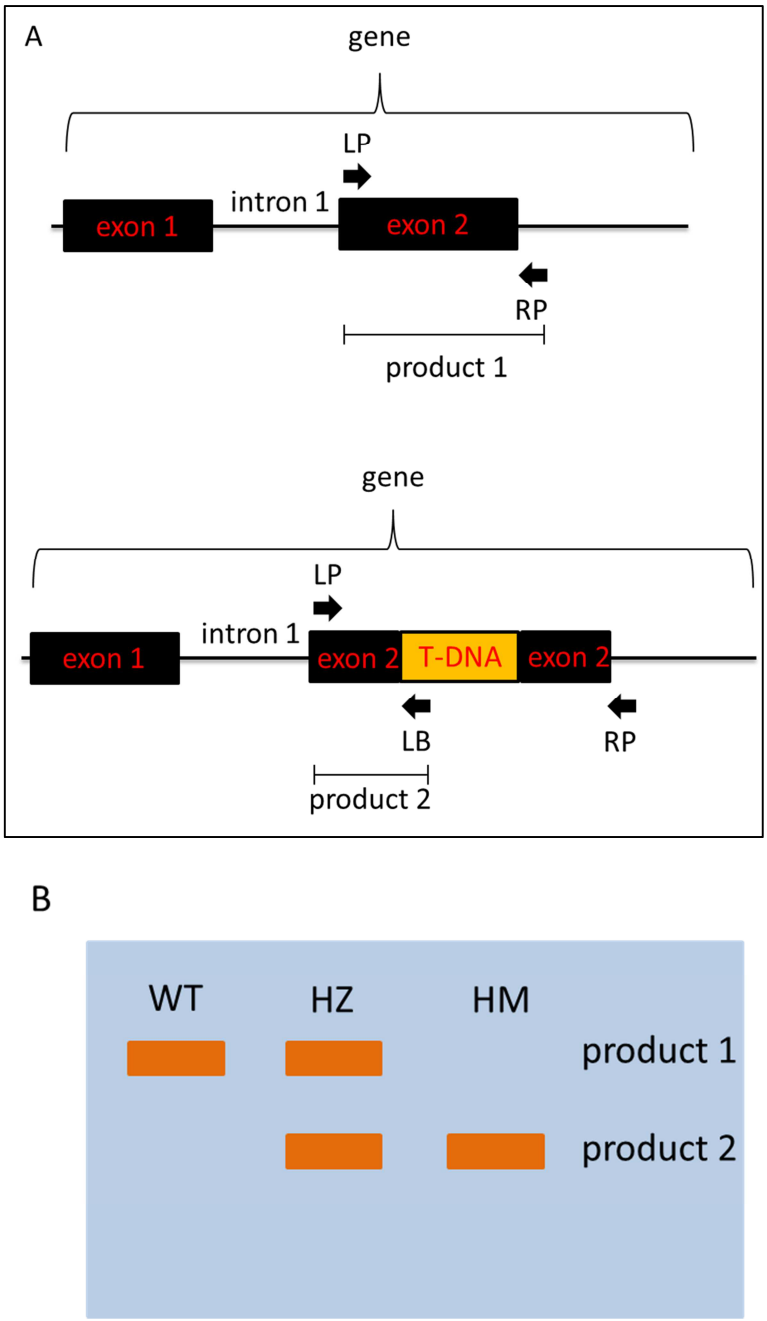

Fig. 11: Functional principle of T-DNA insertion in the genome

A: Schematic presentation of a T-DNA insertion. It is represented a wildtype allele and mutant allele with T-DNA insertion and the position of the primers with the corresponding amplicon size. LP: left genomic primer; RP: right genomic primer; LB: left border primer

B: Schematic presentation of separated possible amplicon products. WT: wildtype; HZ: heterozygous; HM: homozygous

Altered from http://signal.salk.edu/tdnaprimers.2.html

2.2.6.8. Reverse transcription polymerase chain reaction (RT-PCR)

Important information is the quantity of gene transcripts. The method of choice is the RT-PCR. The enzyme reverse transcriptase transcribes the RNA into its compliment DNA by

using oligo $d(T)_{18}$ primers. From the signal intensity of the PCR products a semi-quantitative analysis can be performed.

The RT-PCR was performed with the kit *SuperScript™ III One-Step RT-PCR System with Platinum® Taq-Polymerase* (Invitrogen) in a *Primus 96 advanced thermocycler* (PEQLAB; Erlangen, Germany) according to the manual. The composition of the RT-PCR samples and the temperature program is listed below.

Tab. 5: Composition of *SuperScript™ III One-Step RT-PCR System with Platinum® Taq-Polymerase*

Reagent	Volume [µl]	Concentration (final)
2x Reaction Mix	25	1x
Forward primer (50 µM)	1	0.2 µM
Reverse primer (50 µM)	1	0.2 µM
Template RNA	As required	10 pg – 1 µm
RT/Platinum Taq Mix	1	-
HPLC deionised water	Fill up to 50	-

Tab. 6: : Temperature program of the thermocycler with *SuperScript™ III One-Step RT-PCR System with Platinum® Taq-Polymerase*

Reaction step		Temperatur [°C]	Time
cDNA synthesis		55	30 min
Denaturation		94	2 min
	Denaturation	94	15 s
PCR amplification 35 cycles	Hybridisation	Primer depending	30 s
	Elongation	72	1 min/kbp
Final elongation		72	5 min

2.2.6.9. cDNA synthesis by VILO

According to the protocol of the *SuperScript® VILO cDNA Synthesis Kit and Master Mix* (Invitrogen) the cDNA synthesis was performed.

The composition of the cDNA samples and the temperature program is listed below.

Tab. 7: Composition of *SuperScript® VILO cDNA Synthesis Kit and Master Mix*

Reagent	Volume [µl]	Concentration (final]
5x VILO Reaction Mix	25	1x
Template RNA	As required	Up to 2.5 µg
10x SuperScript® Enzyme Mix	2	-
HPLC deionised water	Fill up to 20	-

Tab. 8: Temperature program of the thermocycler with the *SuperScript® VILO cDNA Synthesis Kit and Master Mix*

Reaction step	Temperatur [°C]	Time
Inhibition of ribonuclease	25	10 min
cDNA synthesis	42	60 min
Inactivation of enzyme	85	5 min

2.2.7. Microbiological approaches

2.2.7.1. Transformation of competent cells of *Escherichia coli*

In order to transfer plasmids *Subcloning Efficiency DH5 α® Competent Cells* (Life Technologies, Darmstadt, Germany) from *Escherichia coli* were used. The transformation of chemical component cells was performed according to the manual. Exactly 10 ng genetic materials were added to the chemical component cells and finally transformed by heat shock in the water bath for 30 seconds. After finishing the incubation time 10 µl, 100 µl and 890 µl aliquots of the transformed chemical component cells were streaked on LB-agar containing appropriate antibiotics. *E. coli* cells incubated on media overnight at 37 °C. In case of entry clone plasmids zeocin (50 µg/ml; Life Technologies, Darmstadt, Germany) or kanamycin (50 µg/ml) for expression clones were used for selection.

2.2.7.2. Preparation of chemical competent *Agrobacterium tumefaciens* cells

Cells of the *Agrobacterium tumefaciens* strain GC3191pMP90 grew on agar plates with LB-media containing rifampicin (10 µg/ml) for two days at 28 °C. Two Erlenmeyer flasks were filled each with 20 ml LB-media containing rifampicin. The LB-media was inoculated by single

colony of *A. tumefaciens*. Pre-culture grew overnight shaking at 170 rpm at 28 °C. On the following day, 20 ml of each pre-culture was added to fresh 200 ml LB-media containing appropriate rifampicin antibiotic. Cells grew for three to four hours at 170 rpm and 28 °C to OD_{600} value between 0.5 and 0.6. Afterwards, the main culture was separated on four 50 ml falcon tubes and centrifuged for 20 minutes at 3,200 and 4 °C g. The supernatant was discarded and the obtained pellets carefully resuspended in 20 ml ice-cold TE-buffer. Two pellets were combined in one falcon tube and 10 ml ice-cold TE-buffer was added to fill up the falcon tube. Cells were centrifuged again at the same conditions. The supernatant was discarded as well. The pellets were resuspended in 1 ml liquid LB-media. Aliquots of 200 µl were prepared and carefully frozen in liquid nitrogen. The prepared chemical competent *Agrobacterium tumefaciens* cells were stored at -80 °C.

2.2.7.3. Transformation of competent cells of *Agrobacterium tumefaciens*

The prepared chemical competent *Agrobacterium tumefaciens* strain GV3101pMP90 was used for the transformation. 200 µl of the chemical competent *A. tumefaciens* cells were thawed on ice. In order to ensure a successful transformation of *A. Tumefaciens* 1 µg of plasmid was added to cell suspension and subsequently frozen in liquid nitrogen for 5 minutes. Afterwards the frozen cells were heat shocked in 37 °C warm water bath for 5 minutes. After heat shocking the *A. tumefaciens* cells 1 ml of SOC-media were added to the cells. The A*. tumefaciens* cells incubated at 28 °C and 300 rpm on a shaker for 3 hours. After incubating 20 µl, 200 µl and 980 µl aliquots of the transformed cells were streaked on LB-agar containing kanamycin (50 µg/ml) and rifampicin (10 µg/ml) and incubated at 28 °C for 48 hours.

2.2.7.4. Preparation, verification and sequencing of bacterial plasmids

The plasmid extraction was performed with the kit *NucleoSpin® Plasmid Miniprep Kits* (Macherey-Nagel, Düren, Germany). According to the instructions manual 5 ml of bacterial cultures were used.
The purified plasmids were verified by PCR likewise the colonies on the LB-agar plates.

Positive plasmids were sequenced with plasmid-specific primers by the company Eurofins MWG Operon (Ebersberg, Germany).

2.2.7.5. Storing of positive transformed bacteria for long-term

Positive sequenced bacteria colonies were stored in glycerol stocks. 700 µl of bacterial culture were added to 50 % (v/v) sterile 300 µl aqueous glycerol. The glycerol stocks were frozen in liquid nitrogen and finally stored in the -80 °C freezer.

2.2.8. Generation of transgenic *Arabidopsis thaliana* plants

Gateway® Technology Systems (Life Technologies, Darmstadt, Germany) was used for the preparation of the cloning procedure and the generation of transformed *Arabidopsis thaliana* plants.
The cloning procedure is divided into two steps. At first an entry clone is generated with the previous amplified DNA area of interest and afterwards an expression clone.

2.2.8.1. Generation of an entry clone by using the BP-reaction

The *Gateway® Technology Systems* uses the recombination system of the bacterial phage λ. Specific enzymes of the bacterial virus help to integrate its own genome into the host genome of *Escherichia coli* cells. These specific enzymes recognise specific *attachment sites* in the DNA (*att*-sequences). By using these *att*-sequences the targeted recombination is performed. The *Gateway® Technology Systems* uses this effect to integrate an amplified gene of interest attached with *att*-sequences into a donor vector. At first the gene or the DNA area of interest is amplified with specific primers containing the complementary *attB*-sequences. A specific set of provided enzymes catalyse the replacement of the *attP*-flanked area in the donor vector with the *attB*-attached amplified DNA area of interest resulting in the entry clone vector. The *attP*-flanked area in the donor vector contains the gene *ccdB* a protein which inhibits the bacterial DNA-gyrase (topoisomerase II). The inhibition of the DNA-gyrase is lethal.

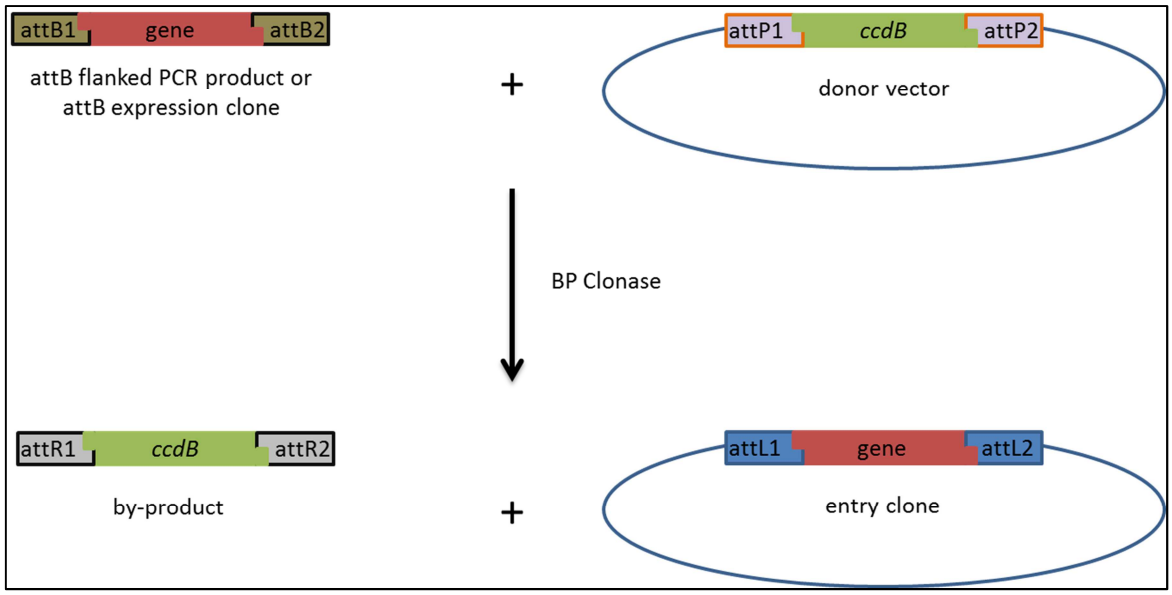

Fig. 12: Schematic principle of the BP-reaction

The attP-flanked sequence of the donor vector is replaced with the gene of interest resulting in an entry clone and a by-product. attB and attP: recombination gateway, *ccdB*: gyrase inhibition gene, donor vector: pDONR®/Zeo; altered from Gateway® Technology user guide.

As described in chapter 2.2.6.5., the gene of interest was amplified with the *Phusion® High Fidelity DNA Polymerase* (Thermo Fisher Scientific; Schwerte, Germany) kit. The specific attachment-sites were generated by specific primers in the PCR. The BP-reaction was performed with the *Gateway® BP Clonase II Enzyme Mix* (Life Technologies, Darmstadt, Germany) according to the manual with the recommended vector pDONR®/Zeo (fig. 12).
After the recombination the entry clone vector was transferred into the chemical component cells of *Escherichia coli* (chapter 2.2.7.1.). Only the replacement of the gene *ccdB* with the gene of interest results in vital *Escherichia coli* cells. Additionally, the transformed cells were selected with the antibiotic zeocin (chapter 2.2.7.1.). The grown colonies were verified by PCR and sequencing (chapter 2.2.7.4.). Positive colonies were incubated in cultures and finally stored in the -80 °C freezer (chapter 2.2.7.5.).

2.2.8.2. Generation of an expression clone by using the LR-reaction

After the successful generation on an entry clone the gene of interest can be transferred to several destination vectors. This reaction is mediated through a λ phage recombination system similar to the BP-reaction as described in chapter 2.2.8.1. The att-sites are recognised

by a set of enzymes which also mediates the replacement of the att-sequences flanked DNA area in the destination vector with the gene of interest.

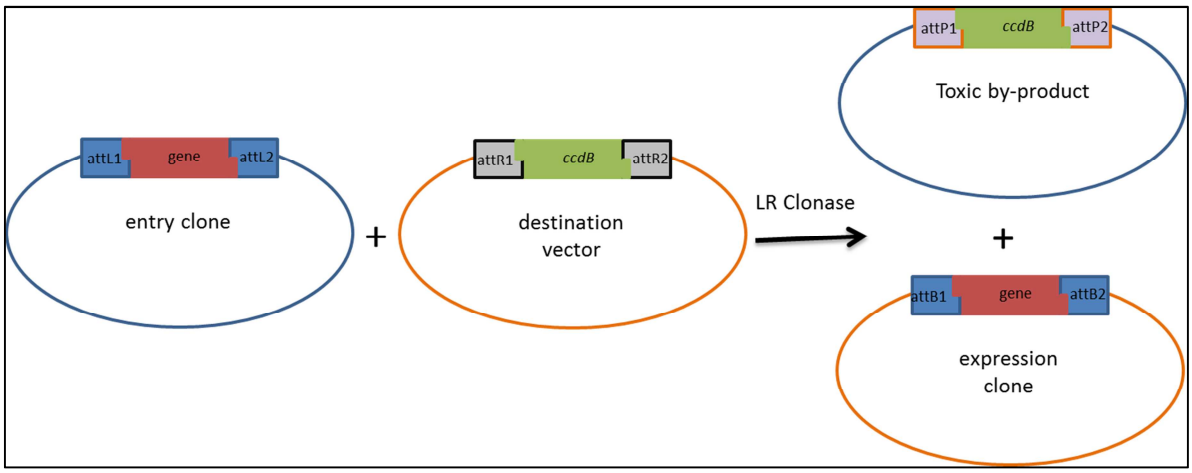

Fig. 13: Schematic principle of the LR-reaction

The attR-flanked sequence of the destination vector is replaced with the gene of interest resulting in an expression clone and a by-product. attL and attR: recombination gateway, *ccdB*: gyrase inhibition gene, destination vector: pMDC; altered from Gateway® Technology userguide.

The LR-reaction was performed with the *Gateway® LR Clonase II Enzyme Mix* (Life Technologies, Darmstadt, Germany) according to the manual. As a destination vector Prom_CYP86B1_pMD (provided by Daniela Nosbüsch, laboratory of Prof. Dr. Lukas Schreiber, University of Bonn) was used.

After the successful recombination the destination vector was transferred into chemical competent cells (chapter 2.2.7.1). The transformed cells were selected with the antibiotic kanamycin (chapter 2.2.7.4.). Positive colonies were incubated in cultures and finally stored in the -80 °C freezer (chapter 2.2.7.5.).

2.2.9. Transformation of *Arabidopsis thaliana* plants with *Agrobacterium tumefaciens*

The transformation of *Arabidopsis thaliana* plants was performed with the bacteria *Agrobacterium tumefaciens* containing the expression clone. The plants were transformed with the called method “floral dip” described by Clough and Bent (1998). The floral organs are dipped into a prepared *Agrobacterium tumefaciens* suspension.

2.2.9.1. Growth of *Agrobacterium tumefaciens* for the "floral dip" procedure

After transformation of *Agrobacterium tumefaciens* (chapter 2.2.7.3.) a pre-culture was performed. One positive colony was transferred to a schikane flask with 10 ml LB-media containing kanamycin (50 µg/ml) and rifampicin (10 µg/ml). The bacteria incubated at 28 °C and 170 rpm overnight. The following day the pre-culture inoculated 300 ml LB-media with the appropriate antibiotics. This main-culture was split into two schikane flasks and incubated at the same conditions as the previous pre-culture.

2.2.9.2. "Floral dip"

Four-week old *Arabidopsis thaliana* plants were used for the "floral dip" method. During the third week the apical stem was cut off to induce the growth of more stems.
The overnight main-cultures were separated into 50 ml falcon tubes and centrifuged. The pellets were resuspended carefully in inoculation media.
The inflorescence of at least 10 plants was dipped twice into the inoculation media for 10 seconds. Subsequently the plants were put in horizontal direction on a tray covered with cling film. The plants were sprinkled with water and covered with cling film. Finally, the tray with the plants were put into a plastic bag and placed back in the growth chamber. After two days the plastic bag and the cling film were removed. The inflorescences were covered with a flat bag to avoid cross-pollination. After the seed maturation the seeds were collected and selected on ½ MS-agar containing hygromycin (25 µg/ml).

2.2.9.3. Selection of transformed *Arabidopsis thaliana* seedlings

After harvesting of the transformed and matured seeds the seeds were sown on ½ MS-agar containing hygromycin (25 µg/ml). The seeds were stratified as described in chapter 2.2.3. On the following day the seeds germinated in the dark at room temperature for five days. Hygromycin-resistant seedlings show an elongated hypocotyl. Afterwards the seedlings were put in the laboratory for two days close to the window to recover slowly by slight light induction (altered from Harrison et al., 2006). Elongated seedlings were put onto new ½ MS-agar without any antibiotics to recover and placed into the growth chamber. After few days

the seedlings could recover and developed long roots and several leaves. Subsequently, the recovered seedlings were placed on earth.

2.2.10. Histological and histochemical analysis

Different microscopes were used to analyse the root structure of *Arabidopsis thaliana*. With respect to suberin and propidium iodide analysis an *Axioplan microscope* (Carl Zeiss, Jena, Germany) was used. The stained suberin root samples were analysed with bright field and fluorescent compounds were visualised via UV-light (filter set: excitation filter BP 450-490 nm, beam splitter FT 510 nm, blocking filter LP 520 nm). The stained apoplast was visualised with UV-light (filter set: excitation filter BP 500-550 nm, beam splitter FT 580 nm, blocking filter LP 590 nm.).
Images were recorded with a *Nikon DXM-1200* digital camera (Nikon, Düsseldorf, Germany).
Casparian strips were visualised by using a *Leica SP5 confocal laser scanning microscope* (Leica, Wetzlar, Germany) and by an *Olympus Fluoview FV1000* (Olympus, Centre Valley, PA, USA).
Suberin ultrastructure was analysed via transmission electron microscopy using *LEO 912AB* (Carl Zeiss, Jena, Germany).

2.2.10.1. Suberin staining with fluorol yellow 088

Fluorol yellow 088 (Life Technologies, Darmstadt, Germany) powder was dissolved in lactic acid (0.01 % w/v) at 70 °C for 30 minutes. Vertically grown seedlings (chapter 2.2.3.) were incubated in 12-well plates containing the freshly prepared fluorol yellow 088 solution at 70 °C for 30 minutes. After the incubation the seedlings were rinsed thrice in water for 5 minutes. Seedlings were counter-stained with aniline blue (0.5 % w/v in distilled water) at room temperature in the dark for 30 minutes. Subsequently, the seedlings were rinsed in water thrice for 10 minutes. Finally, the stained seedlings were mounted on slides using 50 % aqueous glycerol. The stained root samples were visualised under the microscope. Images were taken from the whole root (Pfister et al., 2014).

2.2.10.2. Staining of the apoplastic barrier with propidium iodide

Vertically grown seedlings (chapter 2.2.3.) were incubated in 15 µM (10 µg/ml in distilled water) propidium iodide (PI) (Life Technologies, Darmstadt, Germany) for 10 minutes in the dark. The stained seedlings were rinsed twice in water for seconds. Afterwards the seedlings were mounted on slides with water and staining was visualised by UV-light. For the quantificational analysis the onset of elongation was defined as the point, where endodermal cells in a median optical section are clearly more than twice the width of the previous cell. From this point endodermal cells were counted until the point, where the propidium iodide does not infiltrate the central cylinder (Naseer et al., 2012).

2.2.10.3. Visualising Casparian strips with basic fuchsine

Basic Fuchsine staining was performed according to the protocol of the laboratory of Prof. Dr. Niko Geldner (https://wp.unil.ch/geldnerlab/resources-and-protocols/protocols/). *Arabidopsis thaliana* seedlings were fixed in 4 % paraformaldehyde in one times PBS solution for at least 30 up to 120 minutes at room temperature. Afterwards seedlings were rinsed twice for 1 minute with one time PBS. Seedlings were transferred to ClearSee solution and kept in it overnight. After overnight incubation seedlings were stained directly in 0.2 % basic fuchsine dissolved in ClearSee solution overnight. On the following day basic fuchsine solution was removed and seedlings rinsed once in ClearSee solution for 30 minutes with gentle agitation. After 30 minutes the seedlings were washed again in ClearSee solution overnight. Finally, on the following day the seedlings were mounted on slides with ClearSee solution for imaging. Excitation of basic fuchsine was performed with 550 or 561 nm and detected at 570-650 nm.

2.2.11. Transmissions electron microscopy

The basic of the transmission electron microscopy (TEM) is that an electron beam enables the illustration of an object. The resolution of the TEM goes clearly below the resolution of the light microscopy. The recent resolution of a high-resolution scanning transmission

electron microscope is at 45 pm. In this way, the column between Si-Si atomics were directly resolved (Sawada et al., 2015).

2.2.11.1. Preparation and production of glass knives for the ultra-microtome

For the production of glass knives a bar made of glass (40 x 2.5 x 0.6 cm) was used. The glass bar was washed with soap and then broken into several quadrates (2.5 x 2.5 cm) by using the *LKB 2178 Knifemaker-II* (Reichert-Jung, Vienna, Austria). A diagonal cut with a diamante through the quadrate and a subsequent break resulted into two triangle knives. A trough was stuck with liquid candle wax to the diagonal breakage side underneath the cutting edge. The interface between the trough and the glass knife was sealed with liquid candle wax as well. The trough was filled with distilled water to collect the semi-thin and ultrathin sections.

2.2.11.2. Preparation and production of coated copper grids

The copper grids were coated with a film made of formvar. Formvar is a polyvinylformaldehyde and contributes to stabilise the ultrathin sections on the copper grid. A solution of 1 % of formvar was prepared in $CHCl_3$ and filled into a dropping funnel with an outlet. A cleaned slide was put into the solution and the outlet was opened slowly. The velocity of the flow regulates the thickness of the formvar film. The slower the solution is released the thinner is the film because a slow velocity facilitates to rinse a higher proportion of the formvar solution from the slide. After releasing the solution a formvar film remained on the slide. The formvar film was separated from the slide by cutting off the ends of the film with a razor blade. The slide with the formvar film was put slowly, controlled and diagonal (ca. 45°) into a distilled water bath. In this way, the film was released from the slide and swam on the water surface. The thickness and the quality of the film were examined due to the colour of the film. Only greyish and silvery films were used for the further procedure. After examining the quality of the film copper, grids were put onto the film facing with the rough side to the formvar film. An airmail paper was put onto the film with the copper grids and soaked with distilled water until it was wet. The airmail paper with the attached and coated copper grids was taken out from the water surface with a forceps. The

paper with the copper grids were stored and kept dry in a petri dish (altered from Mahl and Möldner, 1973).

2.2.11.3. The embedding media ERL

In the year 1969 the scientist Spurr developed a low-viscocity epoxy resin embedding media based on ERL-4206 for the transmission electron microscopy. This embedding media is useful for most of the different plant tissues because it shows a high infiltration rate. The structure of the polymer does not influence the plant ultrastructure. The expoxy resin consists of four different compounds: ERL-4206 (vinylcyclohexene dioxide = epoxy monomer), DER 736 (diglycidylether of polypropylene glycol = flexibiliser), NSA (nonenyl succinic anhydride = hardener), DMAE (dimethylaminoethanol = accelerator). The embedding media has to be freshly prepared (Spurr, 1969).

2.2.11.4. Fixation and embedding of *Arabidopsis thaliana* roots for the transmission electron microscopy

Unless otherwise notated, seven day old and one cm long roots from *A. thaliana* seedlings, grown on plates (chapter 2.2.3.), were fixated for 1 h at room temperature by using an aldehyde solution. The aldehyde solution consists of 1.5 % GA and 0.5 % glucose in 50 mM NCP. Afterwards the roots were washed thrice for 10 min in 100 mM NCP in order to remove unbound aldehydes (altered from Karnovsky, 1965). Subsequently, the roots were post-fixed with 2 % OsO_4 in NCP for 1 h at room temperature. Unbound OsO_4 was removed by using two washing steps for 5 min with distilled water. After post-fixation the root samples were dehydrated step by step in acetone (15 %, 30 %, 50 %, 75 %, 90 %, 96 % and 100%). Each step of dehydration from the concentration of 15 % to 90 % acetone was repeated for three times and the roots incubated in each dehydration solution for 10 min. The dehydration steps 96 % and 100 % of acetone were repeated 4 times and the incubation time was 15 min. Afterwards the dehydrated root samples were infiltrated with embedding media. The first infiltration of embedding media (100 % acetone and ERL, ratio 3:1) was performed overnight. The second (100 % acetone and ERL, ratio 1:1) and third (100 % acetone and ERL, 1:3) infiltration was done on the following day for 4 h per infiltration. Overnight the root

samples were infiltrated with pure ERL. On the next day the roots were treated with pure ERL for 4 h again. Afterwards the roots were placed into embedding shapes with pure ERL. Polymerisation was performed at 70 °C for 8 h (Spurr, 1969; altered from Plattner, 1973a).

2.2.11.5. Preparation and performing of ultrathin sections

Polymerised blocks were taken out of the embedding shapes. Excess polymerised material was trimmed by using a sharp razor blade. Subsequently, a pyramid was cut out around the root with a sharp razor blade under the binocular. The section area for the ultra-microtome was cut trapezoidal with the razor blade. In order to perform semi-thin (0.5 – 2 µm) or ultrathin (70 – 100 nm) sections an ultra-microtome (*Ultracut 2*, Reichert – Jung) was used. Sections were collected in the water-filled trough which was placed onto the glass knife. The collected semi-thin sections on the water surface were taken out with a glass stick. The semi-thin sections are transferred onto a glass slide with a drop of water. On a hot plate the sections dried out, were stained with a solution containing 1% toluidine blue and 1% borax, and visualised under the light microscope to assess the quality of the cut. Ultrathin sections were straightened with $CHCl_3$ steam. For this purpose a piece of cotton wool was soaked into $CHCl_3$ and held over the ultrathin sections. After straightening the ultrathin sections were transferred onto copper grids coated with formvar by using an eyelash mounted on a toothpick (altered from Hall, 1978).

2.2.11.6. Enhancement of electron contrast of ultrathin section by using of uranyl acetate and lead citrate

A positive contrasting was performed with heavy metal salts. The most used contrast agents are uranyl acetate and lead citrate. Uranyl acetate is responsible for the staining of nucleic acids and proteins, whereas lead citrate stains membranes. Lead citrate reacts specifically with osmium dioxide ($Os(IV)O_2$) which is bound to the positive charged head groups of phospholipids (Plattner and Zingsheim, 1987).

At first the coated copper grids with the ultrathin sections were put onto a 20 µl drop of 2 % uranyl acetate. The side with the ultrathin sections faced to the uranyl acetate drop. After 5 minutes of staining the copper grid was washed in distilled water for 1 min. Then the

remaining water on the copper grid was removed by a filter paper. Afterwards the copper grid was put onto a 20 µl drop of 1.5 % lead citrate for 5 minutes and then washed in a solution of 0.02 N NaOH. After washing in the NaOH solution the copper grid was finally washed in distilled water for 1 min and the remaining water was again removed by a filter paper. The stained ultrathin sections were stored in a dry box overnight (Plattner and Zingsheim, 1987).

2.2.11.7. Transmission electron microscopy with the *LEO 912AB* from Zeiss

The ultrathin sections of the roots were examined with the transmission electron microscope *LEO 912AB* (Zeiss). Suberin lamellae were visualised with a magnification range from 5,000x to 16,000x and recorded by a CCD-camera (*Proscan HSC2*). The processing of the images was performed by the software "analySIS" (*Soft Imaging System*) and "siViewer" (*Olympus Soft Imaging Viewer*).

2.2.12. Analytical approaches

2.2.12.1. Preparation of roots from *Arabidopsis thaliana*

Unless otherwise notated, roots of five-week old *Arabidopsis* thaliana plants were used for analytical approaches. Soil-grown roots were carefully removed from soil with forceps and paintbrush in a petri dish filled with tap water. Hydroponically-grown plants were removed from the container and the roots were cut off at the transition to the hypocotyl. Afterwards, the cell walls were digested in an enzyme solution (tab. 18) to avoid high sugar signals in the analytical approaches. The roots were digested for one week and the enzyme solution was replaced three times.

Due to the enzymatically digestion lipophilic substances and membrane lipids were released. These lipophilic substances were extracted via a soxhlet-extractor. Enzymatically digested roots were put into cellulose filter bags (ANKOM Technology, Macedon NY, USA) and placed into the soxhlet-extractor. The lipophilic substances were extracted at first with chloroform and then with methanol each for 24 hours. After the extraction the roots were drought in the fume hood and in the oven at 60 °C for 30 minutes.

2.2.12.2. Transesterification with BF_3/MeOH, suberin extraction and derivatisation

Suberin forms complex polyester. Due to this, suberin has to be transesterified by BF3/MeOH to release the single suberin monomers. This reaction is representative presented in figure 14.

Dried, enzymatically digested and extracted root samples were accurately weighed in on the fine balance (Satorius, Göttingen, Germany). Subsequently, 1-2 ml BF_3/MeOH was added to the root samples for the transesterification at 70 °C overnight.

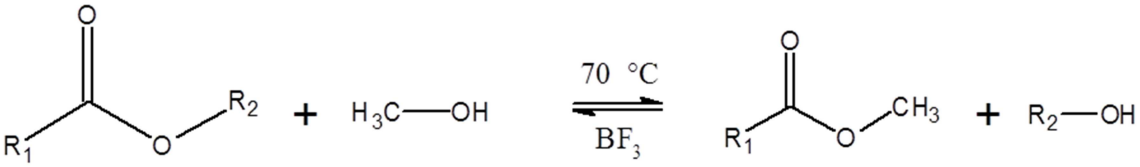

Fig. 14: Transesterification of polyester with BF_3/MeOH at 70 °C.

The boron trifluoride mediates a nucleophilic substitution of the polyester with methanol. It is a reversible reaction but based on the law of Le Chatelier the equilibrium of the reaction is on side of the products (altered from Liu, 1994).

On the following day, 50 µl of C_{32} alkane internal standard (10.02 mg/50 ml) were added to the samples. The transesterification was stopped by pipetting carefully saturated $NaHCO_3/H_2O$. The single suberin monomers were extracted thrice with 1 ml $CHCl_3$. The extracted suberin monomers were collected in a fresh vial and subsequently washed twice with HPLC deionised water. By adding water-free Na_2SO_4 to the extract all remaining water was bonded to the Na_2SO_4 to ensure a water-free sample. Afterwards, the extract was concentrated to 50 µl under nitrogen stream. Finally, the concentrated sample was derivatised with each 20 µl of BSTFA and pyridine.

Derivatisation masks the polar groups as presented in figure 15 and ensures an improved volatility, thermal stability and a separation of the substances through the column according to the molecular weight.

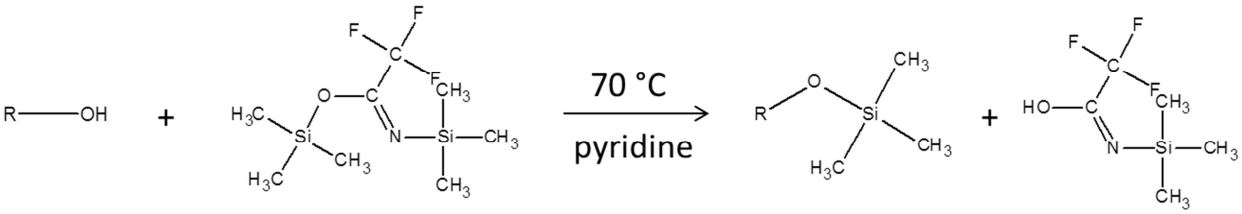

Fig. 15: Derivatisation of a substance with BSTFA

BSTFA mediates an electrophilic substitution at the oxygen atom of the polar group and leads to the formation of a trialkylsilyl-derivative (altered from Knapp, 1979).

2.2.12.3. Thioacidolysis to extract lignin

The main intermonomeric bonds in lignin are the alkyl-aryl-ether linkages. The cleavage of these intermonomeric bonds has intensively studied. Therefore, the lignin polymer is usually degraded to low molecular weight compounds in order to obtain structural information.
By using the nucleophilic ethanethiol and the Lewis-acid boron trifluoride diethyl etherate the β-O-4-aryl-ether linkages are cleaved into thioethylated products (fig. 16).

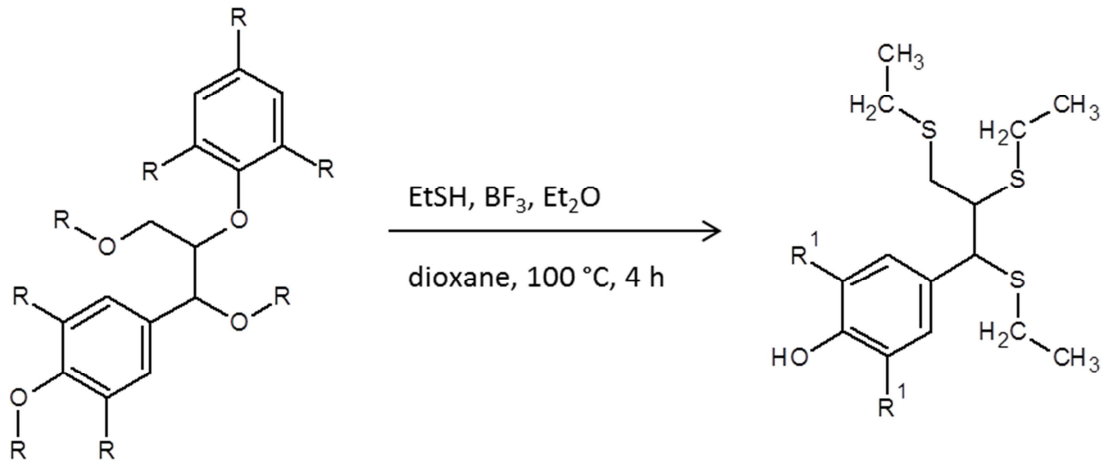

Fig. 16: Cleavage of β-O-4-aryl-ether linkages by thioacidolysis into specific thioethylated products

The nucleophilic ethanethiol together with the borontrifluoride mediates the cleavage of the β-O-4-aryl-ether linkages into thioethylated products (altered from Lapierre et al., 1985).

In detail, lignin of the root material was degraded by cooking at 100 °C for 4 hours in dioxane containing 10 % ethanethiol and 2.5 % boron trifluoride diethyl etherate. The thioethylated lignin monomers were extracted with dichlormethane and subsequently purified in a filter containing water-free sodium sulphate. Under a nitrogen steam the extracted thioethylated lignin monomers were concentrated and finally derivatised by adding BSTFA and pyridine at

70 °C for 40 minutes. Thioethylated lignin monomers were analysed in the GC-FID and identified in the GC-MS.

2.2.12.4. Gas-chromatography and mass spectroscopy

Mixtures of substances were separated by gas-chromatography. The principle of the separation of mixtures is based on the chemical and physical properties of the substances. The combination of the different boiling points of the substances and the reciprocal action with the stationary phase causes characteristic retention times.

In this study, an *Agilent 6890N* gas-chromatograph (Agilent Technologies, Santa Clara, USA) with a *DB1 capillary column* (30 m x 0.32 mm; 0.1 µm coating, J&W Scientific, USA) was used. The inner surface of the capillary column acts as a stationary phase and consists of polydimethylsiloxane. Polydimethylsiloxane is non-polar and therefore suitable for the separation of long-chain aliphatic substances. The substances mixtures were injected into the column via *On-Column-Injection* or *Splitless-Injection*. The following tables represent the temperature programs which were used for suberin and thioacidolysis analysis.

Tab. 9: Temperature program of "suberin_CMH"

ΔT: Temperature increase, T_{max}: maximal temperature of this step

ΔT [°C/min]	T_{max} [°C]	Maintain T [min]
	50	4
10	120	2
2	150	1
3	315	20

Tab. 10: Temperature program of "suberin" used for the thioacidolysis

ΔT: Temperature increase, T_{max}: maximal temperature of this step

ΔT [°C/min]	T_{max} [°C]	Maintain T [min]
	50	2
10	150	1
3	310	30

Qualitatively, the samples were analysed using a mass spectroscopy (*MS 5973 Network Selective Detector*, Agilent Technologies, Santa Clara, USA) coupled to the gas-chromatograph. The gas system in the mass spectroscopy uses helium as a mobile phase. By ionising the separated substances with electrons the substances collapse into characteristic fragments. An electromagnetic field generated by a quadrupole accelerates the fragments. The quadrupole consists of four electrodes, which are arranged in a square. The selection of the fragment occurs according to their mass/charge ratio in particular time intervals caused by the alternating voltage. The mass spectroscopy of each substance is determined by the detector which shows the characteristic fragmentation pattern of the substance. Finally, databanks are used to facilitate the identification of the substances by comparison with fragmentation patterns.

In contrast, the flame ionisation detector (FID) (Agilent Technologies, Santa Clara, USA) was used to analyse quantitatively the mixtures of substances. As a carrier hydrogen gas was used. After separation of the substances by the capillary column the substances are ionised by the oxyhydrogen reaction. The detector determines the released electrons and translates the signal into a digital signal. There is a proportional relationship between the released electrons and the carbon content of a substance. Despite of masking the substances with BSTFA reactions between the derivatised substance and the column may occur. This causes depositions of substances on the inner surface of the column, which impair the quality of the column. Due to this reason, the quality of the column is checked before and after each sample set with a derivatised acid standard. This acid standard is a mixture of three saturated long-chain carbonic acids and an alkane: nonacosanoic acid (C_{29} acid), triacontanoic acid (C_{30} acid), hentriacontanoic acid (C_{31} acid) and tetracosan an alkane (C_{24} alkane). The quality of the column is determined by the ratio of the signal of both the alkane and the longest saturated carbonic acid. Additionally, the peak shape is considered as well as an indicator. Ratios of ≤ 1.3 are considered as “good quality”. Higher ratios lead to appropriate cleaning and rinse methods of the column. The temperature program of the acid standard is listed below.

Tab. 11: Temperature program of “Acid standard”

ΔT: Temperature increase, T_{max}: maximal temperature of this step

ΔT [°C/min]	T_{max} [°C]	Maintain T [min]
	50	1
40	200	2
3	310	15

2.2.12.5. Statistical evaluation

Significant differences between the samples in the analytical approaches were determined by using the student’s t-test. The one-sample and the two-sample t-test are distinguished by the student’s t-test. Differences between the mean of the population from the nominal value are distinguished by the one-sample t-test. The verification of the probability of the means of two independent samples are based on the same population requires the two-sample t-test. With respect to the analytical approaches the two-sample t-test has been used to reveal differences between the WT and the mutants. Probabilities of ≥ 95 % signify the two samples are considered to share not the same population. This result is described as “significant” ($t \leq 0.05$). Probabilities of ≥ 99 % are considered as “high significant” ($t \leq 0.01$).

2.2.13. Physiological approaches

2.2.13.1. Drought stress

Soil-grown plants (chapter 2.2.1.) were used for drought stress experiments. After four or five weeks the plants were transferred into a tray filled with sand to ensure the removal of the remaining water in the soil. Plants were not watered any more in total for 12 or 15 days. After each day the drought phenotype of the plants were documented by a camera (*Canon Powershot G11*, Canon, Tokyo, Japan).

3. Results

3.1. Identification and selection of the putative candidate genes involved in the assembling of the polyaromatic domain in suberin

Synthesis of aromatic compounds is provided by the phenylpropanoid pathway. Due to this, genes involved in the phenylpropanoid pathway were selected and studied. Especially, the synthesis of the crucial aromatic compound for the suberin biosynthesis the ferulic acid was of high interest.

Co-expression of phenylpropanoid pathway genes with respect to suberin biosynthesis genes and tissue specific expression was analysed by using freely available databanks.

The co-expression analysis with *ATTED-II* could not reveal any connection between phenylpropanoid pathway genes and suberin biosynthesis genes (fig. 87 – fig. 93). Only the gene *ASFT* reveals a faint co-expression with phenylpropanoid pathway, casparian strip and suberin specific genes. This result is presented in the table 12.

Tab. 12: Co-expression results of the gene *ASFT* At5g41040 from *ATTED-II*

Position	Locus	Alias	MR
104	At4g34050	CCoAOMT1	92.8
132	At2g36100	CASP1	115.4
138	At4g28110	MYB41	123.3
152	At5g57620	MYB36	136.5
169	At2g28670	ESB1	151.9
172	At5g54160	OMT1	154.1
222	At2g30490	REF3	209.2
234	At1g51680	4CL1	217.8
258	At4g38620	MYB4	250.7

The MR-value reveals the significance of the co-expression with the analysed gene. The smaller the MR-value, the higher is the significance of the co-expression. The listed genes

CCoAOMT1, *OMT1*, *REF3* and *4CL1* are phenylpropanoid pathway genes, whereas *MYB36* and *ESB1* are Casparian strip specific genes and *MYB41* is the only representative of suberin biosynthesis gene.

Tissue specific expression was analysed by using the *Arabidopsis eFP browser*. Focus of this analysis was the root endodermis, the seed coat and stem tissue. In addition, in longitudinal view the root is divided into different zones. Experiments were performed with 5 day old seedlings (Winter et al., 2007). The zones 1 and 2 seem to correspond to apical and basal meristematic zone, whereas the zones 3 and 4 appear to represent the elongation and differentiation zone.

The *REF3* gene reveals a strong gene expression in different tissues of the root. A high gene expression is detectable in the root cortex and endodermis. In the zones 3 and 4 of the root *REF3* is highly expressed. In the seed coat of the pre-globular and globular stage *REF3* is strongly expressed as well (fig. 17). Predominately *REF3* is not expressed in the stem tissue.

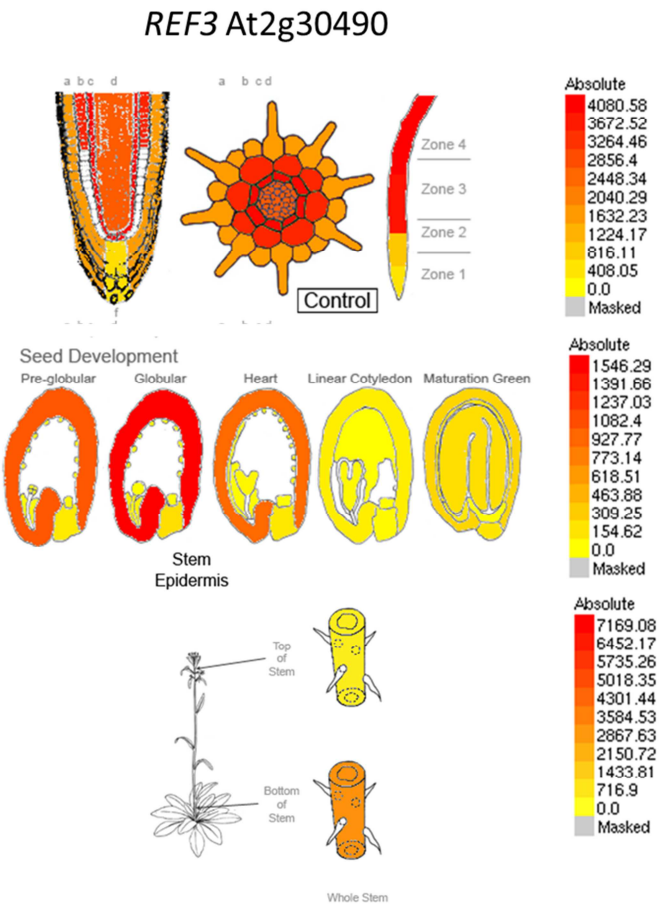

Fig. 17: Localisation of gene expression in the root, seed and stem tissue by using the *Arabidopsis eFP browser*

The Arabidopsis eFP browser graphics are based on expression analysis from microarray studies. Represented is the gene expression of longitudinal and cross sections of roots, longitudinal section of seeds and stem tissue. The intensity of the

staining represents the intensity of the gene expression. Absolute values are depicted in the adjacent scale. *REF3* reveals a cortex, endodermis and seed coat tissue specific gene expression.

The *REF8* gene shows a dominant expression in root endodermis. Especially, in the zone 3 of the root *REF8* gene expression is observable. But also gene expression is detectable in root cortical cells. Only the matured seed coat and bottom stem tissue shows a high gene expression of *REF8* (fig. 18).

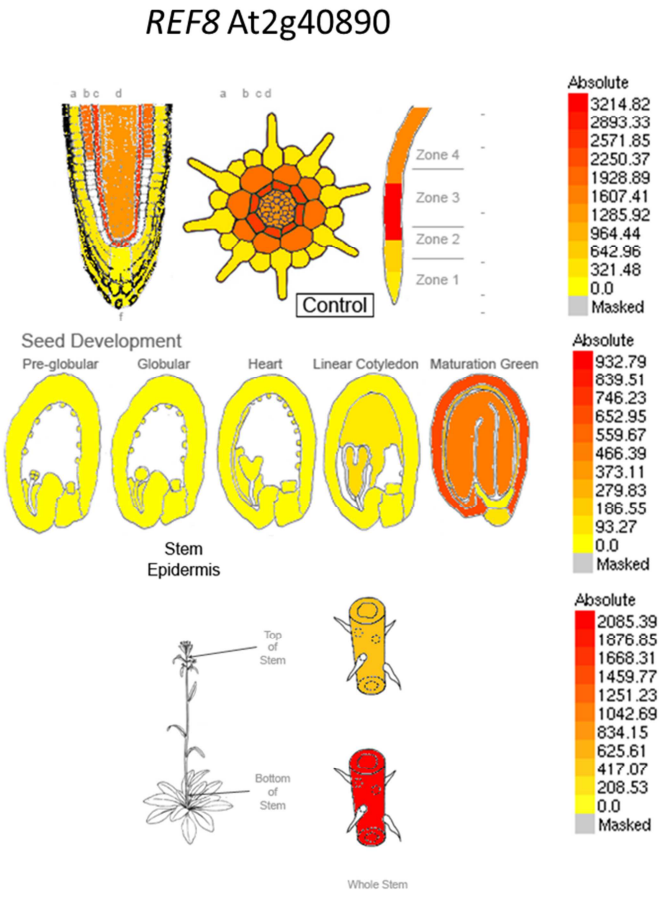

Fig. 18: Localisation of gene expression in the root, seed and stem tissue by using the *Arabidopsis eFP browser*

The Arabidopsis eFP browser graphics are based on expression analysis from microarray studies. Represented is the gene expression of longitudinal and cross sections of roots, longitudinal section of seeds and stem tissue. The intensity of the staining represents the intensity of the gene expression. Absolute values are depicted in the adjacent scale. *REF8* reveals a cortex, endodermis, seed coat and bottom of stem tissue specific gene expression.

As shown in the fig. 19 *HCT* reveals a high gene expression in the root endodermis. *HCT* gene expression is restricted to the zones 3 and 4 of the root. With respect to the seed coat, almost all stages, with the exception of the linear cotyledon stage show a strong gene expression of *HCT*. Furthermore, predominately *HCT* is expressed in bottom stem tissue as well.

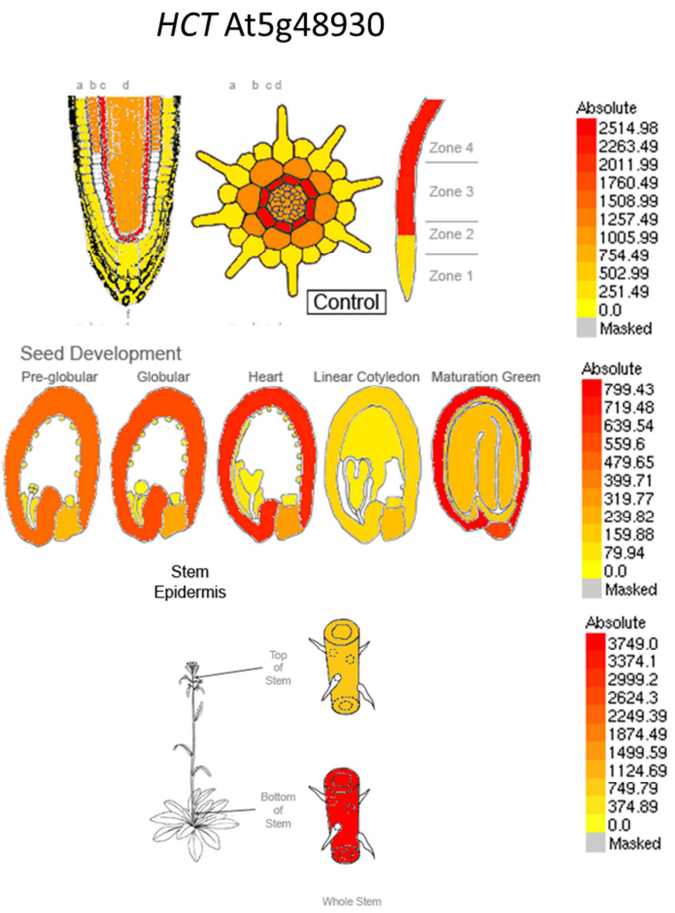

Fig. 19: Localisation of gene expression in the root, seed and stem tissue by using the *Arabidopsis eFP browser*

The Arabidopsis eFP browser graphics are based on expression analysis from microarray studies. Represented is the gene expression of longitudinal and cross sections of roots, longitudinal section of seeds and stem tissue. The intensity of the staining represents the intensity of the gene expression. Absolute values are depicted in the adjacent scale. *HCT* reveals an endodermis, seed coat and bottom of stem tissue specific gene expression.

The gene *CCoAOMT1* which is directly involved in the formation of feruloyl-CoA reveals a high gene expression in the root tissue. Especially, in cortical and endodermal cells of the root zone 3 *CCoAOMT1* is highly expressed. Only the matured seed coat shows a strong gene expression of *CCoAOMT1*. Bottom stem tissue reveals a moderate *CCoAOMT1* gene expression (fig. 20).

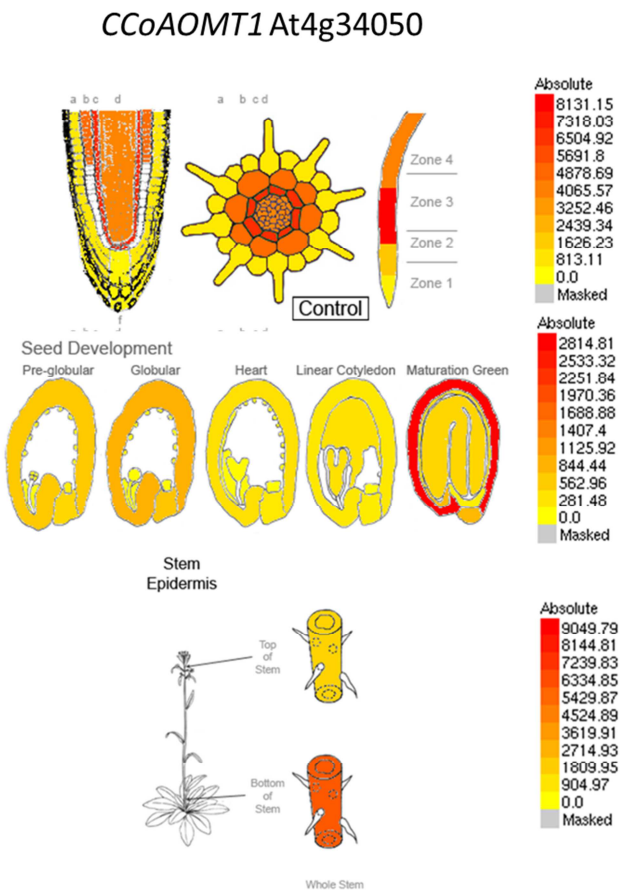

Fig. 20: Localisation of gene expression in the root, seed and stem tissue by using the *Arabidopsis eFP browser*

The Arabidopsis eFP browser graphics are based on expression analysis from microarray studies. Represented is the gene expression of longitudinal and cross sections of roots, longitudinal section of seeds and stem tissue. The intensity of the staining represents the intensity of the gene expression. Absolute values are depicted in the adjacent scale. *CCoAOMT1* shows an endodermis, seed coat and bottom of stem specific gene expression.

COMT1 reveals several strong gene expressions in different tissues. There is an enhanced gene expression in the root central cylinder, endodermis and cortex tissue. Predominately, *COMT1* is expressed in the root zones 3 and 4. During the seed development the chalazal seed coat shows a strong gene expression and in the pre-globular stage of the chalazal endosperm as well. An enhanced expression can be seen in the seedling of the linear cotyledon and maturation green stage. The seed coat shows a strong expression in the maturation green stage (fig. 21).

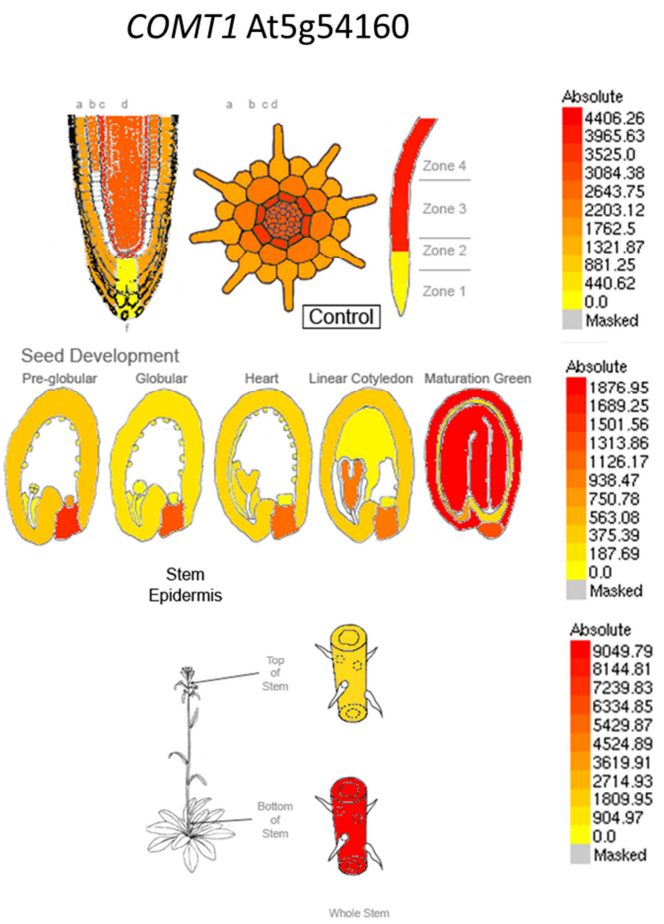

Fig. 21: Localisation of gene expression in the root, seed and stem tissue by using the *Arabidopsis eFP browser*

The Arabidopsis eFP browser graphics are based on expression analysis from microarray studies. Represented is the gene expression of longitudinal and cross sections of roots, longitudinal section of seeds and stem tissue. The intensity of the staining represents the intensity of the gene expression. Absolute values are depicted in the adjacent scale. *COMT1* shows a cortex, endodermis, pre-globular chalazal endosperm, chalazal seed coat, matured seed coat and seedling and bottom of stem specific gene expression.

Predominately the gene *CCR1* is strongly expressed in the root. Root endodermal and central cylinder cells reveal a high *CCR1* gene expression. Root zones 3 and 4 shows a strong *CCR1* gene expression. During seed development, *CCR1* is highly expressed in the matured seed coat and within the seedling. With respect to the stem, *CCR1* is severely expressed in the bottom stem tissue (fig. 22).

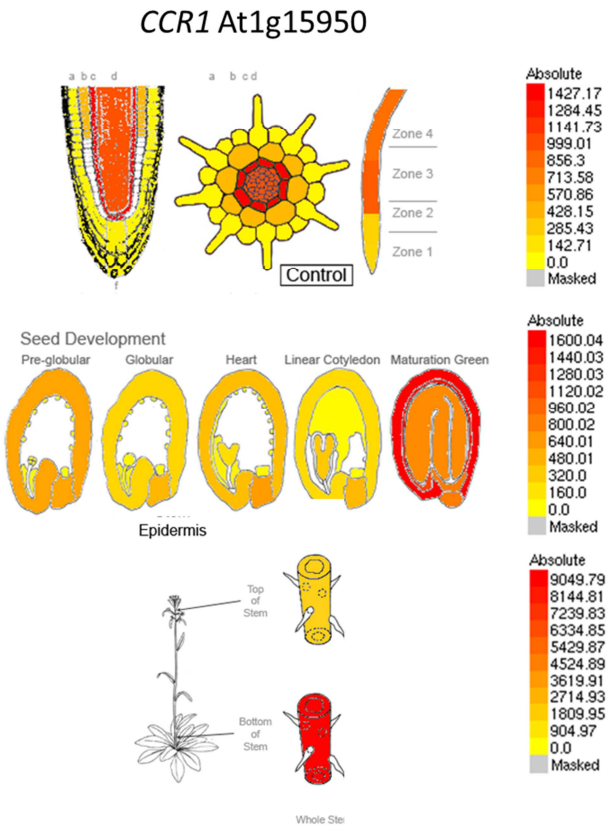

Fig. 22: Localisation of gene expression in the root, seed and stem tissue by using the *Arabidopsis eFP browser*

The Arabidopsis eFP browser graphics are based on expression analysis from microarray studies. Represented is the gene expression of longitudinal and cross sections of roots, longitudinal section of seeds and stem tissue. The intensity of the staining represents the intensity of the gene expression. Absolute values are depicted in the adjacent scale. *CCR1* shows a central cylinder, endodermis, maturation green seedling, seed coat and bottom of stem specific gene expression.

The gene *FAH1* is very specifically expressed. *FAH1* is neither expressed in all root tissues nor significantly during seed development. Only bottom stem tissue shows a strong gene expression of *FAH1* (fig. 23).

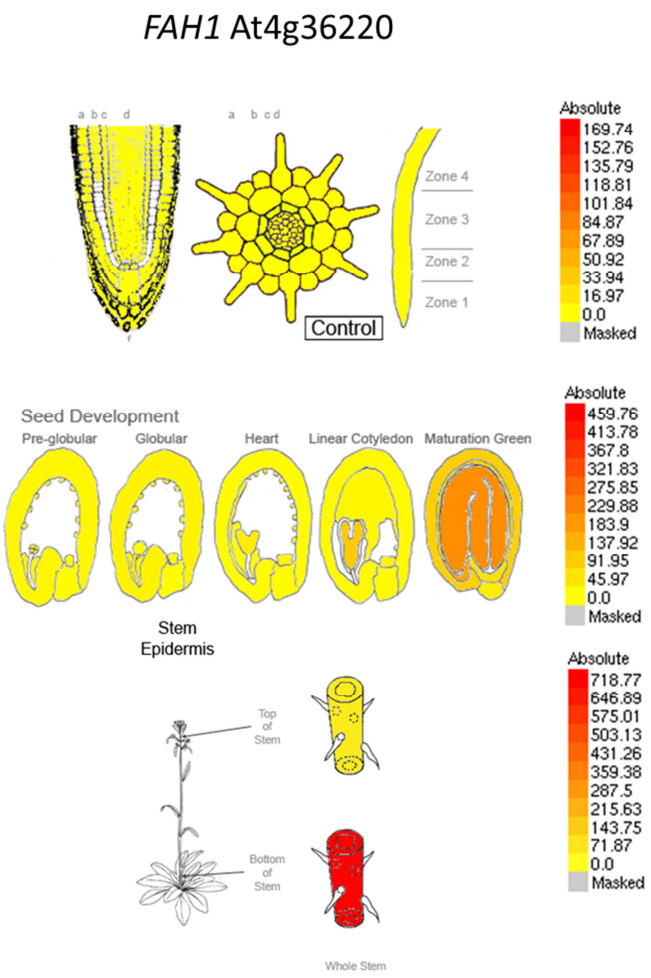

Fig. 23: Localisation of gene expression in the root, seed and stem tissue by using the *Arabidopsis eFP browser*

The Arabidopsis eFP browser graphics are based on expression analysis from microarray studies. Represented is the gene expression of longitudinal and cross sections of roots, longitudinal section of seeds and stem tissue. The intensity of the staining represents the intensity of the gene expression. Absolute values are depicted in the adjacent scale. *FAH1* shows a maturation green seedling and bottom of stem specific gene expression.

CADC gene shows an enhanced gene expression in different tissues. In the root tissue, the endodermis and the central cylinder reveal a high gene expression. This gene expression is observable in the root zones 3 and 4. During all seed developmental stages the gene is highly transcribed in the chalazal seed coat and in the linear cotyledon and maturation green stage of the seedling as well. The seed coat shows an enhanced gene expression in the maturation green stage. A high gene expression of *CADC* can also be seen in the bottom of stem tissue (fig. 24).

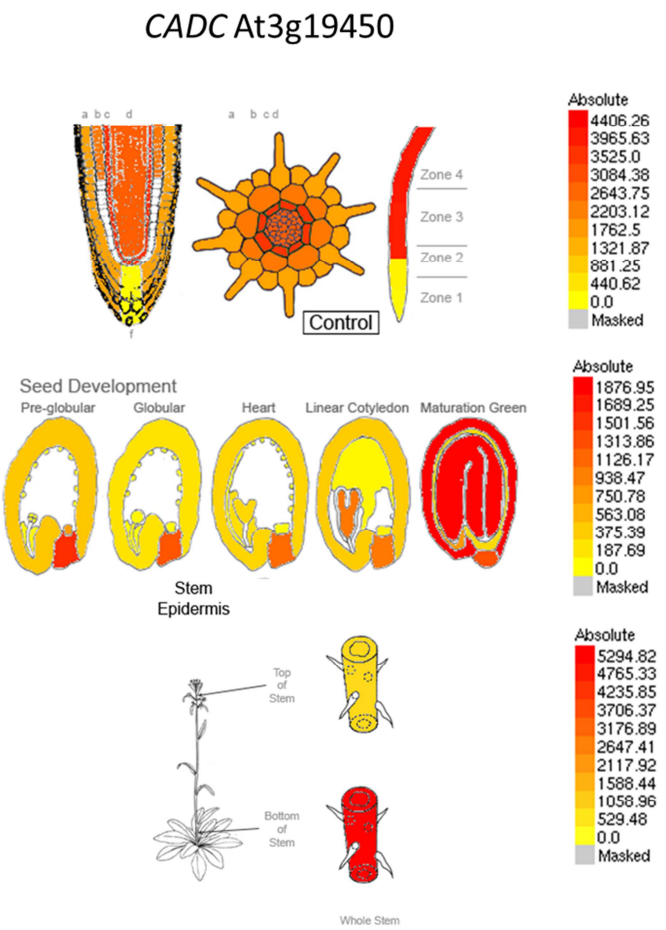

Fig. 24: Localisation of gene expression in the root, seed and stem tissue by using the *Arabidopsis eFP browser*

The Arabidopsis eFP browser graphics are based on expression analysis from microarray studies. Represented is the gene expression of longitudinal and cross sections of roots, longitudinal section of seeds and stem tissue. The intensity of the staining represents the intensity of the gene expression. Absolute values are depicted in the adjacent scale. *CADC* shows a central cylinder, endodermis, chalazal seed coat, linear cotyledon and maturation green seedling, seed coat and bottom of stem specific gene expression.

CADD reveals in comparison to *CADC* a similar tissue specific gene expression but the frequency of the transcripts is decreased. The gene *CADD* is poorly transcribed in root cortex and endodermis tissue. Gene expression of *CADD* is barely detectable in the root zones 3 and 4. High transcript levels can be measured in the chalazal seed coat of all seed developmental stages, especially in the maturation green stage. In the maturation green stage *CADD* is also highly expressed in the seed coat and the chalazal endosperm tissue. The bottom of stem tissue reveals a medium gene expression of *CADD* (fig. 25).

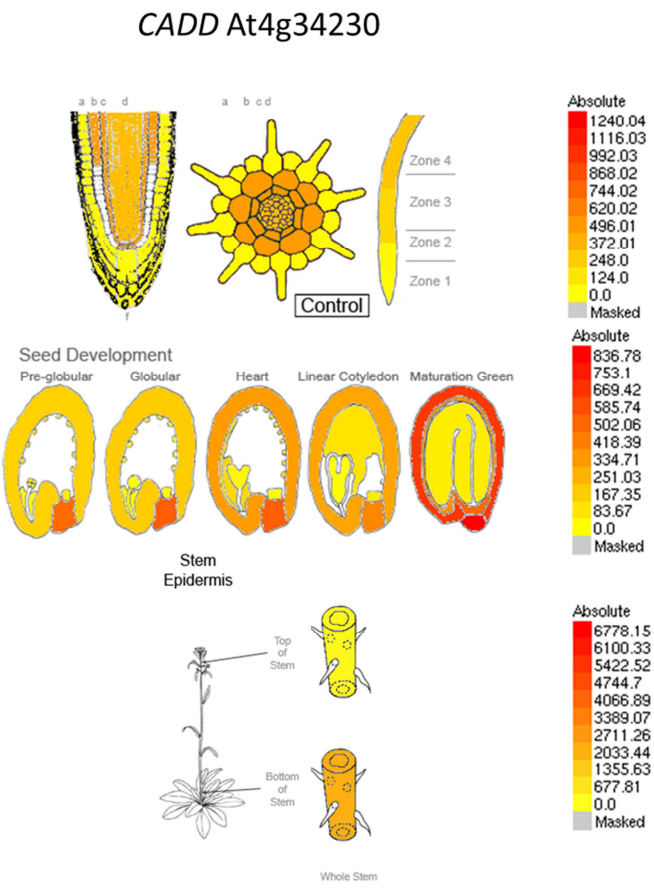

Fig. 25: Localisation of gene expression in the root, seed and stem tissue by using the *Arabidopsis eFP browser*

The Arabidopsis eFP browser graphics are based on expression analysis from microarray studies. Represented is the gene expression of longitudinal and cross sections of roots, longitudinal section of seeds and stem tissue. The intensity of the staining represents the intensity of the gene expression. Absolute values are depicted in the adjacent scale. *CADD* shows a cortex, endodermis, chalazal seed coat, heart, linear cotyledon and maturation green seed coat and bottom of stem specific gene expression.

REF4 reveals a characteristic gene expression in the developing seed. In almost all seed developmental stages a high gene expression is present in the chalazal seed coat and chalazal endosperm tissue. A seed coat specific gene expression can be measured in the globular and maturation green stage. Also, in both stages the embryo proper and the young seedling reveal a high transcription level of *REF4*. Root and stem tissue does not show a strong *REF4* gene expression (fig. 26).

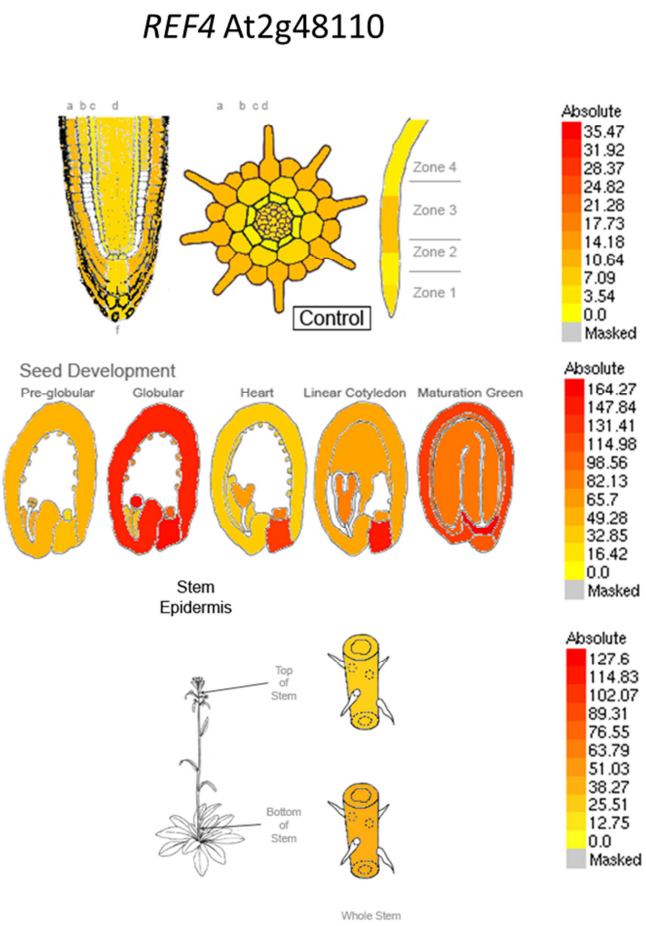

Fig. 26: Localisation of gene expression in the root, seed and stem tissue by using the *Arabidopsis eFP browser*

The Arabidopsis eFP browser graphics are based on expression analysis from microarray studies. Represented is the gene expression of longitudinal and cross sections of roots, longitudinal section of seeds and stem tissue. The intensity of the staining represents the intensity of the gene expression. Absolute values are depicted in the adjacent scale. *REF4* shows an epidermal, chalazal seed coat, chalazal endosperm, embryo proper, globular and maturation green seed coat as well as seedling specific gene expression.

REF1 reveals an epidermal root specific expression. The expression of the gene *REF1* starts in the root zone 3 and increases towards the root zone 4. The seed coat in the linear cotyledon and maturation green stage and the seedling exhibit an induced gene expression as well. *REF1* is not highly transcribed in the stem tissue (fig. 27).

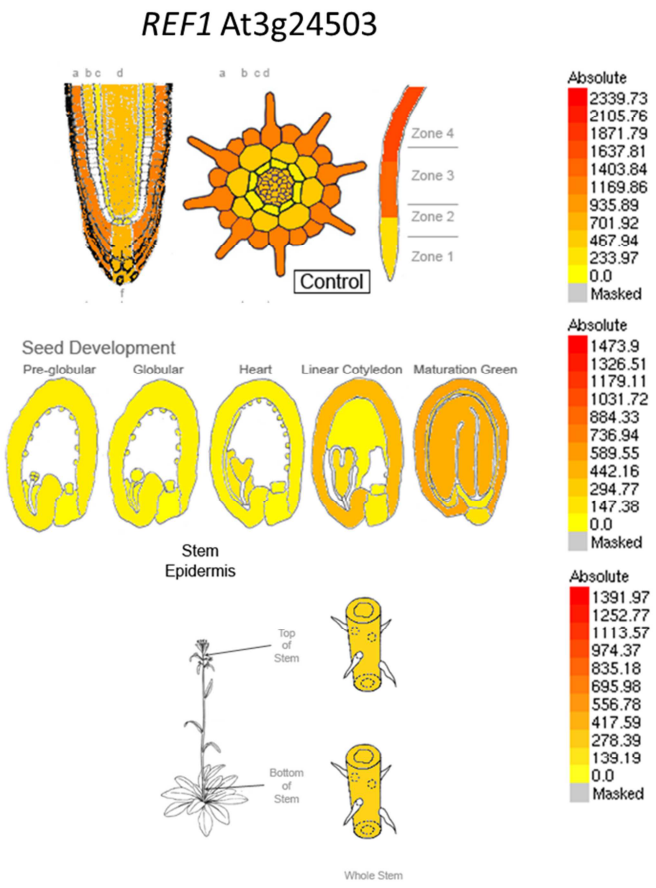

Fig. 27: Localisation of gene expression in the root, seed and stem tissue by using the *Arabidopsis eFP browser*

The Arabidopsis eFP browser graphics are based on expression analysis from microarray studies. Represented is the gene expression of longitudinal and cross sections of roots, longitudinal section of seeds and stem tissue. The intensity of the staining represents the intensity of the gene expression. Absolute values are depicted in the adjacent scale. *REF1* shows an epidermal, linear cotyledon as well as maturation green seed coat and seedling specific gene expression.

The transcription factor MYB4 is highly expressed in root endodermal tissue. However, no specific *MYB4* gene expression is measurable in the root zones. A high gene expression is detectable in all seed developmental stages of the seed coat, especially in the linear cotyledon stage. Stem tissue does not show any characteristic gene expression of *MYB4* (fig. 28).

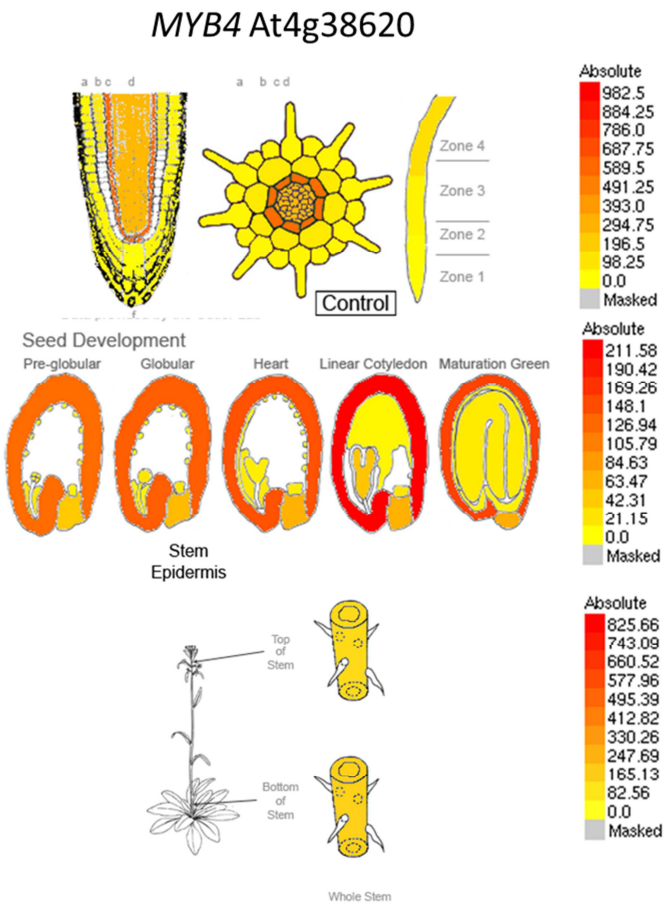

Fig. 28: Localisation of gene expression in the root, seed and stem tissue by using the *Arabidopsis eFP browser*

The Arabidopsis eFP browser graphics are based on expression analysis from microarray studies. Represented is the gene expression of longitudinal and cross sections of roots, longitudinal section of seeds and stem tissue. The intensity of the staining represents the intensity of the gene expression. Absolute values are depicted in the adjacent scale. *MYB4* shows an endodermal and seed coat specific gene expression.

Another transcription factor called MYB7 reveals a similar gene expression pattern like the gene *MYB4*. *MYB7* reveals a root endodermal tissue specific gene expression but in root zones *MYB7* gene expression is barely detectable. During all seed developmental stages, the seed coat exhibits a high *MYB7* gene expression and the chalazal seed coat as well. Especially, the gene is highly transcribed during the early seed developmental stages in the chalazal seed coat. The stem tissue does not show any characteristic gene expression (fig. 29).

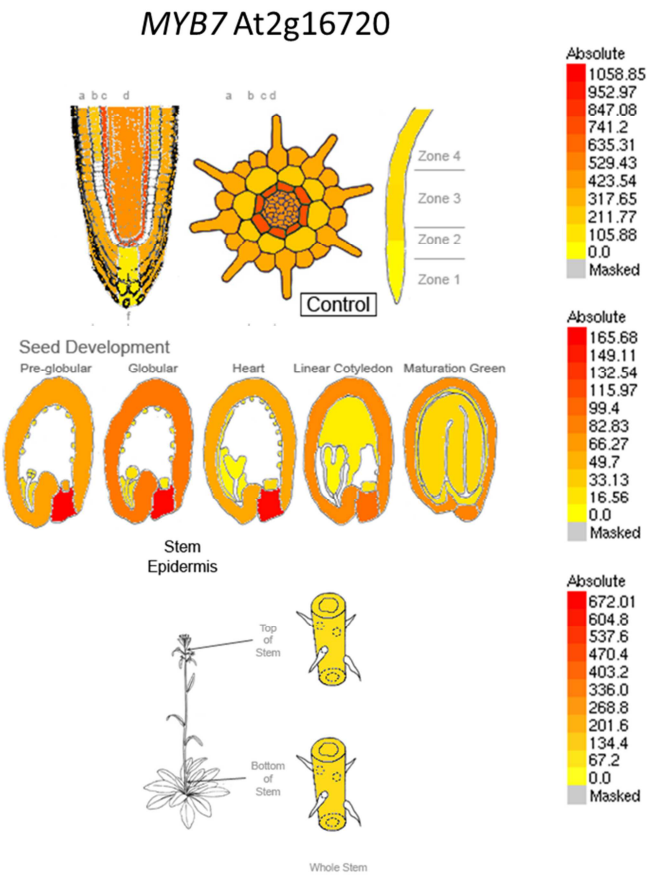

Fig. 29: Localisation of gene expression in the root, seed and stem tissue by using the *Arabidopsis eFP browser*

The Arabidopsis eFP browser graphics are based on expression analysis from microarray studies. Represented is the gene expression of longitudinal and cross sections of roots, longitudinal section of seeds and stem tissue. The intensity of the staining represents the intensity of the gene expression. Absolute values are depicted in the adjacent scale. *MYB7* shows an endodermal, chalazal seed coat and seed coat specific gene expression.

Furthermore, a closely related gene to *HCT* is present in *Solanum tuberosum.* It is called *HQT*. Blast result of *HQT* in *Arabidopsis thaliana* databank reveals the gene At3g53850 with a sequence similarity of 46.23 % (fig. 149). It is described as an uncharacterised protein family (UPF0497) (www.arabidopsis.org), however it was already described by Roppolo et al. in 2014. Here, the gene is notated as *CASPL5B2* (Roppolo et al., 2014). Nonetheless, the gene with the locus number At3g53850 was selected for the further work and mentioned as "*HQT*". There is neither co-expression nor tissue specific expression data available on the websites of the databanks about this gene.

3.2. Genotyping and verification of homozygous knockout transcript expression level of mutants

In order to study the influence of phenylpropanoids to suberisation several transgenic lines of the above mentioned genes (chapter 3.1.) were ordered from the Nottingham Arabidopsis Stock Centre.

T-DNA insertion mutants were selected carefully. Well described and known insertion lines affected in the phenylpropanoid pathway were preferred chosen from the literature whereas undescribed insertion lines were selected carefully. In the case of an undescribed T-DNA insertion line, much attention was directed to the locus of the insertion. If possible, insertions in exons were preferred.

The following figure 30 gives an overview about the insertions in the different phenylpropanoid pathway genes.

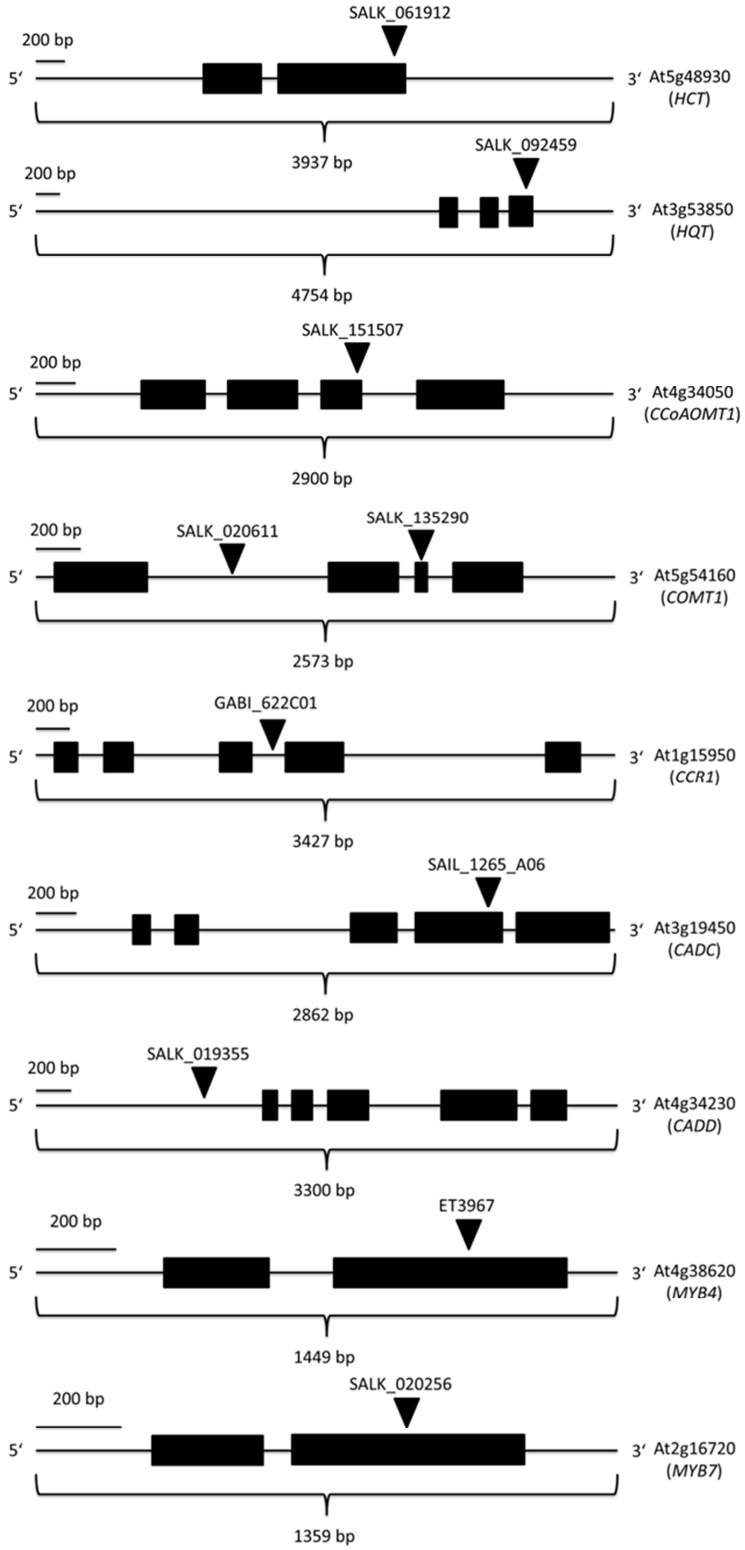

Fig. 30: Schematic view of the gene loci of the candidate genes and the position of the T-DNA insertion

The image represents a schematic view of the eight candidate genes with their corresponding T-DNA insertion. The orientation of the genes is from 5′ to the 3′. Exons are presented as black boxes and T-DNA insertions as triangles.

Genotyping of the different mutant lines was performed by PCR. By using two gene specific and one T-DNA insertion specific primer the T-DNA insertion, the orientation and the position could be verified.

The following figure represents in detail the verification of a T-DNA insertion and the determination of the T-DNA insertion in the gene.

In order to study the knockout of the gene *CCoAOMT1* the T-DNA insertion line SALK_151507 was ordered from the NASC. Seeds of the line SALK_151507 were sown on soil and bred as described in chapter 2.2.1. . After three weeks of growing, one or two leaves of a single plant were cut off to extract the genomic DNA (chapter 2.2.6.1.). Subsequently, the PCR was performed by using the gene specific primers LS1223 and LS1224 and the T-DNA specific primer LS378. The amplicon size of the wildtype product was expected to 1071 bp whereas the amplicon, generated by the primer pair LS1224 and LS1394, was estimated to about 850 bp. Heterozygous mutants would show both amplicon sizes the wildtype one and the mutant one (fig. 31).

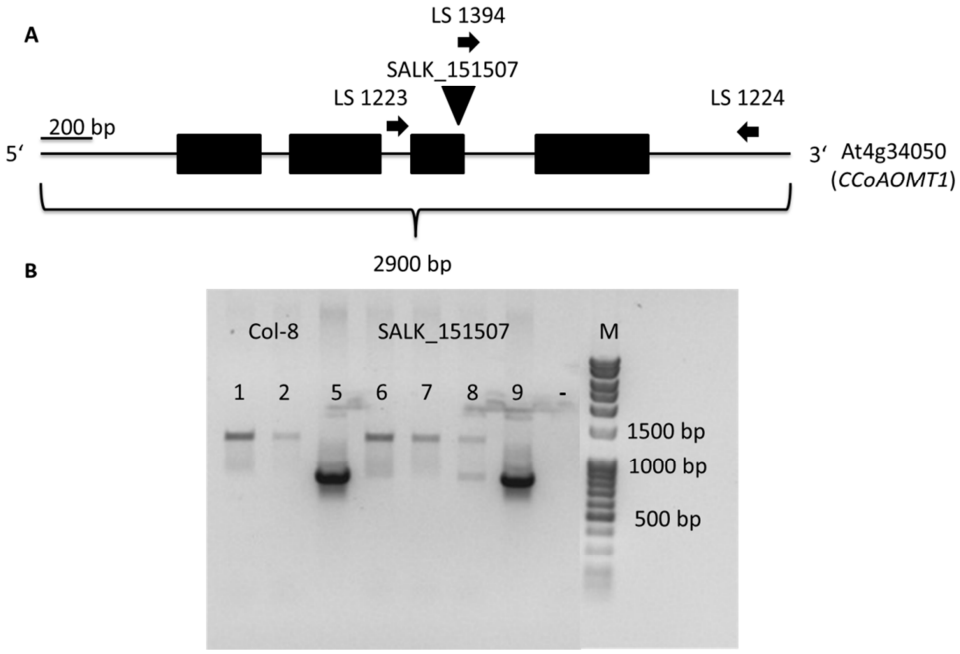

Fig. 31: Genotyping of the mutant line SALK_151507 with T-DNA insertion in *CCoAOMT1*

A: Schematic view of the gene loci CCoAOMT1 with T-DNA insertion. The orientation of the genes is from 5' to the 3'. Exons are presented as black boxes and T-DNA insertions as triangles. Black arrows indicate the position of the genotyping primers. B: Depicted is a representative genotyping PCR. Expected fragment sizes are for WT 1071 bp and for T-DNA insertion about 850 bp. The samples 6 and 7 show the WT expected fragment, whereas samples 5 and 9 exhibit the T-DNA insertion expected product size. Sample 8 shows both products. 1-2: WT genotyping samples, 5-9: SALK_151507 genotyping samples, -: negative control, M: marker.

If only heterozygous plants could be identified, the inflorescences of heterozygous plants were covered with a flat bag to avoid cross-pollination (chapter 2.2.9.2.). After seed maturation the seeds were collected and bred on soil. The following generation was genotyped again to identify at least one homozygous plant.

For all genes at least one homozygous line could be identified. The results are presented in the following table 13.

Tab. 13: Summary of the genotyping results of the different T-DNA insertion lines

Gene locus	T-DNA insertion mutant line	Homozygous	Wildtype
HCT	SALK_061912	X	
(At5g48930)	SALK_063325	X	
HQT	SALK_092459	X	
(At3g53850)		X	
CCoAOMT1	SALK_151507	X	
(At4g34050)			
COMT1	SALK_020611		X
(At5g54160)	SALK_135290	X	
CCR1	GABI_622C01	X	
(At1g15950)			
CADC	SAIL_1265_A06	X	
(At3g19450)			
CADD	SALK_019355	X	
(At4g34230)			
MYB4	ET3967	X	
(At4g38620)			
MYB7	SALK_020256	X	
(At2g16720)			

After the identification of homozygous plants, roots of four weeks old plants were carefully removed from the soil and RNA was extracted (chapter 2.2.6.2.). Semi-quantitative analysis was performed via RT-PCR. As an internal control *actin2* (At3g18780), which is a constitutively expressed gene, was used.

Most of the mutants and the WT reveal a strong *Actin2* PCR product. Only a weak band was obtained for the line SALK_020256. Most of the lines do not show a PCR product of the gene of interest. Only in the case of *HCT* both lines SALK_061912 and SALK_063325 reveal a strong PCR product. Furthermore, the lines SALK_135290 and SALK_019355 exhibit a specific PCR product of the gene of interest, but the intensity of the bands is decreased. Due to this, these two lines are regarded as knockdown lines. All remaining lines are considered as functional knockouts. The results of the RT-PCR are presented in the following figure 32.

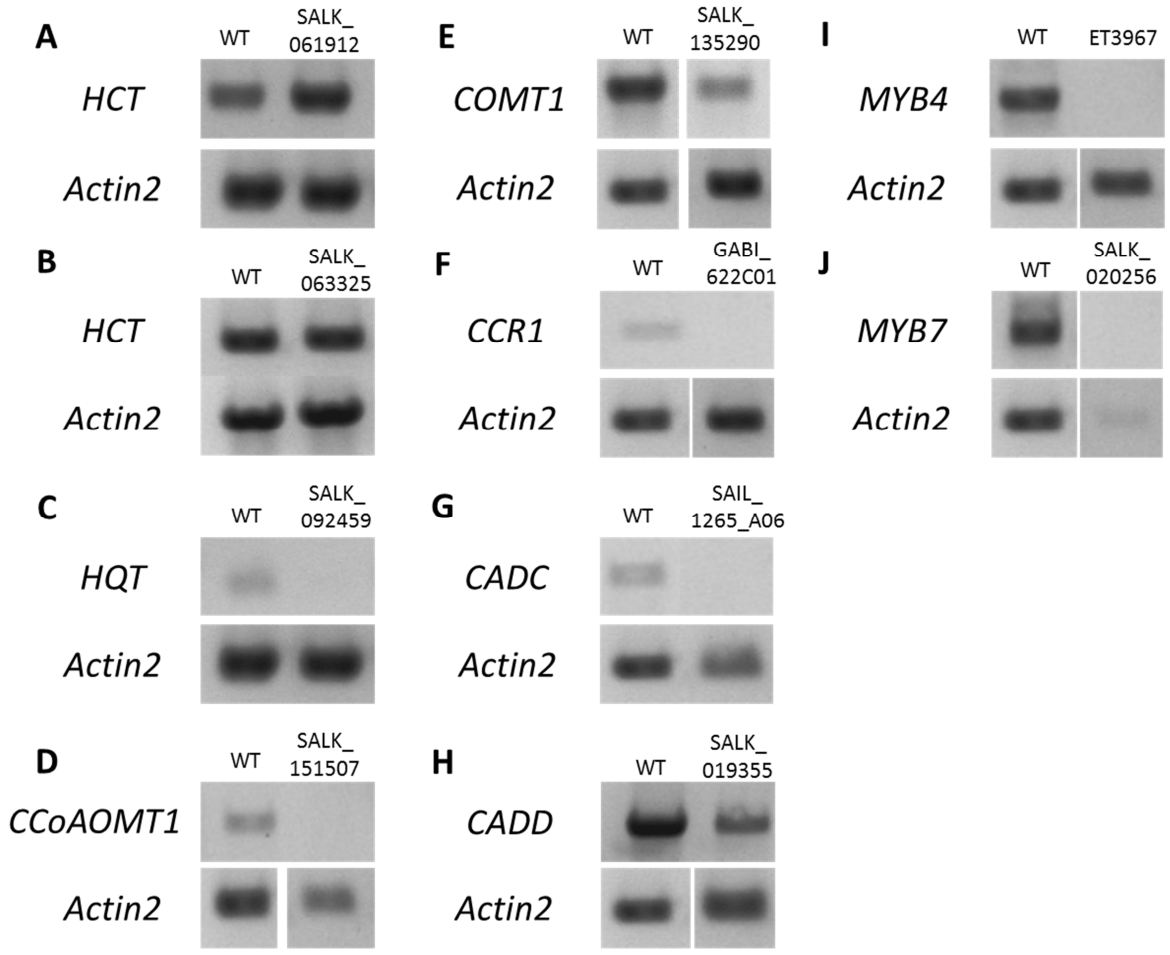

Fig. 32: Determination of the gene expression level in several mutant lines

Depicted is the gene expression level of several T-DNA insertion lines. As a positive control the constitutively expressed gene *Actin 2* was used. Absence of a band is interpreted as a functional knockout, whereas a decreased intensity is interpreted as a knockdown. Functional knockouts are SALK_092459, SALK_151507, GABI_622C01, SAIL_1265_A06, ET3967 and SALK_020256. Knockdowns are SALK_135290 and SALK_019355. Wildtype-like expression level is present in line SALK_061912 and SALK_063325.

The results of the genotyping and RT-PCR analysis are summarised in the following table 14.

Tab. 14: Summary of the genotyping and RT-PCR results of the different T-DNA insertion lines

Gene locus	T-DNA insertion mutant line	Homozygous	Functional knockout
HCT	SALK_061912	yes	no
(At5g48930)		yes	no
HQT	SALK_092459	yes	yes
(At3g53850)		yes	no
CCoAOMT1	SALK_151507	yes	yes
(At4g34050)			
COMT1	SALK_135290	yes	knockdown
(At5g54160)			
CCR1	GABI_622C01	yes	yes
(At1g15950)			
CADC	SAIL_1265_A06	yes	yes
(At3g19450)			
CADD	SALK_019355	yes	knockdown
(At4g34230)			
MYB4	ET3967	yes	yes
(At4g38620)			
MYB7	SALK_020256	yes	yes
(At2g16720)			

Both lines of the gene *HCT* were homozygous but not functional knockout mutants. Due to this the following studies do not involve these T-DNA insertions lines.

3.3. Microscopical analysis of Casparian strip and suberin barrier in seedlings

3.3.1. Determination of a functional apoplastic barrier by staining with propidium iodide

In order to analyse the functionality of the apoplastic barrier one week old seedlings of different mutant lines with a root length of 1 cm were incubated in 15 µM propidium iodide (PI) solutions. After incubation time the seedlings were rinsed in distilled water and the staining was visualised under the microscope by using UV-light (filter set: exication filter BP 500-550 nm, beam splitter FT 580 nm, blocking filter LP 590 nm). From the onset of elongation, the number of endodermal cells was counted until the point where PI does not infiltrate the central cylinder.

The following figure 33 shows the root stained with PI and the blockage of the PI diffusion into the central cylinder. The blockage of the PI into the central cylinder can be clearly seen at the point where the xylem vessels are not stained any more.

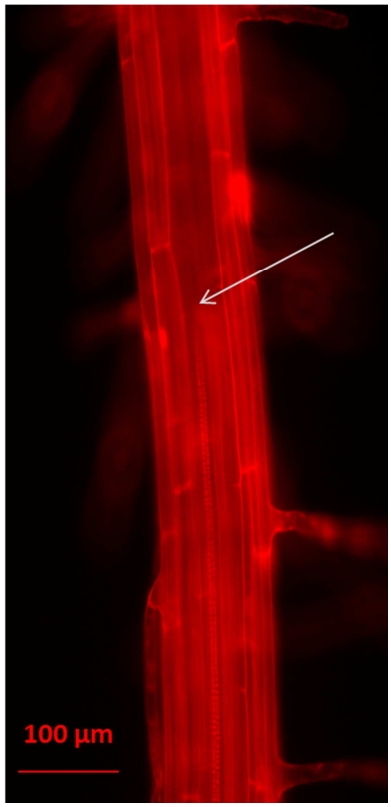

Fig. 33: Propidium iodide stained WT root

This figure visualises a stained root with propidium iodide. The diffusion of PI into the central cylinder can be clearly seen by the stained xylem vessels. The block of the diffusion of the PI is the point where xylem vessels are not stained anymore. The arrow indicates the block of the PI diffusion.

Wildtype (WT) roots of Columbia-8 (Col-8) reveal usually a block of the PI after 10 (± 1.8) endodermal cells. As a positive control of a non-functional apoplastic barrier *enhanced suberin 1* (*esb1*) was used. The PI is blocked in the mutant *esb1* after 19.7 (± 2.0) endodermal cells. The mutant *hqt* develops an apoplastic barrier highly significant earlier as the PI is blocked after 8.5 (± 1.0) endodermal cells. Similar effect is visible in the mutant *RALPH::HQT*. Here, the PI diffusion is blocked after 7.6 (± 1.6) endodermal cells. Mutant lines of *comt1* and *myb7* exhibit a block of PI diffusion into the central cylinder after 13 (± 2.6) and 12 (± 1.6) endodermal cells, which is similar to the wildtype and not significantly altered. In contrast, *ccoaomt1* and *ccr1* reveals a delayed apoplastic diffusion blockage of PI. After 15 (± 3.9) endodermal cells in *ccoaomt1* and 13.8 (± 1.7) endodermal cells in *ccr1* the PI is blocked. This delayed blockage of the PI diffusion is highly significant compared to the wildtype (10 ± 1.8 endodermal cells) (fig. 34).

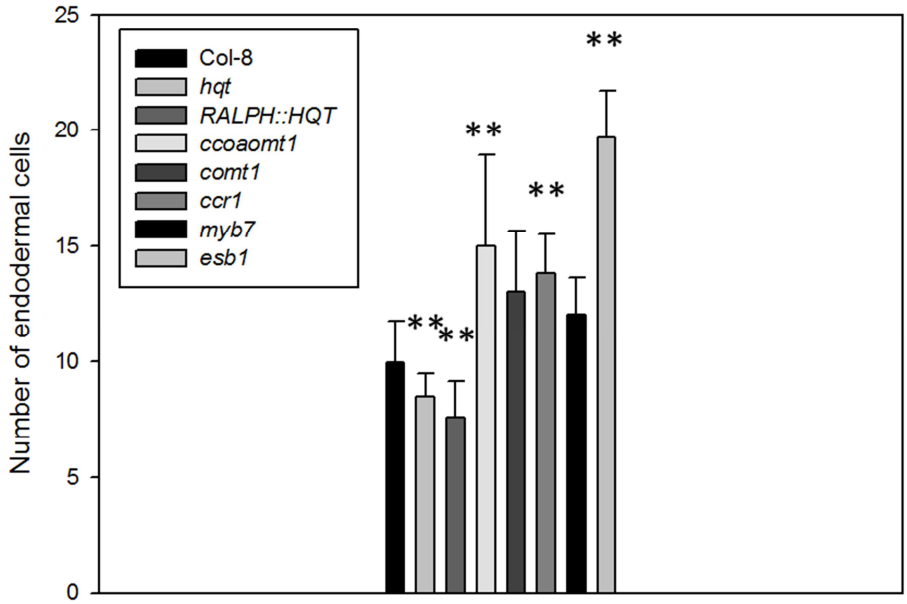

Fig. 34: Establishment of a functional apoplastic diffusion barrier visualised by using PI stained root seedlings of *Arabidopsis thaliana*

The apoplastic diffusion of PI into the central cylinder of Col-8 is blocked after 10 endodermal cells, whereas the blockage of PI occurs after 8.5 in *hqt*, 7.6 in *RALPH::HQT*, 15 in *ccoaomt1*, 13 in *comt1*, 13.8 in *ccr1*, 12 in *myb7* and 19.7 endodermal cells in *esb1*. The represented values are the arithmetic mean of the WT and mutant lines respectively and the calculated standard deviation error bars. The sample amount of each represented value corresponds to 10 seedlings. *: student's t-test, $p \leq 0.05$, **: student's t-test, $p \leq 0.01$.

The *Arabidopsis thaliana* ecotype Landsberg erecta (Ler) shows a blockage of the apoplastic tracer PI after 9.2 (± 1.8) endodermal cells. The mutant *myb4* reveals a slightly delayed blockage of PI after 11.6 (± 2.3) endodermal cells compared to the wildtype. This delayed blockage of PI is significant. The diffusion of PI into the central cylinder of the control *esb1* is highly significant altered. After 19.7 (± 1.6) endodermal cells is the diffusion of PI blocked in the *esb1* (fig. 35).

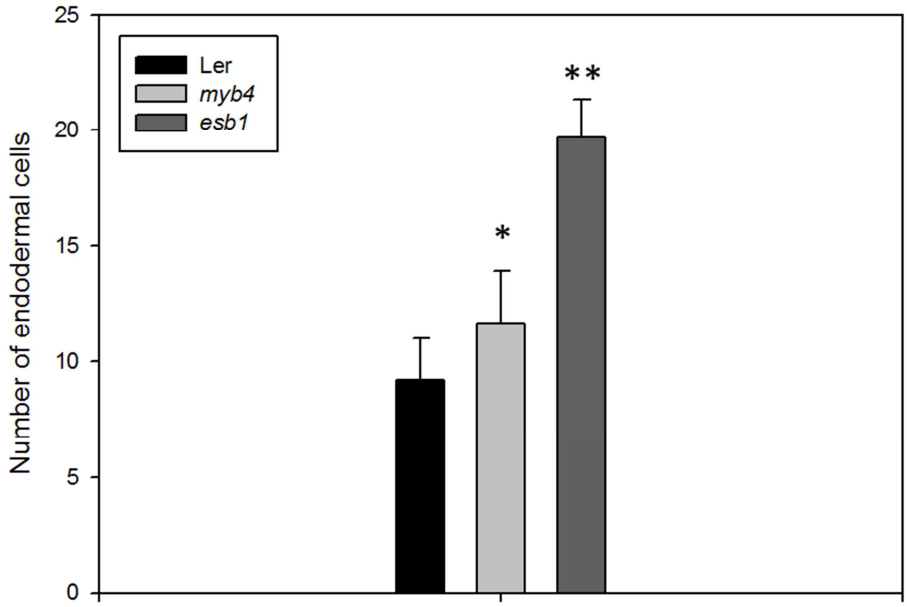

Fig. 35: Establishment of a functional apoplastic diffusion barrier visualised by using PI stained root seedlings of *Arabidopsis thaliana*

The apoplastic diffusion of PI into the central cylinder of Ler is blocked after 9.2 endodermal cells, whereas the blockage of PI occurs after 11.6 in *myb4* and 19.7 endodermal cells in *esb1*. The represented values are the arithmetic mean of the WT and mutant lines respectively and the calculated standard deviation error bars. The sample amount of each represented value corresponds to 10 seedlings. *: student's t-test, $p \leq 0.05$, **: student's t-test, $p \leq 0.01$.

With respect to the *cad*-mutants, single mutants *cadc* (8.6 ± 2.4), *cadd* (10.4 ± 1.8), both double knockout mutant *cadc*cadd* (10 ± 0.9) and *cadc*cadd 2* (10 ± 1.5) and the triple knockout mutant *cadc*cadd*fah1-2* (10.4 ± 1.3) do not show an alteration in the blockage of the PI into the central cylinder compared to the wildtype (9.3 ± 1.6). Only the positive control *esb1* reveals a highly significant delayed blockage of PI after 19.6 (± 1.6) endodermal cells compared to the wildtype (fig. 36).

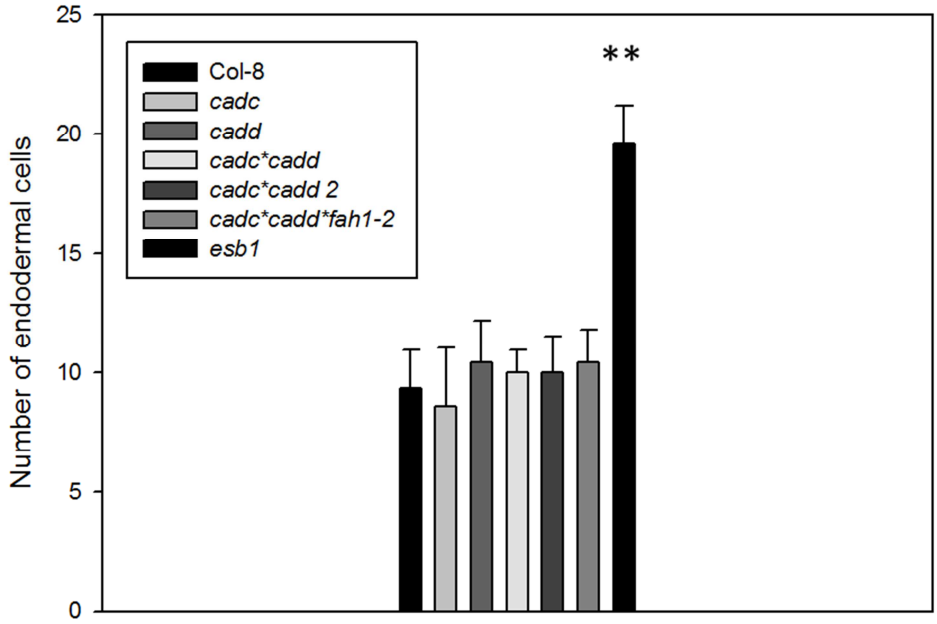

Fig. 36: Establishment of a functional apoplastic diffusion barrier visualised by using PI stained root seedlings of *Arabidopsis thaliana*

The apoplastic diffusion of PI into the central cylinder of Col-8, the *cad* single mutants, both double knockout mutants *cadc*cadd* and the triple knockout mutant *cadc*cadd*fah1-2* are similar. The mutant *esb1* reveals a highly significant delayed establishment of the apoplastic diffusion barrier compared to the WT. The represented values are the arithmetic mean of the WT and mutant lines respectively and the calculated standard deviation error bars. The sample amount of each represented value corresponds to 10 seedlings. *: student's t-test, $p \leq 0.05$, **: student's t-test, $p \leq 0.01$.

In the following figures the apoplastic diffusion barrier of several reduced epidermal fluorescent (*ref*) mutants were analysed. Diffusion of PI into the central cylinder of mutants lines *ref8-1* (9 ± 1.8), *ref8-1*med5a*med5b* (12.4 ± 3.3), *ref8-2*fah1-2*AtC4H::SmF5H* (10.2 ± 3.0) and *fah1-2* (12.3 ± 2.7) is similar in comparison to the wildtype Col-0 (10.2 ± 3.1). As a positive control of an impaired functionality of the apoplastic barrier the mutant *C4H::F5H* was used. This mutant reveals a highly significant delayed functionality of the apoplastic barrier after 25.6 (± 3.3) endodermal cells (fig. 37).

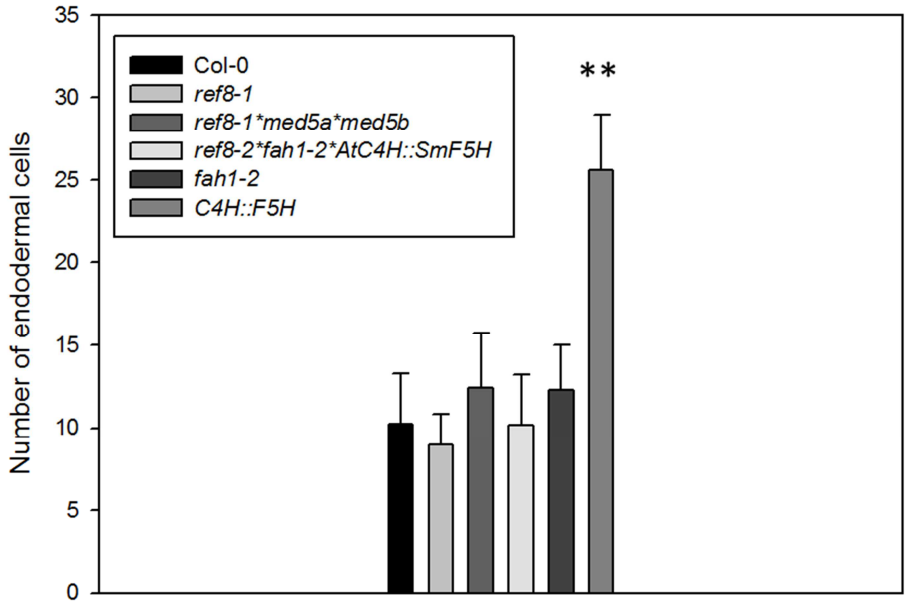

Fig. 37: Establishment of a functional apoplastic diffusion barrier visualised by using PI stained root seedlings of *Arabidopsis thaliana*

The apoplastic diffusion of PI into the central cylinder of Col-0 and the *ref8-1* single mutant, the triple mutant *ref8-1*med5a*med5b,* the mutant *ref8-2*fah1-2*AtC4H::SmF5H* and the *fah1-2* mutant are similar. The mutant *C4H::F5H* reveals a highly significant delayed establishment of a functional apoplastic diffusion barrier compared to the WT. The represented values are the arithmetic mean of the WT and mutant lines respectively and the calculated standard deviation error bars. The sample amount of each represented value corresponds to 10 seedlings. *: student's t-test, $p \leq 0.05$, **: student's t-test, $p \leq 0.01$.

The mutant *ref3-2* reveals the strongest effect of the PI-assay. The apoplastic diffusion of the PI into the central cylinder is not blocked in the mutant *ref3-2*. The number of endodermal cells is highly significant increased by 57.2 (± 8.8) compared to the wildtype Col-0 (10.9 ± 2.1). In contrast, *ref1-4* and *ref4-3* shows a delayed establishment of the apoplastic barrier after 15.8 (± 3.7) and 21.1 (± 3.2) endodermal cells, which is highly significant as well. The control *esb1* reveals a highly significant delayed blockage of PI into the central cylinder after 19.7 (± 2.0) endodermal cells (fig. 38).

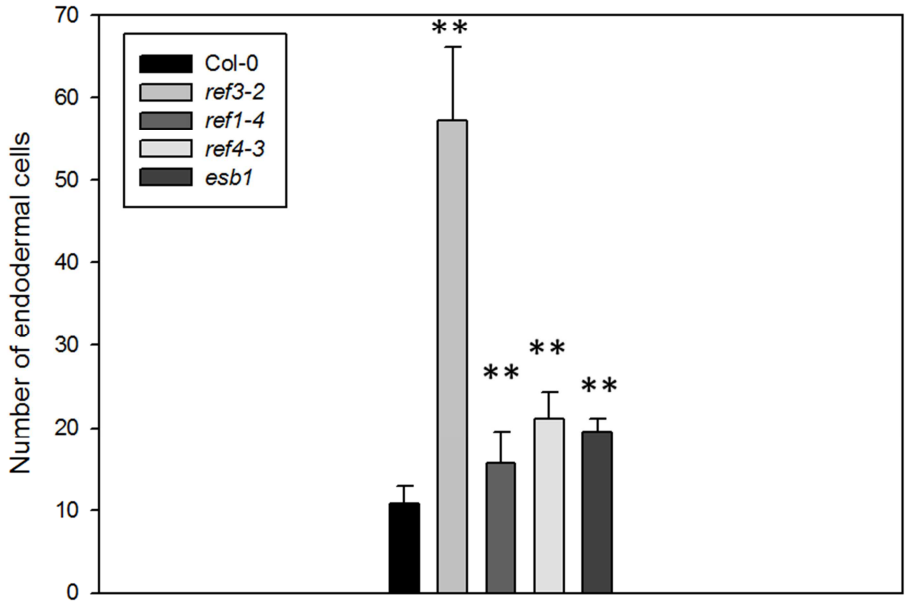

Fig. 38: Establishment of a functional apoplastic diffusion barrier visualised by using PI stained root seedlings of *Arabidopsis thaliana*

The apoplastic diffusion of PI into the central cylinder of Col-0 is blocked after 10.9 endodermal cells, whereas the blockage of PI occurs after 57.2 in *ref3-2*, 15.8 in *ref1-4*, 21.1 in *ref4-3* and 19.7 endodermal cells in *esb1*. The represented values are the arithmetic mean of the WT and mutant lines respectively and the calculated standard deviation error bars. The sample amount of each represented value corresponds to 10 seedlings. *: student's t-test, $p \leq 0.05$, **: student's t-test, $p \leq 0.01$.

Following figure 39 represents the recovery of a defective apoplastic barrier on the one hand by a dexamethasone inducible promoter of the mutant line *ref3-2*DEX::REF3* and on the other hand G-monolignol feeding experiment.

The untreated *ref3-2*DEX::REF3* mutant reveals no blockage of the PI diffusion into the central cylinder. The number of endodermal cells is high significantly altered in the *ref3-2*DEX::REF3* mutant (39.2 ± 7.1) compared to the WT (11 ± 2.2). The diffusion of the PI into the central cylinder is blocked after 22.1 (± 5.4) endodermal cells in the control *C4H::F5H*.

Dexamethasone containing ½ MS-media recovers in *ref3-2*DEX::REF3* the establishment of the apoplastic barrier whereas the WT is not affected by the dexamethasone treatment (*ref3-2*DEX::REF3* 11 ± 3.0, Col-0 9.3 ± 0.9).

Feeding the plant samples with G-monolignol recovers partially the establishment of the apoplastic barrier in *ref3-2*DEX::REF3* and fully in the positive control *C4H::F5H*. Nevertheless, there is a highly significant delayed blockage of PI into the central cylinder in

the *ref3-2*DEX::REF3* (15.2 ± 1.0) mutant compared with the WT (10.3 ± 1.4). *C4H::F5H* shows a similar number of 10.5 (± 1.6) endodermal cells like the WT.

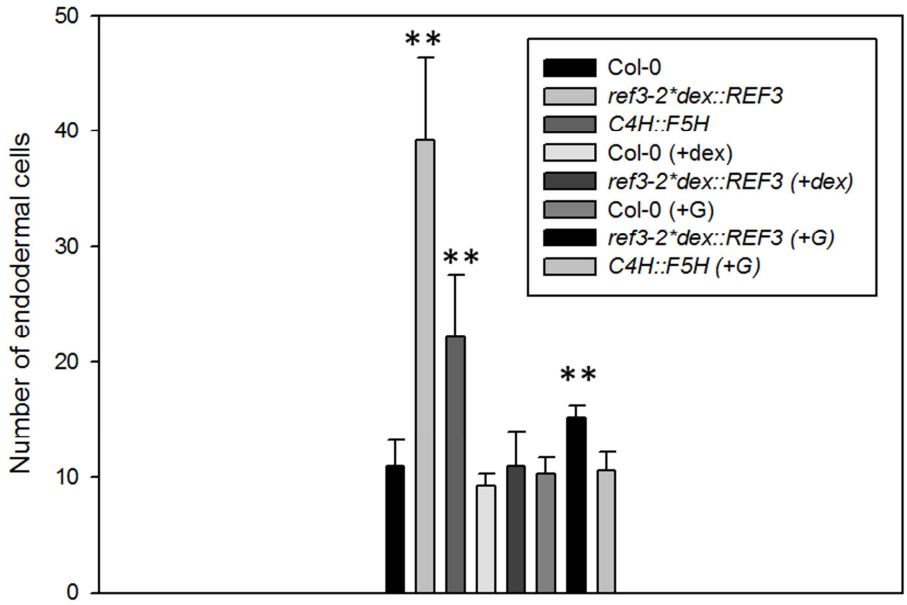

Fig. 39: Establishment of a functional apoplastic diffusion barrier visualised by using PI stained root seedlings of *Arabidopsis thaliana* on either by adding dexamethasone or by feeding with G-monolignol

The apoplastic diffusion of PI into the central cylinder of Col-0 is blocked after 11 endodermal cells, whereas the blockage of PI occur after 39.2 in *ref3-2*DEX::REF3* and 22.1 endodermal cells in *C4H::F5H*. By adding dexamethasone the apoplastic barrier is established after 9.3 in Col-0 and 11 endodermal cells in *ref3-2*DEX::REF3*. Feeding with G-monolignol causes a recovery of the apoplastic barrier. After 10.3 in WT, 15.2 in *ref3-2*DEX::REF3* and 10.5 endodermal cells in *C4H::F5H* the diffusion of PI is blocked into the central cylinder. The represented values are the arithmetic mean of the WT and mutant lines respectively and the calculated standard deviation error bars. The sample amount of each represented value corresponds to 10 seedlings. *: student's t-test, $p \leq 0.05$, **: student's t-test, $p \leq 0.01$.

In general, treating *prx11*, *asft* and *fact3* mutants with PI exhibits a development of the apoplastic barrier similar to the WT. After 8.9 (± 1.2) endodermal cells the apoplastic barrier becomes functional in the WT. The mutants *prx11-1* (9.6 ± 0.7), *asft1* (9.3 ± 1.2), *asft2* (9.8 ± 1.1) and *fact3* (9.2 ± 1.2) do not show a delayed or earlier formation of the apoplastic barrier. Only the mutant *prx11-2* (10.5 ± 1.2) reveals a highly significant delayed established apoplastic barrier. The control *esb1* (17.4 ± 2.1) exhibits a highly significant increased number of endodermal cells until the blockage of the PI into the central cylinder (fig. 40).

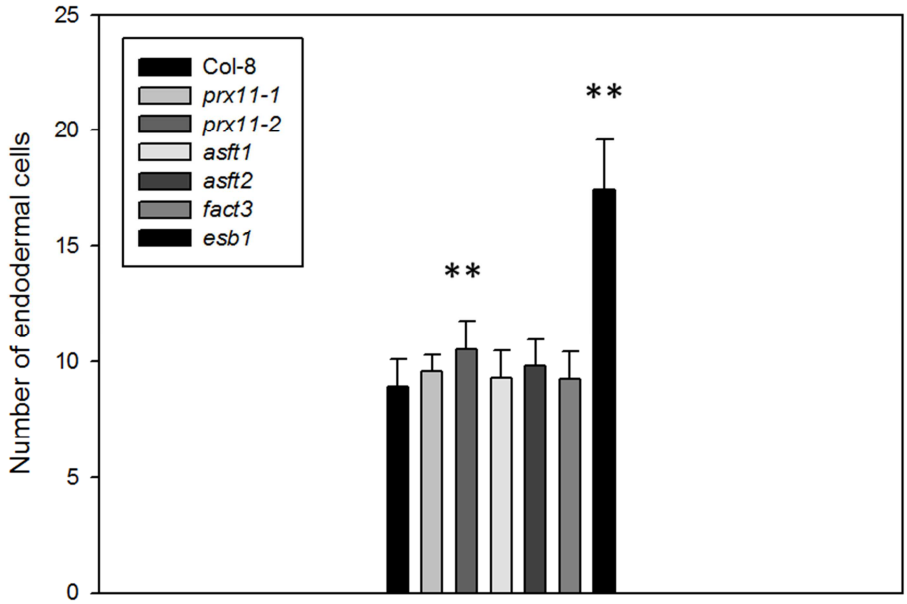

Fig. 40: Establishment of a functional apoplastic diffusion barrier visualised by using PI stained root seedlings of *Arabidopsis thaliana*

The apoplastic diffusion of PI into the central cylinder of Col-8 is blocked after 8.9 endodermal cells, whereas the blockage of PI occur after 9.6 in *prx11-1*, 10.5 in *prx11-2*, 9.3 in *asft1*, 9.8 in *asft2*, 9.2 in *fact3* and 17.4 endodermal cells in *esb1*. The represented values are the arithmetic mean of the WT and mutant lines respectively and the calculated standard deviation error bars. The sample amount of each represented value corresponds to 10 seedlings. *: student's t-test, $p \leq 0.05$, **: student's t-test, $p \leq 0.01$.

3.3.2. Qualitative analysis of the apoplastic barrier by staining with basic fuchsine

The functionality of the apoplastic barrier was qualitatively analysed by staining the one-week old roots with basic fuchsine. After the staining procedure the stained roots were investigated using a Leica SP5 confocal laser scanning microscope. Images were taken after 6, 10 and 15 endodermal cells. The roots are directed from the root tip on the left side to the basal part of the root on the right side.

Images taken at the 6th endodermal cell in the WT reveal a lignified network around the endodermal cells. Localised in the middle of the root the lignified xylem vessels extend along the root. At the 10th endodermal the stained xylem vessels exhibit an increased intensity of the staining. The border of one endodermal cell shows an intensively stained dot. At the 15th

endodermal cell the xylem vessels still reveal a high intensity of the staining. Staining also occurs parallel to the boundary of some endodermal cells (fig. 41, Col-8).

The mutant *hqt* and *RALPH::HQT* reveal a sealed lignified endodermal network at 6th endodermal cell. Below the 6th endodermal cell in *hqt* the endodermal network is still uncompleted, whereas the WT and *RALPH::HQT* already exhibit a completed endodermal network. In comparison to the WT the xylem vessels are less strongly stained but the intensity of the stained xylem vessels seem to increase in direction of the basal part of the root. At 10th endodermal cell the lignified network of the endodermal cells appears functional and the intensity of the stained xylem vessels has been increased. No alterations can be seen at 15th endodermal cell. Compared to the WT *hqt* and *RALPH::HQT* do not reveal any stained material parallel to the boundary of the endodermal cells (fig. 41, *hqt*).

In contrast to the WT, the mutant *ccoaomt1* shows a faint staining in all images. At 6th endodermal cell the lignified endodermal network can only be assumed. Staining is present at the boundary of adjacent endodermal cells and some xylem vessels reveal a weak staining. A faint staining is visible at 10th endodermal cell as well. The endodermal cells show a lignified network but it is hard to argue whether the network is disruptive or not. At 15th endodermal cell holes are existent in the lignified network. Furthermore, intensively stained dot-like parts of the lignified endodermal network might indicate deposited lignin (fig. 41, *ccoaomt1*).

The phenotype of the mutant *ccr1* seems to be similar to *ccoaomt1*. This mutant is also faint stained. An endodermal lignified network is visible at the 6th endodermal cell stage. The intensity of the staining only increases in the boundary of adjacent endodermal cells at the 10th endodermal cell stage. A big dot-like structure is present at the boundary of adjacent endodermal cells. Moreover, the intensity of the staining seems to increase at the 15th endodermal cells. However, the xylem vessels reveal a faint staining. Stained patches close to the boundary of the endodermal cells indicate the presence of lignified material (fig. 41, *ccr1*).

A disruptive lignified endodermal network is existent in the mutant *myb7* at 6th endodermal cell. Xylem vessels appear as dot-like structure in the centre of the root. Holes are sealed and the intensity of the stained xylem vessels is increased when the 10th endodermal cell stage is reached. The 15th endodermal cell stage looks similar to the WT. Only few parts of endodermal cell boundary show an intensively stained structure (fig. 41, *myb7*).

The control *esb1* reveals holes in the lignified endodermal network at 6th endodermal cell. Still, the holes are present at 10th endodermal cell and some deposition of lignin is visible close to the boundary of some endodermal cells. At 15th endodermal cell the holes are not sealed but endodermal cells exhibit multiple deposition of lignin close to the boundary of endodermal cells (fig. 41, *esb1*).

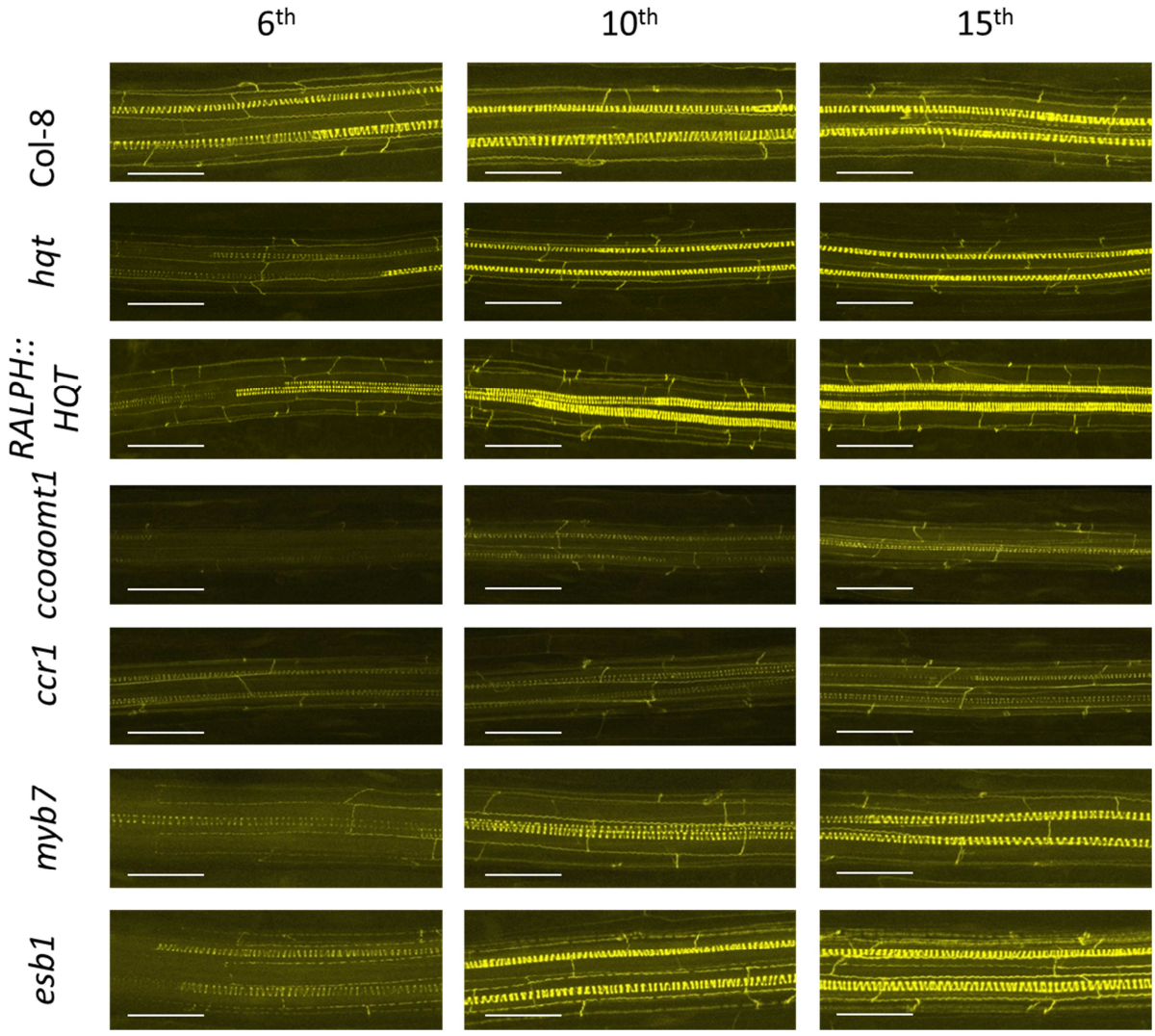

Fig. 41: Basic fuchsine stained roots show lignin deposition in mutant lines *hqt*, *RALPH::HQT*, *ccoaomt1*, *ccr1*, *myb7*, *esb1* and WT

The basic fuchsine staining reveals a lignified endodermal network in the WT. The mutant *hqt* and *RALPH::HQT* reveal a faint staining at 6th endodermal cell but the further developed parts of the root are indistinguishable from the WT. Both mutants *ccoaomt1* and *ccr1* exhibit a faint staining. The mutant *myb7* shows a weak staining at 6th endodermal cell but further developed parts of the root are similar to the WT. The control *esb1* shows a disrupted lignified endodermal network and additionally in the 10th and 15th endodermal cell stage numerous deposition of lignified material is present close to the boundary of endodermal cells. The images are representative for at least two root samples. Scale bar size is 100 µm in Col-8, *hqt*, *ccoaomt1*, *ccr1*, *myb7* and *esb1*. Scale bar size is 150 µm in *RALPH::HQT*.

As described in figure 41 the WT root already shows a lignified endodermal network at the 6th endodermal cell stage. Not all WT roots are lignified at the 6th endodermal cell stage (fig. 42, Col-8). But at 10th endodermal cell the lignified endodermal network is present. The 15th endodermal cell stage does not differ from the 10th endodermal cell stage in the WT (fig. 42, Col-8).

The mutant *cadc* shows a lignified endodermal network at 6th endodermal cell. At 10th endodermal cell stage the lignified endodermal network appears to be washy. Furthermore, at 15th endodermal cell the mutant reveals some stained dots close to the xylem vessels, which are not present in the WT (fig. 42, *cadc*).

The mutant *cadd* also exhibits a lignified endodermal network at 6th endodermal cell. However, the staining reveals weaker compared to the *cadc* mutant and the WT from figure 41. At 10th endodermal cell stage the staining of the lignified endodermal network appears to be washy like in the *cadc* mutant. This washy lignified endodermal network is also present at 15th endodermal cell. Moreover, some stained dots appear close to the xylem vessels.

The double knockout mutant *cadc*cadd* shows at all endodermal cell stages from 6th to 15th a faint staining. Barely detectable is the lignified endodermal network and the xylem vessels at 6th endodermal cell. At 10th and 15th endodermal cell the lignified endodermal network is better visible but not as well compared to the WT. In total the lignified endodermal network does not reveal any holes (fig. 42, *cadd*).

Analysis of *cadc*cadd 2* and *cadc*cadd*fah1-2* was performed by another confocal laser scanning microscope (Olympus Fluoview FV1000). For this reason, the magnification is different. Nevertheless, the second mutant *cadc*cadd 2* shows a weak staining only at 6th endodermal cell stage. Further developed parts of the root are well stained. Some stained lignified material is visible in the boundary of endodermal cells at 15th endodermal cell stage. Furthermore, the staining of the xylem vessels seems to be enhanced in comparison to the WT (fig. 42, *cadc*cadd 2*).

The triple knockout mutant *cadc*cadd*fah1-2* reveals faint staining at 6th and 10th endodermal cell stage. After 15 endodermal cells the staining seems to be still slightly faint in comparison to the WT and some stained lignified material is deposited close to the boundary of endodermal cells. A dot-like structure of the xylem vessels is only present at 10th endodermal cell stage (fig. 42, *cadc*cadd*fah1-2*).

The control *esb1* shows at all endodermal cell stages holes in the lignified endodermal network and furthermore at 15th endodermal cell some lignified material is deposited close to the boundary of the endodermal cells (fig. 42, *esb1*).

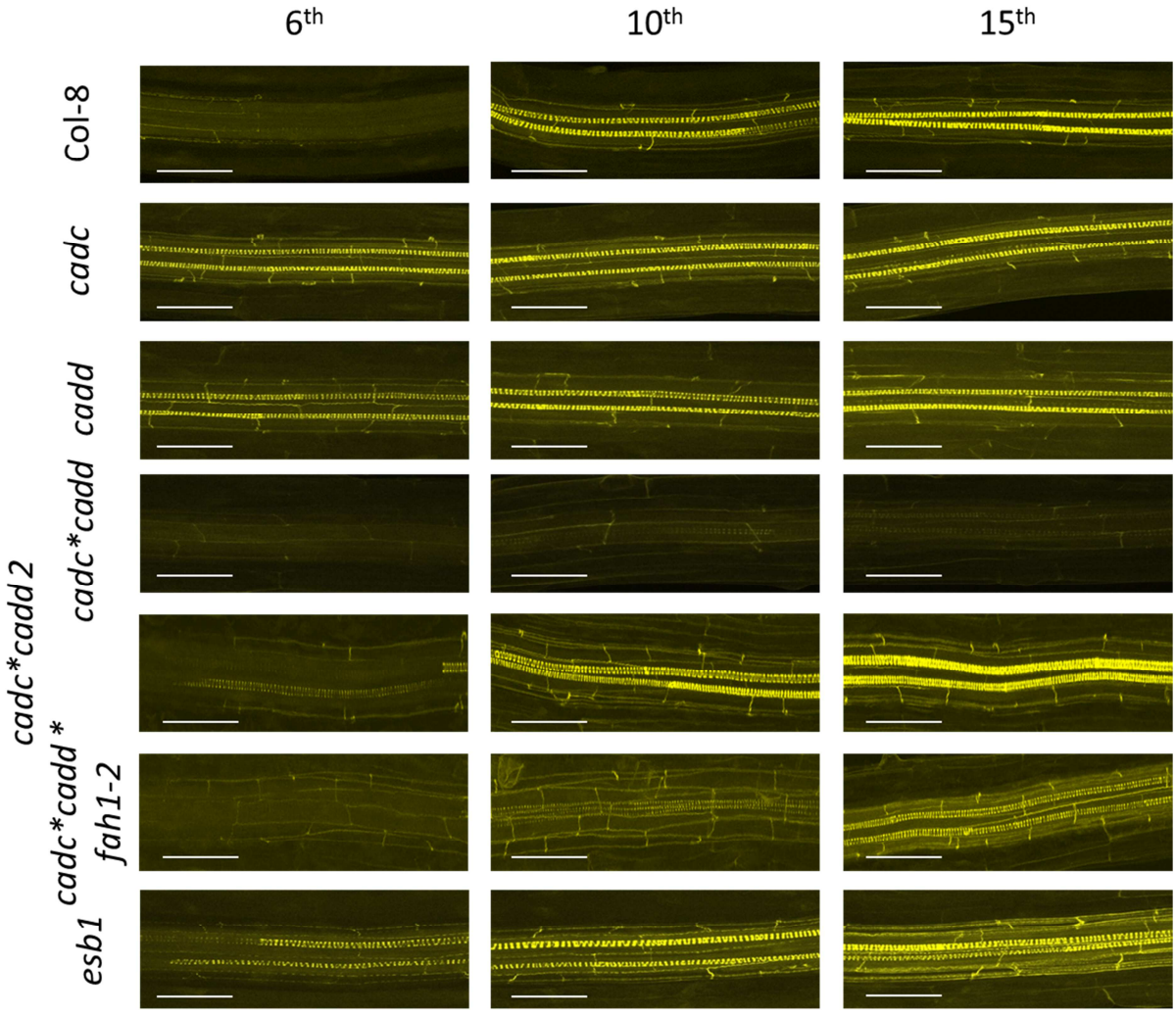

Fig. 42: Basic fuchsine stained roots show lignin deposition in mutant lines *cadc*, *cadd*, *cadc*cadd*, *cadc*cadd 2*, *cadc*cadd*fah1-2*, *esb1* and WT

The basic fuchsine staining reveals a lignified endodermal network in the WT. The mutants *cadc* and *cadd* reveal a similar staining to the WT at 6th endodermal cell but the further developed parts of the roots show a washy staining. The double knockout mutant *cadc*cadd* show a faint staining at all endodermal cell stages but the lignified endodermal network seems to be intact. Similar to *cadc*cadd* the mutant *cadc*cadd2* exhibits faint staining at 6th endodermal cells but further developed parts of the root are similar to the WT. At 15th endodermal cell stage some lignified material is deposited close to the boundary of endodermal cells. The triple knockout mutant *cadc*cadd*fah1-2* reveals weak staining at 6th and 10th endodermal cell. After the 15th endodermal cell the staining intensity is still slightly faint in comparison to the WT. However, some deposited lignified material is visible in the boundary of the endodermal cells. The control *esb1* shows a disrupted lignified endodermal network and additionally in the 10th and especially in the 15th endodermal cell stage numerous deposition of lignified material is present close to the boundary of endodermal cells. The images are representative for at least two root samples. Scale bar size is 100 µm in Col-8, *cadc*, *cadd*, *cadc*cadd* and *esb1*. Scale bar size is 150 µm in *cadc*cadd 2* and *cadc*cadd*fah1-2*.

A strong intensity of the staining is visible in the mutant *ref8-1*. At the beginning of the 6th endodermal cell the lignified endodermal network is still developing. There are some holes in the lignified endodermal network in early endodermal cells but in further developed endodermal cells these holes are sealed. Furthermore, the intensity of the staining of the xylem vessels increases in direction of the basal part of the root. At 10th endodermal cell the xylem vessels reveal a strong overlapping signal. Some stained lignified material seems to be deposited close to the boundary of some endodermal cells.

In contrast, the mutant *ref8-1*med5a*med5b* reveals holes in the lignified endodermal network at 6th endodermal cell stage. At the 10th endodermal cell the holes are sealed. The 15th endodermal cell stage is indistinguishable from the WT (fig. 43).

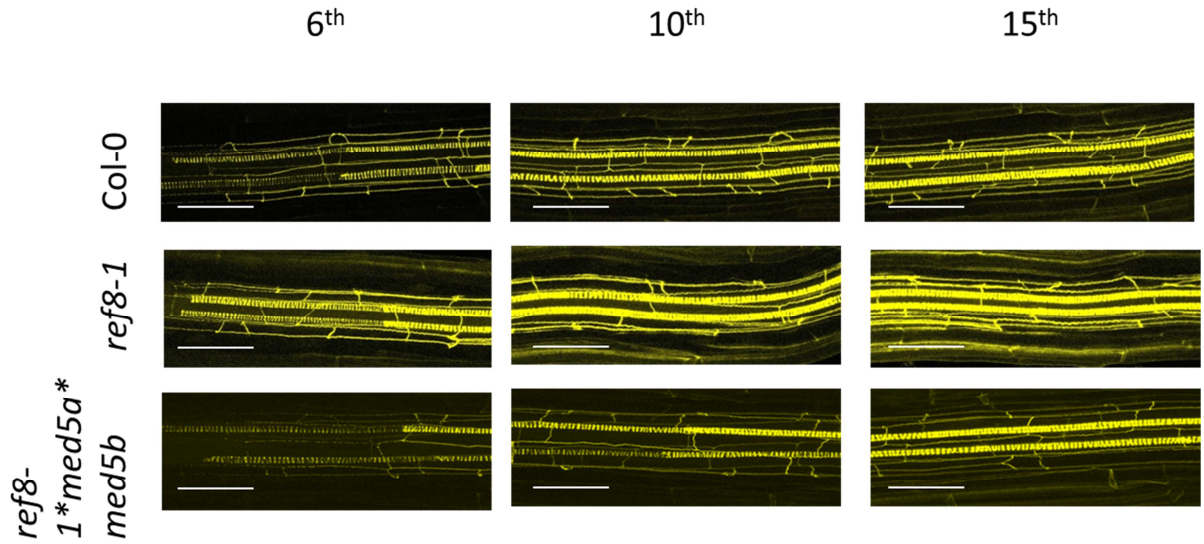

Fig. 43: Basic fuchsine stained roots show lignin deposition in mutant lines *ref8-1*, *ref8-1*med5a*med5b* and WT

The basic fuchsine staining reveals a lignified endodermal network in the WT. The mutant *ref8-1* reveals a lignified endodermal network at 6th endodermal cell. Further developed parts of the roots show a strong signal from the xylem vessels and deposited stained material is visible close to the boundary of endodermal cells. The triple mutant *ref8-1*med5a*med5b* shows at first holes in the lignified endodermal network, which are sealed in the further developed parts of the root. In total the staining reveals a similar phenotype to the WT. The images are representative for at least two root samples. Scale bar size is 100 µm.

Analysis of the second WT, *ref3-2* and *C4H::F5H* was performed with the Olympus Fluoview FV1000, whereas the remaining mutant lines were analysed by using the Leica SP5. This is the reason why, the magnification and the staining are not comparable with the first WT but with the second one. Contours of the endodermal cells at the 6th endodermal cell are not clear visible in the *ref3-2* mutant. At 10th endodermal cell stage the contours of the endodermal cells become more visible and at 15th endodermal cell stage staining is present

within endodermal cells. The xylem vessels appear to be intact and are well stained in all taken images (fig. 44, *ref3-2*).

Both mutant *ref1-4* and *ref4-3* exhibit a similar phenotype. At 6th endodermal cell the lignified endodermal network is not fully developed. Further upstream of the roots the intensity of the staining is increased in total and the lignified endodermal network seems to be intact. However, *ref4-3* reveals deposition of stained material close to the endodermal cell boundary. In contrast, *ref1-4* appears to be similar to the first WT at 10th endodermal cell. At 15th endodermal cell the staining intensity is severely increased. Staining of the xylem vessels overlap in *ref1-4* and in some endodermal cells stained material is deposited close to the stained boundary of the lignified endodermal network. A stronger deposition of stained material within the endodermal cells is observable in the mutant *ref4-3* (fig. 44, *ref1-4* and *ref4-3*).

The control *C4H::F5H* shows deposited lignified material close to the boundary of endodermal cells already at 6th endodermal cell stage. This phenomenon increases in further developed parts of the root. At 10th endodermal cell accumulation of lignified material is present at the interface of two adjacent endodermal cells. After 15 endodermal cells the mutant *C4H::F5H* is severely lignified and the ectopic lignification is clear visible within the endodermal cells and at the interfaces of adjacent endodermal cells (fig. 44, *C4H::F5H*).

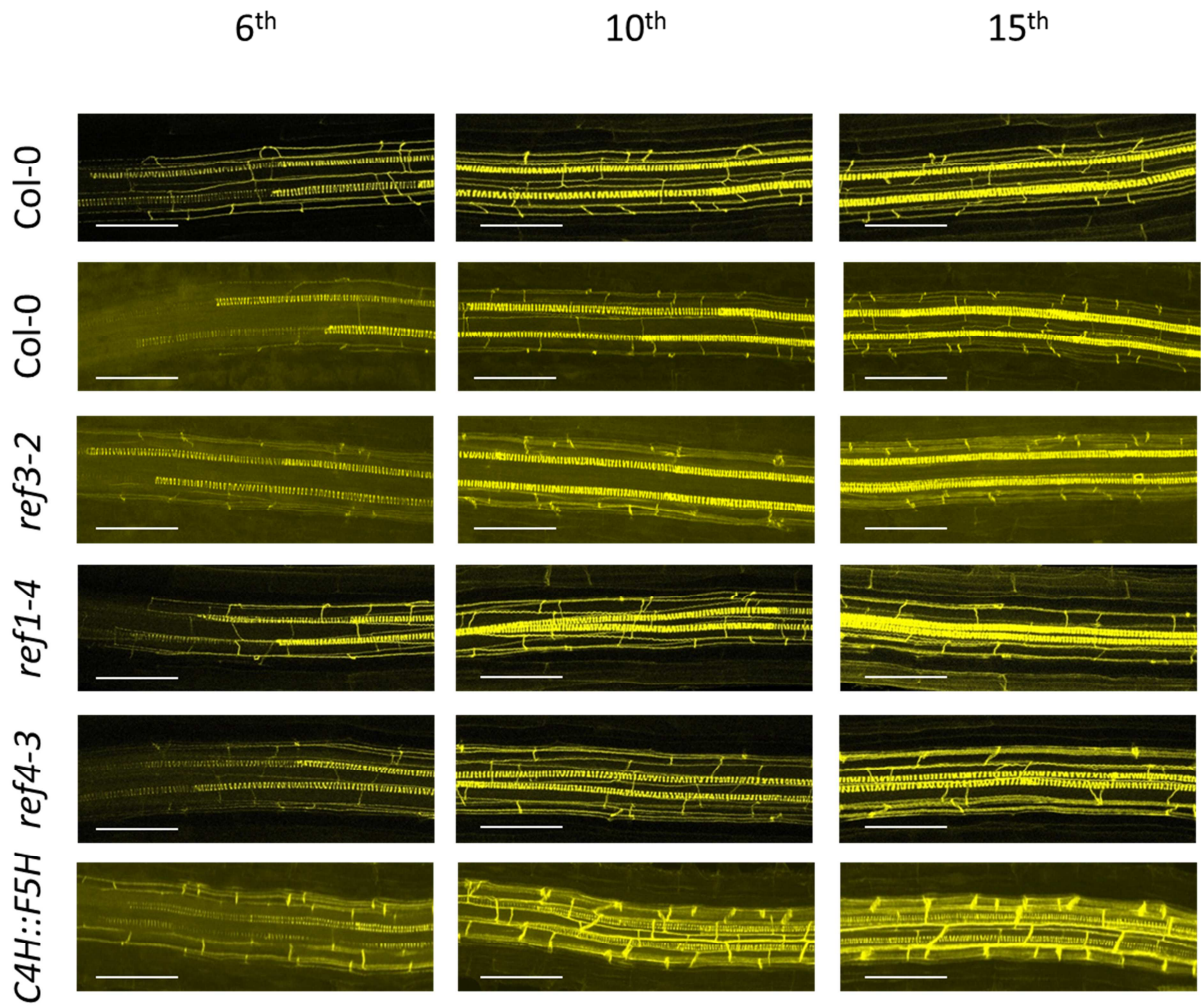

Fig. 44: Basic fuchsine stained roots show lignin deposition in mutant lines *ref3-2*, *ref1-4*, *ref4-3*, *C4H::F5H* and WT

The basic fuchsine staining reveals a lignified endodermal network in the WT. In contrast, contours of endodermal cells are not clear visible at all taken images of *ref3-2*. The contours appear to be washy. Furthermore, deposited stained lignified material is visible within endodermal cells. The mutant *ref1-4* and *ref4-3* reveal an undeveloped lignified endodermal network close to the root tip. At 10th endodermal cell stage the lignified endodermal network is developed but *ref4-3* already indicates first deposited stained material close to the endodermal cell boundary. At 15th endodermal cell stage both mutants *ref1-4* and *ref4-3* show deposited stained material within the endodermal cells. The control *C4H::F5H* exhibits already very early at 6th endodermal cell stage deposited stained lignified material within the endodermal cells. This effect increases in further developed parts of the root. Especially, the interface of adjacent endodermal cells is severely stained. The images are representative for at least two root samples. Scale bar size is 100 µm in Col-0, *ref1-4* and *ref4-3*. Scale bar size is 150 µm in *ref3-2* and *C4H::F5H*.

In figure 45 all mutants reveal at 6th and 10th endodermal cell stage a faint staining compared to the WT. Both *prx11* mutants show a still developing lignified endodermal network at 6th endodermal cell. At 10th endodermal cell the lignified endodermal network is complete present in *prx11-2* but in *prx11-1* it is severely disrupted in one endodermal cell. In some endodermal cells *prx11-2* reveals deposited stained material close to the boundary at 15th

endodermal cell stage. The WT seems to show a similar phenotype. The mutant *prx11-1* does not show any deposited stained material within endodermal cells. Both mutant lines show a fainter staining than the WT at the 15th endodermal cell stage (fig. 45, *prx11-1* and *prx11-2*).

The mutant *asft1* shows an undeveloped lignified endodermal network at the 6th endodermal cell stage whereas *asft2* seems to have a full developed lignified endodermal network already. At the 10th endodermal cell stage *asft1* shows a developed lignified endodermal network similar to *asft2*. Both mutant lines also reveal bright dots in the lignified endodermal network. Bright dots can be seen in the WT as well, but the size is increased in the *asft* mutants (fig. 45, *asft1* and *asft2*).

The mutant *fact3* reveals at the beginning an undeveloped lignified endodermal network. At the 10th and 15th endodermal cell stage the *fact3* mutant is indistinguishable from the WT. There are no specific characteristics visible in the *fact3* mutant (fig. 45, *fact3*).

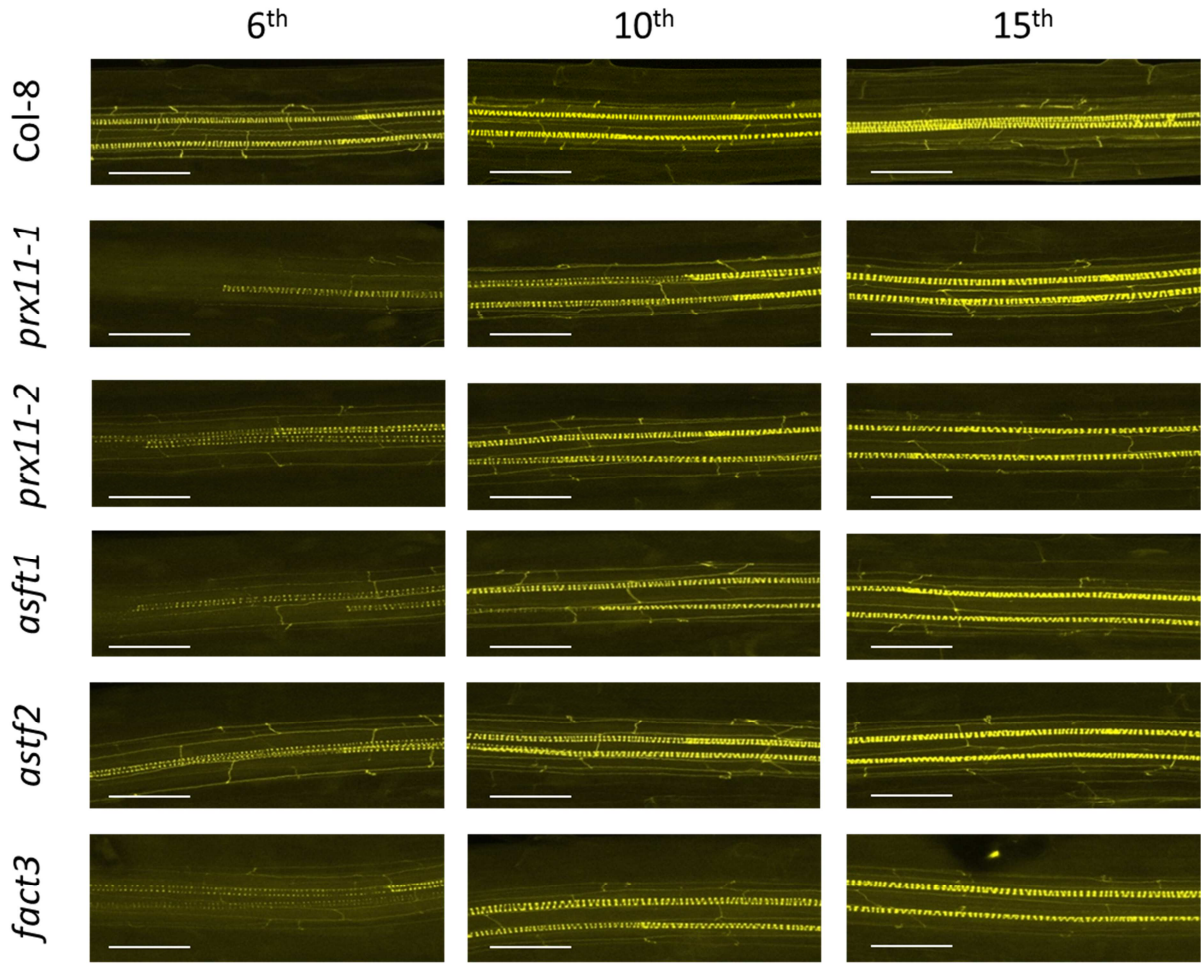

Fig. 45: Basic fuchsine stained roots show lignin deposition in mutant lines *prx11-1*, *prx11-2*, *asft1*, *asft2*, *fact3* and WT

The basic fuchsine staining reveals a lignified endodermal network in the WT. All mutants reveal a fainter staining at 6th and 10th endodermal cell stage than the WT. The mutant *prx11* does not show many alterations compared to the WT. Only

prx11-2 reveals deposited stained material within some endodermal cells. The mutant lines *asft1* and *asft2* do not show specific alterations in the development of the lignified endodermal network. However, there are some bright and large dots in the lignified endodermal network, which also occur in the WT but the size is increased in *asft* mutant lines. The *fact3* mutant does not show any specific characteristics. Only the staining is at the beginning fainter than in the WT. The images are representative for at least two root samples. Scale bar size is 100 µm.

3.3.3. Quantitative and qualitative analysis of the root suberin barrier by staining with fluorol yellow 088

Seven day old roots with a root length of approximately 1 cm were stained with fluorol yellow 088. After staining, the roots were mounted on slides and stained roots were visualised by using UV-light and filter set: excitation filter BP 450-490 nm, beam splitter FT510 nm, blocking filter LP 520 nm. Images were taken along the root. This method enables the visualisation of suberin to analysis the localisation of the suberin deposition and the status of the suberin development.

More than the half of a WT root is not stained (57.0 % ± 1.8 %). This zone is regarded as a non-suberised zone. A WT root consists of approximately 10 % (10.0 % ± 0.9 %) of patchy suberised zone and 33 % (33.1 % ± 1.8 %) of continuously suberised zone (fig. 46 B).

Qualitatively, the development of suberin seems to start earlier in the mutant *hqt*, *RALPH::HQT* and the positive control *esb1*. At the same position the WT is still patchy suberised whereas *hqt*, *RALPH::HQT* and *esb1* exhibits a continuously suberised phenotype. The intensity of the staining is similar to the WT in the taken images of the continuously suberised zone. In contrast, *ccoaomt1*, *comt1* and *ccr1* are not suberised whereas the WT is patchy suberised at the same position. It appears that the three mutant *ccoaomt1*, *comt1* and *ccr1* have a higher degree of uncompleted suberisation. Also further suberised parts of the roots are still patchy suberised whereas the WT reveal a continuously suberised zone. Staining intensity is comparable in mutant lines with WT. Mutant line *myb7* reveal a WT pattern of suberisation. Staining results reveal that suberisation starts at the same point in the *myb7* mutant compared with the WT. The intensity of the staining is similar to the WT (fig. 46 A).

With respect to the quantitative analysis the non-suberised zone is slightly decreased to 40.1 % (± 3.2 %) in *hqt* compared to the WT (46.9 % ± 2.3 %). The size of the patchy suberised zone is similar to the WT in *hqt* (11.8 % ± 3.1 % in *hqt* and 10.9 % ± 0.8 % in WT). Consistent

with a sligthly decreased non-suberised zone the continuously suberised zone is slightly increased to 48.2 % (± 2.7 %) compared to the WT (42.2 % ± 2.2 %) (fig. 46 B).

The quantitative analysis confirms the earlier suberisation of *RALPH::HQT* compared to the WT. The non-suberised zone of *RALPH::HQT* shows a significantly higher decrease in comparison to the WT (33.5 ± 2.6 % in *RALPH::HQT* and 46.9 ± 2.3 % in WT). In contrast, the size of the patchy suberised zone is similar to the WT (14.5 ± 2.5 % in *RALPH::HQT* and 10.9 ± 0.8 % in WT). Consistent with a decreased non-suberised zone the continuously suberised zone is significantly enhanced in *RALPH::HQT* (52.0 ± 3.2 %) compared to the WT (42.2 ± 2.2 %) (fig. 46 B).

Both mutant *ccoaomt1* and *comt1* reveal a similar phenotype. The suberisation appears to start earlier (*ccoaomt1*: 36.1 ± 2.4 %; *comt1*: 39.4 % ± 3.5 %) than in the WT (46.9 % ± 2.3 %). However, the size of the non-suberised zone in *comt1* is not significantly altered from the statistical evaluation. But in contrast, a highly significant increase of the patchy suberised zone in both mutant lines (*ccoaomt1*: 35.9 % ± 3.7 %; *comt1*: 35.6 % ± 3.3 %) results in a decreased continuously suberised zone in *ccoaomt1* (28.0 % ± 2.7 %) and significantly altered one in *comt1* (24.9 % ± 2.7 %) compared to the WT (fig. 46 B).

Roots of *ccr1* are less suberised than the WT. The suberisation is delayed in the mutant. A significantly larger zone of the *ccr1* is not suberised (79.6 % ± 2.9%). The patchy suberised zone is of a similar relative length compared with the WT, but a continuously suberised zone can only be found near the basal part of the root. Only 10.9 % (± 2.5 %) of *ccr1* is continuously suberised. This decrease of the continuously suberised zone is highly significant in comparison to the WT (fig. 46 B).

Statistical evaluation of the three zones of the suberisation stage reveals that *myb7* is similar to the WT and confirms the WT pattern of suberisation.

A patchy suberised zone is only marginal present in *esb1*. Roots of *esb1* reveal a highly significant decrease of the non-suberised (21.4 % ± 0.7 %) and patchy suberised zone (1.2 % ± 0.1 %) but a significantly higher increase of the continuously suberised zone (77.4 % ± 0.7 %) compared with the WT (fig. 46 B).

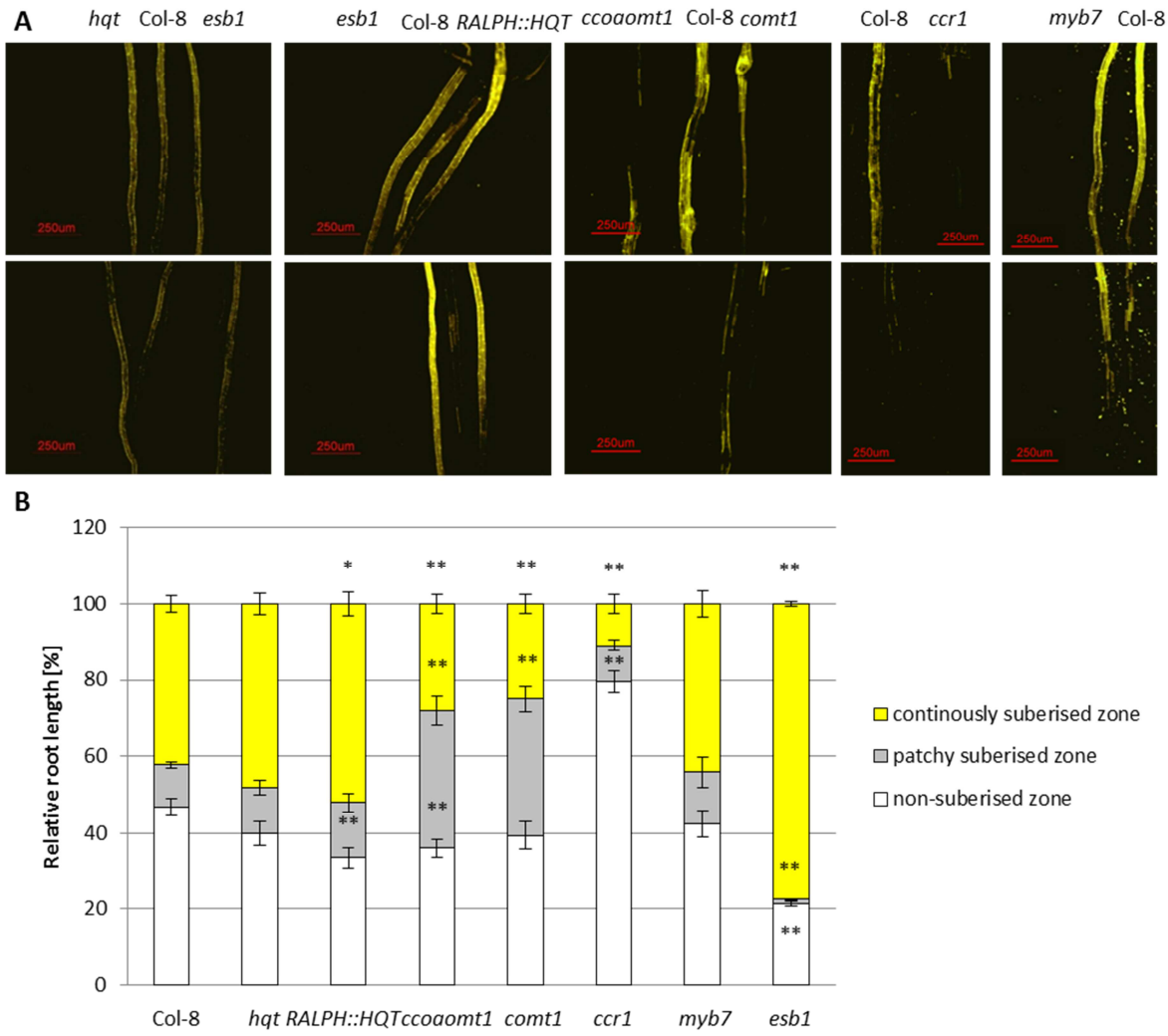

Fig. 46: Stained roots of seedlings with fluorol yellow 088 reveal suberin deposition and qualitative analysis of suberised zones along the roots of *hqt*, *RALPH::HQT*, *ccoaomt1*, *comt1*, *ccr1*, *myb7*, *esb1* and *WT*

A: Depicted are representative stained roots of the different mutants. The upper images reveal the continuously suberised zone, whereas the lower ones represent the patchy suberised zone. Scale bar size is 250 µm.

B: Qualitative analysis of the non-, patchy and continuously suberised zones of WT and mutant lines. The represented values are the arithmetic mean of the WT and mutant lines respectively and the calculated error bars of the standard error. The sample amount corresponds to 58 roots of Col-8, 13 in *hqt*, 12 of *RALPH::HQT*, 14 of *ccoaomt1*, 11 of *comt1* as well as *myb7* and 17 of *esb1*. *: student's t-test, $p \leq 0.05$, **: student's t-test, $p \leq 0.01$.

The development of suberin starts earlier in *myb4* roots than in the WT. Suberisation starts at the same position in *myb4* and *esb1*, whereas the WT is delayed. The intensity of the staining does not differ among all three genotypes (fig. 47 A).

Quantitatively, the non-suberised zone is smaller (33.1 % ± 2.3 %) than in the WT (42.5 % ± 1.5 %) but larger than in *esb1* (24.3 % ± 1.5 %). The patchy suberised zone is similar to the WT (9.1 % ± 3.4 %) in *myb4* (12.8 % ± 2.5 %), whereas *esb1* (0.4 % ± 0.2 %) does barely have a

transition zone between non-suberised and continuously suberised zone. Due to the decreased non-suberised zone the continuously suberised zone is slightly increased in *myb4* (54.2 % ± 2.5 %) but this increase of suberisation is not significant compared with the WT (48.4 % ± 3.5 %). Approximately three-quarter of the positive control *esb1* (75.2 % ± 1.4) reveals a strongly increased continuously suberised zone compared with the WT. This increased continuously suberised zone affects the remaining two zones of the root highly significant (fig. 47 B).

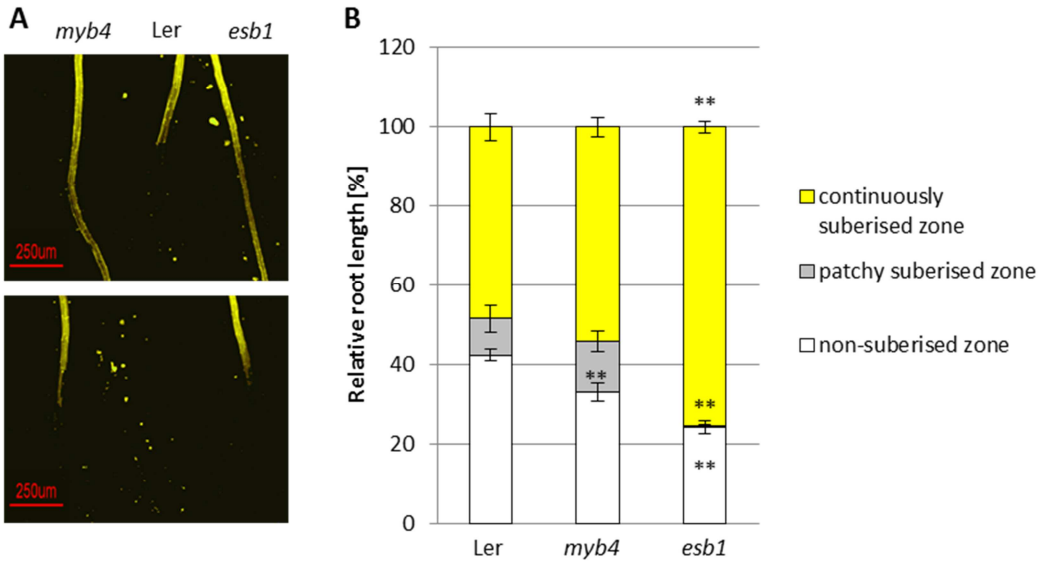

Fig. 47: Stained roots of seedlings with fluorol yellow 088 reveal suberin deposition and qualitative analysis of suberised zones along the roots of *myb4*, *esb1* and WT

A: Depicted are representative stained roots of different mutants. The upper images reveal the continuously suberised zone whereas the lower ones represent the patchy suberised zone. Scale bar size is 250 µm.

B: Qualitative analysis of the non-, patchy and continuously suberised zones of WT and mutant lines. The represented values are the arithmetic mean of the WT and mutant lines respectively and the calculated error bars of the standard error. The sample amount corresponds to 10 roots of Ler, 11 of *myb4* and 8 of *esb1*. *: student's t-test, $p \leq 0.05$, **: student's t-test, $p \leq 0.01$.

Continuously suberisation seems to be severely delayed in *cadc*. Only close to the basal part of the root a continuously suberised zone was observed. But the occurrence of the first suberised endodermal cells takes place at the same position in *cadc* similar as the WT. The mutant *cadd* seems to be delayed in the beginning of the suberisation. The continuously suberised zone is clearly present in the WT but in *cadd* it appears to be slightly delayed. In contrast to the single knockout both double knockout mutant *cadc*cadd* and *cadc*cadd 2* as well as the triple knockout *cadc*cadd*fah1-2* and the positive control *C4H::F5H* start to

suberise earlier than the WT. The continuously suberised zone is similar in the four mutant compared with the WT (fig. 48 A).

Quantitative analysis reveals that the non-suberised zone is similar to the WT in *cadc*. But in *cadd* the non-suberised zone is severely increased to 74.3 % (± 5.1 %) in comparison to the WT (46.9 ± 2.3 %). The patchy suberised zone is in *cadc* significantly increased to 34.2 % (± 4.3 %) but declined to 7.5 % (± 1.1 %) in *cadd* compared to the WT (10.9 ± 0.8 %). In both mutants *cadc* and *cadd* the continuously suberised zone exhibits a decrease to 15.0 % (± 2.4 %) and 18.1 % (± 5.3 %) respectively in comparison to the WT (42.2 ± 2.2 %) (fig. 48 B).

The non suberised zone is in all mutant lines of *cadc*cadd*, *cadc*cadd 2*, *cadc*cadd*fah1-2* and *C4H::F5H* at least significantly declined to 38.8 % (± 3.1 %), 25.0 % (± 1.9 %), 28.3 % (± 1.8 %) and 37.3 % (± 1.4 %) respectively. The size of the patchy suberised zone is generally not affected in these mutant lines with the exception of *cadc*cadd 2*. Here, the patchy suberised zone is increased to 15.5 % (± 1.9 %) compared with the WT. But all show a greater continuously suberised zone (51.6 ± 2.9 % in *cadc*cadd*, 59.5 ± 1.4 % in *cadc*cadd 2*, 60.1 ± 2.6 % in *cadc*cadd*fah1-2* and 53.0 ± 4.8 % in *C4H::F5H*) compared to the WT (fig. 48 B).

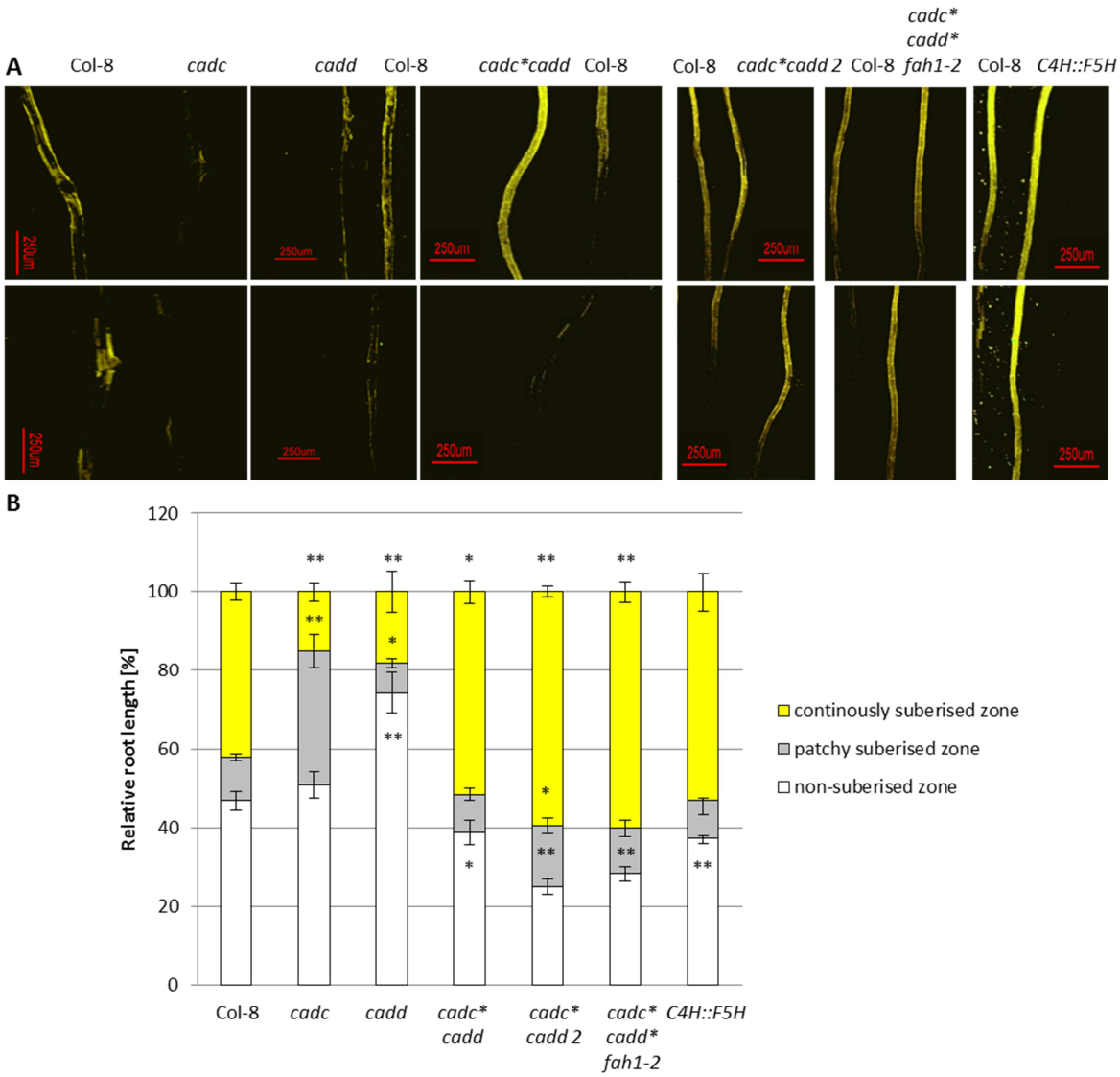

Fig. 48: Stained roots of seedlings with fluorol yellow 088 reveal suberin deposition and qualitative analysis of suberised zones along the roots of *cadc*, *cadd*, *cadc*cadd*, *cadc*cadd 2*, *cadc*cadd*fah1-2*, *C4H::F5H* and WT

A: Depicted are representative stained roots of the different mutants. The upper images reveal the continuously suberised zone, whereas the lower ones represent the patchy suberised zone. Scale bar size is 250 µm.

B: Qualitative analysis of the non-, patchy and continuously suberised zones of WT and mutant lines. The represented values are the arithmetic mean of the WT and mutant lines respectively and the calculated error bars of the standard error. The sample amount corresponds to 58 roots of Col-8, 13 of *cadc*, 9 of *cadd*, 21 of *cadc*cadd*, 10 of *cadc*cadd 2*, *cadc*cadd*fah1-2* and of *C4H::F5H*. *: student's t-test, $p \leq 0.05$, **: student's t-test, $p \leq 0.01$.

The triple knockout mutant *ref8-1*med5a*med5b* and the mutant *ref8-2*fah1-2*AtC4H::SmF5h* show a starting point of suberisation at the same position as the WT. The continuously suberised zone is similar to the WT in both mutant lines. The mutant *fah1-2* and the positive control *esb1* exhibit an early development of suberin compared to the WT. It seems that the staining is more intensive in *fah1-2* in direction to the basal part (fig. 49 A).

Measurement of the length of the non-suberised, patchy and continuously suberised zone indicates no differences between the mutant *ref8-1*med5a*med5b*, *ref8-2*fah1-2*AtC4H::SmF5H* and the WT. The mutant *fah1-2* and the positive control *esb1* reveal at least significant alterations in the size of the three root zones compared with the WT. The non-suberised zone is decreased in both lines to 41.5 % (± 1.5 %) in *fah1-2* and 29.9 % (± 2.2 %) in *esb1* in comparison to the WT (48.5 ± 2.4 %). Furthermore, the patchy suberised zone is decreased as well in both mutant (8.8 ± 2.3 % in *fah1-2*, 1.9 ± 0.5 % in *esb1* and 17.2 ± 1.9 % in WT). Decreased size of non-suberised and patchy suberised zone cause an increase of the suberised zone to 49.7 % (± 3.4 %) in *fah1-2* and 68.2 % (± 2.2 %) in *esb1* compared to the WT (34.3 ± 2.6 %) (fig. 49 B).

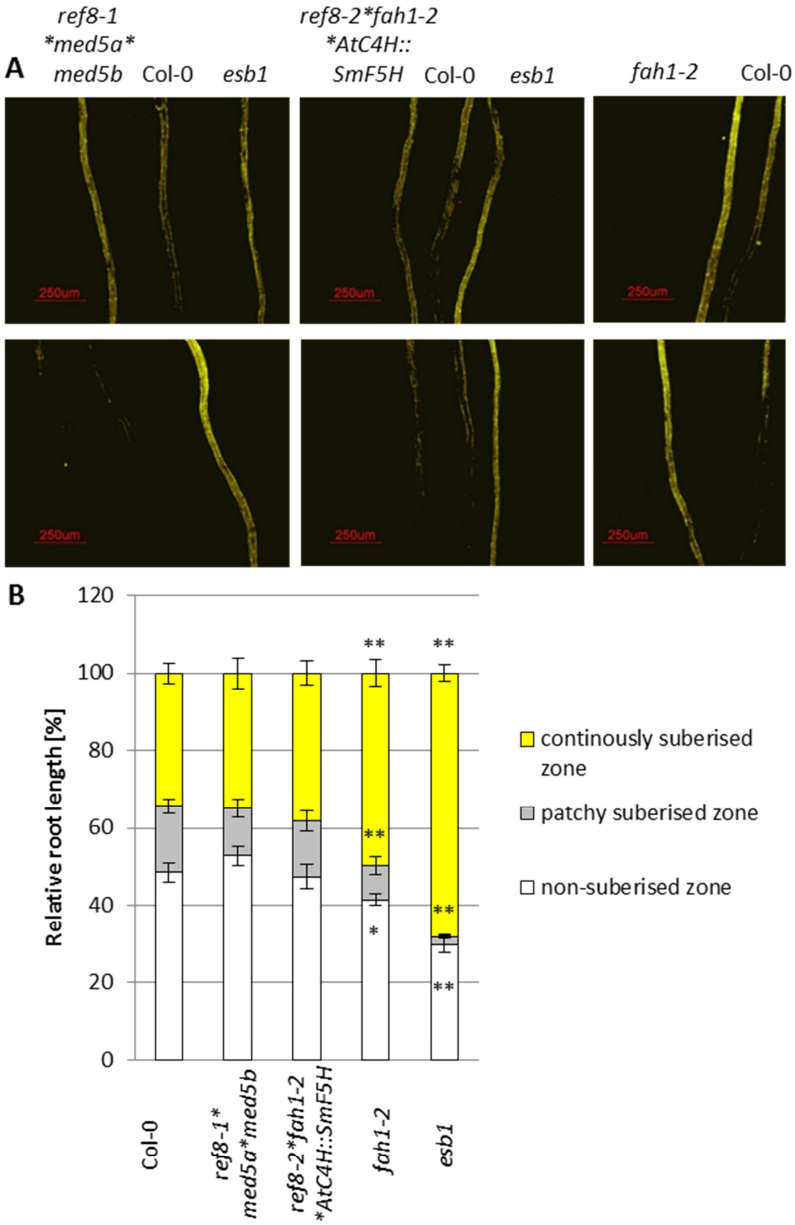

Fig. 49: Stained roots of seedlings with fluorol yellow 088 reveal suberin deposition and qualitative analysis of suberised zones along the roots of *ref8-1*med5a*med5b*, *ref8-2*fah1-2*AtC4H::SmF5H*, *fah1-2*, *esb1* and WT

A: Depicted are representative stained roots of different mutants. The upper images reveal the continuously suberised zone, whereas the lower ones represent the patchy suberised zone. Scale bar size is 250 µm.

B: Qualitative analysis of the non-, patchy and continuously suberised zones of WT and mutant lines. The represented values are the arithmetic mean of the WT and mutant lines respectively and the calculated error bars of the standard error. The sample amount corresponds to 17 roots of Col-0, 20 of *ref8-1*med5a*med5b*, 15 of *ref8-2*fah1-2*AtC4H::SmF5H*, 10 of *fah1-2* and 6 of *esb1*. *: student's t-test, $p \leq 0.05$, **: student's t-test, $p \leq 0.01$.

Suberisation is delayed in the *ref3-2* mutant compared with the WT (fig 50 A). At the beginning of the suberisation in Col-0 the *ref3-2* mutant does not show any suberised endodermal cells, whereas *ref4-3* is already continuously suberised (fig. 50 A). Even in the

area of the continuously suberised zone *ref3-2* only shows few suberised endodermal cells. Also, *ref4-3* reveals some incomplete suberised endodermal cells in the continuously suberised zone. Beginning of the suberisation appears to be similar in *ref1-4* in figure. Staining of the continuously suberised zone does not differ from the WT. The positive control *esb1* exhibits an early development of suberin compared to the WT. Staining intensity of all mutant roots are similar with the WT roots (fig. 50 A)

Quantitative analysis reveals a significantly increased non-suberised and patchy suberised zone in *ref3-2* (non-suberised zone: 62.8 ± 2.7 %; patchy suberised zone: 20.0 ± 2.3 %) mutant compared with the WT (non-suberised zone: 50.4 ± 2.1 %; patchy suberised zone: 14.4 ± 1.1 %). The resulting decrease of the continuously suberised zone is highly significant in *ref3-2* (17.2 ± 1.5 %) compared to the WT (31.9 ± 2.1 %). In contrast all three mutants *ref1-4* (27.8 ± 2.4 %), *ref4-3* (42.8 ± 1.7 %) and *esb1* (36.0 ± 2.3 %) reveal a highly significant decreased non-suberised zone than the WT. The mutant *ref1-4* is the only one mutant, which shows an earlier development of the first suberised endodermal cells than the *esb1* mutant. The size of the patchy suberised zone is significantly increased in *ref1-4* (20.7 ± 2.3 %), whereas the patchy suberised zone is similar in *ref4-3* (14.3 ± 1.8 %) to the WT. Presence of the patchy suberised zone is barely existent in *esb1* (2.0 ± 0.3 %) and therefore highly significant altered than in the WT. All three mutants reveal a highly significant increased continuously suberised zone (51.5 ± 2.4 % in *ref1-4*, 43.0 ± 1.2 % in *ref4-3* and 62.0 % ± 2.3 % in *esb1*) in comparison to the WT (fig. 50 B).

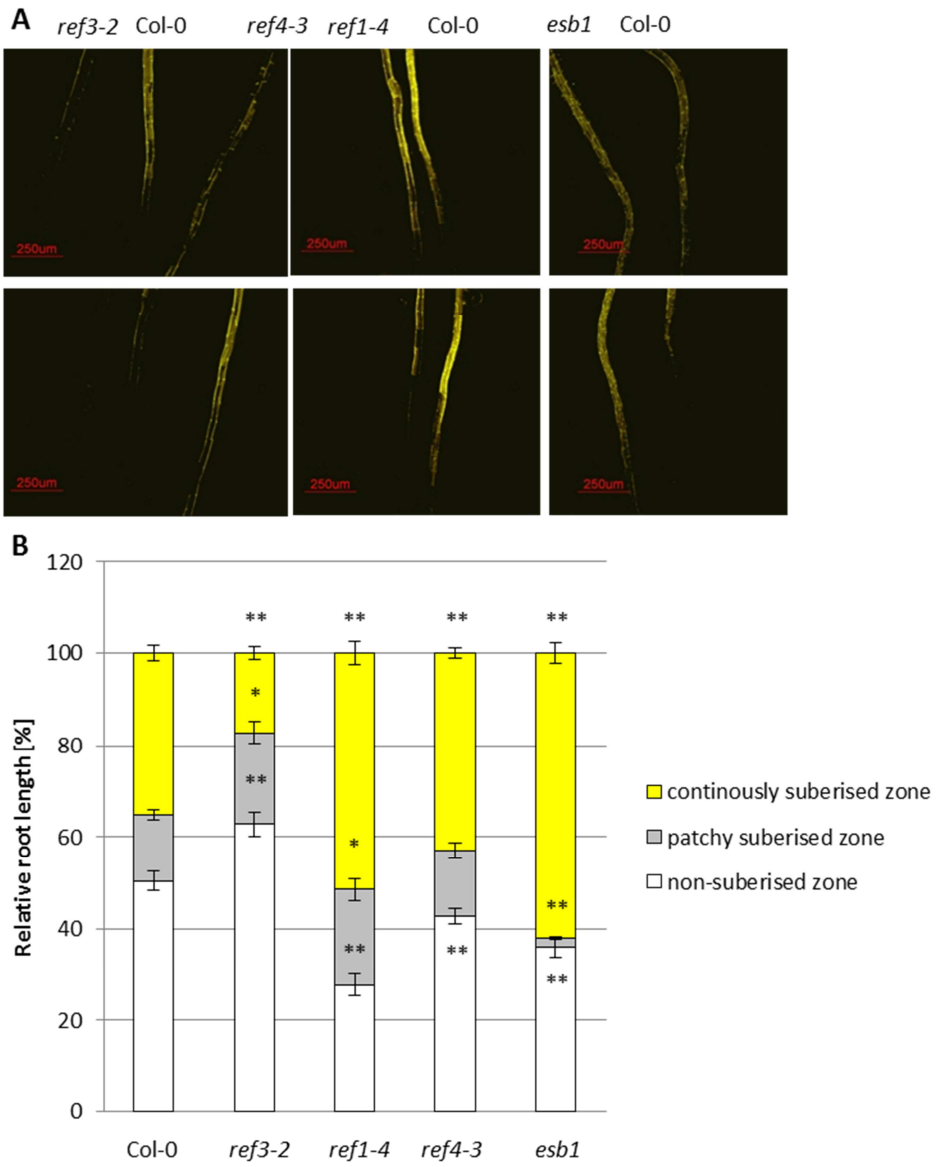

Fig. 50: Stained roots of seedlings with fluorol yellow 088 reveal suberin deposition and qualitative analysis of suberised zones along the roots of *ref3-2*, *ref1-4*, *ref4-3*, *esb1* and WT

A: Depicted are representative stained roots of different mutants. The upper images reveal the continuously suberised zonem, whereas the lower ones represent the patchy suberised zone. Scale bar size is 250 µm.

B: Qualitative analysis of the non-, patchy and continuously suberised zones of WT and mutant lines. The represented values are the arithmetic mean of the WT and mutant lines respectively and the calculated error bars of the standard error. The sample amount corresponds to 45 roots of Col-0, 17 of *ref3-2*, 12 of *ref1-4*, 21 of *ref4-3* and 14 of *esb1*. *: student's t-test, $p \leq 0.05$, **: student's t-test, $p \leq 0.01$.

The mutant *prx11-1* shows the first suberised endodermal cells at the same position as the WT. However, in the area of the continuously suberised zone *prx11-1* remains still in the patchy suberised zone. Unfortunately, in this experimental setup the amount of WT roots was limited and no microscopical images were taken with WT and *prx11-2* together. In

comparison to the positive control *esb1*, *prx11-2* shows a delayed suberisation and the starting point of the continuously suberised zone is very close to the basal part (fig. 51 A). Suberisation in both mutant *asft1* and *asft2* is not delayed compared to the WT. However, both lines reveal a large patchy suberised zone. The mutant *fact3* does not show alterations in the development of suberin compared with the WT. The suberisation starts at the same position in the root and the continuously suberised zone is similar to the WT as well. The WT root is damaged in the continuously suberised zone in the taken image (fig. 51 A).

Quantitatively, both mutants *prx11-1* and *prx11-2* reveal a slightly increased patchy suberised zone (23.1 ± 3.5 % in *prx11-1*, 16.7 ± 3.6 % in *prx11-2* and 16.0 ± 2.3 % in WT) and a small decline in the continuously suberised zone (30.7 ± 2.9 % in prx11-1, 28.8 ± 4.1 % in *prx11-2* and 36.7 ± 3.3 % in WT). However, these decreases are not significant (fig. 51 B).

In contrast, *asft1* (43.3 ± 3.7 %) reveals a highly significant augmented patchy suberised zone compared to the WT (16.0 ± 2.3 %). The mutant *asft2* exhibits a delayed development of suberin since the non-suberised zone is increased to 61.6 % (± 6.7 %). The size of the non-suberised zone in the WT is 47.3 % (± 3.1 %). Due to these alterations in either the non- or patchy suberised zone the continuously suberised zone is significantly smaller (11.8 ± 4.0 % in *asft1*, 24.9 % ± 6.6 % in *asft2*) compared to the WT (36.7 ± 3.3 %). The *fact3* mutant does not show any differences in the size of the non-, patchy or continuously suberised zone in comparison to the WT. The positive control *esb1* shows highly significant alterations in the three zones (non-suberised zone: 24.6 ± 0.6 %; patchy suberised zone: 2.8 ± 0.5 %; continuously suberised zone: 72.6 ± 0.8 %) in comparison to the WT (fig. 51 B).

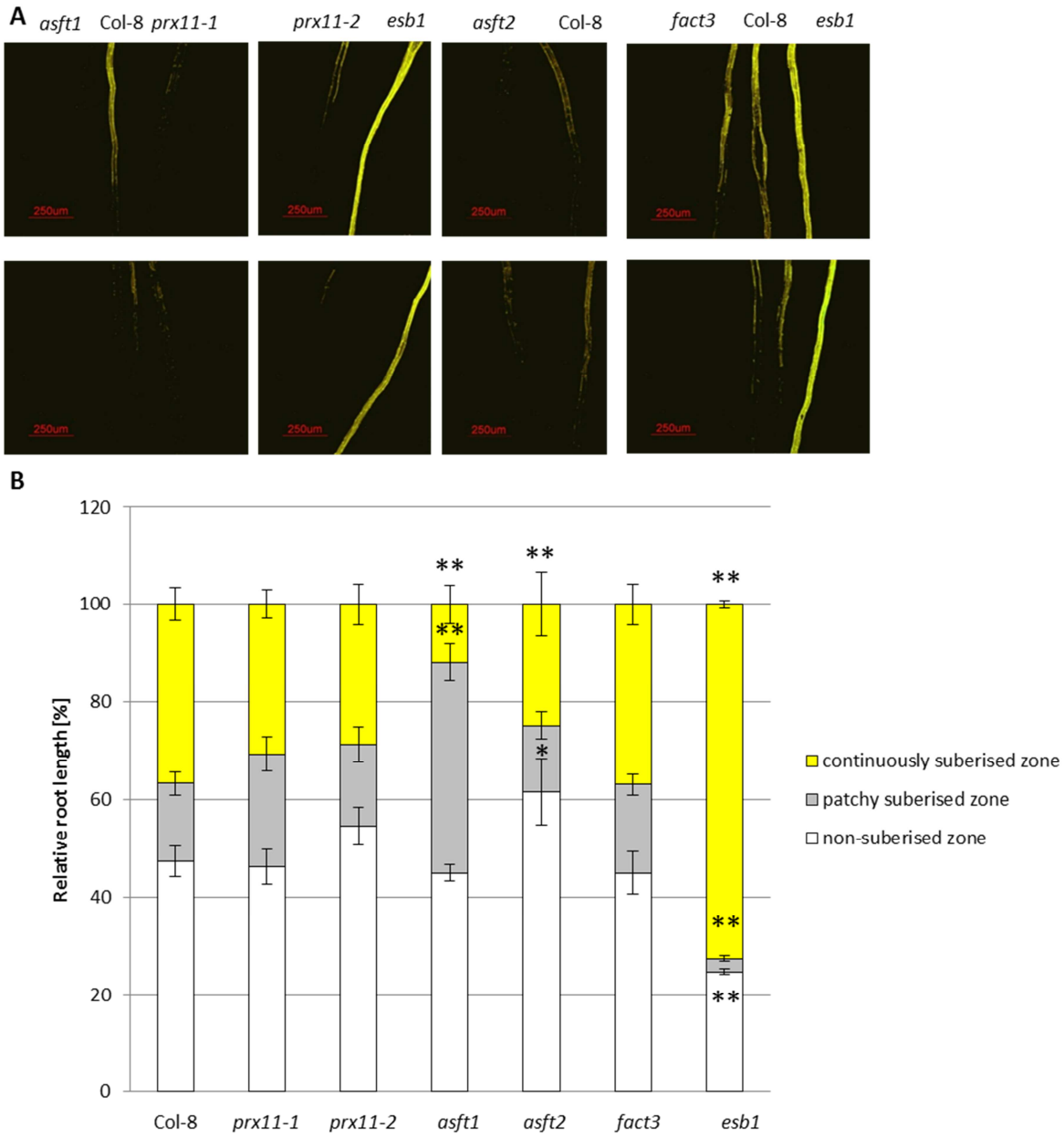

Fig. 51: Stained roots of seedlings with fluorol yellow 088 reveal suberin deposition and qualitative analysis of suberised zones along the roots of *prx11-1*, *prx11-2*, *asft1*, *asft2*, *fact3*, *esb1* and WT

A: Depicted are representative stained roots of different mutants. The upper images reveal the continuously suberised zone, whereas the lower ones represent the patchy suberised zone. Scale bar size is 250 µm.

B: Qualitative analysis of the non-, patchy and continuously suberised zones of WT and mutant lines. The represented values are the arithmetic mean of the WT and mutant lines respectively and the calculated error bars of the standard error. The sample amount corresponds to 9 roots of Col-8, 13 of *prx11-1*, 6 of *prx11-2*, 8 of *asft1*, 11 of *asft2*, 10 of *fact3* and 9 of *esb1*. *: student's t-test, $p \leq 0.05$, **: student's t-test, $p \leq 0.01$.

WT roots were treated with the phenylpropanoid pathway inhibitor piperonylic acid. One group of roots were treated for 24 hours in ½ liquid MS containing 10 µM PA. Another group was transferred onto ½ MS plates containing 10 µM PA on the last two days before

harvesting. The third group germinated and grew on ½ MS plates containing 10 µM PA. As a positive control *esb1* was used. The mutant *esb1* grew only on ½ MS plates without PA.

Treating WT roots with the phenylpropanoid pathway inhibitor piperonylic acid causes an earlier development of suberised endodermal cells. Untreated WT roots are still not suberised at the same position (fig. 52 A).

Evaluation of the quantitative analysis reveals that the treatment with piperonylic acid provokes a decline of the non-suberised zone to 27.2 % (± 4.7 %) in 24h piperonylic acid treated roots, 34.6 % (± 3.7 %) in two days treated roots, 29.5 % (± 3.1 %) in seven days treated roots with PA, while untreated roots exhibit a non-suberised zone of 53.3 % (± 3.9 %). The non-suberised zone of the positive control *esb1* shows a size of 40.3 % (± 3.2 %). Furthermore, the patchy and continuously suberised zone is increased in all PA treated roots compared to the untreated WT (patchy suberised zone: 26.6 ± 4.2 % in Col-8 24h, 34.6 ± 5.0 % in Col-8 2d, 18.6 ± 7.3 % in Col-8 7d and 16.6 ± 2.3 % in WT; continuously suberised zone: 46.2 ± 1.7 % in Col-8 24h, 30.8 ± 4.6 % in Col-8 2d, 51.9 ± 6.2 % in Col-8 7d and 30.3 ± 2.6 % in WT). However, only the patchy suberised zone of two days treated roots with PA is increased significantly higher, but the continuously suberised zone is not significantly increased from the statistical evaluation. The positive control *esb1* shows a barely present patchy suberised zone (3.1 ± 0.4 %) and an enhanced continuously suberised zone (56.7 ± 3.3 %) (fig. 52 B).

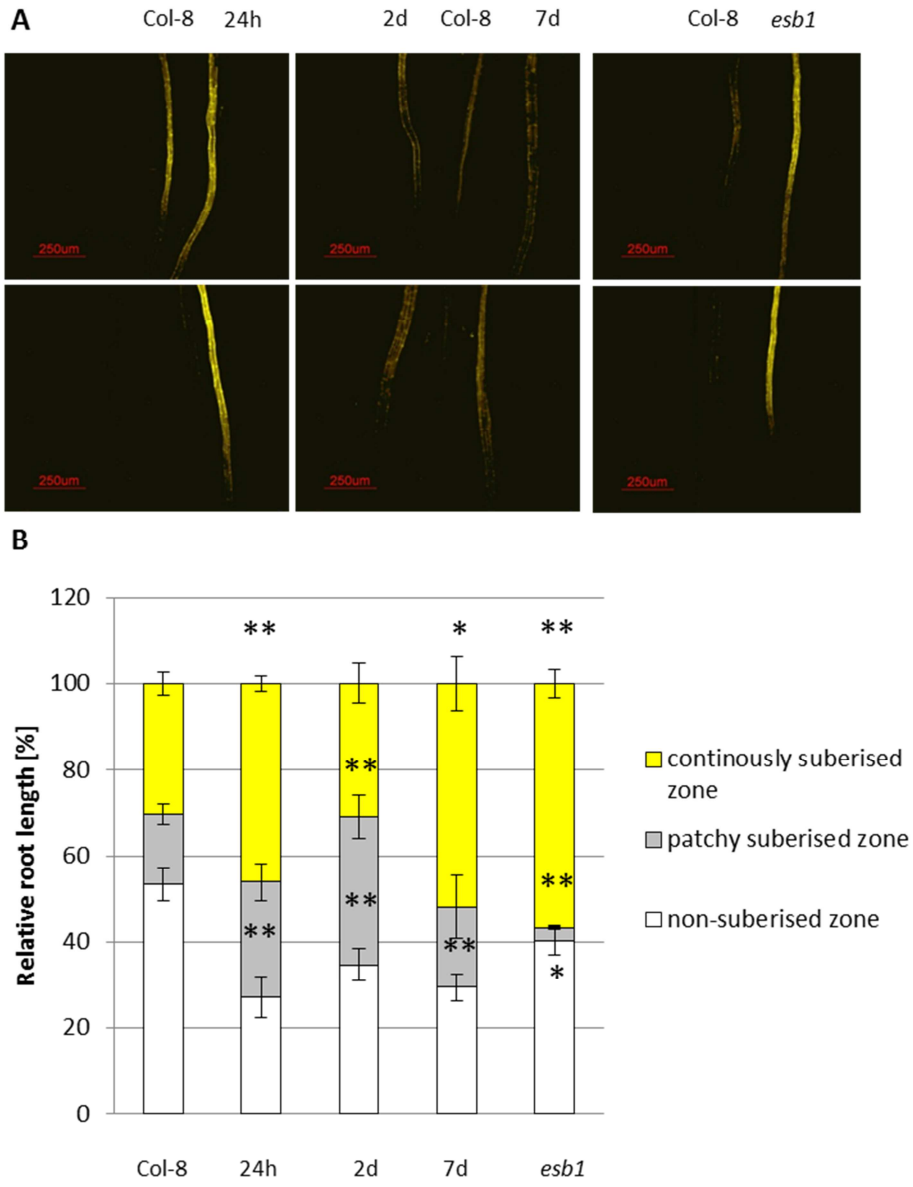

Fig. 52: Stained roots of seedlings with fluorol yellow 088 reveal suberin deposition and qualitative analysis of suberised zones along the roots of WT treated with and without PA

A: Depicted are representative stained roots of PA treated roots. The upper images reveal the continuously suberised zone, whereas the lower ones represent the patchy suberised zone. Scale bar size is 250 µm.

B: Qualitative analysis of the non-, patchy and continuously suberised zones of WT roots treated with and without PA. The represented values are the arithmetic mean of the untreated WT and treated WT samples respectively and the calculated error bars of the standard error. The sample amount corresponds to 14 roots of Col-8, 6 of 24h treated roots with PA, 13 of 2 days treated roots with PA, 7 of 7 days treated roots with PA and 8 of *esb1*. *: student's t-test, $p \leq 0.05$, **: student's t-test, $p \leq 0.01$.

3.3.4. Investigation of the suberin lamellae ultrastructure

3.3.4.1. Suberin lamellae ultrastructure of WT roots

One week old seedlings grown on ½ MS-plates with a root length of about 1 cm were fixated in 50 mM NCP containing 2.5 % glutaraldehyde and 0.025 % calcium chloride. Subsequently the roots were post-fixated in osmium tetroxide and dehydrated gradually in acetone. Afterwards the fixated roots were embedded in ERL-media and cross sections of different zones of the roots were performed. Cross sections were contrasted with uranyl acetate and lead citrate. After contrasting the root cross sections were visualised in the transmission electron microscopy.

A cross section of the root in one mm distance to the root tip shows epidermal, cortical, endodermal, pericycle and cells of the central cylinder (fig. 53 A). Images were taken of cell walls of endodermal and adjacent, cortical and pericycle cells. The red squares indicate the position of the taken image. One cell wall of one endodermal cell exhibits a weak band localised between plasma membrane and primary cell wall. The width of the barely visible band is about 10 and 20 nm. This weak band is not present in the cell wall of the adjacent cortical and endodermal cell (fig. 53 B, images 1 to 3). Furthermore, the weak band could only be visualised with higher magnifications. Other cell walls of endodermal cells do not show a deposited band between plasma membrane and primary cell wall.

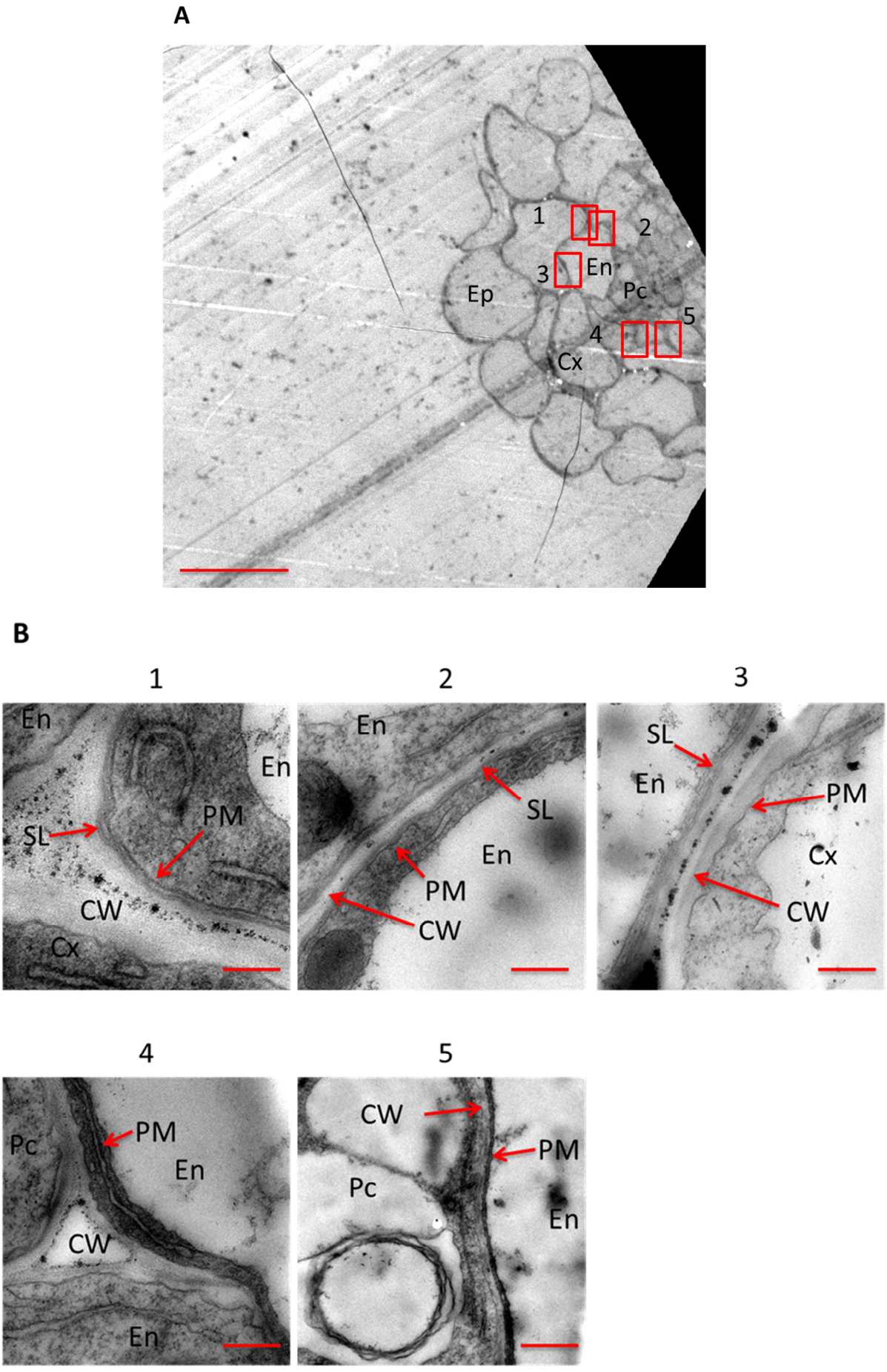
A
1
2
3
En
Ep
Pc
5
4
Cx
B
1
2
3
En
En
SL
PM
CW
Cx
En
SL
En
PM
CW
SL
En
PM
Cx
CW
4
5
Pc
PM
En
CW
En
CW
PM
Pc
En

Fig. 53: Ultrastructure of suberin lamellae one mm distance to the root tip in one-week old WT seedling with a root length of one cm grown on ½ MS-plates

A: Visualised cross section of WT root in one mm distance to the root tip in the TEM. **B**: Taken images of the cell wall ultrastructure. Ep: epidermis cell, Cx: cortex cell, En: endodermis cell, Pc: pericycle cell, CW: primary cell wall, PM: plasma membrane, SL: suberin lamella. Scale bar size in **A**: 20 µm, in **B**: 200 nm.

Organisation and cell shape of a cross section with a distance of 2 ½ mm to the root tip reveals well developed epidermal and cortical cells (fig. 54 A). Endodermal cells appear to be smaller in comparison to the cross section in one mm distance to the root tip. The width of endodermal cells in the cross section in one mm distance to the root tip is around eight µm, whereas the width of the endodermal cells at 2 ½ mm distance to the root tip is about four µm. Cells of the central cylinder seem to be further developed and determined. All endodermal cells in this cross section reveal suberin lamellae in their cell walls. The endodermal cell of the first taken image exhibits a well-formed suberin band with two dark and three bright alternating lamellae. It is exactly tight-fitting between plasma membrane and primary cell wall. The width of the suberin band is about 50 nm (fig. 54 B, image 1). Other endodermal cells reveal smaller suberin bands in their cell wall. Here, the size is about 20 and 30 nm (fig. 54 B, image 2 and 3). Structure divided into alternating dark and bright lamellae is not visible at this stage of magnification. The suberin is not present in the cell wall of cortical and pericycle cells.

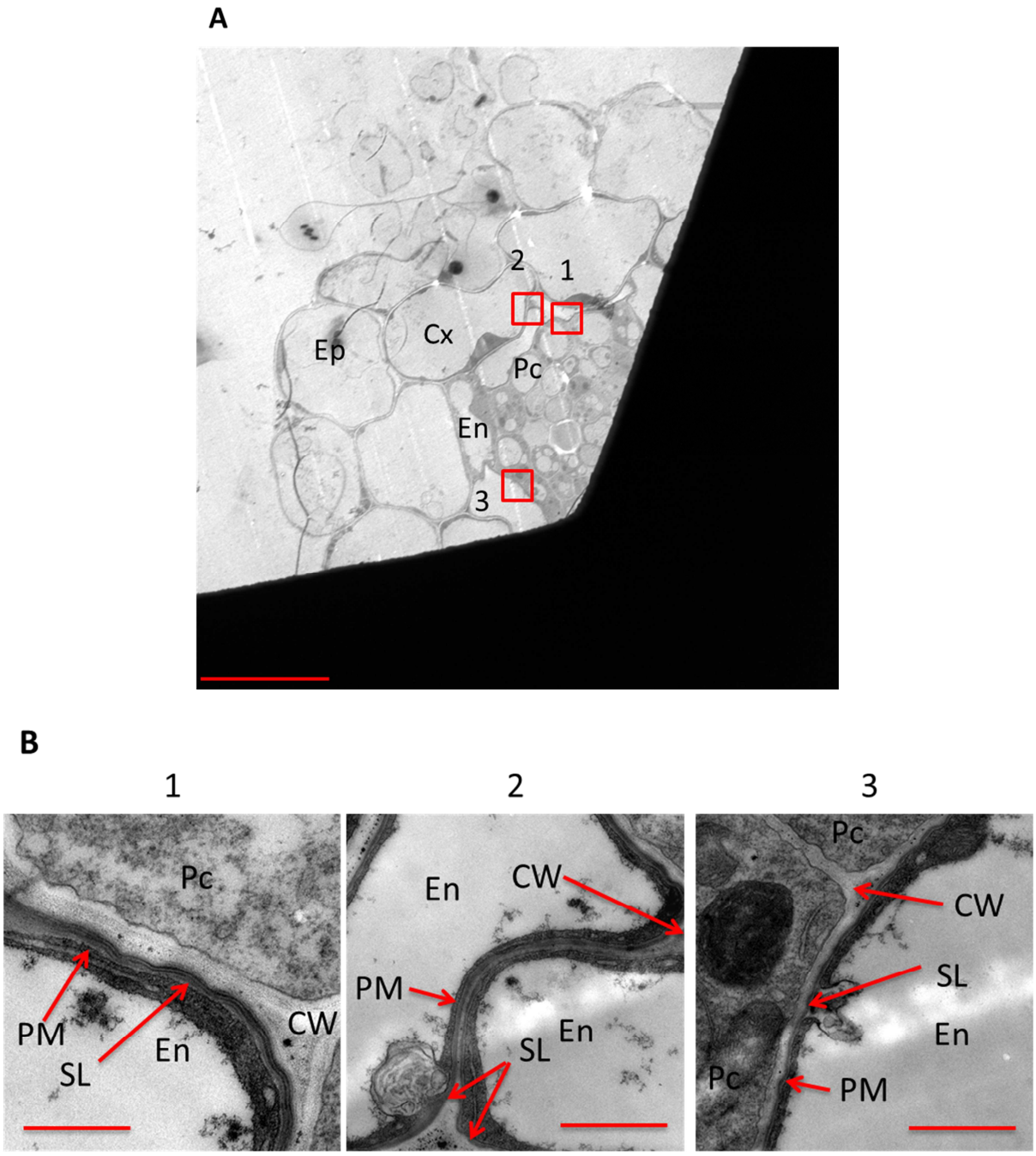

Fig. 54: Ultrastructure of suberin lamellae 2 ½ mm distance to the root tip in one-week old WT seedling with a root length of one cm grown on ½ MS-plates

A: Visualised cross section of WT root at a 2 ½ mm distance from the root tip in the TEM. **B**: Taken images of the cell wall ultrastructure. Ep: epidermis cell, Cx: cortex cell, En: endodermis cell, Pc: pericycle cell, CW: primary cell wall, PM: plasma membrane, SL: suberin lamella. Scale bar size in **A**: 20 µm, in **B**: 500 nm in image 1 and 1 µm in image 2 and 3.

Another cross section was performed at a 3 ½ mm distance to the root tip. At this distance, endodermal cells are barely visible. The size of the endodermal cells is minimised and the width not measurable. In comparison, epidermal and cortical cells are still well developed

(fig. 55 A). But, endodermal cells were visualised at higher magnifications. Cell walls of all endodermal cells show deposited suberin between plasma membrane and primary cell wall. The width of the suberin band is between 40 and 80 nm. A partial lamellation can be observed in the taken images (fig. 55 B, image 1 to 4). The suberin band seems to be not perfectly situated between primary cell wall and plasma membrane in image 2. Above the red arrow the suberin band bends but left and right of this bending the suberin band is perfectly situated again. In image 4 a thickening is visible in the cell walls of two adjacent endodermal cells. This thickening was never observed in the cell wall of other root cells. Therefore, the thickening is considered as Casparian strip. The suberin bands of both endodermal cells surround the thickening within the cell wall. At the thickest point the width is about 145 nm (fig. 55 B, image 4).

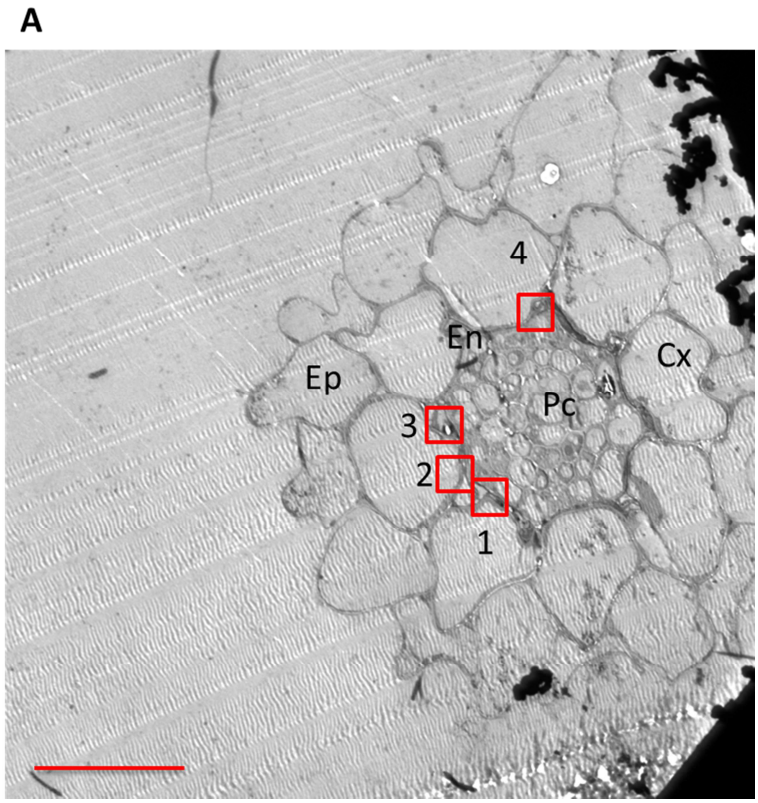

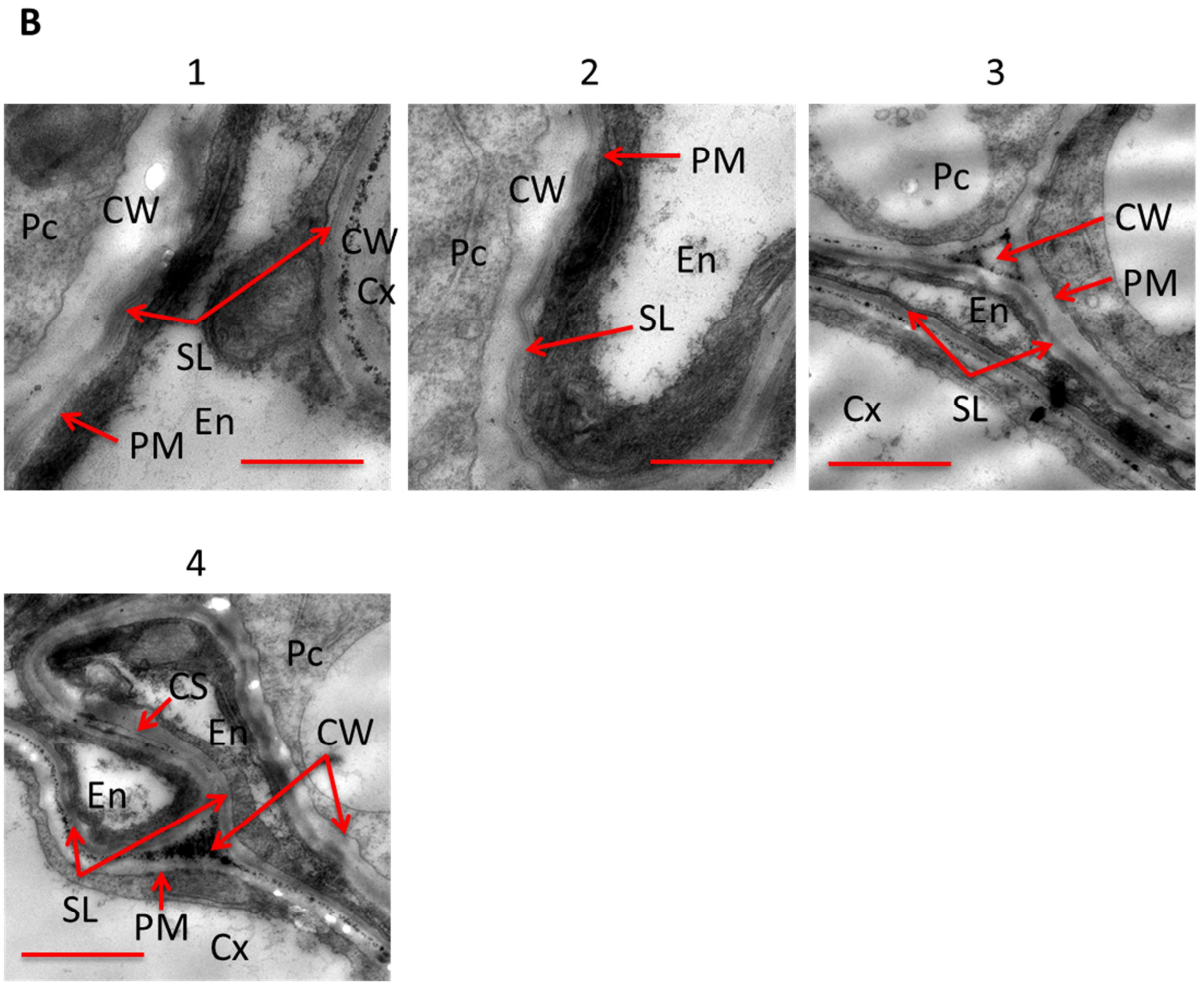

Fig. 55: Ultrastructure of suberin lamellae 3 ½ mm distance to the root tip in one-week old WT seedling with a root length of one cm grown on ½ MS-plates

A: Visualised cross section of WT root at a 3 ½ mm distance to the root tip in the TEM. **B**: Taken images of the cell wall ultrastructure. Ep: epidermis cell, Cx: cortex cell, En: endodermis cell, Pc: pericycle cell, CS: Casparian strip, CW: primary cell wall, PM: plasma membrane, SL: suberin lamella. Scale bar size in **A**: 20 µm, in **B**: 500 nm in image 1 and 2 and 1 µm in image 3 and 4.

At four mm distance to the root tip the cross section is similar to 3 ½ mm to the root tip. The endodermal cells are barely visible in the cross section, while epidermal, cortical, pericycle and cells of the central cylinder can be well observed (fig. 56 A). The cell wall of all endodermal cells reveals suberin. The first cell wall of the endodermal cell shows clearly the lamellar structure of the suberin band, while in the second image the suberin lamellae are barely to see (fig. 56 B, image 1 and 2). Here, the width of the suberin band is between 40 and 70 nm. In the first taken image three dark and four bright lamellae are observable. The second taken image exhibits a Casparian strip between two adjacent endodermal cells.

Especially, at the lower side of the Casparian strip a bulb-like structure is visible. The suberin band appears to curl around the bulb-like structure (fig. 56 B, image 2).

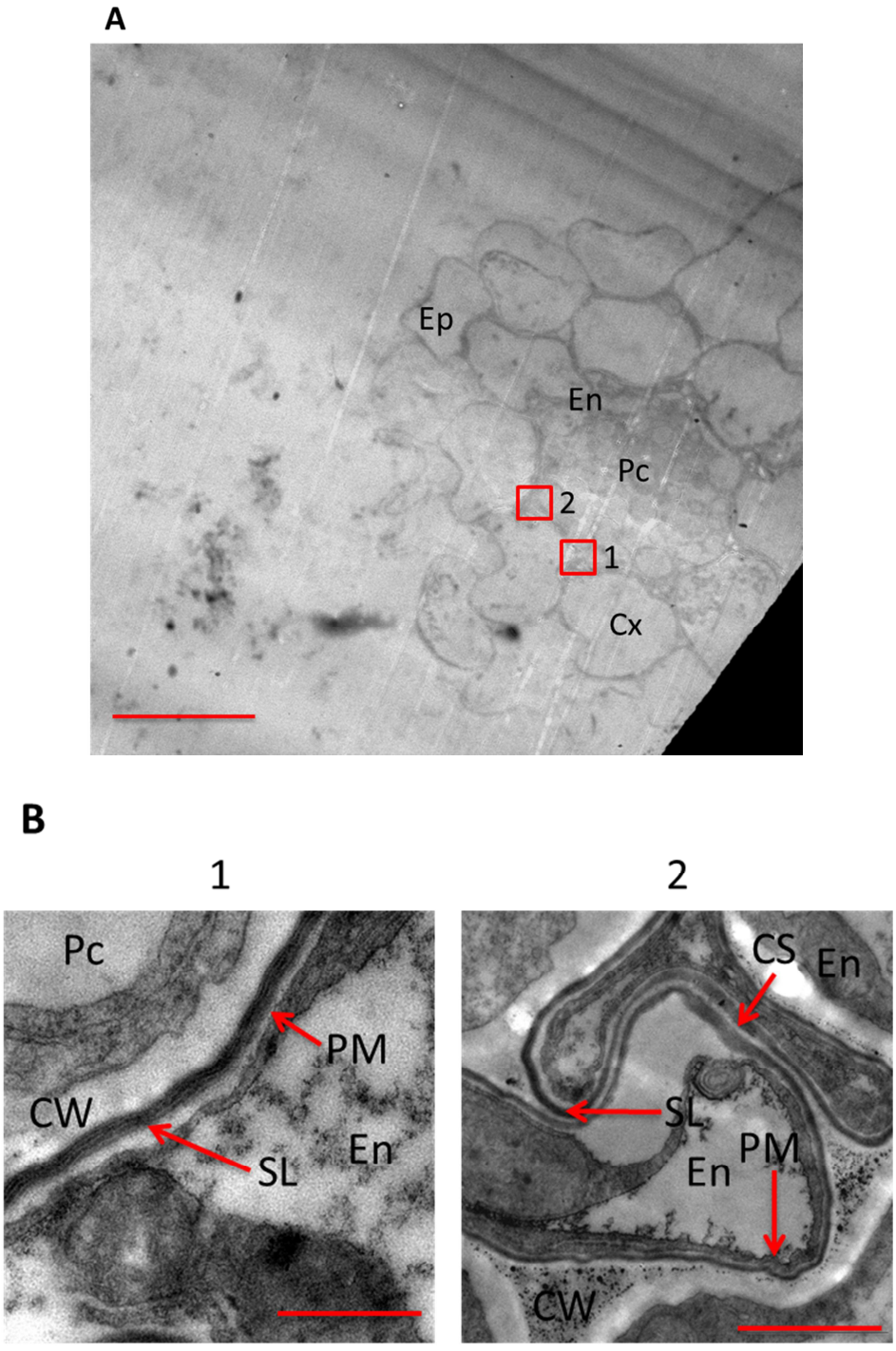

Fig. 56: Ultrastructure of suberin lamellae four mm distance to the root tip in one-week old WT seedling with a root length of one cm grown on ½ MS-plates

A: Visualised cross section of WT root at a four mm distance to the root tip in the TEM. **B**: Taken images of the cell wall ultrastructure. Ep: epidermis cell, Cx: cortex cell, En: endodermis cell, Pc: pericycle cell, CS: Casparian strip, CW: primary cell wall, PM: plasma membrane, SL: suberin lamella. Scale bar size in **A**: 20 µm, in **B**: 500 nm in image 1 and 1 µm in image 2.

Moreover, cross sections were performed with a one mm distance to the hypocotyl. Epidermal and cortical cells are well developed and pericycle cells as well as cells of the central cylinder are clearly visible, while endodermal cells are barely to identify in the clear view of the cross section (fig. 57 A). But, by using higher magnifications endodermal cells were identified and investigated. The cell walls of all endodermal cells are suberised. Image 1 and 2 of figure 57 B shows a Casparian strip between endodermal cells. The magnification of the second Casparian strip reveals a bulb-like structure of the Casparian strip (fig. 57 B, image 3). It appears that the suberin band is attached to the bulb-like structure. On both sides there is no lamellar-like structure of the suberin band visible close to the bulb-like structure. The width of the suberin band in the taken images is between 50 and 60 nm. Two or three dark as well as three or four bright lamellae are observable in the suberin band (fig. 57 B, image 3 and 4).

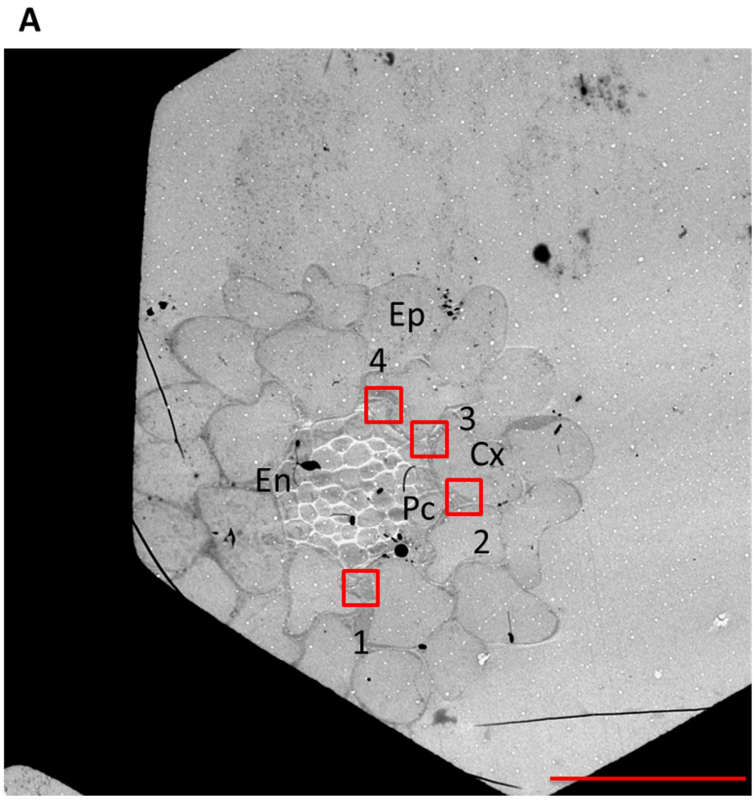

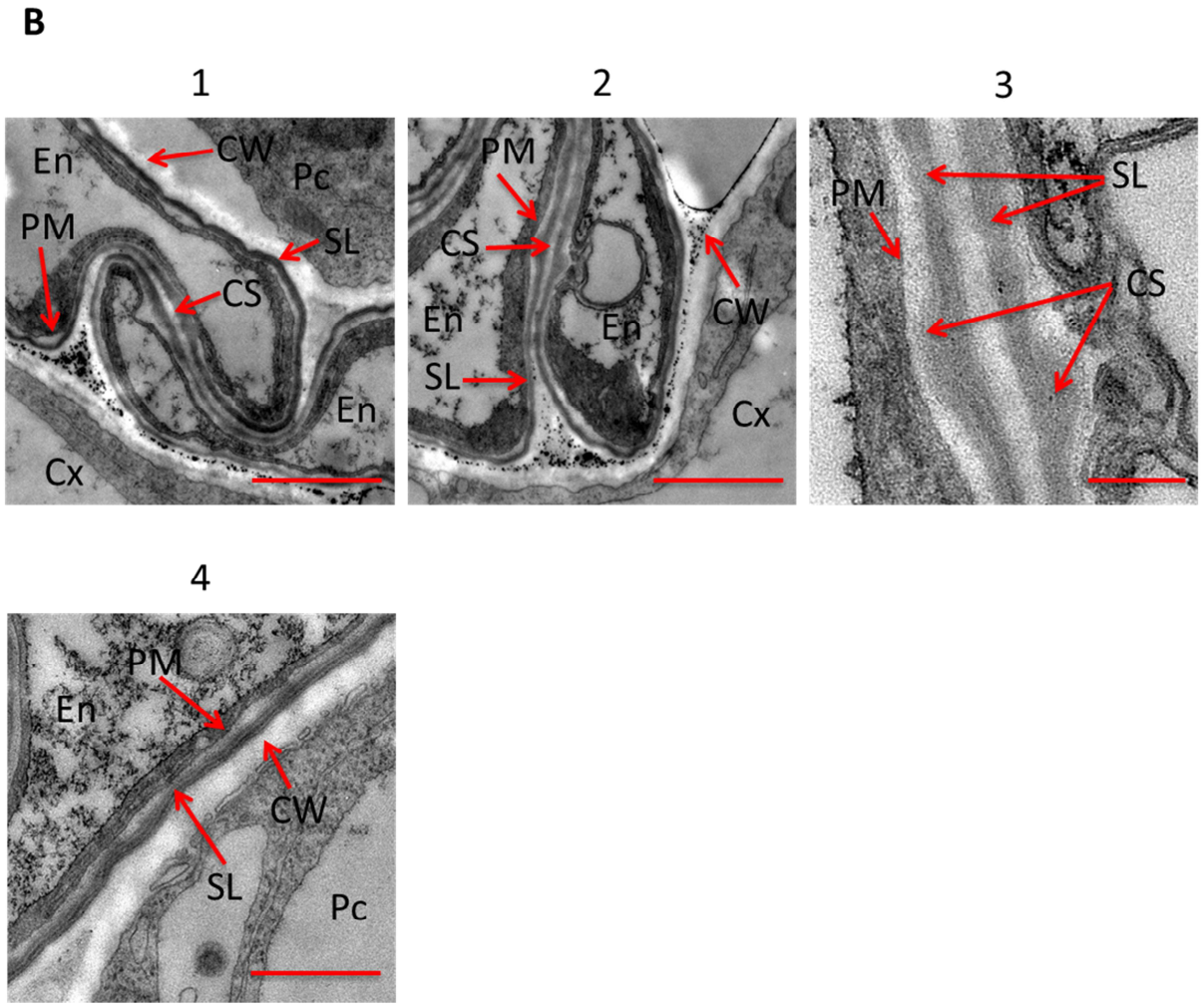

Fig. 57: Ultrastructure of suberin lamellae one mm distance to the hypocotyl in one-week old WT seedling with a root length of one cm grown on ½ MS-plates

A: Visualised cross section of WT root at a one mm distance to the hypocotyl in the TEM. **B**: Taken images of the cell wall ultrastructure. Ep: epidermis cell, Cx: cortex cell, En: endodermis cell, Pc: pericycle cell, CS: Casparian strip, CW: primary cell wall, PM: plasma membrane, SL: suberin lamella. Scale bar size in **A**: 20 µm, in **B**: 1 µm in image 1 and 2, 200 nm in image 3 and 500 nm in image 4.

3.3.4.2. Suberin lamellae ultrastructure of *asft1*

Ultrastructure of the suberin was analysed in the mutant line *asft1* as well. Cross section at a one mm distance to the root tip shows a clear structure of epidermal, cortical, endodermal, pericycle and cells of the central cylinder. The width of endodermal cells is around eight µm (fig. 58 A). The cell wall of the endodermal cells does not exhibit a suberin band (fig. 58 B, image 1 to 2).

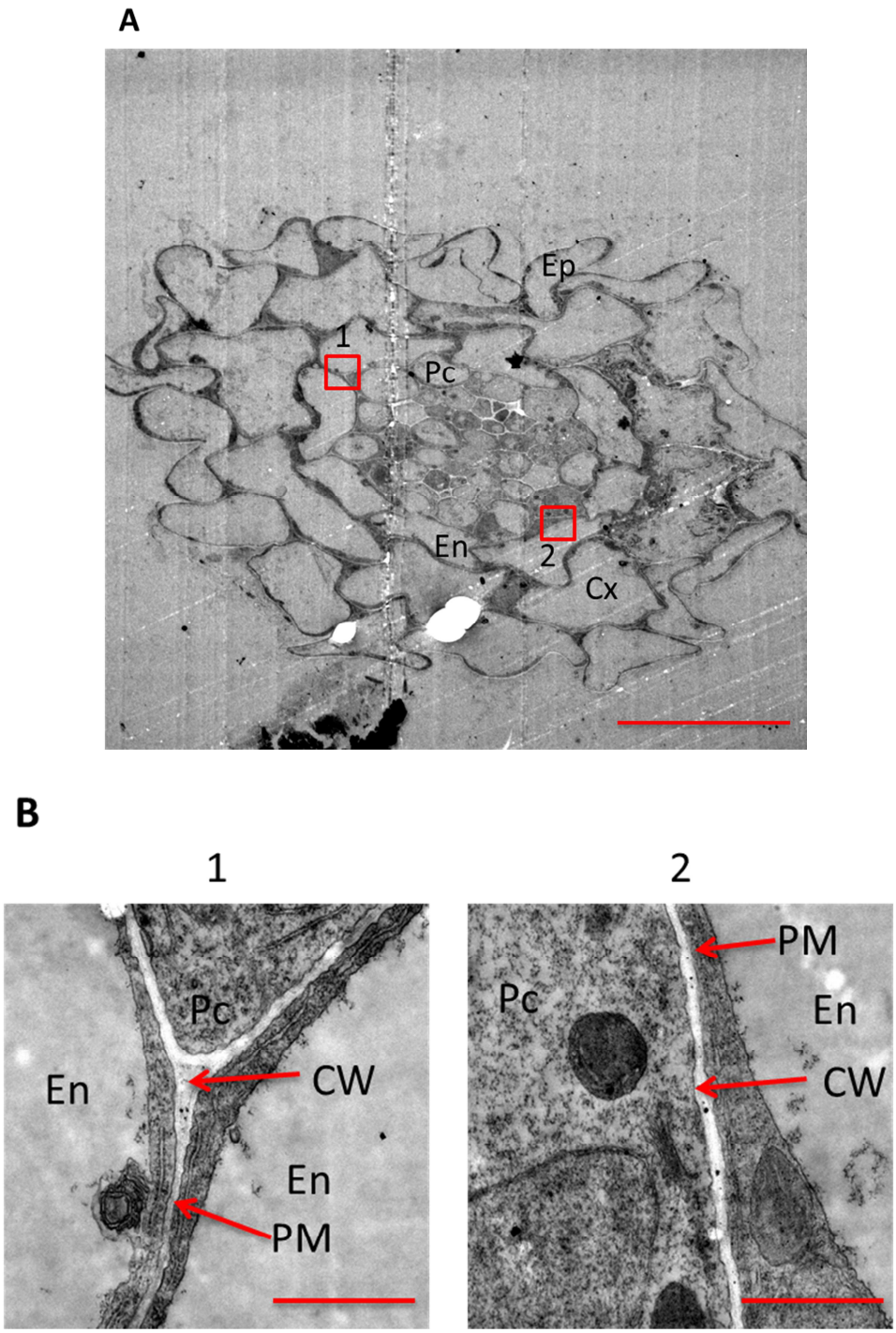

Fig. 58: Ultrastructure of suberin lamellae one mm distance to the root tip in one-week old *asft1* seedling with a root length of one cm grown on ½ MS-plates

A: Visualised cross section of *asft1* root at a one mm distance to the root tip in the TEM. **B**: Taken images of the cell wall ultrastructure. Ep: epidermis cell, Cx: cortex cell, En: endodermis cell, Pc: pericycle cell, CS: Casparian strip, CW: primary cell wall, PM: plasma membrane, SL: suberin lamella. Scale bar size in **A**: 20 µm, in **B**: 1 µm in image 1 and 2.

The same root was further trimmed to three mm distance tp the root tip. Here, the cross section still reveals well developed endodermal cells. The width of non-suberised cells is around eight µm, whereas the one suberised cell has a width about three µm. In contrast,

the size of the endodermal cells was minimised in WT already at a 2 ½ mm to the root tip (fig. 59 A).

The cell wall of one endodermal cell is suberised. The suberin band is wavy situated between primary cell wall and plasma membrane in the cell wall next to the pericycle cell. In the cell wall of the adjacent cortical cell the suberin band is perfectly fitted between primary cell wall and plasma membrane. The width of the suberin band in the first taken image is variable. At the wavy point of the suberin band the width is about 15 nm, whereas further on the right side the width is approximately 30 nm (fig. 59 B, image 1). In the second image the width is on the right side of the image around 20 nm and on the left side at the thickest point 35 nm. Lamellation is at this width of the suberin band not possible to see (fig. 59 B, image 2). Other endodermal cells do not show a suberin band in their cell wall. But in the third image a golgi-apparatus with dictyosomes and two vesicles are visible. The first vesicle seems to merge with the plasma membrane, whereas the second one is either on the way to the plasma membrane or the direction is to the mitochondria (fig. 59 B, image 3). The fourth image reveals the cell wall between two adjacent endodermal cells. The cell wall is stained dark compared with the cell wall in the cell wall edges. A thickening is not observable. This point is the supposed position of a Casparian strip (fig. 59 B, image 4).

A

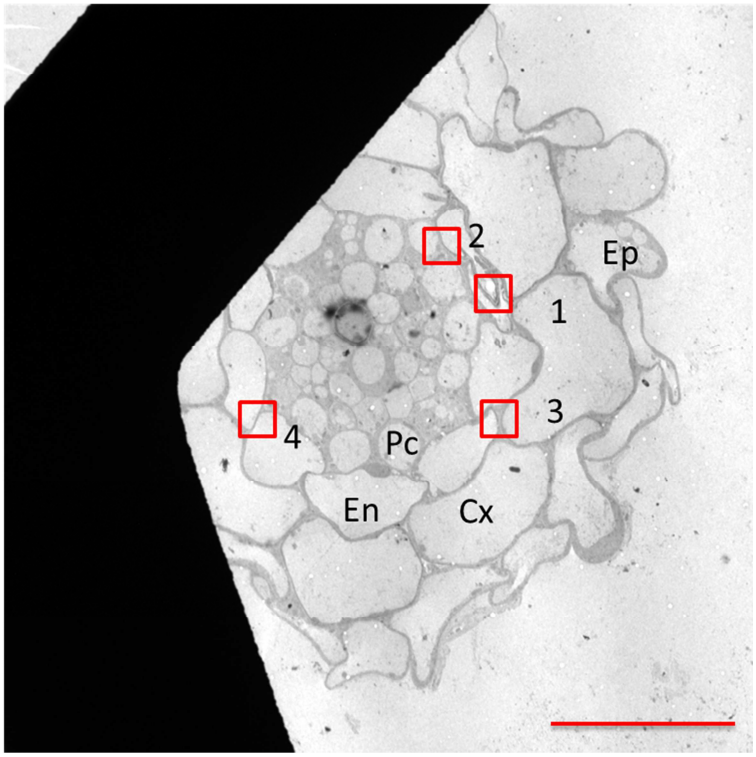

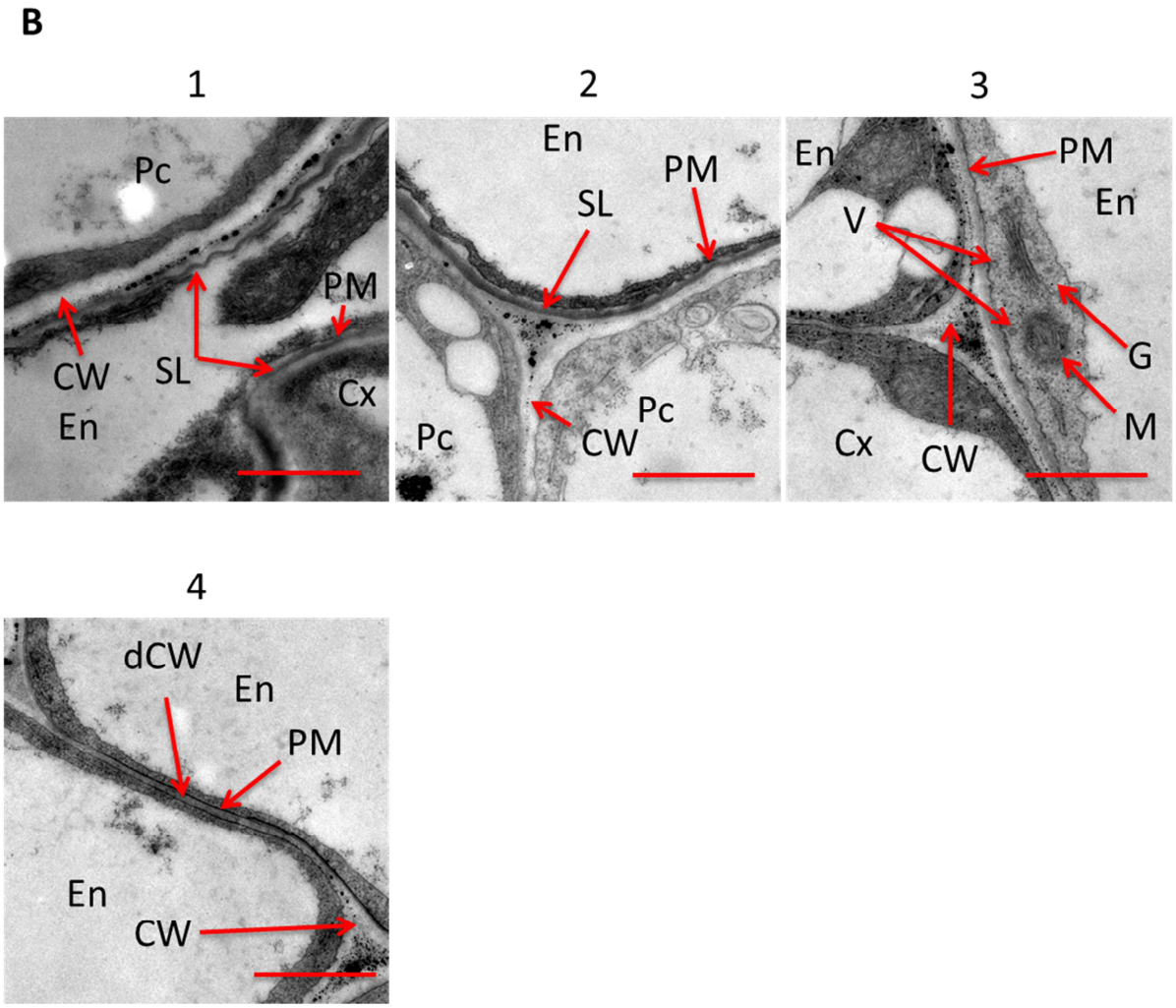

Fig. 59: Ultrastructure of suberin lamellae at a three mm distance to the root tip in one-week old *asft1* seedling with a root length of one cm grown on ½ MS-plates

A: Visualised cross section of *asft1* root at a three mm distance to the root tip in the TEM. **B**: Taken images of the cell wall ultrastructure. Ep: epidermis cell, Cx: cortex cell, En: endodermis cell, Pc: pericycle cell, CS: Casparian strip, dCW: dark primary cell wall, CW: primary cell wall, G: golgi-apparatus, M: mitochondria, PM: plasma membrane, SL: suberin lamella, V: vesicle. Scale bar size in **A**: 20 µm, in **B**: 500 nm in image 1 to 4.

At a Five mm distance to the root tip the size of all endodermal cells seems to minimise now. The width is about three and five µm. Epidermal, cortical, pericycle and cells of the central cylinder are still well developed (fig. 60 A).

The cell wall of all endodermal cells reveals suberin. In the first taken image a Casparian strip with suberin is visible. A bulb-like structure in the cell wall with the Casparian strip and the suberin is observable. Furthermore, it seems that the suberin band goes around the Casparian strip. Lamellation is visible and it appears to be divided into four dark and five bright bands. The width is variable. Close to the Casparian strip the width is about 90 nm,

while away from the Casparian strip the width decreases to about 45 nm. At the Casparian strip the suberin band together with the Casparian strip shows a width of about 180 nm (fig. 60 B, image 1). In the second image the width of the suberin band away from the Casparian strip is around 55 nm (fig. 60 B, image 2). In the third and the last image the width of the suberin band is smaller. It is about 30 and 40 nm. But now the number of dark and bright lamellae is decreased. Two dark and three bright lamellae are visible (fig. 60 B, image 3 and 4).

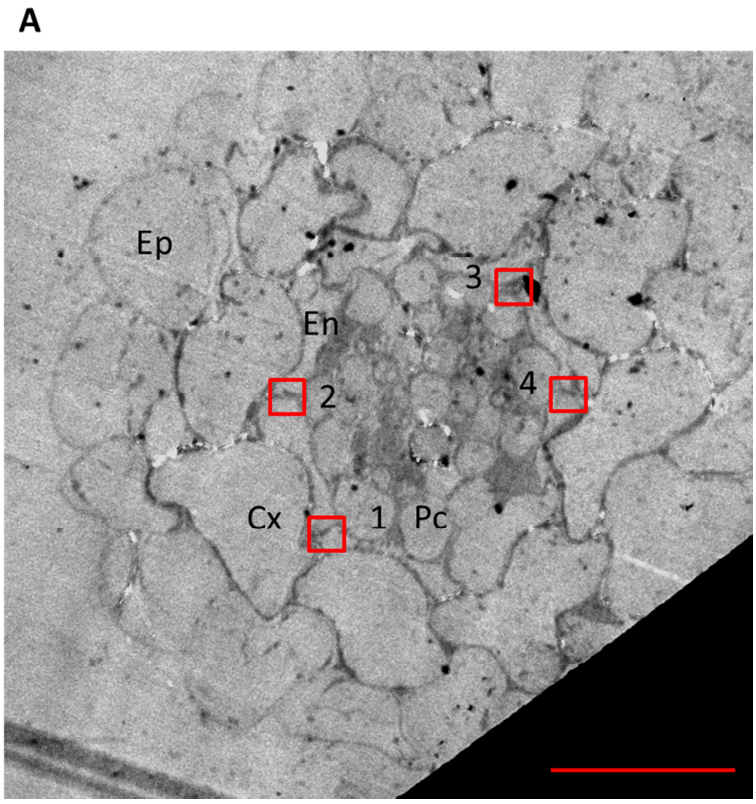

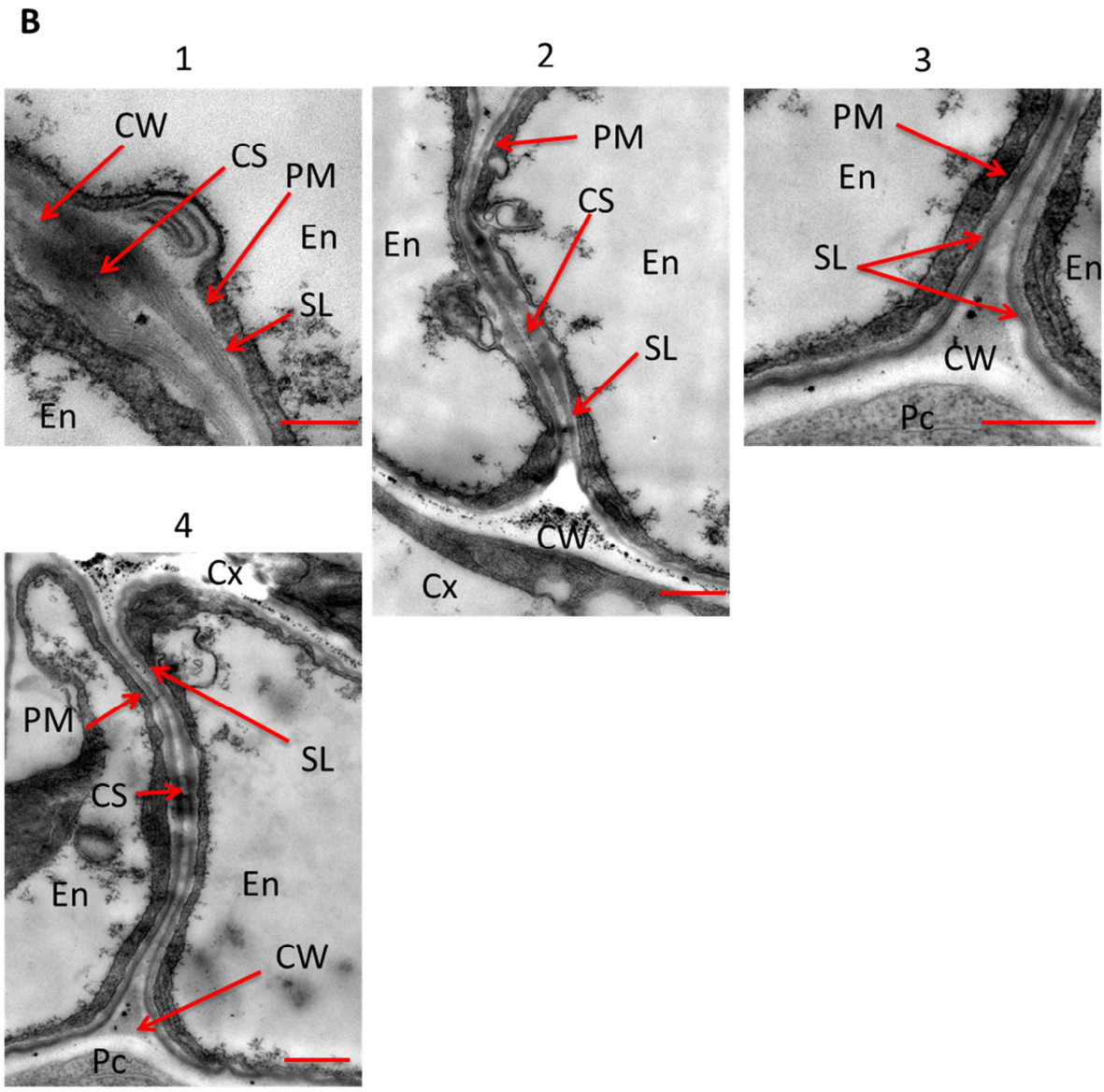

Fig. 60: Ultrastructure of suberin lamellae at a five mm distance to the root tip in one-week old *asft1* seedling with a root length of one cm grown on ½ MS-plates

A: Visualised cross section of *asft1* root at a five mm distance to the root tip in the TEM. **B**: Taken images of the cell wall ultrastructure. Ep: epidermis cell, Cx: cortex cell, En: endodermis cell, Pc: pericycle cell, CS: Casparian strip, CW: primary cell wall, PM: plasma membrane, SL: suberin lamella. Scale bar size in **A**: 20 µm, in **B**: 300 nm in image 1 and 500 nm in image 2 to 4.

Cross section of a distance of one mm to the hypocotyl reveals decreased size of endodermal cells. The width of the endodermal cells is about three µm. All other types of cells reveal to be well developed (fig. 61 A).

All cell walls of endodermal cells exhibit a suberin band. The suberin band shows a wavy structure in the cell wall next to the adjacent cortical cell (fig. 61 B, image 1). Another point of a wavy situated suberin band is in image 3 visible (fig. 61 B, image 3). Again, the suberin

band in the cell wall next to the adjacent cortical cell shows the wavy structure. In the last image a wavy structure of the suberin band is observable. However, now the plasma membrane is folded as well. The width of the suberin bands is between 40 and 60 nm in the taken images (fig. 61 B, image 4). Only the second image reveal suberin bands in the cell wall of endodermal cells, which are perfectly situated between primary cell wall and plasma membrane (fig. 61 B, image 2).

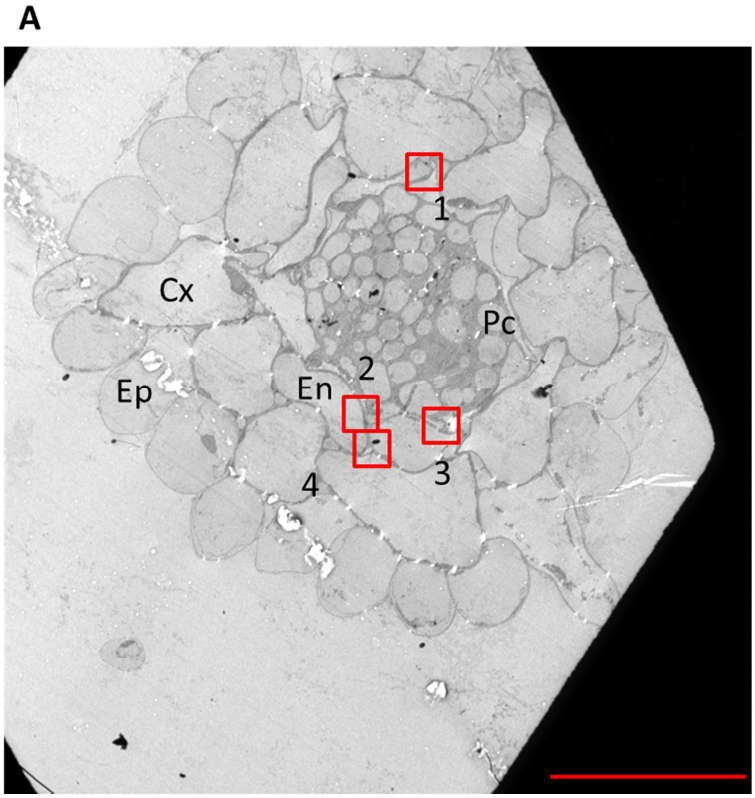

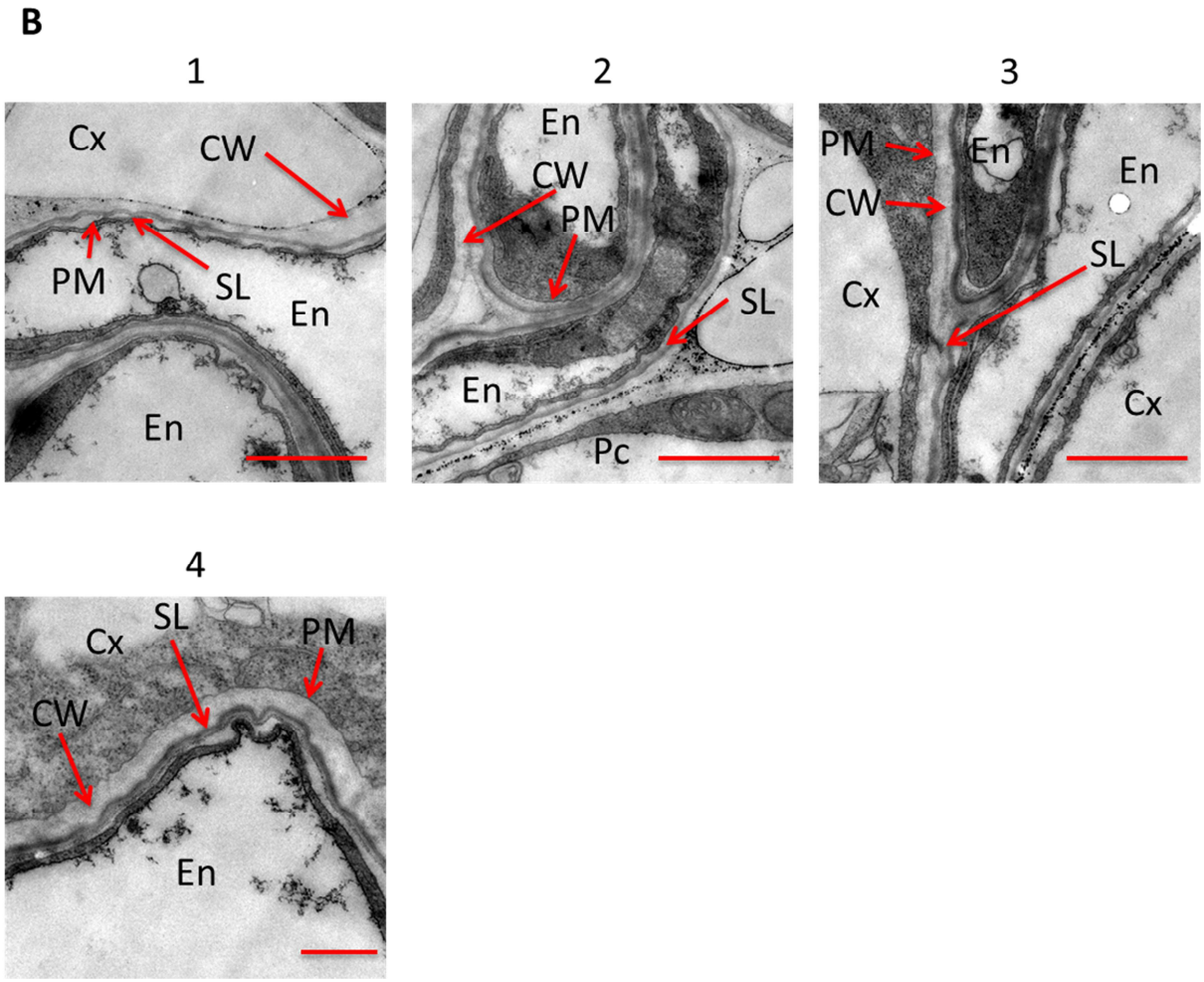

Fig. 61: Ultrastructure of suberin lamellae at a one mm distance to the hypocotyl in one-week old *asft1* seedling with a root length of one cm grown on ½ MS-plates

A: Visualised cross section of *asft1* root with one mm distance apart from the hypocotyl in the TEM. **B**: Taken images of the cell wall ultrastructure. Ep: epidermis cell, Cx: cortex cell, En: endodermis cell, Pc: pericycle cell, CS: Casparian strip, CW: primary cell wall, PM: plasma membrane, SL: suberin lamella. Scale bar size in **A**: 20 µm, in **B**: 1 µm in image 1 to 3 and 500 nm in image 4.

3.3.4.3. Suberin lamellae ultrastructure of *prx11-1*

A cross section of *prx11-1* at a 2 ½ mm distance to the root tip shows well developed epidermal, cortical and endodermal cells. Unfortunately, the central cylinder is covered by the grid (fig. 62 A). The cell walls of almost all endodermal cells are not suberised. In the first image in the cell walls of two adjacent endodermal cells dark stained cell walls are visible, exactly at the position of a supposed Casparian strip (fig. 62 B, image 1). However, these dark stained cell walls are not always present in the cell walls of adjacent endodermal cells as image 2 shows (fig. 62 B, image 2). One cell wall of one endodermal cell shows a weak

dark band between primary cell wall and plasma membrane. This dark band is absent in the cell wall of the adjacent cortical cell. It is considered to be suberin. The width of the suberin band is approximately 15 nm (fig. 62 B, image 3).

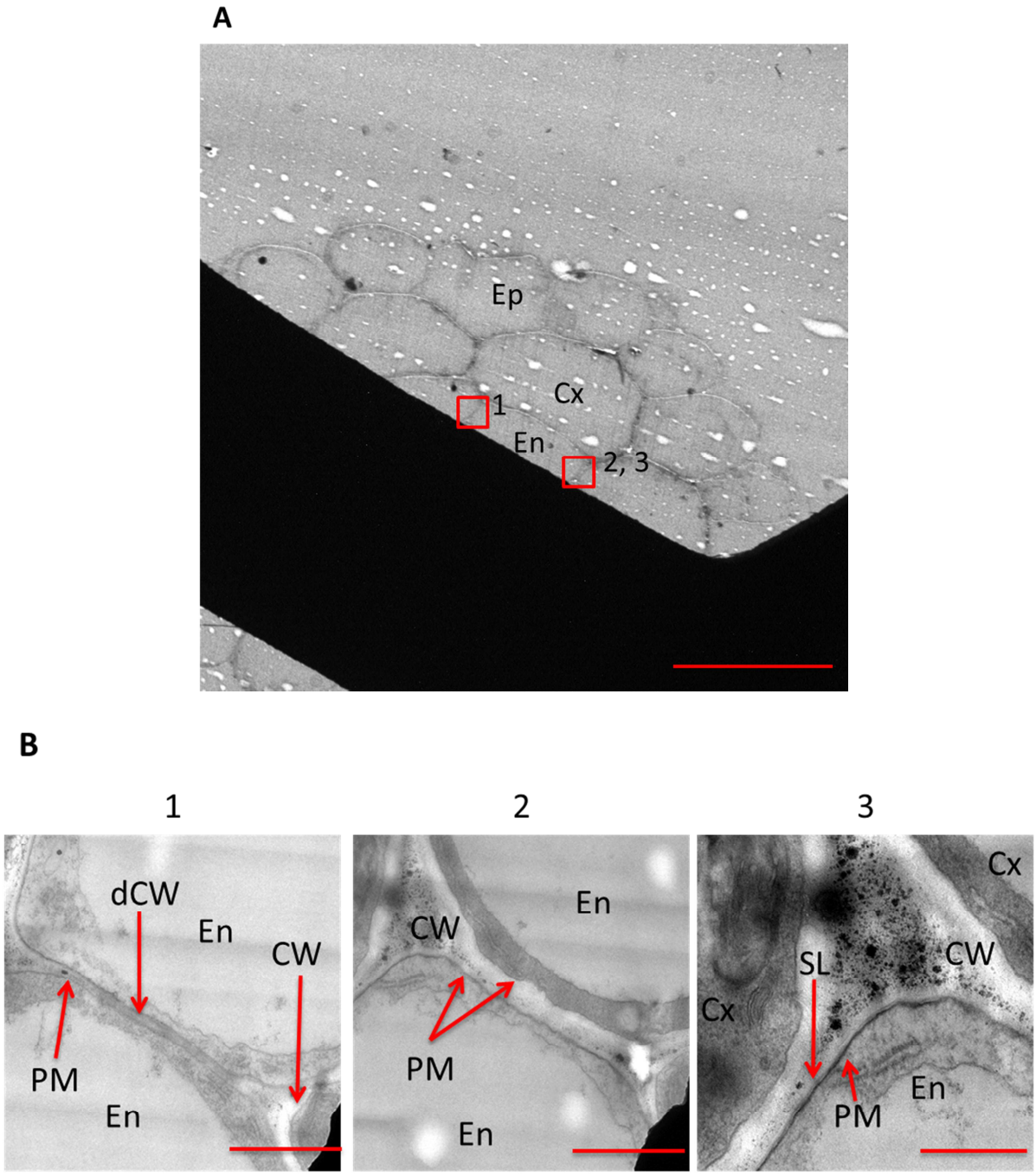

Fig. 62: Ultrastructure of suberin lamellae at a 2 ½ mm distance to the root tip in one-week old *prx11-1* seedling with a root length of one cm grown on ½ MS-plates

A: Visualised cross section of *prx11-1* root at a 2 ½ mm distance to the root tip in the TEM. **B**: Taken images of the cell wall ultrastructure. Ep: epidermis cell, Cx: cortex cell, En: endodermis cell, Pc: pericycle cell, CS: Casparian strip, dCW: dark primary cell wall, CW: primary cell wall, PM: plasma membrane, SL: suberin lamella. Scale bar size in **A**: 20 µm, in **B**: 1 µm in image 1 and 2 and 500 nm in image 3.

At a three mm distance to the root tip all cells of the root are well developed. The width of the endodermal cells is between four and six µm (fig. 63 A). Cell wall of one endodermal cell seems to be suberised. One dark and two bright bands are observable. The width of the suberin band is around 20 nm. The suberin band does not show a wavy phenotype. It is perfectly situated between primary cell wall and plasma membrane (fig. 63 B, image 1 and 2). Other cell walls of endodermal cells are not suberised (fig. 63 B, image 3 and 4).

A

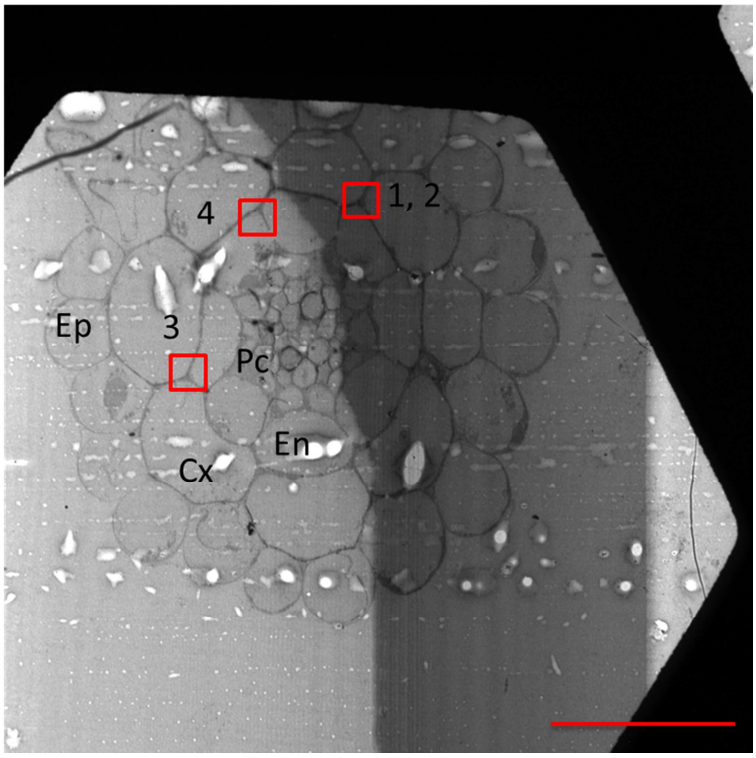

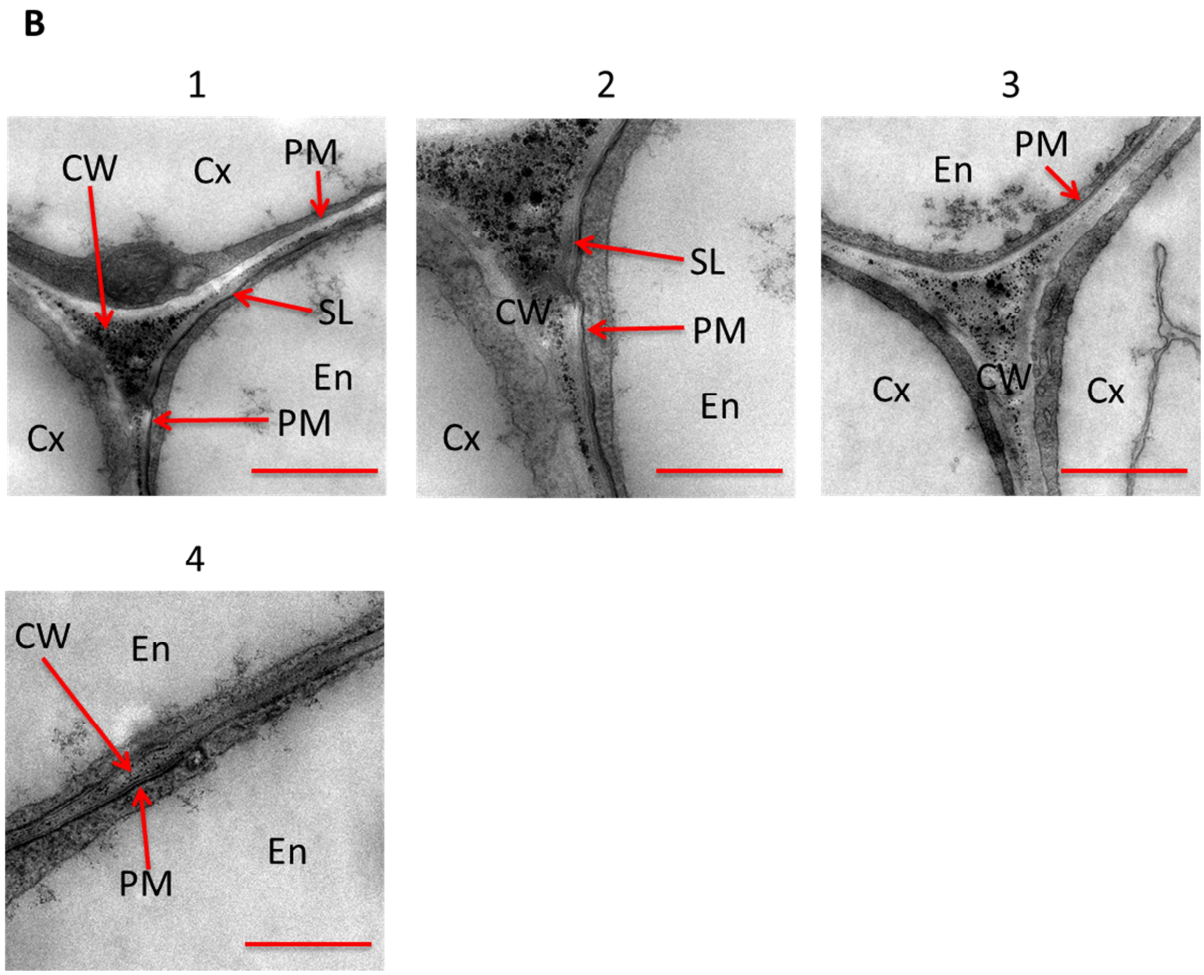

Fig. 63: Ultrastructure of suberin lamellae at a three mm distance to the root tip in one-week old *prx11-1* seedling with a root length of one cm grown on ½ MS-plates

A: Visualised cross section of *prx11-1* root at a three mm distance to the root tip in the TEM. **B**: Taken images of the cell wall ultrastructure. Ep: epidermis cell, Cx: cortex cell, En: endodermis cell, Pc: pericycle cell, CS: Casparian strip, CW: primary cell wall, PM: plasma membrane, SL: suberin lamella. Scale bar size in **A**: 20 µm, in **B**: 1 µm in image 1 and 3 and 500 nm in image 2 and 4.

At a 3 ½ mm distance to the root tip all cells of the root are well developed. The width of the endodermal cells is between six and eight µm (fig. 64 A).

Also, at a 3 ½ mm distance to the root tip the cell wall of one endodermal cell is suberised. One dark and two bright lamellae are visible. The red arrow indicates one point, where two dark bands are observable. The width of the suberin band is about 25 nm (fig. 64 B, image 1). Cell walls of the remaining endodermal cells do not show a suberin band in the cell wall (fig. 64 B, image 2 and 3). The third image shows dark stained cell walls of adjacent endodermal cells. The presence of a Casparian strip is not clear (fig. 64 B, image 3).

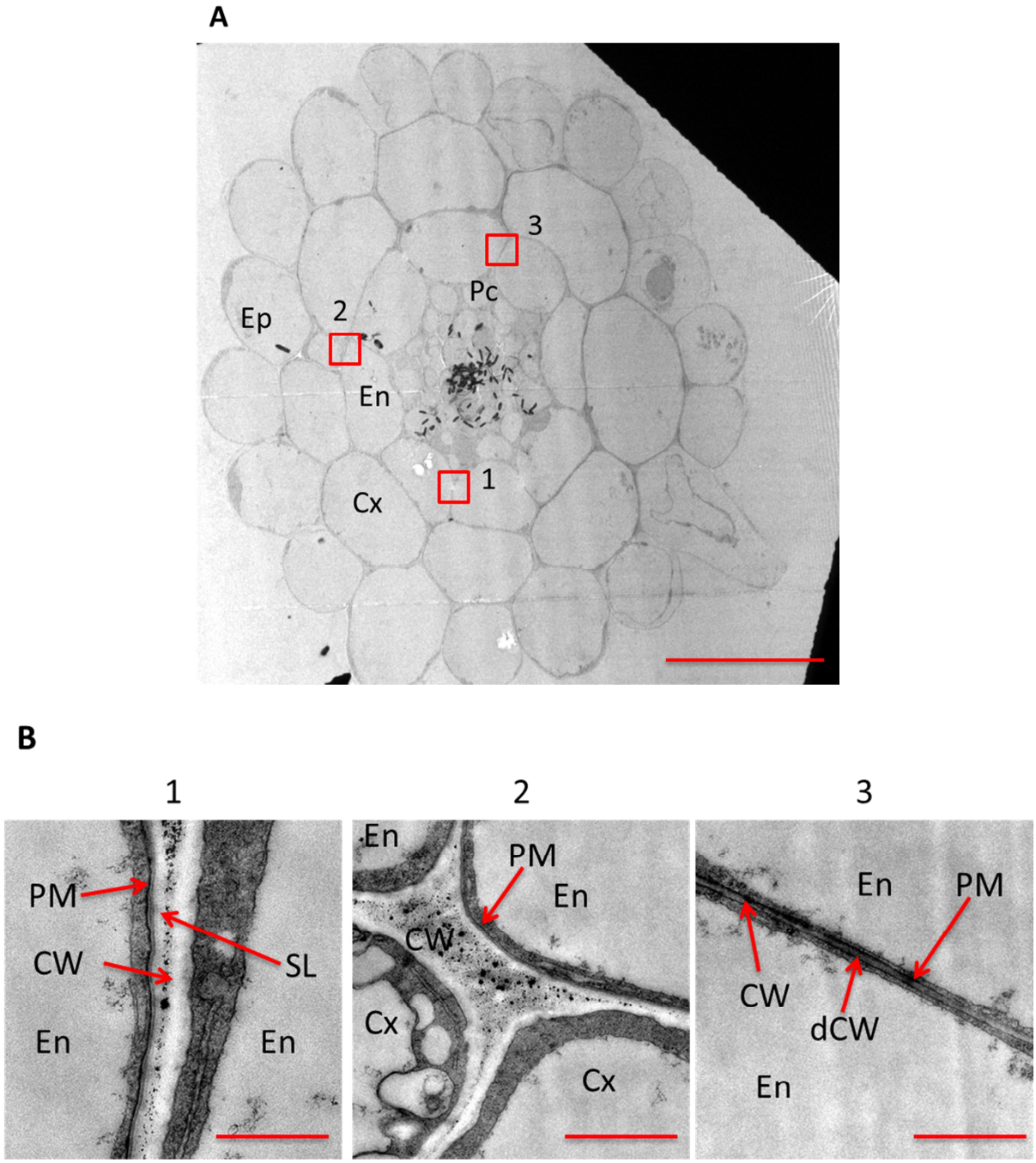

Fig. 64: Ultrastructure of suberin lamellae at a 3 ½ mm distance to the root tip in one-week old *prx11-1* seedling with a root length of one cm grown on ½ MS-plates

A: Visualised cross section of *prx11-1* root at a 3 ½ mm distance to the root tip in the TEM. **B**: Taken images of the cell wall ultrastructure. Ep: epidermis cell, Cx: cortex cell, En: endodermis cell, Pc: pericycle cell, CS: Casparian strip, dCW: dark primary cell wall, CW: primary cell wall, PM: plasma membrane, SL: suberin lamella. Scale bar size in **A**: 20 µm, in **B**: 500 nm in image 1 and 1 µm in image 2 and 3.

A cross section at a one mm distance to the hypocotyl reveals decreased size of endodermal cells. The width is about four to five µm. Epidermal, cortical, pericycle and cells of the central

cylinder are clear visible and well developed (fig. 65 A). Unfortunately, in this cross section only two endodermal cells could be analysed.

The cell walls of these two endodermal cells are suberised. Lamellation is observable. Three dark and two bright lamellae can be recognised. The width of the suberin band is around 50 nm (fig. 65 B, image 1). In the cell walls of these two endodermal cells there is one thickening present, which is considered as a Casparian strip (fig. 65 B, image 2).

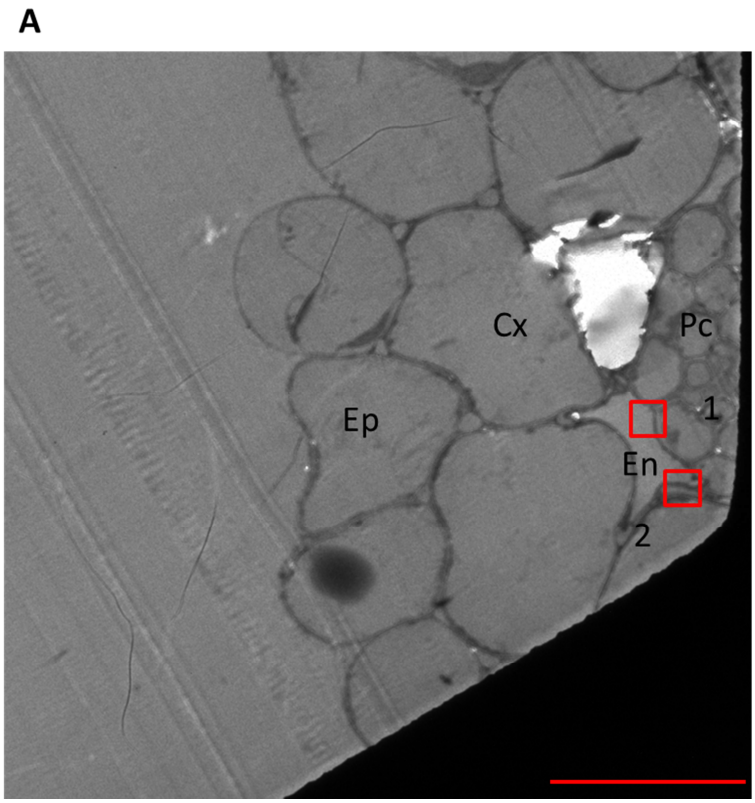

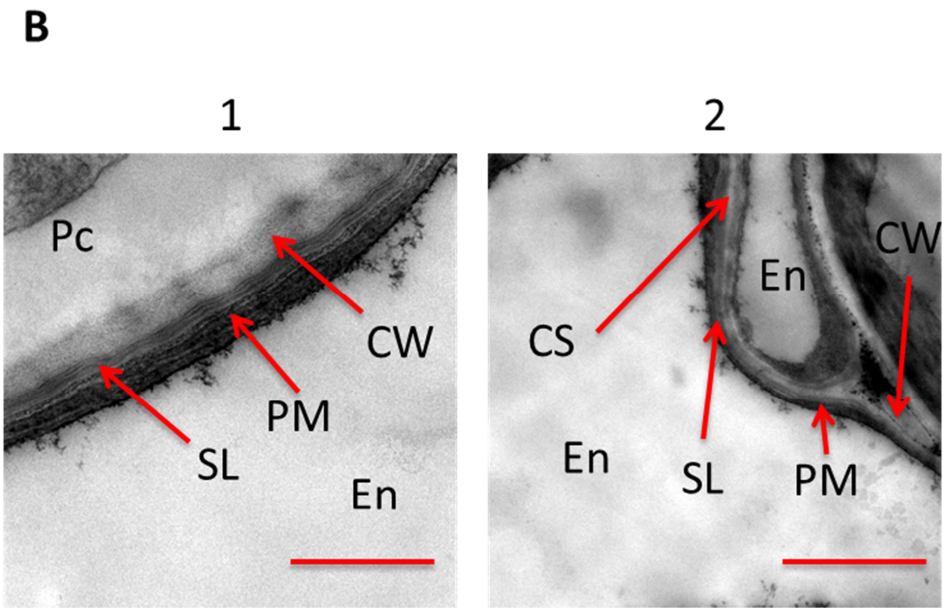

Fig. 65: Ultrastructure of suberin lamellae at a one mm distance to the hypocotyl in one week old *prx11-1* seedling with a root length of one cm grown on ½ MS-plates

A: Visualised cross section of *prx11-1* root at a one mm distance to the hypocotyl in the TEM. **B**: Taken images of the cell wall ultrastructure. Ep: epidermis cell, Cx: cortex cell, En: endodermis cell, Pc: pericycle cell, CS: Casparian strip, CW: primary cell wall, PM: plasma membrane, SL: suberin lamella. Scale bar size in **A**: 20 µm, in **B**: 500 nm in image 1 and 1 µm in image 2.

3.3.4.4. Suberin lamellae ultrastructure of *prx11-2*

The second mutant *prx11-2* was analysed as well. The first cross section was investigated at a two mm distance to the root tip. The cross section reveals well developed epidermal, cortical, endodermal, pericycle and central cylinder cells. The width of the endodermal cells is between eight and twelve µm (fig 66 A). The cell walls of endodermal cells do not show a suberised band (fig. 66 B, image 1 and 2).

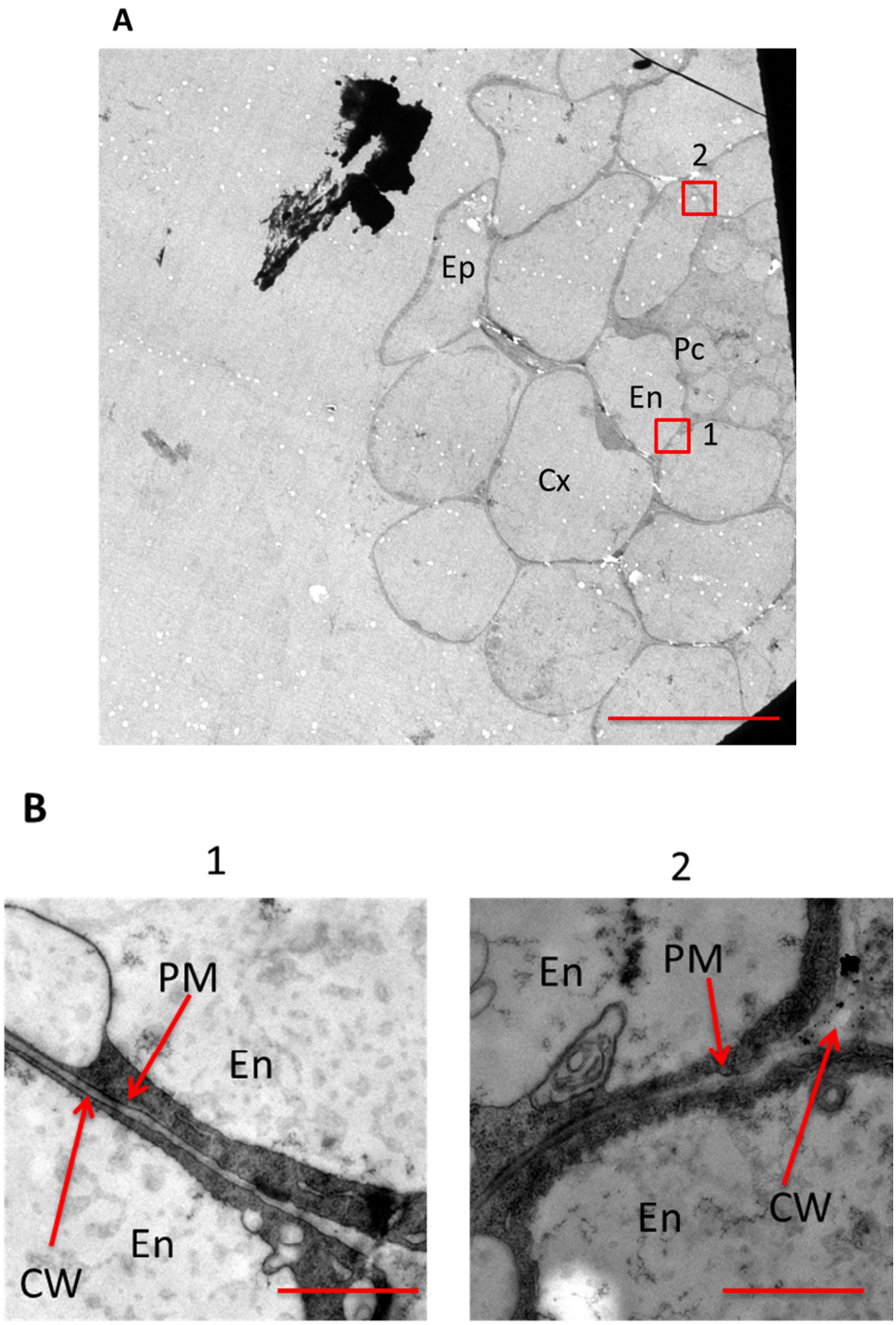

Fig. 66: Ultrastructure of suberin lamellae at a two mm distance to the root tip in one-week old *prx11-2* seedling with a root length of one cm grown on ½ MS-plates

A: Visualised cross section of *prx11-2* root at a two mm distance to the root tip in the TEM. **B**: Taken images of the cell wall ultrastructure. Ep: epidermis cell, Cx: cortex cell, En: endodermis cell, Pc: pericycle cell, CS: Casparian strip, CW: primary cell wall, PM: plasma membrane, SL: suberin lamella. Scale bar size in **A**: 20 µm, in **B**: 1 µm.

At a 2 ½ mm distance to the root tip all cells are well developed. The width of the endodermal cells is around seven µm (fig. 67 A).

One cell wall of one endodermal cell seems to be suberised. Lamellar-like structure is barely to see. The width of the suberin band is about 20 nm (fig. 67 B, image 1). Other cell walls of endodermal cells are not suberised. In the second image the cell walls of adjacent endodermal cells are stained dark at the supposed position of the Casparian strip (fig. 67 B, image 2).

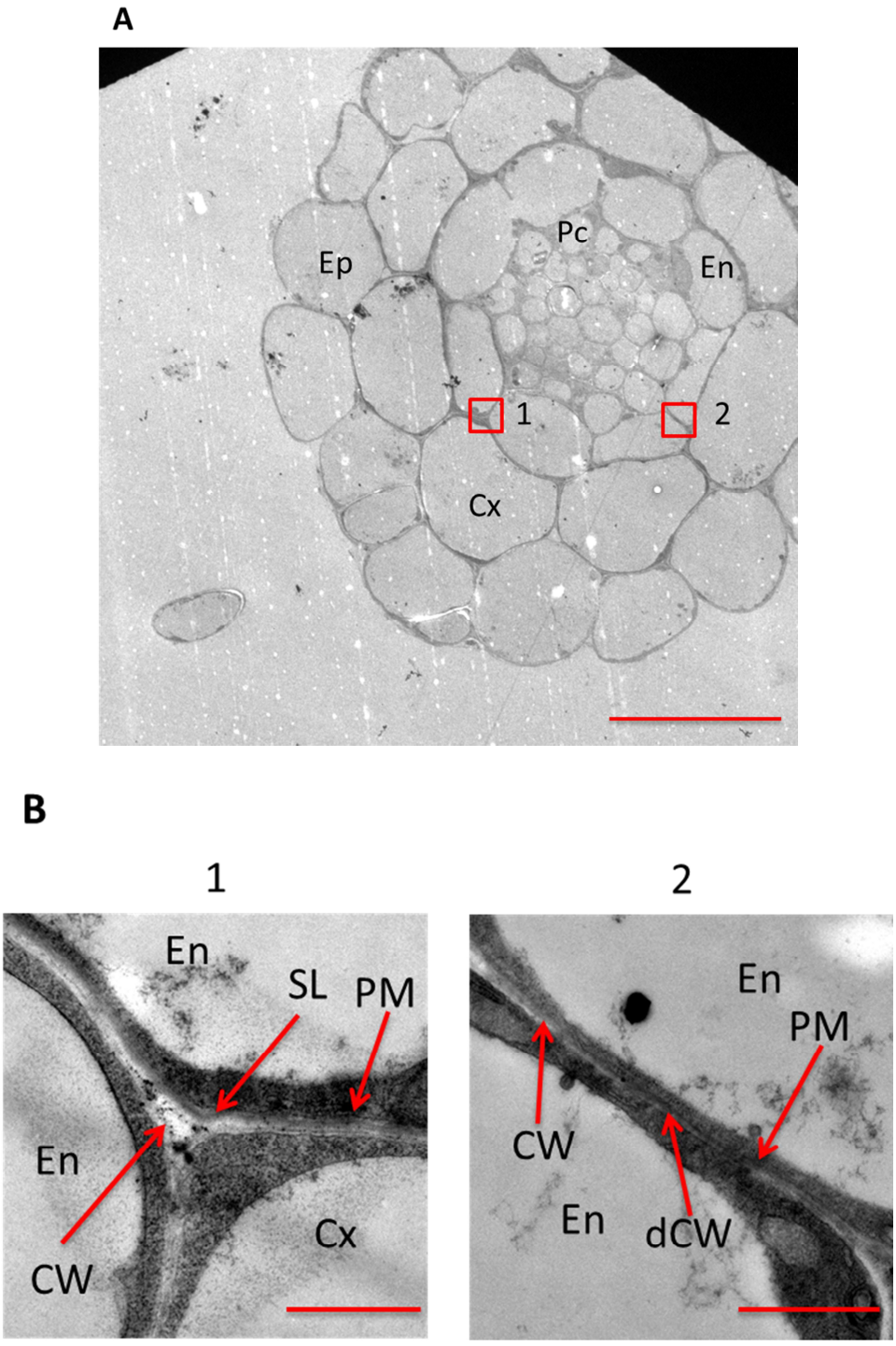

Fig. 67: Ultrastructure of suberin lamellae at a 2 ½ mm to the root tip in one-week old *prx11-2* seedling with a root length of one cm grown on ½ MS-plates

A: Visualised cross section of *prx11-2* root at a 2 ½ mm distance to the root tip in the TEM. **B**: Taken images of the cell wall ultrastructure. Ep: epidermis cell, Cx: cortex cell, En: endodermis cell, Pc: pericycle cell, CS: Casparian strip, CW: primary cell wall, PM: plasma membrane, SL: suberin lamella. Scale bar size in **A**: 20 µm, in **B**: 500 nm in image 1 and 1 µm in image 2.

Further upstream towards the hypocotyl at a four mm distance to the root tip the width of the endodermal cells seems to decrease. The width is between five and seven µm (fig. 68 A). A close-up view shows that the cell walls of some endodermal cells are suberised and others are non-suberised. In the first image a wavy phenotype of the suberin band is visible. One or two dark and two or three bright lamellae are observable in the suberin band. The width of the suberin band is about 45 nm (fig. 68 B, image 1). In the second image only one endodermal cell is suberised whereas the second one is non-suberised (fig. 68 B, image 2). The third image shows a thin dark suberin band, while the adjacent endodermal cell seems not to be suberised. At the thickest point, the width is about 15 nm. The thickness of the suberin band decreases in the direction of the central point of the cell walls of the adjacent endodermal cells (fig. 68 B, image 3).

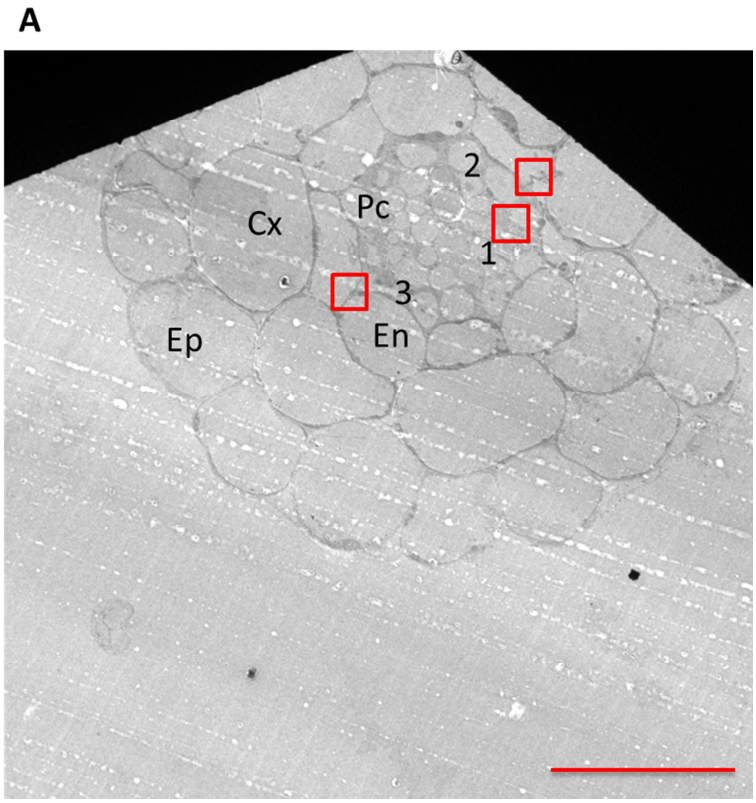

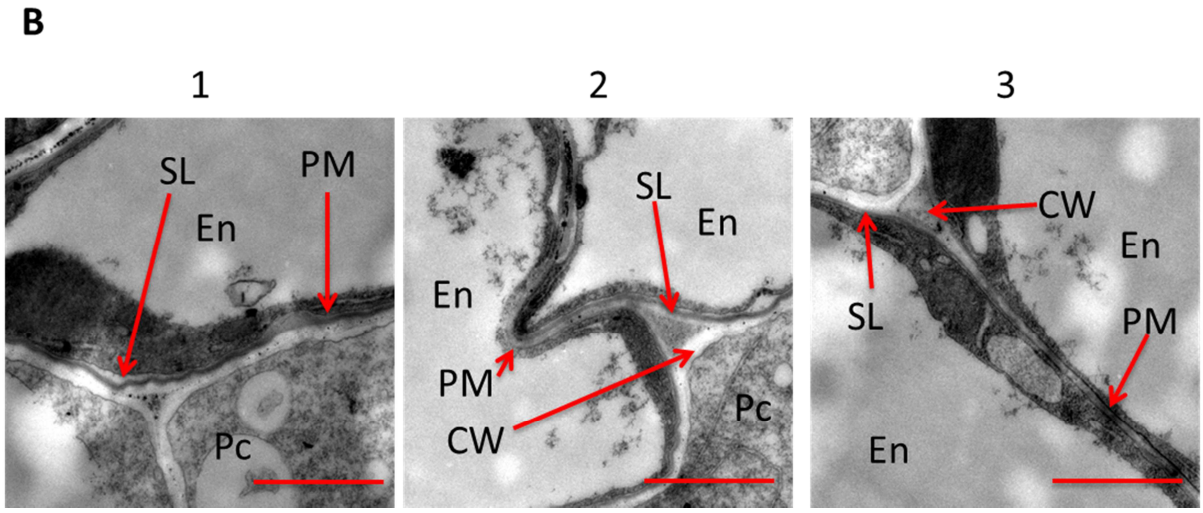

Fig. 68: Ultrastructure of suberin lamellae at a four mm distance to the root tip in one-week old *prx11-2* seedling with a root length of one cm grown on ½ MS-plates

A: Visualised cross section of *prx11-2* root at a four mm distance to the root tip in the TEM. **B**: Taken images of the cell wall ultrastructure. Ep: epidermis cell, Cx: cortex cell, En: endodermis cell, Pc: pericycle cell, CS: Casparian strip, CW: primary cell wall, PM: plasma membrane, SL: suberin lamella. Scale bar size in **A**: 20 µm, in **B**: 1 µm.

Cross section at a five mm distance to the root exhibits well developed epidermal, cortical, pericycle and central cylinder cells. The size of endodermal cells seems to decrease further. The width is about three and five µm (fig. 69 A).

Most cell walls of endodermal cells seem to be suberised. In the first and second close-up image the suberin band shows a wavy structure. Apart from the wavy structure the suberin band is perfectly situated between primary cell wall and plasma membrane. Some parts of the suberin band show one or two dark and two or three bright lamellae (fig. 69 B, image 1 and 2). In the first three close-up images the width of the suberin band is between 40 and 65 nm (fig. 69 B, image 1 to 3), while in the last image the width of the suberin band is about 15 nm (fig. 69 B, image 4). Lamellar-like structure is not observable in the last image. Furthermore, between the endodermal cells a Casparian strip is visible in their cell walls. Here, the width of the suberin band with the Casparian strip is about 55 nm (fig. 69 B, image 4).

A

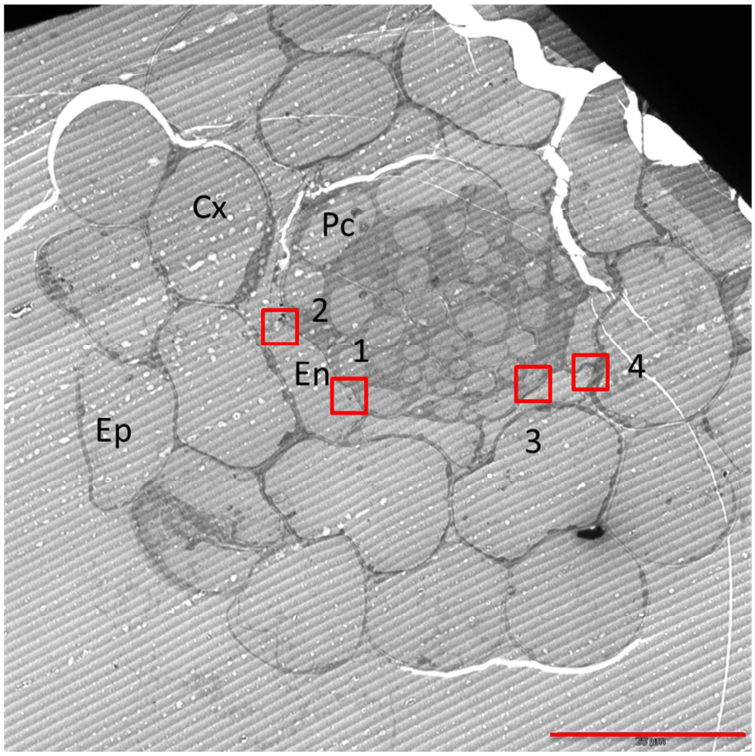

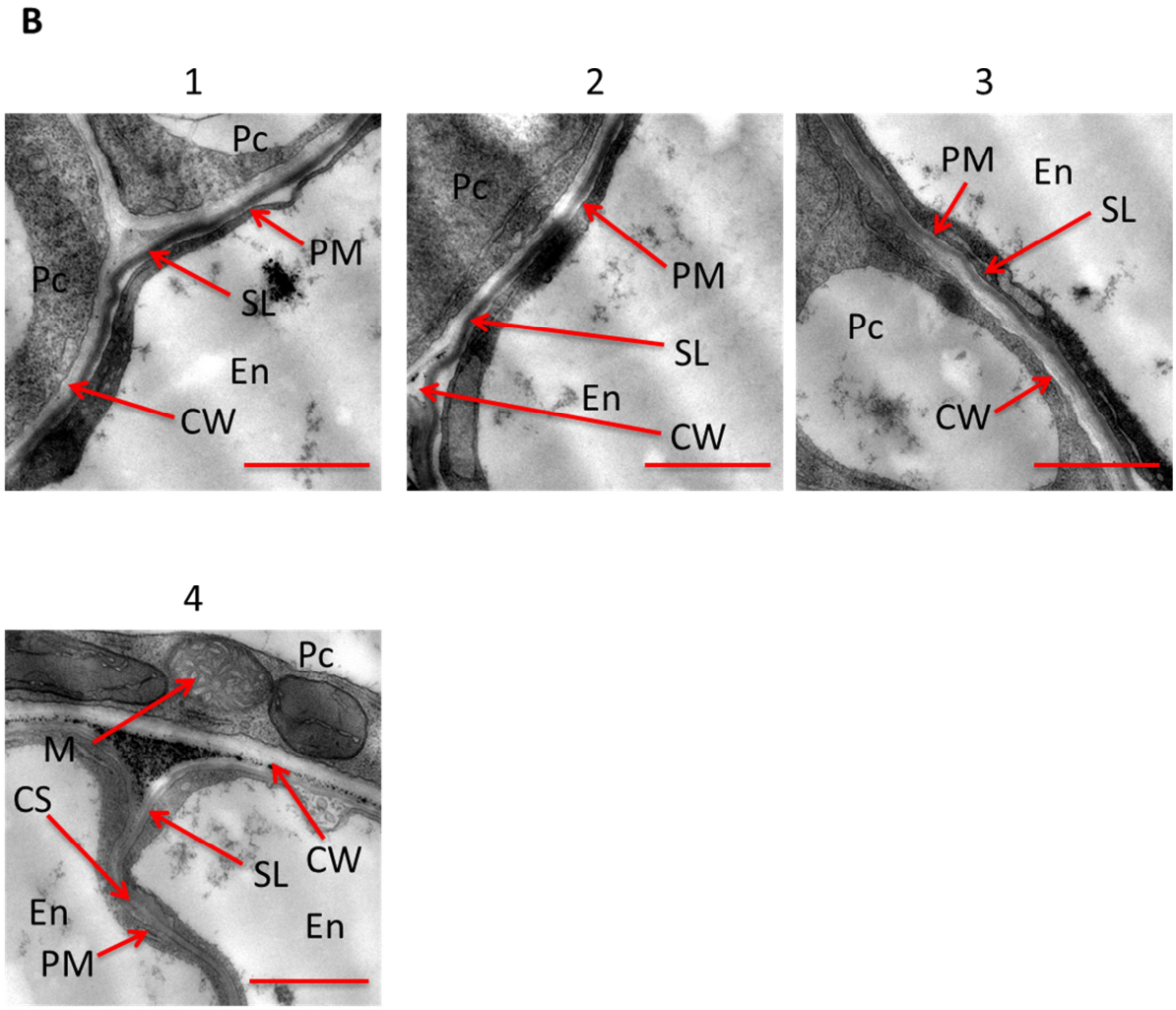

Fig. 69: Ultrastructure of suberin lamellae at a five mm distance to the root tip in one-week old *prx11-2* seedling with a root length of one cm grown on ½ MS-plates

A: Visualised cross section of *prx11-2* root at a five mm distance to the root tip in the TEM. **B**: Taken images of the cell wall ultrastructure. Ep: epidermis cell, Cx: cortex cell, En: endodermis cell, Pc: pericycle cell, CS: Casparian strip, CW: primary cell wall, PM: plasma membrane, SL: suberin lamella. Scale bar size in **A**: 20 µm, in **B**: 1 µm in image 1 to 3 and 500 nm in image 4.

Cross sections at a two mm distance to the hypocotyl were performed as well. Here, the width of the endodermal cells is decreased in comparison to the previous cross section at a five mm distance to the root tip. The shape of endodermal cells can barely be observed (fig. 70 A).

The close-up images show that the cell wall of all endodermal cells is suberised. The wavy phenotype of the suberin band is still recognisable but now it appears that the suberin band is situated between primary cell wall and plasma membrane. In the first image two dark and three bright lamellae are observable. The width is about 50 nm (figure… image 1). In the

second image a Casparian strip with a bulb-like structure is visible (fig. 70 B, image 2). The last image shows again the wavy phenotype of the suberin band (fig. 70 B, image 3).

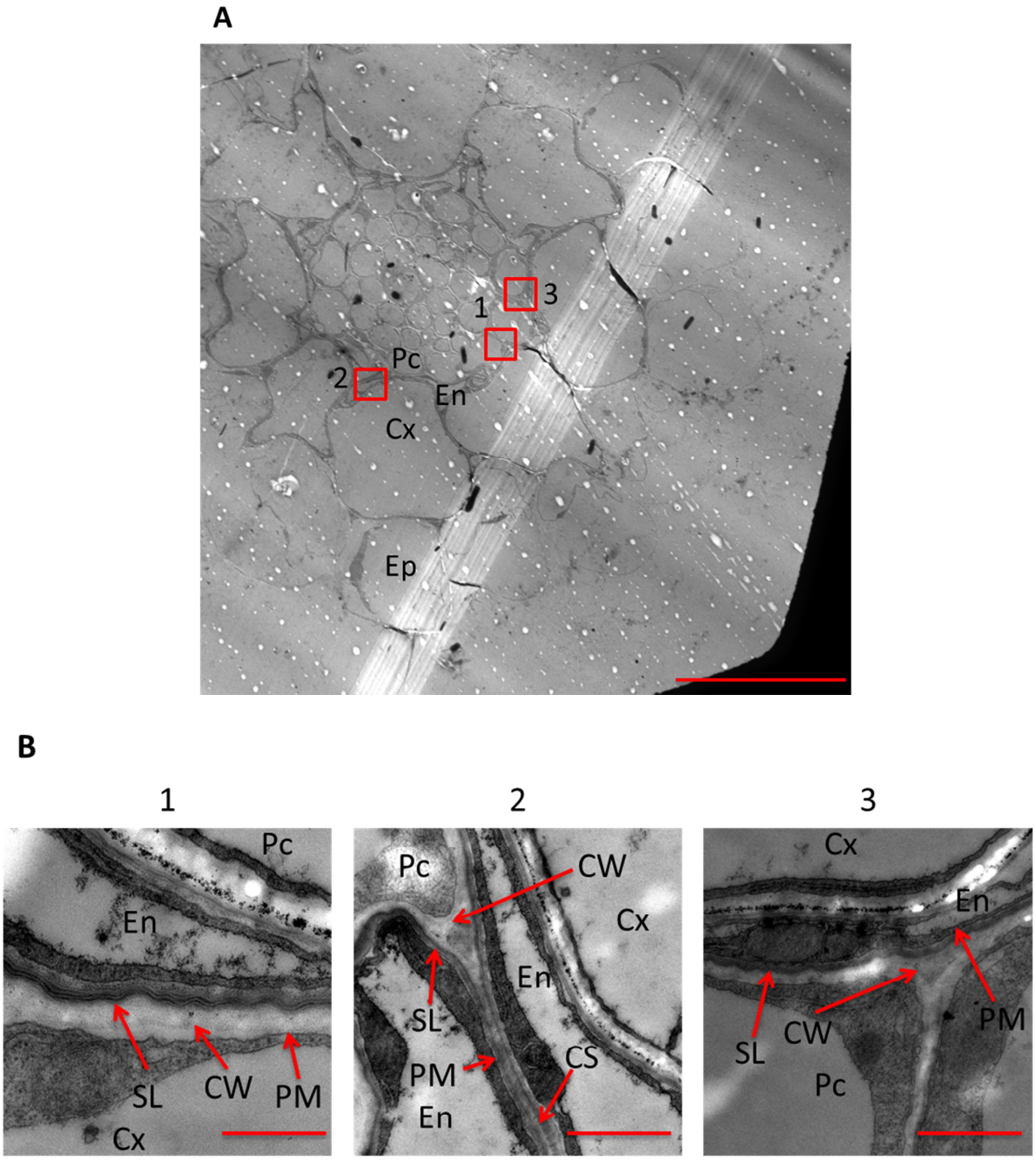

Fig. 70: Ultrastructure of suberin lamellae at a two mm distance to the hypocotyl in one week old *prx11-2* seedling with a root length of one cm grown on ½ MS-plates

A: Visualised cross section of *prx11-2* root at a two mm distance to the hypocotyl in the TEM. **B**: Taken images of the cell wall ultrastructure. Ep: epidermis cell, Cx: cortex cell, En: endodermis cell, Pc: pericycle cell, CS: Casparian strip, CW: primary cell wall, PM: plasma membrane, SL: suberin lamella. Scale bar size in **A**: 20 µm, in **B**: 500 nm in image 1 and 1 µm in image 2 and 3.

3.3.4.5. Suberin lamellae ultrastructure of *C4H::F5H*

Investigation of cross sections at a two mm distance to the root tip in *C4H::F5H* shows different sizes of endodermal cells. Also, the size of cortical and epidermal cells seems to be not homogenous like in the WT. The width of the endodermal cells is between two and six µm (fig. 71 A).

Higher magnifications of endodermal cells show that many, but not all cell walls of endodermal cells are suberised. Lamellar-like structure is well observable. The suberin band in the first image seems to consist of three dark and four bright lamellae. The width of the suberin band is between 75 and 85 nm. The second endodermal cell is not suberised (fig. 71 B, image 1). The next close-up image presents a larger part of the cross section. The cell wall of both endodermal cells is suberised. Above the red arrow of the identification mark of the suberin lamellae the suberin band is slightly wavy organised. But in general, the suberin band is perfectly situated between primary cell wall and plasma membrane. Both adjacent cells the cortical and the pericycle cell reveal mitochondria and smooth and rough endoplasmatic reticula. Additionally, in the pericycle cell a vacuole is present (fig. 71 B, image 2). Larger magnification of the cell walls of the adjacent endodermal cells exhibits a thickening between the endodermal cells. This thickening is considered as a Casparian strip. Here, the width of suberin band is between 25 and 30 nm. The width of the Casparian strip together with the suberin band is around 50 nm (fig. 71 B, image 3).

A

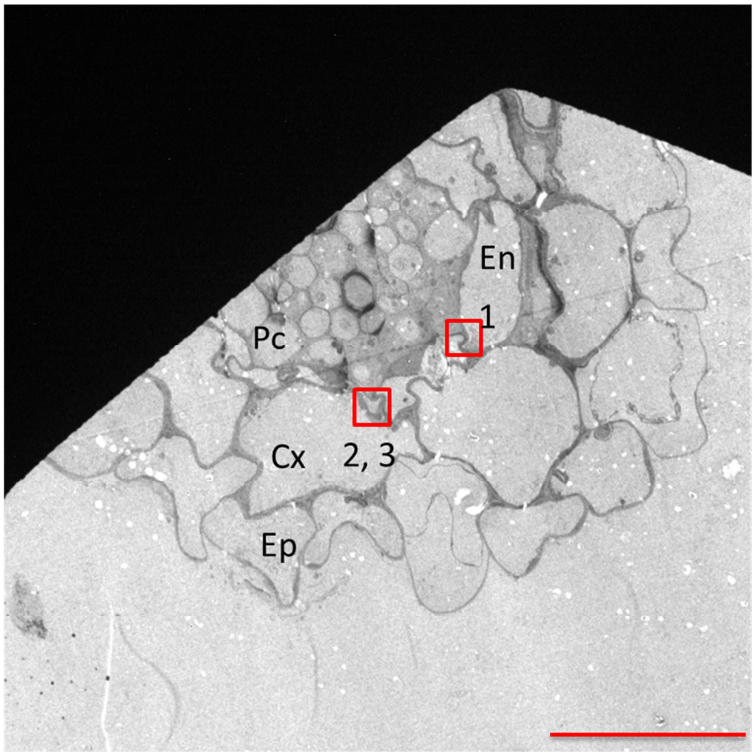

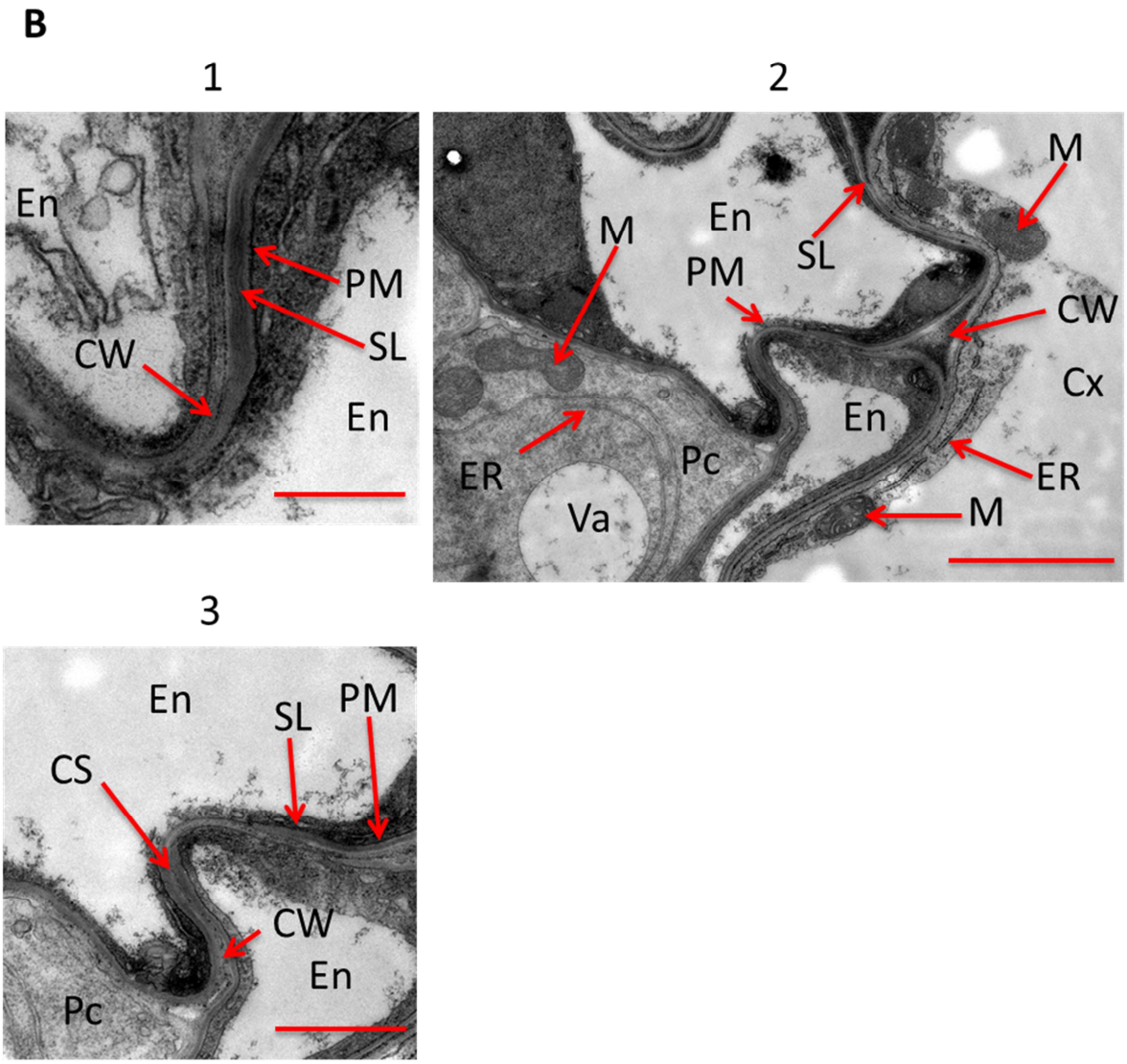

Fig. 71: Ultrastructure of suberin lamellae at a two mm distance to the root tip in one-week old *C4H::F5H* seedling with a root length of one cm grown on ½ MS-plates

A: Visualised cross section of *C4H::F5H* root at a two mm distance to the root tip in the TEM. **B**: Taken images of the cell wall ultrastructure. Ep: epidermis cell, Cx: cortex cell, En: endodermis cell, Pc: pericycle cell, CS: Casparian strip, CW: primary cell wall, ER: endoplasmatic reticulum, M: mitochondria, PM: plasma membrane, SL: suberin lamella, Va: vacuole. Scale bar size in **A**: 20 µm, in **B**: 500 nm in image 1 and 3 and 2 µm in image 2.

The last cross section was performed at a three mm to the hypocotyl. Now, the mutant *C4H::F5H* shows an additional layer of cortical cells. The size and shape of epidermal, cortical, endodermal, pericycle and central cylinder cells appear to be well developed and more homogenous than in the cross section of the root tip (fig. 72 A).

Cell walls of all endodermal cells are suberised. The close-up image reveals the lamellar-like structure of the suberin band, which consist of three dark and four bright lamellae on the left side of the endodermal cell, whereas on the right sight four dark and five bright lamellae

are present. The width of the suberin band on the left side is between 45 and 55 nm. In contrast, on the right side it is between 75 and 90 nm (fig. 72 B, image 1).

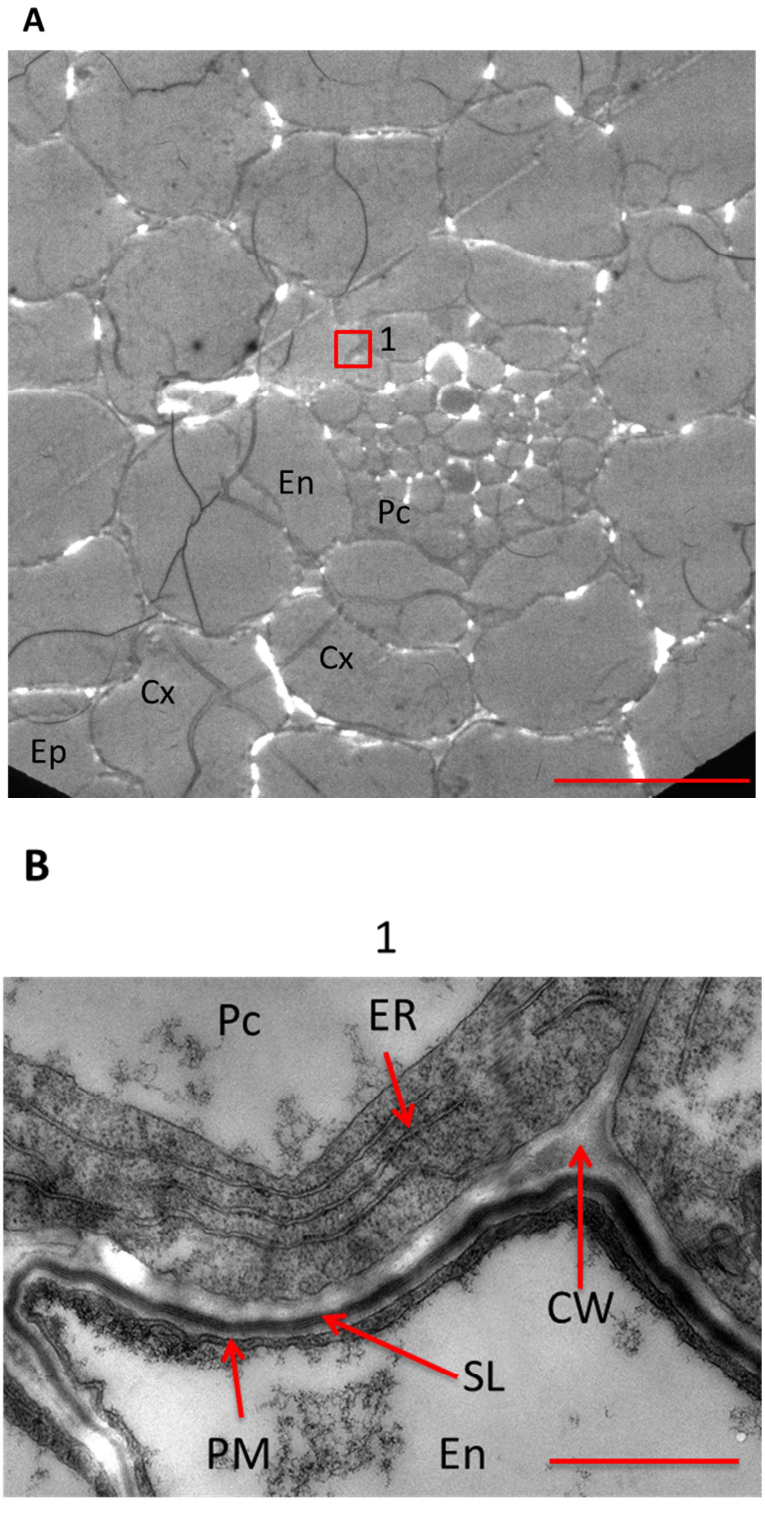

Fig. 72: Ultrastructure of suberin lamellae at a three mm distance to the hypocotyl in one week old *C4H::F5H* seedling with a root length of one cm grown on ½ MS-plates

A: Visualised cross section of *C4H::F5H* root at a three mm distance to the hypocotyl in the TEM. **B**: Taken images of the cell wall ultrastructure. Ep: epidermis cell, Cx: cortex cell, En: endodermis cell, Pc: pericycle cell, CW: primary cell wall, ER: endoplasmatic reticulum, PM: plasma membrane, SL: suberin lamella. Scale bar size in **A**: 20 µm, in **B**: 1 µm.

3.3.5. Summary of the study results of seedlings

The following table summarises the study results of the apoplastic barriers in the different mutated seedlings. The mutant lines are put into order from disrupted/delayed development of Casparian strip to functional and earlier formed CS barrier.

Tab. 15: Summary of the obtained results from microscopical analysis of the apoplastic barriers put into order from disrupted, delayed to functional and earlier formed Casparian strip barrier

Genotype	PI	BF	FY	TEM
WT	functional	sealed network	0	lamellar-like structure
ref3-2	disrupted	faint stained	delayed	
ccoaomt1	delayed	faint stained	delayed	
ccr1	delayed	faint stained	delayed	
comt1	slightly delayed		delayed	
myb4	slightly delayed		0	
ref1-4	delayed	ectopic lignification	enhanced	
ref4-3	delayed	ectopic lignification	enhanced	
C4H::F5H	delayed	ectopic lignification	enhanced	lamellar-like structure, thicker suberin band with more lamellae
esb1	delayed	disrupted network	enhanced	
cadc	functional	sealed network	delayed	
cadd	functional	sealed network	delayed	
prx11-1	functional	sealed network	slightly delayed	lamellar like structure
prx11-2	functional	sealed network	slightly delayed	wavy phenotype Llmellar-like structure

asft1	functional	sealed network	delayed	wavy phenotype lamellar-like structure
asft2	functional	sealed network	delayed	
ref8-1	functional	increased staining		
ref8-1 med5a*med5b*	functional	sealed network	0	
myb7	functional	sealed network	0	
fact3	functional	sealed network	0	
*ref8-2*fah1-2* AtC4H::SmF5H*	functional		0	
fah1-2	functional		enhanced	
*cadc*cadd*	functional	faint stained	enhanced	
*cadc*cadd2*	functional	faint stained	enhanced	
*cadc*cadd* fah1-2*	functional	faint stained	enhanced	
hqt	earlier formed	sealed network	0	
RALPH::HQT	earlier formed	sealed network	enhanced	

3.4. Analysis of the chemical composition of lignified and suberised root endodermal network

3.4.1. Determination of lignin content and composition of whole root systems in different phenylpropanoid pathway mutants

Hydroponically grown roots of five-week old plants were either digested in enzymatic solution or kept in citrate solution with sodium azide. Mutant lines sensitive to cell wall degrading enzymes were not digested but only kept in citrate buffer with sodium azide. After digestion lipophilic soluble compounds were extracted in a soxhlet-extractor with chloroform at first and followed by methanol, each for 24 hours. Finally, the structure of lignin of the either digested or undigested roots was depolymerised by cooking in a dioxane

solution containing 10 % ethanethiol and 2.5 % boron trifluoride diethyl etherate at 100 °C for 4 hours. The thioethylated lignin monomers were extracted with dichlormethane and subsequently purified in a filter containing water-free sodium sulphate. Under a nitrogen steam the extracted thioethylated lignin monomers were concentrated and finally derivatised by adding BSTFA and pyridine at 70 °C for 40 minutes. Lignin monomers were analysed in the GC-FID and identified in the GC-MS.

Three thioethylated aromatic compounds could be identified and quantified: thioethylated coumaryl, coniferyl and sinapyl monomer. These three identified compounds are also known in lignin analysis as H-, G-, and S-compounds.

The major compound in the WT is the coniferyl monomer, followed by sinapyl and coumaryl monomer. The digested root samples of the WT contain 0.6 µg/mg dw (± 0.3 µg/mg dw) of coumaryl monomers, 16.3 µg/mg dw (± 1.1 µg/mg dw) of coniferyl monomers and 3.3 µg/mg dw (± 0.3 µg/mg dw) of sinapyl monomers (fig. 73 A). The relative composition of the WT is 2.8 % (± 1.3 %) H-, 80.7 % (± 3.4 %) G- and 16.4 % (± 2.1 %) S-lignin (fig. 73 B). With respect to the mutant *hqt* the content of the single monomers and the relative composition has not changed compared with the WT (fig. 73 A and B). In contrast, the mutant *ccoaomt1* shows a significant decline of coniferyl monomers by 37 % (10.3 ± 2.0 µg/mg dw in *ccoaomt1* and 16.3 ± 1.1 µg/mg dw in WT). This causes a significant decrease of total lignin by 34 % (13.2 ± 2.8 µg/mg dw in *ccoaomt1* and 20.1 ± 0.9 µg/mg dw in WT) (fig. 73 A). Considering the relative composition there is no alteration compared with the WT. The mutant *comt1* shows a significant decrease in coniferyl monomers by 20 % (12.4 ± 1.6 µg/mg dw in *comt1* and 16.3 ± 1.1 µg/mg dw in WT) and a highly significant reduction in sinapyl monomers by 88 % (0.4 ± 0.1 µg/mg dw in *comt1* and 3.3 ± 0.3 µg/mg dw in WT). The reduced content of coniferyl and sinapyl monomers leads to a significant decline of the total lignin content by 34 % (13.2 ± 1.8 µg/mg dw in *comt1* and 20.1 ± 0.5 µg/mg dw in WT) in *comt1* (fig. 73 A). Especially, the reduction of sinapyl monomers causes a shift in the relative composition of lignin. The relative proportion of G-monomers is by 13.3 % significantly higher increased in comparison to the WT (94.0 ± 1.0 % in *comt1* and 80.7 ± 3.4 % in WT), whereas S-monomers reveal a highly significant reduction by 13.3 % (2.7 ± 0.5 % in *comt1* and 16.4 ± 2.1 % in WT) compared with the WT (fig. 73 B). The mutant *ccr1* exhibits the strongest reduction in lignin. The coumaryl content is reduced by 50 % (0.3 ± 0.1 µg/mg dw in *ccr1* and 0.6 ± 0.3 µg/mg dw in WT), while coniferyl and sinapyl monomers are highly significant decreased by 45 %

(9.0 ± 1.5 µg/mg dw in *ccr1* and 16.3 ± 1.1 µg/mg dw in WT) and 76 % (0.8 ± 0.2 µg/mg dw in *ccr1* and 3.3 ± 0.3 µg/mg dw in WT) respectively. The total lignin content is reduced by 50 % (10.1 ± 1.7 µg/mg dw in *ccr1* and 20.1 ± 0.5 µg/mg dw in WT) in *ccr1* (fig. 73 A). This strong reduction in sinapyl monomers primarily causes a shift in the relative lignin composition. G-monomers are significantly increased by 8.4 % (89.1 ± 1.0 % in *ccr1* and 80.7 ± 3.4 % in WT), while S-monomers are decreased by 8.1 % (8.3 ± 0.4 % in *ccr1* and 16.4 ± 2.1 % in WT) (fig. 73 B). The mutant *esb1* shows a significantly higher altered sinapyl monomer content compared to the WT. Sinapyl monomers are reduced by 30 % (2.3 ± 0.3 µg/mg dw in *esb1* and 3.3 ± 0.3 µg/mg dw in WT) (fig. 73 A). The total lignin content is slightly and significantly reduced by 6 % (18.9 ± 0.7 µg/mg dw in *esb1* and 20.1 ± 0.5 µg/mg dw in WT). The decline of sinapyl monomers causes a significant reduction by 4 % (12.4 ± 1.1 % in *esb1* and 16.4 ± 2.1 % in WT) in S-lignin compared with the WT (fig. 73 B).

A

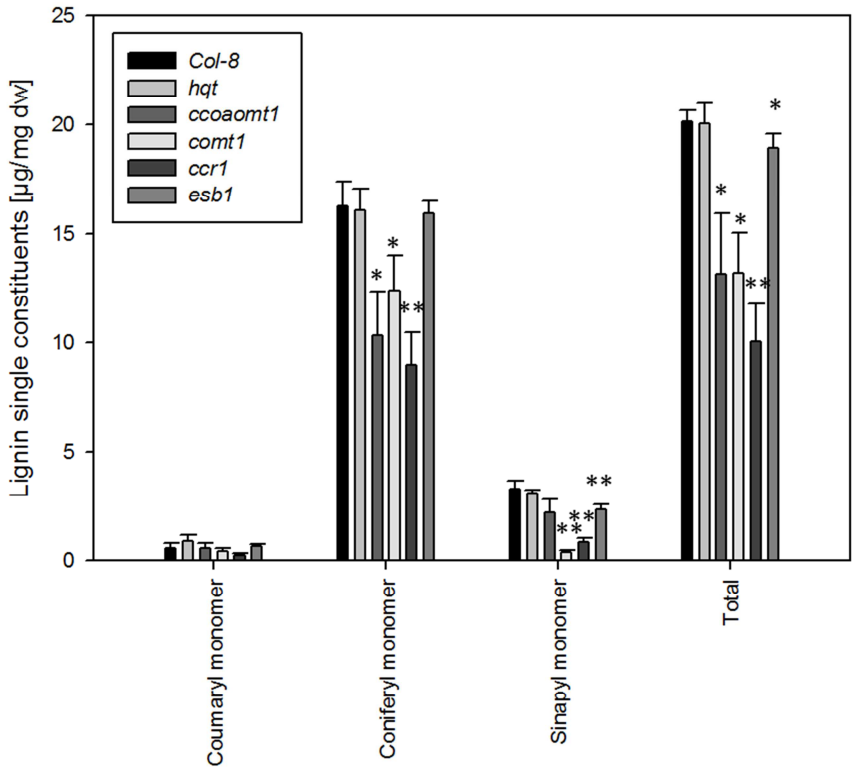

B

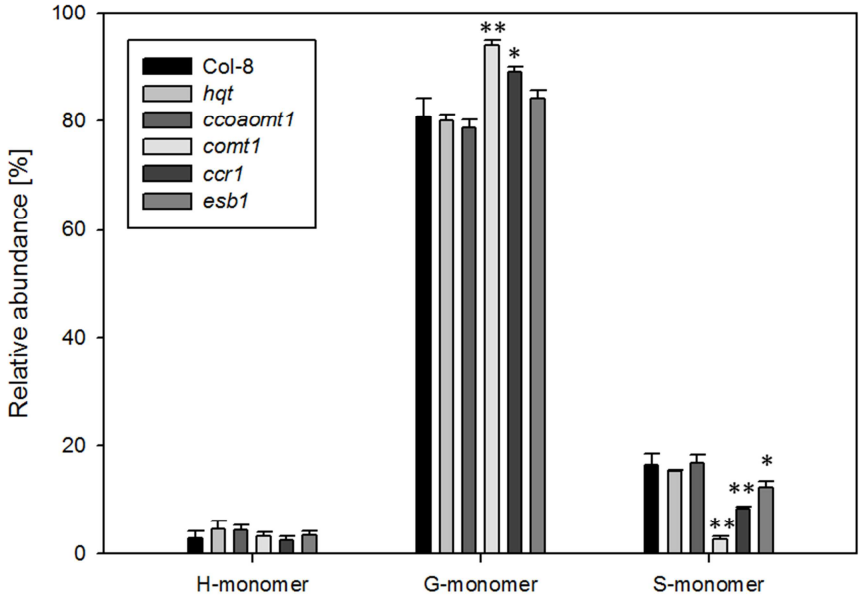

Fig. 73: Comparison of root lignin composition of the mutant lines *hqt*, *ccoaomt1*, *comt1*, *ccr1* and *esb1* with the corresponding WT

Five-week old hydroponically grown roots treated with cell wall degrading enzymes were analysed. **A**: Absolute lignin composition related to the root dry weight. **B**: Relative lignin composition related to the root dry weight. The represented values are the arithmetic mean of the WT and mutant lines respectively and the calculated standard deviation error bars. The sample amount corresponds to four roots of Col-8, two of *hqt*, three of *ccoaomt1*, *comt1* and *ccr1* and four roots of *esb1*. H-monomer: hydroxycinnamyl-monomer, G-monomer: guiacyl-monomer, S-monomer: sinapyl-monomer. *: student's t-test, $p \leq 0.05$, **: student's t-test, $p \leq 0.01$.

Root samples untreated with cell wall degrading enzymes show less lignin related to the root dry weight than digested ones. Undigested root samples of WT exhibit 0.06 µg/mg dw (± 0.03 µg/mg dw) of coumaryl monomers, 2.9 µg/mg dw (0.4 µg/mg dw) of coniferyl monomers and 0.3 µg/mg dw (0.1 µg/mg dw) of sinapyl monomers. This amount of the three lignin monomers leads to a relative composition of 1.7 % (± 0.5 %) of H-, 89.0 % (± 2.9 %) of G- and 9.3 % (± 2.7 %) of S-monomers (fig. 74 A). Both mutants *cadc* and *cadd* show similar amounts of lignin monomers like the WT and the composition is also not altered. Primarily, lignin monomers are found in less amount in double and triple knockout mutant *cadc*cadd* and *cadc*cadd*fah1-2*. Coniferyl and sinapyl monomers are significantly reduced by 57 % (1.2 ± 0.8 µg/mg dw in *cadc*cadd* and 2.9 ± 0.4 µg/mg dw in WT) and 67 % (0.1 ± 0.06 µg/mg dw in *cadc*cadd* and 0.3 ± 0.1 µg/mg dw in WT) respectively in *cadc*cadd*. The

absolute lignin content is significantly decreased by 61 % (1.3 ± 0.7 µg/mg dw in *cadc*cadd* and 3.3 ± 0.5 µg/mg dw in WT) (fig. 74 A). However, this reduction of coniferyl and sinapyl monomers does not affect the relative composition of lignin compared to the WT. The triple knockout mutant *cadc*cadd*fah1-2* shows a significantly higher decline of coniferyl monomers by 66 % (1.0 ± 0.6 µg/mg dw in *cadc*cadd*fah1-2* and 2.9 ± 0.4 µg/mg dw in WT), a significant loss of sinapyl monomers by 83 % (0.05 ± 0.01 µg/mg dw in *cadc*d*fah1-2* and 0.3 ± 0.1 µg/mg dw in WT) and a total reduction of lignin by 67 % (1.1 ± 0.5 µg/mg dw in *cadc*cadd*fah1-2* and 3.3 ± 0.5 µg/mg dw in WT) (fig. 74 A). The loss of sinapyl monomers causes a shift in the relative lignin composition. S-monomers are significantly reduced to 4.7 % (± 2.4 %), whereas 9.3 % (± 2.7 %) of the total lignin corresponds to S-monomers in the WT (fig. 74 B). Relative content of H- and G-monomers are not altered in the triple knockout mutant *cadc*cadd*fah1-2*. The mutant *esb1* shows a significantly higher increased content of coniferyl monomers by 59 % (4.6 ± 0.5 µg/mg dw in *esb1* and 2.9 ± 0.4 µg/mg dw in WT). The increased content of coniferyl monomers leads to a significantly higher content of 52 % (5.0 ± 0.5 µg/mg dw in *esb1* and 3.3 ± 0.5 µg/mg dw in WT) lignin than in the WT. However, the increased content of coniferyl monomers does not change the relative lignin monomer composition (fig. 74 B).

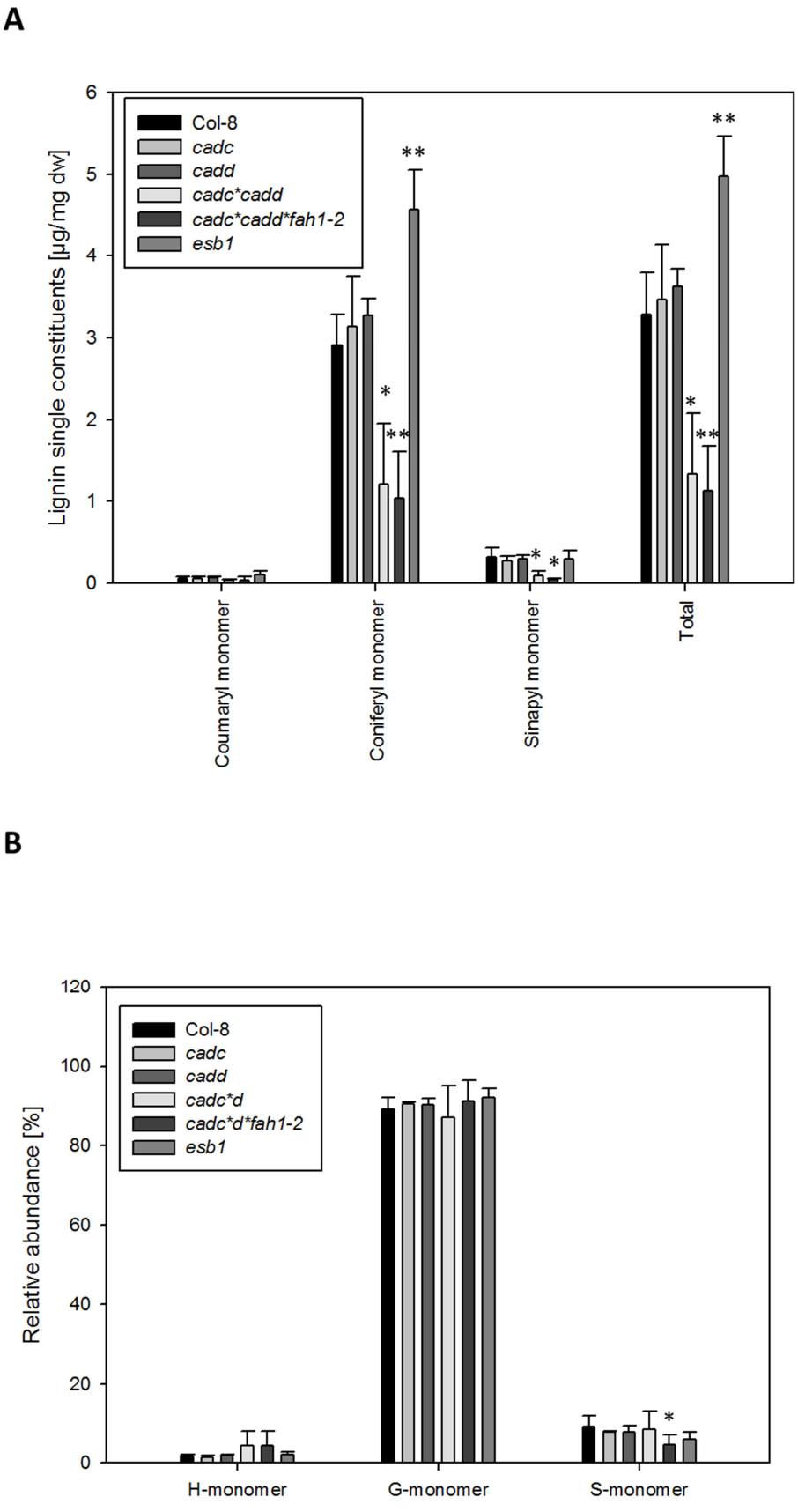

Fig. 74: Comparison of root lignin composition of the mutant lines *cadc*, *cadd*, *cadc*cadd*, *cadc*cadd*fah1-2* and *esb1* with the corresponding WT

Five-week old hydroponically grown roots untreated with cell wall degrading enzymes were analysed. A: Absolute lignin composition related to the root dry weight. B: Relative lignin composition related to the root dry weight. The represented values are the arithmetic mean of the WT and mutant lines respectively and the calculated standard deviation error bars. The sample amount corresponds to four roots of Col-8, *cadc*, *cadd*, three of *cadc*cadd* and *cadc*cadd*fah1-2* and four roots of *esb1*. H-monomer: hydroxycinnamyl-monomer, G-monomer: guiacyl-monomer, S-monomer: sinapyl-monomer. *: student's t-test, $p \leq 0.05$, **: student's t-test, $p \leq 0.01$.

The following set of mutants was untreated with cell wall degrading enzymes as well. The triple knockout mutant *ref8-1*med5a*med5b* shows the strongest increase of lignin. Coniferyl monomers show a 3.3 fold increase, which is highly significant (9.6 ± 1.2 µg/mg dw in *ref8-1*med5a*med5b* and 2.9 ± 0.7 µg/mg dw in WT). Due to this increased coniferyl content the absolute lignin content is significantly increased by 3.2 fold (10.9 ± 1.3 µg/mg dw in *ref8-1*med5a*med5b* and 3.4 ± 1.2 µg/mg dw in WT) as well (fig. 75 A). The relative proportions of the lignin monomers are not altered in *ref8-1*med5a*med5b* (fig. 75 B). The mutant *ref8-2*fah1-2*AtC4H::SmF5H* shows a similar lignin composition as the mutant *C4H::F5H*. Coniferyl monomers are decreased but not significantly by 51 % (1.2 ± 0.5 µg/mg dw in *ref8-2*fah1-2*AtC4H::SmF5H* and 2.9 ± 0.7 µg/mg dw in WT). In contrast to the loss of coniferyl monomers the sinapyl monomers are 7.3 fold-increased, which is highly significant (2.9 ± 1.2 µg/mg dw in *ref8-2*fah1-2*AtC4H::SmF5H* and 0.4 ± 0.3 µg/mg dw in WT) (fig. 75 A). However, total lignin content is not significantly altered in the mutant line compared with the WT. The massive rise of sinapyl monomers generates a shift from the dominant G-compounds to S-compounds. G-monomers reveal a significantly higher decline by 55.8 % (27.1 ± 2.0 % in *ref8-2*fah1-2*AtC4H::SmF5H* and 82.9 ± 7.6 % in WT). In contrast to the relative decline of G-monomers S-monomers are highly significant increased by 54.8 % (67.0 ± 3.3 % in *ref8-2*fah1-2*AtC4H::SmF5H* and 12.2 ± 5.2 % in WT) (fig. 75 B). The single knockout *fah1-2* does not show any alterations in the lignin content and the relative composition to the WT (fig. 75 A and B). *C4H::F5H* shows a deficiency in coniferyl monomers by 86 % (0.4 ± 0.1 µg/mg dw in *C4H::F5H* and 2.9 ± 0.7 µg/mg dw in WT) and the strongest increase of sinapyl monomers by 19.8 fold (7.9 ± 0.2 µg/mg dw in *C4H::F5H* and 0.4 ±0.3 µg/mg dw in WT) which is highly significant. The total lignin content is enhanced by 2.6 fold (8.7 ± 0.4 µg/mg dw in *C4H::F5H* and 3.4 ± 1.2 µg/mg dw in WT) (fig. 75 A). The severely enhanced content of sinapyl-monomers provokes a shift from dominant G-monomers to S-monomers. G-monomers are high significantly decreased by 77.8 % (5.1 ± 1.5 % in *C4H::F5H*

and 82.9 ± 7.6 % in WT), while S-monomers are high significantly increased by 77.9 % (90.1 ± 3.2 % in *C4H::F5H* and 12.2 ± 5.2 % in WT) (fig. 75 B).

In this experimental set one isolated peridermal tissue from roots of *Arabidopsis thaliana* were analysed as well. The same thioethylated aromatic compounds are identified and quantified like in the whole root sample. One mg dry weight of *Arabidopsis thaliana's* peridermal tissue consists of 0.7 µg coumaryl, 6.8 µg coniferyl and 0.6 µg sinapyl monomers. The total aromatic content corresponds to 8.2 µg (fig. 75 A). This leads to a relative composition of 8.5 % H-, 83.6 % G- and 7.9 % S-monomers similar to whole root lignin composition (fig. 75 B).

A

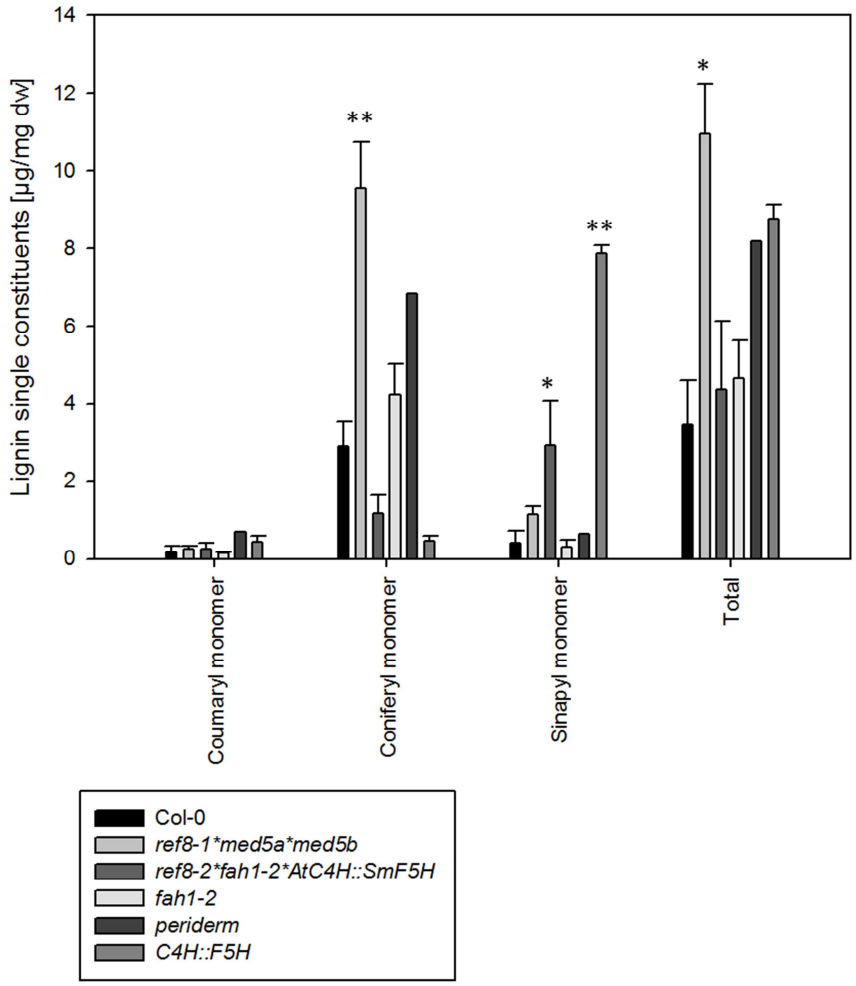

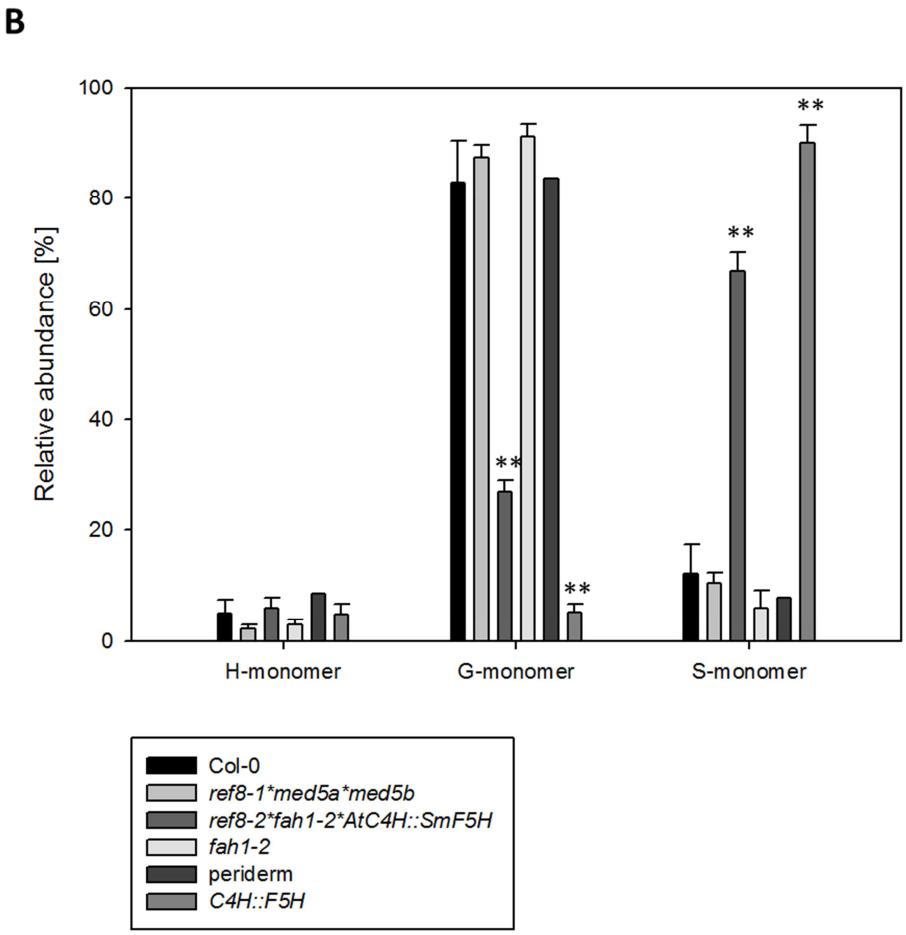

Fig. 75: Comparison of root lignin composition of the mutant lines *ref8-1*med5a*med5b*, *ref8-2*fah1-2*AtC4H::SmF5H*, *fah1-2*, periderm and *C4H::F5H* with the corresponding WT

Five-week old hydroponically grown roots untreated with cell wall degrading enzymes were analysed. A: Absolute lignin composition related to the root dry weight. B: Relative lignin composition related to the root dry weight. The represented values are the arithmetic mean of the WT and mutant lines respectively and the calculated standard deviation error bars. The sample amount corresponds to two roots of Col-0, four of *ref8-1*med5a*med5b*, *ref8-2*fah1-2*AtC4H::SmF5H*, *fah1-2*, one of peridermal tissue and three of *C4H::*F5H. H-monomer: hydroxycinnamyl-monomer, G-monomer: guiacyl-monomer, S-monomer: sinapyl-monomer. *: student's t-test, $p \leq 0.05$, **: student's t-test, $p \leq 0.01$.

Both mutant *ref3-2* and *ref4-3* show highly significant declines in coniferyl and sinapyl monomers. Coniferyl monomers are reduced by 69 % (4.8 ± 0.1 µg/mg dw in *ref3-2* and 15.3 ± 2.6 µg/mg dw in WT) in *ref3-2* and 63 % (5.6 ± 0.5 µg/mg dw in *ref4-3* and 15.3 ± 2.6 µg/mg dw in WT) in *ref4-3*. Sinapyl monomers decline by 81 % (0.5 ± 0.2 µg/mg dw in *ref3-2* and 2.6 ± 0.4 µg/mg dw in WT) in *ref3-2* and 92 % (0.2 ± 0.02 µg/mg dw in *ref4-3* and 2.6 ± 0.4 µg/mg dw in WT) in *ref4-3*. The loss of coniferyl and sinapyl monomers causes a highly significant decline in the total lignin content in *ref3-2* by 69 % (5.7 ± 0.01 µg/mg dw in *ref3-2* and 18.6 ± 3.1 µg/mg dw in WT) in by 66 % (6.3 ± 0.6 µg/mg dw in *ref4-3* and 18.6 ± 3.1 µg/mg dw in

WT) in *ref4-3* less total lignin content compared with the WT (fig. 76 A). The relative composition of *ref3-2* does not change significantly but the high loss of sinapyl monomers in the *ref4-3* mutant provokes significant alterations. H-monomers are increased by 4.9 % (8.0 ± 0.7 % in ref4-3 and 3.1 ± 0.4 µg/mg dw in WT), G-monomers are increased by 5.9 % (88.6 ± 0.1 % in ref4-3 and 82.7 ± 1.2 % in WT) and S-monomers are decreased by 10.7 % (3.4 ± 0.6 % in ref4-3 and 14.1 ± 1.0 % in WT) (fig. 76 B). The mutant *ref1-4* does not show any alterations in the lignin content and relative composition compared with the WT (fig. 76 A and B). The lignin mutant *C4H::F5H* shows a 2.3 fold increased coumaryl monomer content (1.4 ± 0.7 µg/mg dw in *C4H::F5H* and 0.6 ± 0.2 µg/mg dw in WT). Coniferyl monomers are significantly higher decreased by 90 % (1.6 ± 1.1 µg/mg dw in *C4H::F5H* and 15.3 ± 2.6 µg/mg dw in WT), while a 7.8 fold increase of the sinapyl monomers is highly significant enhanced (20.2 ± 4.5 µg/mg dw in *C4H::F5H* and 2.6 ± 0.4 µg/mg dw in WT). Total lignin content is slightly increased by 24.7 % (23.2 ± 5.3 µg/mg dw in *C4H::F5H* and 18.6 ± 3.1 µg/mg dw in WT) (fig. 76 A). The high significant loss of G-monomers and enhanced S-monomers causes a shift in the relative lignin composition from dominant G-monomers to S-monomers. G-monomers show a highly significant reduction by 75.9 % (6.8 ± 3.7 % in *C4H::F5H* and 82.7 ± 1.2 % in WT), whereas S-monomers show a high significant rise by 73.2 % (87.3 ± 1.9 % in *C4H::F5H* and 14.1 ± 1.0 % in WT) (fig. 76 B).

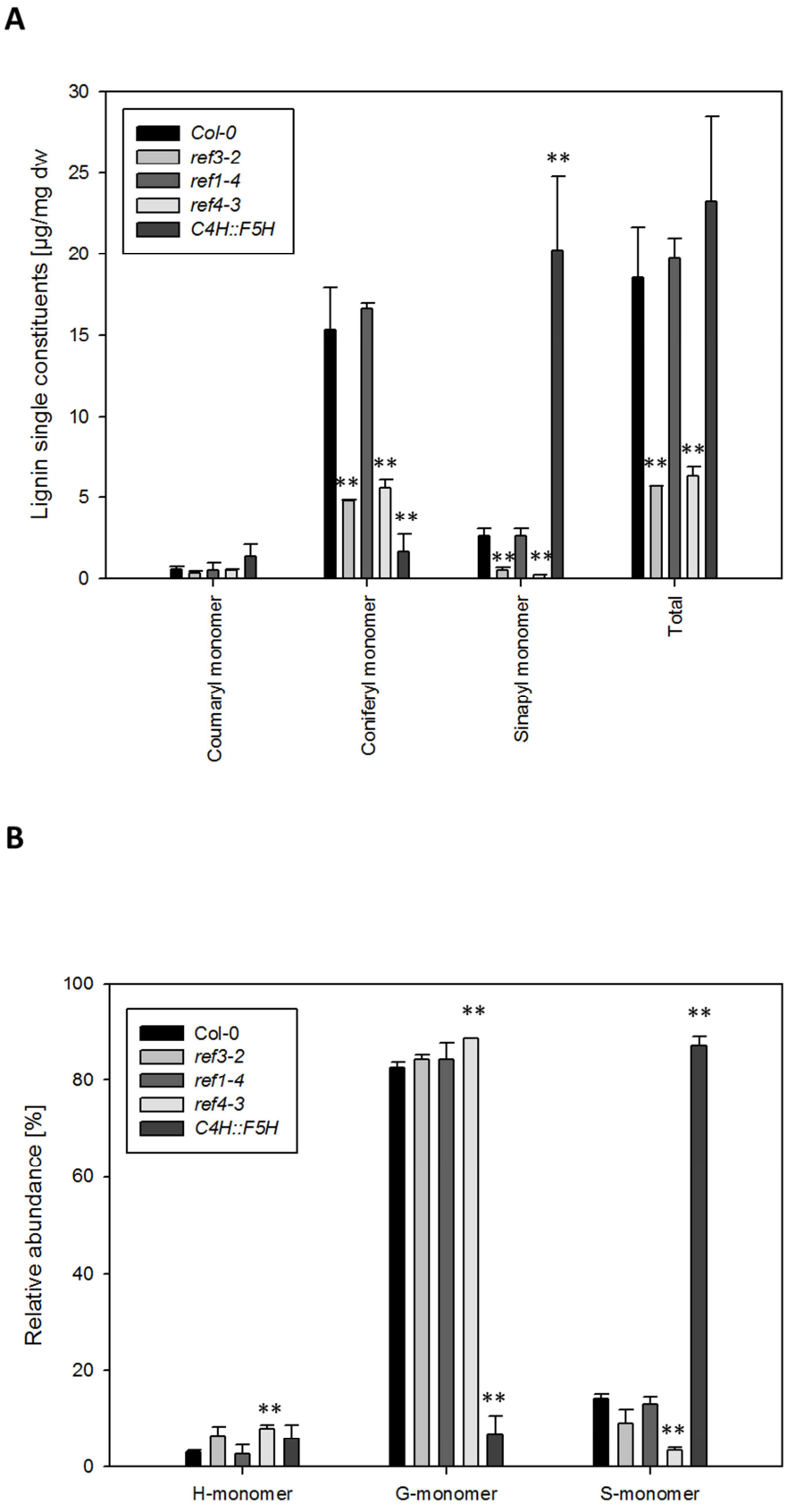

Fig. 76: Comparison of root lignin composition of the mutant lines *ref3-2*, *ref1-4*, *ref4-2* and *C4H::F5H* with the corresponding WT

Five-week old hydroponically grown roots untreated with cell wall degrading enzymes were analysed. A: Absolute lignin composition related to the root dry weight. B: Relative lignin composition related to the root dry weight. The represented values are the arithmetic mean of the WT and mutant lines respectively and the calculated standard deviation error bars. The sample amount corresponds to four roots of Col-0, two of *ref3-2*, three of *ref1-4* and *ref4-3* and four of *C4H::*F5H. H-monomer: hydroxycinnamyl-monomer, G-monomer: guiacyl-monomer, S-monomer: sinapyl-monomer. *: student's t-test, $p \leq 0.05$, **: student's t-test, $p \leq 0.01$.

3.4.2. Determination of the suberin content and composition of whole root systems in different phenylpropanoid pathway mutants

3.4.2.1. Soil-grown roots

Suberin was extracted from five-week old soil-grown roots. The roots were digested with cell wall degrading enzymes. After this treatment lipophilic substances were extracted at first with chloroform and followed by methanol each for 24 hours in a soxhlet-extractor. Afterwards the roots were transesterified by heating the roots in a solution of boron trifluoride in methanol at 70 °C overnight. Transesterification was stopped by adding saturated sodium hydrogen carbonate solution to the samples. Transesterified compounds were extracted with chloroform and the lipophilic phase was washed with HPLC water. The lipophilic phase was dried by water-free sodium sulphate and concentrated under a nitrogen steam. Extracted lipophilic substances were derivatised by using pyridine and BSTFA at 70 °C for 40 minutes. Derivatised lipophilic substances were quantitatively and qualitatively analysed by GC-FID and GC-MS.

In soil-grown roots 23 different aliphatic and aromatic substances were identified. 19 of these substances were identified as suberin aliphatic specific compounds. The remaining four compounds were aromatics. The single constituents of the aliphatic suberin can be divided into the following classes: monocarboxylic acids (C_{16}-C_{24}), primary alcohols (C_{18}-C_{22}), ω-hydroxyacids (C_{16}-C_{24}) and α, ω-dicarboxylic acids (C_{16}-C_{22}). The identified aromatic compounds were *cis* and *trans* coumaric acid as well as *cis* and *trans* ferulic acid.

The evaluation of the data reveals few significant alterations in the content of aliphatic suberin constituents. The mutant line *hqt* exhibits an increased acid content by 59 % (2.7 ± 0.4 µg/mg dw in *hqt* and 1.7 ± 0.6 µg/mg dw in WT) (fig. 77 C). Furthermore, only two minor compounds show significant alterations. The C_{22} alcohol is increased by 2.5 fold (0.32 ± 0.06

µg/mg dw in *hqt* and 0.13 ± 0.06 µg/mg dw in WT) and the C_{24} ω-hydroxy acid is decreased by 50 % (0.04 ± 0.01 µg/mg dw in *hqt* and 0.08 ± 0.03 µg/mg dw in WT) (fig. 77 A). Regarding the aromatic compounds only the *cis* ferulic acid is increased by 4.2 fold (0.88 ± 0.2 µg/mg dw in *hqt* and 0.21 ± 0.08 µg/mg dw in WT) (fig. 77 D).

The mutant line *ccoaomt1* does not show significant alterations in the suberin classes (fig. 77 C). However, the total aliphatic suberin content shows a decline by 30 % (8.9 ± 3.9 µg/mg dw in *ccoaomt1* and 12.6 ± 3.8 µg/mg dw in WT). Only minor compounds are significantly decreased. For example the C_{22} ω-hydroxy acid content shows 50 % (0.48 ± 0.18 µg/mg dw in *ccoaomt1* and 0.96 ± 0.36 µg/mg dw in WT) less content than the WT (fig. 77 A). Highly significant alterations are found in the composition of aromatic substances. The total aromatic substances are decreased by 47 % (1.7 ± 0.8 µg/mg dw in *ccoaomt1* and 3.2 ± 1.1 µg/mg dw in WT). This decline in the aromatic content is caused by the severe decline of *cis* coumaric acid by 80 % (0.04 ± 0.03 µg/mg dw in *ccoaomt* and 0.20 ± 0.10 µg/mg dw in WT), *cis* ferulic acid by 71 % (0.06 ± 0.03 µg/mg dw in *ccoaomt1* and 0.21 ± 0.08 µg/mg dw in WT) and *trans* ferulic acid by 53 % (0.49 ± 0.20 µg/mg dw in *ccoaomt1* and 1.04 ± 0.35 µg/mg dw in WT) (fig. 77 D).

Statistical evaluation of the data from *comt1* does not show any significant alterations. Nevertheless, with respect to the main suberin aliphatic constituents the $C_{18:1}$ ω-hydroxy acid and α, ω-dicarboxylic acid both seem to be enhanced by 28 % ($C_{18:1}$ ω-hydroxy acid: 5.0 ± 2.5 µg/mg dw in *comt1* and 3.9 ± 1.2 µg/mg dw in WT; $C_{18:1}$ α, ω-dicarboxylic acid: 2.3 ± 1.1 µg/mg dw in *comt1* and 1.8 ± 0.5 µg/mg dw in WT) (fig. 77 A). This causes slightly enhanced total suberin content by 29 % (16.3 ± 7.6 µg/mg dw in *comt1* and 12.6 ± 3.8 µg/mg dw in WT) (fig. 77 B). The content of aromatics is slightly induced by 59 % (5.1 ± 2.5 µg/mg dw in *comt1* and 3.2 ± 1.1 µg/mg dw in WT), which is mainly provoked by the increased content of *trans* coumaric acid (3.0 ± 1.8 µg/mg dw in *comt1* and 1.8 ± 0.8 µg/mg dw in WT) (fig. 77 D).

The mutant line *ccr1* is indistinguishable from the WT regarding the suberin as well as aromatic composition and content. The evaluation of the data does not show any significant alterations (fig. 77 B, C and D).

In contrast, the mutant line *myb7* shows slightly enhanced suberin content by 38 % (17.4 ± 4.9 µg/mg dw in *myb7* and 12.6 ± 3.8 µg/mg dw in WT) (fig. 77 C). This increase is linked to the significant and not significant increased content in monocarboxylic acids (C_{18}, C_{22}), primary alcohols (C_{20}, C_{22}), ω-hydroxy acids (C_{18}, $C_{18:1}$, C_{20}, C_{22}) and α, ω-dicarboxylic acids

(C_{16}, $C_{18:1}$, C_{20} and C_{22}). A significantly decreased content is found in C_{20} monocarboxylic acids (0.11 ± 0.08 µg/mg dw in *myb7* and 0.36 ± 0.17 µg/mg dw in WT) (fig. 77 B). Considering the aromatic constituents the *trans* coumaric acid is enhanced by 50 % (2.7 ± 0.4 µg/mg dw in *myb7* and 1.8 ± 0.8 µg/mg dw in WT) and *cis* ferulic acid by 2.1 fold (0.44 ± 0.04 µg/mg dw in *myb7* and 0.21 ± 0.08 µg/mg dw in WT). In total the aromatics are enhanced by 29 % (4.4 ± 0.6 µg/mg dw in *myb7* and 3.4 ± 1.1 µg/mg dw in WT) (fig. 77 D).

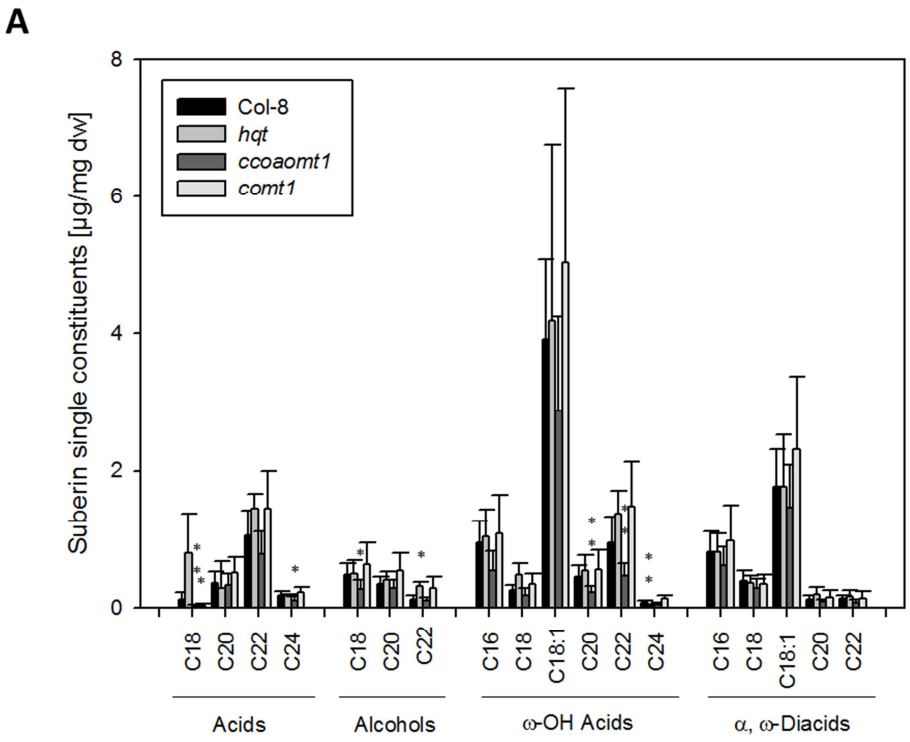

B

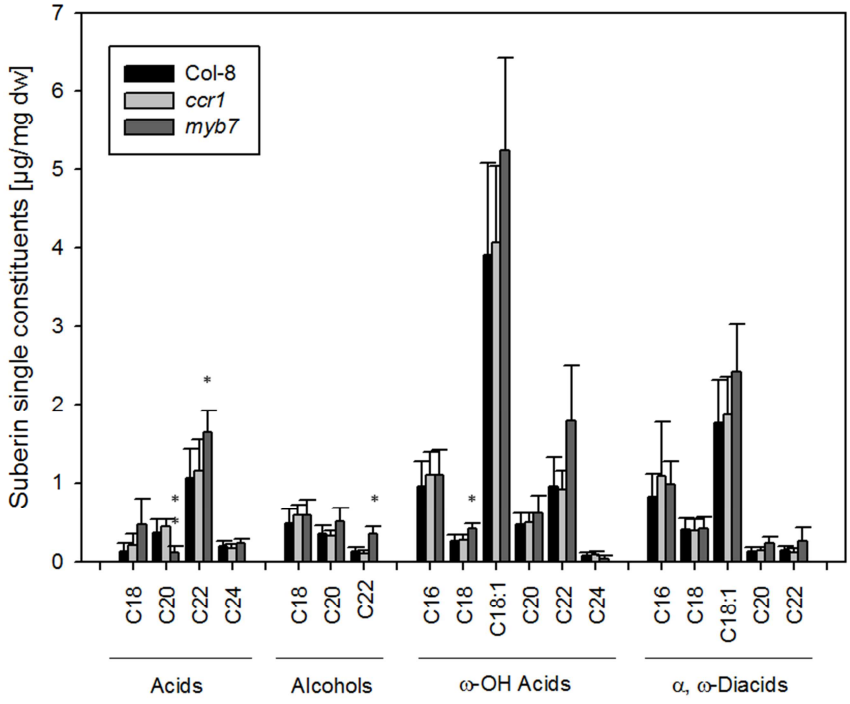
Suberin single constituents [µg/mg dw]
Col-8
ccr1
myb7
C18
C20
C22
C24
C16
C18:1
Acids
Alcohols
ω-OH Acids
α, ω-Diacids

C

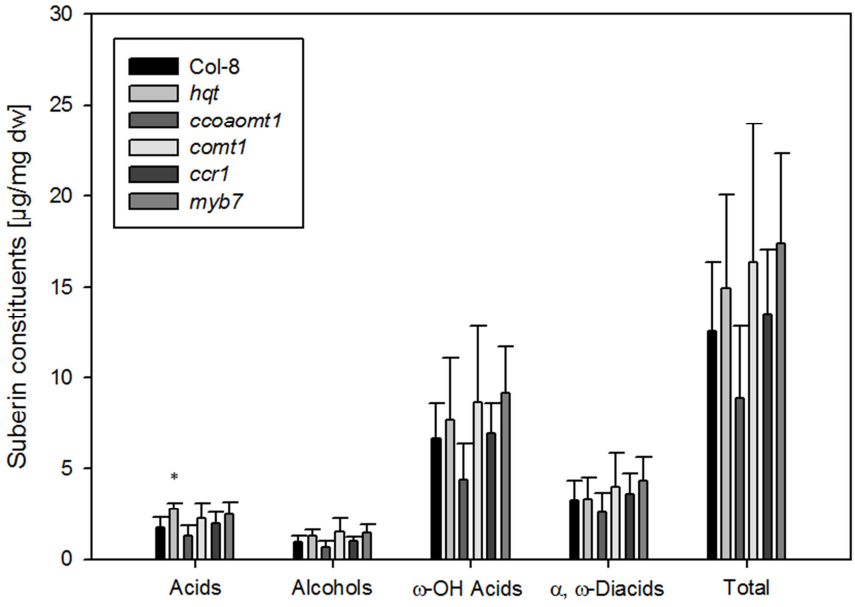
Suberin constituents [µg/mg dw]
Col-8
hqt
ccoaomt1
comt1
ccr1
myb7
Acids
Alcohols
ω-OH Acids
α, ω-Diacids
Total

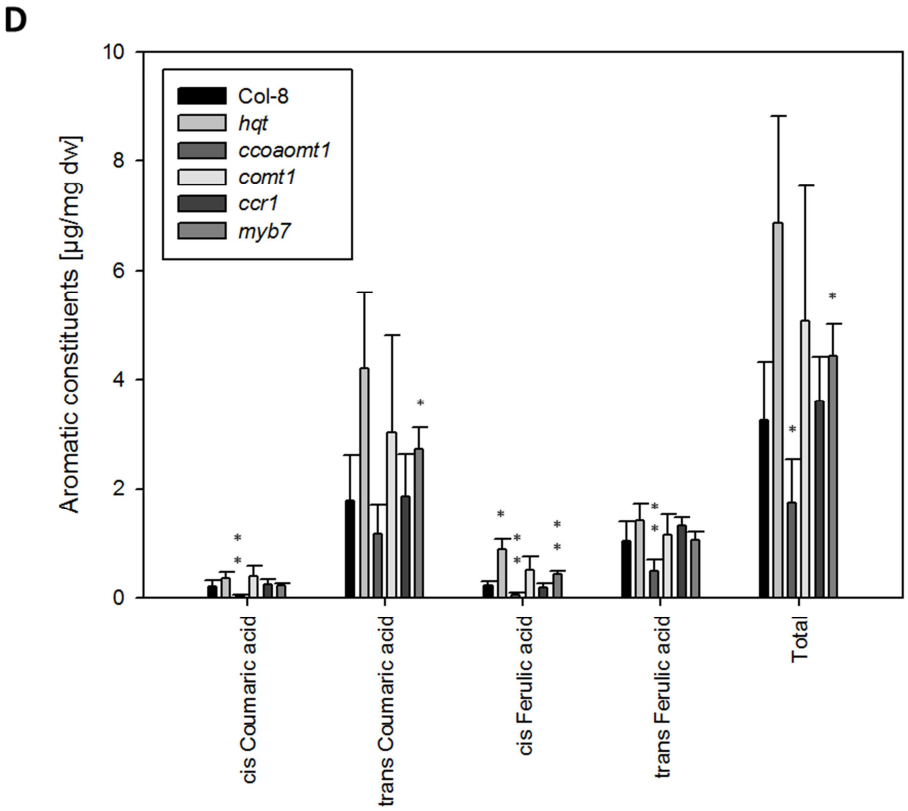

Fig. 77: Comparison of root aliphatic suberin and aromatic compounds of the mutant lines *hqt*, *ccoaomt1*, *comt1*, *ccr1* and *myb7* with the corresponding WT

Five weeks old soil-grown roots treated with cell wall degrading enzymes were analysed. **A**: Composition of the suberin aliphatic single constituents of *hqt*, *ccoaomt1*, *comt1* and WT related to the root dry weight. **B**: Composition of the suberin aliphatic single constituents of ccr1, myb7 and WT related to the root dry weight. **C**: Composition of the suberin aliphatic substance classes related to the root dry weight. **D**: Composition of the aromatic compounds related to the root dry weight. The represented values are the arithmetic mean of the WT and mutant lines respectively and the calculated standard deviation error bars. The sample amount corresponds to 15 roots of WT, three of *hqt*, four of *ccoaomt1*, four of *comt1*, ten of *ccr1* and three of *myb7*. Acids: monocarboxylic acids, Alcohols: primary alcohols, ω-OH Acids: ω-hydroxy acids, α, ω-Diacids: α, ω-dicarboxylic acids, *: student's t-test, $p \leq 0.05$, **: student's t-test, $p \leq 0.01$.

Suberin analysis of *myb4* does not show significant alterations in the total suberin content, the suberin classes and the aromatic constituents. Only the minor compound C_{18} ω-hydroxy acid is significantly increased by 79 % (0.34 ± 0.06 µg/mg dw in *myb4* and 0.19 ± 0.04 µg/mg dw in WT) (fig. 78 A, B and C).

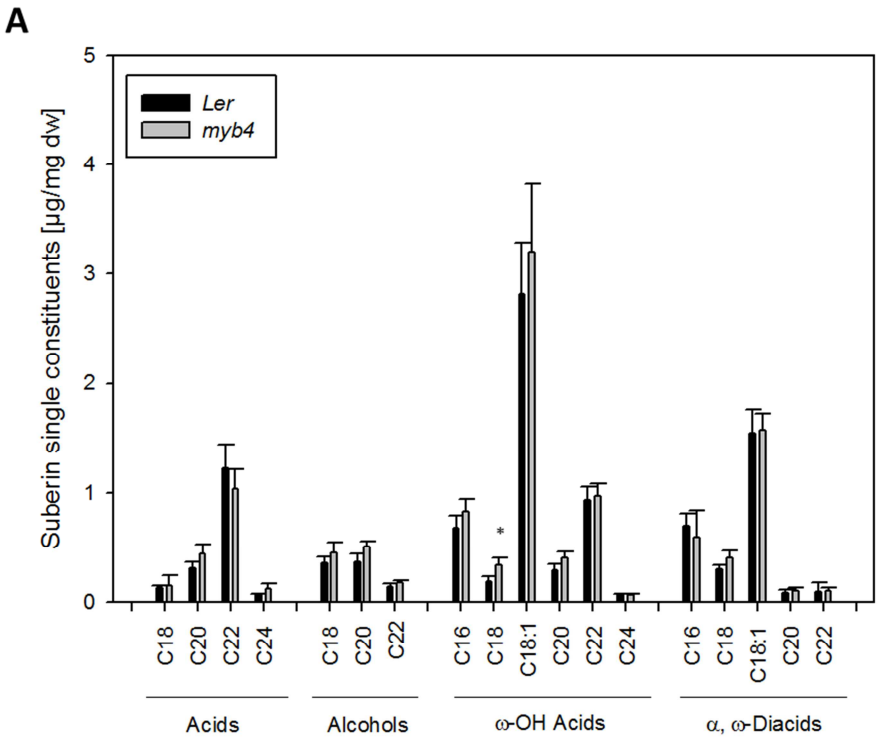
A
Suberin single constituents [µg/mg dw]
Ler
myb4
0
1
2
3
4
5
*
C18
C20
C22
C24
C18
C20
C22
C16
C18
C18:1
C20
C22
C24
C16
C18
C18:1
C20
C22
Acids
Alcohols
ω-OH Acids
α, ω-Diacids

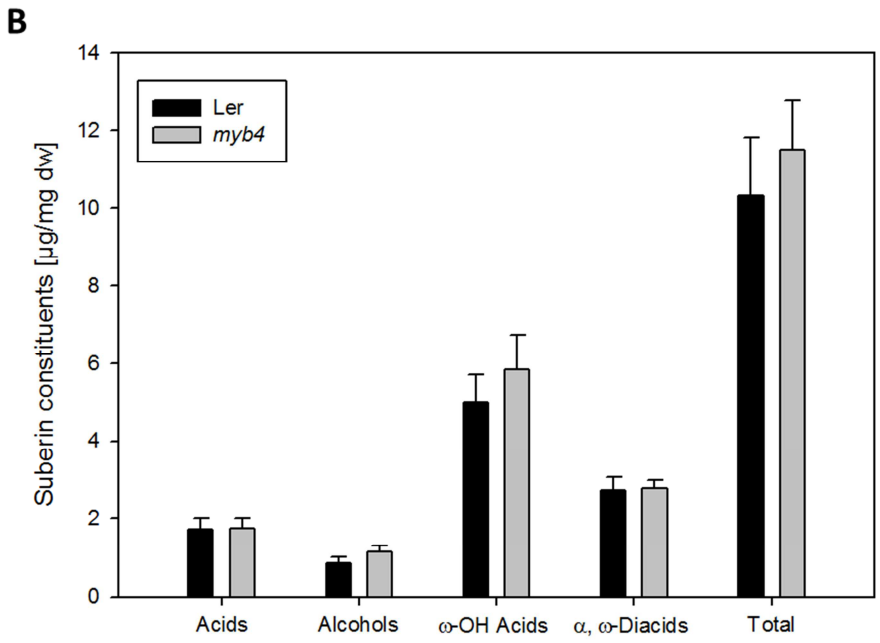
B
Suberin constituents [µg/mg dw]
Ler
myb4
0
2
4
6
8
10
12
14
Acids
Alcohols
ω-OH Acids
α, ω-Diacids
Total

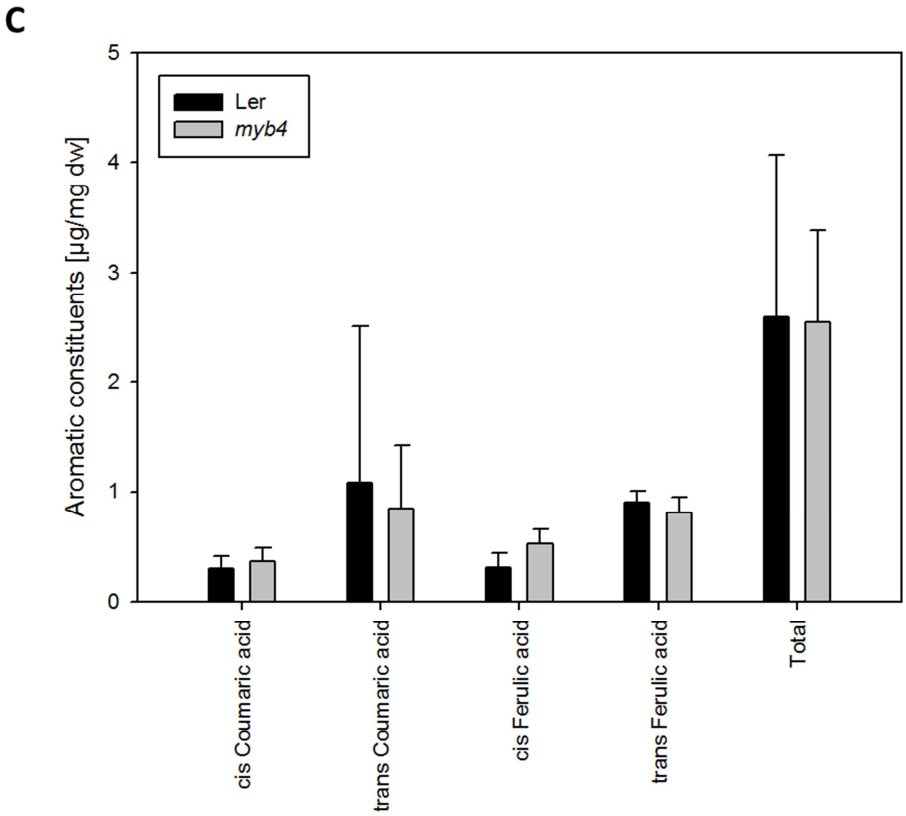

Fig. 78: Comparison of root aliphatic suberin and aromatic compounds of the mutant line *myb4* with the corresponding WT

Five weeks old soil-grown roots treated with cell wall degrading enzymes were analysed. **A**: Composition of the suberin aliphatic single constituents of *myb4* and WT related to the root dry weight. **B**: Composition of the suberin aliphatic substance classes related to the root dry weight. **C**: Composition of the aromatic compounds related to the root dry weight. The represented values are the arithmetic mean of the WT and mutant line respectively and the calculated standard deviation error bars. The sample amount corresponds to three roots of WT and *myb4*. Acids: monocarboxylic acids, Alcohols: primary alcohols, ω-OH Acids: ω-hydroxy acids, α, ω-Diacids: α, ω-dicarboxylic acids*: student's t-test, $p \leq 0.05$, **: student's t-test, $p \leq 0.01$.

The evaluation of suberin analysis reveals statistical significant alterations in the suberin content of *cadc* mutant. The total suberin content is decreased by 31 % (10.2 ± 2.3 µg/mg dw in *cadc* and 14.7 ± 4.7 µg/mg dw in WT). The decline in suberin content is mainly linked to the monocarboxylic acids and ω-hydroxy acids. The monocarboxylic acids are decreased by 26 % (1.4 ± 0.2 µg/mg dw in *cadc* and 1.9 ± 0.5 µg/mg dw in WT) and ω-hydroxy acids by 35 % (5.4 ± 1.7 µg/mg dw in *cadc* and 8.3 ± 3.1 µg/mg dw in WT) (fig. 79 B). This effect is especially found in the C_{18} monocarboxylic acid, $C_{18:1}$ and C_{22} ω-hydroxy acid and $C_{18:1}$ as well as C_{22} α, ω-dicarboxylic acid. However, the main substance both $C_{18:1}$ ω-hydroxy acid and α, ω-dicarboxylic acid do not show significant alterations compared to the WT (fig. 79 A). With

respect to the aromatics the *trans* coumaric acid is significantly decreased by 72 % (0.37 ± 0.25 µg/mg dw in *cadc* and 1.34 ± 0.98 µg/mg dw in WT). This provoked a decline of aromatic content by 27 % (2.2 ± 0.2 µg/mg dw in *cadc* and 3.0 ± 1.2 µg/mg dw in WT). However, the content of *trans* ferulic acid is not affected but the minor compound *cis* ferulic acid seems to be significantly increased by 73 % (0.64 ± 0.07 µg/mg dw in *cadc* and 0.37 ± 0.34 µg/mg dw in WT) (fig. 79 C).

High similarity in the suberin composition and content between *cadd* mutant and WT is determinable. Only minor compounds like C_{18}, C_{20} monocarboxylic acid and C_{18} α, ω-dicarboxylic acid reveal significant alterations. But these alterations do not influence the suberin content or composition. The content of aromatics is enhanced by 53% (4.6 ± 1.0 µg/mg dw in *cadd* and 3.0 ± 1.2 µg/mg dw in WT). However, the increased content is not significant. But significant alterations are found in *cis* and *trans* coumaric acid content. Both contents are increased by 3.2 fold (0.35 ± 0.1 µg/mg dw in *cadd* and 0.11 ± 0.08 µg/mg dw in WT) and by 2.1 fold (2.7 ± 0.7 µg/mg dw in *cadd* and 1.3 ± 1.0 µg/mg dw in WT) (fig. 79 A, B and C).

The double knockout *cadc*cadd* shows no significant alterations in the suberin aliphatic classes and content. There is only one significantly decreased content of C_{24} monocarboxylic acid (0.10 ± 0.05 µg/mg dw in *cadc*cadd* and 0.18 ± 0.05 µg/mg dw in WT). The content of *cis* coumaric acid is increased by 2.2 fold (0.24 ± 0.04 µg/mg dw in *cadc*cadd* and 0.11 ± 0.08 µg/mg dw in WT), whereas the content of *cis* ferulic acid is decreased by 78 % (0.08 ± 0.07 µg/mg dw in *cadc*cadd* and 0.37 ± 0.34 µg/mg dw in WT) (fig. 79 A, B and C)).

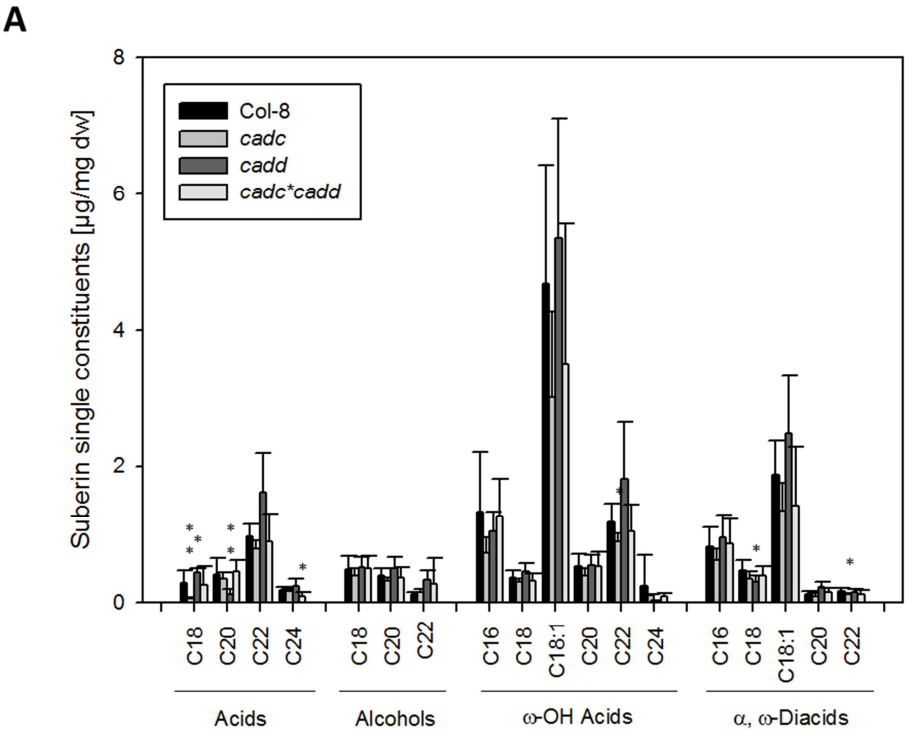
A
Suberin single constituents [µg/mg dw]
Col-8
cadc
cadd
cadc*cadd
C18
C20
C22
C24
C18
C20
C22
C16
C18
C18:1
C20
C22
C24
C16
C18
C18:1
C20
C22
Acids
Alcohols
ω-OH Acids
α, ω-Diacids

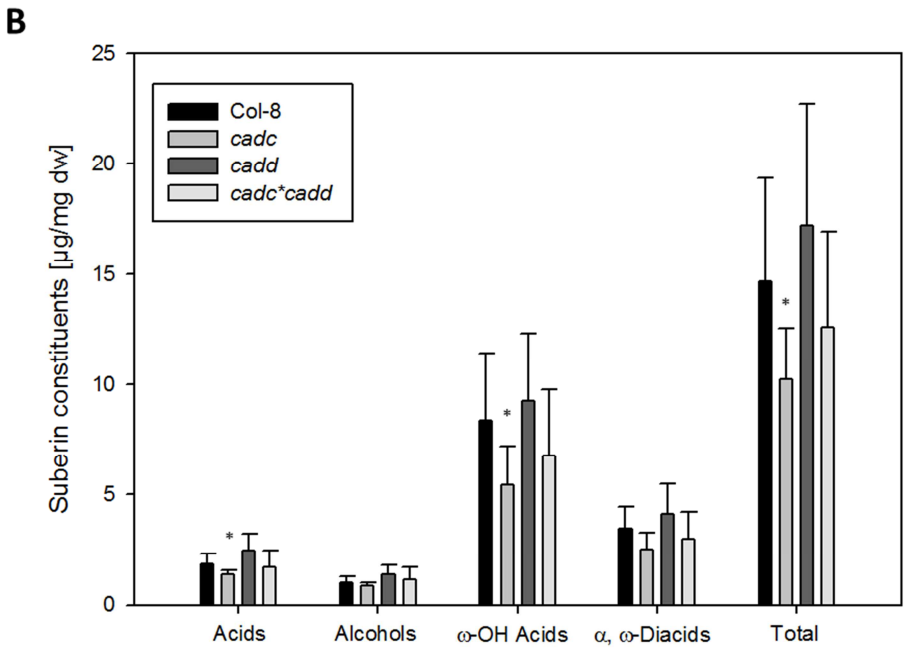
B
Suberin constituents [µg/mg dw]
Col-8
cadc
cadd
cadc*cadd
Acids
Alcohols
ω-OH Acids
α, ω-Diacids
Total

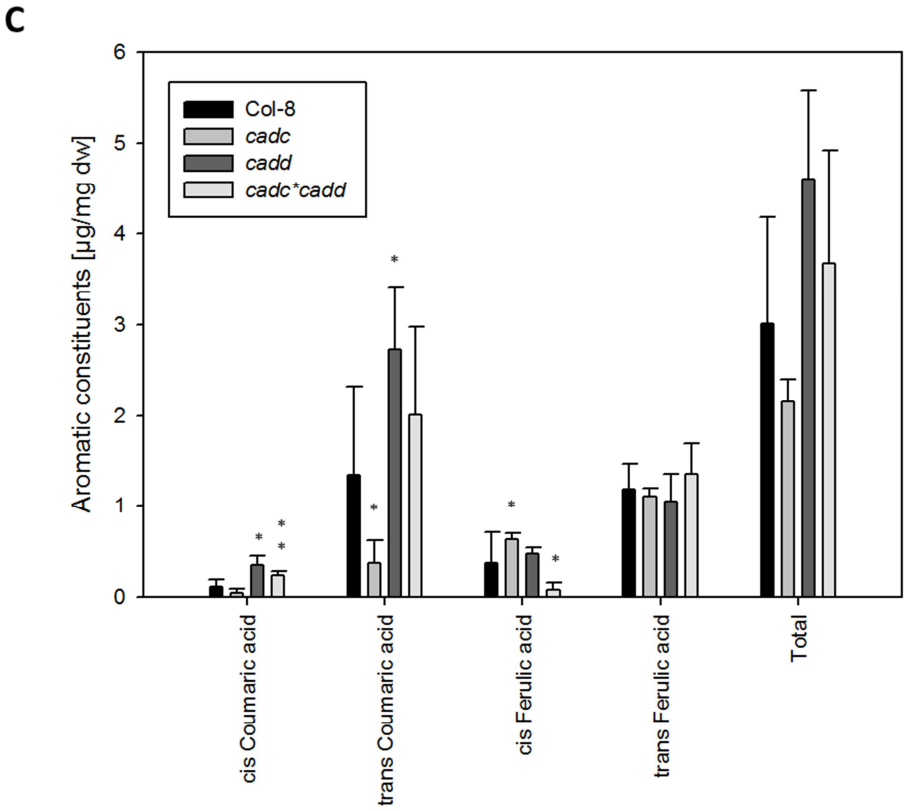

Fig. 79: Comparison of root aliphatic suberin and aromatic compounds of the mutant lines *cadc*, *cadd* and *cadc*cadd* with the corresponding WT

Five weeks old soil-grown roots treated with cell wall degrading enzymes were analysed. **A**: Composition of the suberin aliphatic single constituents of *cadc*, *cadd*, *cadc*cadd* and WT related to the root dry weight. **B**: Composition of the suberin aliphatic substance classes related to the root dry weight. **C**: Composition of the aromatic compounds related to the root dry weight. The represented values are the arithmetic mean of the WT and mutant lines respectively and the calculated standard deviation error bars. The sample amount corresponds to ten roots of WT, four of *cadc*, three of *cadd* and four of *cadc*cadd*. Acids: monocarboxylic acids, Alcohols: primary alcohols, ω-OH Acids: ω-hydroxy acids, α, ω-Diacids: α, ω-dicarboxylic acids*: student's t-test, $p \leq 0.05$, **: student's t-test, $p \leq 0.01$.

The statistical evaluation of *ref8-1* shows an enhanced suberin content by 36 % (14.3 ± 5.0 µg/mg dw in *ref8-1* and 10.5 ± 4.7 µg/mg dw in WT). Significantly increased content of monocarboxylic acids by 2.3 fold (3.2 ± 1.5 µg/mg dw in *ref8-1* and 1.4 ± 0.5 µg/mg dw in WT) causes mainly the enhanced content of suberin (fig. 80 B). Chain length of C_{18} and C_{22} contribute to the increased content of monocarboxylic acid. Furthermore, the content of C_{16} α, ω-dicarboxylic acid is significantly enhanced by 65 % (0.99 ± 0.33 µg/mg dw in *ref8-1* and 0.60 ± 0.30 µg/mg dw in WT) (fig. 80 A). The aromatics are decreased by 27 % (2.4 ± 0.8 µg/mg dw in *ref8-1* and 3.3 ± 1.2 µg/mg dw in WT). Especially, the content of *trans* ferulic

acid reveals a significant decline by 30 % (0.77 ± 0.20 µg/mg dw in *ref8-1* and 1.1 ± 0.2 µg/mg dw in WT) (fig. 80 C).

The triple knockout mutant *ref8-1*med5a*med5b* shows a significantly decreased content of α, ω-dicarboxylic acids by 29 % (2.4 ± 0.5 µg/mg dw in *ref8-1*med5a*med5b* and 3.4 ± 0.4 µg/mg dw in WT) (fig. 80 B). In contrast to the decreased content of α, ω-dicarboxylic acids the content of C_{18} and C_{24} ω-hydroxy acid is high significantly raised by 66 % (0.4 ± 0.07 µg/mg dw in *ref8-1*med5a*med5b* and 0.24 ± 0.08 µg/mg dw in WT) and 3.1 fold (0.22 ± 0.18 µg/mg dw in *ref8-1*med5a*med5b* and 0.07 ± 0.03 µg/mg dw in WT) respectively (fig. 80 A). With respect to the aromatics the total content is significantly decreased by 36 % (2.1 ± 0.4 µg/mg dw in *ref8-1*med5a*med5b* and 3.3 ± 1.2 µg/mg dw in WT). This is linked to the decline of *trans* coumaric acid by 45 % (1.1 ± 0.3 µg/mg dw in *ref8-1*med5a*med5b* and 2.0 ± 0.9 µg/mg dw in WT) and *cis* ferulic acid by 75 % (0.02 ± 0.01 µg/mg dw in *ref8-1*med5a*med5b* and 0.08 ± 0.07 µg/mg dw in WT) (fig. 80 C).

Based on the statistical evaluation the mutant *ref8-2*fah1-2*AtC4H::SmF5H* does not show significant alterations. However, it seems that the total suberin content is enhanced by 2.6 fold (27.0 ± 12.0 µg/mg dw in *ref8-2*fah1-2*AtC4H::SmF5H* and 10.5 ± 4.7 µg/mg dw in WT) (fig. 80 B). Both main compounds $C_{18:1}$ ω-hydroxy acid and α, ω-dicarboxylic acid appears to be increased by 2.3 fold (8.2 ± 2.3 µg/mg dw in *ref8-2*fah1-2*AtC4H::SmF5H* and 3.5 ± 1.9 µg/mg dw in WT) and by 2.9 fold (4.0 ± 1.9 µg/mg dw in *ref8-2*fah1-2*AtC4H::SmF5H* and 1.4 ± 0.6 µg/mg dw in WT). At least significantly increased content are detected in chain length of C_{18} and C_{20} α, ω-dicarboxylic acid (C_{18}: 0.63 ± 0.06 µg/mg dw in *ref8-2*fah1-2*AtC4H::SmF5H* and 0.32 ± 0.19 µg/mg dw in WT, C_{20}: 0.21 ± 0.03 µg/mg dw in *ref8-2*fah1-2*AtC4H::SmF5H* and 0.09 ± 0.04 µg/mg dw in WT) (fig. 80 A). Considering the aromatics the total content seems to be slightly decreased by 21 % (2.6 ± 0.4 µg/mg dw in *ref8-2*fah1-2*AtC4H::SmF5H* and 3.3 ± 1.2 µg/mg dw in WT). This is provoked by the decline of *trans* coumaric acid by 50 % (1.0 ± 0.5 µg/mg dw in *ref8-2*fah1-2*AtC4H::SmF5H* and 2.0 ± 0.9 µg/mg dw in WT) (fig. 80 C).

The mutant line *fah1-2* does not show significant alterations in the suberin aliphatic and aromatic composition and content from the statistical evaluation (fig. 80 A, B and C).

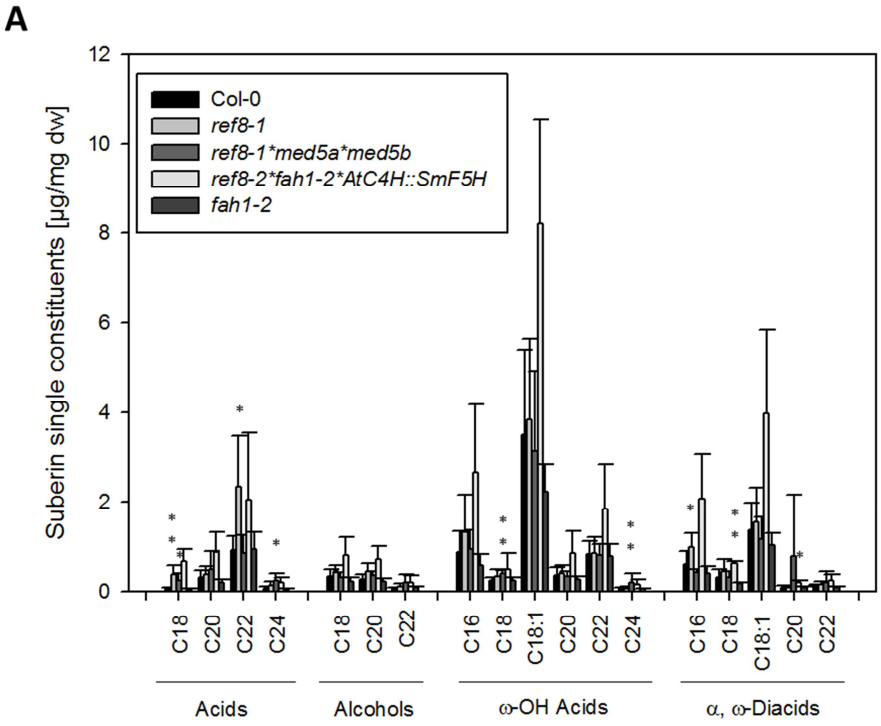
A
Suberin single constituents [µg/mg dw]
Col-0
ref8-1
ref8-1*med5a*med5b
ref8-2*fah1-2*AtC4H::SmF5H
fah1-2
C18
C20
C22
C24
C18
C20
C22
C16
C18
C18:1
C20
C22
C24
C16
C18
C18:1
C20
C22
Acids
Alcohols
ω-OH Acids
α, ω-Diacids

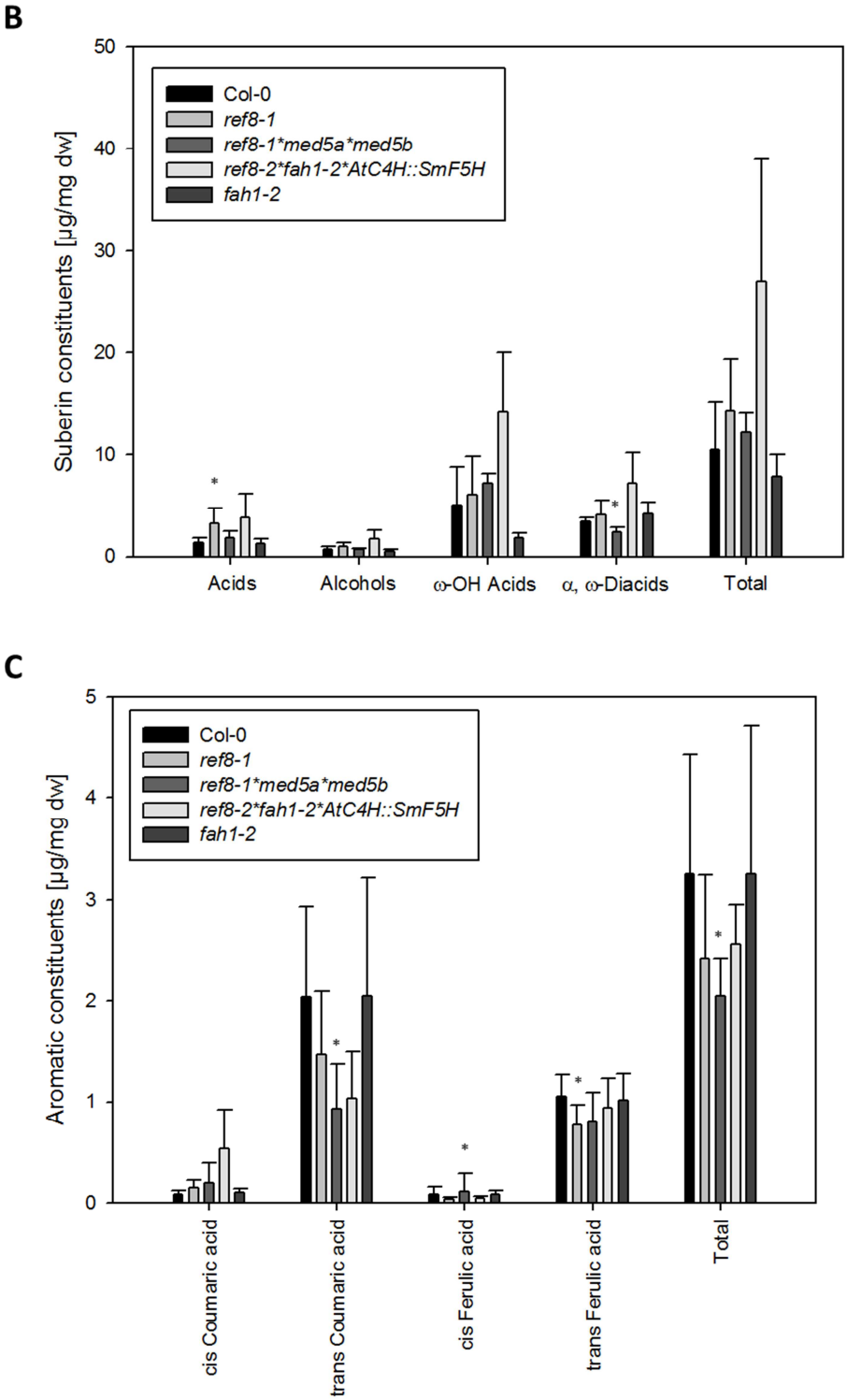

Fig. 80: Comparison of root aliphatic suberin and aromatic compounds of the mutant line *ref8-1*, *ref8-1*med5a*med5b*, *ref8-2*fah1-2*AtC4H::SmF5H* and *fah1-2* with the corresponding WT

Five weeks old soil-grown roots treated with cell wall degrading enzymes were analysed. **A**: Composition of the suberin aliphatic single constituents of *ref8-1*, *ref8-1*med5a*med5b*, *ref8-2*fah1-2*AtC4H::SmF5H*, *fah1-2* and WT related to the root dry weight. **B**: Composition of the suberin aliphatic substance classes related to the root dry weight. **C**: Composition of the aromatic compounds related to the root dry weight. The represented values are the arithmetic mean of the WT and mutant lines respectively and the calculated standard deviation error bars. The sample amount corresponds to eight roots

of WT, six of *ref8-1*, four of *ref8-1*med5a*med5b*, two of *ref8-2*fah1-2*AtC4H::SmF5H* and four of *fah1-2*. Acids: monocarboxylic acids, Alcohols: primary alcohols, ω-OH Acids: ω-hydroxy acids, α, ω-Diacids: α, ω-dicarboxylic acids*: student's t-test, $p \leq 0.05$, **: student's t-test, $p \leq 0.01$.

The suberin content is significantly increased in *ref3-2*. About 3.0 fold (33.7 ± 11.8 µg/mg dw in *ref3-2* and 11.4 ± 2.6 µg/mg dw in WT) more suberin is found in *ref3-2* in comparison to the WT (fig. 81 B). All aliphatic suberin classes show higher proportions than the WT. Significant higher amounts are detected in ω-hydroxy (15.3 ± 4.7 µg/mg dw in *ref3-2* and 6.2 ± 1.6 µg/mg dw in WT) and α, ω-dicarboxylic acids (11.6 ± 4.1 µg/mg dw in *ref3-2* and 3.0 ± 0.63 µg/mg dw in WT) (fig. 81 B). Many single constituents of suberin are significantly increased. For instance, C_{22} monocarboxylic acid is increased by 3.4 fold (2.9 ± 1.3 µg/mg dw in *ref3-2* and 0.86 ± 0.17 µg/mg dw in WT), C_{20} primary alcohol by 3.2 fold (0.98 ± 0.35 µg/mg dw in *ref3-2* and 0.31 ± 0.09 µg/mg dw in WT), $C_{18:1}$ ω-hydroxy acid by 2.4 fold (8.5 ± 2.1 µg/mg dw in *ref3-2* and 3.5 ± 1.1 µg/mg dw in WT) and $C_{18:1}$ α, ω-dicarboxylic acid by 3.6 fold (5.7 ± 1.4 µg/mg dw in *ref3-2* and 1.6 ± 0.3 µg/mg dw in WT) (fig. 81 A). With respect to the aromatic constituents almost all aromatics are significantly increased. Only the amount of *trans* ferulic acid is not significantly altered in *ref3-2* in comparison to the WT. Due to the increased proportions of aromatics, the total aromatic content is increased by 90 % (3.7 ± 0.56 µg/mg dw in *ref3-2* and 2.0 ± 1.3 µg/mg dw in WT) (fig. 81 C).

Neither the content of suberin aliphatic classes and aromatics nor the composition is altered in *ref1-4*. Only the C_{20} monocarboxylic acid shows a significantly increase by 43 % (0.50 ± 0.08 µg/mg dw in *ref1-4* and 0.35 ± 0.09 µg/mg dw in WT) (fig. 81 A).

All suberin aliphatic classes show a significant rise in *ref4-3* in comparison to the WT. The content of monocarboxylic acids is increased by 36 % (1.9 ± 0.13 µg/mg dw in *ref4-3* and 1.4 ± 0.28 µg/mg dw in WT), primary alcohols by 48 % (1.3 ± 0.17 µg/mg dw in *ref4-3* and 0.88 ± 0.20 µg/mg dw in WT), ω-hydroxy acids by 73 % (10.7 ± 2.3 µg/mg dw in *ref4-3* and 6.2 ± 1.6 µg/mg dw in WT) and α, ω-dicarboxylic acids by 50 % (4.5 ± 0.70 µg/mg dw in *ref4-3* and 3.0 ± 0.63 µg/mg dw in WT). In total 61 % (18.4 ± 3.2 µg/mg dw in *ref4-3* and 11.4 ± 2.6 µg/mg dw in WT) more suberin is found in *ref4-3* than in the WT (fig. 81 B). Similar to *ref3-2* many suberin single constituents are significantly increased. For instance, significant higher amounts are found in C_{20} monocarboxylic acid (0.58 ± 0.06 µg/mg dw in *ref4-3* and 0.35 ± 0.09 µg/mg dw in WT), C_{20} primary alcohol (0.48 ± 0.04 µg/mg dw in *ref4-3* and 0.31 ± 0.09 µg/mg dw in WT), $C_{18:1}$ ω-hydroxy acid (6.6 ± 1.6 µg/mg dw in *ref4-3* and 3.5 ± 1.1 µg/mg dw

in WT) and $C_{18:1}$ α, ω-dicarboxylic acid (2.4 ± 0.39 µg/mg dw in *ref4-3* and 1.6 ± 0.33 µg/mg dw in WT) (fig. 81 A). In general, the content of aromatic constituents is significantly increased by 70 % (3.4 ± 0.71 µg/mg dw in ref4-3 and 2.0 ± 1.3 µg/mg dw in WT). The content of *cis* coumaric and *cis* ferulic acid are increased by 3.3 fold (0.26 ± 0.06 µg/mg dw in *ref4-3* and 0.08 ± 0.06 µg/mg dw in WT) and by 2.8 fold (0.31 ± 0.08 µg/mg dw in *ref4-3* and 0.11 ± 0.08 µg/mg dw in WT) respectively, whereas *trans* coumaric and *trans* ferulic acid tend to show higher amounts than the WT (fig. 81 C).

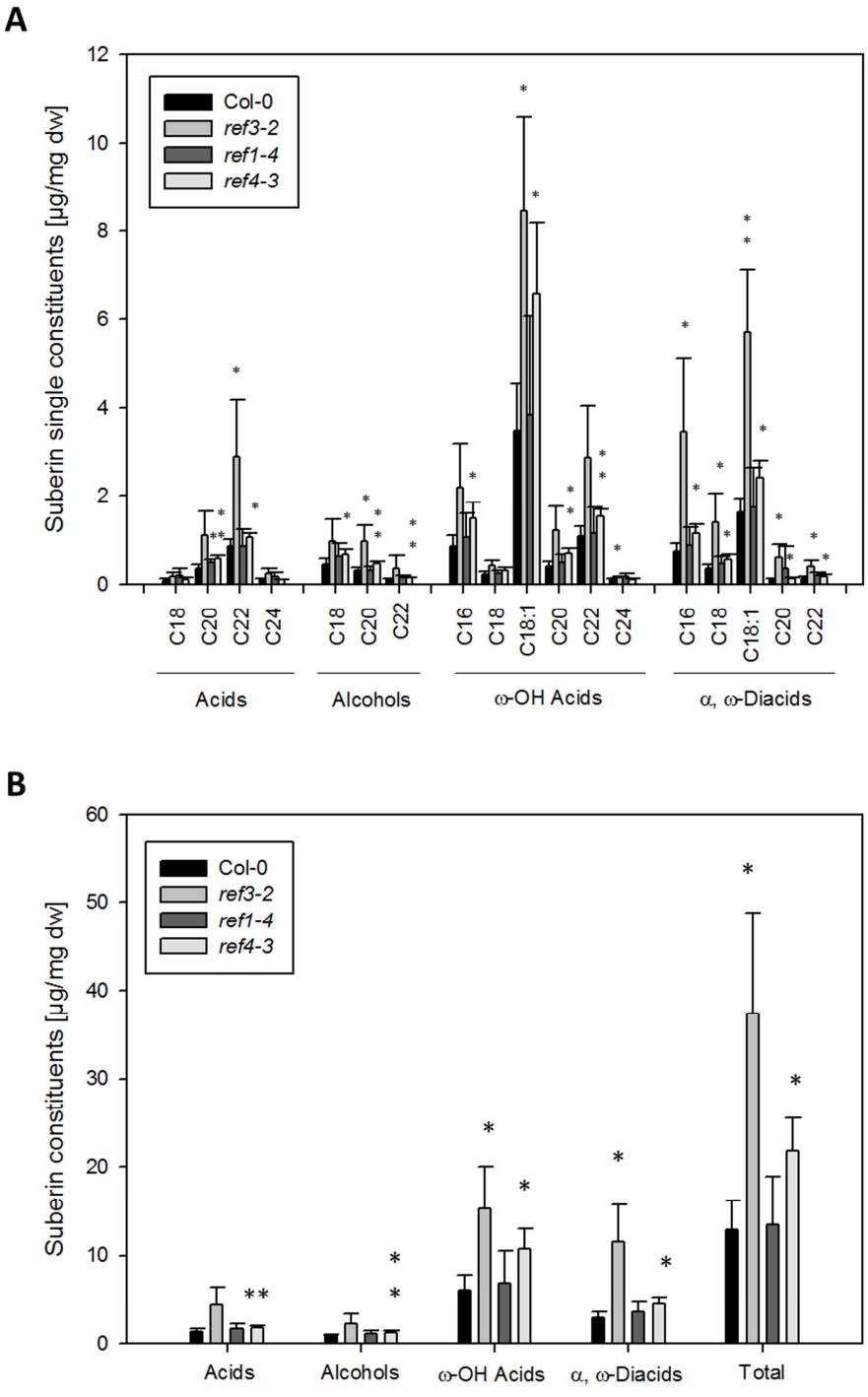

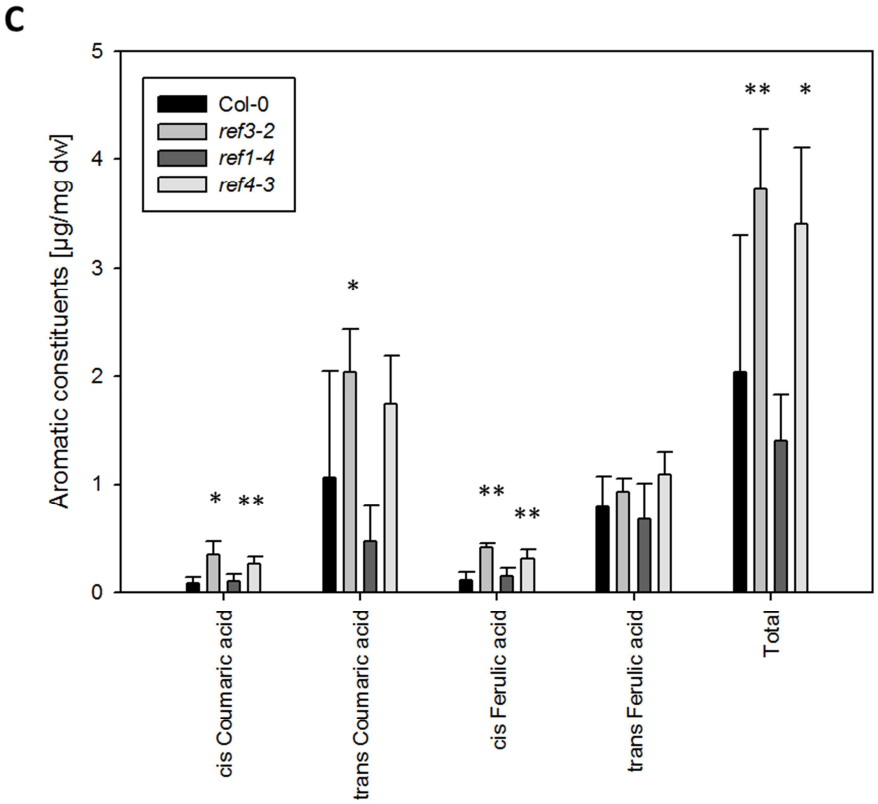

Fig. 81: Comparison of root aliphatic suberin and aromatic compounds of the mutant line *ref3-2*, *ref1-4* and *ref4-3* with the corresponding WT

Five weeks old soil-grown roots treated with cell wall degrading enzymes were analysed. **A**: Composition of the suberin aliphatic single constituents of *ref3*-2, *ref1-4*, *ref4-3* and WT related to the root dry weight. **B**: Composition of the suberin aliphatic substance classes related to the root dry weight. **C**: Composition of the aromatic compounds related to the root dry weight. The represented values are the arithmetic mean of the WT and mutant lines respectively and the calculated standard deviation error bars. The sample amount corresponds to nine roots of WT, four of *ref3-2*, five of *ref1-4*, four of *ref4-3*. Acids: monocarboxylic acids, Alcohols: primary alcohols, ω-OH Acids: ω-hydroxy acids, α, ω-Diacids: α, ω-dicarboxylic acids*: student's t-test, $p \leq 0.05$, **: student's t-test, $p \leq 0.01$.

3.4.2.2. Hydroponically grown roots

Suberin was extracted from the same experimental set of hydroponically grown roots as well. As already described in 3.4.1., some experimental sets were treated with cell wall degrading enzymes and mutant sets sensitive to cell wall degrading enzymes were not digested. In contrast to soil-grown roots focus of the suberin analysis of hydroponically grown roots was on aromatic constituents as well. In total 27 components were identified. 19 of these components are aliphatic substances and eight substances are aromatics. The same aliphatic constituents as in the soil-grown roots were identified. The identified

aromatic constituents are *trans* coumaric acid, vanillin, vanillic acid, *cis* ferulic acid, *trans* ferulic acid, diferulic acid, syringa aldehyde and syringic acid.

Statistical analysis of the mutant line *hqt* reveals there are no significant alterations in the aliphatic suberin content (fig. 82 C). Only the minor compound C_{16} ω-hydroxy acid shows a significantly decreased content by 49 % (0.42 ± 0.19 µg/mg dw in *hqt* and 0.82 ± 0.37 µg/mg dw in WT) (fig. 82 A). Considering the aromatic constituents *cis* ferulic acid is significantly decreased by 88 % (0.006 ± 0.002 µg/mg dw in *hqt* and 0.05 ± 0.05 µg/mg dw in WT) and syringa aldehyde by 44 % (0.05 ± 0.02 µg/mg dw in *hqt* and 0.09 ± 0.05 µg/mg dw in WT) (fig. 82 E).

The mutant line *ccoaomt1* shows decreased suberin content by 20 % (7.4 ± 0.1 µg/mg dw in *ccoaomt1* and 9.2 ± 2.8 µg/mg dw in WT). However, this decreased suberin content is not significant. Nevertheless, the decreased suberin content is linked to the significant decline of ω-hydroxy acids by 32 % (3.2 ± 0.5 µg/mg dw in *ccoaomt1* and 4.7 ± 1.8 µg/mg dw in WT) (fig. 82 C). Especially, chain length of C_{20}, C_{22} and C_{24} are affected in the ω-hydroxy acids (fig. 82 A). Furthermore, the statistical evaluation reveals significant alterations in the aromatic constituents. The content of *trans* coumaric acid is enhanced by 3.4 fold (0.17 ± 0.02 µg/mg dw in *ccoaomt1* and 0.05 ± 0.02 µg/mg dw in WT), whereas the content of *cis* ferulic acid, *trans* ferulic acid, diferulic acid and syringa aldehyde are decreased between 45 % and 80 % (*cis* ferulic acid: 0.01 ± 0.003 µg/mg dw in *ccoaomt1* and 0.05 ± 0.05 µg/mg dw in WT, *trans* ferulic acid: 0.06 ± 0.02 µg/mg dw in *ccoaomt1* and 0.11 ± 0.04 µg/mg dw in WT, diferulic acid: 0.02 ± 0.01 µg/mg dw in *ccoaomt1* and 0.08 ± 0.02 µg/mg dw in WT, syringa aldehyde: 0.05 ± 0.01 µg/mg dw in *ccoaomt1* and 0.09 ± 0.05 µg/mg dw in WT) (fig. 82 E).

The mutant *comt1* does show few significant alterations in minor compounds like C_{18} primary alcohol (0.41 ± 0.05 µg/mg dw in *comt1* and 0.29 ± 0.09 µg/mg dw in WT) or in the major compound $C_{18:1}$ ω-hydroxy acid (3.6 ± 0.4 µg/mg dw in *comt1* and 2.7 ± 1.2 µg/mg dw in WT) (fig. 82 A). The most dominant effects of *comt1* are detectable in the aromatic constituents. The content of *trans* coumaric acid, *trans* ferulic acid and diferulic acid are increased between 1.8 to 2.4 fold (*trans* coumaric acid: 0.09 ± 0.03 µg/mg dw in *comt1* and 0.05 ± 0.02 µg/mg dw in WT, *trans* ferulic acid: 0.26 ± 0.07 µg/mg dw in *comt1* and 0.11 ± 0.04 µg/mg dw in WT, diferulic acid: 0.14 ± 0.03 µg/mg dw in *comt1* and 0.08 ± 0.02 µg/mg dw in WT), whereas syringa aldehyde and syringic acid are decreased between 50 to 67 %

(syringa aldehyde: 0.03 ± 0.01 µg/mg dw in *comt1* and 0.09 ± 0.05 µg/mg dw in WT, syringic acid: 0.04 ± 0.02 µg/mg dw in *comt1* and 0.08 ± 0.06 µg/mg dw in WT) (fig. 82 E).

The mutant *C4H::F5H* shows highly significant alteration in all aliphatic classes of suberin. The total suberin content is enhanced by 2.1 fold (19.4 ± 2.8 µg/mg dw in *C4H::F5H* and 9.2 ± 2.8 µg/mg dw in WT). Suberin aliphatic classes are significantly increased between 1.7 and 3.0 fold (monocarboxylic acids: 4.5 ± 0.8 µg/mg dw in *C4H::F5H* and 2.1 ± 0.6 µg/mg dw in WT, primary alcohols: 1.1 ± 0.1 µg/mg dw in *C4H::F5H* and 0.53 ± 0.15 µg/mg dw in WT, ω-hydroxy acids: 8.1 ± 1.3 µg/mg dw in *C4H::F5H* and 4.7 ± 1.8 µg/mg dw in WT, α, ω-dicarboxylic acids: 5.7 ± 1.1 µg/mg dw in *C4H::F5H* and 1.9 ± 0.84 µg/mg dw in WT) (fig. 82 C). Statistical evaluation of the aromatic constituents reveals significant alterations in five of eight compounds. *Trans* coumaric acid, *trans* ferulic acid, diferulic acid and syringic acid are enhanced by 1.9 to 15 fold (*trans* coumaric acid: 0.14 ± 0.03 µg/mg dw in *C4H::F5H* and 0.05 ± 0.02 µg/mg dw in WT, *trans* ferulic acid: 0.96 ± 0.36 µg/mg dw in *C4H::F5H* and 0.11 ± 0.04 µg/mg dw in WT, diferulic acid: 0.15 ± 0.05 µg/mg dw in *C4H::F5H* and 0.08 ± 0.02 µg/mg dw in WT, syringic acid: 1.2 ± 0.4 µg/mg dw in *C4H::F5H* and 0.08 ± 0.06 µg/mg dw in WT). Only vanillin is significantly reduced by 50 % (0.02 ± 0.01 µg/mg dw in *C4H::F5H* and 0.04 ± 0.04 µg/mg dw in WT). In total the content of aromatic compounds is enhanced by 4.3 fold (3.4 ± 0.6 µg/mg dw in *C4H::F5H* and 0.79 ± 0.18 µg/mg dw in WT) (fig. 82 E).

Statistical evaluation of the suberin data from *ccr1* shows that *ccr1* does not differ from WT with respect to content of suberin classes and the total aliphatic suberin content. There are significant alterations in three compounds. The C_{16} ω-hydroxy acid is decreased by 34 % (0.54 ± 0.05 µg/mg dw in *ccr1* and 0.82 ± 0.37 µg/mg dw in WT) or C_{22} α, ω-dicarboxylic acid is increased by 70 % (0.17 ± 0.05 µg/mg dw in *ccr1* and 0.10 ± 0.05 µg/mg dw in WT) (fig. 82 B). With respect to the aromatic constituents only the content of *trans* ferulic acid is severely enhanced by 2.2 fold (0.24 ± 0.06 µg/mg dw in *ccr1* and 0.11 ± 0.04 µg/mg dw in WT). Total aromatic content is not affected (fig. 82 F).

The mutant *myb7* does neither exhibit significant alterations in the composition of suberin aliphatic nor aromatic constituents (fig. 82 B, D and F).

The positive control *esb1* shows significant higher content of all suberin aliphatic classes compared to the WT. For example the content of ω-hydroxy acids is enhanced by 43 % (6.7 ± 1.2 µg/mg dw in *esb1* and 4.7 ± 1.8 µg/mg dw in WT) and α, ω-dicarboxylic acids by 2.4 fold (4.5 ± 1.0 µg/mg dw in *esb1* and 1.9 ± 0.8 µg/mg dw in WT) (fig. 82 D). The total aromatic

content has not changed. But the content of *cis* ferulic acid and syringic acid show declines by 80 % (0.01 ± 0.004 µg/mg dw in *esb1* and 0.05 ± 0.05 µg/mg dw in WT) and by 62 % (0.03 ± 0.02 µg/mg dw in *esb1* and 0.08 ± 0.06 µg/mg dw in WT) respectively. In contrast to this, the content of *trans* ferulic acid and diferulic acid show a rise by 55 % (0.17 ± 0.03 µg/mg dw in *esb1* and 0.11 ± 0.04 µg/mg dw in WT) and by 75 % (0.14 ± 0.03 µg/mg dw in *esb1* and 0.08 ± 0.02 µg/mg dw in WT) respectively (fig. 82 F).

Due to eight different aromatic constituents it is possible to calculate the ratio of the aromatic composition similar to the lignin extraction. *Trans* coumaric acid has the scaffold of hydroxycinnamyl-monomers, whereas vanillin, vanillic acid, *trans* and *cis* ferulic acid and as well as diferulic acid belong to guiacyl-monomers. Syringa aldehyde and syringic acid are sinapyl-monomers. Considering the hydroxycinnamyl-monomers three mutant lines show significant alterations. The content of hydroxycinnamyl monomers is enhanced by 19.1 % in *ccoaomt1* and by 3.8 % (26.1 ± 7.2 % in *ccoaomt1*, 10.8 ± 2.5 % in *esb1* and 7.0 ± 1.7 % in WT) in *esb1*. *C4H::F5H* reveals a decline of hydroxyl-cinnamyl-monomers by 2.9 % (4.1 ± 0.3 % in *C4H::F5H* and 7.0 ± 1.7 % in WT). Significant alterations in guiacyl-monomers are detectable in *ccoaomt1*, *comt1*, *ccr1* and *C4H::F5H*. G-monomers are decreased in *ccoaomt1* by 16.3 % and in *C4H::F5H* by 33.2 % (55.4 ± 4.9 % in *ccoaomt1*, 38.5 ± 6.8 % in *C4H::F5H* and 71.7 ± 7.7 % in WT). In contrast, *comt1* reveals an increased content by 9.9 % and *ccr1* by 10.0 % (81.6 ± 3.7 % in *comt1*, 81.7 ± 4.1 % in *ccr1* and 71.7 ± 7.7 % in WT). Sinapyl-monomers are reduced in *comt1* by 13.3 %, in both *ccr1* and *esb1* by 9.4 % (8.0 ± 1.4 % in *comt1*, 11.9 ± 3.1 in *ccr1*, 11.9 ± 1.6 % in *esb1* and 21.3 ± 8.0 % in WT). An increase of the sinapyl-monomer content by 36.1 % (57.4 ± 7.0 % in *C4H::F5H* and 21.3 ± 8.0 % in WT) is detectable in *C4H::F5H* (fig. 82 G).

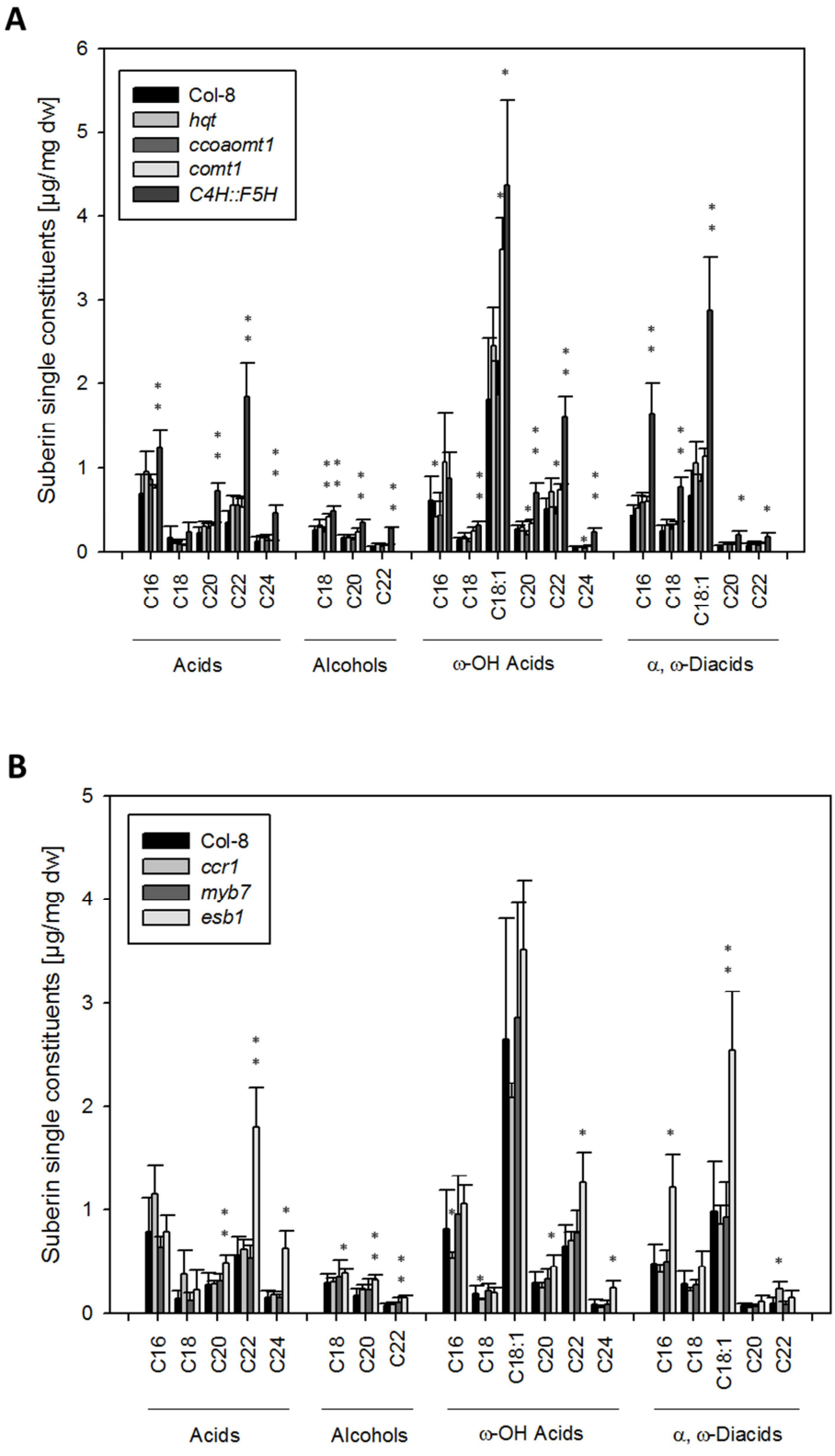
A
Suberin single constituents [µg/mg dw]
Col-8
hqt
ccoaomt1
comt1
C4H::F5H
C16
C18
C20
C22
C24
C18
C20
C22
C16
C18
C18:1
C20
C22
C24
C16
C18
C18:1
C20
C22
Acids
Alcohols
ω-OH Acids
α, ω-Diacids
B
Suberin single constituents [µg/mg dw]
Col-8
ccr1
myb7
esb1
Acids
Alcohols
ω-OH Acids
α, ω-Diacids

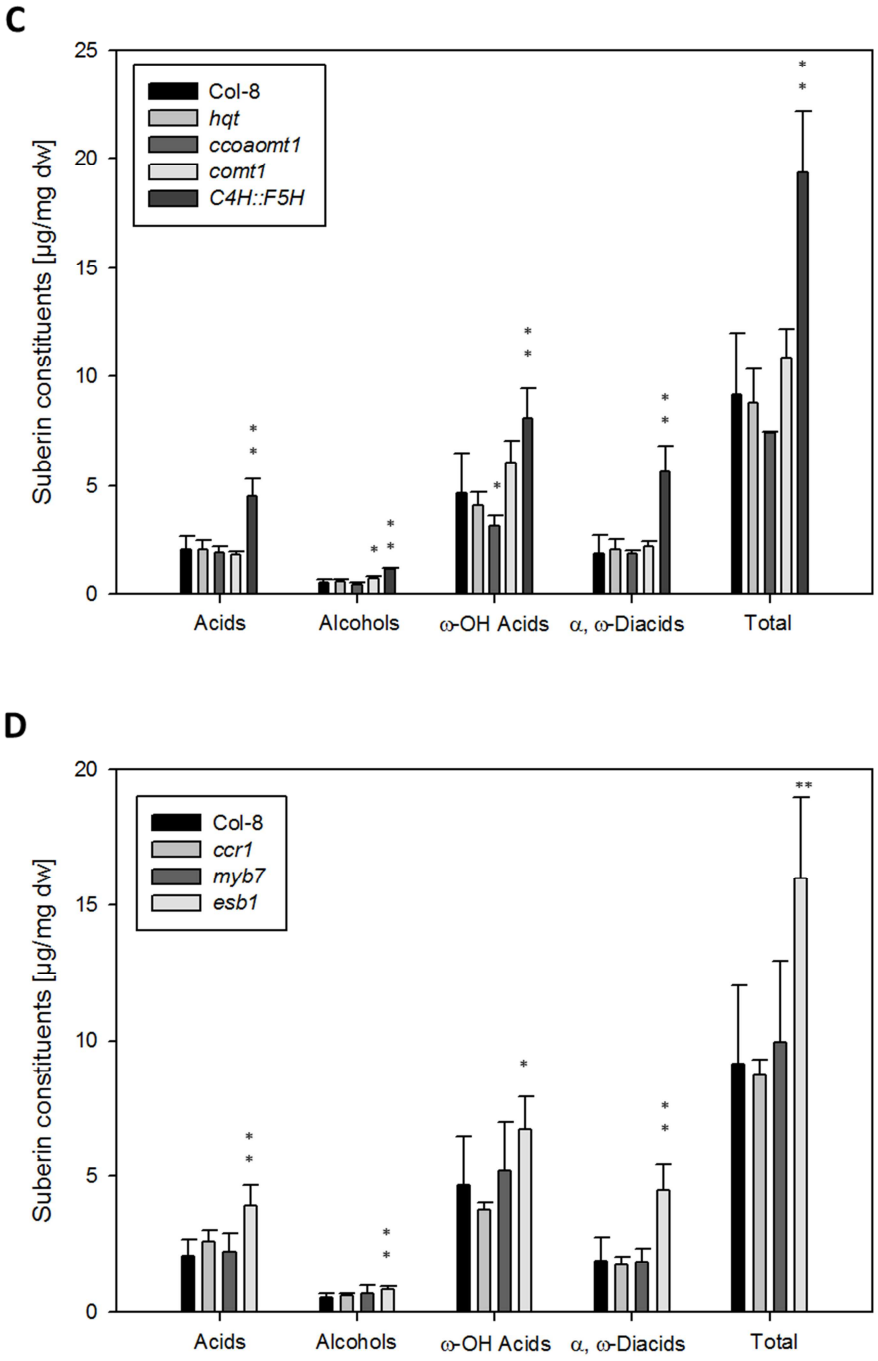
C
Suberin constituents [µg/mg dw]
25
20
15
10
5
0
Col-8
hqt
ccoaomt1
comt1
C4H::F5H
Acids
Alcohols
ω-OH Acids
α, ω-Diacids
Total
D
Suberin constituents [µg/mg dw]
20
15
10
5
0
Col-8
ccr1
myb7
esb1
Acids
Alcohols
ω-OH Acids
α, ω-Diacids
Total

E

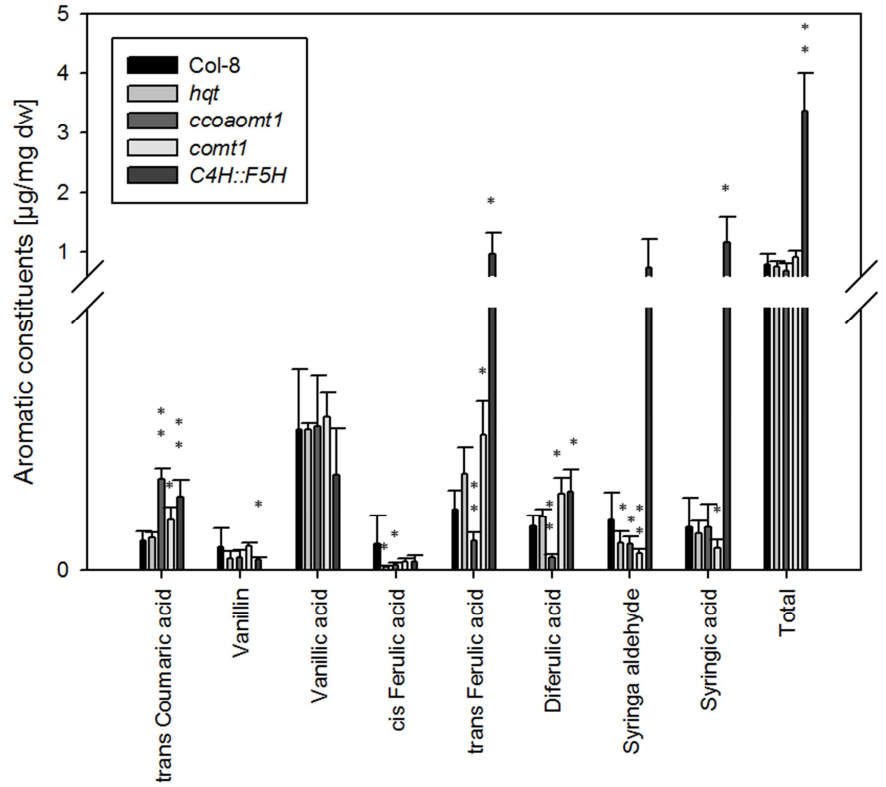
Aromatic constituents [µg/mg dw]
Col-8
hqt
ccoaomt1
comt1
C4H::F5H
trans Coumaric acid
Vanillin
Vanillic acid
cis Ferulic acid
trans Ferulic acid
Diferulic acid
Syringa aldehyde
Syringic acid
Total

F

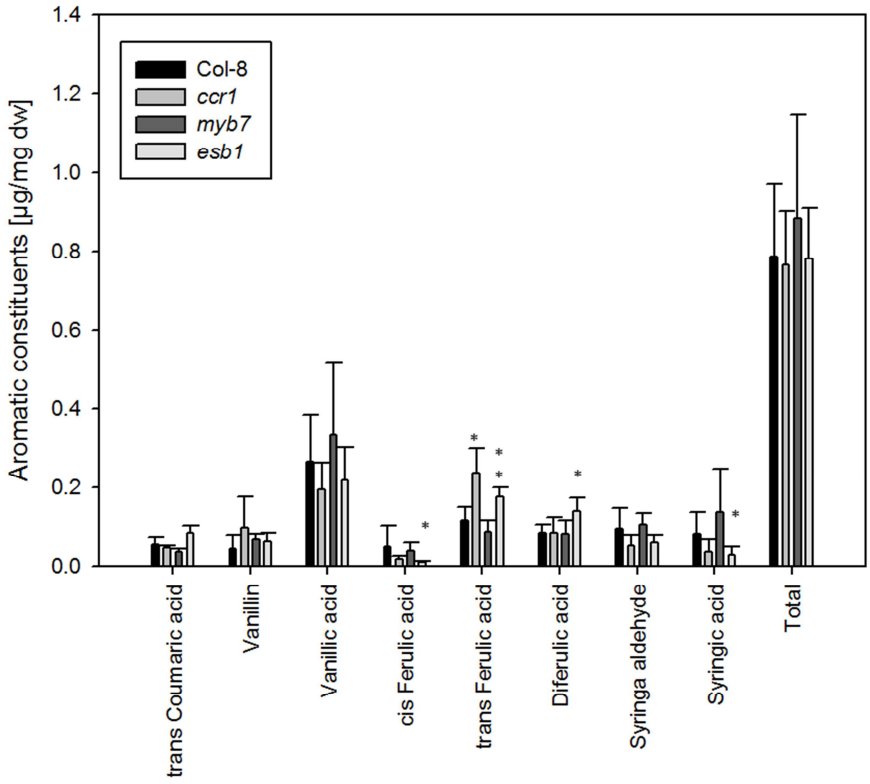
Aromatic constituents [µg/mg dw]
Col-8
ccr1
myb7
esb1
trans Coumaric acid
Vanillin
Vanillic acid
cis Ferulic acid
trans Ferulic acid
Diferulic acid
Syringa aldehyde
Syringic acid
Total

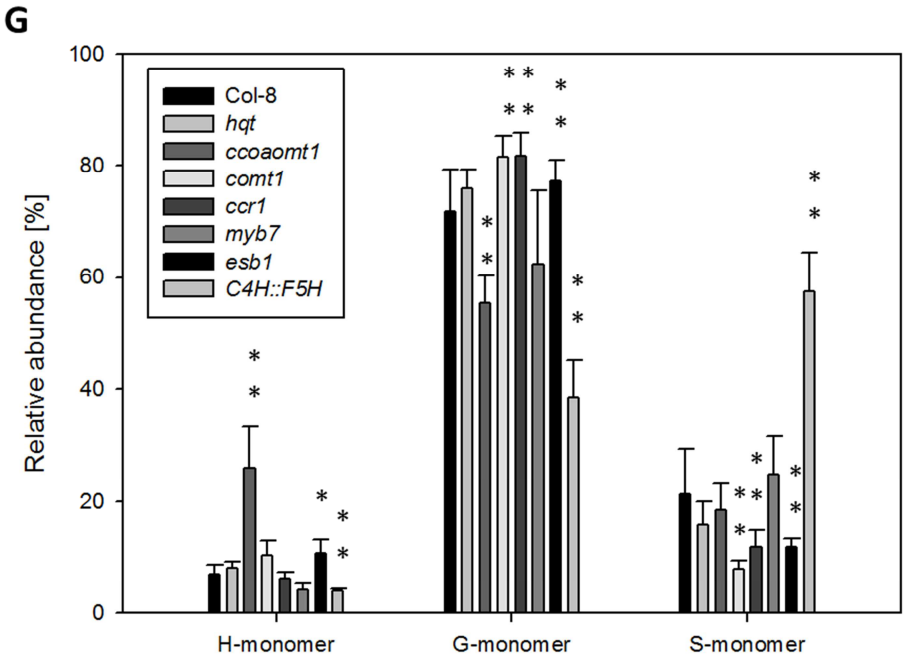

Fig. 82: Comparison of root aliphatic suberin and absolute and relative aromatic composition of the mutant lines *hqt*, *ccoaomt1*, *comt1*, *ccr1*, *myb7*, *esb1* and *C4H::F5H* with the corresponding WT

Five weeks old hydroponically grown roots treated with cell wall degrading enzymes were analysed. **A**: Composition of the suberin aliphatic single constituents of *hqt*, *ccoaomt1*, *comt1*, *C4H::F5H* and WT related to the root dry weight. **B**: Composition of the suberin aliphatic single constituents of *ccr1*, *myb7*, *esb1* and WT related to the root dry weight. **C**: Composition of the suberin aliphatic substance classes of *hqt*, *ccoaomt1*, *comt1*, *C4H::F5H* and WT related to the root dry weight. **D**: Composition of the suberin aliphatic substance classes of *ccr1*, *myb7*, *esb1* and WT related to the root dry weight. **E**: Composition of the aromatic compounds of *hqt*, *ccoaomt1*, *comt1*, *C4H::F5H* and WT related to the root dry weight. **F**: Composition of the aromatic compounds of *ccr1*, *myb7*, *esb1* and WT related to the root dry weight. **G**: Relative aromatic composition related to the root dry weight. The represented values are the arithmetic mean of the WT and mutant lines respectively and the calculated error bars of standard deviation. The sample amount corresponds to 12 roots of WT and four of *hqt*, *ccoaomt1*, *comt1*, *ccr1*, *myb7*, *esb1* and *C4H::F5H*. Acids: monocarboxylic acids, Alcohols: primary alcohols, ω-OH Acids: ω-hydroxy acids, α, ω-Diacids: α, ω-dicarboxylic acids. H-monomer: hydroxycinnamyl-monomer, G-monomer: guiacyl-monomer, S-monomer: sinapyl-monomer. *: student's t-test, $p \leq 0.05$, **: student's t-test, $p \leq 0.01$.

Statistical evaluation of the data shows that the content of the primary alcohol C_{20} is increased by 82 % (0.31 ± 0.06 µg/mg dw in *myb4* and 0.17 ± 0.06 µg/mg dw in WT) and C_{22} by 71 % (0.12 ± 0.02 µg/mg dw in *myb4* and 0.07 ± 0.03 µg/mg dw in WT) in *myb4* (fig. 82 A). In total the substance class of primary alcohols is significantly enhanced by 55 % (0.76 ± 0.1 µg/mg dw in *myb4* and 0.49 ± 0.15 µg/mg dw in WT) (fig. 83 B). Considering the aromatic compounds statistical significant alterations are found in vanillic acid, syringa aldehyde and syringic acid. The content of vanillic acid is increased by 1.6 fold (0.50 ± 0.10 µg/mg dw in *myb4* and 0.31 ± 0.04 µg/mg dw in WT), by 2.6 fold (0.29 ± 0.11 µg/mg dw in *myb4* and 0.11

± 0.03 µg/mg dw in WT) in syringa aldehyde and by 2.9 fold (0.23 ± 0.08 µg/mg dw in *myb4* and 0.08 ± 0.01 µg/mg dw in WT) in syringic acid (fig. 83 C). The suberin enhanced mutant *C4H::F5H* reveals several statistically significant alterations in all suberin specific substances (fig. 82 A), classes and in almost all aromatic compounds. The total aliphatic suberin content is significantly higher enhanced by 2.3 fold (20.3 ± 4.2 µg/mg dw in *C4H::F5H* and 9.0 ± 1.5 µg/mg dw in WT) in comparison to the WT. This enhanced suberin content is caused by significantly increased amounts of the in monocarboxylic acids (4.5 ± 0.8 µg/mg dw in *C4H::F5H* and 2.6 ± 0.8 µg/mg dw in WT), primary alcohols (0.96 ± 0.24 µg/mg dw in *C4H::F5H* and 0.49 ± 0.15 µg/mg dw in WT), ω-hydroxy acids (8.9 ± 2.1 µg/mg dw in *C4H::F5H* and 3.4 ± 1.8 µg/mg dw in WT) and α, ω-dicarboxylic acids (5.9 ± 1.1 µg/mg dw in *C4H::F5H* and 2.5 ± 0.4 µg/mg dw in WT) content (fig. 83 B). The total aromatic content is significantly enhanced by 3.3 fold (3.3 ± 1.1 µg/mg dw in *C4H::F5H* and 1.0 ± 0.1 µg/mg dw in WT). Guiacyl related compounds like vanillin and vanillic acid are decreased by 40 % (0.03 ± 0.01 µg/mg dw in *C4H::F5H* and 0.05 ± 0.01 µg/mg dw in WT) and 68 % (0.10 ± 0.05 µg/mg dw in *C4H::F5H* and 0.31 ± 0.04 µg/mg dw in WT) respectively. In contrast to guiacyl related compounds syringyl related compounds like syringa aldehyde and syringic acid are increased by 10 fold (1.1 ± 0.3 µg/mg dw in *C4H::F5H* and 0.11 ± 0.03 µg/mg dw in WT) and by 10.8 fold (0.86 ± 0.41 µg/mg dw in *C4H::F5H* and 0.08 ± 0.01 µg/mg dw in WT). The content of *trans* ferulic acid is enhanced by 3.0 fold (0.72 ± 0.29 µg/mg dw *in C4H::F5H* and 0.24 ± 0.07 µg/mg dw in WT) and diferulic acid by 1.6 fold (0.13 ± 0.03 µg/mg dw in *C4H::F5H* and 0.08 ± 0.04 µg/mg dw in WT). However, the content of diferulic acid is not significantly increased (fig. 83 C).

Considering the ratio of aromatic constituents sinapyl-monomers are enhanced by 12.8 % in *myb4* and by 41 % (32.5 ± 7.1 % in *myb4*, 60.7 ± 6.9 % in *C4H::F5H* and 19.7 ± 5.1 % in WT) in *C4H::F5H*. Guiacyl-monomers are reduced by 9.2 % in *myb4* and by 36 % (61.9 ± 6.8 % in *myb4*, 35.1 ± 7.9 % in *C4H::F5H* and 71.1 ± 4.1 % in WT) in *C4H::F5H*. Hydroxycinnamyl-monomers show a decline by 3.5 % in *myb4* and 4.9 % (5.6 ± 0.5 % in *myb4*, 4.2 ± 2.0 % in *C4H::F5H* and 9.1 ± 2.7 % in WT) in *C4H::F5H*. But the reduced ratio of hydroxycinnamyl- and guiacyl-monomers is not significantly altered in *myb4* (fig. 83 D).

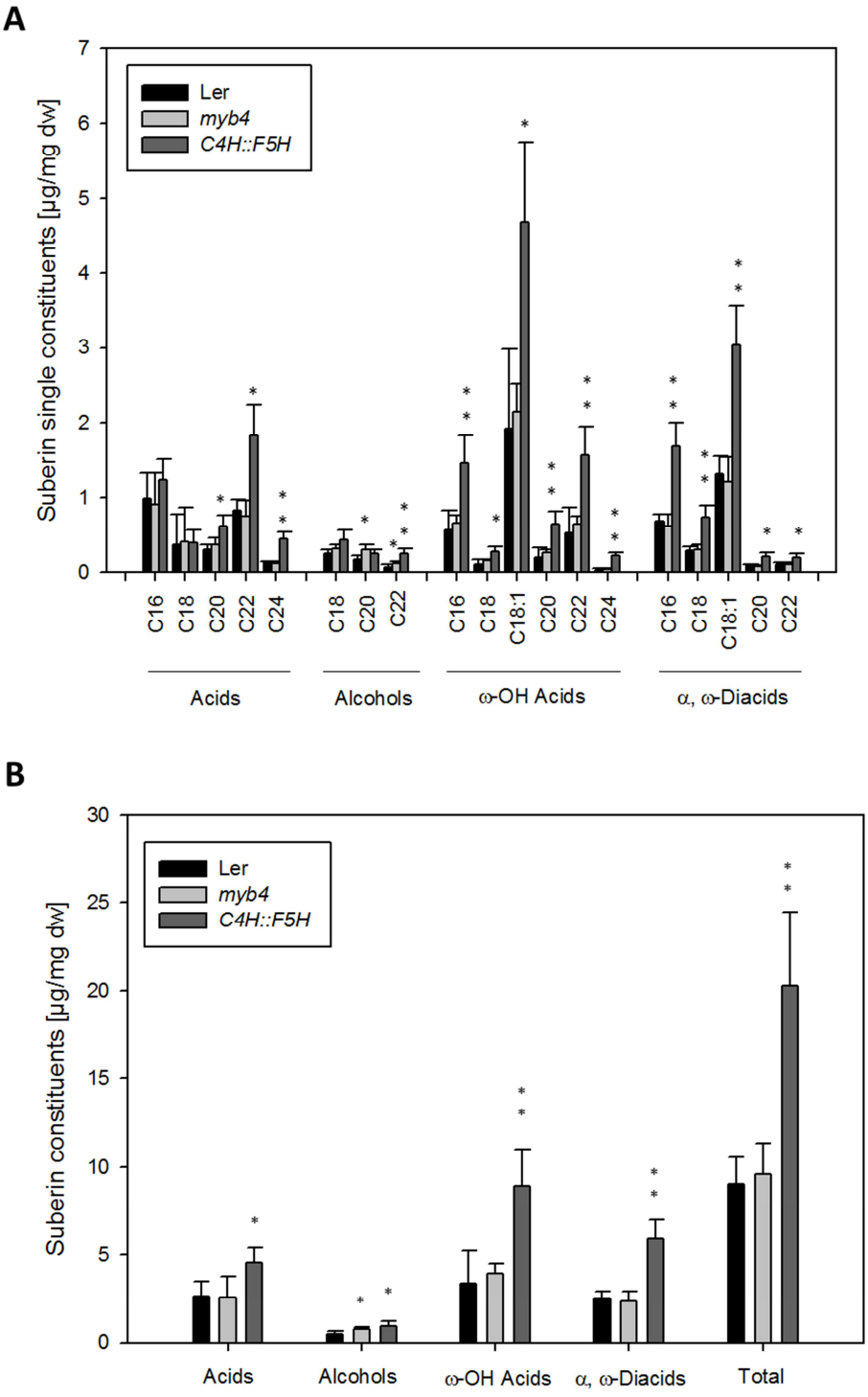
A
Suberin single constituents [µg/mg dw]
Ler
myb4
C4H::F5H
C16
C18
C20
C22
C24
C18
C20
C22
C16
C18
C18:1
C20
C22
C24
C16
C18
C18:1
C20
C22
Acids
Alcohols
ω-OH Acids
α, ω-Diacids
B
Suberin constituents [µg/mg dw]
Ler
myb4
C4H::F5H
Acids
Alcohols
ω-OH Acids
α, ω-Diacids
Total

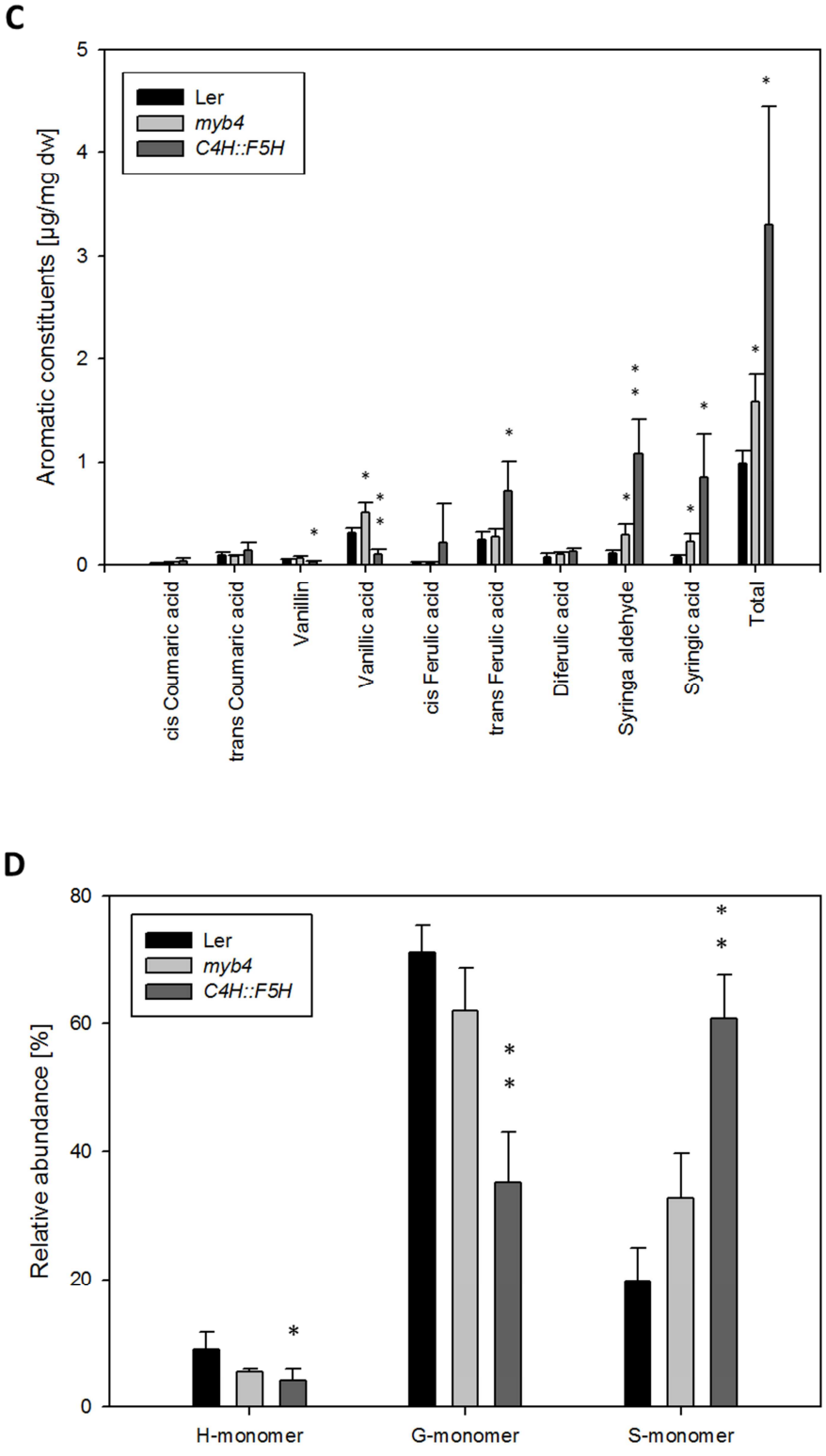

Fig. 83: Comparison of root aliphatic suberin and aromatic compounds of the mutant lines *myb4* and *C4H::F5H* with the corresponding WT

Five weeks old hydroponically grown roots treated with cell wall degrading enzymes were analysed. **A**: Composition of the suberin aliphatic single constituents of *myb4* and *C4H::F5H* and WT related to the root dry weight. **B**: Composition of the suberin aliphatic substance classes related to the root dry weight. **C**: Composition of the aromatic compounds related to the root dry weight. **D**: Relative aromatic composition related to the root dry weight. The represented values are the arithmetic

mean of the WT and mutant lines respectively and the calculated error bars of standard deviation. The sample amount corresponds to four roots of WT, *myb4* and *C4H::F5H* respectively. Acids: monocarboxylic acids, Alcohols: primary alcohols, ω-OH Acids: ω-hydroxy acids, α, ω-Diacids: α, ω-dicarboxylic acids. H-monomer: hydroxycinnamyl-monomer, G-monomer: guiacyl-monomer, S-monomer: sinapyl-monomer. *: student's t-test, $p \leq 0.05$, **: student's t-test, $p \leq 0.01$.

The following set of mutants was not treated with cell wall degrading enzymes. Knockout in *cadc* and knock-down of *cadd* do neither influence suberin total, suberin aliphatic class's content and aromatic constituents nor aromatic relative composition (fig. 84 A, C, D and E). There are only two significant alterations detectable in *cadc*. Both minor compounds C_{20} and C_{22} α, ω-dicarboxylic acid are decreased by 17 % (0.05 ± 0.003 µg/mg dw in *cadc* and 0.06 ± 0.008 µg/mg dw in WT) and by 29 % (0.05 ± 0.01 µg/mg dw in *cadc* and 0.07 ± 0.01 µg/mg dw in WT) respectively (fig. 84 A).

The double knockout mutant *cadc*cadd* and the triple knockout mutant *cadc*cadd*fah1-2* do not show significant alterations in the suberin aliphatic classes and suberin content (fig. 84 B and C). Only *cadc*cadd* exhibits significant alterations in three suberin single constituents. The content of C_{20} acid, C_{18} and C_{20} α, ω-dicarboxylic acid are reduced by 30 % (0.14 ± 0.02 µg/mg dw in *cadc*cadd* and 0.20 ± 0.02 µg/mg dw in WT), by 22 % (0.18 ± 0.02 µg/mg dw in *cadc*cadd* and 0.23 ± 0.03 µg/mg dw in WT) and by 33 % (0.04 ± 0.01 µg/mg dw in *cadc*cadd* and 0.06 ± 0.01 µg/mg dw in WT) respectively (fig. 84 B).

The positive control *esb1* shows similar results as already described in the set of *hqt*, *ccoaomt1*, *comt1*, *ccr1* and *myb7*. Therefore, a detailed description of this mutant is not present in this paragraph. All suberin aliphatic classes reveal highly significant alterations (fig. 84 B, C).

Considering the aromatic constituents only the double knockout *cadc*cadd* and the triple knockout *cadc*cadd*fah1-2* indicate significant alterations in the content. In *cadc*cadd* the total aromatic content is enhanced by 77 % (0.76 ± 0.09 µg/mg dw in *cadc*cadd* and 0.43 ± 0.07 µg/mg dw in WT) and by 23 % (0.53 ± 0.09 µg/mg dw in *cadc*cadd*fah1-2* and 0.43 ± 0.07 µg/mg dw in WT) in *cadc*cadd*fah1-2*. However, the slightly increased content of aromatics is not significant. An increased content is evaluated from the statistical analysis in *trans* ferulic acid, diferulic acid and syringa aldehyde in *cadc*cadd*. The content of *trans* ferulic acid is increased by 3.6 fold (0.36 ± 0.07 µg/mg dw in *cadc*cadd* and 0.10 ± 0.04 µg/mg dw in WT), diferulic acid and syringa aldehyde by 2.0 fold (diferulic acid: 0.08 ± 0.02 µg/mg dw in *cadc*cadd* and 0.04 ± 0.02 µg/mg dw in WT, syringa aldehyde: 0.06 ± 0.01

µg/mg dw in *cadc*cadd* and 0.03 ± 0.01 µg/mg dw in WT). In *cadc*cadd*fah1-2* the content of *trans* ferulic acid is increased by 2.4 fold (024 ± 0.07 µg/mg dw in *cadc*cadd*fah1-2* and 0.10 ± 0.04 µg/mg dw in WT). Syringa aldehyde and syringic acid show a decline by 67 % (0.01 ± 0.003 µg/mg dw in *cadc*cadd*fah1-2* and 0.03 ± 0.01 µg/mg dw in WT) and by 50 % (0.01 ± 0.001 µg/mg dw in *cadc*cadd*fah1-2* and 0.02 ± 0.005 µg/mg dw in WT) (fig. 84 D).

The loss of syringa aldehyde and syringic acid causes a shift in the G- and S-monomer ratio. Guiacyl-monomers are enhanced by 9.8 % (89.7 ± 1.9 % in *cadc*cadd*fah1-2* and 79.9 ± 3.5 % in WT), whereas sinapyl-monomers are reduced by 8.9 % (3.8 ± 1.3 % in *cadc*cadd*fah1-2* and 12.7 ± 2.3 % in WT) (fig. 84 E).

The positive control *esb1* reveals an increased aromatic content as well. *Trans* coumaric acid is enhanced by 2.3 fold (0.07 ± 0.01 µg/mg dw in *esb1* and 0.03 ± 0.01 µg/mg dw in WT), *cis* ferulic acid by 2.0 fold (0.04 ± 0.02 µg/mg dw in *esb1* and 0.02 ± 0.002 µg/mg dw in WT) and diferulic acid by 2.8 fold (0.11 ± 0.01 µg/mg dw in *esb1* and 0.04 ± 0.02 µg/mg dw in WT). The total aromatic content is enhanced by 51 % (0.65 ± 0.05 µg/mg dw in *esb1* and 0.43 ± 0.07 µg/mg dw in WT). These alterations cause decreased relative sinapyl-monomer content by 4.3 % (8.4 ± 1.5 % in *esb1* and 12.7 ± 2.3 % in WT), while hydroxycinnamyl-monomers are increased by 3.5 % (10.9 ± 1.1 % in *esb1* and 7.4 ± 1.7 % in WT) (fig. 84 D, E).

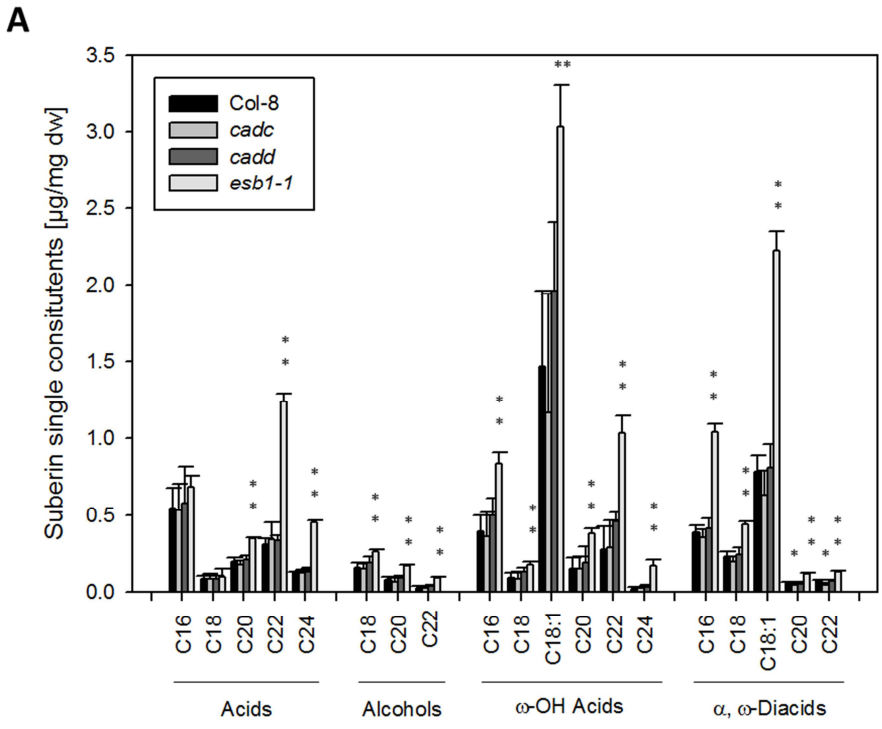

B

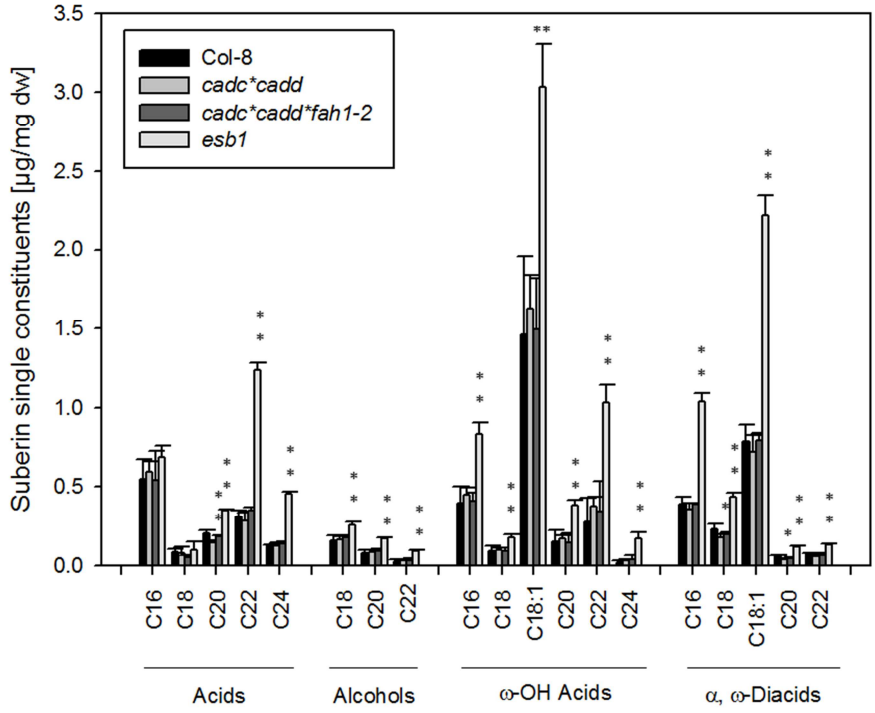
Suberin single constituents [µg/mg dw]
Col-8
cadc*cadd
cadc*cadd*fah1-2
esb1
C16
C18
C20
C22
C24
C18
C20
C22
C16
C18
C18:1
C20
C22
C24
C16
C18
C18:1
C20
C22
Acids
Alcohols
ω-OH Acids
α, ω-Diacids

C

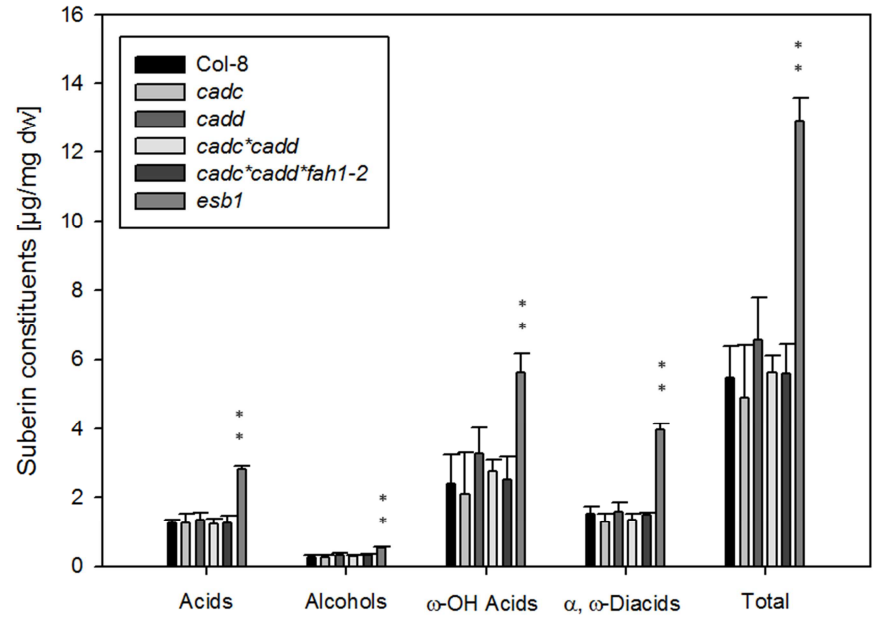
Suberin constituents [µg/mg dw]
Col-8
cadc
cadd
cadc*cadd
cadc*cadd*fah1-2
esb1
Acids
Alcohols
ω-OH Acids
α, ω-Diacids
Total

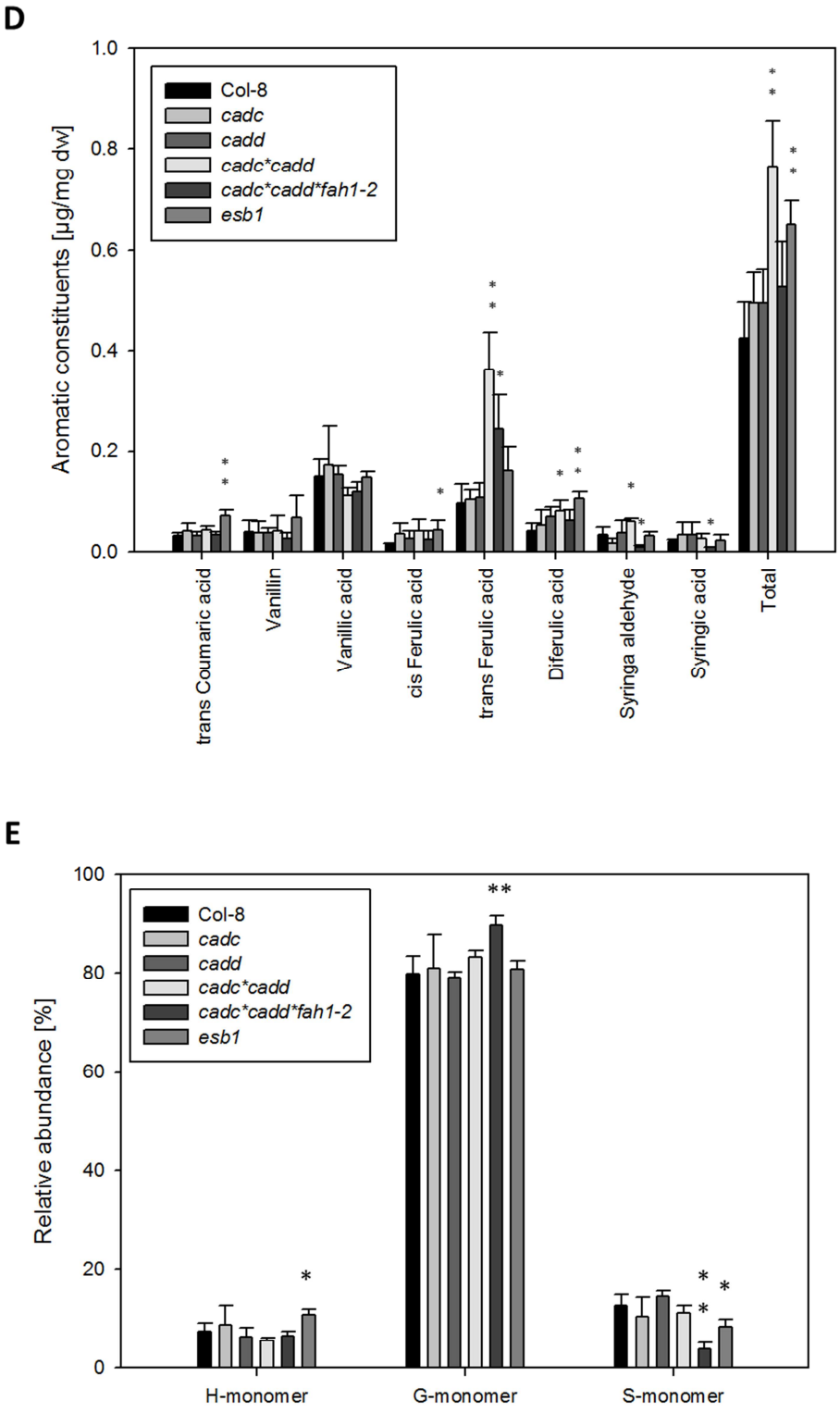

Fig. 84: Comparison of root aliphatic suberin and aromatic compounds of the mutant line *cadc*, *cadd*, *cadc*cadd*, *cadc*cadd*fah1-2* and *esb1* with the corresponding WT

Five weeks old hydroponically grown roots untreated with cell wall degrading enzymes were analysed. **A**: Composition of the suberin aliphatic single constituents of *cadc*, *cadd*, *esb1* and WT related to the root dry weight. **B**: Composition of the suberin aliphatic single constituents of *cadc*cadd*, *cadc*cadd*fah1-2*, *esb1* and WT related to the root dry weight. **C**: Composition of the suberin aliphatic substance classes related to the root dry weight. **D**: Composition of the aromatic

compounds related to the root dry weight. **E**: Relative aromatic composition related to the root dry weight. The represented values are the arithmetic mean of the WT and mutant lines respectively and the calculated error bars of standard deviation. The sample amount corresponds to four roots of WT, *cadc*, *cadd*, *cadc*cadd*, *cadc*cadd*fah1-2*, and *esb1* respectively. Acids: monocarboxylic acids, Alcohols: primary alcohols, ω-OH Acids: ω-hydroxy acids, α, ω-Diacids: α, ω-dicarboxylic acids. H-monomer: hydroxycinnamyl-monomer, G-monomer: guiacyl-monomer, S-monomer: sinapyl-monomer. *: student's t-test, $p \leq 0.05$, **: student's t-test, $p \leq 0.01$.

Extraction of suberin of this set of mutants untreated with cell wall degrading enzymes show small amounts of all compounds. Nevertheless, significant alterations are detectable and comparable due to the use of the positive control *C4H::F5H*. Unfortunately, sown seeds of a heterozygous *ref8-1* plant did not provide enough homozygous *ref8-1* mutants for a suberin analysis. Due to this, *ref8-1* could not be analysed in this set of mutants.

At first, the triple knockout mutant *ref8-1*med5a*med5b* exhibits an increased suberin content by 62 % (4.7 ± 1.3 µg/mg dw in *ref8-1*med5a*med5b* and 2.9 ± 0.3 µg/mg dw in WT). However, the increased suberin content is not significant. Only the content of the primary alcohol classes is significantly increased by 47 % (0.28 ± 0.05 µg/mg dw in *ref8-1*med5a*med5b* and 0.19 ± 0.02 µg/mg dw in WT) (fig. 85 C). Significant alterations are evaluated in five suberin single constituents. The C_{22} monocarboxylic acid is enhanced by 2.3 fold (0.42 ± 0.06 µg/mg dw in *ref8-1*med5a*med5b* and 0.18 ± 0.05 µg/mg dw in WT), C_{20} and C_{22} primary alcohol by 63 % (0.13 ± 0.03 µg/mg dw in *ref8-1*med5a*med5b* and 0.08 ± 0.01 µg/mg dw in WT) and by 75 % (0.07 ± 0.01 µg/mg dw in *ref8-1*med5a*med5b* and 0.04 ± 0.01 µg/mg dw in WT) respectively, C_{24} ω-hydroxy acid by 2.7 fold (0.08 ± 0.03 µg/mg dw in *ref8-1*med5a*med5b* and 0.03 ± 0.01 µg/mg dw in WT) and C_{22} α, ω-dicarboxylic acid by 67 % (0.05 ± 0.01 µg/mg dw in *ref8-1*med5a*med5b* and 0.03 ± 0.01 µg/mg dw in WT) (fig. 84 A). Regarding the aromatics the total content is increased by 66 % (0.53 ± 0.27 µg/mg dw in *ref8-1*med5a*med5b* and 0.32 ± 0.07 µg/mg dw in WT) but the enhanced content is not significant. A significantly increased amount is statistically evaluated in the content of diferulic acid. Diferulic acid is enhanced by 2.0 fold (0.06 ± 0.01 µg/mg dw in *ref8-1*med5a*med5b* and 0.03 ± 0.01 µg/mg dw in WT) (fig. 85 D). The relative ratio of different aromatic monomers does not show significant alterations (fig. 85 E).

Suberin content, composition as well as aromatic constituents and composition has not significantly altered in the mutant *ref8-2*fah1-2*AtC4H::SmF5H* (fig. 85 A, C and D). Relative composition of the aromatic monomers reveals a shift from guiacyl-monomers to sinapyl-monomers. Guiacyl-monomers are decreased by 20.8 % (57.2 ± 14.2 % in *ref8-2*fah1-*

*2*AtC4H::SmF5H* and 83.1 ± 6.4 % in WT), while sinapyl monomers are increased by 17.4 % (33.6 ± 22.6 % in *ref8-2*fah1-2*AtC4H::SmF5H* and 16.2 ± 4.8 % in WT) (fig. 85 E).

The *fah1-2* mutant is indistinguishable from the suberin phenotype compared with the WT. Suberin content, composition as well as aromatic content and composition do not differ significantly from the WT (fig. 85 A, C, D and E). Nonetheless, one significant alteration is detectable in the content of C_{20} α, ω-dicarboxylic acid. Here, the content exhibits a decline by 67 % (0.04 ± 0.01 µg/mg dw in *fah1-2* and 0.12 ± 0.02 µg/mg dw in WT) (fig. 85 A).

Isolated peridermal tissue from roots *Arabidopsis thaliana* reveal a high content of suberin aliphatic monomers as well as aromatic constituents. However, only one sample of isolated peridermal tissue could be analysed. Compared with a whole root system isolated peridermal tissue exhibit a 19.7 fold increase of suberin (57.2 µg/mg dw in peridermal tissue and 2.9 ± 0.3 µg/mg dw in whole WT root). Monocarboxylic acids are increased by 11.5 fold (9.3 µg/mg dw in peridermal tissue and 0.81 ± 0.08 µg/mg dw in whole WT root), primary alcohols by 72.1 fold (13.7 µg/mg dw in peridermal tissue and 0.19 ± 0.02 µg/mg dw in whole WT root), ω-hydroxy acids by 19.3 fold (25.1 µg/mg dw in peridermal tissue and 1.3 ± 0.05 µg/mg dw in whole WT root) and α, ω-dicarboxylic acids by 15.9 fold (9.2 µg/mg dw in peridermal tissue and 0.58 ± 0.18 µg/mg dw in whole WT root) (fig. 85 C). Considering the aliphatic single constituents it is remarkable that the unsaturated fatty acid $C_{18:1}$ ω-hydroxy acid and α, ω-dicarboxylic acid are not present. The three dominant single constituents are C_{22} monocarboxylic acid (6.1 µg/mg dw), C_{16} and C_{22} ω-hydroxy acid (C_{16} ω-hydroxy acid: 7.0 µg/mg dw, C_{22} ω-hydroxy acid: 12.6 µg/mg dw) (fig. 85 B). The aromatic content is increased by 9.4 fold (3.0 µg/mg dw in peridermal tissue and 0.32 ± 0.07 µg/mg dw in whole WT root) in comparison to WT whole root system. Half of the aromatic content is contributed by vanillin (1.6 µg/mg dw). The two followed dominant aromatic constituents are *trans* coumaric acid (0.19 µg/mg dw) and *trans* ferulic acid (0.27 µg/mg dw) (fig. 85 D). The relative aromatic composition is dominated by guiacyl-monomers (87.4 %). Hydroxycinnamyl- and sinapyl-monomers are almost equally distributed (hydroxycinnamyl-monomers: 6.2 %, sinapyl-monomers: 6.4 %) (fig. 85 E).

The positive control *C4H::F5H* was already detailed described in the mutant set of *hqt*,*ccoaomt1*, *comt1*, *ccr1*, *myb7* and the mutant set of *myb4*. All suberin aliphatic classes are at least significantly enhanced. *Cis*, *trans* ferulic and diferulic acid are increased as well as both sinapyl-monomers syringa aldehyde and syringic acid. This causes a shift in the ratio of

guiacyl- and sinapyl-monomers. Sinapyl monomers are enhanced, while guiacyl-monomers reveal a decline (fig. 85 A, B, C, D, E).

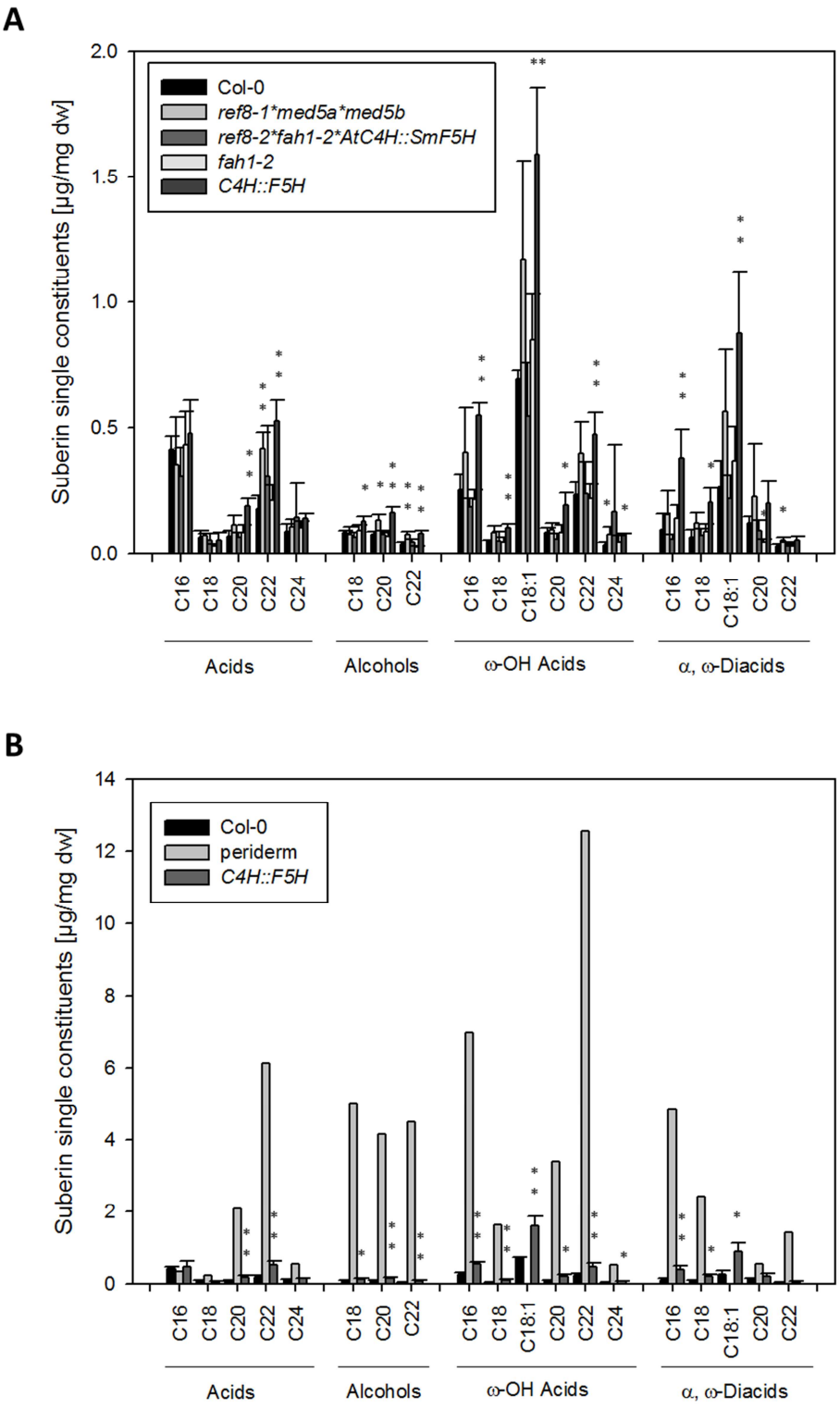

C

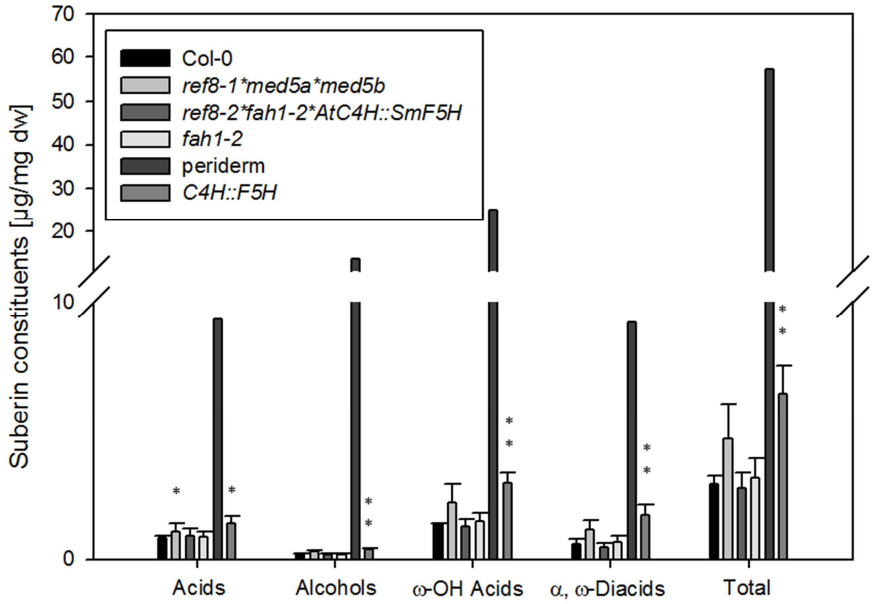
Suberin constituents [µg/mg dw]
70
60
50
40
30
20
10
0
Col-0
ref8-1*med5a*med5b
ref8-2*fah1-2*AtC4H::SmF5H
fah1-2
periderm
C4H::F5H
Acids
Alcohols
ω-OH Acids
α, ω-Diacids
Total

D

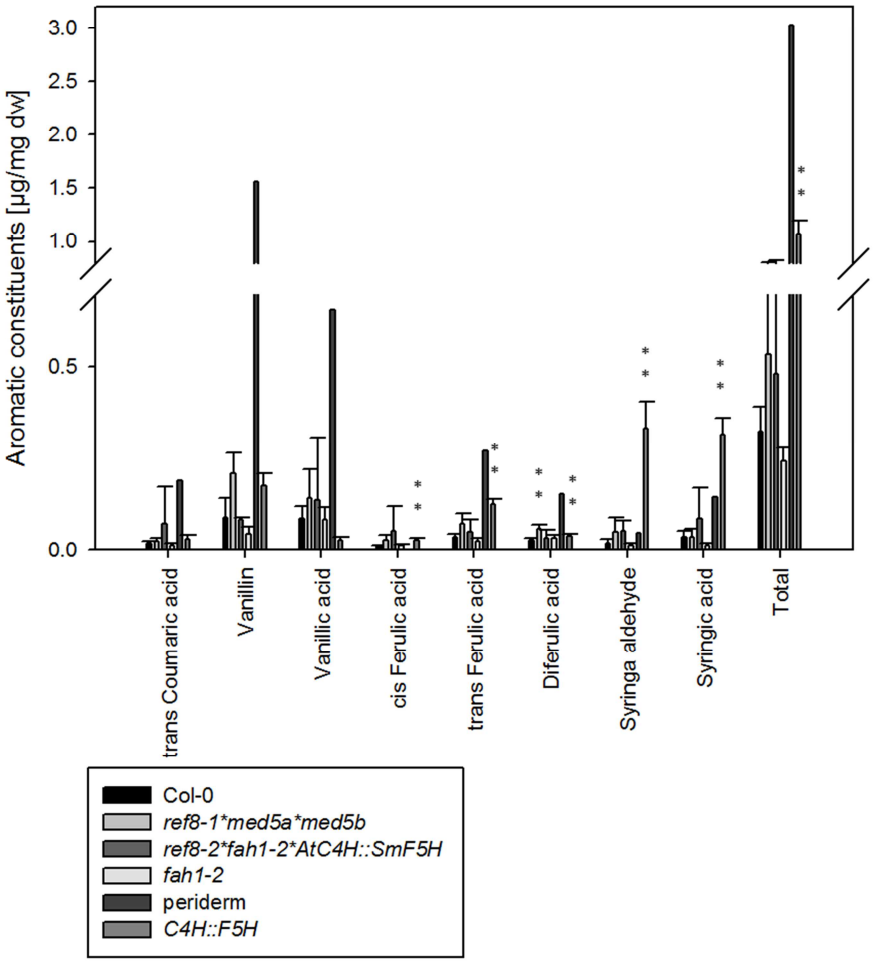
Aromatic constituents [µg/mg dw]
3.0
2.5
2.0
1.5
1.0
0.5
0.0
trans Coumaric acid
Vanillin
Vanillic acid
cis Ferulic acid
trans Ferulic acid
Diferulic acid
Syringa aldehyde
Syringic acid
Total
Col-0
ref8-1*med5a*med5b
ref8-2*fah1-2*AtC4H::SmF5H
fah1-2
periderm
C4H::F5H

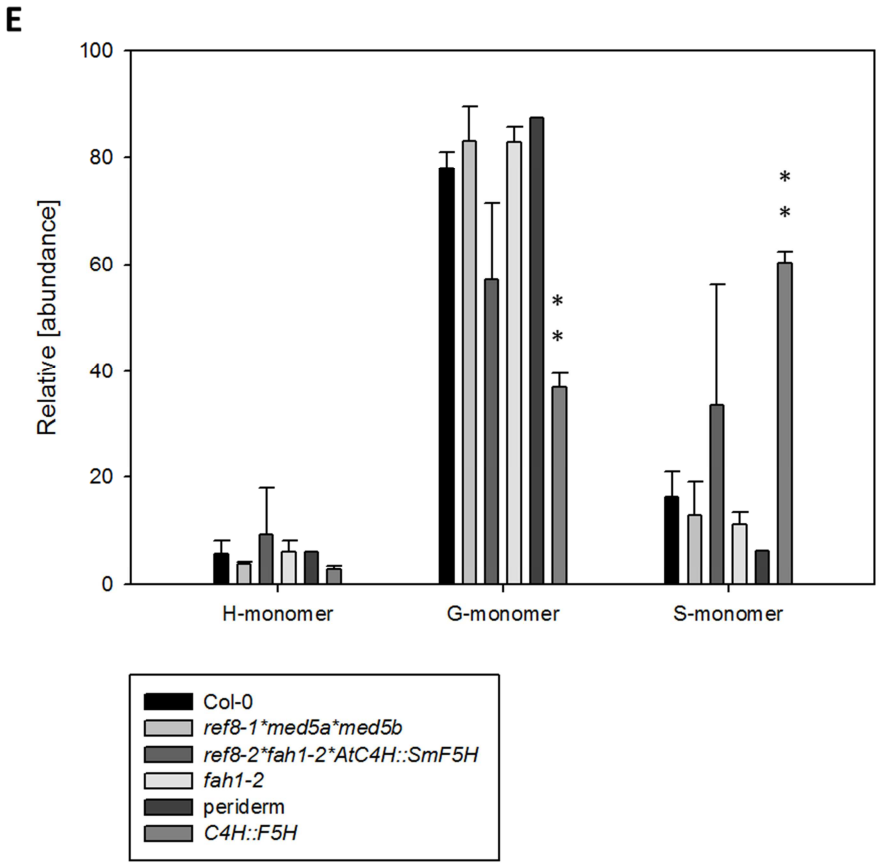

Fig. 85: Comparison of root aliphatic suberin and aromatic compounds of the mutant lines *ref8-1*med5a*med5b*, *ref8-2*fah1-2*AtC4H::SmF5H*, *fah1-2*, periderm and *C4H::F5H* with the corresponding WT

Five weeks old hydroponically grown roots untreated with cell wall degrading enzymes were analysed. **A**: Composition of the suberin aliphatic single constituents of *ref8-1*med5a*med5b*, *ref8-2*fah1-2*AtC4H::SmF5H*, *fah1-2*, *C4H::F5H* and WT related to the root dry weight. **B**: Composition of the suberin aliphatic single constituents of periderm, *C4H::F5H* and WT related to the root dry weight. **C**: Composition of the suberin aliphatic substance classes related to the root dry weight. **D**: Composition of the aromatic compounds related to the root dry weight. **E**: Relative aromatic composition related to the root dry weight. The represented values are the arithmetic mean of the WT and mutant lines respectively and the calculated error bars of standard deviation. The sample amount corresponds to three roots of WT, four of *ref8-1*med5a*med5b*, *ref8-2*fah1-2*AtC4H::SmF5H*, *fah1-2*, *C4H::F5H* respectively and one peridermal tissue sample. Acids: monocarboxylic acids, Alcohols: primary alcohols, ω-OH Acids: ω-hydroxy acids, α, ω-Diacids: α, ω-dicarboxylic acids. H-monomer: hydroxycinnamyl-monomer, G-monomer: guiacyl-monomer, S-monomer: sinapyl-monomer. *: student's t-test, $p \leq 0.05$, **: student's t-test, $p \leq 0.01$.

Statistical evaluation of the suberin content and composition of *ref3-2* reveals significant alterations. The total suberin content is enhanced by 70 % (16.5 ± 4.5 µg/mg dw in *ref3-2* and 9.7 ± 1.6 µg/mg dw in WT). This is linked to the increased content of monocarboxylic acids by 90 % (4.0 ± 1.2 µg/mg dw in *ref3-2* and 2.1 ± 0.3 µg/mg dw in WT) and α, ω-dicarboxylic acids by 2.2 fold (4.0 ± 1.0 µg/mg dw in *ref3-2* and 1.8 ± 0.3 µg/mg dw in WT) (fig. 86 B). Considering the suberin single constituents many compounds exhibit an increased

content compared with the WT. However, there is one compound with a decreased content. The C_{16} monocarboxylic acid is decreased by 30 % (0.77 ± 0.13 µg/mg dw in *ref3-2* and 1.1 ± 0.14 µg/mg dw in WT) (fig. 86 A). All other significantly altered substances are increased. For instance, C_{20} monocarboxylic acid shows a rise by 2.2 fold (0.67 ± 0.08 µg/mg dw in *ref3-2* and 0.30 ± 0.04 µg/mg dw WT), C_{22} ω-hydroxy acid by 55 % (0.96 ± 0.19 µg/mg dw in *ref3-2* and 0.62 ± 0.08 µg/mg dw in WT) and $C_{18:1}$ α, ω-dicarboxylic acid by 2.2 fold (2.2 ± 0.60 µg/mg dw in *ref3-2* and 1.0 ± 0.17 µg/mg dw in WT) (fig. 86 A). With respect to the aromatic constituents the aromatic content is decreased by 30 % (0.64 ± 0.08 µg/mg dw in *ref3-2* and 0.91 ± 0.08 µg/mg dw in WT). This decline in aromatic content is provoked by the decline in vanillin by 61 % (0.11 ± 0.02 µg/mg dw in *ref3-2* and 0.28 ± 0.02 µg/mg dw in WT), *trans* ferulic acid by 37 % (0.10 ± 0.02 µg/mg dw in *ref3-2* and 0.16 ± 0.03 µg/mg dw in WT) and diferulic acid by 55 % (0.05 ± 0.02 µg/mg dw in *ref3-2* and 0.11 ± 0.03 µg/mg dw in WT) (fig. 86 C). This loss of guiacyl-monomers causes a shift in the guiacyl- and sinapyl-monomer ratio. Guiacyl-monomers are decreased by 21.8 % (49.8 ± 12.6 % in *ref3-2* and 71.6 ± 3.4 % in WT), while sinapyl-monomers are increased by 21.1 % (42.6 ± 11.7 % in *ref3-2* and 21.5 ± 2.6 % in WT) (fig. 86 D).

In contrast to the *ref3-2* mutant, the mutant *ref1-4* does neither exhibit significant alterations in the suberin content, composition nor in the aromatic constituents and relative composition (fig. 86 A, B, C and D).

The mutant *ref4-3* does not show many significant alterations like the *ref3-2* mutant. The total suberin content is not altered but the content of primary alcohols reveals an increase by 47 % (0.88 ± 0.10 µg/mg dw in *ref4-3* and 0.60 ± 0.10 µg/mg dw in WT) (fig. 86 B). Moreover, four single constituents exhibit at least significant alterations. The content of C_{16} monocarboxylic acid is decreased by 35 % (0.72 ± 0.23 µg/mg dw in *ref4-3* and 1.1 ± 0.14 µg/mg dw in WT), whereas the content of C_{20} and C_{22} primary alcohol are increased by 43 % (0.30 ± 0.05 µg/mg dw in *ref4-3* and) and by 86 % (0.13 ± 0.01 µg/mg dw in *ref4-3* and 0.07 ± 0.002 µg/mg dw in WT) respectively as well as C_{16} ω-hydroxy acid by 68 % (1.41 ± 0.16 µg/mg dw in *ref4-3* and 0.84 ± 0.21 µg/mg dw in WT) (fig. 86 A). Considering the aromatic content it is increased by 65 % (1.5 ± 1.7 µg/mg dw in *ref4-3* and 0.91 ± 0.08 µg/mg dw in WT). However, this increased content is not significant. Due to the 3.1 fold rise in vanillin (086 ± 1.5 µg/mg dw in *ref4-3* and 0.28 ± 0.02 µg/mg dw in WT) the total aromatic content is

increased (fig. 86 C). Regarding the relative aromatic composition no significant differences were statistically evaluated (fig. 86 D).

The positive control *C4H::F5H* reveals significant increases in all suberin aliphatic classes and the suberin content. The guiacyl-monomer vanillic acid is decreased, while sinapyl-monomers like syringa aldehyde and syringic acid are enhanced. This causes the shift from dominant guiacyl-monomers to sinapyl-monomers in *C4H::F5H* (fig. 86 A, B, C, D).

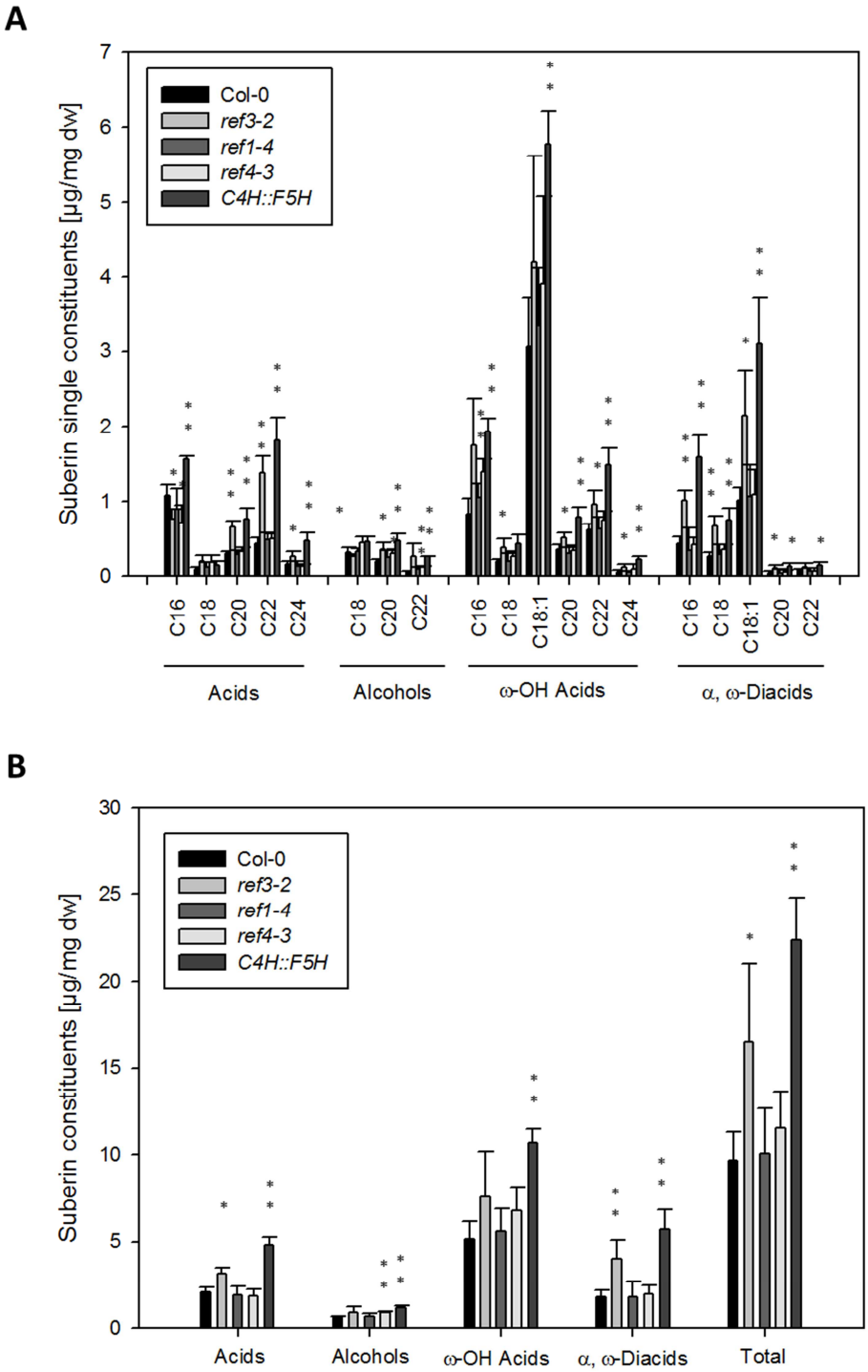

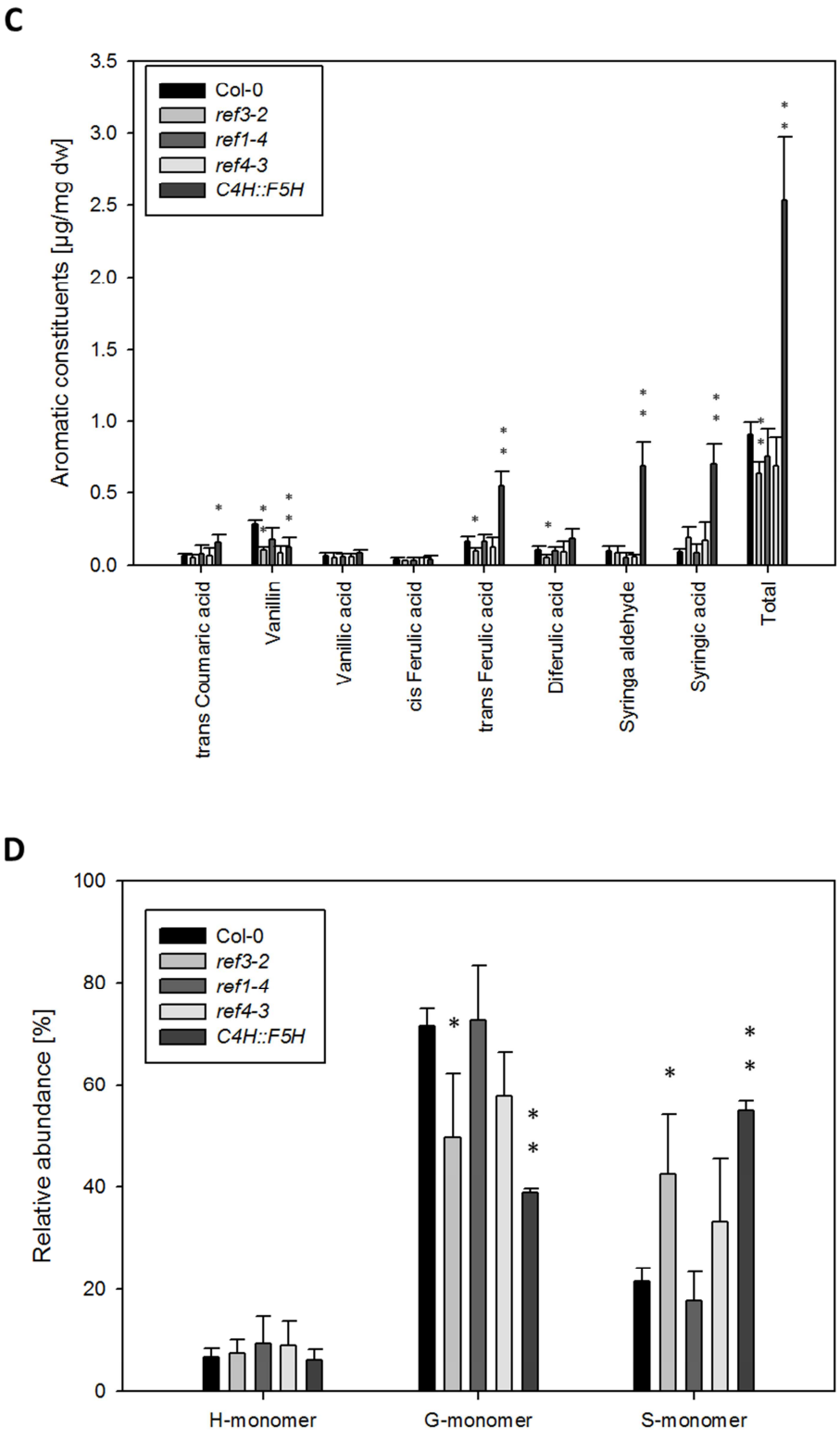

Fig. 86: Comparison of root aliphatic suberin and aromatic compounds of the mutant lines *ref3-2*, *ref1-4*, *ref4-3* and *C4H::F5H* with the corresponding WT

Five weeks old hydroponically grown roots untreated with cell wall degrading enzymes were analysed. **A**: Composition of the suberin aliphatic single constituents of *ref3-2*, *ref1-4*, *ref4-3*, *C4H::F5H* and WT related to the root dry weight. **B**: Composition of the suberin aliphatic substance classes related to the root dry weight. **C**: Composition of the aromatic compounds related to the root dry weight. **D**: Relative aromatic composition related to the root dry weight. The

represented values are the arithmetic mean of the WT and mutant lines respectively and the calculated error bars of standard deviation. The sample amount corresponds to four roots of WT and *ref3-2*, three of *ref1-4*, four of *ref4-3* and *C4H::F5H* respectively. Acids: monocarboxylic acids, Alcohols: primary alcohols, ω-OH Acids: ω-hydroxy acids, α, ω-Diacids: α, ω-dicarboxylic acids. H-monomer: hydroxycinnamyl-monomer, G-monomer: guiacyl-monomer, S-monomer: sinapyl-monomer. *: student's t-test, $p \leq 0.05$, **: student's t-test, $p \leq 0.01$.

Extraction of suberin monomers of the mutant *prx11-1* does neither show significant alterations in the suberin classes nor suberin content (fig. 87 C). Only the C_{16} monocarboxylic acid reveals a decline by 46 % (0.43 ± 0.16 µg/mg dw in *prx11-1* and 0.73 ± 0.33 µg/mg dw in WT) (fig. 86 A). Although the aromatic content is not significantly enhanced, an increase by 52 % (1.14 ± 0.34 µg/mg dw in *prx11-1* and 0.73 ± 0.19 µg/mg dw in WT) is visible. The content of *trans* ferulic acid is enhanced by 2.1 fold (0.21 ± 0.10 µg/mg dw in *prx11-1* and 0.10 ± 0.03 µg/mg dw in WT), while the amount of diferulic acid is decreased by 25 % (0.06 ± 0.02 µg/mg dw in *prx11-1* and 0.08 ± 0.02 µg/mg dw in WT) (fig. 87 D). Even though the increase of *trans* ferulic acid and decrease of diferulic acid is not significant, similar but significant effect is detectable in the *prx11-2* mutant. Here, the content of *trans* ferulic acid is increased by 2 fold (0.20 ± 0.01 µg/mg dw in *prx11-2* and 0.10 ± 0.03 µg/mg dw in WT) and diferulic acid shows a decline by 38 % (0.05 ± 0.01 µg/mg dw in *prx11-2* and 0.08 ± 0.02 µg/mg dw in WT). Furthermore, the content of *trans* coumaric acid is decreased by 25 % (0.03 ± 0.01 µg/mg dw in *prx11-2* and 0.04 ± 0.01 µg/mg dw in WT). The total aromatic content is indistinguishable from the WT (fig. 87 D). The mutation in *prx11-1* does not influence the relative aromatic composition. The mutant *prx11-2* reveals a decrease in hydroxycinnamyl-monomers by 4.7 % (3.8 ± 1.3 % in *prx11-2* and 8.5 ± 5.9 % in WT) (fig. 86 E). Considering the aliphatic suberin the ω-hydroxy acids exhibit a rise by 32 % (6.2 ± 0.48 µg/mg dw in *prx11-2* and 4.7 ± 1.8 µg/mg dw in WT) (fig. 87 C). Significant alterations are evaluated in three suberin single constituents. The C_{16} monocarboxylic acid is decreased by 28 % (0.57 ± 0.03 µg/mg dw in *prx11-2* and 0.79 ± 0.33 µg/mg dw in WT), the C_{20} primary alcohol and the $C_{18:1}$ ω-hydroxy acid are increased by 41 % (C_{20} primary alcohol: 0.24 ± 0.01 µg/mg dw in *prx11-2* and 0.17 ± 0.06 µg/mg dw in WT, $C_{18:1}$ ω-hydroxy acid: 3.8 ± 0.47 µg/mg dw in *prx11-2* and 2.7 ± 1.2 µg/mg dw in WT) (fig. 87 A).

The mutant *asft1* reveals significant alterations in the suberin single constituents. The total suberin content and the aliphatic classes are not significantly altered in comparison to the WT (fig. 87 C). The C_{16} monocarboxylic acid is increased by 39 % (1.1 ± 0.09 µg/mg dw in

asft1 and 0.79 ± 0.33 µg/mg dw in WT) and the C_{16} α, ω-dicarboxylic acid by 42 % (0.68 ± 0.06 µg/mg dw in *asft1* and 0.48 ± 0.19 µg/mg dw in WT). The content of C_{18} and C_{24} ω-hydroxy acid are reduced by 33 % (0.12 ± 0.03 µg/mg dw in *asft1* and 0.18 ± 0.08 µg/mg dw in WT) and by 50 % (0.04 ± 0.01 µg/mg dw in *asft1* and 0.08 ± 0.05 µg/mg dw in WT) (fig. 87 B). With respect to the aromatics the content of *trans* coumaric acid is increased by 75 % (0.07 ± 0.01 µg/mg dw in *asft1* and 0.04 ± 0.01 µg/mg dw in WT). *Trans* ferulic acid is decreased by 82 % (0.02 ± 0.02 µg/mg dw in *asft1* and 0.11 ± 0.04 µg/mg dw in WT) and diferulic acid by 75 % (0.02 ± 0.001 µg/mg dw in *asft1* and 0.08 ± 0.02 µg/mg dw in WT) (fig. 86 D). Due to the increased content of *trans* coumaric acid the relative amount of hydroxycinnamyl-monomers are increased by 5.3 % (12.3 ± 3.1 % in *asft1* and 7.0 ± 1.7 % in WT) (fig. 87 E).

The aliphatic content and composition of the suberin is not altered in the mutant *asft2* in comparison to the WT (fig. 87 B). But significant alterations are found in the aromatic constituents of *asft2*. The total aromatic content is not significantly altered. But the content of *trans* ferulic acid is decreased by 73 % (0.03 ± 0.01 µg/mg dw in *asft2* and 0.11 ± 0.04 µg/mg dw in WT) and diferulic acid by 37 % (0.05 ± 0.01 µg/mg dw in *asft2* and 0.08 ± 0.02 µg/mg dw in WT) (fig. 87 D). The relative aromatic composition is not affected by the alterations in the aromatic constituents (fig. 87 E).

The mutant *fact3* does not exhibit significant alterations in the suberin content and aliphatic classes (fig. 87 C). There are only two significant alterations detectable in the suberin single constituents. C_{20} primary alcohol is increased by 35 % (0.23 ± 0.04 µg/mg dw in *fact3* and 0.17 ± 0.06 µg/mg dw in WT) and C_{18} ω-hydroxy acid by 33 % (0.24 ± 0.03 µg/mg dw in *fact3* and 0.18 ± 0.08 µg/mg dw in WT) (fig. 87 B). *Trans* coumaric acid reveals a decline by 25 % (0.03 ± 0.01 µg/mg dw in *fact3* and 0.04 ± 0.01 µg/mg dw in WT) (fig. 87 D). The loss of *trans* coumaric acid causes a decline in the relative hydroxycinnamyl-monomer content by 2.7 % (4.3 ± 1.3 % in *fact3* and 7.0 ± 1.7 % in WT) (fig. 87 E).

C4H::F5H reveals similar effects in the suberin aliphatic classes and the aromatic composition like in the previous sets. All suberin aliphatic classes exhibit an increased amount. Guiacyl-monomers are reduced, while sinapyl-monomers are enhanced (fig. 87 A, B, C, D, E).

A

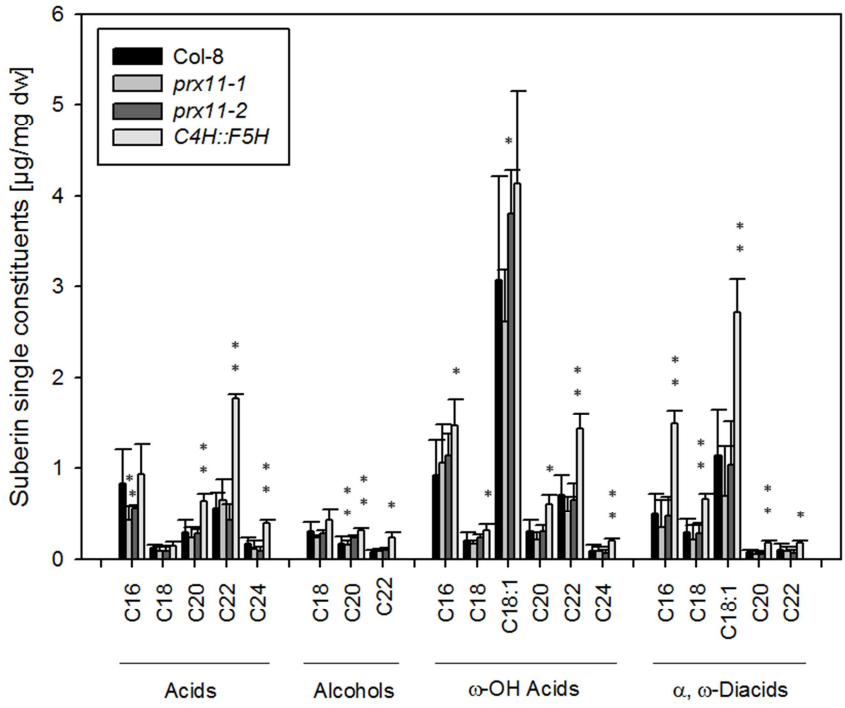
Suberin single constituents [µg/mg dw]
Col-8
prx11-1
prx11-2
C4H::F5H
C16
C18
C20
C22
C24
C18
C20
C22
C16
C18
C18:1
C20
C22
C24
C16
C18
C18:1
C20
C22
Acids
Alcohols
ω-OH Acids
α, ω-Diacids

B

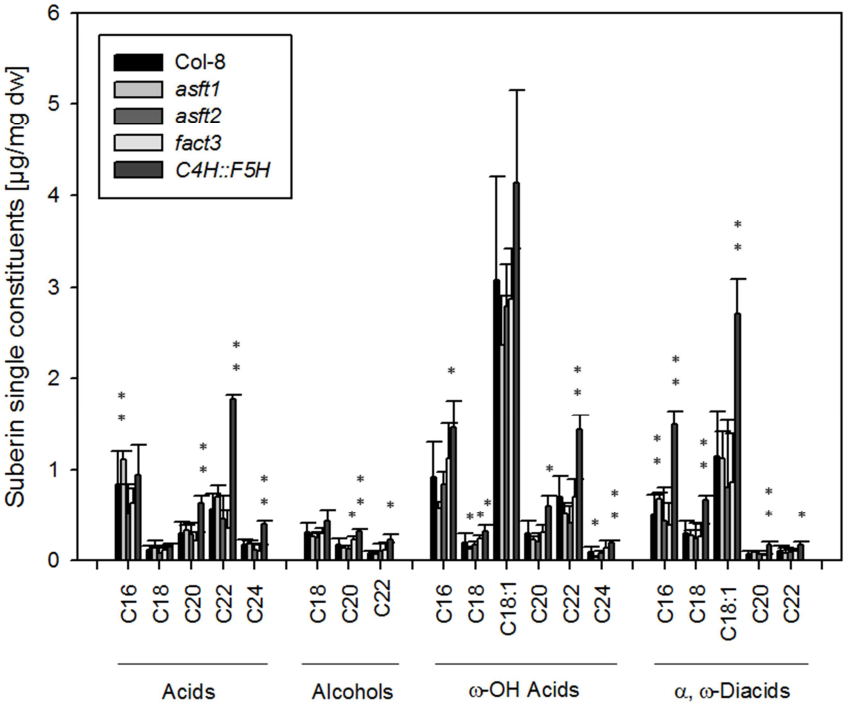
Suberin single constituents [µg/mg dw]
Col-8
asft1
asft2
fact3
C4H::F5H
C16
C18
C20
C22
C24
C18
C20
C22
C16
C18
C18:1
C20
C22
C24
C16
C18
C18:1
C20
C22
Acids
Alcohols
ω-OH Acids
α, ω-Diacids

C

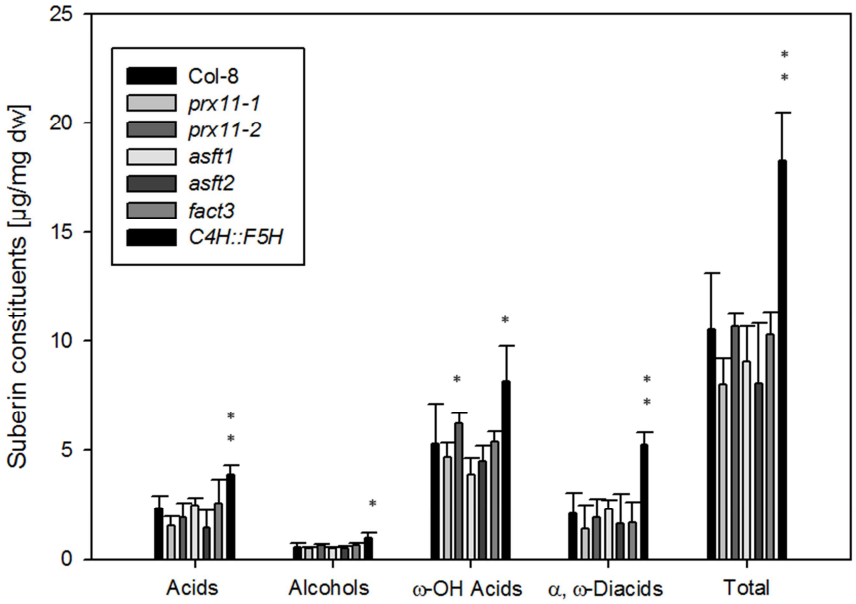
Suberin constituents [µg/mg dw]
25
20
15
10
5
0
Col-8
prx11-1
prx11-2
asft1
asft2
fact3
C4H::F5H
Acids
Alcohols
ω-OH Acids
α, ω-Diacids
Total

D

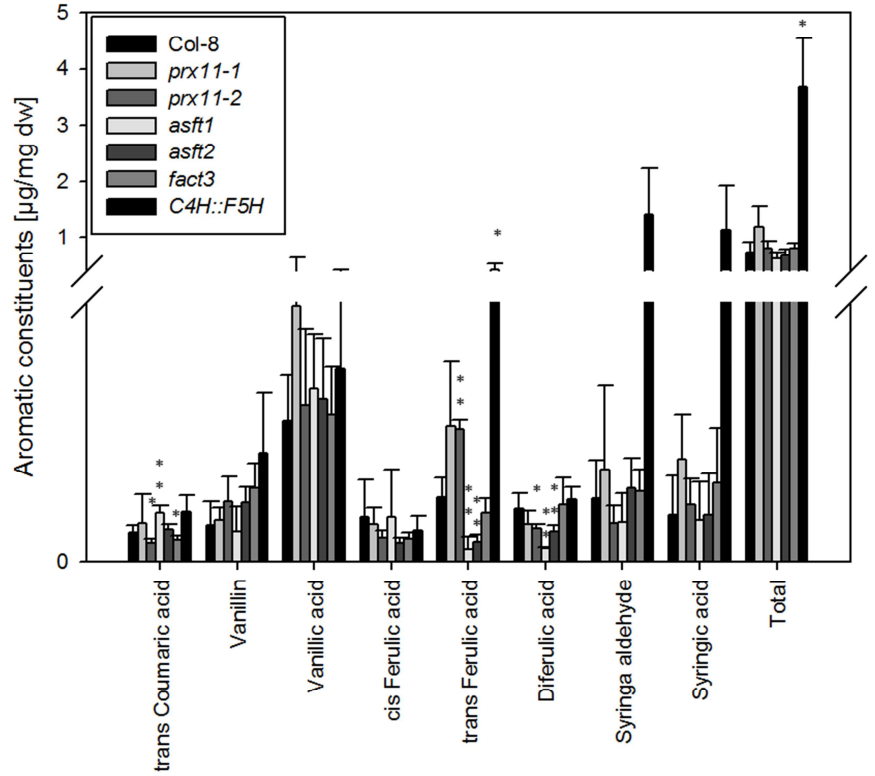
Aromatic constituents [µg/mg dw]
5
4
3
2
1
0
Col-8
prx11-1
prx11-2
asft1
asft2
fact3
C4H::F5H
trans Coumaric acid
Vanillin
Vanillic acid
cis Ferulic acid
trans Ferulic acid
Diferulic acid
Syringa aldehyde
Syringic acid
Total

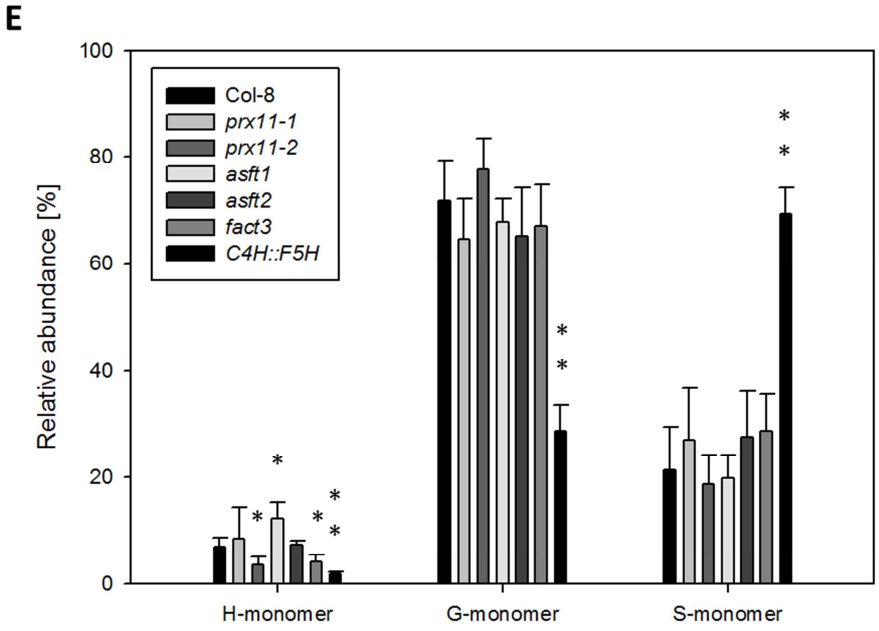

Fig. 87: Comparison of root aliphatic suberin and aromatic compounds of the mutant lines *prx11-1*, *prx11-2*, *asft1*, *asft2*, *fact3* and *C4H::F5H* with the corresponding WT

Five weeks old hydroponically grown roots treated with cell wall degrading enzymes were analysed. **A**: Composition of the suberin aliphatic single constituents of *prx11-1*, *prx11-2*, *C4H::F5H* and WT related to the root dry weight. B: Composition of the suberin aliphatic single constituents of *asft1*, *asft2*, *fact3*, *C4H::F5H* and WT related to the root dry weight. **C**: Composition of the suberin aliphatic substance classes related to the root dry weight. **D**: Composition of the aromatic compounds related to the root dry weight. **E**: Relative aromatic composition related to the root dry weight. The represented values are the arithmetic mean of the WT and mutant lines respectively and the calculated error bars of standard deviation. The sample amount corresponds to 12 roots of WT, four of *prx11-1*, three of *prx11-2*, four of *asft1*, *asft2*, *fact3* and three of *C4H::F5H* respectively. Acids: monocarboxylic acids, Alcohols: primary alcohols, ω-OH Acids: ω-hydroxy acids, α, ω-Diacids: α, ω-dicarboxylic acids. H-monomer: hydroxycinnamyl-monomer, G-monomer: guiacyl-monomer, S-monomer: sinapyl-monomer. *: student's t-test, $p \leq 0.05$, **: student's t-test, $p \leq 0.01$.

3.4.3. Summary of the chemical analysis of the lignified and suberised endodermal network

The following table summarises the obtained results from the chemical analysis of the lignified and suberised endodermal network. The mutant lines are put into order based on the lignin content. It starts with unaltered amount of lignin, continues with reduced content and ends with increased lignin content.

Tab. 16: Summary of the obtained results from the chemical analysis of the lignified and suberised endodermal network in soil- and hydroponically grown roots

Genotype	Total lignin	G/S ratio of lignin	Aliphatic suberin	Esterified aromatics
WT		more G, less S		
periderm	WT-like	WT-like	unsatured aliphatic compounds not present	high amount of guiacyl-related monomers
myb7			WT-like	WT-like
myb4			WT-like	WT-like
fact3			WT-like	WT-like
cadc	WT-like	WT-like	WT-like	WT-like
cadd	WT-like	WT-like	WT-like	WT-like
hqt	WT-like	WT-like	WT-like	WT-like
ref1-4	WT-like	WT-like	WT-like	WT-like
asft1			WT-like	less ferulic acid, less diferulic acid
asft2			WT-like	less ferulic acid, less diferulic acid
prx11-1			WT-like	more ferulic acid, less vanillic acid Less diferulic acid
prx11-2			WT-like	more ferulic acid, less vanillic acid less diferulic acid
esb1	WT-like	WT-like	enhanced	more ferulic acid, more diferulic acid
ref8-2*fah1-2* AtC4H::SmF5H	WT-like	more S, less G	WT-like	WT-like
fah1-2	WT-like	less S, more G	WT-like	WT-like
ref8-1			more monocarboxylic	less ferulic acid

			acids	
ccoaomt1	reduced	WT-like	ω-OH Acids reduced	less ferulic acid, less diferulic acid
comt1	reduced	less S, more G	WT-like	more ferulic acid
ccr1	reduced	less S, more G	WT-like	more ferulic acid
cadc*cadd* fah1-2	reduced	less S, more G	WT-like	more ferulic acid
ref4-3	reduced	less S, more G	WT-like	WT-like
cadc*cadd	reduced	WT-like	WT-like	more ferulic acid
ref3-2	reduced	WT-like	enhanced	less ferulic acid
ref8-1* med5a*med5b	enhanced	WT-like	slightly enhanced	slightly enhanced
C4H::F5H	enhanced	more S, less G	enhanced	more ferulic acid, more syringyl-monomers

4. Discussion

4.1. Selection of putative candidate genes

Suberin research was focused on the aliphatic constituents. The knowledge about the aromatics involvement in the suberin polymer is still limited. The phenylpropanoid pathway allocates *trans* ferulic acid for the suberin polymer. Co-expression analysis has been conducted with phenylpropanoid pathway genes to elucidate a suberin tissue specific expression. At first, databank analysis of typical suberin and Casparian strip genes does not show any co-expression with phenylpropanoid genes. When querying for genes co-expressed with phenylpropanoid pathway and suberin the only suberin associated gene identified is *ASFT* (tab. 12). Substrate of ASFT is feruloyl-CoA and involvement in suberin biosynthesis has been shown (Molina et al., 2009). Expression of *CCoAOMT1* is similar to expression of *ASFT* but there are more than 100 genes more closely co-expressed with *ASFT*. This indicates not direct relationship between the suberin gene *ASFT* and the phenylpropanoid pathway gene *CCoAOMT1*. It demonstrates that phenylpropanoid biosynthesis appears to be independent from suberin aliphatic biosynthesis. Phenylpropanoid pathway provides several products used for example for plant defence, act against damage of UV irradiation and attract pollinators (Holton and Cornish, 1995; Jin et al., 2000; Dixon et al., 2002). Due to this, the phenylpropanoid pathway has to be independent and is not directly associated to suberin synthesis. Additionally, typical Casparian strip genes are not co-expressed with phenylpropanoid biosynthesis genes, indicating the CS formation to be independent from biosynthesis of phenylpropanoids. Typical phenylpropanoid biosynthesis genes are primarily co-expressed with other biosynthesis genes of the secondary metabolism like flavonoid biosynthesis (fig. 98 to 106). Consequently, the focus of phenylpropanoid biosynthesis genes was on tissue specific expression instead of information from co-expression. Of high interest was the gene expression in endodermal and seed coat tissue because both are impregnated with suberin (Franke et al., 2005; Beisson et al, 2007). High expression just in stem tissue indicates genes to be lignin associated. Most of the phenylpropanoid biosynthesis genes are highly expressed in the endodermal and seed coat tissue indicating that phenylpropanoids might be involved in the suberin biosynthesis. The

two exceptions are *FAH1* and *REF1*. Both are neither endodermal nor seed coat specific expressed (fig. 23 and fig. 27). *FAH1* and *REF1* contribute to the synthesis of sinapate esters. Furthermore, *fah1* mutants fail to deposit S-lignin in stem tissue. Expression of *FAH1* under the promoter of the phenylpropanoid pathway gene *C4H* in *fah1-2* background (designated as *C4H::F5H*) leads to almost exclusive deposition of S-lignin in the stem tissue but also to a disrupted Casparian strip barrier, which is accompanied by ectopic suberisation. Therefore, the mutant *C4H::F5H* was used in this study as a positive control for suberisation and as a negative control for the formation of a functional Casparian strip barrier (Chapple et al., 1992; Meyer et al., 1998; Fraser and Chapple, 2011). REF1 is responsible for the $NADP^+$-dependent oxidation of coniferaldehyde and sinapaldehyde to the corresponding ferulate and sinapate. It has been demonstrated that *ref1* plants produce 10 % less sinapate esters in the leaf epidermis and the mutant plants contain reduced amounts of cell wall esterified ferulic acid (Nair et al., 2004; Fraser and Chapple, 2011). Due to the tissue specific expression as well as the biochemical function of FAH1 and REF1 it is unlikely that both enzymes might contribute to the suberin biosynthesis. Nevertheless, both were selected for the work.

The following genes show all a high endodermal and seed coat tissue specific expression, which is associated with suberin. C4H is one of the first enzymes in the phenylpropanoid pathway and therefore a key enzyme for downstream products. The *ref3* mutants, affected in *C4H*, show a strong decrease in the lignin content and collapsed xylem. Moreover, the mutants is characterised by a dwarfed phenotype, male sterility and reduced in apical dominance (Schilmiller et al., 2009). Thus, *REF3* mutation causes a severe phenotype and consequently, the mutation might affect the suberisation and the development of Casparian strips as well.

The genes *C3H* and *HCT* are both located upstream of feruloyl-CoA synthesis. Mutations in both genes show a dwarfed phenotype and decreased lignin content in stems. But *ref8* mutant plants, affected in *C3H*, deposit less G- and S-lignin and H-lignin instead, whereas *HCT-RNAi* mutant plants exhibit reduction in S-lignin in stem tissue (Franke et al., 2002b; Hoffmann et al., 2004; Fraser and Chapple, 2011). However, it has been demonstrated that *C3H*-deficient mutants still contain substantial proportion of G- and S-lignin in the lignified root tissue, indicating a C3H-independent route of *meta*-hydroxylation (Abdulrazzak et al., 2006). Both genes, *C3H* and *HCT*, are highly expressed in the endodermal and seed coat tissue. Due to this, both genes are good candidates for the study. Unfortunately, no

knockout mutant was found for *HCT* and therefore this gene cannot be studied in this work further.

The gene *CCoAOMT1* is considered to be a crucial gene in providing feruloyl-CoA for the assembly of the polyaromatic domain. Down regulation of *CCoAOMT* in alfalfa causes a decline in G-lignin and increases as a result the S/G ratio (Guo et al., 2001). Thus, a decrease in the ferulic acid content of the suberin might be possible by loss of function mutation in *CCoAOMT1* and furthermore, the formation of Casparian strips might be affected as well.

CCR1 is an important gene for the lignification of stem and xylem tissue. Mutation in the gene causes a decreased lignin content, dwarfed phenotype and delayed senescence. The enzyme is located downstream of feruloyl-CoA (Jones et al., 2001; Derikvand et al., 2008; Fraser and Chapple, 2011). Consequently, *ccr1* mutant might accumulate feruloyl-CoA which possibly would provide more ferulic acid to the suberin assembly. Due to the lack of lignin the Casparian strip might be disrupted in the mutant line.

The two cinnamyl alcohol dehydrogenases CADC and CADD are both specific for the synthesis of coumaryl, coniferyl and sinapyl alcohol (Kim et al., 2004). Single knockout mutation of the *CAD* genes does not affect the lignin content and composition, but double knockout leads to unusual accumulation of conifer- and sinapaldehyde (Sibout et al., 2003; Sibout et al., 2005; Anderson et al., 2015). It is highly questionable whether a Casparian strip barrier is functional only built by aldehydes and whether suberisation is affected by the double knockout mutation as well. Possibly, feruloyl-CoA accumulates in the double knockout mutant since in total less lignin is synthesis, which may cause a reflux of the phenylpropanoid pathway towards feruloyl-CoA synthesis.

T-DNA insertion mutation in *COMT1* reduces the S-lignin content in the stem tissue (Goujon et al., 2003). Casparian strip formation might not be affected by the mutation but feruoyl-CoA synthesis could be enhanced by the accumulation of guiacyl associated compounds and finally redirected to feruloyl-CoA synthesis.

The two transcription factors *MYB4* and *MYB7* were chosen due to their regulatory function of the phenylpropanoid pathway. *MYB4* controls the formation of sinapate esters. The knockout mutant *myb4* accumulates sinapate esters and arouses higher tolerance against UV-B radiation. Additionally, the expression of *C4H* is increased in the *myb4* mutant (Jin et al., 2000). Thus, it might be possible that the *myb4* mutant also provides more ferulic acid to suberin biosynthesis than the WT. *MYB7* acts as a repressor of the flavonoid biosynthesis.

The mutant *myb7* shows an increased flavonoid content, whereas anthocyanins are decreased (Fornalé et al., 2014). Possibly, a lack of MYB7 might drive the phenylpropanoids to the synthesis of flavonoids and thereby may reduce the amount of ferulic acid for the suberin biosynthesis.

With respect to peroxidases, some of them (At1g68850/PRX11, At5g14130, At2g35380, At5g66390, At5g42180/PER64, At1g05260/RCI3) are notated as to be involved in phenylpropanoid biosynthesis (fig. 90, 92 and 96). As demonstrated in the master thesis of Matthias Brands and in this work PRX11 appears to be not involved in the phenylpropanoid pathway biosynthesis, rather it is associated with linking ferulic acids to diferulic compounds (Brands, 2014). PER64 is involved in the Casparian strip formation (Lee et al., 2013) and therefore also not a phenylpropanoid biosynthesis gene. Rare Cold Inducible gene 3 (RCI3) seems to play a crucial role during potassium-deprivation. Under conditions of low potassium RCI3 is upregulated, enhances the reactive oxygen species (ROS) concentration in the root and subsequently expression of a potassium transporter (Kim et al., 2010). Thus, RCI3 does not seem to be connected with lignin or suberin synthesis. The peroxidase At5g14130 was found to be expressed in the embryo sac (Yu et al., 2005), At2g35380 expression appears to be increased through salicylic acid signalling caused by pathogen infiltration (Lee et al., 2006), At5g66390 called PRX72 participates in lignification process of interfascicular fibres (Férnandez-Pérez et al, 2015). Taken together, some peroxidases like PRX11, PER64 and PRX72 seem to use phenylpropanoids as substrates and At5g14130 as well as At2g35380 are either indirectly associated with phenylpropanoids or relationship between phenylpropanoids and peroxidase is still unclear. Thus, the annotation from the databank is partial correct.

4.2. Mutant lines *esb1* and *C4H::F5H* show a non-functional Casparian strip barrier accompanied by ectopic lignification and suberisation

In this work *esb1* and *C4H::F5H* were used as positive controls for enhanced suberisation and as negative controls for a functional Casparian strip barrier. The non-functionality of the Casparian strip barrier in *esb1* has been demonstrated already by Hosmani et al. (2013). In

the ERA-CAPS collaboration the mutant *C4H::F5H* was identified as a Casparian strip mutant. However, the reason for the delayed blockage of the apoplastic tracer PI is different in both mutants. The mutant *esb1* shows holes in the Casparian strip network. Due to the loss of the dirigent domain-containing protein ESB1, lignin accumulates in the corner of the endodermal cells (fig. 41 and 42; Kamiya et al., 2015). It is assumed that this ectopic lignification is an attempt to compensate for the disrupted Casparian strip network. Ectopic lignification is accompanied by ectopic suberisation (Hosmani et al., 2013). In *C4H::F5H* the accumulation and polymerisation of S-monolignols seems to impair the Casparian strip barrier (fig. 37). Furthermore, lignin is ectopically deposited in the cell wall (fig. 44) and suberisation starts earlier in the mutant as well (fig. 48 B). However, with respect to the lignin content and composition in *esb1* contradictory results were obtained. Digestion of the root cell walls by cellulase and pectinase causes a slightly decrease in lignin content (fig. 73 A), whereas undigested roots contain more lignin polymer than the WT (fig. 74 A). The assumption that the ectopic lignification may influence the cell wall degradability is refuted by the root dry weight of digested and undigested samples. Both dry weights are similar to WT root dry weights (fig. 135 and 136). Due to the ectopic lignification it is expected that *esb1* contains more lignin, corresponding to results from undigested samples. Possibly, digestion causes loss of ectopically lignified root parts, because the ectopic lignification consists of patchy deposited lignin islands instead of a stable network (Hosmani et al., 2013). What remains is the disrupted Casparian strip barrier, which in total contains less lignin than the intact one in WT roots (fig. 73 A). Therefore, ectopically deposited lignin is also extracted in undigested *esb1* roots. Here, the amount of G-monolignols is increased indicating that Casparian strips are possibly exclusively made of G-monolignol (fig. 74 A). In contrast, in *C4H::F5H* an accumulation of S-monolignols and a decrease of G-monolignols are measured, indicating a shift towards S-monolignols disrupts the Casparian strip. The total lignin content is slightly increased, which is consistent with the ectopic lignification (fig. 75 A, B). Taken together, these results demonstrate that a functional Casparian strip barrier is exclusively or predominately made of G-monolignol. Feeding experiments of Guilhem Reyt (laboratory of Prof. Dr. David Salt, University of Nottingham) support the assumption that a functional CS barrier is achieved by G-monolignol and not by S-monolignol polymerisation (unpublished data from Guilhem Reyt).

Chemical composition of the suberin polymer of both mutants shows an increase in the aliphatic suberin content (fig. 82 A, B, C and D). In *esb1* only the content of *trans* ferulic and diferulic acid is increased. In *C4H::F5H* *trans* coumaric acid, *trans* ferulic and diferulic acid, syringa aldehyde as well as syringic acid contents are found in higher amounts (fig. 82 E and F). Combining the results indicate that an increased aliphatic suberin content is accompanied by an elevated amount of *trans* ferulic and diferulic acid. The mutations in *C4H::F5H* also influence the composition of cell wall bond phenolic compounds. As described in the following chapter 4.3., *trans* coumaric acid, vanillin, vanillic acid, syringa aldehyde and syringic acid do not seem to be part of the suberin polymer. Furthermore, the ultrastructure of the suberin polymer is still similar to the WT. Lamellar-like structure is still well formed and demonstrates the specificity of the *trans* ferulic acid as a substrate of the polymer. Only the diameter of the suberin seems to be increased in the further developed part of the root (fig. 72 B). It might be possible that *trans* ferulic acid acts as a cross-linker and ensures the growth of the suberin diameter. The increased amounts of aliphatic constituents are linked to the additional *trans* ferulic acid and may built a new lamella. Furthermore, *C4H::F5H* reveals in the cross section close to the hypocotyl an additional cortical cell layer (fig. 72 A), whereas the WT still contains one cortical cell layer (fig. 57 A). During maturation process another cortical cell layer is developed (Dolan et al., 1993). It appears that *C4H::F5H* develops faster than the WT.

4.3. Cell wall bond aromatic compounds

Partial depolymerisation of cork oak suberin was able to demonstrate that transesterified ferulic acid is part of the suberin polymer (Santos and Graça, 2006). The analytical approach of suberin analysis extracts many different aromatic compounds beside *trans* ferulic acid from the digested root tissue. Other aromatic compounds are *trans* coumaric acid, vanillin, vanillic acid, diferulic acid, syringa aldehyde and syringic acid (fig. 82 E and F). Passardi et al. (2004) demonstrated that several hydroxycinnamates are covalently attached to the cell wall. Ferulic acid is the major compound found in the cell wall of most plants. In stem tissue of cereals however *p*-coumaric acid tends to be predominant. Also, vanillin and vanillic acid are found in good quantities in stem tissue of the wheat *Triticum vulgare*. The aromatic compounds are esterified to pectin in dicots and to arabinoxylans in monocots. Cell

differentiation seems to start with the accumulation of ferulic and diferulic acid content in the primary cell wall. Accumulation of both compounds also inhibits cell elongation and cell wall extensibility. Both compounds contribute to cell wall rigidity (Passardi et al., 2004). Dimers of ferulic acid seem to act as cross-linkers of cell wall components (Eraso and Hartley, 1990; Iiyama et al., 1994; Waldron et al., 1996). As cross-linking feature, the ferulic acid dimers have been implicated in either polysaccharide-polysaccharide or polysaccharide-lignin interactions (Iiyama et al., 1994; Ralph et al., 1995). The ferulic acid monomers seem to be oxidatively coupled within the cytosol. But apoplastic dimerisation is not disregarded (Lindsay and Fry, 2008). Furthermore, the monomeric ferulic acid bond to the cell wall may act as target site for lignification. In cell walls of grass, ferulic acid is associated to the β position of coniferyl alcohol. This provided evidence that ferulic acid monomers serve as growth points for the lignin polymer and besides as anchoring point to the polysaccharides (Jacquet et al., 1995). Moreover, ferulic acid and diferulic acid may provide an antimicrobial barrier in the wall (Faulds and Williamson, 1999). This might be due to the fact that, for instance, high concentrations of ferulic acid are toxic to microorganisms. Ferulic acid inhibits the growth of the production strain or causes even cell lysis (Gallage and Møller et al., 2015). Enzymes of the biosynthetic production of vanillin, vanillic acid, syringa aldehyde and syringic acid remained unknown until the year 2014. Vanillin is the key component of the vanilla flavour. In *Vanilla planifolia* a single enzyme belonging to the hydratase/lyase type catalyses direct conversion of ferulic acid and its glucoside into vanillin and its glucoside, respectively. The discovered gene is named vanillin synthase (*VpVAN*) (Gallage et al., 2014). A homolog gene sequence with 80.9 % identity has been found by blast result as well in *Arabidopsis thaliana* (fig. 152). This gene is highly transcribed in the root tissue, seed coat and stem tissue (fig. 153). The function of vanillin and vanillic acid in the cell wall is still unknown. Due to the chemical structure, vanillin cannot act as a cross-linker. Cross-linking activity appears to be possible for vanillic acid. It might be possible that vanillic acid, similar to ferulic acid, serve as growth point for the lignin or suberin polymer. Syringa aldehyde and syringic acid are known to accumulate in response to manipulation of the phenylpropanoid pathway towards the preferred synthesis of S-lignin in the mutant *C4H::F5H* (fig. 82 E and G, fig. 83 C and D, fig. 85 D and E, fig. 86 D and E, fig. 87 D and E). This indicates that both compounds are derived from sinapate compounds. However, vanillin and syringa aldehyde cannot be cross-linkers of a polymer, because vanillin and syringa aldehyde only contain one

hydroxy-group. Thus, vanillin and syringa aldehyde might be derivatives of vanillic acid and syringic acid generated by the chemical transesterification process during suberin sample preparation. But it is also possible that both compounds are positioned at the ends of the suberin polymer. Summarising, it might be possible that a similar enzyme like the vanillin synthase from *Vanilla planifolia* is present and active in *Arabidopsis thaliana* and may catalyse the reaction from sinapates to syringic acid and from *trans* ferulic acid to vanillic acid. Respective enzymes involved in synthesis of aromatic compounds isolated from suberin might be interesting to research further in the context of suberin synthesis.

4.4. Knockout of *HQT* appears to influence Casparian strips development

The gene *HQT* was found based on sequence similarity with the *HQT* gene in *Solanum tuberosum*. *HQT* is a gene closely related to *HCT* in *Solanum tuberosum* (fig. 148). For example, it is involved in the formation of chlorogenic acid in tobacco and tomato (Niggeweg et al., 2004). This organic acid is caffeoyl quinic acid. It has been demonstrated that HCT is able to esterify coumaroyl CoA with either shikimic acid or quinic acid. *Meta*-hydroxylation of the coumaryol quinic acid leads to the formation of caffeoyl quinic acid. HCT is also able to disestablish the ester bond between both but HQT has that ability as well (Hoffmann et al., 2004; Payyavula et al., 2014). In *Arabidopsis thaliana* a phenylpropanoid pathway route via the enzyme HQT neither has been described yet nor has been excluded. However, *Arabidopsis thaliana* does not seem to contain chlorogenic acid (Payyavula et al., 2014). Therefore, it is of interest to elucidate this alternative pathway within the phenylpropanoid pathway in *Arabidopsis thaliana*.

Microscopical analysis of *hqt* and *RALPH::HQT* show earlier formation of an apoplastic barrier by staining with PI (fig. 34). Qualitative analysis of the Casparian strip formation by staining with basic fuchsine does not show an earlier establishment of the Casparian strip barrier (fig. 41). However, the lignified endodermal network below the 6^{th} endodermal cell is uncompleted in *hqt*, whereas the lignified endodermal network is already completed in WT *RALPH::HQT*. Since the establishment of the Casparian strip barrier in both mutants *hqt* and *RALPH::HQT* is similar to the WT, results of the lignin-specific staining and the staining of the

apoplastic tracer PI appear to be contradictory. But, the lignin-specific staining shows that the development of the xylem vessels is delayed in *hqt* and *RALPH::HQT* in comparison to the WT (fig. 41). A delayed development of xylem vessels may impair the vascular transport, which has to be considered for the PI staining as well. Propidium iodide diffuses through the uncompleted Casparian strip barrier into the vascular tissue. From there the propidium iodide diffuses further upstream to the basal part of the root. Thus, it might be possible that the root hydraulic conductance is impaired in both mutants due to the less developed xylem vessels and therefore the uptake of propidium iodide is blocked earlier in both mutants. Surely, the obtained results from PI staining are a combination of both PI blockage by apoplastic barrier formation and basal transport of taken up PI in the xylem vessels.

With respect to the tissue specific expression of HQT results were obtained by Roppolo et al. in 2014. HQT protein is notated as a CASP-like protein (CASPL5B2), which is found in the stele of the meristematic zone, in the lateral root primordia and young leaves (Roppolo et al., 2014). A particular involvement of HQT/CASPL5B2 in the formation of xylem vessels cannot be excluded and might influence the PI phenotype, causing the observed difference between completion of lignin network and PI blockage.

The suberisation in *hqt* does not seem to be affected. However, expression of *HQT* in endodermal cells under the suberin specific promoter of *RALPH* enhances slightly and significantly the suberisation (fig. 46 B). Although a high number of WT and also a substantial number of *hqt* and *RALPH::HQT* roots were used, the increase in suberisation is not convincing in comparison to the positive control *esb1*. The slight increase in suberisation in *RALPH::HQT* is not comparable with an ectopic suberisation found in *esb1*. A repetition of the fluorol yellow 088 staining with the mutant line *anac038-1*, which shows an increased suberin content (Frenger, 2014), might validate the shown data. Furthermore, an analysis of the chemical composition of the suberin polymer of *RALPH::HQT* is required, which might elucidate an elevated suberisation.

Analysis of the chemical composition of lignin and suberin in five-week old roots of *hqt* does not show any alterations compared to the WT (fig. 73 A and B; fig. 77 A, C and D; fig. 82 A, C, E and G). This is consistent with the histochemical analysis of the lignified endodermal network and the suberised zones. But roots of *hqt* and *RALPH::HQT* showed a delayed formation of xylem vessels. The delayed development of the xylem vessels cannot be studied in fully matured roots, since developmental processes may compensated by time.

Thus, a lignin extraction of *hqt* seedlings is required to emphasise an expected delay in formation of the xylem vessels, which might influence the root hydraulic conductance. Another option is to analyse the root hydraulic conductance system by histochemical analysis of root cross sections.

Since, the putative HQT gene does not show any specific effect in the lignin composition it is arguable whether the found HQT gene is closely related with the *HQT* gene in *Solanum tuberosum*. Therefore, a new sequence blast was performed and another gene was found with the exact same sequence similarity of 42.23 % as the previous found one *HQT* gene (fig. 150). The enzyme belongs to the HXXXD-type acyl-transferase protein family. It seems to be related to a benzoyl-CoA:anthranilate N-benzoyltransferase *Dianthus caryophyllus* (Yang et al., 1997). Databank analysis shows endodermal, chalazal seed coat and bottom of stem specific analysis (fig. 151). This gene might be another good candidate for further analysis to give evidence about the existence of this alternative route of caffeoyl-CoA synthesis.

4.5. *CCoAOMT1*, *COMT1* and *CCR1* contribute to the development of apoplastic barriers

Knockout of the genes *CCoAOMT1, COMT1* and *CCR1* influence the formation of the Casparian strip barrier. The PI blockage is delayed in all three knockout mutants (fig. 34). Furthermore, qualitative analysis of the Casparian strips shows a faint staining in *ccoaomt1* and *ccr1* (fig. 41). Unfortunately, lignin specific staining of *comt1* failed and has to be repeated in the future. The mutant *comt1* shows a delayed blockage of the PI diffusion into the vascular tissue similar to the mutant lines *ccoaomt1* and *ccr1*, it is speculated that *comt1* may reveal a faint staining as well. Consistent with this, the lignin content in mature roots is decreased in all three mutants. Especially *ccr1* and *comt1* exhibit a lack of S-lignin, whereas in *ccoaomt1* amounts of G-monomers are decreased (fig. 73 A and B). Suberin specific staining of seedlings shows a delayed suberisation process in *ccoaomt1*, *comt1* and *ccr1*. However, in *ccoaomt1* and *comt1* suberisation starts at the same position like in the WT, whereas *ccr1* is completely delayed (fig. 46 B). Chemical analysis of the suberin polymer shows that amounts of the suberin aliphatic monomers in *comt1* and *ccr1* are unaffected. This might be explained by the reason that suberisation is a time-dependent process. In five-

week old fully matured roots the temporal delay of suberisation appears to be compensated. But *ccoaomt1* exhibits a decrease in especially ω-hydroxy acids which is accompanied by a decrease of ferulic and diferulic acid (fig. 77 A, B, C and D; fig. 82 A, B, C, D, E, F and G). These results demonstrate several points. The first one is that a delayed formation of the Casparian strip barrier is not always accompanied by ectopic suberisation like in *esb1*. So far, only mutants were described with a defective Casparian strip barrier and accompanied ectopic suberisation like *esb1*, *casp1-1*casp3-1*, *myb36* (Baxter et al., 2009; Hosmani et al., 2013; Kamiya et al., 2015). The exception is *sgn3* with completely disrupted Casparian strip barrier without ectopic suberisation, which is affected in ectopic suberin signalling (Pfister et al., 2014). Secondly, both transesterified ferulic and polymerised diferulic acid are crucial for the suberisation. Deficiency of both limits suberisation, but excess does not enhance suberisation. This indicates that the additional ferulic and diferulic acid are not part of suberin. Maybe the excess of both is transesterified to the cell wall. Furthermore, only excess of *trans* ferulic and diferulic acid does not induce enhanced suberisation. Appropriately, in a *ccr1* knockout line more cell wall bond ferulic acids were found (Derikvand et al., 2008), which is consistent with the results from this work (fig. 82 F). As already described in chapter 4.3., it is speculated that also syringa aldehyde and syringic acid are esterified components within the cell wall. Amounts of both aromatic compounds are reduced in *comt1*. Nonetheless, the suberin content is not affected by the decrease of both compounds (fig. 82 E) indicating that syringa aldehyde and syringic acid are not part of the suberin polymer and rather exclusively cell wall bond phenolic compounds. Additionally, coumaric acid content is enhanced in *ccoaomt1*, but ω-hydroxy acid compounds are decreased and other aliphatic classes are unaltered. Thus, it can be concluded that coumaric acid is bond to the cell wall as well.

With respect to the lignin content, in all three mutants the three typical monolignol classes were found. Knockout of *ccoaomt1* decreases the synthesis of G-monolignols in the root tissue (fig. 73 A). The synthesised G- and S-monolignols have to be rerouted via CCR1 yielding into the formation of caffealdehyde, which is catalysed by COMT1 to coniferaldehyde. This route of the phenylpropanoid pathway was found in alfalfa (Guo et al., 2001; Parvathi et al., 2001). Based on lignin analysis of stem tissue in another *ccoaomt1*-deficient mutant of *Arabidopsis thaliana* an alternative route has been also speculated (Do et al., 2007). These results emphasise the existence of an alternative pathway for the

synthesis of G- and S-monolignols not only in the stem, but also in the root tissue. However, this alternative pathway can be described as a non-efficient pathway, demonstrated by the delayed formation of the Casparian strip barrier in *ccoaomt1*. The gene *COMT1* is also important for the synthesis of S-monolignols in the root tissue. Knockout mutation decreases the G- and S-monolignols in the stem (Goujon et al., 2003). As this work demonstrates G- and S-monolignols are decreased in the root tissue as well (fig. 73 A and B). Again these results emphasise the alternative route of the synthesis of G-monolignols via the reduction of caffeoyl CoA to caffealdehyde by CCR1. A small proportion of G-monolignols is synthesised via this alternative way. This may explain the delayed formation of a functional Casparian strip barrier in *comt1* mutant. CCR1 is crucial for the synthesis of G- and S-monolignols in both the stem and root tissue (fig. 73 A and B; Derikvand et al., 2008). Loss of function mutation causes a dwarfed phenotype and a delayed formation of the Casparian strip barrier. How exactly *COMT1* and *CCR1* influence the suberisation in seedlings remains unclear, whereas in the *ccoaomt1* mutant the delayed formation of a continuously suberised zone is caused by the limited formation of feruloyl-CoA.

4.6. Lack of functional MYB7 and MYB4 appears neither influence Casparian strip nor suberin development

MYB transcriptions factors are involved in several processes within the plant, for instance primary and secondary metabolism, development, determination of cell fate and identity as well as responses to environmental stresses (Zhou et al., 2015; Kim et al., 2015). Both transcription factors *MYB7* and *MYB4*, were chosen for their role as regulators in the phenylpropanoid pathway (Jin et al., 2000; Fornalé et al., 2014).

The obtained results from both mutant lines *myb7* and *myb4* do not show any participation in the development of suberin and Casparian strip. However, based on the statistical evaluation the blockage of the PI is significantly delayed in *myb4* (fig. 35). In comparison to WT the *myb4* mutant shows a delay in the blockage of the PI diffusion into the stele. Compared to the *esb1* mutant the difference is not that striking. It can be argued that the formation of the Casparian strip barrier is not delayed in *myb4*, as these differences might also appear in WT roots. However, the assumption that the development of Casparian strips

is delayed in *myb4* is supported by the suberin specific staining. Here, the non-suberised zone is significantly decreased (fig. 47 A and B). However, both patchy and continuously suberised zones are not significantly increased. Nonetheless, the suberisation seems to start earlier in *myb4* than in the WT.

Analysis of the chemical composition of the lignin polymer was not performed with the mutants. As the focus of the lignin analysis was on mutant lines with delayed formation of the Casparian strip or enhanced suberisation. However, the suberin polymer was analysed of both mutant lines. With respect to the aliphatic suberin monomers no significant alterations were detected. But the aromatic composition seems to be slightly altered in both mutant lines. The mutant *myb7* tends towards an increased *trans* coumaric acid content, whereas *myb4* shows slightly elevated amounts of syringa aldehyde and syringic acid (fig. 77 D; fig. 83 C). These results are also supported by the known facts about *myb4* plants. Knockout mutation of *MYB4* causes an accumulation of sinapate esters in leaves. Additionally, the transcript level of *C4H* is elevated. Conversely, this implies that MYB4 acts as a repressor of *C4H*. *MYB4* is mediated by the protein Sensitive to ABA and Drought 2 (SAD2) to the nucleus, where it represses the gene expression of *C4H* (Zhou et al., 2015). Furthermore, the transcript level of *CCoAOMT1* is decreased (Jin et al., 2000). Therefore, it was expected that the amount of feruloyl CoA is reduced in the root of *myb4* and influences negatively the suberisation. The results may indicate that *MYB4* is not the only regulator of *CCoAOMT1* expression in the root endodermis. The transcription factor MYB7 acts as a repressor of the flavonoid biosynthesis. Knockout mutation of *MYB7* results in decreased levels of anthocyanins, but increased amounts of flavonols. Especially, the expression of *PAL*, *C4H* and *4Cl* is induced by the lack of MYB7 (Fornalé et al., 2014; Kim et al., 2015). Key product of the flavonoid synthesis is the *p*-coumaroyl CoA. As already described *myb7* tends to accumulate *trans* coumaric acid. It might be possible that elevated amounts of *trans* coumaric acid are esterified to the cell wall. It was suggested that the flux of phenylpropanoids is driven to the flavonoids and may cause a lack of feruloyl-CoA. However, due to the normal suberisation pattern a lack of feruloyl-CoA is not expected. Although knockout mutations of both genes *MYB4* and *MYB7* did not influence the suberisation process further studies with both genes should be conducted.

Overexpression of *MYB7* leads to ectopically deposited lignin in the stem (Kim, 2016) and wounded leaf tissue, where suberin is deposited, down-regulates the transcript level of

MYB4 to ensure monolignol biosynthesis (Zhao and Dixon, 2011). Therefore, endodermal specific overexpression is proposed of both genes *MYB7* and *MYB4*, which might reveal result not observed in knockout mutants. Promoter of *RALPH* and *CASP1* are proposed to drive the expression of *MYB7* and *MYB4* in endodermal cells (Compagnon et al., 2009; Roppolo et al., 2011; Naseer et al., 2012).

4.7. Mutated *CAD* genes alter suberisation

All single mutated CAD genes (knockout of *CADC* and knockdown of *CADD*) as well as the double knockout mutants *cadc*cadd* plus *cadc*cadd 2* and the triple knockout mutant *cadc*cadd*fah1-2* do not affect the functionality of the Casparian strip barrier (fig. 36). However, staining of the lignified endodermal barrier shows only a faint staining in the double knockout mutant *cadc*cadd* and the triple knockout mutant, whereas the lignified endodermal barrier in *cadc*cadd 2* appears to be well developed (fig. 42). The double mutant *cadc*cadd 2* was created by the hybridisation of the single knockout mutant *cadc* and the knockdown *cadd* of this work. Possibly, the knockdown of *CADD* is not severe as the knockout. Sufficient amounts of *CADD* transcripts might still ensure a WT phenotype in *cadd* and the double mutant *cadc*cadd 2*. It appears that Casparian strip functionality is not influenced by the accumulation of aldehydes derived from monolignols as described for the both mutants *cadc*cadd* and *cadc*cadd*fah1-2* (Sibout et al., 2005; Anderson et al., 2015). The synthesis of monolignols is blocked in both mutants due to the loss of function of both genes *CADC* and *CADD*. This causes an accumulation of aldehydes derived from monolignols (Sibout et al., 2005; Anderson et al., 2015). The decreased staining might be caused by the specificity of the staining dye basic fuchsine or by decreased lignin content. How the basic fuchsine reacts with the lignin polymer is not clear. It is only supposed to be specific for phenolic substances similar to safranin staining (Kraus et al., 1997). The faint staining might also be linked to the decreased lignin content as the thioacidolytic analysis of the lignin polymer shows a decrease in the double and triple knockout mutant (fig. 74 A). A chemical analysis of *cadc*cadd 2* roots may elucidate the unaltered lignin-specific staining. Depending on the result, the mutant line *cadc*cadd 2* may help to interpret the faint staining in *cadc*cadd* and *cadc*cadd*fah1-2* mutant lines as well. An accumulation of *p*-coumaraldehyde, coniferaldehyde and sinapaldehyde could not be detected with the applied

method. But still, it is of high interest to proof the accumulation of “monolignaldehydes” instead of monolignols in the root tissue. This might demonstrate that a functional Casparian strip barrier does not exclusively require monolignols. Accumulation of monolignaldehydes in the lignin polymer of stem tissue has already been provided evidence (Anderson et al., 2015).

Process of suberisation is different among single and double as well as triple mutants. Both single mutants show a delayed suberisation. In detail, the suberisation in *cadc* starts at the same position as in the WT, but *cadd* is further delayed. In contrast, both double and the triple mutant develop earlier a suberin barrier than the WT (fig. 48 A and B). Fully matured roots of single, double and triple knockout lines have unaltered aliphatic suberin content. Only *cadc* shows a decrease in monocarboxylic, ω-hydroxy and few α, ω-dicarboxylic acids, matching the significant suberisation delay (fig. 79 C). The aromatic composition does not show any alterations in the single mutants. But the double and triple knockout mutants show a higher amount of *trans* ferulic acid and the amount of diferulic acid is in both at least slightly increased. This indicates that a higher amount of *trans* ferulic and diferulic acid do not enhance the suberisation without other components. But how is it possible that the single mutants delay the suberisation process and the double and triple knockout mutant enhances the process? None of the mutations seem to delay the Casparian strip development as the plants provide sufficient substrates for the formation. It might be possible that the proposed generation and accumulation of monolignaldehydes activates a stress-related response within the plant. Aldehydes are highly reactive molecules and can stimulate the formation of reactive oxygen species (ROS) (Kirch et al., 2001; Sunkar et al., 2003). Furthermore, aldehydes can form Schiff bases and thereby possibly inhibiting enzymatic activity and show toxic effects in organisms (Gallage and Møller, 2015). ROS are highly reactive as well and cause damage to lipids, proteins, carbohydrates and nucleic acids (Gill and Tuteja, 2010). Oxidative stress is connected with the synthesis of the phytohormone abscisic acid (ABA) which is involved in plant growth, development and stress signalling. Specifically, environmental stress can elevate the ABA production (Taylor et al., 2000). Small amounts of ABA, which do not influence the root growth, induce the suberisation process already (Barberon et al., 2016). Taken together, it might be possible that the accumulation of monolignaldehydes provokes a stress-related response which enhances the suberisation of the seedlings in double and triple knockout mutants.

However, how the single mutants cause a delay in suberisation remains unclear.

4.8. Typical lignin mutants *ref8-1*, *ref8-1*med5a*med5b*, *ref8-2*fah1-2*AtC4H::SmF5H* and *fah1-2* show normal suberisation and an alternative route of G-monolignol synthesis in roots

The *ref8-1* mutant is a typical lignin mutant. This mutant shows a defect in the *p*-coumarate 3-hydroxylase (C3H). Because of the defective C3H protein the mutant accumulates *p*-coumarate esters in the leaves and the lignin in the stem tissue consists of *p*-coumaryl alcohol instead of predominately coniferyl alcohol. Furthermore, the plant is sterile (Franke et al., 2002a; Franke et al., 2002b). Due to the defective C3H protein, it was expected that *ref8-1* mutant plants are not able to synthesise feruloyl-CoA for suberisation.

Growth, lignin deficiency and fertility are recovered in the triple mutant with defective C3H and both disrupted mediator subunit MED5a and MED5b. However, the guiacyl and syringyl monomer biosynthesis is not restored in the triple mutant. Still, it accumulates H-lignin (Bonawitz et al., 2014).

In the mutant *fah1-2* a lack of S-lignin is detected. Consequently, leaves show a red fluorescence under UV-light because of the missing sinapoyl malate (Chapple et al., 1992; Humphreys et al., 1999).

The mutant *ref8-2*fah1-2*AtC4H::SmF5H* allows partial rescue of *ref8-2* and *fah1-2* mutant plants by rerouting the phenylpropanoid pathway. The mutant *ref8-2*fah1-2*AtC4H::SmF5H* shows a defective C3H and FAH1 enzyme. However, the *F5H* gene from *Selaginella moellendorffii* under the control of the *Arabidopsis C4H* promoter enables S-lignin synthesis via a new route in the phenylpropanoid pathway not present in angiosperms. The new route of S-lignin synthesis recovers partially the growth phenotype. But, female sterility is still present in the mutant suggesting that either the SmF5H enzyme is not sufficient to compensate the loss of C3H activity in flower development or the *Arabidopsis C4H* promoter does not promote the expression of *SmF5H* in the required tissues or cells for the flower development (Weng et al., 2008a). Due to the new route of S-lignin synthesis the formation of feruloyl-CoA is not required and independent. Summarising the lignin composition of all mutants, the single *ref8-1* mutant and the triple mutant *ref8-1*med5a*med5b* show

exclusively H-lignin (Bonawitz et al., 2014), whereas the *ref8-2*fah1-2*AtC4H::SmF5H* contains both H- and S-lignin and the content of G-lignin is minimised. The *fah1-2* only contains H- and G-lignin (Weng et al. 2010a). Thus, the questions arise whether the mutants are able to form a functional Casparian strip barrier with H-lignin instead of G-lignin. Furthermore, how is the suberisation affected if the production of feruloyl-CoA is expected to be not synthesised?

Based on the PI staining all four mutants are able to build a functional Casparian strip barrier similar to the WT (fig. 37). Lignin specific staining shows an ectopic lignification in *ref8-1* and a normal lignified endodermal network in *ref8-1*med5a*med5b* (fig. 43). Unfortunately, there are no results of *ref8-2*fah1-2*AtC4H::SmF5H* and *fah1-2* available. The focus of this work was on lignin-specific staining especially in mutants with defective and delayed Casparian strip formation. Nonetheless, chemical analysis of the lignin composition was conducted for all mutants except *ref8-1* and obtained results are contradictory to literature. Analysis reveals that triple mutant *ref8-1*med5a*med5b* contains large amounts of G-monolignol, whereas amounts of H- and S-monolignol are similar to WT. The mutant *ref8-2*fah1-2*AtC4H::SmF5H* contains less G-monolignol but increased content of S-monolignol. The mutant *fah1-2* is not significantly altered in the monolignol composition compared with the WT. S-lignin is still present (fig. 75 A and B). A chemical analysis of the lignin polymer in roots of *ref8-1* mutants could not be performed as the mutant line is not able to grow well in hydroponic cultures due to its growth deficit. Furthermore, a suberin specific staining failed since an appropriate number of homozygous *ref8-1* seedlings were not achieved for analysis. Therefore, fluorol yellow staining of *ref8-1* seedlings has to be repeated. The results of *ref8-1*med5a*med5b* and *fah1-2* are surprising. Although the lignin polymer in the stem tissue of *ref8-1*med5a*med5b* consists predominantly of H-lignin, whereas G- and S-lignin are only present in traces (Bonawitz et al., 2014), measured lignin composition of the root in this work shows large content of G-monolignol. An explanation of the supposedly absent G- and S-monolignols might be the partial rerouting of G- and S-monolignol synthesis (Abdulrazzak et al. 2006). Null mutation in *CYP98A3* exhibits a similar effect as is observed in *ref8-1* with deposition of H-lignin in stem tissue (Franke et al., 2002b). But root tissue shows ectopic lignification and chemical analysis presents an accumulation of H-lignin, but still more than the half of the lignin polymer constitute of G- and S-monolignols. Therefore, it was proposed that there is an alternative C3H-independent *meta*-hydroxylation mechanism active mainly

in roots (Abdulrazzak et al., 2006). Assuming a C3H-independent *meta*-hydroxylation in the root tissue exists, which can partially restore G- and S-monolignol synthesis, may explain the establishment of a functional Casparian strip barrier in the mutant *ref8-1*med5a*med5b* and *ref8-2*fah1-2*AtC4H::SmF5H*. But presence of mainly H-monolignols is sufficient for establishing a functional Casparian strip barrier as well. This was discovered by feeding Casparian strip defective mutant *C4H::F5H* with H-monolignol (unpublished data from Guilhem Reyt, laboratory of Prof. Dr. David Salt, University of Nottingham). Consequently, the functional Casparian strip barrier in the mutants might be due to rerouting G- and S-monolignol synthesis or simply by presence of sufficient H-monolignols. However, especially the mutant *ref8-2*fah1-2*AtC4H::SmF5H* was expected to have a defective Casparian strip barrier similar to *C4H::F5H*. Albeit *C4H::F5H* contains in comparison to the complemented *ref8-2*fah1-2*AtC4H::SmF5h* mutant line more S- and less G-monolignol. Thereby, the complemented *ref8-2*fah1-2*AtC4H::SmF5H* mutant line appears to contain sufficient amounts of H- and G-monolignol to build a functional Casparian strip barrier.

The mutant *fah1-2*, while lacking in S-lignin synthesis and sinapoyl malate production in leaves (Chapple et al., 1992; Humphreys et al., 1999), still shows S-lignin in the root tissue similar to the WT. With respect to tissue specific gene expression analysis of *FAH1*, the *FAH1* gene is only highly transcribed in the stem tissue (fig. 23). This implicates that *FAH1* cannot be responsible for the production of S-lignin in the root tissue. Another unknown enzyme with 5-hydroxylation activity must exist in the root tissue.

These new insights help to interpret the suberisation in seedlings and the chemical analysis of the suberin polymer. No alterations were detected in the suberisation pattern *ref8-1*med5a*med5b* and *ref8-2*fah1-2*AtC4H::SmF5H* roots. Only *fah1-2* starts to suberise earlier than the WT (fig. 49 A and B). Also, the chemical analysis of the suberin polymer does not show severe alterations in the suberin aliphatic classes or the aromatic composition in any of the lines. This absence of suberin effects in *ref8-1*, *ref8-1*med5a*med5b* and *ref8-2*fah1-2*AtC4H::SmF5H* roots might be explained by a potential C3H-independent route for the *meta*-hydroxylation in root tissue, which was already described in this chapter. In the aromatic fraction only the amount of diferulic acid is increased in *ref8-1*med5a*med5b*, which does not lead to an enhanced suberisation. As already described in chapter 4.3., diferulic acid is part of the primary cell wall and strengthens cell walls. But in endodermal tissue it could be part of the polyaromatic domain and acts as an anchor point for the next

growing lamella according to the model of Graça (2015). Due to the reason that the suberisation is not affected in *ref8-1*med5a*med5b* the increased content of diferulic acid might be not extracted from endodermal cell walls. The increased diferulic acid content might be located in the cell walls of the vascular tissue. Also, in both mutants *ref8-2*fah1-2*AtC4H::SmF5H* and *fah1-2* no alterations in the aromatic composition are found. It was expected that *FAH1* limits the synthesis of syringa aldehyde and syringic acid and finally resulting in less S-monolignols. Inversely, *ref8-2*fah1-2*AtC4H::SmF5H* may accumulate both derived S-compounds. None of this is the case. This indicates on the one hand that the enzyme SmF5H in *ref8-2*fah1-2*AtC4H::SmF5H* is not able to synthesise the specific precursor for the production of syringa aldehyde and syringic acid and on the other hand there is a F5H-independent mechanism of 5-hydroxylation as already suggested for the S-lignin synthesis.

4.9. In *reduced epidermal fluorescence* mutants Casparian strip and suberisation in seedlings is affected

The *ref3* mutants with affected functionality of C4H are severely affected in the lignin composition and content. In agreement with the early position of the C4H enzyme within the phenylpropanoid pathway the mutants show a lack of several phenylpropanoid end-products. Furthermore, the leaf tissue accumulates cinnamoyl malate resulting in a reddish leaf epidermal fluorescence (fig. 117). Due to the decreased activity of C4H the mutants have a pleiotropic phenotype. The *ref3* mutants are characterised by dwarfed phenotype, male sterility and the development of swellings at branch junctions (Schilmiller et al., 2009).
The *ref1* mutant encodes an aldehyde dehydrogenase which catalyses the oxidation of aldehydes to the corresponding carboxylic acids in a $NADP^+$-dependent manner. This mutation affects a small proportion of sinpate ester synthesis and the mutant has small amounts of cell wall esterified ferulic acid (Nair et al., 2004).
Plants of *ref4-3* contain a disrupted MED5b subunit. This mutation causes a reduction in lignin content, less sinapoyl malate to be found in leaf tissue and reduced growth (Stout et al., 2008). Additionally, *ref4-3* seeds are yellowish similar to the transparent testa mutants (Winkel-Shirley, 2001), indicating an effect on flavonoid biosynthesis (Stout et al., 2008). The

protein REF4 controls the phenylpropanoid biosynthesis on a transcriptional level. REF4 and RFR1 (known as MED5a) are both physically associated with the conserved transcriptional co-regulator complex Mediator, which mediates information from *cis*-acting DNA elements to RNA polymerase II at the core promoter (Bonawitz et al., 2012). It is proposed that REF4 and RFR1 act to suppress the expression of phenylpropanoid biosynthetic genes in response to environmental or developmental factors. Absence of REF4 and RFR1 leads to an accumulation of phenylpropanoids. In contrast, in *ref4-3* the substitution of a single glycine to serine may stabilise the interaction between REF4 and one of its binding partners (Bonawitz et al., 2012) causing the depression of lignin. Another reason might be that the amino acid substitution alters the interaction between Mediator5b and other Mediator subunits, transcription factors, transcription co-regulators, or components of the general transcription machinery (Dolan et al., 2017).

All three *ref*-mutants have a PI-phenotype. The *ref1-4* and *ref4-3* mutant show both a delayed formation of a functional apoplastic barrier for the PI diffusion into the stele. However, *ref3-2* does not show any blockage of PI diffusion into the vascular tissue in one-week old seedlings (fig. 38). Casparian strip functionality is recovered in *ref3-2*dex::REF3* by promoting the transcription of the REF3 gene with dexamethasone and by feeding the root with G-monolignols (fig. 39). Lignin specific staining shows a weak staining of *ref3-2* mutant, whereas *ref1-4* and *ref4-3* show ectopic deposition of lignin (fig. 44). Similar to *C4H::F5H* and *esb1*, the delayed establishment of Casparian strip and the ectopic lignification in both mutant lines *ref1-4* and *ref4-3* is accompanied by ectopic suberisation. Only *ref3-2* mutants show a delayed developed suberin barrier in combination with no apparent Casparian strip barrier (fig. 50 A and B). Thioacidolytic analysis of the lignin polymer shows a decreased total lignin content in *ref3-2* without affecting the relative composition of the monolignol classes. The mutant *ref4-3* also shows reduced lignin content but additionally the composition is shifted to be more G-monolignol dominant than the WT. Mutation of the aldehyde dehydrogenase in *ref1-4* does neither affect the lignin content nor the composition (fig. 76 A and B).

Due to the early position of the C4H enzyme in the phenylpropanoid pathway a decline of phenylpropanoid end-products has already been described for *ref3* plants (Schilmiller et al., 2009). Therefore, it is consistent that the lignin content is reduced as well and the Casparian strip barrier is not functional. The reason for a defective Casparian strip barrier in *ref4-3* can

also be the decrease of lignin monomers. But how is the position of the REF1 enzyme, the hydroxycinnamaldehyde dehydrogenase (HCALDH), able to influence the formation of the Casparian strip barrier? Furthermore, according to the databank analysis *REF1* gene is not highly expressed in the root tissue (fig. 27). The lignin content and the composition are not affected. It might be possible that the loss of REF1 leads to an uncontrolled synthesis of monolignols which impairs the correct development of the Casparian strip barrier. Although the mutant *ref1-4* shows an ectopic lignification same amount of lignin monomers are found in the root tissue. This indicates that the ectopic lignification forms patchy island within the cell wall, therefore it is lost during sample preparation. Root samples not treated with cell wall degrading enzymes may show an increased content of lignin as *esb1* (fig. 74 A).

Ectopic suberisation is found by suberin-specific staining in seedlings of *ref1-4* and *ref4-3* (fig. 50 A and B). The chemical analysis of the suberin polymer in *ref1-4* and *ref4-3* mutant does not show an increased content (fig. 85 A and B). Possibly, the suberisation process starts earlier in seedlings of both mutant lines, but in matured roots the ectopically deposition of suberin appears to be stopped. In contrast, the *ref3-2* mutant is delayed in the suberin development, but mature roots have more monocarboxylic and α, ω-dicarboxylic acids (fig. 85 A and B). Nonetheless, the content of aromatics is still decreased. Especially, amounts of vanillin, *trans* ferulic and diferulic acid are reduced (fig. 85 C). Possibly, the lack of *trans* ferulic acid may cause the delayed suberisation in seedlings of *ref3-2*. How is it possible that still more monocarboxylic and α, ω-dicarboxylic acids are found in the suberin polymer? Probably, the mutated roots try to compensate the disrupted Casparian strip barrier by ectopic suberisation. However, decreased amounts of *trans* ferulic acid seems to limit the incorporated amount of ω-hydroxy acids. Therefore, only more monocarboxylic and α, ω-dicarboxylic acids are found. A feeding experiment with *trans* ferulic acid might enhance the suberisation. Feeding Casparian strip deficient mutants with *trans* ferulic acid does not recover the functionality of the apoplastic barrier (fig. 144). This indicates that *trans* ferulic acid is not part of the Casparian strip and that external provided *trans* ferulic acid is not further synthesised to coniferyl alcohol.

4.10. Loss of function mutations in *PRX11* and *ASFT* delay suberin development and *FACT3* does neither contribute to the Casparian strip nor suberin barrier

The mutants (*prx11-1*, *prx11-2*, *asft1*, *asft2* and *fact3*) show a functional Casparian strip barrier similar to the WT. However, based on the statistical evaluation of *prx11-2* the Casparian strip development is slightly delayed. But in comparison to the *esb1* mutant the blockage of the apoplastic diffusion of the PI is rather similar to the WT. The difference is only 1.6 endodermal cells between WT and *prx11-2* (fig. 40). Since WT values are also measured in the range of *prx11-2* in other experimental sets of PI staining, this delayed establishment of the Casparian strip barrier is high arguable. Specific staining of the lignified endodermal network does not show any alterations in the Casparian strip development for any mutant (fig. 45). Consequently, all mutants show the same Casparian strip phenotype, indicating that in *prx11-2* the CS barrier is correctly formed as well. Suberin-specific staining shows slightly delayed suberisation in *prx11* mutants and severely decreased continuously suberised zones in *asft* mutants. The mutant *fact3* is not affected in the suberisation process (fig. 51 A and B). Analysis of the ultrastructure reveals a wavy suberin band in both *prx11-2* and *asft1* (fig. 59 B, image 1; fig. 61 B, image 2; fig. 68 B, image 1; fig. 69 B, image 2; fig. 70 B, image 1). Additionally, the thickness of the suberin band appears to be smaller. But lamellar-like structure is still present in both mutant lines (fig. 60 B, image 1; fig. 70 B, image 1). A lignin analysis was not performed of this mutant set, because the development of the Casparian strip is not affected in all mutants. Chemical analysis of suberin in matured roots show a tendency of decreased ω-hydroxy acids in *asft* mutant lines as well as a decline in *trans* ferulic and diferulic acid, correlating with significant suberisation delay (fig. 87 B, C, D). The *prx11* mutants and *fact3* do not show any significant alterations in the aliphatic suberin monomer composition (fig. 87 A and B). But the aromatic composition is altered. In both *prx11* mutants the amount of *trans* ferulic acid is increased, whereas diferulic acid content is decreased. Furthermore, vanillin content seems to be slightly elevated, while vanillic acid is decreased as well. In *fact3*, amounts of *trans* coumaric acid, vanillic acid and *trans* ferulic acid are decreased, while vanillin is increased (fig. 87 D).

Delayed suberisation in *prx11* mutants (fig. 51 B) was already observed by Mathias Brands and the increased amounts of *trans* ferulic as well as decreased content of diferulic acid (Brands, 2014). Due to the amino acid sequence of the *PRX11* gene it is speculated to be a peroxidase superfamily protein. It might be possible that PRX11 dimerises *trans* ferulic acid to diferulic acid. Loss of function mutation would decrease polymerisation of *trans* ferulic acid and consequently either abolish or at least minimise the polyaromatic domain in suberin. This might provoke a delayed suberisation as it is determined (fig. 51 B; Brands, 2014). An enzymatic assay may elucidate the functionality of the PRX11 enzyme. The *PRX11* gene has to be cloned and overexpressed in *Escherichia coli* cells. Positive colonies will be propagated and overexpressed PRX11 enzymes will be extracted and purified. As an educt *trans* ferulic acid will be used. In order to test for a function linking esterified aromatics to each other, another educt is extracted waxes of tuber peridermal tissue of *Solanum tuberosum*. Peridermal wax of *S. tuberosum* is enriched in feruloylated aliphatic compounds (Serra et al., 2009). For instance, the measurement of the educts and products can be done analytically by gas chromatography. If the enzymatic activity of PRX11 has been confirmed, a fluorescent tagged PRX11 protein will solve the localisation of the PRX11 protein within the cell or in the apoplastic space. At the moment it is predicted to be cell wall localised.

The *asft* mutants are crucial mutants because these are the first identified mutants with decreased transesterified ferulic acid content. Due to the loss of esterified ferulic acid it is assumed that free ferulic acid is accumulated within the plant. Extraction of free phenolic compounds may elucidate an accumulation of free soluble ferulic acid. Furthermore, *asft* mutant lines help to analyse the ultrastructure of suberin. But at first it is necessary to summarise the known facts about *asft* mutation. The major effect of *asft* knockout mutation was discovered in *Arabidopsis thaliana* seed suberin. Here, the amount of ferulates is decreased and in concordance the content of C_{22} and C_{24} ω-hydroxy acids as well. Also, the suberin composition in seeds of *CYP86B1* knockout mutants, also known as *ralph*, show a correlation between the decrease of long-chain ω-hydroxy acids and ferulates. However, the published chemical analysis of the suberin composition in matured roots of *asft* exhibit a decline in ferulate but ω-hydroxy acid content is unaffected (Molina et al., 2009). Still, a tendentious correlation between aromatic and ω-hydroxy acid content in *rwp*/*asft* was showed by the chemical analysis of suberin published by Gou et al. (2009). Additionally, the

composition of cell wall bond aromatics was analysed in stem tissue showing decreased content of ferulates (Gou et al., 2009).

In the *ccoaomt1* mutant evidence suggests that *trans* ferulic acid and ω-hydroxy acids are strongly associated. Furthermore, partial depolymerisation of cork and potato tuber suberin reveals esterified ferulic acid with ω-hydroxy acids (Santos and Graça, 2006; Graça et al., 2015). As already described, the most severe effects on suberin are found after suberin staining in many mutant seedlings. A chemical analysis of the suberin polymer in seedlings may elucidate whether ω-hydroxy acids are significantly reduced by the various mutations as well. It appears to be possible that some mutations are well observable in the developing root system. Matured roots may compensate for the mutation or a delayed development is compensated by time.

New insight regarding suberin of *asft* mutants is the loss of diferulic acid. Together with *prx11* mutants, it has been speculated whether diferulic acid is part of the polyaromatic domain, which may anchor the suberin polymer to the cell wall. Furthermore, the electron-opaque lamellae were assumed to be aromatic-rich zones or are the polyaromatic domain (Bernards, 2002; Graça and Santos, 2007; Graça, 2015). With respect to the lamellar-like structure no differences are observable between the WT and the investigated mutants. This is consistent with TEM investigations of the suberin ultrastructure in peridermal tissue in *asft1* and in *FHT*-RNAi mutants in potato (Molina et al., 2009; Serra et al., 2010). FHT is the potato orthologue to *Arabidopsis'* ASFT (Serra et al., 2010). Several times a wavily situated suberin band was observed in especially *prx11-2* and *asft1* mutant. This wavy structure of the suberin was only observed to be local and not global around the endodermal cell. It might be possible that this wavy phenotype of the suberin band is associated with the decrease of diferulic acid content. To assume that diferulic acid may anchor suberin to the cell wall is possible and also supported by literature (Faulds and Williamson, 1999). Nonetheless, diferulic acid contributes to cell wall rigidity as well (Passardi et al., 2004) and loss of diferulic acid may cause a weak cell wall. As a consequence of this the suberin appears to be loosely in the cell wall. To proof that this phenotype is associated with the loss of diferulic acid, it is of high interest to analyse the ultrastructure of the suberin in the mutant *ccoaomt1*, which is also characterised by a decreased content of both *trans* ferulic and diferulic acid. Since esterified ferulic acid does not contribute to the lamellar-like structure of the suberin and additionally diferulic acid content is decreased, it is arguable

whether aromatic compounds really cause the electron-opaque lamellae as also disputed by Molina et al. (2009). Another idea of what contributes to the electron-opaque lamellae is further discussed in the chapter 4.12.

Taken together the function of ASFT and PRX11 is likely related to aromatic suberin synthesis. It is possible that ASFT connects ω-hydroxy acids with *trans* ferulic acid by ester bonds and PRX11 polymerises *trans* ferulic acids to diferulic acid. PRX11 might also connect the dimer of esterified ferulic acid and ω-hydroxy acid to a single *trans* ferulic acid in order to obtain dimerised diferulic acid with an esterified ω-hydroxy acid. Another possibility is that two *trans* ferulic acids esterified with ω-hydroxy acids polymerise to diferulic acids with esterified ω-hydroxy acids at each end. The latter and second possibility seems to be more likely because *asft* knockout lines show a strong decrease of diferulic acid as well.

Not many ultrastructural differences of the suberin polymer in literature were found. The first one was obtained by treating green cotton fibers with an endoplasmatic reticulum-associated fatty acid elongase. Thinner electron-translucent lamellae were found and chemical analysis revealed decreased carbon chain length, which corresponded with the decreased diameter of the elctron-translucent lamellae (Schmutz et al., 1996). The second was found in *CYP86A33* RNAi-silenced potato tuber. The RNAi-silencing caused especially a decrease of $C_{18:1}$ ω-hydroxy and α, ω-dicarboxylic acid. This decrease of the main compounds was accompanied by a decline in primary alcohols, monocarboxylic acids and aromatic compounds. Therefore, the typical lamellar-like structure of suberin disappeared but the size of the primary cell wall was increased (Serra et al., 2009b). Thus, the composition of the electron-opaque lamellae is still unknown.

The *fact3* mutant was found by Daniela Nosbüsch during her work in the department of ecophysiology. The FACT protein is responsible for the esterification of mainly caffeoyl-CoA to a primary alcohol, which is found in suberin associated waxes (Kosma et al., 2012). Mutant lines of FACT show a lack of chloroform-soluble alkyl caffeate esters. Only minor changes were found in the aliphatic suberin polymer. In vitro assays demonstrated that FACT uses caffeoyl-CoA as acyl donor but also coumaryol- and feruloyl-CoA (Kosma et al., 2012; Domergue and Kosma, 2017). The result of the in vitro assay appears to be confirmed by the chemical analysis of cell wall composition in *fact3* in this work. The mutant *fact3* exhibits decreased amounts of esterified *trans* coumaric acid, vanillic acid and *trans* ferulic acid. In contrast, more vanillin is found in its cell wall. However, the content of primary alcohols is

not decreased. Instead, the content of C_{20} primary alcohol is significantly increased as well as the amount of C_{18} ω-hydroxy acid. Possibly, the C_{20} primary alcohol and C_{18} ω-hydroxy acid are associated with coumarates, caffeates and ferulates. But due to the knockout mutation in *FACT* more primary alcohols were used as substrates for the suberin polymer. Finally, these results emphasise that *trans* coumaric, vanillic acid and also a small proportion of *trans* ferulic acid are incorporated into other structures than the suberin polymer.

4.11. Suberised peridermal tissue exhibits typical lignin monomers

Isolated peridermal tissue of *Arabidopsis thaliana* was obtained by PD Dr. Rochus Benni Franke. The isolated peridermal tissue is highly suberised. Approximately, 5.7 % of its dry weight consists of suberin (fig. 85 C). Although only one sample has been used for the suberin analysis the obtained values are similar to the published data (Franke et al., 2005). However, no unsaturated ω-hydroxy and α, ω-dicarboxylic acid were found in the sample (fig. 85 B). This might be reasoned by the age of the isolated peridermal tissue. The isolated peridermal tissue was not freshly harvested. By time it is possible that the unsaturated compounds may oxidise further to saturated derived fatty acids. The composition of the suberin classes appears to be similar to whole root extracted suberin. Only the amount of primary alcohols seems to be relative higher than in the whole root (fig. 85 C). Primary alcohols and monocarboxylic acids can be not used to extend the suberin polymer. These compounds have to be present at the ends of the polymer. It might be possible that the suberin polymer in the peridermal tissue is from its chemical structure different in comparison to endodermal located suberin. However, ultrastructural organisation is lamellar-like as well (Franke et al., 2005). Thioacidolytic analysis reveals typical lignin monomers. The thioacidolytic degradation of lignin cleaves specifically only 8-*O*-4' ethers of monolignol (Lapierre et al., 1986). Peridermal tissue of *Arabidopsis thaliana* seems to consist almost of 1 % lignin-like polymer. This lignin-like polymer is mainly composed of G-monomers, whereas H- and S-monomers are minor compounds (fig. 75 A). Also, the relative proportion of this lignin-like polymer resembles the relative proportion of whole root extracted lignin (fig. 75 B). Thioacidolytic degradation was also performed in samples of suberised *Quercus suber* bark tissue and wound-healing peridermal *Solanum tuberosum* tissue (Lapierre et al., 1996; Marques et al., 1999). About one-tenth of lignin-like polymer

was found in wound-healing peridermal tissue. Furthermore, it is assumed that this lignin-like polymer is highly cross-linked in the wound-healing peridermal tissue because of the low frequency of β-*O*-4 and β-1 bonds (Lapierre et al., 1996). Bark tissue of *Quercus suber* consists of predominately G-monomers. H- and S-monomers are only minor compounds. Due to the comparison with spruce milled wood lignin it is supposed that the lignin-like polymer in *Quercus suber* is highly cross-linked as well (Marques et al., 1999). Applying the analytical approach "derivatization followed by a reductive cleavage" (DFRC) developed by Lu and Ralph (1997) results in the identification of guiacyl- and syringyl-monomers. In comparison to lignified tissue, the amount of lignin-like polymer in wound-healing tissue is 5 to 6 % of that of lignified tissue from pine and basswood xylem (Razem and Bernards, 2002). In conclusion, suberised material contains a lignin-like polymer. Aromatic compounds are cross-linked with each other. Maybe this lignin-like polymer is the speculated polyaromatic domain. This lignin-like polymer may provide an anchor point for the suberin to attach to the primary cell wall. Furthermore, the lignin-like polymer may contribute to cell wall rigidity as well. Targeted manipulation of the lignin-like polymer may elucidate the functionality of the lignin-like polymer. One possibility might be feeding WT roots with a phenylpropanoid pathway inhibitor like piperonylic acid. Ultrastructural analysis of suberin may demonstrate loss and consequence of the lignin-like polymer.

4.12. Inhibition of the phenylpropanoid pathway enhances suberisation

Piperonylic acid (PA) is a natural molecule which is extracted from bark tissue of the tree *Ocotea pseudo-coto*. It contains a methylenedioxyphenyl function at a position suitable for P450 cytochrome oxidation (Schalk et al., 1998). P450 enzymes of animals have a high specificity to bind to molecules with methylenedioxyphenyl function (Franklin, 1977; Ortiz de Montellano and Correia, 1995). PA seems to bind irreversible to the P450 enzyme C4H of the phenylpropanoid pathway, inhibiting its function. Thereby, in case of treating tobacco cells in suspension with PA an accumulation of cinnamic acid and a sharp decline of *p*-coumaric acid are measured (Schalk et al., 1998).

Treating *Arabidopsis thaliana* roots with PA results in a delayed formation of the Casparian strip barrier. However, suberisation is not affected by the inhibition of the phenylpropanoid pathway by PA treatment (Naseer et al., 2012). This is not consistent with the results of this work. Incubation of *Arabidopsis thaliana* seedlings for 24h in ½ liquid MS containing 10 µM PA causes earlier suberisation and an increased continuously suberised zone. Growing plants for two or seven days on ½ MS-agar plates containing 10 µM PA also enhances the suberisation by earlier development of the suberin barrier similar to the Casparian strip defective mutant *esb1* (fig. 52 A and B). Nonetheless, this result raises the question how is it possible to increase the suberisation if the phenylpropanoid pathway is inhibited? Due to the inhibition of the C4H enzyme it was expected that the PA treatment does not lead to an enhanced suberisation after 24 hours treatment. In addition, it was expected to observe a decline of WT suberin deposition by continuously longer treatment with PA similar to the suberisation pattern in *ref3-2* seedlings. Due to the involvement of *trans* ferulic acid within the suberin polymer it has to be synthesised in order to generate a functional suberin barrier. No other enzyme is known to catalyse the *para*-hydroxylation of the cinnamic acid to *p*-coumaric acid. One possibility, explaining earlier suberisation, when C4H is inhibited might be that the amino acid L-tyrosine, which is already *para*-hydroxylated, is catalysed to *p*-coumaric acid. However, all four PAL enzymes that are possibly involved in this reaction in *Arabidopsis thaliana* use as substrate L-phenylalanine, not L-tyrosine. However, under high alkaline conditions as well as high concentrations of L-tyrosine showed the synthesis of *p*-coumaric acid in vitro (Cochrane et al., 2004). Although the possibility that PAL uses under conditions of C4H inhibition L-tyrosine as a substrate is unlikely, it is not possible to exclude this alternative synthesis of *p*-coumaric acid. Even if this assumption can be confirmed, the defective Casparian strip barrier cannot be recovered by this alternative pathway since PI diffusion was delayed in plants subjected to PA treatment (Naseer et al., 2012). On the other hand, the synthesis origin of the *trans* ferulic acid in the suberin polymer is arguable. Is it exclusively derived from the amino acid L-phenylalanine or L-tyrosine? Maybe a feeding experiment with L-tyrosine could elucidate the possible existence of an alternative route in the phenylpropanoid pathway for the synthesis of *trans* ferulic acid. Mutants of *ref3-2* only grown on media containing the amino acid L-tyrosine and WT seedlings grown on media containing both PA and L-tyrosine may elucidate an alternative route within the

phenylpropanoid pathway. In both treated mutant and WT roots an ectopic suberisation is expected.

Another idea of the use of a phenylpropanoid pathway inhibitor was already discussed in chapter 4.11. . Treated roots with PA revealed close to the root tip suberised endodermal cells. An ultrastructural analysis of these early suberised endodermal cells might elucidate how the suberin is positioned within the cell wall. If a lignin-like polymer provides an anchor point for the suberin in the primary cell wall the suberin would be loosely situated in the cell wall. Nonetheless, cell wall rigidity may also contribute to a straight situated suberin in the cell wall as well. Finally, a loosely suberin cannot exclusively referred to the loss of an anchor point.

4.13. TEM shows lamellar-like structure of the suberin polymer

Analysing the ultrastructure of a single cell was made possible by the development of the transmission electron microscopy in the years 1945 to 1950. The advantage of the TEM is the higher resolution in comparison to the light microscopy. The optical resolution of the light microscopy is limited by the wavelength of the light and by the numerical aperture. Due to this, the optical resolution of a light microscope is limited to ≈ 0.3 µm. In contrast, the TEM exhibits an optical resolution of ≈ 0.3 nm (Roland, 1978; Plattner and Zingsheim, 1987).

Analysis of the ultrastructure of suberin shows a lamellar-like structure (fig. 56 B, image 1). The first occurrence of suberin has been reported already at a one mm distance from the root tip (fig. 53 B, image 1 to 3). In contrast, at approximately five mm distance to the root tip first suberin staining is detectable by fluorol yellow staining (fig. 46 B). At four mm distance to the root tip the suberin consists already of several lamellae (fig. 56 B, image 1), indicating that fluorol yellow staining seems to stain only well-developed suberin. The observation of this lamellar-like structure is caused by contrasting the samples with heavy metals, then subjecting the contrasted sample to an electron beam. Biological material contains light elements with light atom nuclei, which causes an impaired scattering of electrons. The principle mechanism of the TEM is that the incident electron beam is scattered by atoms of the sample and the emergent electron beam is detected and translated into a topographic map. The incident electrons are scattered either elastic or inelastic by an atom. Elastic scattering occurs by the interaction of the incident electrons

with the nuclear charge. Thereby, the angle of the emergent electron beam is altered, whereas the velocity is not affected. The scattering effect is proportional to the atomic number. In contrast, inelastic scattering occurs by the interaction of the incident electrons with the electron shell of an atom. Thereby, the angle of the emergent electron beam is slightly altered but the velocity of the electron beam is decelerated. This scattering effect is also proportional to the atomic number (Plattner and Zingsheim, 1987). To achieve a higher contrast of the biological material, contrasting with heavy metals is required. Due to the high atomic number of heavy metals, the scattering effect is increased in comparison to non-contrasted samples (Plattner and Zingsheim, 1987).

In order to explain the visualisation of the characteristic lamellar-like structure of suberin with TEM, comprehension of the sample preparation process is necessary. Possibility of visualising specifically ferulic acid with the respective method is discussed in the following.

The first step of the preparation of biological material is the fixation with formaldehyde and glutaraldehyde. Formaldehyde and glutaraldehyde react with the amino and guanidyl group of proteins to establish cross-linkages (Fraenkel-Conrat et al., 1946; Fraenkel-Conrat and Olcott, 1948; Richard and Knowles, 1968). Furthermore, amino-lipids like phosphatidyl ethanolamine also react with both aldehydes (Gigg and Payne, 1969; Roozemond, 1969). Only in the potato suberin polymer feruloyl- and coumaroyltiramines have been detected (Bernards, 2002). The amide of the feruloyl- and coumaroyltiramine might react with formaldehyde and glutaraldehyde in a similar way, as it is proposed for the amide in tryptophane (Fraenkel-Conrat et al., 1946). However, in the suberin composition of *Arabidopsis thaliana* no feruloyl- and coumaroyltiramines have been found yet.

The next step is the fixation and contrasting with osmium tetroxide [$Os(VIII)O_4$]. Osmium tetroxide reacts with the double bond of unsaturated fatty acids resulting in the formation of glycol and osmium trioxide [$Os(VI)O_3$]. One part of osmium trioxide oxidises to osmium tetroxide [$Os(VIII)O_4$] and another part reduces to osmium dioxide [$Os(IV)O_2$]. Furthermore, cross-linkages occur in lipids between adjacent unsaturated fatty tails via osmate esters. However, the osmate esters are not considered to contribute much to the contrasting. Additionally, charged osmium dioxide [$Os(IV)O_3^{2-}$] is formed as well and binds to the positively charged head groups of lipids (Plattner and Zingsheim, 1987). The osmium atom is regarded as the constituent giving significant contrast in very thin sections (Bahr, 1954). Aromatic compounds with two adjacent hydroxyl-groups in *ortho*-position also react with

osmium tetroxide, leading to the formation of osmate esters. This reaction has been demonstrated for plant aromatic compounds such as D-catechin, quercetin, caffeic acid and *o*-dihydroxyl coumarin. Two adjacent hydroxyl-groups with an olefinic double bond of the carbon atoms are necessary for the reaction with osmium tetroxide. For instance, one hydroxyl-group in vanillaaldehyde, one hydroxyl- and one carbonyl-group in salicylic acid, *o*-dimethoxy groups in veratrole or *m*-dihydroxyl-groups in resorcinol fail the reaction with osmium tetroxide (Nielson and Griffith, 1978). Consequently, it is highly arguable whether ferulic acid may react with osmium tetroxide since it does not contain two adjacent hydroxyl groups. Based on the results from Nielson and Griffith ferulic acid does not seem to react with osmium tetroxide. However, *trans* ferulic acid contains a double bond in the carbon chain of the carboxyl residue. It has not been demonstrated that this double bond, also present in caffeic acid, can react with osmium tetroxide, but nonetheless it remains possible. Probably, due to the aromatic ring and the carboxyl group electrons of this double bond may be detracted and the reaction with osmium tetroxide becomes unlikely. Furthermore, the aromatic ring may prevent sterically the reaction of this double bond with the osmium tetroxide. However, the olefinic double bonds of non-substituted aromatic rings can react with osmium tetroxide (Badger and Reed, 1948). But, H magnetic resonance spectra analysis shows that osmium tetroxide preferentially attacks the two adjacent hydroxyl-groups in substituted aromatic molecules instead of the olefinic double bonds within the aromatic ring (Nielson and Griffith, 1978). Therefore, a reaction of osmium tetroxide with the olefinic double bonds within the aromatic ring of ferulic acid becomes more unlikely.

Casparian strips predominately consisted of G-monolignols show to be highly contrasted, when investigated with TEM (Hosmani et al., 2013). Also, in the obtained results of this work a darkened cell wall between endodermal cells was observed (fig. 59 B, image 4; fig. 62 B, image 1; fig. 64 B, image 3; fig. 67 B, image 2). The contrasting of the section performed by Hosmani et al. was also performed with osmium tetroxide and afterwards the sections were stained with lead citrate and uranyl acetate according to the manual of Kolosova et al. (2001). Uranyl acetate and lead citrate dissociate to the corresponding lead and uranyl ions. These ions bind to negatively charged regions like phosphate in DNA (Stoeckenius, 1961; Frasca and Parks, 1965) or phospholipids (Silva et al., 1971; Ginsburg and Wolosin, 1979), to the ionic bond of osmium ions (Plattner and Zingsheim, 1987) and to proteins (Reynolds, 1963; Soloff, 1973; Klotz et al., 1978). However, according to the fixation and contrasting

experiments of Bahr (1954) lignin, cellulose and pectin do not react with osmium tetroxide. Therefore, primary cell walls, consisting of cellulose and pectin, appear to be electron-translucent. Lignin is usually visualised by contrasting and fixation with potassium permanganate (Wooding and Northcote, 1964; Bland et al., 1971; Donaldson, 2001; Anderson et al., 2015). In histochemistry, staining of lignin with potassium permanganate, which is specific for S-lignin, is established as Mäule-staining (Atanassova et al., 1995; Hoffmann et al., 2004). But how is it possible that the Casparian strip barrier is contrasted if S-lignin is not present? One reason might be that the Casparian strip barrier is not exclusively made of lignin. Proteins could be involved as supporting elements. For example, ESB1 is localised within the Casparian strip, which has been demonstrated by immunogold electron microscopy (Hosmani et al., 2013). It is supposed that osmium tetroxide may bind by hydrogen bonds directly to proteins (Litman and Barrnett, 1972) and as already described uranyl and lead ions also bind to proteins (Reynolds, 1963; Soloff, 1973; Klotz et al., 1978).

Thus, visualisation of the Casparian strip might be possible by the presence of proteins within the Casparian strip and probably not caused by the monolignols because lignin does not react with osmium tetroxide.

Incidentally, whether *trans* ferulic acid reacts with osmium tetroxide remains doubtful. The knockout mutation of *asft1* shows an abolished content of esterified ferulic acid and diferulic acid content (fig. 87 D). Nonetheless, the lamellar-like structure of suberin is maintained (fig. 60 B, image 1; Molina et al., 2009; Serra et al., 2010). Therefore, it might be possible that the assumption the electron-opaque lamellae consist either of the polyaromatic domain or an aromatic rich zone is not correct. But what else can cause this distinct contrast? Is it an accumulation of osmium tetroxide molecules together with lead and uranyl ions? From the chemical composition of suberin an electric charge can be excluded. The osmium tetroxide molecules will bind to the unsaturated ω-hydroxy and α, ω-dicarboxylic acids and cross link them if unsaturated fatty acids are stacked like in the model of Graça (2015). However, one row of transesterified osmates does not cause a dark lamella of a size of ca. 10 nm (fig. 56 B, image 1). A possible explanation for the visualised macromolecular structure of suberin is crystallisation. Crystallisation of polymers is known to result in a lamellar-like structure (Mandelkern, 1985; Wittmann and Lotz, 1985; Mandelkern, 1990; Strobl, 2000). For example, synthetic organic polymers like polyethylene and nylon are crystalline and show chain folding. Also, natural polymers like rubber crystallise with chain folding (Hoffman et al.,

1976). The molecules are orientated parallel to the fold direction (Wittmann and Lotz, 1985). A lamellar-like structure is found in amphiphilic molecules like lipids but also in block copolymers (Alsayed et al., 2004). A copolymer is a heteropolymer, which consists of different monomers (Sfatos and Shakhnovich, 1997). The suberin itself consists of many different lipids, alcohols and aromatic compounds. Thus, suberin can be considered as a copolymer. Copolymers are able to self-assembly resulting in a lamellar-like structure (Kim et al., 2003). Therefore, it might be possible that the lamellar-like structure of the suberin polymer is caused by the physical properties of self-assembly process of copolymers. For instance, cutin, a polymer found on the leaf surface, also shows a lamellar-like structure (Wattendorff and Holloway, 1982). It is an insoluble biopolymer composed of aliphatic compounds which are cross-linked via ester bonds. Typical are fatty acids with ω-hydroxy- and carboxyl-groups (Franke et al., 2005). The lipid barrier in the stratum corneum of mammalian skin also exhibits a lamellar-like structure (Madison et al., 1987; Pilgram et al., 1999; Warner et al., 2003). Here, the proposed molecular model consists of ω-hydroxy acids in amide linkage with sphingosine (Swartzendruber et al., 1989). Aromatics are not necessarily part of a copolymer. Therefore, the observed lamellar-like structure may form independently.

Taken all together, ferulic and diferulic acid do not seem to contribute to the lamellar-like structure. According to polymer research crystallised polymers show a lamellar-like structure and crystallised copolymers are able to self-assemble to a lamellar-like structure. Suberin is a heteropolymer. It might be possible that suberin crystallises in the cell wall and is able to self-assemble to a lamellar-like structure. Based on these information further researches on the ultrastructure of suberin is possible and can contribute to appropriate experiment finally elucidating the origin of the lamellar-like structure.

4.14. Drought tolerance may be also associated with lignin

The mutant *ccr1* shows a dwarfed phenotype and a delayed formation of the Casparian strip barrier (fig. 34; fig. 41). Furthermore, *ccr1* mutants show to be drought tolerant (fig. 111; fig. 112). Drought tolerance can be excluded from the suberisation since matured roots do not contain more suberin than the WT (fig. 77 D; fig. 82 D). The mutant *ccr1* shows collapsed xylem in stem tissue due to the loss of lignin (Jones et al., 2001; Patten et al., 2005). The

absolute content of lignin in the root tissue is decreased, but the G/S ratio is not altered (fig. 73 A and B). A similar drought tolerance feature can be observed in the mutant *ref8-2*fah1-2*AtC4H::SmF5H* (fig. 114). Also, the suberin content is unaltered in five-week old matured roots of *ref8-2*fah1-2*AtC4H::SmF5H* (fig. 85 C), whereas the G/S ratio of lignin is affected (fig. 75 A and B). It might be possible that *ref8-2*fah1-2*AtC4H::SmF5H* is also affected in the xylem organisation. Disturbed xylem organisation of *ccr1* may impair root hydraulic conductance. But it might be possible that the water efflux out of the root forced by drought stress is also impaired by the collapsed xylem elements. Xylem vessels appear to be less lignified than the WT (fig. 41). Another reason might be caused by less transpiration. Stomatal aperture might be affected in both mutants. This might influence the transpiration and might contribute to an increased drought tolerance. Measurements of the root hydraulic conductance value and analysis of stomatal aperture could help to solve the reason of drought tolerance in both mutants *ccr1* and *ref8-2*fah1-2*AtC4H::SmF5H*.

4.15. Contribution of root barriers to water and nutrient transport as well as leaf ion homeostasis

Manipulating of the phenylpropanoid pathway causes different effects on Casparian strip and suberin development. Studying water and nutrient transport through the root or ion homeostasis within the leaf tissue is challenging if both endodermal barriers are affected by mutations. For instance, it seems that Casparian strip defective mutants (*esb1*, *C4H::F5H*, *ref3-2*) have an increased content of sodium and magnesia, whereas calcium is decreased. However, in the case of *sgn3-3* the Casparian strip barrier is completely disrupted (Pfister et al., 2014), but sodium concentration is decreased and calcium concentration is unaltered within the leaf tissue (tab. 17). This might indicate that sodium accumulation within the leaf tissue is independent from Casparian strip barrier functionality. But most of the Casparian strip deficient mutants (*esb1*, *C4H::F5H*, *myb36-2*, *ref3-2*, *ref4-3* and *sgn3-3*) show an increased content of magnesia (tab. 17). Casparian strip deficiency appears to be associated with magnesia concentration. Possibly, the Casparian strip barrier stops the apoplastic diffusion of magnesia into the vascular tissue. A suberin deficient mutant like *horst*ralph* exhibits an increased content of sodium and magnesia as well (tab. 17), suggesting the

importance of suberin for respective ion uptake. Roles of Casparian strips and suberin in uptake and retention of various solutes and water remain to be elucidated. By using the different phenylpropanoid pathway mutants, a tool box is available to study the influence of each endodermal barrier to both water transport and ion homeostasis. It is proposed to use the different *cad*-mutants with a functional Casparian strip barrier but different suberisation. The mutants provide on the one hand delayed suberisation in single *cad*-mutants and on the other hand increased suberisation in double and triple mutants. They will allow studying the contribution of the suberin barrier to ion homeostasis, water and nutrient transport. Mutants like *ccooaomt1*, *ccr1*, *comt1*, *ref3-2* may elucidate the importance of both Casparian strips and suberin as a functional endodermal barrier to the apoplastic and coupled trans-cellular pathway of both water and nutrients. Due to PI staining it is supposed that Casparian strips act as an apoplastic barrier, whereas blockage of FDA staining is associated with suberisation. Based on this experiment suberin is supposed to block the coupled trans-cellular pathway (Barberon et al., 2016). Measuring the root hydraulic conductance of roots of *cadc*cadd* with ectopic suberisation shows an impaired root hydraulic conductance (fig. 147 B). Thus, ectopic suberisation might influence water flux within the root. However, it is also important to ensure functionality of xylem elements in the *cadc*cadd* mutant to exclude the possibility of non-functional conducting elements as the reason of impaired root hydraulic conductance. Further investigations by using phenylpropanoid pathway mutants will help to increase our recent knowledge about the contribution of endodermal barriers to water and nutrient transport as well as ion homeostasis.

5. Summary

This study demonstrated that manipulation of the phenylpropanoid pathway results into altered suberisation of seedlings and influences the development of the Casparian strip barrier. Manipulation of the early positioned enzyme C4H within the biosynthesis of phenylpropanoids in *ref3-2* causes decreased content of phenylpropanoid end-products such as lignin and feruloyl-CoA and therefore a delayed suberisation as well as a non-functional Casparian strip barrier. Loss of function mutations in crucial enzymes of lignin biosynthesis positioned in the middle of the phenylpropanoid pathway like in *ccoaomt1*, *ccr1* and *comt1* provoke both delayed development of Casparian strip barrier and suberisation due to the lack of monomers for the assembly of both polymers. Especially, *ccoaomt1* demonstrates that ω-hydroxy acids are associated with *trans* ferulic acid. Manipulated enzymes directly involved in the synthesis of monolignols like in *cadc* and *cadd* do neither influence the Casparian strip development nor the functionality. Suberisation seems to be delayed. But double *cadc*cadd* mutants and triple knockout mutant *cadc*cadd*fah1-2* enhance the suberisation without affecting the Casparian strip barrier. Also manipulated HCALDH enzyme in *ref1-4* delays the Casparian strip development which provokes an ectopic suberisation. The mutated phenylpropanoid pathway Mediator subunit Mediator5b in *ref4-3* decreases phenylpropanoids and delays the Casparian strip development as well, which is accompanied by ectopic suberisation. Two other regulators MYB4 and MYB7 do not influence the development of Casparian strips and suberisation. Loss of function mutation in *fah1-2* also does not reveal any effect on CS and suberin development. Only in seedlings the suberisation seems to start earlier. Surprisingly, S-monolignol synthesis is not affected by the *fah1-2* mutant indicating a possible F5H-independent pathway exists in the root tissue. Expressing *FAH1* gene under the promoter of *C4H* leads to an accumulation of S-derived aromatic compounds which impairs the Casparian strip development and causes an ectopic suberisation. However, S-derived aromatic compounds appear to be not incorporated into the suberin polymer. Furthermore, ultrastructural analysis reveals lamellar-like structure of the suberin, but apparently there are more lamellae present. Surprisingly, the mutants *ref8-1*, *ref8-1*med5a*med5b*, *ref8-2*fah1-2*AtC4H::SmF5H* have an unaltered development of Casparian strips and suberin. Thioacidolytic analysis of the lignin composition exhibits G-monolignol synthesis in *ref8-1*med5a*med5b* roots, which underlines the assumption that a

C3H-independent pathway exists in the root tissue. Both the knockout mutation of *HQT* as well as transcription of *HQT* under the control of the promoter of *RALPH* in *hqt* mutant background show an earlier development of Casparian strip barrier in both lines. However, suberisation is not affected by both mutations. The contribution of the possible *HQT* gene to the phenylpropanoid pathway remains doubtful. Loss of function mutations in *PRX11* and *ASFT* reveal unaltered development of Casparian strip but delayed suberisation. This seems to be caused by the lack of diferulic acid. Ultrastructural analysis shows a local wavy phenotype of suberin in the cell wall. Possibly, suberin is anchored via diferulic in the cell wall. Furthermore, loss of esterified ferulic acid or diferulic acid does not influence the lamellar-like structure of suberin. Due to the chemical properties of the contrasting the electron-opaque lamellae can neither consist of a polyaromatic domain nor an aromatic rich zone. Probably, suberin is crystallised in the cell wall and able to self-assemble to the lamellar-like structure like other copolymers. Mutation in *fact3* does neither influence the Casparian strip development nor the suberisation.

Finally, the different phenylpropanoid pathway mutants enable the study of the contribution of both endodermal barriers to physiological phenomena like water as well as nutrient transport and ion homeostasis.

6. Further Research

6.1. Basic fuchsine staining of *comt1*, *fah1-2* and *ref8-2*fah1-2*AtC4H::SmF5H*

The visualisation of the Casparian strip barrier was mainly focused on mutant lines that are severely affected in the Casparian strip development. Nonetheless, it is expected that *comt1* exhibits a faint staining of the lignified Casparian strip barrier similar to *ccr1* and *ccoaomt1*. The mutant *fah1-2* shows a functional Casparian strip barrier and unaltered lignin composition. Visualisation of the lignified Casparian strips supports the idea of a F5H-independent pathway of S-monolignol synthesis in the root tissue. The mutant *ref8-2*fah1-2*AtC4H::SmF5H* was expected to show an impaired Casparian strip barrier similar to *C4H::F5H*, but a basic fuchsine staining would show alterations. The lignin content is severely affected in the root tissue but blockage of PI is similar to the WT. Qualitative analysis of the Casparian strip barrier may help to understand its functionality.

6.2. Fluorol yellow staining and analysis of lignin composition of *ref8-1* roots

The suberin staining of one-week old roots of *ref8-1* seedlings has to be repeated since an appropriate number of homozygous *ref8-1* seedlings were not achieved by the last experiment. Chemical suberin analysis reveals no alterations in the composition compared to the WT. This was unexpected and may indicate that *meta*-hydroxylation in the phenylpropanoid pathway in the roots is performed by another enzyme than in the stem tissue. Furthermore, thioacidolytic analysis of the lignin composition in *ref8-1* might emphasise the hypothesis of the C3H-independent pathway in the root tissue.

6.3. Ultrastructural analysis of suberin in *ccoaomt1*

Similar to *asft* mutant lines *ccoaomt1* reveals a decreased content of both *trans* ferulic acid and diferulic acid in the chemical analysis of suberin. Ultrastructural analysis of suberised endodermal cells by TEM might show evidence of a wavy suberin band. If this has been confirmed three different mutant lines with decreased diferulic acid content would further support the idea that suberin is anchored in the primary cell wall via diferulic acid.

6.4. Localisation of PRX11 and its analysis of enzymatic feature

The enzymatic activity of PRX11 was not analysed yet. It is proposed that PRX11 is able to polymerise *trans* ferulic acid to diferulic acid. Due to the reason that *asft* mutant lines reveal a decline of diferulic acid, it might be possible that PRX11 uses as substrate esterified ferulic acid monomers. Synthesis of PRX11 enzyme can be achieved by overexpression of *PRX11* gene in *Escherichia coli* cells. Isolated and purified PRX11 enzymes can be used in an enzymatic assay. As substrates *trans* ferulic acid and extracted alkyl ferulates from *Solanum tuberosum* peridermal tissue can be used. Yielded products of the enzymatic reaction could be either analysed by gas chromatography or by thin-layer chromatography. UV-light fluorescence might detect the polymerised diferulic acid molecules onto a coated silica-plate. The possible polymerised alkyl ferulates might be too heavy to become volatile and therefore not detectable via gas chromatography. Another possibility is the separation via high-performance liquid chromatography.

If the enzymatic activity of PRX11 has been confirmed, a fluorescent tagged PRX11 protein might provide evidence for the localisation of PRX11 in the cell wall. Furthermore, counting the number of endodermal cells after the onset of elongation up to the first occurrence of fluorescent tagged PRX11 protein could also elucidate the association of PRX11 with ASFT.

6.5. Role of suberin with respect to apoplastic and coupled trans-cellular pathway

The characterisation of the different phenylpropanoid pathway mutants employed a tool box to study the contribution of both endodermal barriers to the apoplastic and trans-cellullar pathway. The influence of a delayed and enhanced suberisation may be studied in the different *cad*-mutants without interference of a delayed or disrupted Casparian strip barrier. The contribution of the delayed formation of both endodermal barriers may also be analysed by using mutants like *ccoaomt1*, *ccr1* and *comt1*. Influence of delayed formed Casparian strip barrier and accompanied ectopic suberisation is possible to study in *ref4-3* and *ref1-4* mutants. Before studying the root hydraulic conductance, the functionality of xylem elements has to be confirmed by histochemical analysis of root cross sections. This might elucidate the drought tolerance in *ccr1* and *ref8-2*fah1-2*AtC4H::SmF5H* plants.

6.6. Combination of piperonylic acid treatment and feeding experiments

Inhibition of the phenylpropanoid pathway seems to follow the pattern of disrupted Casparian strip with accompanied ectopic suberisation. However, it is arguable how suberisation is enhanced if feruloyl-CoA synthesis seems to be inhibited. Treating seedlings with PA and simultaneously feeding seedlings with L-tyrosine might elucidate the participation of L-tyrosine as a substrate for the phenylpropanoid pathway and the origin of the feruloyl-CoA synthesis. Furthermore, *ref3-2* plants were expected to simulate the PA treatment. It is of high interest to investigate if feeding *ref3-2* plants with either L-tyrosine or *trans* ferulic acid might trigger the ectopic suberisation phenotype.

7. References

1. **Abdulrazzak, N., Pollet, B., Ehlting, J., Larsen, K., Asnaghi, C., Ronseau, S., Proux, C., Erhardt, M., Seltzer, V., Renou, J.-P., Ullmann, P., Pauly, M., Lapierre, C. & Werck-Reichhart, D.** (2006) A coumaroyl-ester-3-hydroxylase insertion mutant reveals the existence of nonredudant meta-hydroxylation pathways and essential roles for phenolic precursors in cell expansion and plant growth. Plant Physiology **140**: 30-48
2. **Alassimone, J., Naseer, S. & Geldner, N.** (2010) A developmental framework for endodermal differentiation and polarity. PNAS **107**: 5214-5219
3. **Allen, R. C.** (2010) The British industrial revolution in global perspective. Reviews on History, Cambridge, UK, Cambridge University Press: 344-347
4. **Alsayed, A. M., Dogic, Z. & Yodh, A. G.** (2004) Melting of lamellar phases in temperature sensitive colloid-polymer suspension. Physical Review Letters **96**: 1-4
5. **Andersen, T. G., Barberon, M. & Geldner, N.** (2015) Suberization – the second life of an endodermal cell. Current Opinion in Plant Biology **28**: 9-15
6. **Anderson, N. A., Tobimatsu, Y., Ciesielski, P. N., Ximines, E., Ralph, J., Donohoe, B. S., Ladisch, M. & Chapple, C.** (2015) Manipulation of guiacyl and syringyl monomer biosynthesis in an Arabidopsis cinnamyl alcohol dehydrogenase mutant results in atypical lignin biosynthesis and modified cell wall structure. The Plant Cell **27**: 2195-2209
7. **Atanassova, R., Favet, N., Martz, F., Chabbert, B., Tollier, M.-T., Monties, B., Fritig, B. & Legrand, M.** (1995) Altered lignin composition in transgenic tobacco expressing O-methyltransferase sequences in sense and antisense orientation. The Plant Journal **8**: 465-477
8. **Badger, G. M. & Reed, R. I.** (1948) Relative reactivity of aromatic double bonds. Nature **161**: 238
9. **Bahr, G. F.** (1954) Osmium tetroxide and ruthenium tetroxide and their reactions with biologically important substances. Experimental Cell Research **7**: 457-479
10. **Barberon, M. & Geldner, N.** (2014): Radial transport of nutrients: the plant root as a polarized epithelium. Plant Physiology **166**: 528-537
11. **Barberon, M., Vermeer, J. E. M., De Bellis, D., Wang, P., Naseer, S., Andersen, T. G., Humbel, B. M., Nawrath, C., Takano, J., Salt, D. E. & Geldner, N.** (2016) Adaption of

root function by nutrient-induced plasticity of endodermal differentiation. Cell **164**: 447-459

12. **Barberon, M.** (2017) The endodermis as a checkpoint for nutrient. New Phytologist **213**: 1604-1610
13. **Barthlott, W.** (1990) Geschichte des Botanischen Gartens der Universität Bonn. In: Heijo Klein: Bonn – Universität in der Stadt. Publications of the city archive **48**: 41-60
14. **Bateman, R. M., Crane, P. R., DiMichele, W. A., Kenrick P. R., Rowe, N. P., Speck, T. & Stein, W. E.** (1998) Early evolution of land plants: phylogeny, physiology, and ecology of the primary terrestrial radiation. Annual Review of Ecology and Systematics **29**: 263-292
15. **Baxter, I., Hosmani, P. S., Rus, A., Lahner, B., Borevitz, J. O., Muthukumar, B., Mickelbart, M. V., Schreiber, L., Franke, R. B. & Salt, D. E.** (2009) Root suberin forms an extracellular barrier that affects water relations and mineral nutrition in Arabidopsis. PLoS Genetics **5**: 1-12
16. **Beisson, F., Li, Y., Bonaventure, G., Pollard, M. & Ohlrogge, J. B.** (2007) The acyltransferase GPAT5 is required for the synthesis of suberin in seed coat and root of *Arabidopsis*. The Plant Cell **19**: 351-368
17. **Bernards, M. A., Lopez, M. L., Zajicek & Lewis, N. G.** (1995) Hydroxycinnamic acid-derived polymers constitute the polyaromatic domain of suberin. The Journal of Biological Chemistry **270**: 7382-7386
18. **Bernards, M. A. & Razem, F. A.** (2001) The poly(phenolic) domain of potato suberin: a non-lignin cell wall bio polymer. Phytochemistry **57**: 1115-1122
19. **Bernards, M. A.** (2002) Demystifying suberin. Canadian Journal of Botany **80**: 227-240
20. **Biggs, A. R. & Miles, N. W.** (1988) Association of suberin formation in uninoculated wounds with susceptibility to Leucostoma cincta and L. personii in various peach cultivars. Phytopathology **78**: 1070-1074
21. **Bland, D. E., Foster, R. C. & Logan, A. F.** (1971) The mechanism of permanganate and osmium tetroxide fixation and the distribution of lignin in the cell wall of *Pinus radiata*. Holzforschung **25**: 137-143
22. **Boerjan, W., Ralph, J. & Baucher M.** (2003) Lignin biosynthesis. Annual Review of Plant Physiology and Plant Molecular Biology **54**: 519-546

23. **Bonawitz, N. D., Soltau, W. L., Blatchley, M. r., Powers, B. L., Hurlock, A. K., Seals, L. A., Weng, J.-K., Stout, J. & Chapple, C.** (2012) REF4 and RFR1, subunits of the transcriptional coregulatory complex Mediator, are required for phenylpropanoid homeostasis in *Arabidopsis*. Journal of Biological Chemistry **287**: 5434-5445
24. **Bonawitz, N. D., Kim, J. I., Tobimatsu, Y., Ciesielski, P. N., Anderson, N. A., Ximines, E., Maeda, J., Ralph, J., Donohoe, B. S., Ladisch, M. & Chapple, C.** (2014) Disruption of mediator rescues the stunted growth of a lignin-deficient *Arabidopsis* mutant. Nature **509**: 376-380
25. **Brands, M.** (2014) Functional genomics of At1g68850 provides evidence for the involvement of perixidases in suberin deposition in the root endodermis and the seed coat. Master thesis, Mathematisch-Naturwisssenschaftliche Fakultät der Rheinischen Friedrich-Wilhelms-Universität-Bonn
26. **Campbell, N. A., Reece, J. B., Urry, Cain, Wasserman, Minorsky & Jackson** (2011) Biologie. Pearson Studium, München, Germany, 8th edition: 587
27. **Caspary, R.** (1866) Bermerkungen über die Schutzscheide und die Bildung des Stammes und der Wurzel. Jahrbücher für wissenschaftliche Botanik **4**: 101-124
28. **Chapple, C. C. S., Vogt, T., Ellis, B. E. & Somerville, C. R.** (1992) An Arabidopsis mutant defective in the general phenylpropanoid pathway. Plant Cell **4**: 1413-1424
29. **Clough, S. J. & Bent, A. F.** (1998) Floral dip: a simplified method for Agrobacterium-mediated transformation of Arabidopsis thaliana. The Plant Journal **16**: 735-743
30. **Cochrane, F. C., Davin, L. B. & Lewis, N. G.** (2004) The Arabidopsis phenylalanine ammonia-lyase gene family: kinetic characterization of the four PAL isoforms. Phytochemistry **65**: 1557-1564
31. **Compagnon, V., Diehl, P., Benveniste, I., Meyer, D., Schaller, H., Schreiber, L., Franke, R. & Pinot, F.** (2009) CYP86B1 is required for very long chain ω-hydroxyacid and α,ω-dicarboxylic acid synthesis in root and seed suberin polyester. Plant Physiology **150**: 1831-1843
32. **Corpet, F.** (1988) Multiple sequence alignment with hierarchical clustering. Nucleic acids research **16**: 10881-10890
33. **De Smet, S., Cuypers, A., Vangronsveld, J. & Remans, T.** (2015) Gene networks involved in hormonal control of root development in *Arabidopsis thaliana*: A

framework for studying its disturbance by metal stress. International Journal of Molecular Sciences **16**: 19195-19224

34. **Derikvand, M. M., Sierra, J. B., Ruel, K., Pollet, B., Do, C.-T., Thévenin, J., Buffard, D., Jouanin, L. & Lapierre, C.** (2008) Redirection of the phenylpropanoid pathway to feruloyl malate in *Arabidopsis* mutants deficient for cinnamoyl-CoA reductase 1. Planta **227**: 943-956
35. **Dharmawardhana, D. P., Ellis, B. E. & Carlson, J. E.** (1992) Characterization of vascular lignification in *Arabidopsis thaliana*. Canadian Journal of Botany **70**: 2238-2244
36. **Di Laurenzio, L., Wysocka-Diller, J., Malamy, J. E., Pysh, L., Helanriutta, Y., Freshour, G., Hahn, M. G., Feldmann, K. A. & Benfey, P. N.** (1996) The *SCARECROW* gene regulates an asymmetric cell division that is essential for generating the radial organization of the *Arabidopsis* root. Cell **86**: 423-433
37. **Dixon, R. A., Achnine, L., Kota, P., Liu, C.-J., Reddy, M. S. S. & Wang, L.** (2002) The phenylpropanoid pathway and plant defence – a genomics perspective. Molecular Plant Pathology **3**: 371-390
38. **Do, C.-T., Pollet, B., Thévenin, J., Sibout, R., Denoue, D., Barrière, Y., Lapierre, C. & Jouanin, L.** (2007) Both caffeoyl coenzyme A 3-*O*-methyltransferse 1 and caffeic acid *O*-methyltransferase 1 are involved in redundant functions for lignin, flavonoids and sinapoyl malate biosynthesis in Arabidopsis. Planta **226**: 1117-1129
39. **Doblas, V. G., Smakowska-Luzan, E., Fujita, S., Alassimone, J., Barberon, M., Madalinski, M., Belkhadir, Y. & Geldner, N.** (2017) Root diffusion barrier contol by a vasculature-derived peptide binding to the SGN3 receptor. Plant Science **355**: 280-284
40. **Dolan, L., Janmaat, K., Willemsen, V., Linstead, P., Poethig, S., Roberts, K. & Scheres, B.** (1993) Cellular organisation of the *Arabidopsis thaliana* root. Development **119**: 71-84
41. **Dolan, W. L., Dilkes, B. P., Stout, J. M., Bonawitz, N. D. & Chapple, C.** (2017) Mediator complex subunits MED2, MED5, MED16, and MED23 genetically interact in the regulation of phenylpropanoid biosynthesis. The Plant Cell **29**: 3269-3285
42. **Domergue, F. & Kosma, D. K.** (2017) Occurrence and biosynthesis of alkyl hydroxycinnamates in plant lipid barriers. Plants **6**: 1-17

43. **Donaldson, L. A.** (2001) Lignification and lignin topochemistry – an ultrastructural view. Phytochemistry **57**: 859-873
44. **Eraso, F. & Hartley, R. D.** (1990) Monomeric and dimeric phenolic constituents of plant cell walls – possible factors influencing wall biodegradability. Journal of the Science of Food and Agriculture **51**: 163-170
45. **Espelie, K. E., Sadek, N. Z. & Kolattukudy, P. E.** (1980) Composition of suberin-associated waxes from the subterranean storage organs of seven plants, parsnip, carrot, rutabaga, turnip, red beet, sweet potato and potato. Planta **148**: 468-476
46. **Espelie, K. E. & Kolattukudy, P. E.** (1985) Purification and characterization of an abscisic acid-inducible anionic peroxidase associated with suberization in potato (*Solanum tuberosum*). Archives of Biochemistry and Biophysics **240**: 539-545
47. **Falk, H. & Sitte, P.** (1963) Untersuchungen am Caspary-Streifen. In: Houwink AL, Spit BJ (eds) The proceedings of the European regional conferece on electron microscopy, Delft 1960. De Nederlandse Vereniging Voor Electronenmicroscopie Delft, Delft: 1063-1066
48. **Faulds, C. B. & Williamson, G.** (1999) The role of hydroxycinnamates in the plant cell wall. Journal of the Science of Food and Agriculture **79**: 393-395
49. **Férnandez-Pérez, F., Pomar, F., Pedreño, M. A. & Novo-Uzal, E.** (2015) Suppression of Arabidopsis peroxidase 72 alters cell wall and phenylpropanoid metabolism. Plant Science **239**: 192-199
50. **Fraenkel-Conrat, H., Brandon, B. A. & Olcott, H. S.** (1946) The reaction of formaldehyde with proteins: IV. Participation of indole groups. Gramicidin. Journal of Biological Chemistry **168**: 99-118
51. **Fraenkel-Conrat, H. & Olcott, H. S.** (1948) The reaction of formalaldehyde with proteins. V. Cross-linking between amino and primary amide or guanidyl groups. Journal of the American Chemical Society **70**: 2673-2684
52. **Franke, R., Humphreys, J. M., Hemm, M. R., Denault, J. W., Ruegger, M. O., Cusumano, J. C. & Chapple, C.** (2002a) The *Arabidopsis REF8* gene encodes the 3-hydroxylase of phenylpropanoid metabolism. The Plant Journal **30**: 33-45
53. **Franke, R., Hemm, M. R., Denault, J. W., Ruegger, M. O., Humphreys, J. M. & Chapple, C.** (2002b) Changes in secondary metabolism and deposition of an unusual lignin in the *ref8* mutant of *Arabidopsis*. The Plant Journal **30**: 47-59

54. **Franke, R., Briesen, I., Wojciechowski, T., Faust, A., Yephremov, A., Nawrath, C. & Schreiber, L.** (2005) Apoplastic polyester in *Arabidopsis* surface tissue – A typical suberin and a particular cutin. Phytochemistry **66**: 2643-2658

55. **Franke, R. & Schreiber, L.** (2007) Suberin – a biopolyester forming apoplastic plant interfaces. Current Opinion in Plant Biology **10**: 252-259

56. **Franklin, M. R.** (1977) Inhibition of mixed-function oxidations by substrates forming reduced cytochrome P-450 metabolic-intermediate complexes. Pharmacoloy & Therapeutics **2**: 227-245

57. **Frasca, J. M. & Parks, V. R.** (1965) A routine technique for double-staining ultrathin sections using uranyl and lead salts. The Journal of Cell Biology **25**: 157-161

58. **Fraser, C. & Chapple, C.** (2011) The phenylpropanoid pathway in Arabidopsis. The Arabidopsis Book, American Society of Plant Biologist: 1-19

59. **Frenger, M. S.** (2014) Untersuchung zur Regulation und Biosynthese apoplastischer Polyester in höheren Pflanzen. Dissertation, Mathematisch-Naturwisssenschaftliche Fakultät der Rheinischen Friedrich-Wilhelms-Universität-Bonn

60. **Fornalé, S., Lopez, E., Salazar-Henao, J. E., Fernández-Nohales, P., Rigau, J. & Caparros-Ruiz, D.** (2014) AtMYB7, a new player in the regulation of UV-sunscreens in *Arabidopsis thaliana*. Plant Cell Physiology **55**: 507-516

61. **Gallage, N. J., Hansen, E. H., Kannangara, R., Olsen, C. E., Motawia, M. S., Jørgensen, K., Holme, I., Hebelstrup, K., Grisoni, M. & Møller, B. L.** (2013) Vanillin formation from ferulic acid in Vanilla planifolia is catalysed by a single enzyme. Nature Communications **5**:4037

62. **Gallage, N. J. & Møller, B. L.** (2015) Vanillin-bioconversion and bioengineering of the most popular plant flavour and its de novo biosynthesis in the vanilla orchid. Molecular Plant **8**: 40-57

63. **García-Vallejo, M. C., Conde, E., Cadahía, E. & Fernández de Simón, B.** (1997) Suberin composition of reproduction cork from Quercus suber. Holzforschung **51**: 219-224

64. **Gensel, P. G. & Edwards, D.** (2001) Plants invade the land: evolutionary and environmental perspectives. New York, NY, USA: Columbia University Press.

65. **Gigg, R. & Payne, S.** (1969) The reaction of glutaraldehyde with tissue lipids. Chemistry and Physics of Lipids **3**: 292-295

66. **Gill, S. S. & Tuteja, N.** (2010) Reactive oxygen species and antioxidant machinery in abiotic stress tolerance in crop plants. Plant Physiology and Biochemistry **48**: 909-930
67. **Ginsburg, H. & Wolosin, J. M.** (1979) Effects of uranyl ions on lipid bilayer membranes. Chemistry and Physics of Lipids **23**: 125-131
68. **Goujon, T., Sibout, R., Pollet, B., Maba, B., Nussaume, L., Bechtold, N., Lu, F., Ralph, J., Mila, I., Barrière, Y., Lapierre, C. & Jouanin, L.** (2003) A new *Arabidopsis thaliana* mutant deficient in the expression of *O*-methyltransferase impacts lignins and sinpoyl esters. Plant Molecular Biology **51**: 973-989
69. **Graça, J. & Santos, S.** (2007) Suberin: a biopolyester of plant's skin. Macromolecular Bioscience **7**: 128-135
70. **Graça, J.** (2010) Hydroxycinnamates in suberin formation. Phytochemistry Review **9**: 85-91
71. **Graça, J., Cabral, V., Santos, S., Lamosa, P., Serra, O., Molinas, M., Schreiber, L., Kauder, F. & Franke, R.** (2015) Partial depolymerization of genetically modifed potato tuber periderm reveals intermolecular linkages in suberin polyester. Phytochemistry **117**: 209-219
72. **Graça, J.** (2015) Suberin: the biopolyester at the frontier of plants. Frontiers in Chemistry **3**: 1-11
73. **Guo, D., Chen, F., Inoue, K., Blount, J. W. & Dixon, R. A.** (2001) Downregulation of caffeic acid 3-*O*-methyltransferase and caffeoyl CoA 3-*O*-methyltransferase in transgenic alfalfa: impacts on lignin structure and implications for the biosynthesis of G and S lignin. The Plant Cell **13**: 76-88
74. **Hall, J. L.** (1978) Electron microscopy and cytochemistry of plant cells. pp. 14-15 Elsevier/North-Holland Biomedical Press, New York
75. **Harrison, S. J., Mott, E. K., Parsley, K., Aspinall, S., Gray, J. C. & Cottage, A.** (2006) A rapid and robust method of identifying transformed Arabidopsis thaliana seedlings following floral dip transformation. Plant Methods **2**: 1-7
76. **Hayatsu, R., Winans, R. E., McBeth, R. L., Scott, R. G., Moore, L. P. & Studier, M. H.** (1979) Lignin-like polymers in coals. Nature **278**: 41-43
77. **Helanriutta, Y., Fukaki, H., Wysocka-Diller, J., Nakajima, K., Jung, J., Sena, G., Hauser, M. T. & Benfey, P. N.** (2000) The SHORT-ROOT gene controls radial patterning of the *Arabidopsis* root through radial signaling. Cell **101**: 555-567

78. **Higgins, C. F. & Linton, K. J.** (2004) The ATP switch model for ABC transporters. Nature Structural & Molecular Biology **11**: 918-926

79. **Hoffman, J. D., Davis, G. T. & Lauritzen, Jr., J. I.** (1976) The rate of crystallization of linear polymers with chain folding. Treatise on Solid State Chemistry, edited by N. B. Hannay, Bell Telephone Laboratories: 497-498

80. **Hoffmann, L., Maury, S., Martz, F., Geoffroy, P. & Legrand, M.** (2003) Purification, cloning, and properties of an acyltransferase controlling shikimate and quinate ester intermediates in phenylpropanoid metabolism. The Journal of Biological Chemistry **278**: 95-103

81. **Hoffmann, L., Besseau, S., Geoffroy, P., Ritzenthaler, C., Meyer, D., Lapierre, C., Pollet, B & Legrand, M.** (2004) Silencing of hydroxycinnamoyl-coenzyme A shikimate/quinate hydroxycinnamoyltransferase affects phenylpropanoid biosynthesis. The Plant Cell **16**: 1446-1465

82. **Holton, T. A., Brugliera, F. & Tanaka, Y.** (1993) Cloning and expression of flavonol synthase from *Petunia hybrida*. The Plant Journal **4**: 1003-1010

83. **Holton, T. A. & Cornish, E. C.** (1995) Genetics and biochemistry of anthocyanin biosynthesis. The Plant Cell **7**: 1071-1083

84. **Hosmani, P. S., Kamiya, T., Danku, J., Naseer, S., Geldner, N., Guerinot, M. L. & Salt, D. E.** (2013) Dirigent domain-containing protein is part of the machinery required for formation of the lignin-based casparian strip in the root. PNAS **110**: 14498-14503

85. **Höfer, R., Briesen, I., Beck, M., Pinot, F., Schreiber & Franke, R.** (2008) The Arabidopsis cytochrome P450 CYP86A1 encodes a fatty acid ω-hydroxylase involved in suberin monomer biosynthesis. Journal of Experimental Botany **59**: 2347-2360

86. **Humphreys, J. M., Hemm, M. R. & Chapple, C.** (1999) New routes for lignin biosynthesis defined by biochemical characterization of recombinant ferulate 5-hydroxylase, a multifunctional cytochrome P450-dependent monooxygenase. PNAS **96**: 10045-10050

87. **Iiyama, K., Lam, T. B.-T. & Stone, B. A.** (1994) Covalent cross-links in the cell wall. Plant Physiology **104**: 315-320

88. **Jacquet, G., Pollet, B. & Lapierre, C.** (1995) New ether-linked ferulic acid – coniferyl alcohol dimers identified in grass straws. Journal of Agricultural Food Chemistry **43**: 2746-2751

89. **Jin, H., Cominelli, E., Bailey, P., Parr, A., Mehrtens, F., Jones, J., Tonelli, C., Weisshaar, B. & Martin, C.** (2000) Transcriptional repression by AtMYB4 controls production of UV-protecting sunscreens in *Arabidopsis*. The EMBO Journal **19**: 6150-6161

90. **Jones, L., Ennos, A. R. & Turner, S. R.** (2001) Cloning and characterization of *irregular xylem4* (*irx4*): a severely lignin-deficient mutant of *Arabidopsis*. The Plant Journal **26**: 205-216

91. **Kamiya, T., Borghi, M., Wang, P., Danku, J. M. C., Kalmbach, L., Hosmani, P. S., Naseer, S., Fujiwara, T., Geldner, N. & Salt, D. E.** (2015) The MYB36 transcription factor orchestrates Casparian strip formation. PNAS **112**: 10533-10538

92. **Karnovsky, M. J.** (1965) A formaldehyde-glutaraldehyde fixative of high osmolarity for use in electron microscopy. The Journal of Cell Biology **27**: 137A-138A

93. **Kempken, F. & Kempken, R.** (2012) Gentechnik bei Pflanzen – Chancen und Risiken. Springer-Verlag Berlin, Heidelberg, 4th edition: 63-64

94. **Khan, W., Prithiviraj, B. & Smith, D. L.** (2003) Chitosan and chitin oligomers increase phenylalanine ammonia-lyase and tyrosine ammonia-lyase activities in soybean leaves. Journal of Plant Physiology **160**: 859-863

95. **Kim, J. H., Hyun, W. Y., Nguyen, H. N., Jeong, C. Y., Xiong, L., Hong, S.-W. & Lee, H.** (2015) AtMyb7, a subgroup 4 R2R3 Myb, negatively regulates ABA-induced inhibition of seed germination by blocking the expression of the bZIP transcription factor ABI5. Plant, Cell and Environment **38**: 559-571

96. **Kim, M. J., Ciani, S. & Schachtman, D. P.** (2010) A peroxidase contributes to ROS production during *Arabidopsis* root response to potassium deficiency. Molecular Plant **3**: 420-427

97. **Kim, S.-J., Kim, M.-R., Bedgar, D. L., Moinuddin, S. G. A., Cardenas, C. L., Davin, L. B., Kang, C. H. & Lewis, N. G.** (2004) Functional reclassification of the putative cinnamyl alcohol dehydrogenase multigene family in Arabidopsis. PNAS **101**: 1455-1460

98. **Kim, S. O., Solak, H. H., Stoykovich, M. P., Ferrier, N. J., de Pablo, J. J. & Nealey, P. F.** (2003) Epitaxial self-assembly of block copolymers on lithographically defined nanopatterned substrates. Nature **424**: 411-414

99. **Kim, W.-C.** (2016) AtMYB7 acts as a repressor of lignin biosynthesis in Arabidopsis. Journal of Applied Biological Chemistry **59**: 215-220

100. **Kirch, H.-H., Nair, A. & Bartels, D.** (2001) Novel ABA- and dehydration-inducible aldehyde dehydrogenase genes isolated from the resurrection plant *Craterostigma plantagineum* and *Arabidopsis thaliana*. The Plant Journal **28**: 555-567

101. **Klotz, G., Kleinschmidt, A. K. & Goebel, W.** (1978) Counting superhelical turns in electron micrographs of large plasmids. Electron Microscopy **2**: 196-197

102. **Knapp, D. R.** (1979) Handbook of analytical derivatization reactions. New York: John Wiley & Sons, Ltd.

103. **Kolattukudy, P. E.** (1980) Biopolyester membranes of plants: cutin and suberin. Science **208**: 990-1000

104. **Kolattukudy, P. E.** (1981) Structure, biosynthesis, and biodegradation of cutin and suberin. Annual Review of Plant Physiology and Plant Molecular Biology **32**: 539-567

105. **Kolattukudy, P. E.** (2001) Biopolyester membranes of plants: cutin and suberin. Science **208**: 990-1000

106. **Kolosova, N., Sherman, D., Karlson, D. & Dudareva, N.** (2001) Cellular and subcellular localization of S-adenosyl-L-methionine:benzoic acid carboxyl methyltransferase, the enzyme responsible for biosynthesis of the volatile ester methylbenzoate in snapdragon flowers. Plant Physiology **126**: 956-964

107. **Koornneef, M., Rolff, E. & Spruit, C. J. P.** (1980) Genetic control of light-inhibited hypocotyl elongation in Arabidopsis thaliana (L.) Heynh. Zeitschrift für Pflanzenphysiologie **100**: 147-160

108. **Koornneef, M., van Eden, J., Hanhart, C. J., Stam, P., Braaksma, F. J. & Feenstra, W. J.** (1983) Linkage map of *Arabidopsis thaliana*. Journal of Heredity **74**: 265-272

109. **Kosma, D. K., Molina, I., Ohlrogge, J. B. & Pollard, M.** (2012) Identification of an Arabidopsis fatty alcohol:caffeoyl-Coenzyme A acyltransferase required for the synthesis of alkyl hydroxycinnamates in root waxes. Plant Physiology **160**: 237-248

110. **Kosma, D. K., Murmu, J., Razeq, F. M., Santos, P., Bourgault, R., Molina I. & Rowland, O.** (2014) AtMYB41 activates ectopic suberin synthesis and assembly in multiple plant species and cell types. The Plant Journal **80**: 216-229

111. **Kraus, J. E., de Sousa, H. C., Rezende, M. H., Castro, N. M., Vecchi, C. & Luque, R.** (1997) Astra blue and basic fuchsin double staining of plant materials. Biotechnic & Histochemistry **98**: 235-243

112. **Kroemer, K.** (1903) Wurzelhaut, Hypodermis und Endodermis der Angiospermenwurzel. Bibliotheca Botanica **59**: 1-148

113. **Laibach, F.** (1943) Zur Ätiologie der Blütenbildung. Bot. Arch. **44**: 439

114. **Lapierre, C., Monties, B. & Rolando, C.** (1985) Thioacidolysis of lignin: comparison with acidolysis. Journal of Wood Chemistry and Technology **5**: 277-292

115. **Lapierre, C., Monties, B. & Rolando, C.** (1986) Preparative thioacidolysis of spruce lignin: isolation and identification of main monomeric products. Holzforschung **40**: 47-50

116. **Lee, J., Nam, J., Park, H. C., Na, G., Miura, K., Jin, J. B., Yoo, C. Y., Baek, D., Kim, D. H., Jeong, J. C., Kim, D., Lee, S. Y., Salt, D. E., Meningste, T., Gong, Q., Ma, S., Bohnert, H. J., Kwak, S.-S., Bressan, R. A., Hasegawa, P. M. & Yun, D.-J.** (2006) Salicylic acid-mediated innate immunity in Arabidopsis is regulated by SIZ1 SUMO E3 ligase. The Plant Journal **49**: 79-90

117. **Lee, S. B., Jung, S. J., Go, Y. S., Kim, H. U., Kim, J. K., Cho, H. J., Park, O. K. & Suh, M. C.** (2009) Two Arabidopsis 3-ketoacyl CoA synthase genes, *KCS20* and *KCS2/DAISY*, are functionally redundant in cuticular wax and root suberin biosynthesis, but differentially controlled by osmotic stress. The Plant Journal **60**: 462-475

118. **Lee, Y., Rubio, M. C., Alassimone, J. & Geldner, N.** (2013) A mechanism for localized lignin deposition in the endodermis. Cell **153**: 402-412

119. **Lenz, H., Dombinov, V., Dreistein, J., Reinhard, M. R., Gebert, M. & Knoop, V.** (2013) Magnesium deficiency phenotypes upon multiple knockout of Arabidopsis thaliana MRS2 clade B genes can be ameliorated by concomitantly reduced calcium supply. Plant and Cell Physiology **54**: 1118-113

120. **Li, Y., Beisson F., Ohlrogge, J. & Pollard, M.** (2007b) Monoacylglycerols are components of root waxes and can be produced in the aerial cuticle by ectopic expression of a suberin associated acyltransferase. Plant Physiology **144**: 1267-1277

121. **Lindsay, S. E. & Fry, S. C.** (2008) Control of diferulate formation in dicotyledonous and gramineous cell-suspension cultures. Planta **227**: 439-452

122. **Litman, R. B. & Barnett, R. J.** (1972) The mechanism of the fixation of tissue components by osmium tetroxide via hydrogen bonding. The Journal of Ultrastructure Research **38**: 63-86

123. **Liu, K. S.** (1994) Preparation of fatty acid methyl esters for gas-chromatographic analysis of lipids in biological materials. Journal of the American Oil Chemists' Society **71**: 1179-1187

124. **Lobreaux, S., Massenet, O., Briat, J. F.** (1992) Iron induces ferritin synthesis in maize plantlets. Plant Molecular Biology **19**: 563-575

125. **Lowry, B., Hebant, C. & Lee, D.** (1980) The origin of land plants – a new look at an old problem. Taxon **29**: 183-197

126. **Löfke, C., Luschnig, C. & Kleine-Vehn, J.** (2013) Posttranslational modification and trafficking of PIN auxin efflux carriers. Mechanisms of Development **130**: 82-94

127. **Lu, F. & Ralph, J.** (1997) Derivatization followed by reductive cleavage (DFRC method), a new method for lignin analysis: protocol for analysis of DFRC monomers. Journal of Agricultural Food Chemistry **45**: 2590-2592

128. **Luo, J., Butelli, E., Hill, L., Parr, A., Niggeweg, R., Bailey, P., Weisshaar, B. & Martin, C.** (2008) AtMYB12 regulates caffeoyl quinic acid and flavonol synthesis in tomato: expression in fruit results in very high levels of both types of polyphenol. The Plant Journal **56**: 316-326

129. **Madison, K. C., Swartzendruber, D. C., Wertz, P. W. & Downing, D. T.** (1987) Presence of intact intercellular lipid lamellae in the upper layers of the stratum corneum. The Journal of Investigative Dermatology **88**: 714-718

130. **Maher, E. A., Bate, N. J., Ni, W., Elkind, Y., Dixon, R. A. & Lamb, C. J.** (1994) Increased disease susceptibility of transgenic tobacco plants with suppressed levels of preformed phenylpropanoid products. Plant Biology **91**: 7802-7806

131. **Mahl, H. & Möldner, K.** (1973a) Herstellung von Formvar-Objektträger-Filmen nach dem Eintauchverfahren. Methodensammlung der Elektronenmikroskopie (G. Schimmel and W. Vogell, editors) pp. 1-6, Wissenschaftliche Verlagsgesellschaft, Stuttgart

132. **Manach, C., Monrad, C., Crespy, V., Demigné, C., Texier, O., Régérat, F. & Rémésy, C.** (1998) Quercetin is recovered in human plasma as conjugated derivatives which retain antioxidant properties. FEBS letters **426**: 331-336

133. **Mandelkern, L.** (1985) The relation between structure and properties of crystalline polymers. Polymer Journal **17**: 337-350

134. **Mandelkern, L.** (1990) The structure of crystalline polymers. Accounts of Chemical Research **23**: 380-386

135. **Markus, K.** (2018) Characterization of the transcription factor *ANAC058* and its role in suberin regulation. Dissertation, Mathematisch-Naturwisssenschaftliche Fakultät der Rheinischen Friedrich-Wilhelms-Universität-Bonn

136. **Marques, A. V., Pereira, H., Meier, D. & Faix, O.** (1999) Structural characterization of cork lignin by thioacidolysis and permanganate oxidation. Holzforschung **53**: 167-174

137. **Meinke, D. W. & Sussex, I. M.** (1979) Embryo-lethal mutants of Arabidopsis thaliana: A model system for genetic analysis of plant embryo development. Developmental Biology **72**: 50-61

138. **Meinke, D. W., Cherry, J. M., Dean, C., Rounsley, S. D. & Koornneef, M.** (1998) Arabidopsis thaliana: A model plant for genome analysis. Science **282**: 662-682

139. **Meinke, D. & Scholl, R.** (2003) The preservation of plant genetic resources. Experiences with Arabidopsis. Plant Physiology **133**: 1046-1050

140. **Mendel, G.** (1866) Versuche über Pflanzenhybride. Verhandlungen über des Naturforschenden Vereines in Brünn **4**: 3-47

141. **Meyer, C. J., Peterson, C. A. & Bernards, M. A.** (2011) A comparision of suberin monomers from the multiseriate exodermis of *Iris germanica* during maturation under differing growth conditions. Planta **233**: 773-786

142. **Meyer, K., Shirley, A. M., Cusumano, J. C., Bell-Lelong, D. A. & Chapple, C.** (1998) Lignin monomer composition is determined by the expression of a cytochrome P450-dependent monooxygenase in *Arabidopsis*. PNAS **95**: 6619-6623

143. **Millán Hidalgo, C.** (2015) Analysis of HCT RNAi lines in potato (*Solanum tuberosum* L.) tubers with respect to the suberin formation. Master thesis, Rheinische Friedich-Wilhelms-Universität Bonn

144. **Mohnen, D.** (2008) Pectin structure and biosynthesis. Current Opinion in Plant Biology **11**: 266-277

145. **Molina, I., Bonaventure, G., Ohlrogge, J. & Pollard, M.** (2006): The lipid polyester composition of *Arabidopsis thaliana* and *Brassica napus* seeds. Phytochemistry **67**: 2597-2610

146. **Molina, I., Li-Beisson, Y., Beisson, F., Ohlrogge, J. B. & Pollard, M.** (2009) Identification of an Arabidopsis feruloyl-coenzyme A transferase required for suberin synthesis. Plant Physiology **151**: 1317-1328

147. **Nair, R. B., Bastress, K. L., Ruegger, M. O., Denault, J. W. & Chapple, C.** (2004) The *Arabidopsis thaliana REDUCED EPIDERMAL FLUORESCENCE1* gene encodes an aldehyde dehydrogenase involved in ferulic acid and sinapic acid biosynthesis. The Plant Cell **16**: 544-554

148. **Naseer, S., Lee, Y., Lapierre, C., Franke, R., Nawrath, C. & Geldner, N.** (2012) Casparian strip diffusion barrier in Arabidopsis is made of a lignin polymer without suberin. PNAS **109**: 10101-10106

149. **Nielson, A. J. & Griffith, W. P.** (1978) Tissue fixation and staining with osmium tetroxide: the role of phenolic compounds. The Journal of Histochemistry and Cytochemistry **26**: 138-140

150. **Niggeweg, R., Michael, A. J. & Martin, C.** (2004) Engineering plants with increased levels of the antioxidant chlorogenic acid. Nature Biotechnology **22**: 746-754

151. **Nobel, P. S.** (1999) Physicochemical and environmental plant physiology. San Diego: Academic Press Inc.

152. **North, G. B. & Nobel, P. S.** (1994) Changes in root hydraulic conductivity for two tropical epiphytic cacti as soil moisture varies. American Journal of Botany **81**: 46-53

153. **Nover, L.** (2002) Comeback von Arabidopsis. Forschung Frankfurt **1**: 1-2

154. **Obayashi, T., Kinoshita, K., Nakai, K., Shibaoka, M., Hayashi, S., Saeki, M., Shibata, D., Saito, K. & Ohta, H.** (2007) ATTED-II: a database of co-expressed genes and cis elements for identifying co-regulated gene groups in Arabidopsis. Nucleic Acid Research **35**: D863-D869

155. **Olthof, M. R., Hollman, P. C. H. & Katan, M. B.** (2000) Chlorogenic acid and caffeic acid are absorbed in humans. The Journal of Nutrition **131**: 66-71

156. **Olthof, M. R., Hollman, P. C. H., Buijsman, M. N. C. P., van Amelsvoort, J. M. M. & Katan, M. B.** (2003) Chlorogenic acid, quercetin-3-rutinoside and black tea phenols are extensively metabolized in humans. The Journal of Nutrition **133**: 1806-1815

157. **Oparka, K. J., Duckett, C. M., Prior, D. A. M. & Fisher, D. B.** (1994): Real-time imaging of phloem unloading in the root tip of *Arabidopsis*. The Plant Journal **6**: 759-766

158. **Ortiz de Montellano, P. R. & Correia M. A.** (1995) Inhibition of cytochrome P450 enzymes. Plenum Press, New York: 305-364

159. **Pandey, K. B. & Rizvi, S. I.** (2009) Plant polyphenols as dietary antioxidants in human health and disease. Oxidative Medicine and Cellular Longevity **2**: 270-278

160. **Passardi, F., Penel, C. & Dunand, C.** (2004) Performing the paradoxical: how plant peroxidases modify the cell wall. Trends in Plant Science **9**: 534-540

161. **Patten, A. M., Cardenas, C. L., Cochrane, F. C., Laskar, D. D., Bedgar, D. L., Davin, L. B. & Lewis, N. G.** (2005) Reassessment of effects on lignification and vascular development in the *irx4 Arabidopsis* mutant. Phytochemistry **66**: 2092-2107

162. **Parvathi, K., Chen, F., Guo, D., Blount, J. W. & Dixon, R. A.** (2001) Substrate preferences of *O*-methyltransferases in alfalfa suggest new pathways for 3-*O*-methylation of monolignols. The Plant Journal **25**: 193-202

163. **Payyavula, R. S., Shakya, R., Sengoda, V. G., Munyaneza, J. E., Swamy, P. & Navarre, D. A.** (2014) Synthesis and regulation of chlorogenic acid in potato: rerouting phenylpropanoid flux in *HQT*-silencing lines. Plant Biotechnology Journal: 1-14

164. **Péret, B., De Rybel, B., Casimiro, I., Benková, E., Swarup, R., Laplaze, L., Beeckman, T. & Bennett, M. J.** (2009) Arabidopsis lateral root development: an emerging story. Trends in Plant Science **14**: 399-408

165. **Peterson, C. A. & Cholewa, E.** (1998) Structural modifications of the apoplast and their potential impact on ion uptake. Zeitschrift Pflanzenernährung und Bodenkunde **161**: 521-531

166. **Pfister, A., Barberon, M., Alassimone, J., Kalmbach, L., Lee, Y., Vermeer, J. E. M., Yamazaki, M., Li, G., Maurel, C., Takano, J., Kamiya, T., Salt, D. E., Roppolo, D. & Geldner, N.** (2014) A receptor-like kinase mutant with absent endodermal diffusion barrier displays selective nutrient homeostasis defects. eLife 3, e03115.

167. **Pilgram, G. S. K., van Pelt, A. M. E., Bouwstra, J. A. & Koerten, H. K.** (1999) Electron diffraction provides new information on human stratum corneum lipid organization studied in relation to depth and temperature. The Journal of Investigative Dermatology **113**: 403-409

168. **Plattner, H.** (1973a) Die Entwässerung und Einbettung von biologischen Objekten für die Elektronenmikroskopie. Methodensammlung der Elektronenmikroskopie (G.

Schimmel and W. Vogell, editors) pp. 1-51, Wissenschaftliche Verlagsgesellschaft, Stuttgart

169. **Plattner, H. & Zingsheim, H. P.** (1987) Elektronenmikroskopische Methodik in der Zell- und Molekularbiologie. pp. 48-49 Gustav-Fischer Verlag, Stuttgart
170. **Pfister, A., Barberon, M., Alassimone, J., Kalmbach, L., Lee, Y., Vermeer, J. E. M., Yamazaki, M., Li, G., Maurel, C., Takano, J., Kamiya, T., Salt, D. E., Roppolo, D. & Geldner, N.** (2014) A receptor-like kinase mutant with absent endodermal diffusion barrier displays selective nutrient homeostasis defects. eLife **3**: 1-20
171. **Quiroga, M., Guerrero, C., Botella, M. A., Barcelo, A., Amaga, I., Medina, M. I., Alfonso, F. J., de Forchetto, S. M., Tigier, M. & Valpnesta, V.** (2000) A tomato peroxidase involved in the synthesis of lignin and suberin. Plant Physiology **122**: 1119-1127
172. **Ralph, J., Grabber, J. H. & Hatfield, R. D.** (1995) Lignin-ferulate cross-links in grasses: active incorporation of ferulate polysaccharide esters into ryegrass lignins. Carbohydrate Research **275**: 167-178
173. **Ranathunge, K. & Schreiber, L.** (2011) Water and solute permeabilities of *Arabidopsis* roots in relation to the amount and composition of aliphatic suberin. Journal of Experimental Botany **62**: 1961-1974
174. **Raven, J. A.** (1984) Physiological correlates of the morphology of early vascular plants. Botanical Journal of the Linnean Society **88**: 105-126
175. **Razeq, F. M., Kosma, D. K., Rowland, O. & Molina, I.** (2014) Extracellular lipids of Camelina sativa: characterization of extractable waxes from aerial and subterranean surfaces. Phytochemistry **106**: 188-196
176. **Razem, F. A. & Bernards, M. A.** (2002) Hydrogen peroxide is required for poly(phenolic) domain formation during wound-induced suberization. Journal of Agricultural and Food Chemistry **50**: 1009-1015
177. **rbb24** (5/7/2018) Ernteausfälle beim Getreide existenzbedrohend. Last time invoked the website on 6/7/2018, https://www.rbb24.de/wirtschaft/beitrag/2018/07/ernte-brandenburg-getreide-ausfaelle-bauernverband-existenzbedrohend-rukwied-trockenheit-landwirtschaft.html
178. **Rédei, G. P**. (1970) *Arabidopsis thaliana* (L.) *Heynh*. A review of the genetics and biology. Biobligraphia Genetica **20**: 151

179. **Reinhardt, D. H. & Rost, T. L.** (1995) Salinity accelerates endodermal development and induces an exodermis in cotton seedling roots. Environmental and Experimental Botany **35**: 563-574

180. **Reynolds, E. S.** (1963) The use of lead citrate at high pH as an electron-opaque stain in electron microscopy. The Journal of Cell Biology **17**: 208-212

181. **Richards, F. M. & Knowles, J. R.** (1968) Glutaraldehyde as a protein cross-linking reagent. Journal of Molecular Biology **37**: 231-233

182. **Roland, J.-C.** (1978) General preparation and staining of thin sections. Electron Microscopy and Cytochemistry of Plant Cells, edited by J. L. Hall, Elsevier/North-Holland Biomedical Press, Amsterdam – Oxford – New York

183. **Roozemond, R. C.** (1969) The effect of fixation with formaldehyde and glutaraldehyde on the composition of phospholipids extractable from rat hypothalamus. The Journal of Histochemistry and Cytochemistry **17**: 482-486

184. **Roppolo, D., De Rybel, B., Tendron, V. D., Pfister, A., Alassimone, J., Vermeer, J. E. M., Yamazaki, M., Stierhof, Y. D., Beeckman, T. & Geldner, N.** (2011) A novel protein family mediates Casparian strip formation in the endodermis. Nature **473**: 380-384

185. **Rösler, J., Krekel, F., Amrhein, N. & Schmid, J.** (1997) Maize phenylalanine ammonia-lyase has tyrosine ammonia-lyase activity. Plant Physiology **113**: 175-179

186. **Sanz, L., Murray, J. A. H. & Dewitte, W.** (2012) To divide and to rule; regulating cell division in roots during post-embryonic growth. Progress in Botany **73**: 57-80

187. **Sawada, H., Shimura, N., Hosokawa, F., Shibata, N. & Ikuhara, Y.** (2015) Resolving 45-pm-separated Si-Si atomic columns with an aberration-corrected STEM. The Japanese Society of Microscopy **64**: 213-217

188. **Schalk, M., Cabello-Hurtado, F., Pierrel, M.-A., Atanossova, R., Saindrenan, P. & Werck-Reichhart, D.** (1998) Piperonylic acid, a selective, mechansim-based inactivator of the *trans*-cinnamate 4-hydroxylase: a new tool to control the flux of metabolites in the phenylpropanoid pathway. Plant Physiology **118**: 209-218

189. **Schilmiller, A. L., Stout, J., Weng, J.-K., Humphreys, J., Ruegger, M. O. & Chapple, C.** (2009) Mutations in the cinnamate 4-hydroxylase gene impact metabolism, growth and development in Arabidopsis. The Plant Journal **60**: 771-782

190. **Schmutz, A., Buchala, A. J. & Ryser, U.** (1996) Changing the dimensions of suberin lamellae of green cotton fibers with a specific inhibitor of the endoplasmic reticulum-associated fatty acid elongases. Plant Physiology **110**: 403-411

191. **Schreiber, L., Breitner, H. W., Riederer, M., Düggelin, M. & Guggenheim, R.** (1994) The casparian strip of *Clivia miniata* Reg. Roots: isolation, fine structure and chemical nature. Botanica Acta **107**: 353-361

192. **Schreiber, L.** (1996) Chemical composition of casparian strips isolated from *Clivia miniata* Reg. roots: evidence for lignin. Planta **199**: 596-601

193. **Schreiber, L., Franke, R. & Hartmann, K.** (2005) Wax and suberin development of native and wound periderm of potato (*Solanum tuberosum* L.) and its relation to peridermal transpiration. Planta **220**: 520-530

194. **Schreiber, L.** (2010) Transport barriers made of cutin, suberin and associated waxes. Trends in Plant Science **15**: 546-553

195. **Scholl, R. L., May, S. T. & Ware, D. H.** (2000) Seed and molecular resources for Arabidopsis. Plant Physiology **124**: 1477-1480

196. **Seago Jr., J. L. & Fernando, D. D.** (2013) Anatomical aspects of angiosperm root evolution. Annals of Botany **112**: 223-238

197. **Serra, O., Soler, M., Hohn, C., Franke, R., Schreiber, L., Prat, S., Molinas, M. & Figueras, M.** (2009) Silencing of StKCS6 in potato periderm leads to reduced chain lengths of suberin and wax compounds and increased peridermal transpiration. Journal of Experimental Botany **60**: 697-707

198. **Serra, O., Soler, M., Hohn, C., Sauveplane, V., Pinot, F., Franke, R., Schreiber, L., Prat, S., Molinas, M. & Figueras, M.** (2009b) CYP86A33-targeted gene silencing in potato tuber alters suberin composition, distorts suberin lamellae, and impairs the periderm's water barrier function. Plant Physiology **149**: 1050-1060

199. **Serra, O., Hohn, C., Franke, R., Prat, S., Molinas, M. & Figueras, M.** (2010) A feruloyl transferase involved in the biosynthesis of suberin and suberin-associated wax is required for maturation and sealing properties of potato periderm. The Plant Journal **62**: 277-290

200. **Sfatos, C. D. & Shakhnovich, E. I.** (1997) Statistical mechanics of random heteropolymers. Physics Reports **288**: 77-108

201. **Sibout, R., Eudes, A., Pollet, B., Goujon, T., Mila, I., Granier, F., Séguin, A., Lapierre, C. & Jouanin L.** (2003) Expression pattern of two paralogs encoding cinnamyl alcohol dehydrogenases in Arabidopsis. Isolation and characterization of the corresponding mutants. Plant Physiology **132**: 848-860

202. **Sibout, R., Eudes, A., Mouille, G., Pollet, B., Lapierre, C., Jouanin, L. & Séguin, A.** (2005) CINNAMYL ALCOHOL DEHYDROGENASE-C and –D are the primary genes involved in lignin biosynthesis in the floral stem of Arabidopsis. The Plant Cell **17**: 2059-2076

203. **Silva, M. T., Santos Mota, J. M., Melo & Carvalho Guerra, F.** (1971) Uranyl salts as fixatives for electron microscopy study of the membrane ultrastructure and phospholipid loss in bacilli. Biochimica et Biophysica Acta **233**: 513-520

204. **Soloff, B. L.** (1973) Buffered potassium permanganate-uranyl acetate-lead citrate staining sequence for ultrathin sections. Stain Technology **48**: 159-165

205. **Sonnante, G., D'Amore, R., Blanco, E., Pierri, C. L., De Palma, M., Luo, J., Tucci, M. & Martin, C.** (2010) Novel hydroxycinnamoyl-coenzyme A quinate transferase genes from artichoke are involved in the synthesis of chlorogenic acid. Plant Physiology **153**: 1224-1238

206. **Spurr, A. R.** (1969) A low-viscosity epoxy resin embedding medium for electron microscopy. Journal of Ultrastructure Research **26**: 31-43

207. **Stoeckenius, W.** (1961) Electron microscopy of DNA molecules "stained" with heavy metal salts. The Journal of Biophysical and Biochemical Cytology **11**: 297-310

208. **Stout, J., Romero-Severson, E., Ruegger, M. O. & Chapple, C.** (2008) Semidominant mutations in *reduced epidermal fluorescence 4* reduce phenylpropanoid content in Arabidopsis. Genetics **178**: 2237-2251

209. **Strobl, G.** (2000) From the melt via mesomorphic and granular crystalline to lamellar crystallites: a major route followed in polymer crystallization? The European Physical Journal E **3**: 165-183

210. **Sunkar, R., Bartels, D. & Kirch, H.-H.** (2003) Overexpression of a stress-inducible aldehyde dehydrogenase gene from *Arabidopsis thaliana* in transgenic plants improves stress tolerance. The Plant Journal **35**: 452-464

211. **Swartzendruber, D. C., Wertz, P. W., Kitko, D. J., Madison, K. C. & Downing, D. T.** (1989) Molecular models of the intercellular lipid lamellae in mammalian stratum corneum. The Journal of Investigative Dermatology **92**: 251-257

212. **Taylor, I. B., Burbidge, A. & Thompson, A. J.** (2000) Control of abscisic acid synthesis. Journal of Experimental Botany **51**: 1563-1574

213. **Teixeira, R. T. & Pereira, H.** (2010) Suberized cell walls of cork from cork oak differ from other species. Microscopy and Microanalysis **16**: 569-575

214. **The Arabidopsis Genome Initiative** (2000) Analysis of the genome sequence of the flowering plant Arabidopsis thaliana. Nature **408**: 796-815

215. **Thomas, R., Fang, X., Ranathunge, K., Anderson, T. R., Peterson, C. A. & Bernards, M.** (2007) Soybean root suberin: Anatomical distribution, chemical composition, and relationship to partial resistance to *Phytophtora sojae*. Plant Physiology **144**: 299-311

216. **Tobimatsu, Y., Chen, F., Nakashima, J., Escamilla-Treviño, L. L., Jackson, L., Dixon, R. A. & Ralph, J.** (2013) Coexistence but independent biosynthesis of catechyl and guiacyl/syringyl lignin polymers in seed coats. The Plant Cell **25**: 2587-2600

217. **Vishwanath, S. J., Delude, C., Domergue, F. & Rowland, O.** (2015) Suberin: biosynthesis, regulation, and polymer assembly of a protective extracellular barrier. Plant Cell Report **34**: 573-586

218. **Wang, Y., Stass, A. & Horst, W. J.** (2004) Apoplastic binding of aluminium is involved in silicon-induced amelioration of aluminium toxicity in maize. Plant Physiology **136**: 3762-3770

219. **Warner, R. R., Stone, K. J. & Boissy, Y. L.** (2003) Hydration disrupts human stratum corneum ultrastructure. The Journal of Investigative Dermatology **120**: 275-284

220. **Watanabe, K., Nishiuchi, S., Kulichikhin, K. & Nakazono, M.** (2013) Does suberin accumulation in plant roots contribute to waterlogging tolerance? Frontiers in Plant Science **4**: 1-7

221. **Wattendorff, J. & Holloway, P. J.** (1982) Studies on the ultrastructure and histochemistry of plant cuticles: isolated cuticular membrane preparations of agave Americana L. and the effects of various extraction procedures. Annals of Botany **49**: 769-804

222. **Weng, J. K., Li, X., Stout, J. & Chapple, C.** (2008b) Independent origins of syringyl lignin in vascular plants. Proceedings of the National Academy of Sciences **105**: 7887-7892

223. **Weng, J. K. & Chapple, C.** (2010) The origin and evolution of lignin biosynthesis. New Phytologist **187**: 273-285

224. **Wilson, C. A. & Peterson, C. A.** (1983) Chemical composition of the epidermal, hypodermal, endodermal and intervening cortical cell walls of various plant roots. Annals of Botany **51**: 759-769

225. **Winkel-Shirley, B.** (2001) Flavonoid biosynthesis. A colorful model for genetics, biochemistry, cell biology, and biotechnology. Plant Physiology **236**: 485-493

226. **Winter, D., Vinegar, B., Nahal, H., Ammar, R., Wilson, G. V. & Provart, N. J.** (2007) An "electronic fluorescent pictograph" browser for exploring and analyzing largescale biological data sets. PloS ONE **2**

227. **Wittmann, J. C. & Lotz, B.** (1985) Polymer decoration: the orientation of polymer folds as revealed by the crystallization of polymer vapors. Journal of Polymer Science **23**: 205-226

228. **Wooding, F. B. P. & Northcote, D. H.** (1964) The development of the secondary wall of the xylem in *Acer pseudoplatanus*. The Journal of Cell Biology **23**: 327-337

229. **Yadav, V., Molina, I., Ranathunge, K., Castillo, I. Q., Rothstein, S. J. & Reed, J. W.** (2014) ABCG transporters are required for suberin and pollen wall extracellular barriers in *Arabidopsis*. The Plant Cell **26**: 3569-3588

230. **Yan, B. & Stark, R. E.** (2000) Biosynthesis, molecular structure, and domain architecture of potato suberin: a C-13 NMR study using isotopically labeled precursors. Journal of Agricultural and Food Chemistry **48**: 3298-3304

231. **Yang, Q., Reinhardt, K., Schiltz, E. & Matern, U.** (1997) Characterization and heterologous expression of hydroxycinnamoyl/benzoyl-CoA:anthranilate N-hydroxycinnamoyl/benzoyltransferase from elicited cell cultures of carnation, *Dianthus caryophyllus* L. Plant Molecular Biology **35**: 777-789

232. **Yu, H. J., Hogan, P. & Sundaresan, V.** (2005) Analysis of the female gametophyte transcriptome of Arabidopsis by comparative expression profiling. Plant Physiology **139**: 1853-1869

233. **Zeier, J. & Schreiber, L.** (1997) Plant Physiology **113**: 1223-1231

234. **Zhao, Q., Nakashima, J., Chen, F., Yin, Y., Fu, C., Yun, J., Shao, H., Wang, X., Wang, Z. Y. & Dixon, R. A.** (2013) LACCASE is necessary and nonredudant with PEROXIDASE for lignin polymerization during vascular development in *Arabidopsis*. The Plant Cell **25**: 3976-3987

235. **Zhao, Q. & Dixon, R. A.** (2010) Transcriptional networks for lignin biosynthesis: more complex than we thought? Trends in Plant Science **16**: 227-233

236. **Zhao, Q.** (2016) Lignification: flexibility, biosynthesis and regulation. Trends in Plant Science **21**: 713-721

237. **Zhou, M., Sun, Z., Wang, C., Zhang, X., Tang, Y., Zhu, X., Shao, J. & Wu, Y.** (2015) Changing a conserved amino acid in R2R3-MYB transcription repressors results in cytoplasmic accumulation and abolishes their repressive activity in *Arabidopsis*. The Plant Journal **84**: 395-403

238. **Ziegenspeck, H.** (1921): Über die Rolle des Casparyschen Streifens der Endodermis und analoge Bildungen. Berichte der Deutschen Botanischen Gesellschaft **39**: 302-310

239. **Zimmermann, H. M., Hartmann, K., Schreiber, L. & Streudle E.** (2000): Chemical composition of apoplastic transport barriers in relation to radial hydraulic conductivity of corn roots (*Zea mays* L.). Planta **210**: 302-311

8. Acknowledgement

At first I am deeply grateful to PD Dr. Rochus Benni Franke for promoting and demanding of my scientific career since my Bachelor study. During my education Mr. PD Dr. Rochus Benni Franke promoted my expertise in molecular biology, analytics and microscopy. My Ph.D. education was characterised by mental liberty and harmonic collaboration. My own ideas were always supported, which resulted in one of the most important features of a scientist: to be curious.

Also I am deeply grateful for the ERA-CAPS project, which allowed working on an interesting and applicable topic. Due to the ERA-CAPS project I became acquainted with many European scientists. The personal communication and the exchange of scientific expertise elevated my scientific knowledge about plant biology. The different tasks of each scientist illustrated the common topic from another perspective and demonstrated the different paradigm to solve scientific questions. This collaboration was a mental enrichment and demonstrated the efficient team work within the group on the common topic.

Due to the ERA-CAPS project I could visit the laboratory of Prof. Dr. David Salt at the University of Nottingham. His postdoc Dr. Guilhem Reyt taught me how to analyse Casparian strips. Quickly, I became a group member and I achieved a lot of interesting results for my Ph.D. thesis. I thank both for the friendly integration in the group and the acquisition of the new methods to analyse Casparian strips.

I would like to express my gratitude to Ursula Mettbach for teaching me the whole procedure of transmission electron microscopy. Always, she advised and helped me with the correct handling of the TEM and the samples.

Besides, I thank to Dr. Jeong Im-Kim and Prof. Dr. Clint Chapple for providing important and interesting lignin mutants, which allowed a deeper analysis of the Casparian strip and suberin barrier development.

I appreciate Prof. Dr. Peter Dörmann for taking the time as second referee.

Furthermore, I would like to thank to Prof. Dr. Lukas Schreiber who piqued my interest in research of plant interface and gave me the opportunity to work in his group. Special thanks are addressed to the group members of the department of ecophysiology, who were always helpful and provided advices to me. I am also grateful for the BBQ evenings, which we spent together.

Acknowledgement

I am grateful to Dr. Katharina Markus for her expertise in cloning techniques and suberin research.

For the support and the interest in my work I appreciate Britta Migdal, Sindrela Shrestha and Marcel Kohlstock.

My deepest gratitude is addressed to my fiancée Sanu Shrestha, my parents Gertrud and Miguel Millán Hidalgo, my grandparents Josefine and Horst Tillack and to my “second” parents Mery Thapa-Shrestha and Prachanda Thapa. Their support enabled my academic education. Always, they believed in my capabilities mastering the academic education. Finally, I am happy about that I decided to study Biology in the year 2010.

9. Appendix

9.1. Selection of putative candidate genes involved in the assembling of the polyaromatic domain

Based on freely available databanks putative candidate genes involved in the synthesis of the polyaromatic domain were selected. Co-expression networks of typical suberin, Casparian strip, lignin and phenylpropanoid biosynthesis genes reveal the relationship among the genes. Co-expression study of CYP86A1 is not available on the website http://atted.jp/.

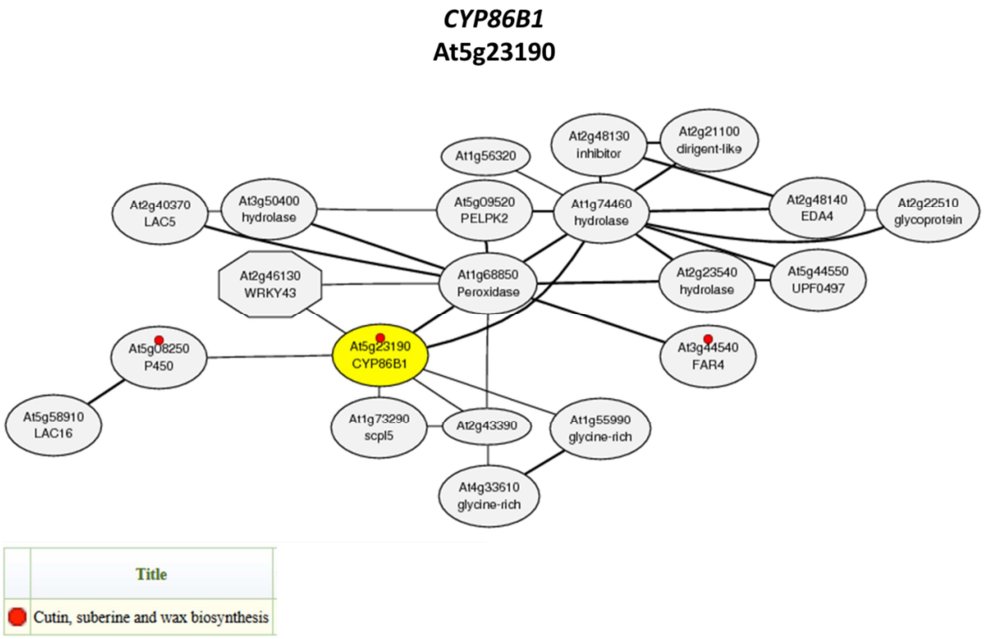

Fig. 88: Co-expression network of *CYP86B1*

Co-expression network reveals associated transcription of *CYP86B1*. This co-expression network is represented on the website http://atted.jp/.

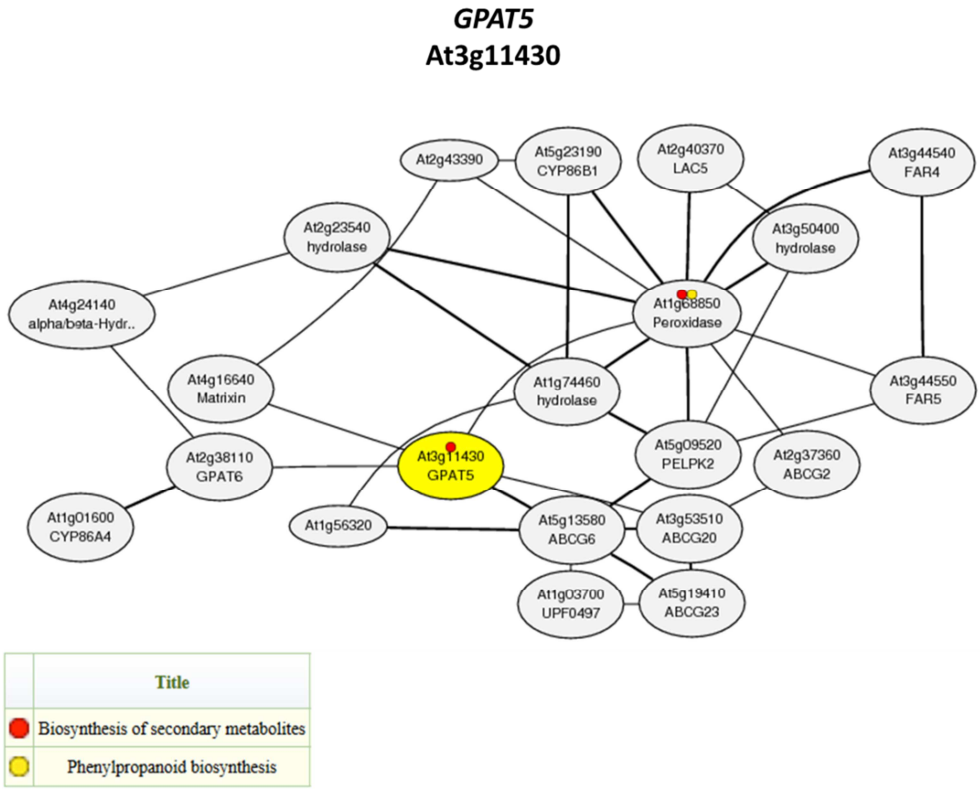

Fig. 89: Co-expression network of *GPAT5*

Co-expression network reveals associated transcription of *GPAT5*. This co-expression network is represented on the website http://atted.jp/.

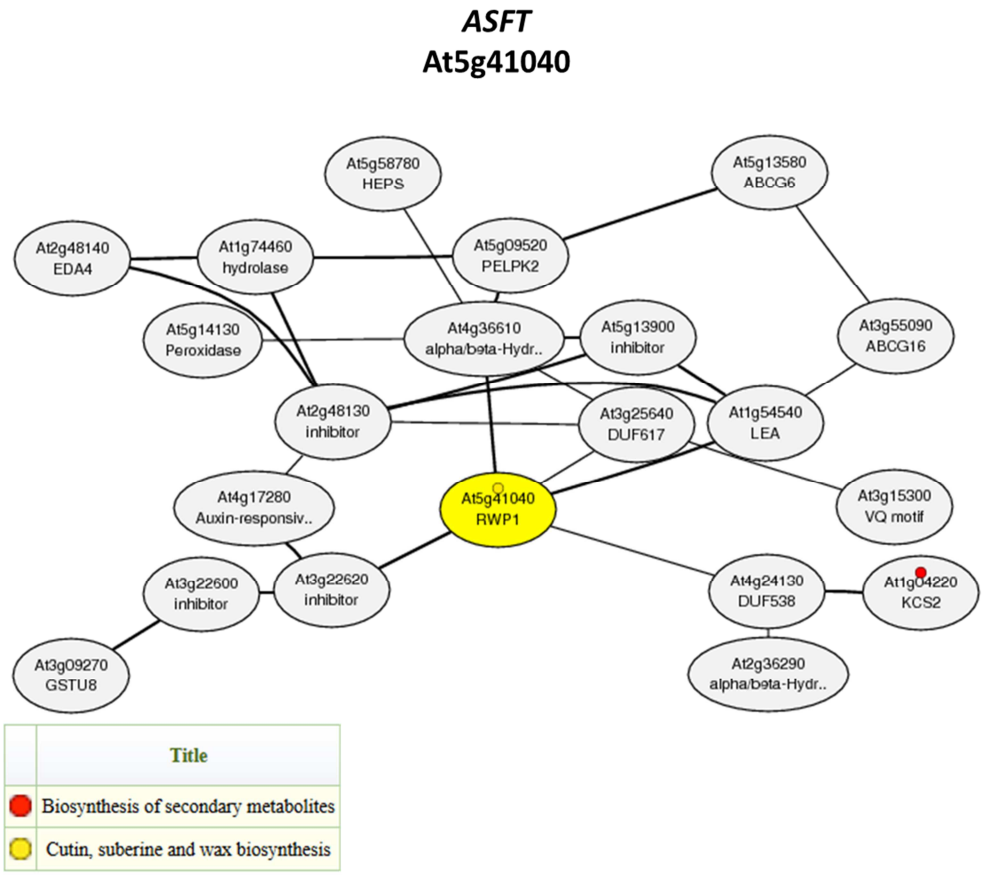

Fig. 90: Co-expression network of *ASFT*

Co-expression network reveals associated transcription of *ASFT*. This co-expression network is represented on the website http://atted.jp/.

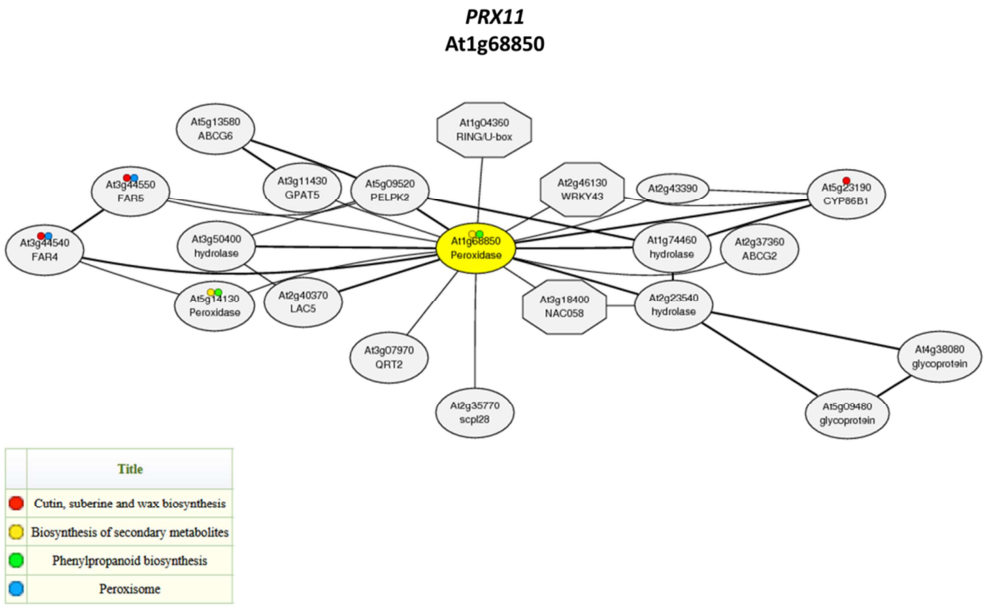

Fig. 91: Co-expression network of *PRX11*

Co-expression network reveals associated transcription of *PRX11*. This co-expression network is represented on the website http://atted.jp/.

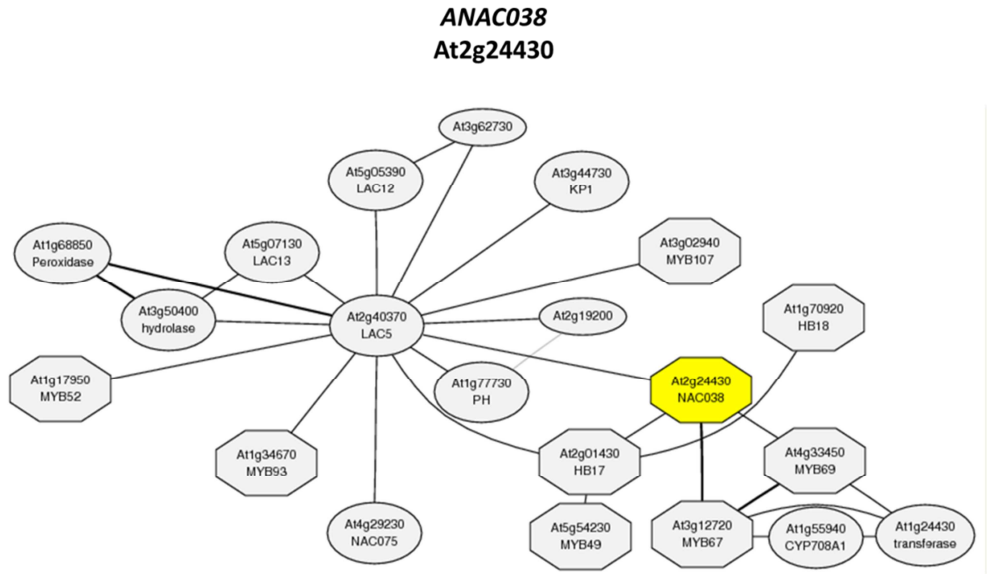

Fig. 92: Co-expression network of *ANAC038*

Co-expression network reveals associated transcription of *ANAC038*. This co-expression network is represented on the website http://atted.jp/.

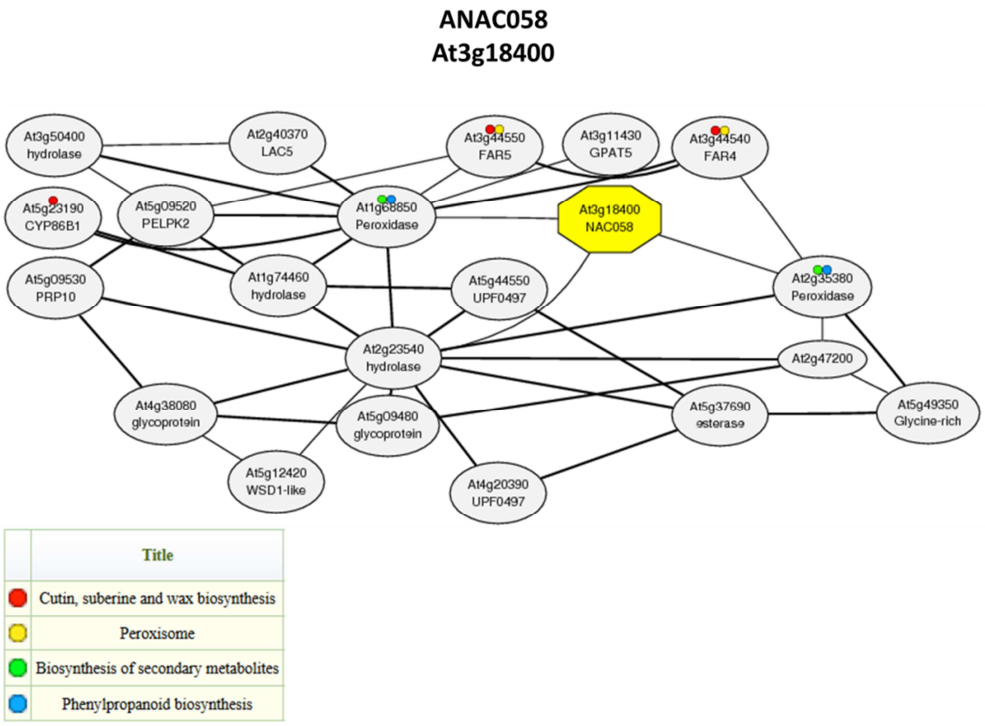

Fig. 93: Co-expression network of *ANAC058*

Co-expression network reveals associated transcription of *ANAC058*. This co-expression network is represented on the website http://atted.jp/.

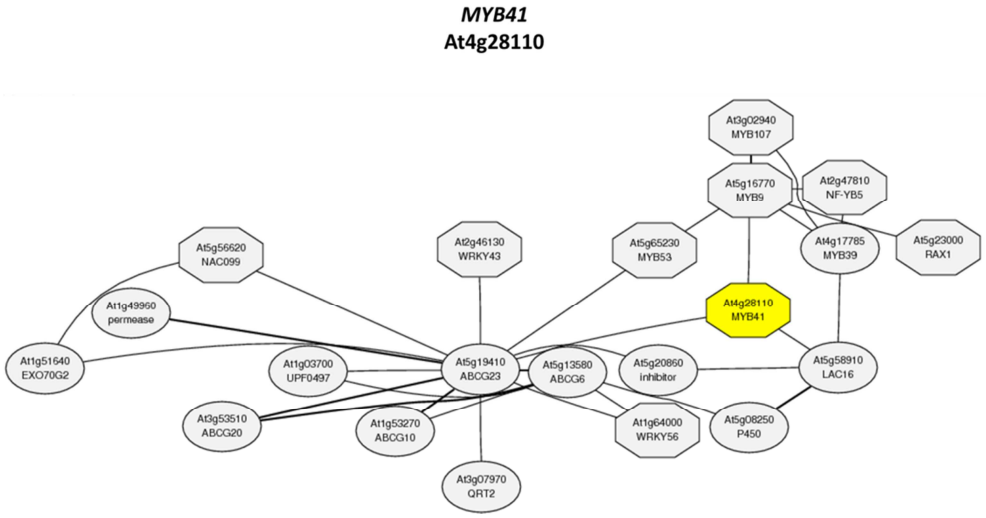

Fig. 94: Co-expression network of *MYB41*

Co-expression network reveals associated transcription of *MYB41*. This co-expression network is represented on the website http://atted.jp/.

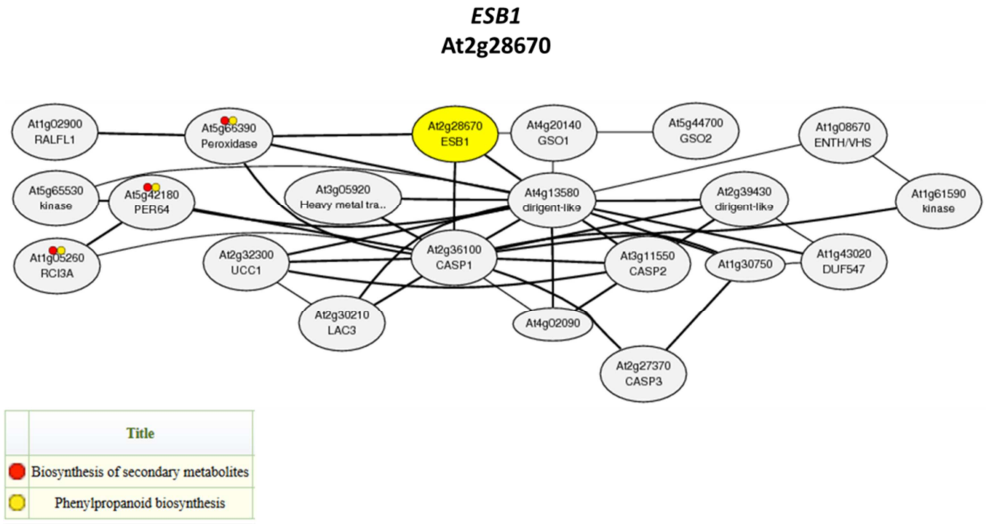

Fig. 95: Co-expression network of *ESB1*

Co-expression network reveals associated transcription of *ESB1*. This co-expression network is represented on the website http://atted.jp/.

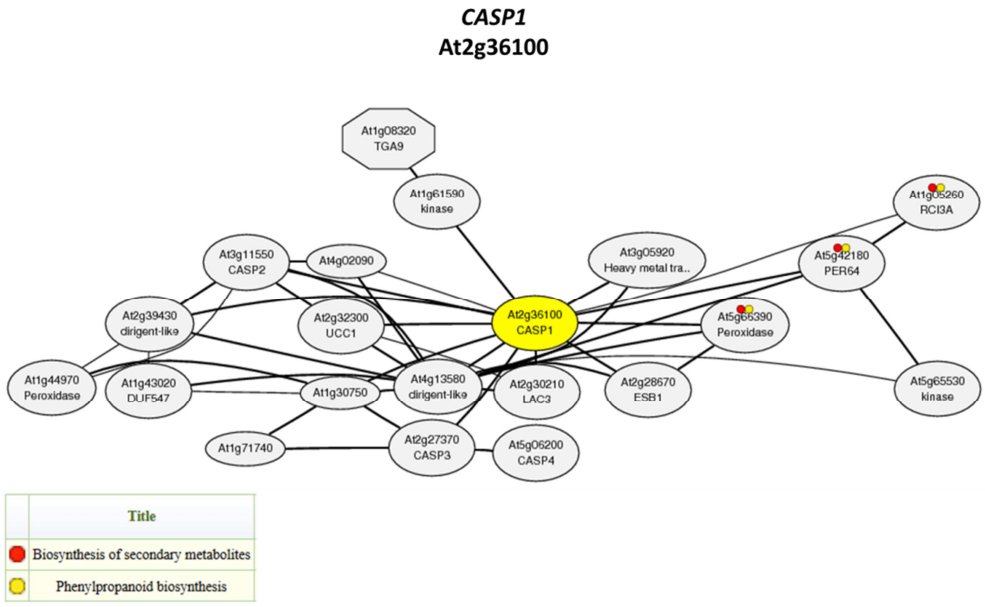

Fig. 96: Co-expression network of *CAPS1*

Co-expression network reveals associated transcription of *CASP1*. This co-expression network is represented on the website http://atted.jp/.

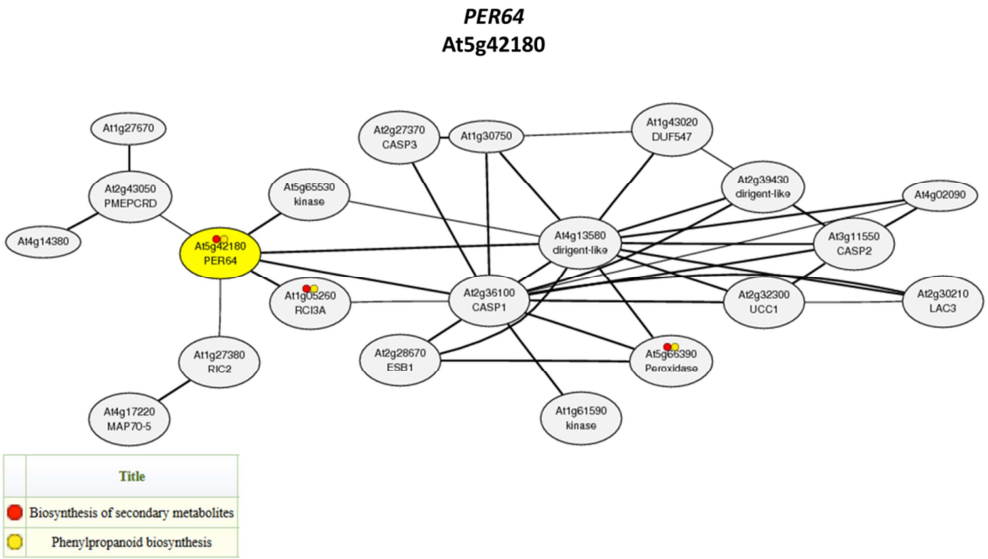

Fig. 97: Co-expression network of *PER64*

Co-expression network reveals associated transcription of *PER64*. This co-expression network is represented on the website http://atted.jp/.

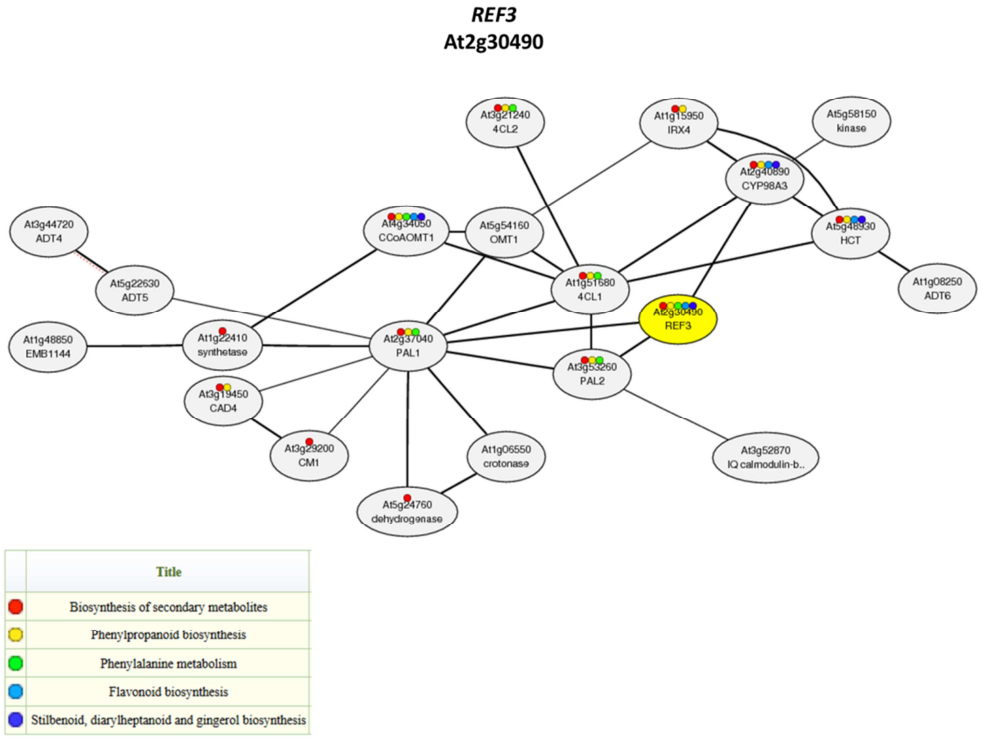

Fig. 98: Co-expression network of *REF3*

Co-expression network reveals associated transcription of *REF3*. This co-expression network is represented on the website http://atted.jp/.

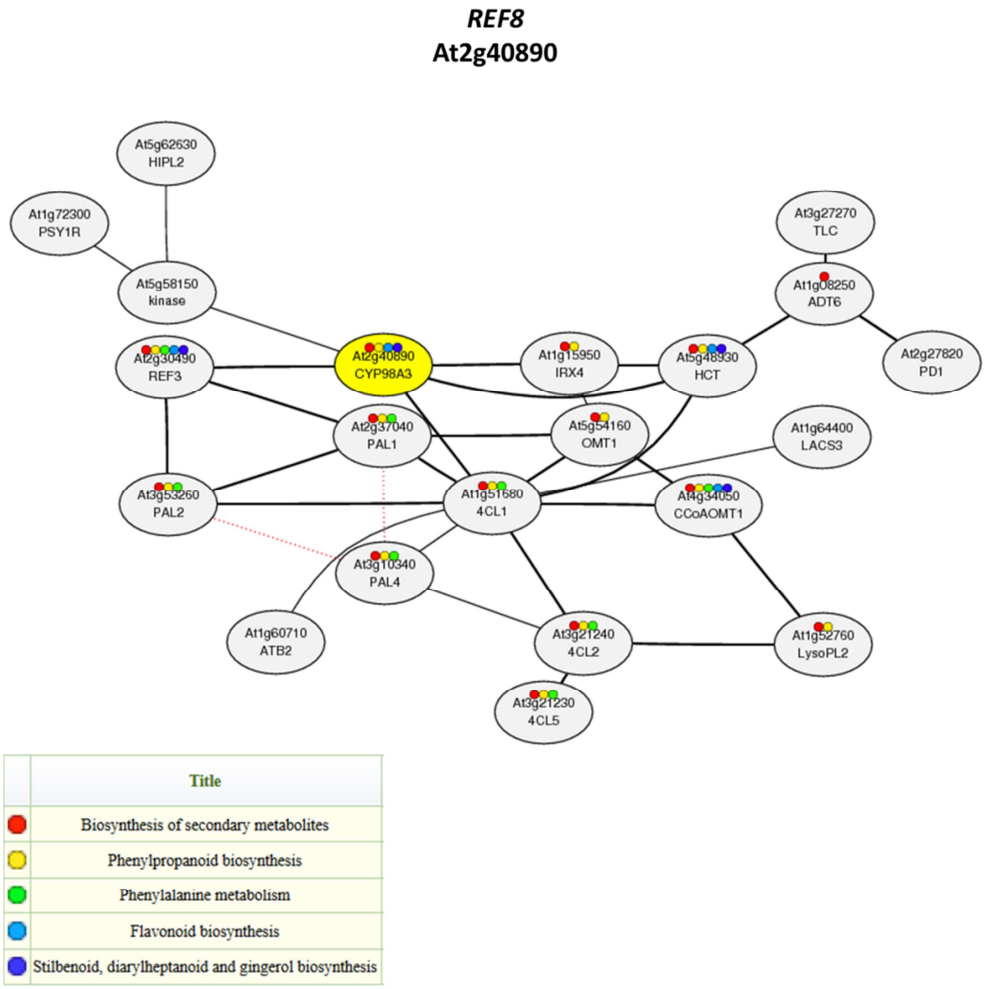

Fig. 99: Co-expression network of *REF8*

Co-expression network reveals associated transcription of *REF8*. This co-expression network is represented on the website http://atted.jp/.

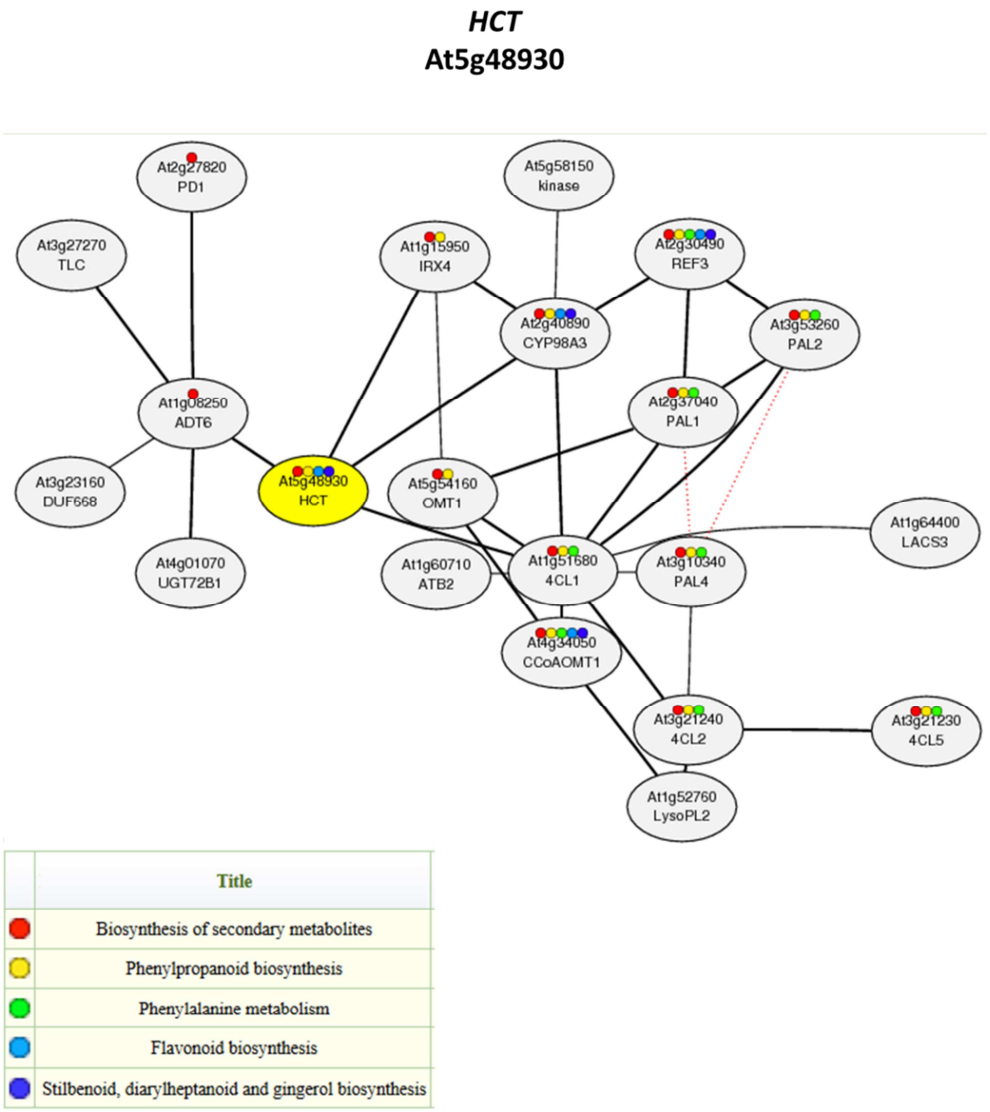

Fig. 100: Co-expression network of *HCT*

Co-expression network reveals associated transcription of *HCT*. This co-expression network is represented on the website http://atted.jp/.

Fig. 101: Co-expression network of *CCoAOMT1*

Co-expression network reveals associated transcription of *CCoAOMT1*. This co-expression network is represented on the website http://atted.jp/.

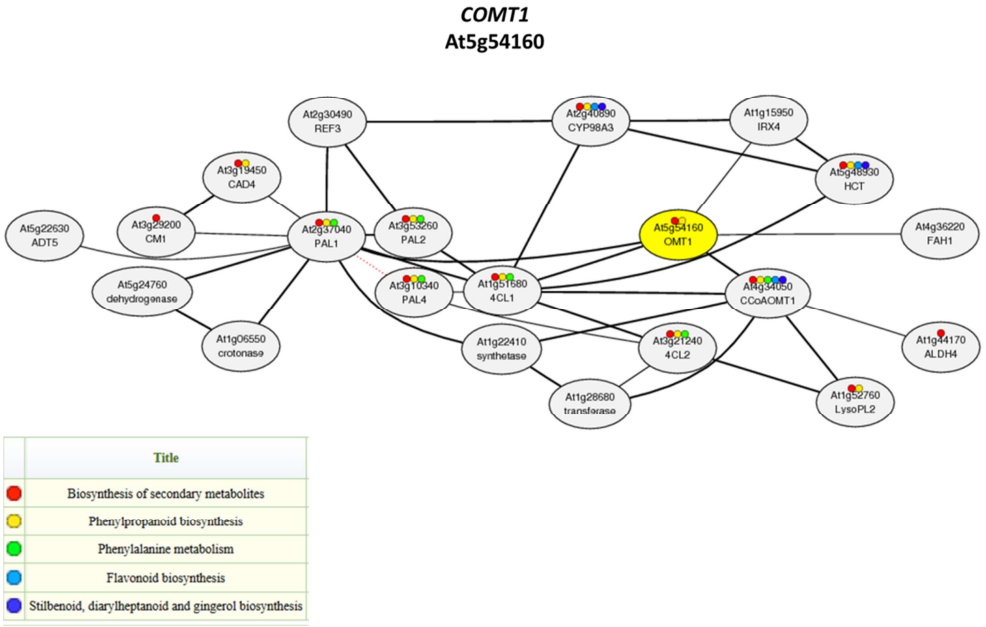

Fig. 102: Co-expression network of *COMT1*

Co-expression network reveals associated transcription of *COMT1*. This co-expression network is represented on the website http://atted.jp/.

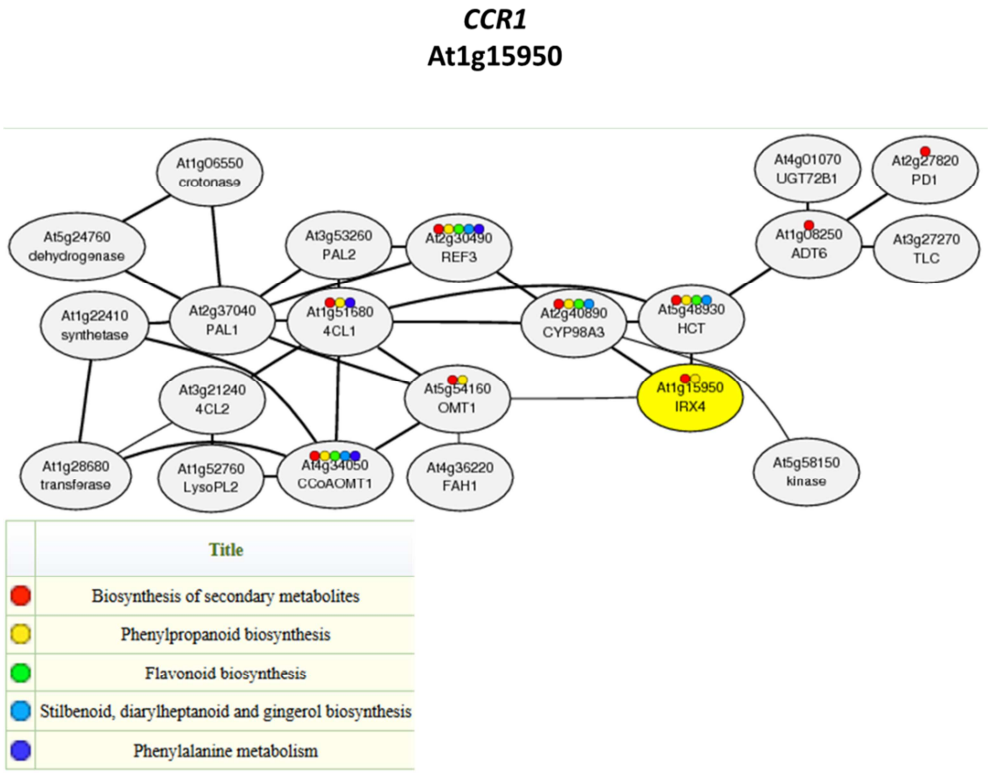

Fig. 103: Co-expression network of *CCR1*

Co-expression network reveals associated transcription of *CCR1*. This co-expression network is represented on the website http://atted.jp/.

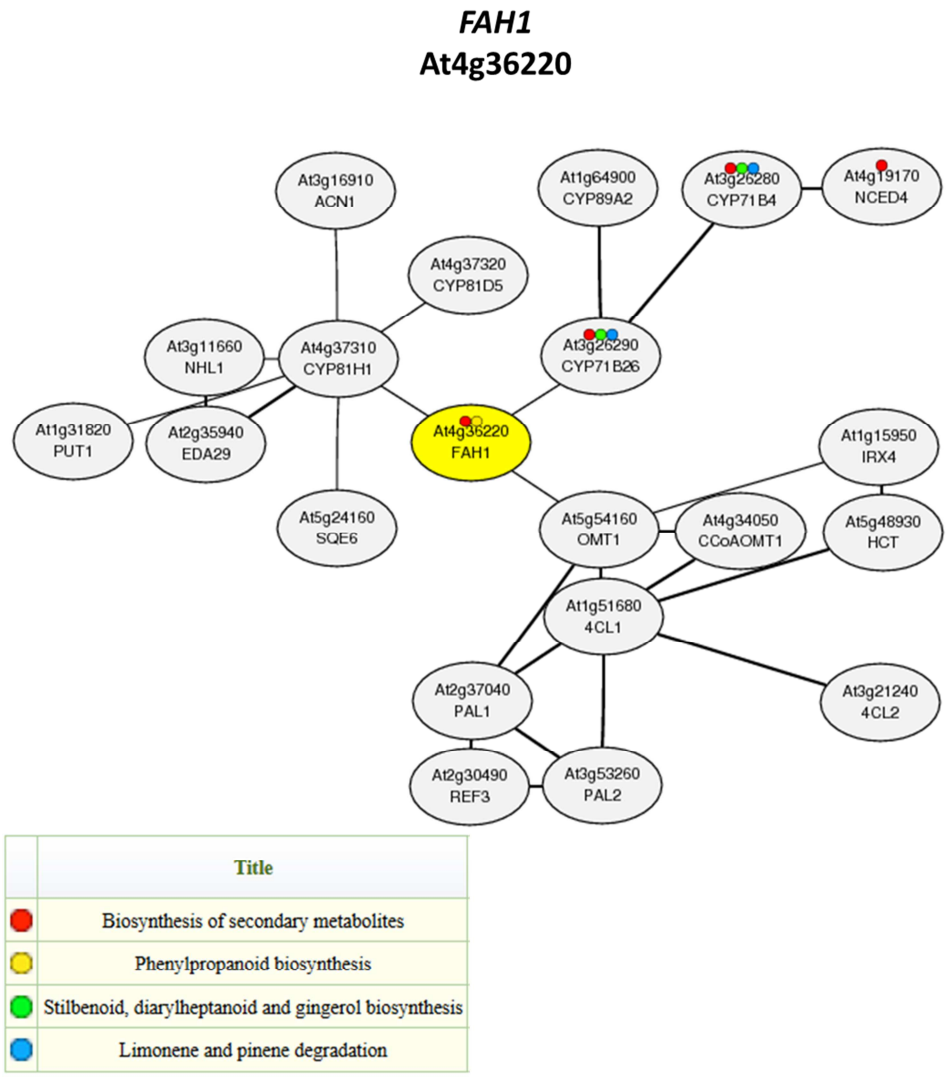

Fig. 104: Co-expression network of *FAH1*

Co-expression network reveals associated transcription of *FAH1*. This co-expression network is represented on the website http://atted.jp/.

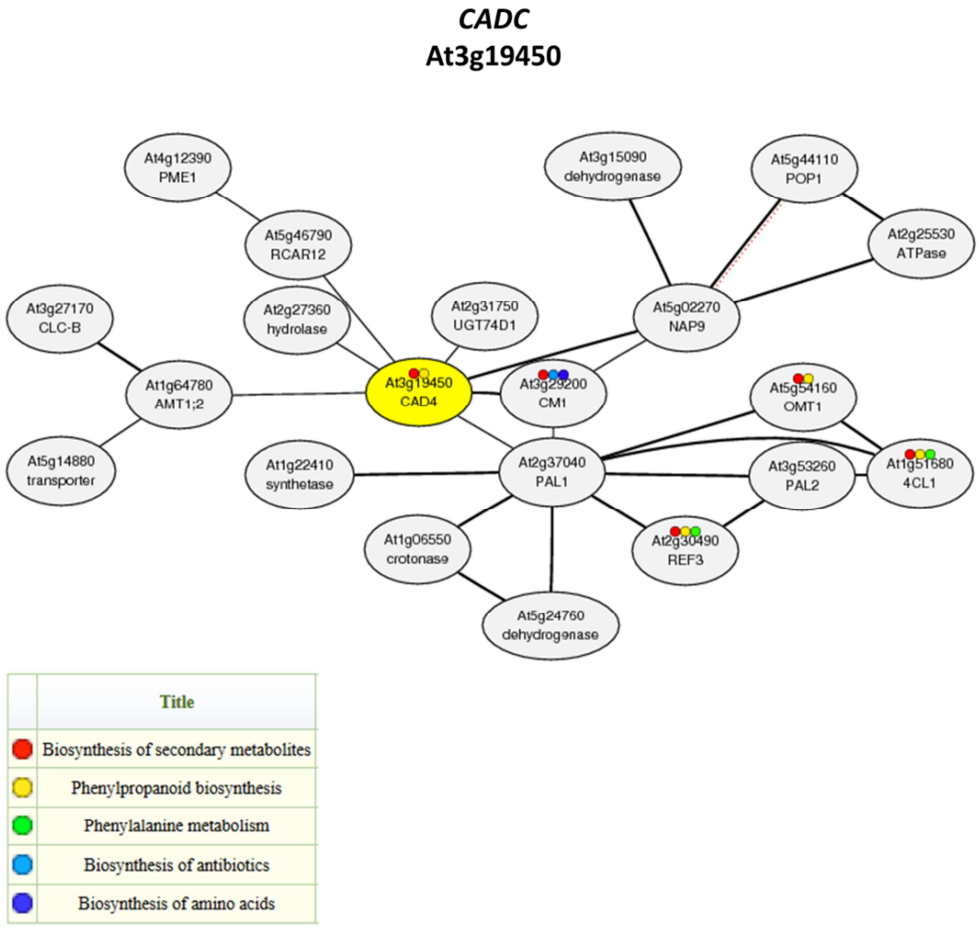

Fig. 105: Co-expression network of *CADC*

Co-expression network reveals associated transcription of *CADC*. This co-expression network is represented on the website http://atted.jp/.

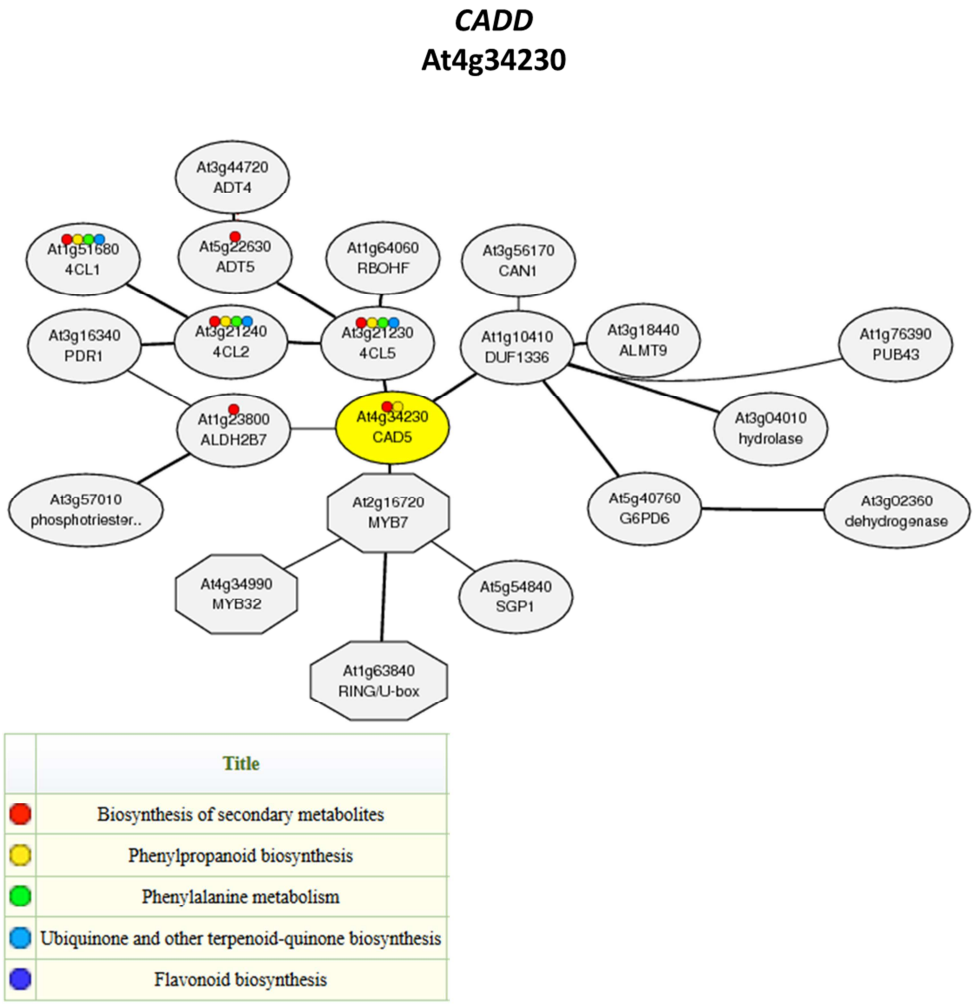

Fig. 106: Co-expression network of *CADD*

Co-expression network reveals associated transcription of *CADD*. This co-expression network is represented on the website http://atted.jp/.

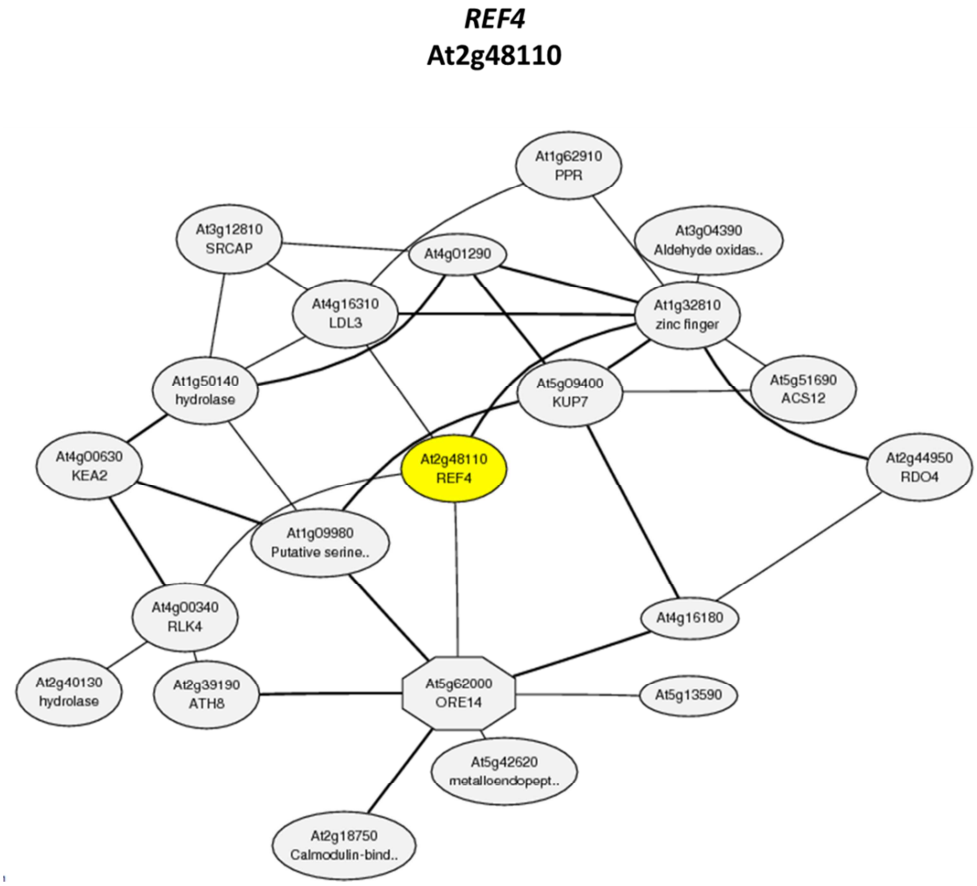

Fig. 107: Co-expression network of *REF4*

Co-expression network reveals associated transcription of *REF4*. This co-expression network is represented on the website http://atted.jp/.

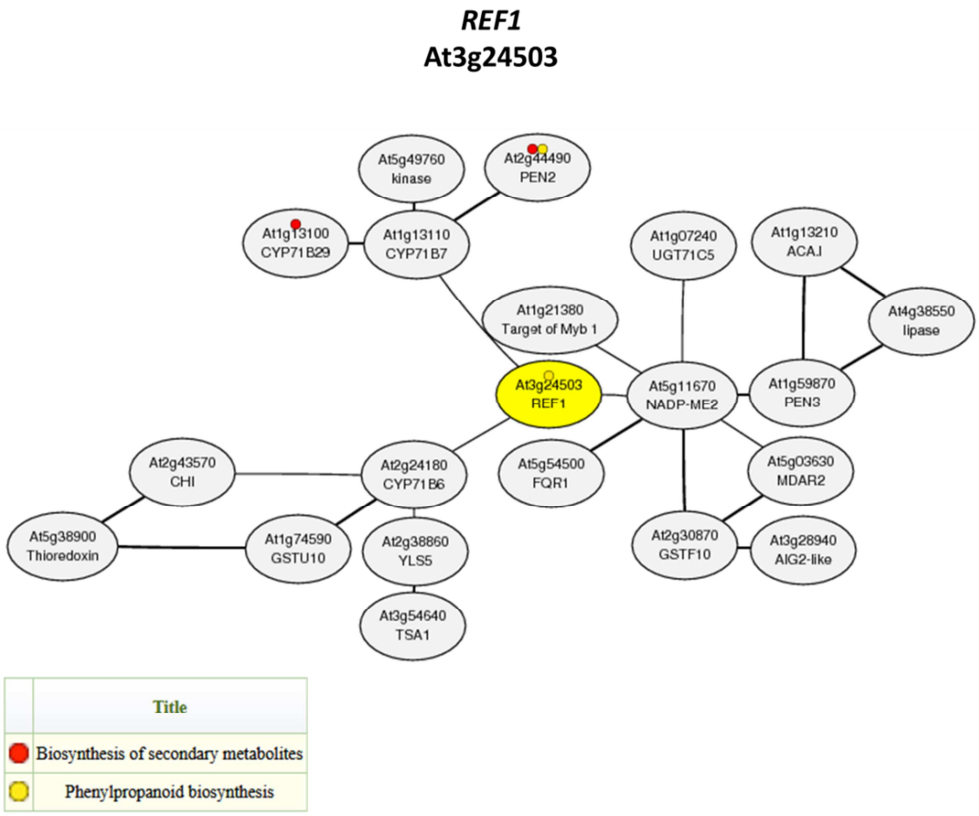

Fig. 108: Co-expression network of *REF1*

Co-expression network reveals associated transcription of *REF1*. This co-expression network is represented on the website http://atted.jp/.

Fig. 109: Co-expression network of *MYB4*

Co-expression network reveals associated transcription of *MYB4*. This co-expression network is represented on the website http://atted.jp/.

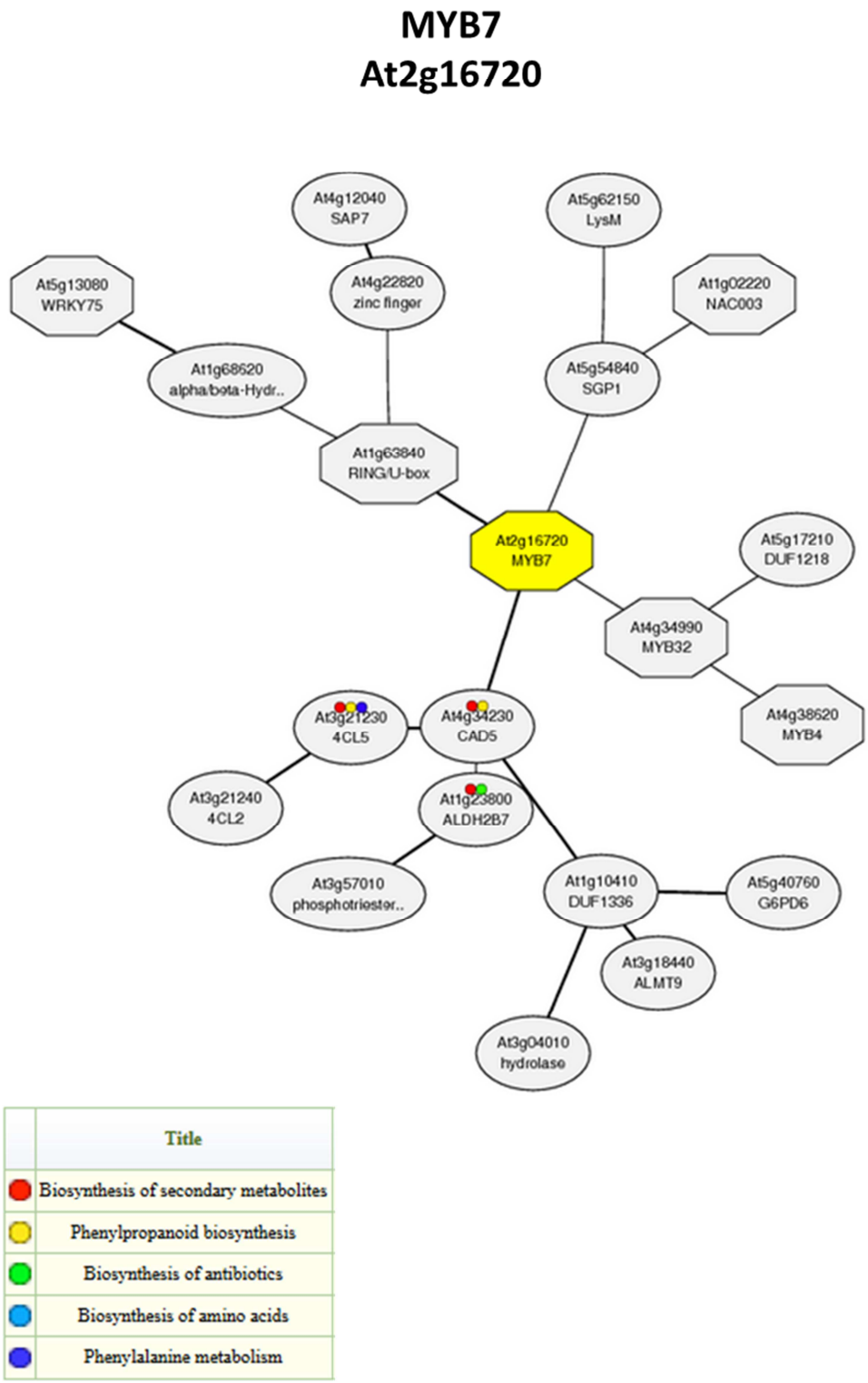

Fig. 110: Co-expression network of *MYB7*

Co-expression network reveals associated transcription of *MYB7*. This co-expression network is represented on the website http://atted.jp/.

Focus of the previous master thesis was the gene *HCT* in *Solanum tuberosum*. The closely related gene to *HCT* is *HQT* in potato itself. Sequence similarity between both genes is about

87 %. Blast result of HQT in *Arabidopsis thaliana* databank reveals the gene At3g53850 with a sequence similarity of 46.23 %. In the databank it is described as an uncharacterised protein family (UPF0497) (www.arabidopsis.org), however 2014 it was already described by Roppolo et al.. Here, the gene is notated as CASPL5B2 (Roppolo et al., 2014).

9.2. Drought stress experiment

Several drought stress experiments show that the mutation in *ccr1* cause a stronger tolerance against drought stress. A similar effect is visible in the mutant *ref8-2*fah1-2*AtC4H::SmF5H*. Only plants of *ref8-1*med5*med5b* seem to be more sensitive against drought stress.

Fig. 111: Drought stress experiment of *ccr1*, *ralph*horst*, *esb1* and WT after 12 days without watering

The mutant line *ccr1* and WT were not watered for 12 days. As a suberin-rich positive control *esb1* and as a suberin-deficient negative control *ralph*horst* was used.

Fig. 112: Drought stress experiment of *ccr1*, *ralph*horst*, *esb1* and WT after 15 days without watering

The mutant line *ccr1* and WT were not watered for 15 days. As a suberin-rich positive control *esb1* and as a suberin-deficient negative control *ralph*horst* was used.

Fig. 113: Drought stress experiment of *ref8-1*med5a*med5b*, *ralph*horst*, *esb1* and WT after 15 days without watering

The mutant line *ref8-1*med5a*med5b* and WT were not watered for 15 days. As a suberin-rich positive control *esb1* and as a suberin-deficient negative control *ralph*horst* was used.

Fig. 114: Drought stress experiment of *ref8-2*fah1-2*AtC4H::SmF5H*, *ralph*horst*, *esb1* and WT after 15 days without watering

The mutant line *ref8-2*fah1-2*AtC4H::SmF5H* and WT were not watered for 15 days. As a suberin-rich positive control *esb1* and as a suberin-deficient negative control *ralph*horst* was used.

9.3. Root phenotype

After extraction of soluble compounds the double knockout mutant *cadc*cadd* and the triple knockout mutant *cadc*cadd*fah1-2* reveal a yellowish root colour. Roots of *cadc* appear to be slightly yellowish, whereas WT roots are white.

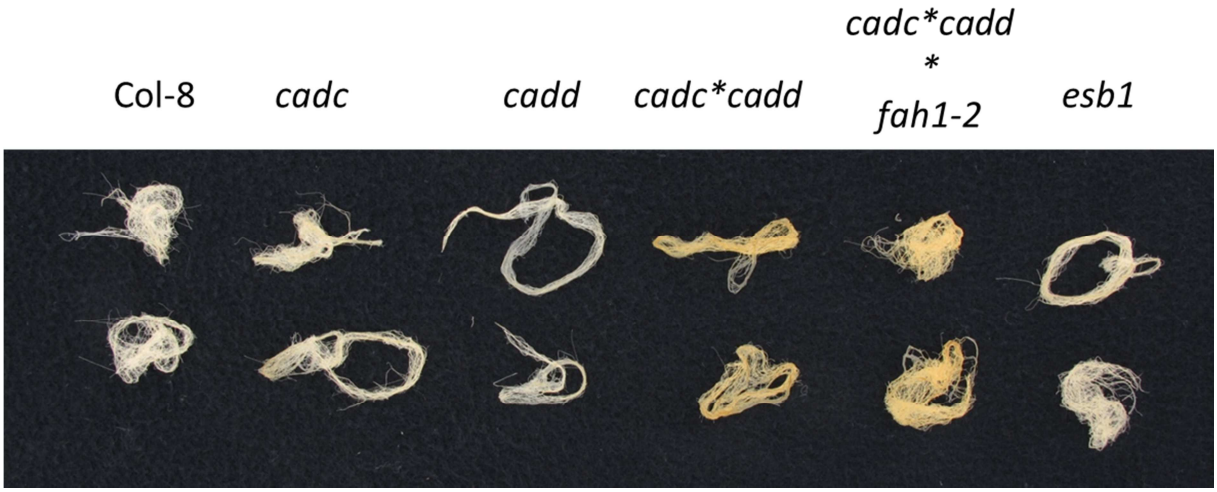

Fig. 115: Root phenotype of *cadc*, *cadd*, *cadc*cadd*, *cadc*cadd*fah1-2*, *esb1* and WT after extraction of soluble compounds in chloroform and methanol

Roots of *cadc* reveal to be slightly yellowish. The yellow colour is clearly observable in the double knockout mutant *cadc*cadd* and in the triple knockout mutant *cadc*cadd*fah1-2*. The mutant line *cadd*, *esb1* and the WT exhibit rather a white root colour.

9.4. Leaf epidermal fluorescence phenotype

The following images were taken with the help of Yannic Müller. Under UV-light *ref*-mutants and only *fah1-2* mutants exhibit a reddish leaf epidermal fluorescence.

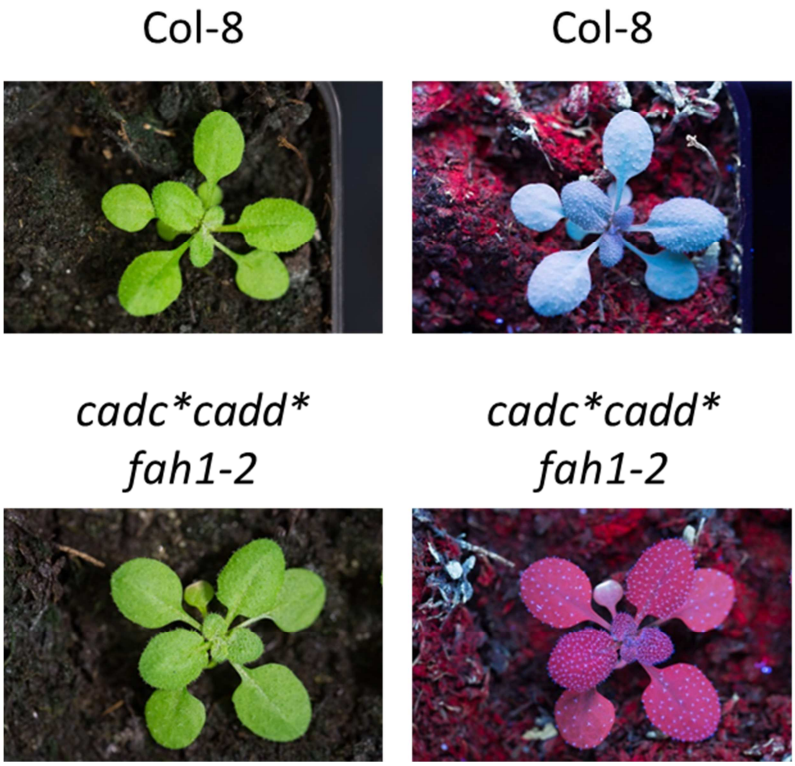

Fig. 116: Leaf epidermal fluorescence phenotype of *cadc*cadd*fah1-2* and WT under UV-light

The triple knockout mutant *cadc*cadd*fah1-2* reveals a red fluorescence colour on the leaf surface, while the leaf surface of the WT seems to be white-blue-greenish under UV-light.

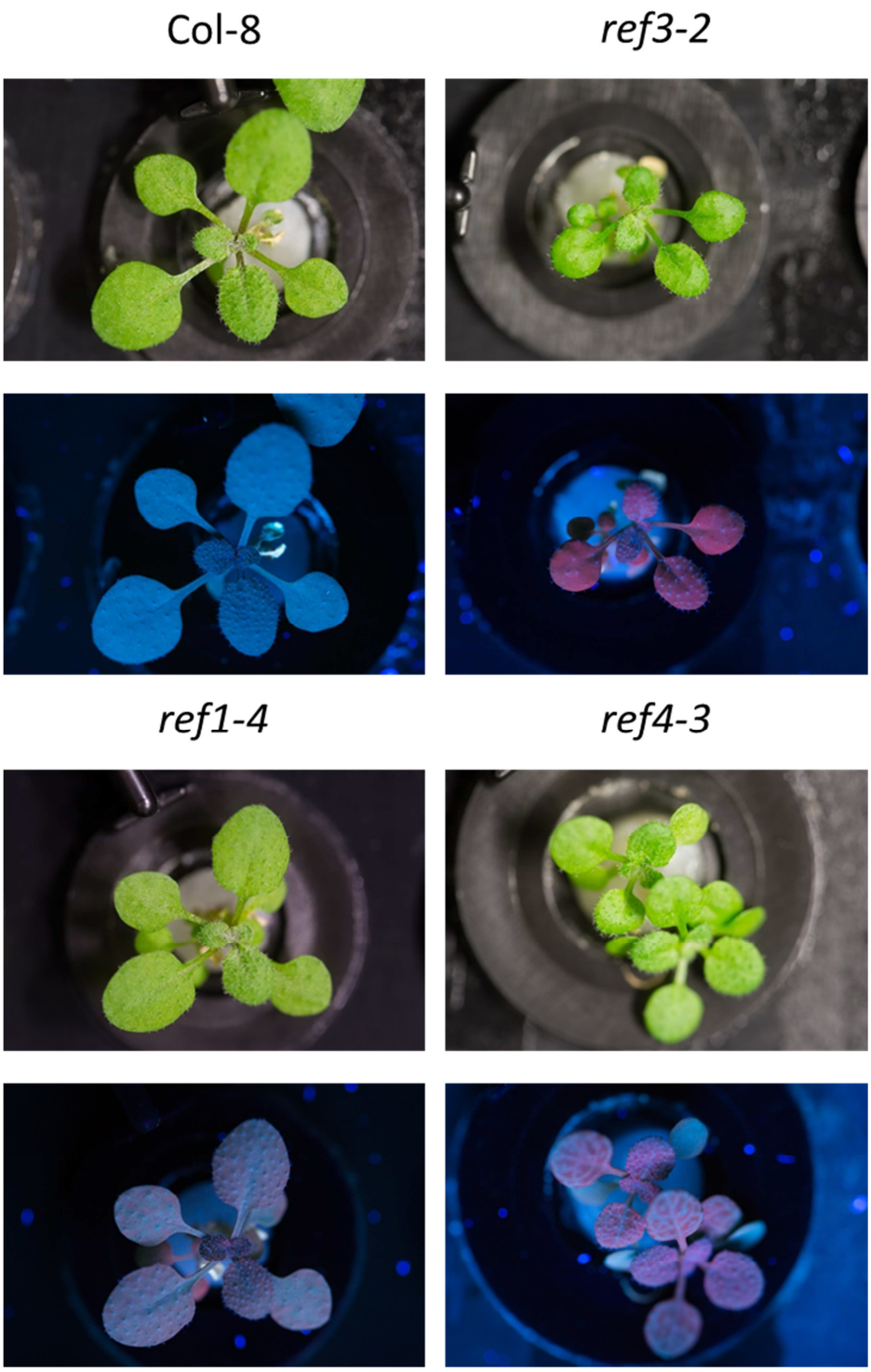

Fig. 117: Leaf epidermal fluorescence phenotype of *ref3-2*, *ref1-4*, *ref4-3* and WT under UV-light

Leaf epidermal fluorescence of ref3-2 is red under UV-light. The mutant ref4-3 ins only shows a red colour at the position where is not a leaf vein present. The mutant ref1-4 reveals weak red colour. Most part of the leaf surface is rather whitish. In contrast to the mutants, the leaf surface of the WT is rather blue-greenish under UV-light.

9.5. Ionomic profile

The ionomic profile was investigated of different casparian strip and suberin mutants. Total elemental composition was analysed of leaves. The results were obtained from the website http://www.ionomicshub.org/arabidopsis/piims/showIndex.action.

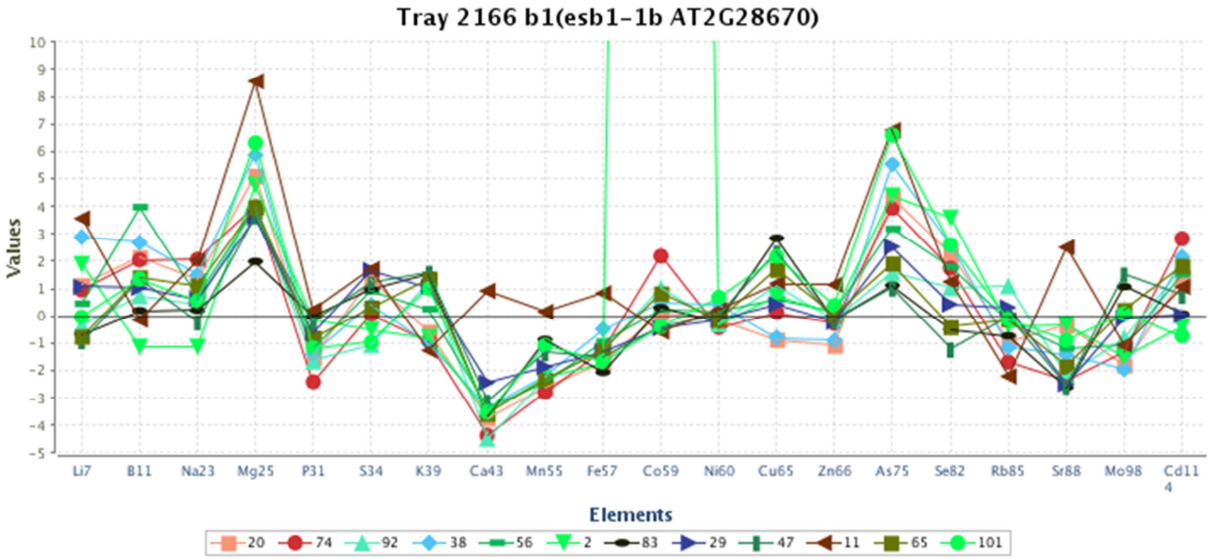

Fig. 118: Z-score graph of the leaf ionomic profile of *esb1*

Leaf elemental composition was analysed of *esb1*. The ionomic content of each single element was set to 0 for the WT. Presented are the values of each single mutant sample. As more deviate the value from the 0 as stronger is the difference between the WT and the mutant. Sample number: 12. Growing condition: 10h day length, 100 µE light intensity, 21 °C, 65 % humidty. Li7: lithium 7, B11: boron 11, Na23: Sodium 23, Mg25: magnesium 25, P31: phosphor 31, S34: sulphur 34, K39: potassium 39, Ca43: calcium 43, Mn55: manganese 55, Fe57: iron 57, Co59: cobalt 59, Ni60: nickel 60, Cu65: copper 65, Zn66: zinc 66, As75: arsenic 75, Se82: selenium 82, Rb85: rubidium 85, Sr88: strontium 88, Mo98: molybdenum 98, Cd114: cadmium 114.

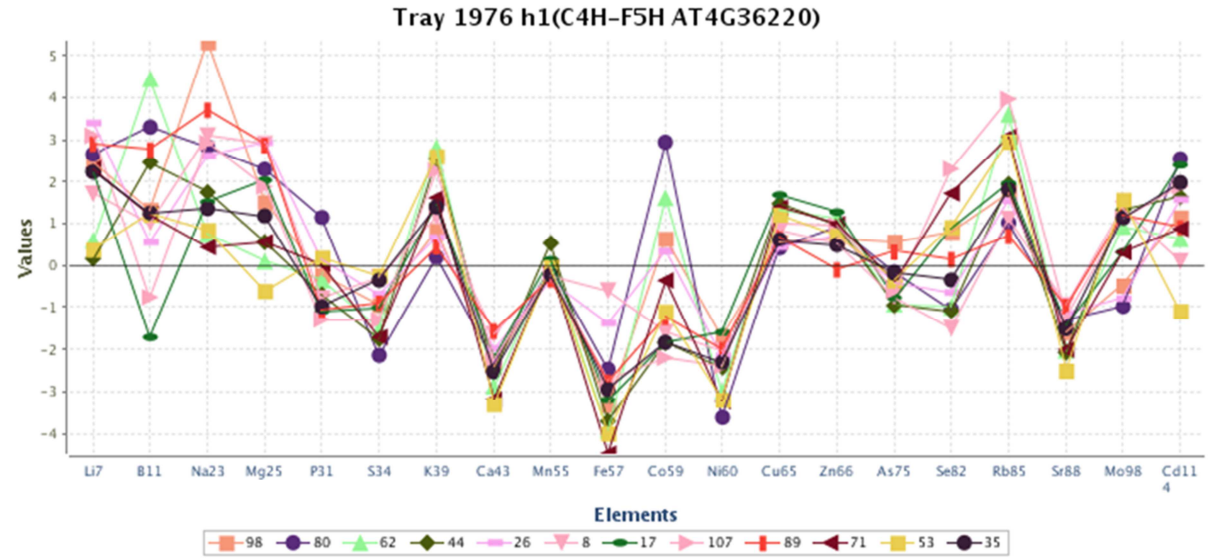

Fig. 119: Z-score graph of the leaf ionomic profile of *C4H::F5H*

Leaf elemental composition was analysed of *C4H::F5H*. The ionomic content of each single element was set to 0 for the WT. Presented are the values of each single mutant sample. As more deviate the value from the 0 as stronger is the difference between the WT and the mutant. Sample number: 12. Growing condition: 10h day length, 90 µE light intensity, 19 °C, 38 % humidty. Li7: lithium 7, B11: boron 11, Na23: Sodium 23, Mg25: magnesium 25, P31: phosphor 31, S34: sulphur 34, K39: potassium 39, Ca43: calcium 43, Mn55: manganese 55, Fe57: iron 57, Co59: cobalt 59, Ni60: nickel 60, Cu65: copper 65, Zn66: zinc 66, As75: arsenic 75, Se82: selenium 82, Rb85: rubidium 85, Sr88: strontium 88, Mo98: molybdenum 98, Cd114: cadmium 114.

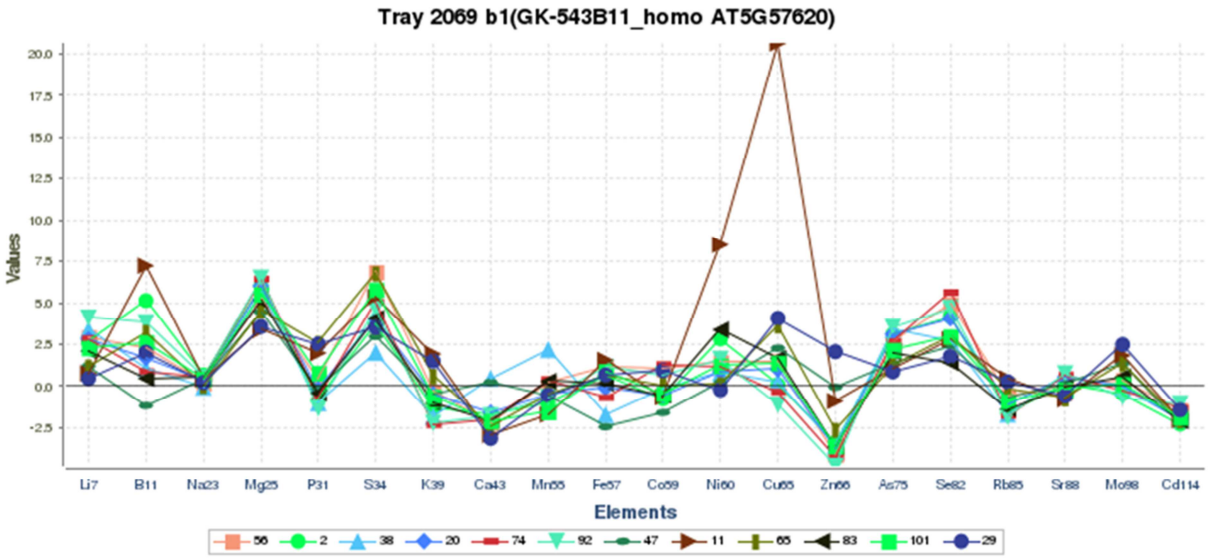

Fig. 120: Z-score graph of the leaf ionomic profile of *myb36-2*

Leaf elemental composition was analysed of *myb36-2*. The ionomic content of each single element was set to 0 for the WT. Presented are the values of each single mutant sample. As more deviate the value from the 0 as stronger is the difference between the WT and the mutant. Sample number: 12. Growing condition: 10h day length, 90 µE light intensity, 21 °C, 57 % humidty. Li7: lithium 7, B11: boron 11, Na23: Sodium 23, Mg25: magnesium 25, P31: phosphor 31, S34: sulphur 34, K39: potassium 39, Ca43: calcium 43, Mn55: manganese 55, Fe57: iron 57, Co59: cobalt 59, Ni60: nickel 60, Cu65: copper 65, Zn66: zinc 66, As75: arsenic 75, Se82: selenium 82, Rb85: rubidium 85, Sr88: strontium 88, Mo98: molybdenum 98, Cd114: cadmium 114.

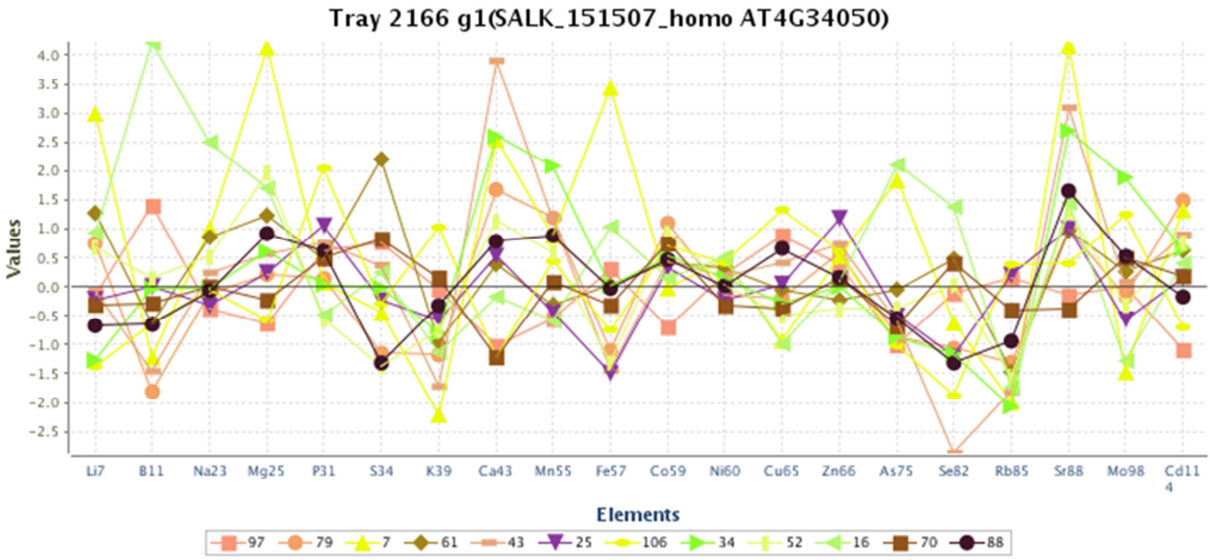

Fig. 121: Z-score graph of the leaf ionomic profile of *ccoaomt1*

Leaf elemental composition was analysed of *ccoaomt1*. The ionomic content of each single element was set to 0 for the WT. Presented are the values of each single mutant sample. As more deviate the value from the 0 as stronger is the difference between the WT and the mutant. Sample number: 12. Growing condition: 10h day length, 100 µE light intensity, 21 °C, 65 % humidty. Li7: lithium 7, B11: boron 11, Na23: Sodium 23, Mg25: magnesium 25, P31: phosphor 31, S34: sulphur 34, K39: potassium 39, Ca43: calcium 43, Mn55: manganese 55, Fe57: iron 57, Co59: cobalt 59, Ni60: nickel 60, Cu65: copper 65, Zn66: zinc 66, As75: arsenic 75, Se82: selenium 82, Rb85: rubidium 85, Sr88: strontium 88, Mo98: molybdenum 98, Cd114: cadmium 114.

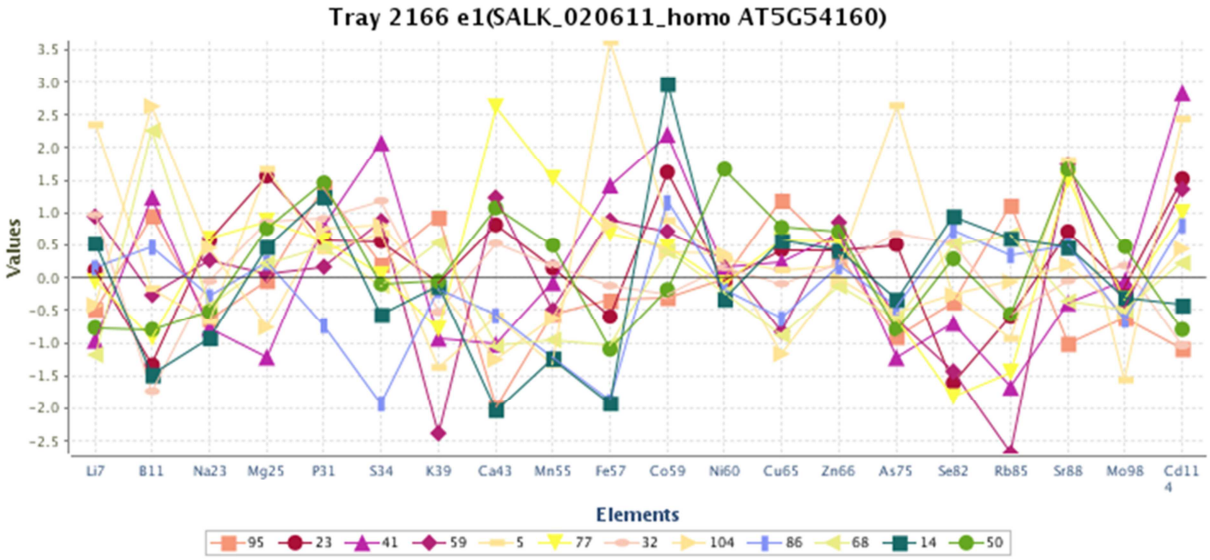

Fig. 122: Z-score graph of the leaf ionomic profile of SALK_020611 a *comt1* mutant

Leaf elemental composition was analysed of SALK_020611 a *comt1* mutant. The ionomic content of each single element was set to 0 for the WT. Presented are the values of each single mutant sample. As more deviate the value from the 0 as stronger is the difference between the WT and the mutant. Sample number: 12. Growing condition: 10h day length, 100 µE light intensity, 21 °C, 65 % humidty. Li7: lithium 7, B11: boron 11, Na23: Sodium 23, Mg25: magnesium 25, P31: phosphor 31, S34: sulphur 34, K39: potassium 39, Ca43: calcium 43, Mn55: manganese 55, Fe57: iron 57, Co59: cobalt 59, Ni60: nickel

60, Cu65: copper 65, Zn66: zinc 66, As75: arsenic 75, Se82: selenium 82, Rb85: rubidium 85, Sr88: strontium 88, Mo98: molybdenum 98, Cd114: cadmium 114.

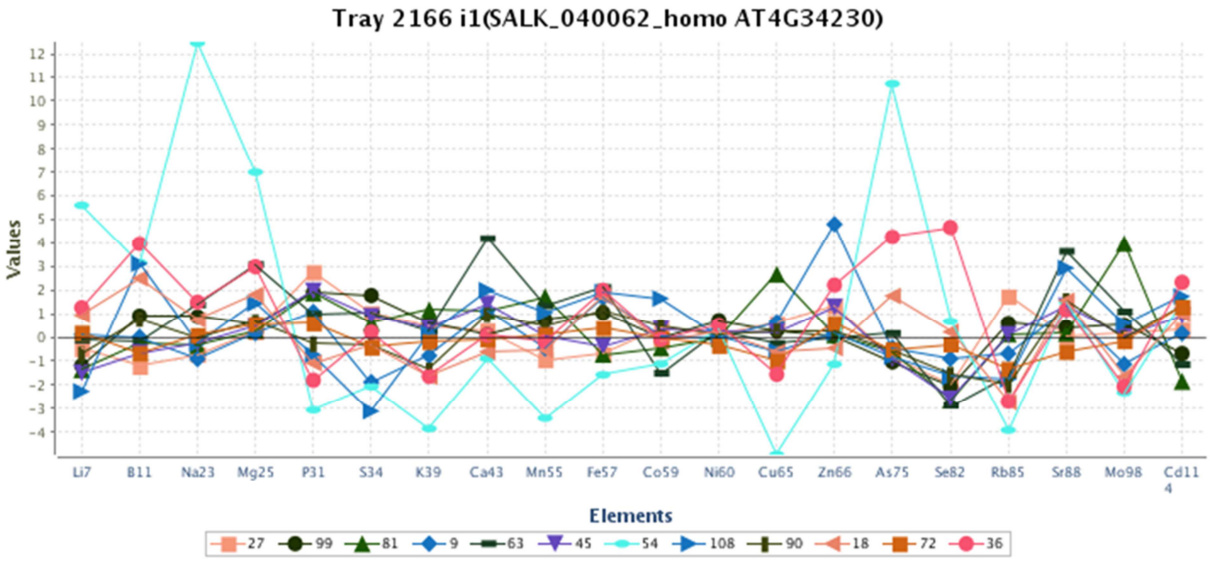

Fig. 123: Z-score graph of the leaf ionomic profile of SALK_040062 a *cadd* mutant

Leaf elemental composition was analysed of SALK_040062 a *cadd* mutant. The ionomic content of each single element was set to 0 for the WT. Presented are the values of each single mutant sample. As more deviate the value from the 0 as stronger is the difference between the WT and the mutant. Sample number: 12. Growing condition: 10h day length, 100 µE light intensity, 21 °C, 65 % humidty. Li7: lithium 7, B11: boron 11, Na23: Sodium 23, Mg25: magnesium 25, P31: phosphor 31, S34: sulphur 34, K39: potassium 39, Ca43: calcium 43, Mn55: manganese 55, Fe57: iron 57, Co59: cobalt 59, Ni60: nickel 60, Cu65: copper 65, Zn66: zinc 66, As75: arsenic 75, Se82: selenium 82, Rb85: rubidium 85, Sr88: strontium 88, Mo98: molybdenum 98, Cd114: cadmium 114.

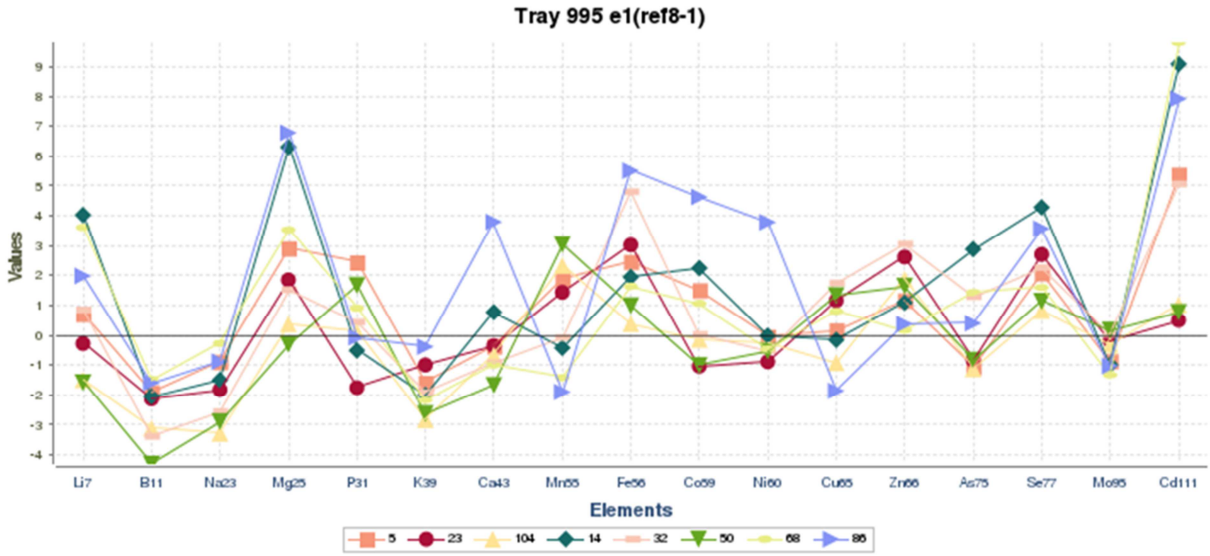

Fig. 124: Z-score graph of the leaf ionomic profile of *ref8-1*

Leaf elemental composition was analysed of *ref8-1*. The ionomic content of each single element was set to 0 for the WT. Presented are the values of each single mutant sample. As more deviate the value from the 0 as stronger is the difference between the WT and the mutant. Sample number: 8. Growing condition: 10h day length, 100 µE light intensity, 18 °C, 50 % humidty. Li7: lithium 7, B11: boron 11, Na23: Sodium 23, Mg25: magnesium 25, P31: phosphor 31, S34: sulphur 34, K39:

potassium 39, Ca43: calcium 43, Mn55: manganese 55, Fe57: iron 57, Co59: cobalt 59, Ni60: nickel 60, Cu65: copper 65, Zn66: zinc 66, As75: arsenic 75, Se82: selenium 82, Rb85: rubidium 85, Sr88: strontium 88, Mo98: molybdenum 98, Cd114: cadmium 114.

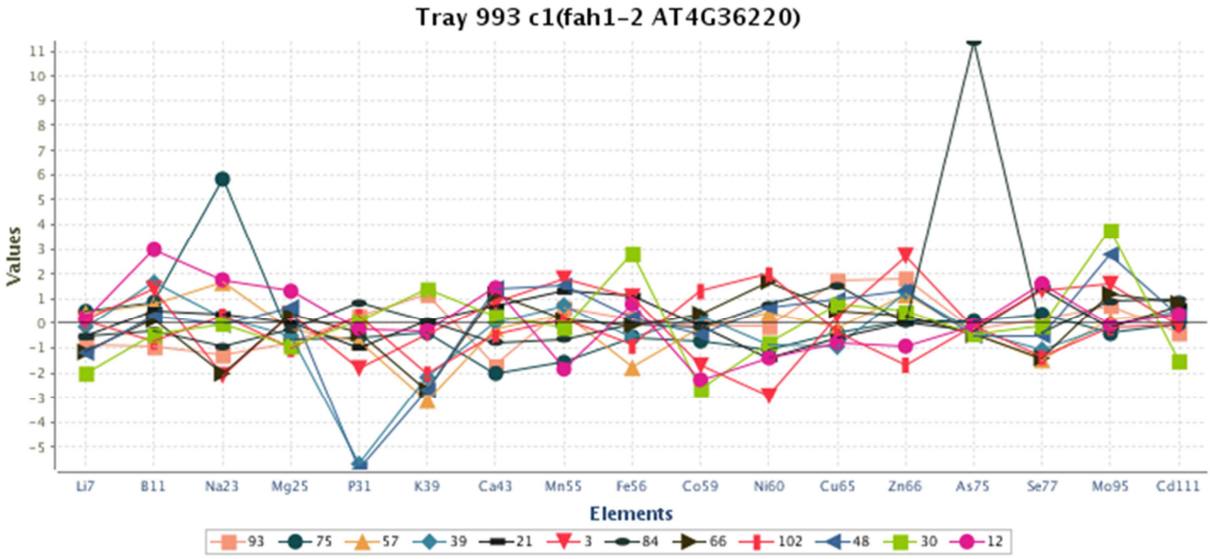

Fig. 125: Z-score graph of the leaf ionomic profile of *fah1-2*

Leaf elemental composition was analysed of *fah1-2*. The ionomic content of each single element was set to 0 for the WT. Presented are the values of each single mutant sample. As more deviate the value from the 0 as stronger is the difference between the WT and the mutant. Sample number: 12. Growing condition: 10h day length, 100 µE light intensity, 18 °C, 50 % humidty. Li7: lithium 7, B11: boron 11, Na23: Sodium 23, Mg25: magnesium 25, P31: phosphor 31, S34: sulphur 34, K39: potassium 39, Ca43: calcium 43, Mn55: manganese 55, Fe57: iron 57, Co59: cobalt 59, Ni60: nickel 60, Cu65: copper 65, Zn66: zinc 66, As75: arsenic 75, Se82: selenium 82, Rb85: rubidium 85, Sr88: strontium 88, Mo98: molybdenum 98, Cd114: cadmium 114.

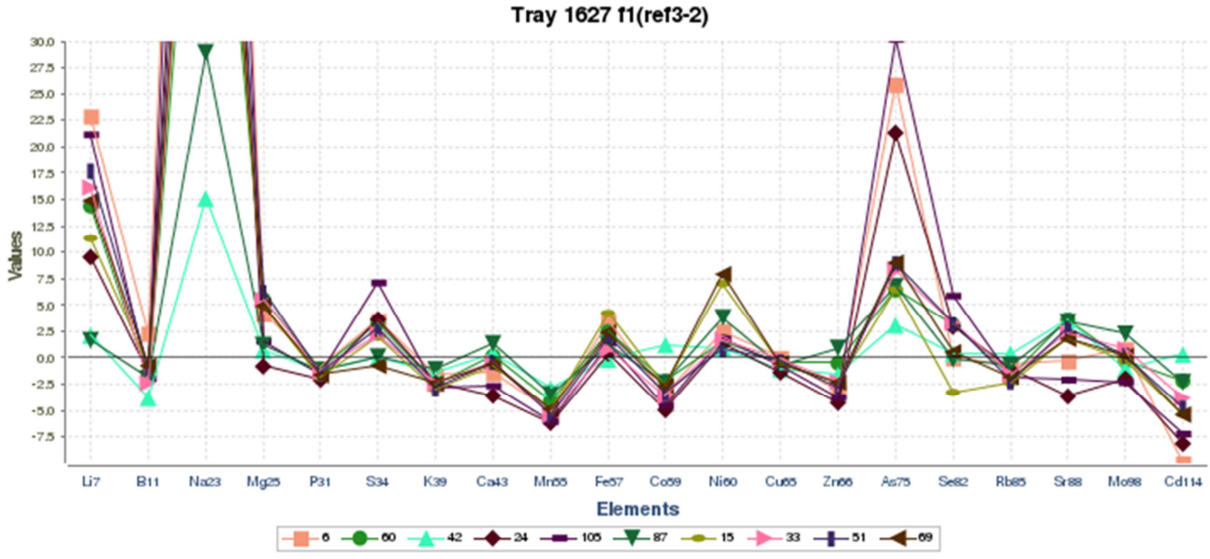

Fig. 126: Z-score graph of the leaf ionomic profile of *ref3-2*

Leaf elemental composition was analysed of *ref3-2*. The ionomic content of each single element was set to 0 for the WT. Presented are the values of each single mutant sample. As more deviate the value from the 0 as stronger is the difference between the WT and the mutant. Sample number: 10. Growing condition: 10h day length, 90 µE light intensity, 21 °C, 72 %

humidty. Li7: lithium 7, B11: boron 11, Na23: Sodium 23, Mg25: magnesium 25, P31: phosphor 31, S34: sulphur 34, K39: potassium 39, Ca43: calcium 43, Mn55: manganese 55, Fe57: iron 57, Co59: cobalt 59, Ni60: nickel 60, Cu65: copper 65, Zn66: zinc 66, As75: arsenic 75, Se82: selenium 82, Rb85: rubidium 85, Sr88: strontium 88, Mo98: molybdenum 98, Cd114: cadmium 114.

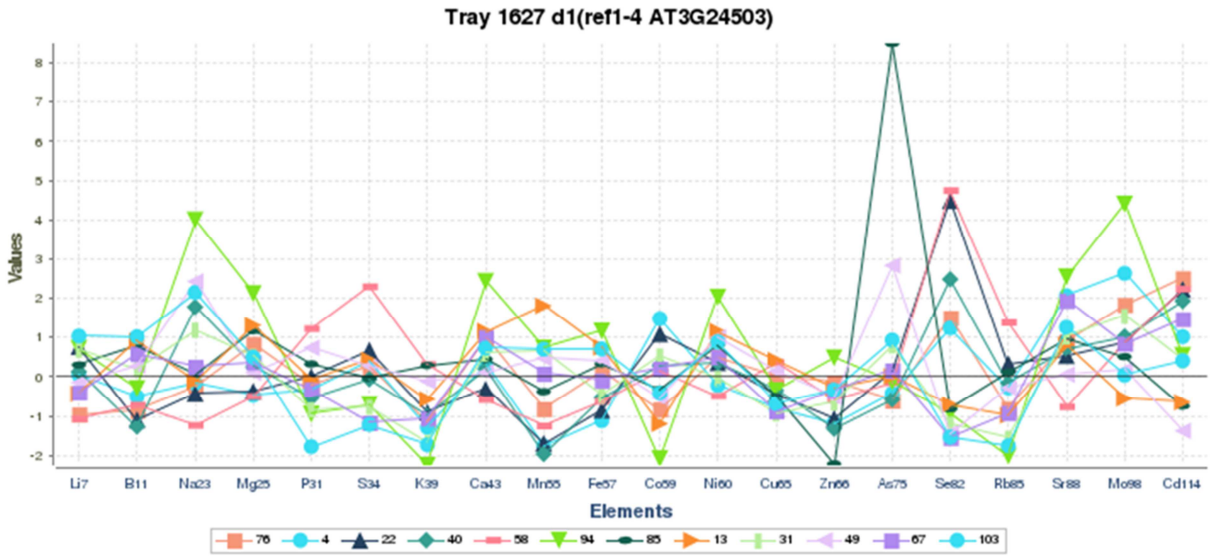

Fig. 127: Z-score graph of the leaf ionomic profile of *ref1-4*

Leaf elemental composition was analysed of *ref1-4*. The ionomic content of each single element was set to 0 for the WT. Presented are the values of each single mutant sample. As more deviate the value from the 0 as stronger is the difference between the WT and the mutant. Sample number: 12. Growing condition: 10h day length, 90 µE light intensity, 21 °C, 72 % humidty. Li7: lithium 7, B11: boron 11, Na23: Sodium 23, Mg25: magnesium 25, P31: phosphor 31, S34: sulphur 34, K39: potassium 39, Ca43: calcium 43, Mn55: manganese 55, Fe57: iron 57, Co59: cobalt 59, Ni60: nickel 60, Cu65: copper 65, Zn66: zinc 66, As75: arsenic 75, Se82: selenium 82, Rb85: rubidium 85, Sr88: strontium 88, Mo98: molybdenum 98, Cd114: cadmium 114.

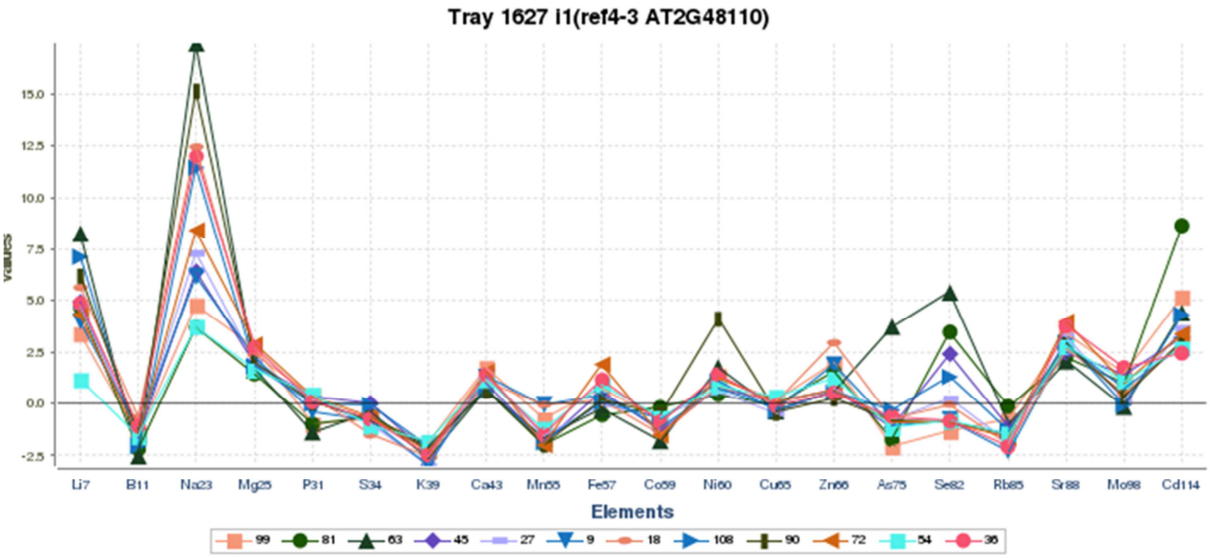

Fig. 128: Z-score graph of the leaf ionomic profile of *ref4-3*

Leaf elemental composition was analysed of *ref4-3*. The ionomic content of each single element was set to 0 for the WT. Presented are the values of each single mutant sample. As more deviate the value from the 0 as stronger is the difference

between the WT and the mutant. Sample number: 12. Growing condition: 10h day length, 90 µE light intensity, 21 °C, 72 % humidty. Li7: lithium 7, B11: boron 11, Na23: Sodium 23, Mg25: magnesium 25, P31: phosphor 31, S34: sulphur 34, K39: potassium 39, Ca43: calcium 43, Mn55: manganese 55, Fe57: iron 57, Co59: cobalt 59, Ni60: nickel 60, Cu65: copper 65, Zn66: zinc 66, As75: arsenic 75, Se82: selenium 82, Rb85: rubidium 85, Sr88: strontium 88, Mo98: molybdenum 98, Cd114: cadmium 114.

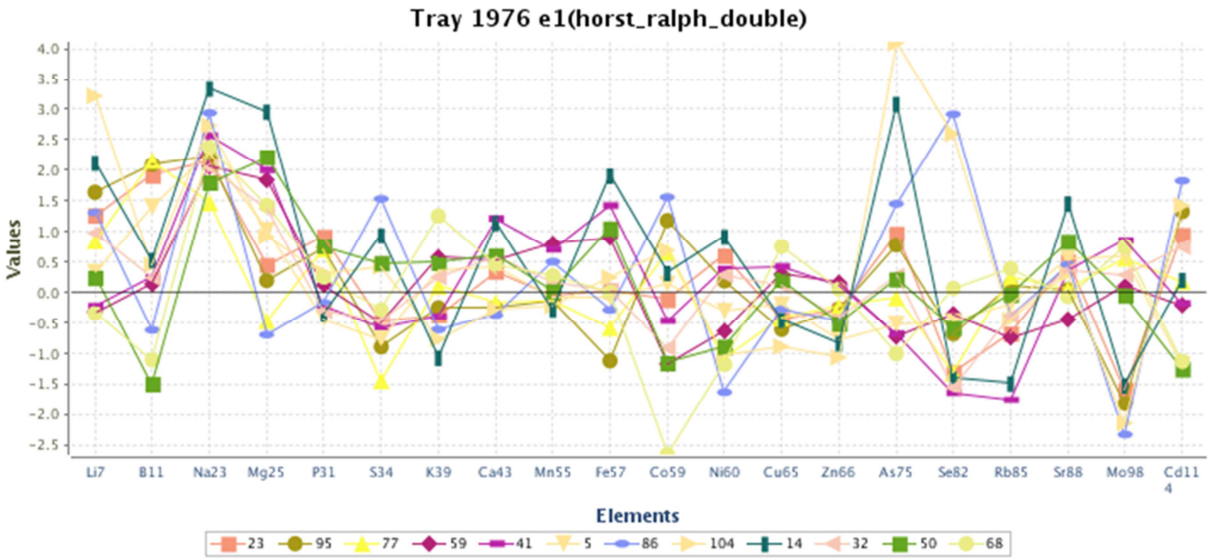

Fig. 129: Z-score graph of the leaf ionomic profile of *horst*ralph*

Leaf elemental composition was analysed of *horst*ralph*. The ionomic content of each single element was set to 0 for the WT. Presented are the values of each single mutant sample. As more deviate the value from the 0 as stronger is the difference between the WT and the mutant. Sample number: 12. Growing condition: 10h day length, 100 µE light intensity, 18 °C, 50 % humidty. Li7: lithium 7, B11: boron 11, Na23: Sodium 23, Mg25: magnesium 25, P31: phosphor 31, S34: sulphur 34, K39: potassium 39, Ca43: calcium 43, Mn55: manganese 55, Fe57: iron 57, Co59: cobalt 59, Ni60: nickel 60, Cu65: copper 65, Zn66: zinc 66, As75: arsenic 75, Se82: selenium 82, Rb85: rubidium 85, Sr88: strontium 88, Mo98: molybdenum 98, Cd114: cadmium 114.

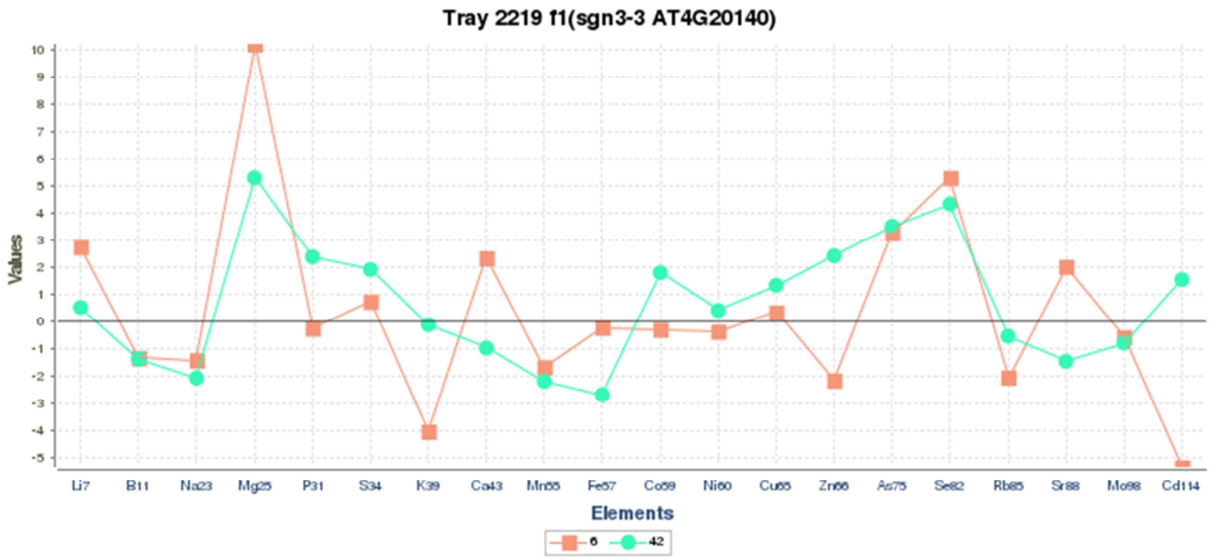

Fig. 130: Z-score graph of the leaf ionomic profile of *sgn3-3*

Leaf elemental composition was analysed of *sgn3-3*. The ionomic content of each single element was set to 0 for the WT. Presented are the values of each single mutant sample. As more deviate the value from the 0 as stronger is the difference between the WT and the mutant. Sample number: 2. Growing condition: 10h day length, 100 µE light intensity, 21 °C, 39 % humidty. Li7: lithium 7, B11: boron 11, Na23: Sodium 23, Mg25: magnesium 25, P31: phosphor 31, S34: sulphur 34, K39: potassium 39, Ca43: calcium 43, Mn55: manganese 55, Fe57: iron 57, Co59: cobalt 59, Ni60: nickel 60, Cu65: copper 65, Zn66: zinc 66, As75: arsenic 75, Se82: selenium 82, Rb85: rubidium 85, Sr88: strontium 88, Mo98: molybdenum 98, Cd114: cadmium 114.

Tab. 17: Summary of the elemental composition of different casparian strip, suberin and phenylpropanoid pathway mutants

+: significantly increased, -: significantly decreased, student's t-test $p \leq 0.05$.

Genotype	Na23	Mg25	P31	K39	Ca43	Fe57	Cu65	As75
esb1	+	+	-	0	-	-	+	+
C4H::F5H	+	+	0	+	-	-	+	-
myb36-2	0	+	0	0	-	0	+	+
ccoaomt1	0	0	0	-	+	0	0	0
SALK_020611	0	0	0	0	0	0	0	0
SALK_040062	0	+	0	0	+	0	0	0
ref8-1	-	+	0	-	0	+	0	0
fah1-2	0	0	0	0	0	0	0	0
ref3-2	+	+	-	-	-	+	-	+
ref1-4	0	0	0	-	0	0	0	0
ref4-3	-	+	0	-	+	0	0	0
horst*ralph	+	+	0	0	0	0	0	0
sgn3-3	-	+	0	-	0	0	0	+

9.6. Tissue specific gene expression of *HQT*

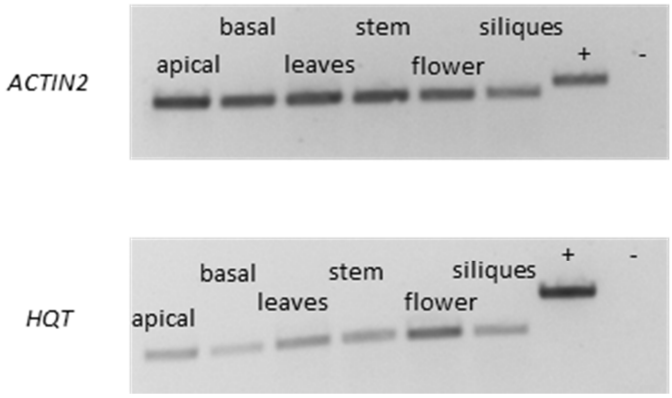

Fig. 131: Tissue specific gene expression of HQT in *Arabidopsis thaliana*

Depicted is the tissue specific gene expression of HQT. As a positive control the constitutively expressed gene Actin2 was used. A hydroponically grown Arabidopsis thaliana plant was used for the tissue specific analysis. The root was divided into two parts: an apical and a basal part. Furthermore, leaf, stem, whole flower and silique tissue were harvested. HQT is predominately expressed in the flower. A high gene expression is observable in apical part of the root, the leaves, stem and the siliques. A weak gene expression is found in the basal part of the root.

9.7. Root dry weight

Root dry weights of either treated with cell wall degrading enzymes or untreated with cell wall degrading enzymes are presented in the following images.

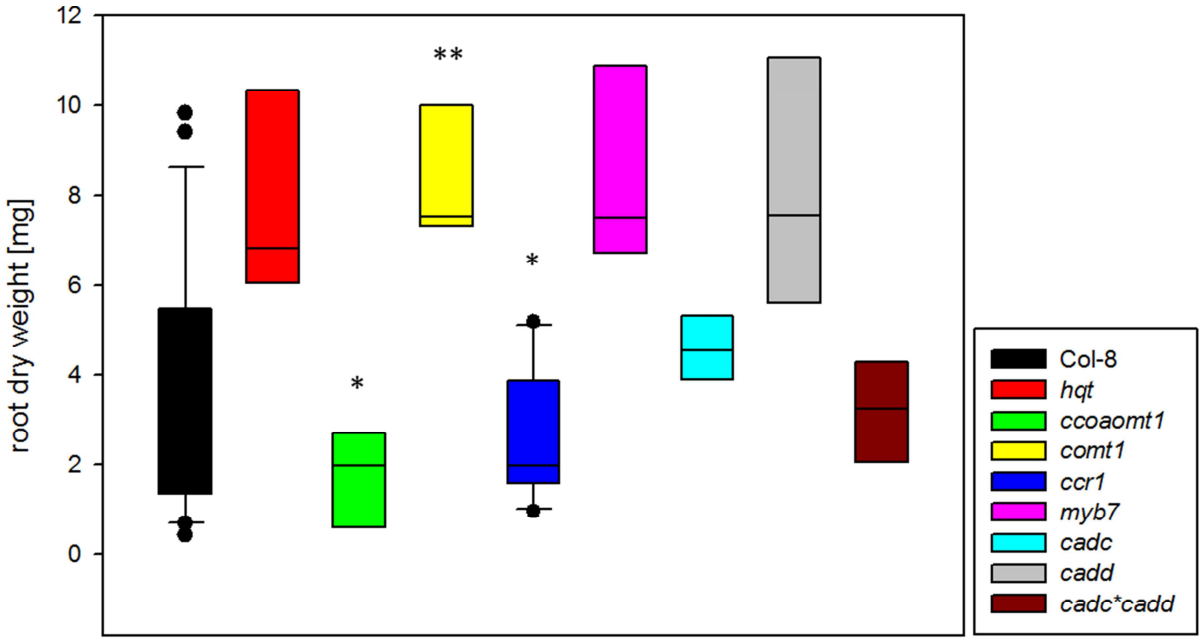

Fig. 132: Root dry weight of soil-grown roots Col-8, *hqt*, *ccoaomt1*, *comt1*, *ccr1*, *myb7*, *cadc*, *cadd* and *cadc*cadd* treated with cell wall degrading enzymes

Represented is the root dry weight of all soil-grown plants treated with cell wall degrading enzymes and after extraction of chloroform and methanol soluble compounds. The sample amount corresponds to 27 of WT, 3 of *hqt* and *ccoaomt1*, 4 of *comt1*, 10 of *ccr1*, 3 of *myb7*, 4 of *cadc*, 3 of *cadd* and 4 of *cadc*cadd*. *: student's t-test, $p \leq 0.05$, **: student's t-test, $p \leq 0.01$.

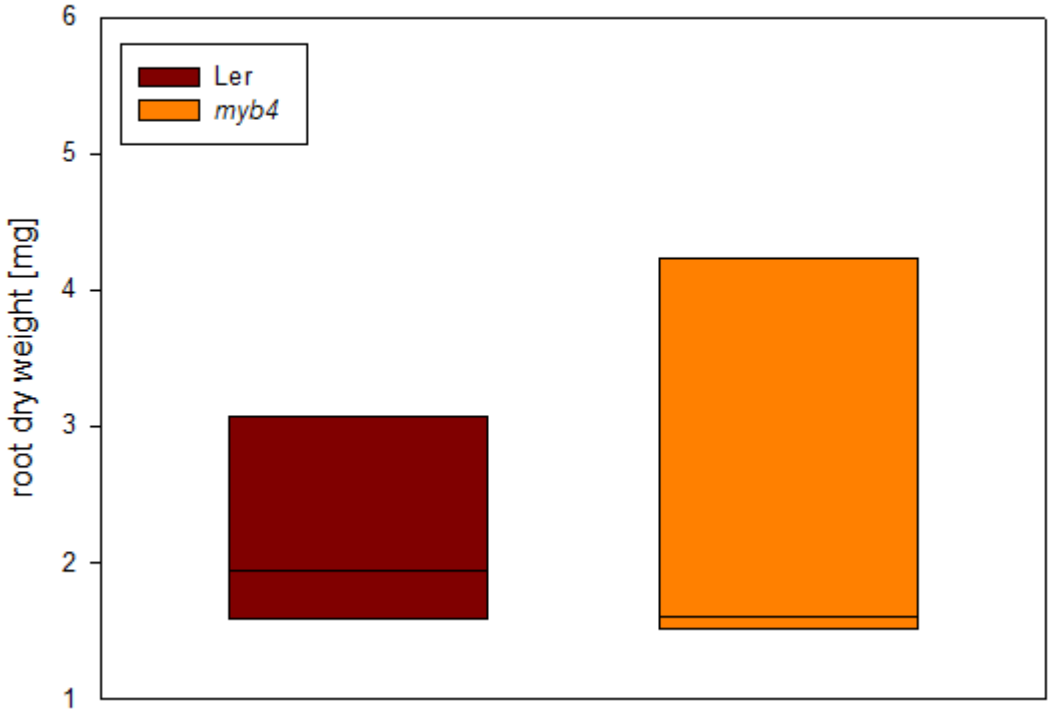

Fig. 133: Root dry weight of soil-grown roots of Ler and *myb4* treated with cell wall degrading enzymes

Represented is the root dry weight of all soil-grown plants treated with cell wall degrading enzymes and after extraction of chloroform and methanol soluble compounds. The sample amount corresponds to 4 of WT and *myb4*. *: student's t-test, p ≤ 0.05, **: student's t-test, p ≤ 0.01.

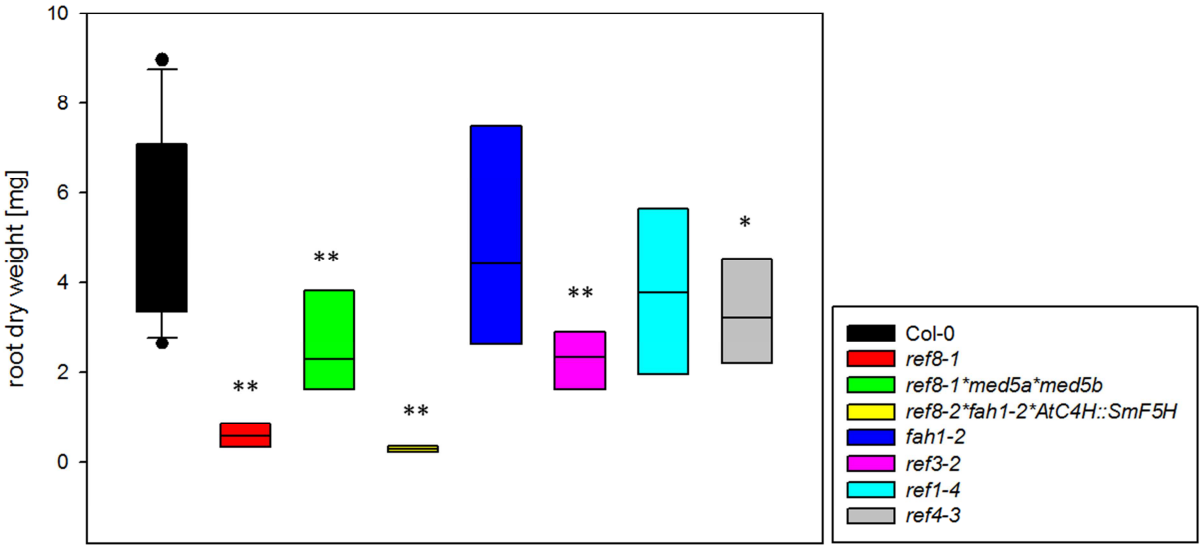

Fig. 134: Root dry weight of soil-grown roots of Col-0, *ref8-1*, *ref8-1*med5a*med5b*, *ref8-2*fah1-2*AtC4H::SmF5H*, *fah1-2*, *ref3-2*, *ref1-4*, *ref4-3* treated with cell wall degrading enzymes

Represented is the root dry weight of all soil-grown plants treated with cell wall degrading enzymes and after extraction of chloroform and methanol soluble compounds. The sample amount corresponds to 17 of WT, 7 of *ref8-1*, 4 of *ref8-1*med5a*med5b*, *ref8-2*fah1-2*AtC4H::SmF5H*, *fah1-2* as well as *ref3-2*, 5 of *ref1-4* and 4 of *ref4-3*. *: student's t-test, $p \leq 0.05$, **: student's t-test, $p \leq 0.01$.

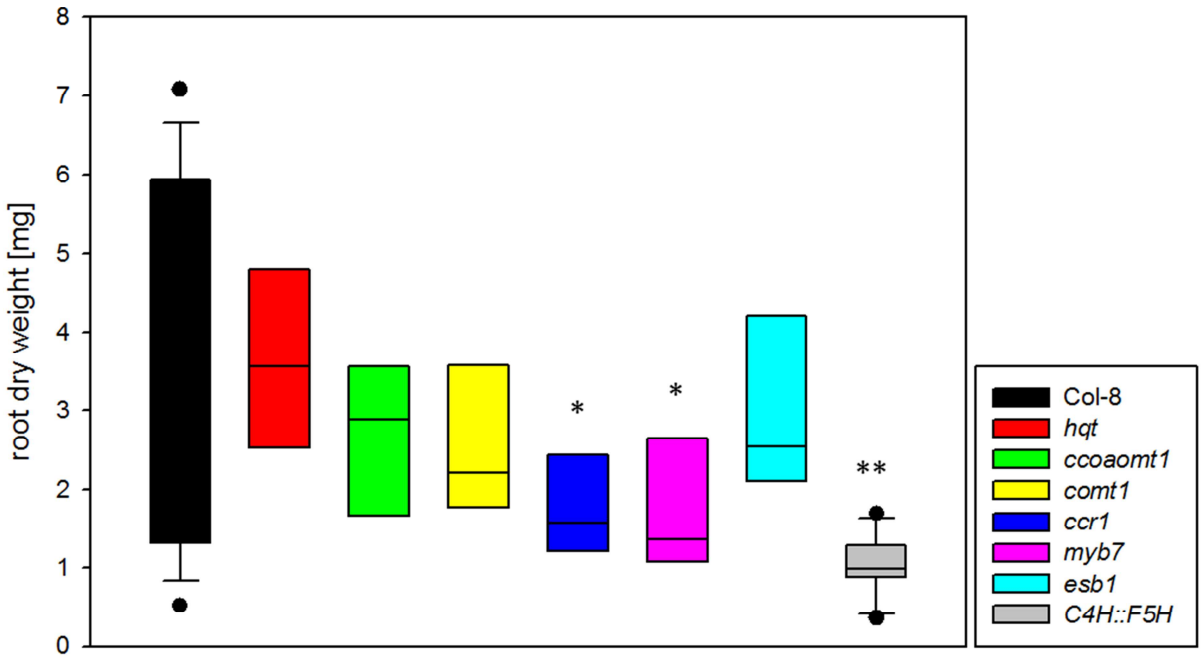

Fig. 135: Root dry weight of hydroponically grown roots of Col-8, *hqt*, *ccoaomt1*, *comt1*, *ccr1*, *myb7*, *esb1* and *C4H::F5H* treated with cell wall degrading enzymes

Represented is the root dry weight of all hydroponically grown plants treated with cell wall degrading enzymes and after extraction of chloroform and methanol soluble compounds. The sample amount corresponds to 16 of WT, 6 of *hqt*, 7 of *ccoaomt1* and *comt1*, 8 of *ccr1*, 4 of *myb7*, 8 of *esb1* and 11 of *C4H::F5H*. *: student's t-test, $p \leq 0.05$, **: student's t-test, $p \leq 0.01$.

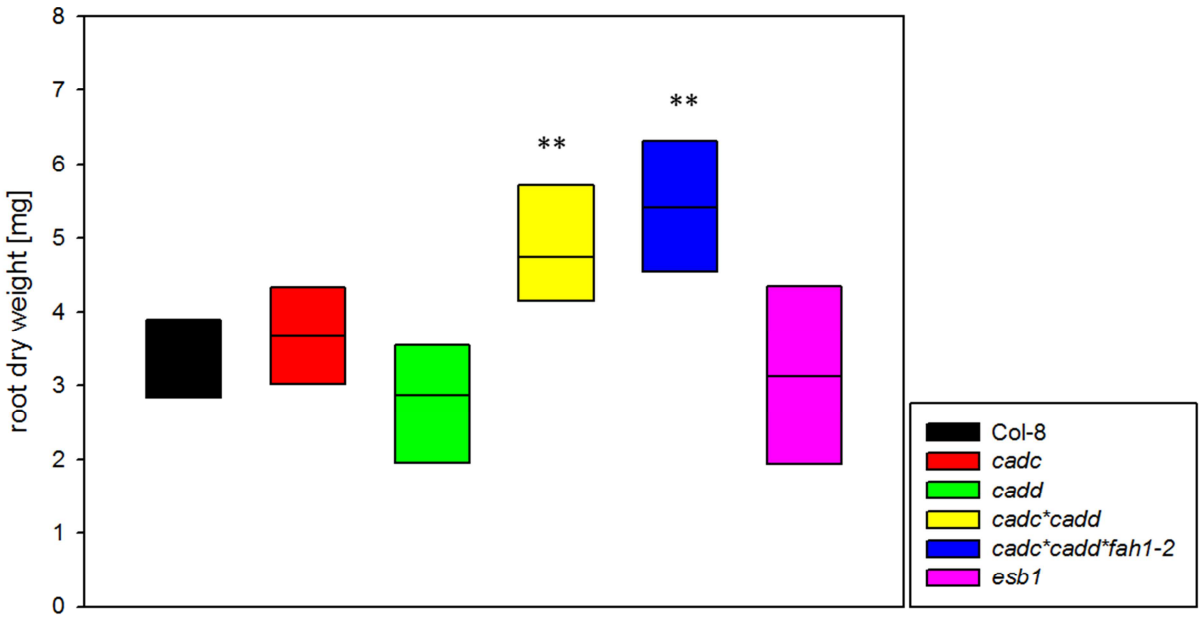

Fig. 136: Root dry weight of hydroponically grown roots of Col-8, *cadc*, *cadd*, *cadc*cadd*, *cadc*cadd*fah1-2* and *esb1* untreated with cell wall degrading enzymes

Represented is the root dry weight of all hydroponically grown plants treated with cell wall degrading enzymes and after extraction of chloroform and methanol soluble compounds. The sample amount corresponds to 8 of WT, *cadc* as well as *cadd*, 7 of *cadc*cadd*, 8 of *cadc*cadd*fah1-2* and *esb1*. *: student's t-test, $p \leq 0.05$, **: student's t-test, $p \leq 0.01$.

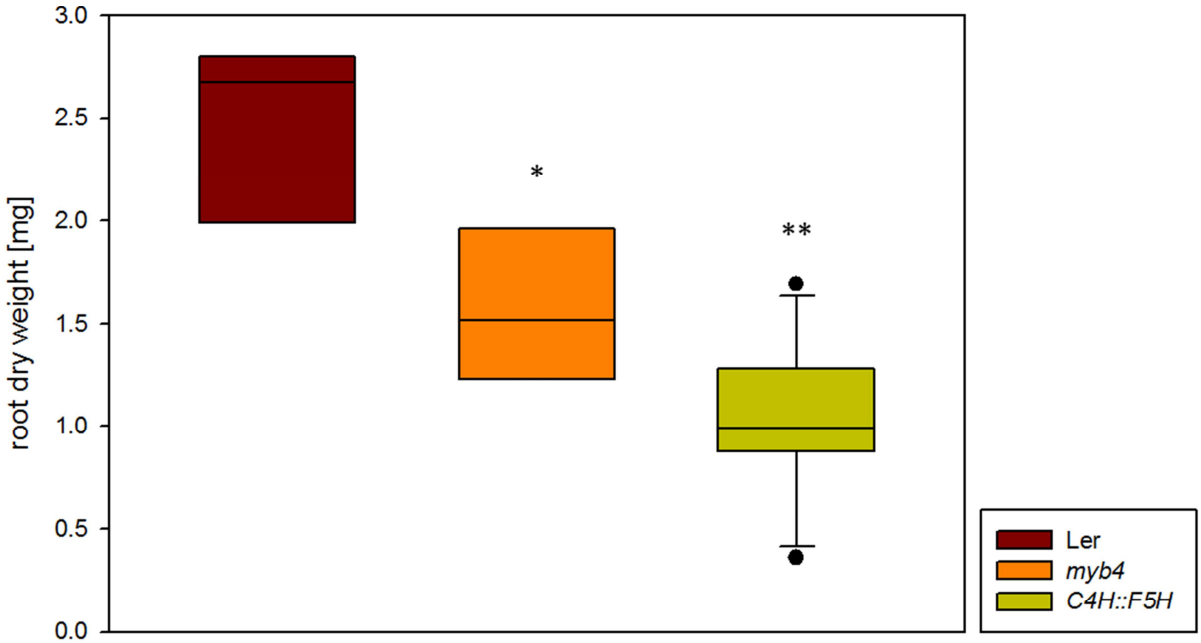

Fig. 137: Root dry weight of hydroponically grown roots of Ler, *myb4* and *C4H::F5H* treated with cell wall degrading enzymes

Represented is the root dry weight of all hydroponically grown plants treated with cell wall degrading enzymes and after extraction of chloroform and methanol soluble compounds. The sample amount corresponds to 4 of WT as well as *myb4* and 11 of *C4H::F5H*. *: student's t-test, $p \leq 0.05$, **: student's t-test, $p \leq 0.01$.

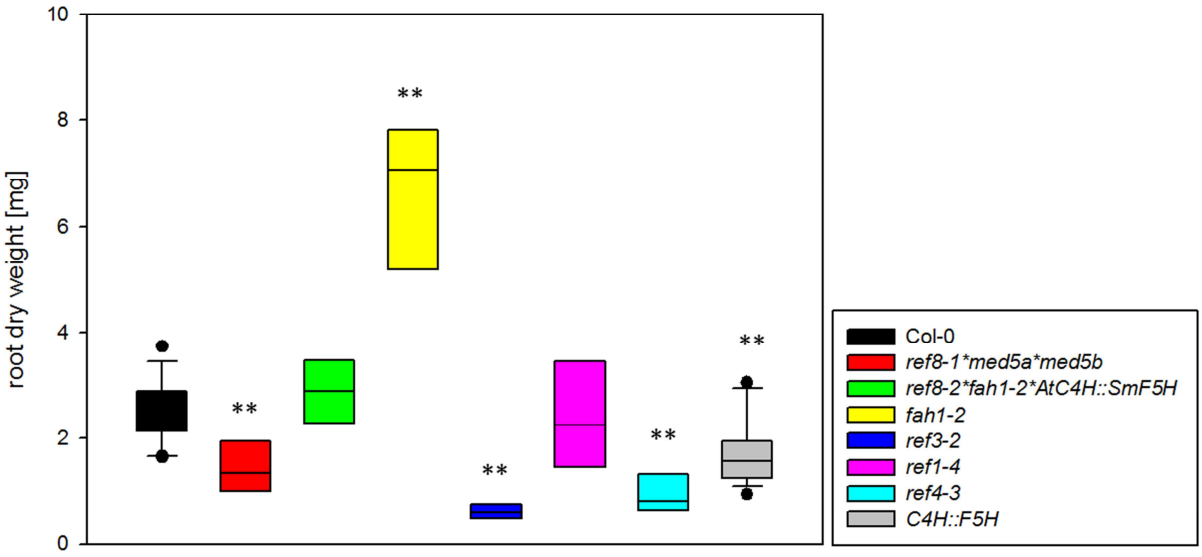

Fig. 138: Root dry weight of hydroponically grown roots of Col-0, *ref8-1*med5a*med5b*, *ref8-2*fah1-2*AtC4H::SmF5H*, *fah1-2*, *ref3-2*, *ref1-4*, *ref4-3* and *C4H::F5H* untreated with cell wall degrading enzymes

Represented is the root dry weight of all hydroponically grown plants treated with cell wall degrading enzymes and after extraction of chloroform and methanol soluble compounds. The sample amount corresponds to 13 of WT, 8 of *ref8-1*med5a*med5b*, *ref8-2*fah1-2*AtC4H::SmF5H*, *fah1-2*, 6 of *ref3-2* as well as *ref1-4*, 7 of *ref4-3* and 15 of *C4H::F5H*. *: student's t-test, $p \leq 0.05$, **: student's t-test, $p \leq 0.01$.

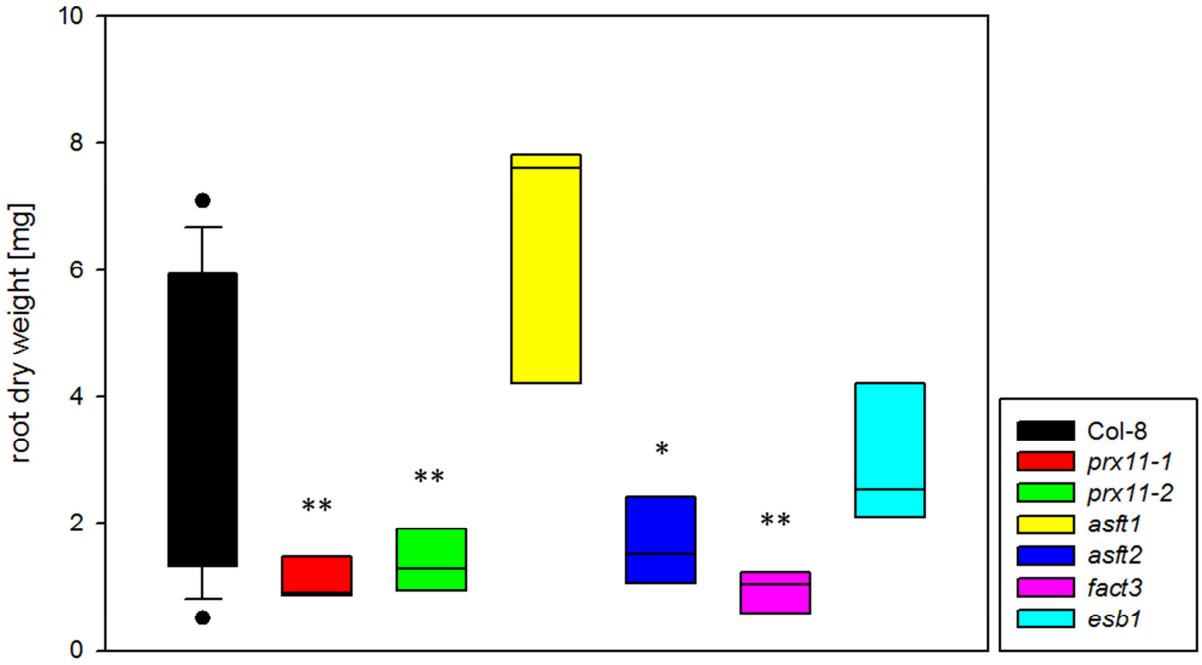

Fig. 139: Root dry weight of hydroponically grown roots of Col-8, *prx11-1*, *prx11-2*, *asft1*, *asft2*, *fact3* and *esb1* treated with cell wall degrading enzymes

Represented is the root dry weight of all hydroponically grown plants treated with cell wall degrading enzymes and after extraction of chloroform and methanol soluble compounds. The sample amount corresponds to 16 of WT, 4 of *prx11-1*, 3 of *prx11-2*, 4 of *asft1*, *asft2* as well as *fact3* and 8 of *esb1**: student's t-test, $p \leq 0.05$, **: student's t-test, $p \leq 0.01$.

9.8. Suberin extraction followed by lignin extraction

At first suberin was extracted by transesterification with boron trifluoride and methanol. Afterwards, thioacidolytic approach was performed with the suberin extracted roots. Chromatograms of extracted lignin monomers and quantified results of the lignin extraction are represented.

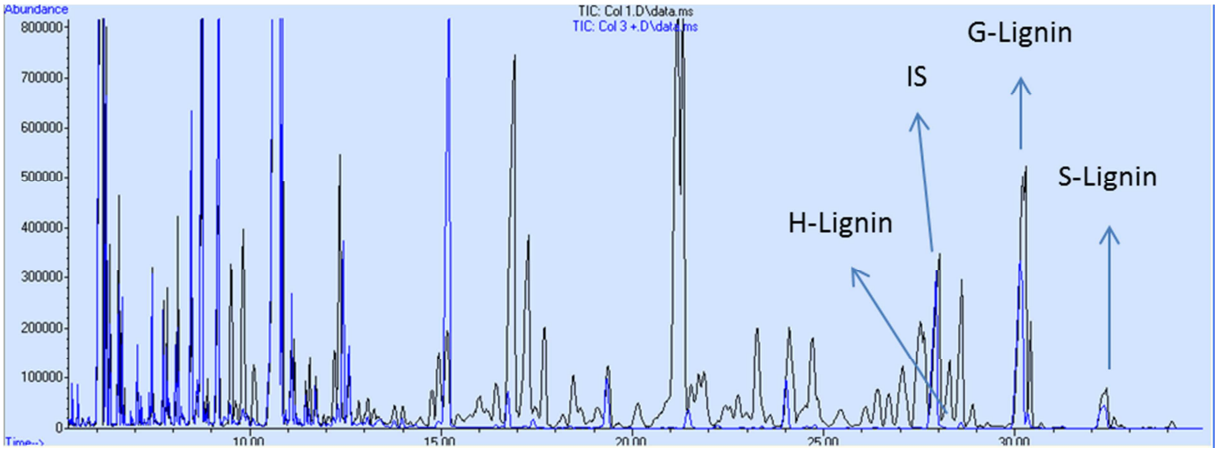

Fig. 140: Chromatogram of thioacidolytic released products of WT roots

The chromatogram reveals thioacidolytic released products of WT root either suberin extracted or without suberin extraction. The sample in black represents the suberin non-extracted root, whereas the blue sample is the suberin extracted root. Suberin extraction seems to partially degrade the lignin polymer.

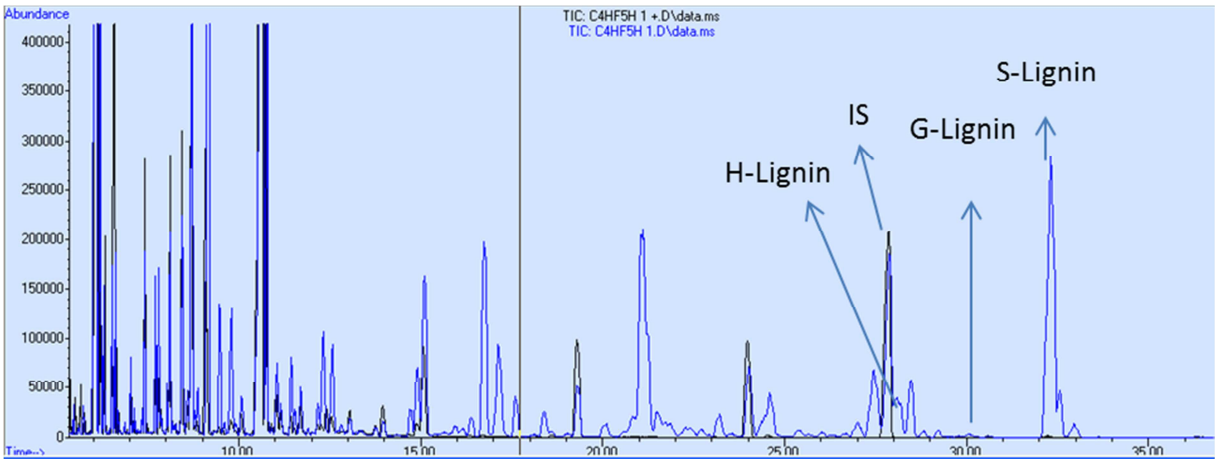

Fig. 141: Chromatogram of thioacidolytic released products of *C4H::F5H* roots

The chromatogram reveals thioacidolytic released products of *C4H::F5H* root either suberin extracted or without suberin extraction. The sample in black represents the suberin extracted root, whereas the blue sample is the suberin non-extracted root. Suberin extraction appears to degrade almost the whole lignin polymer in *C4H::F5H*.

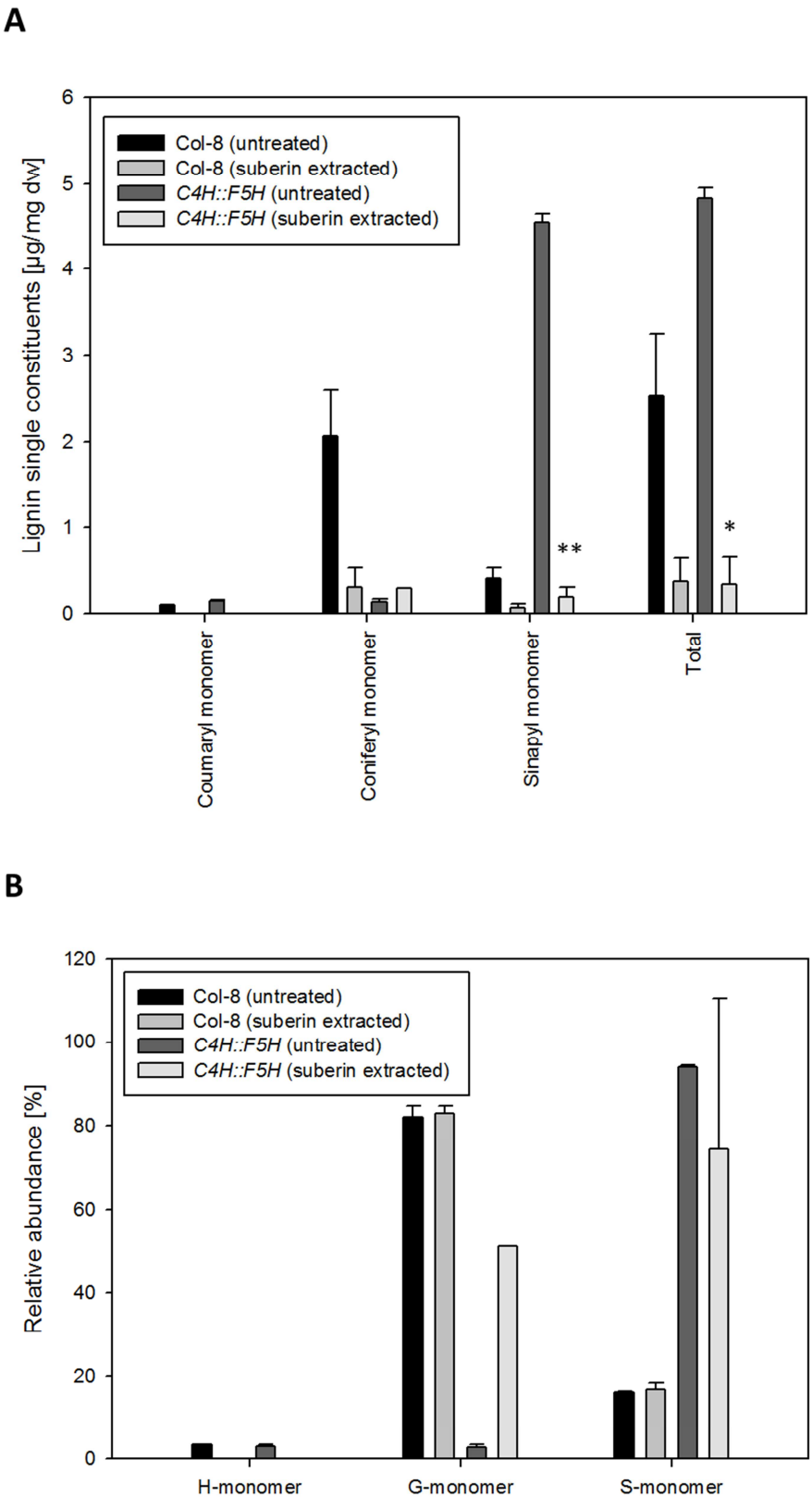

Fig. 142: Comparison of root lignin composition of suberin extracted and suberin non-extracted roots

Five weeks old hydroponically grown roots treated with cell wall degrading enzymes were analysed. A: Absolute lignin composition related to the root dry weight. B: Relative lignin composition related to the root dry weight. The represented values are the arithmetic mean of the WT and mutant lines respectively and the calculated standard error bars. The sample

amount corresponds to two samples for WT and *C4H::F5H*. H-monomer: hydroxycinnamyl-monomer, G-monomer: guiacyl-monomer, S-monomer: sinapyl-monomer. *: student's t-test, $p \leq 0.05$, **: student's t-test, $p \leq 0.01$.

A

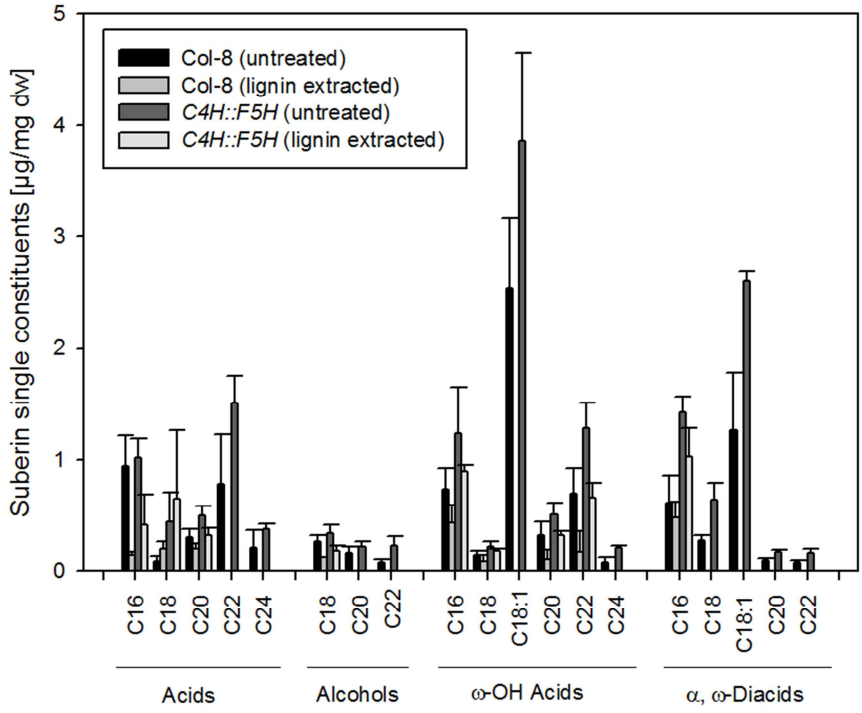

B

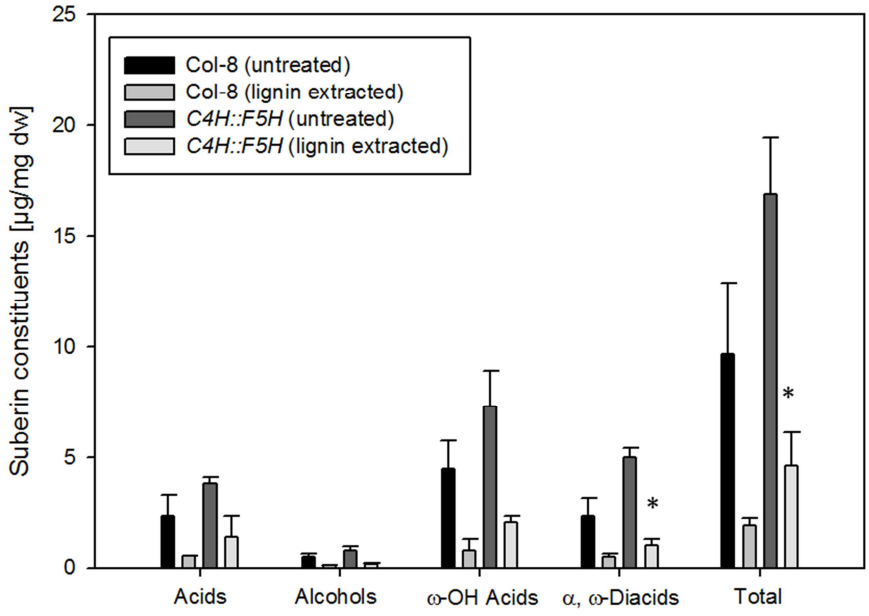

C

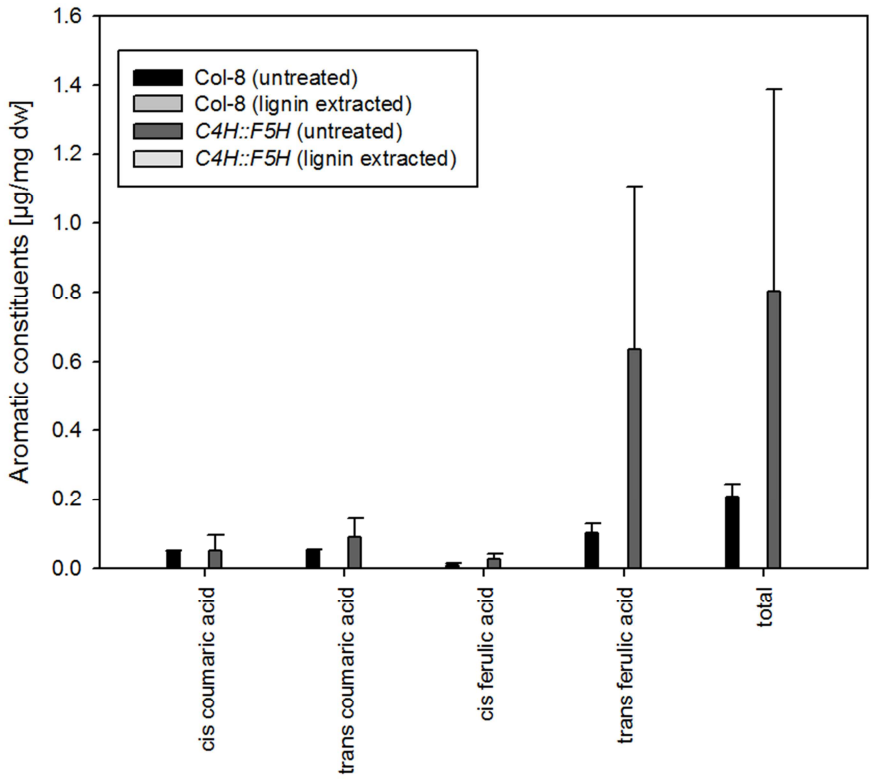

Fig. 143: Comparison of root aliphatic suberin and aromatic compounds of suberin extracted and lignin non-extracted roots

Five weeks old hydroponically grown roots treated with cell wall degrading enzymes were analysed. **A**: Composition of the suberin aliphatic single constituents of suberin extracted and lignin non-extracted WT and *C4H::F5H* roots related to the root dry weight. **B**: Composition of the suberin aliphatic substance classes of suberin extracted and lignin non-extracted WT and *C4H::F5H* roots related to the root dry weight. **C**: Composition of the aromatic compounds of suberin extracted and lignin non-extracted WT and *C4H::F5H* roots related to the root dry weight. The represented values are the arithmetic mean of the WT and mutant lines respectively and the calculated error bars of standard deviation. The sample amount corresponds to two roots for WT and *C4H::F5H*. Acids: monocarboxylic acids, Alcohols: primary alcohols, ω-OH Acids: ω-hydroxy acids, α, ω-Diacids: α, ω-dicarboxylic acids. *: student's t-test, $p \leq 0.05$, **: student's t-test, $p \leq 0.01$.

9.9. Feeding with *trans* ferulic acid does not recover PI phenotype

Feeding *ccoaomt1* and *C4H::F5H* with *trans* ferulic acid does not recover the PI phenotype.

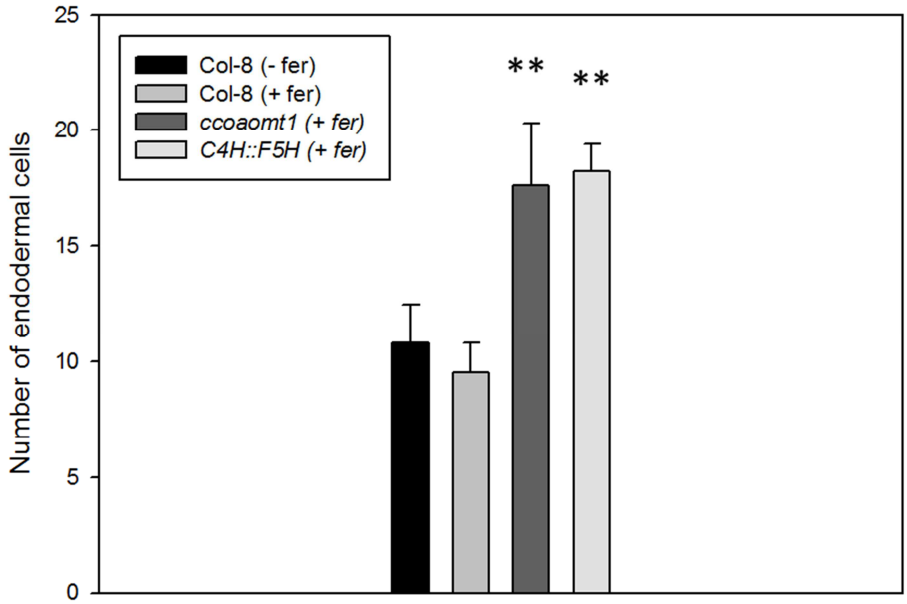

Fig. 144: Establishment of a functional apoplastic diffusion barrier is not achieved by feeding seedlings with *trans* ferulic acid

The apoplastic diffusion of PI into the central cylinder of Col-8 is blocked after 10.8 endodermal cells. Feeding seedlings with trans ferulic acid does not alter the establishment of the apoplastic diffusion barrier in WT. The PI is blocked after 9.5 endodermal cells whereas the blockage of PI occurs after 17.6 endodermal cells in *ccoaomt1* and after 18.2 in *C4H::F5H*. The represented values are the arithmetic mean of the WT and mutant lines respectively and the calculated standard deviation error bars. The sample amount of each represented value corresponds to 10 seedlings. *: student's t-test, $p \leq 0.05$, **: student's t-test, $p \leq 0.01$.

9.10. Qualitative analysis of Casparian strips in roots fed with *trans* ferulic acid

Feeding mutant lines *ccoaomt1* and *ccr1* with *trans* ferulic acid does not recover the Casparian strip barrier. Furthermore, it appears that the outer cell wall of the endodermal cells is not lignified. This phenotype was not observed without treating roots *with* trans ferulic acid. WT is not affected by feeding experiment.

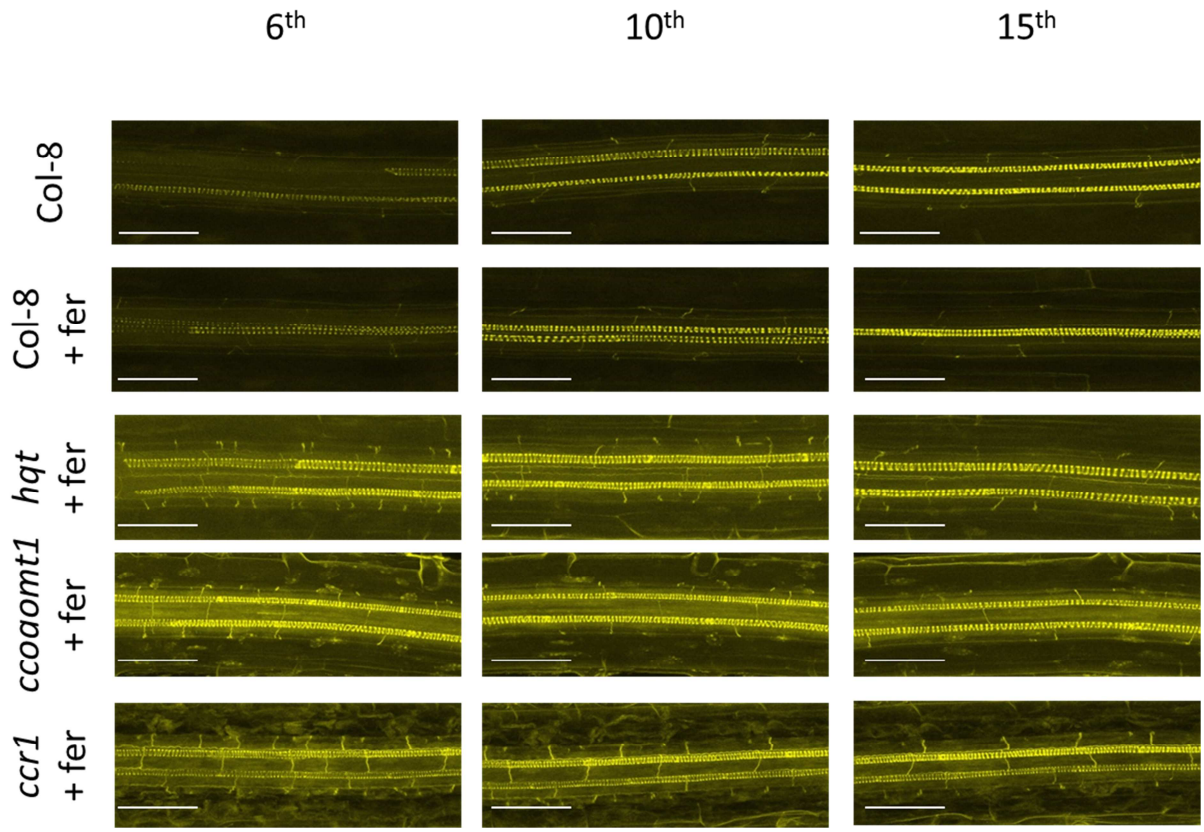

Fig. 145: Basic fuchsine stained roots of WT and mutated *Arabidopsis thaliana* fed with *trans* ferulic acid

The basic fuchsine staining reveals a lignified endodermal network in the WT treated with *trans* ferulic acid or without. The mutant line *hqt* seems to be not affected by the treatment. In contrast *ccoaomt1* and *ccr1* still reveal an impaired lignified endodermal network. Especially in *ccr1* it appears that the outer endodermal cell wall is not lignified. Scale bar size is 100 µm.

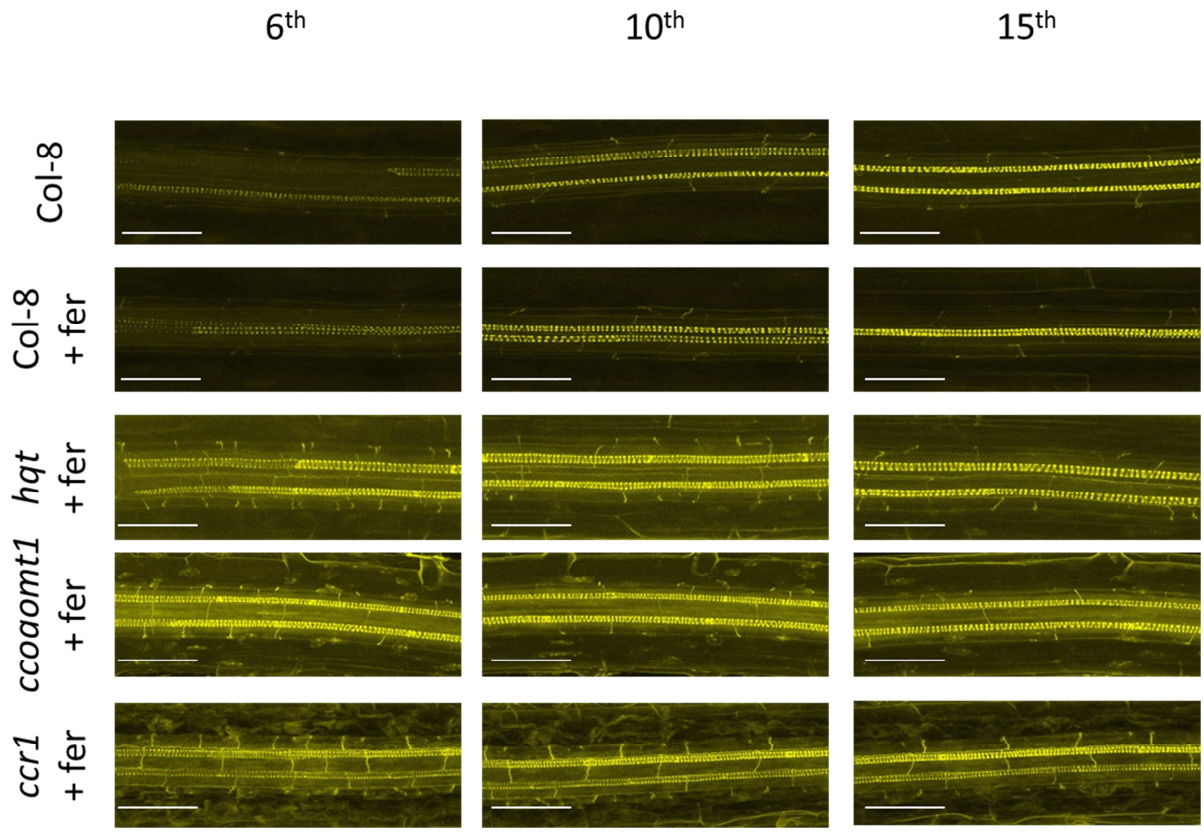

Fig. 146: Basic fuchsine stained roots of WT and mutated *Arabidopsis thaliana* fed with *trans* ferulic acid

The basic fuchsine staining reveals a lignified endodermal network in the WT treated with *trans* ferulic acid or without. The mutant lines *prx11-1*, *asft1* and *asft2* seem to be not affected by the treatment. Scale bar size is 100 µm.

9.11. Root hydraulic conductance

Water transport through the root of *hqt*, *myb7*, *cadc*, *cadd* and *cadc*cadd* were measured by Katharina Markus. The roots were four weeks old. Only *cadc*cadd* reveals an impaired root hydraulic conductance value.

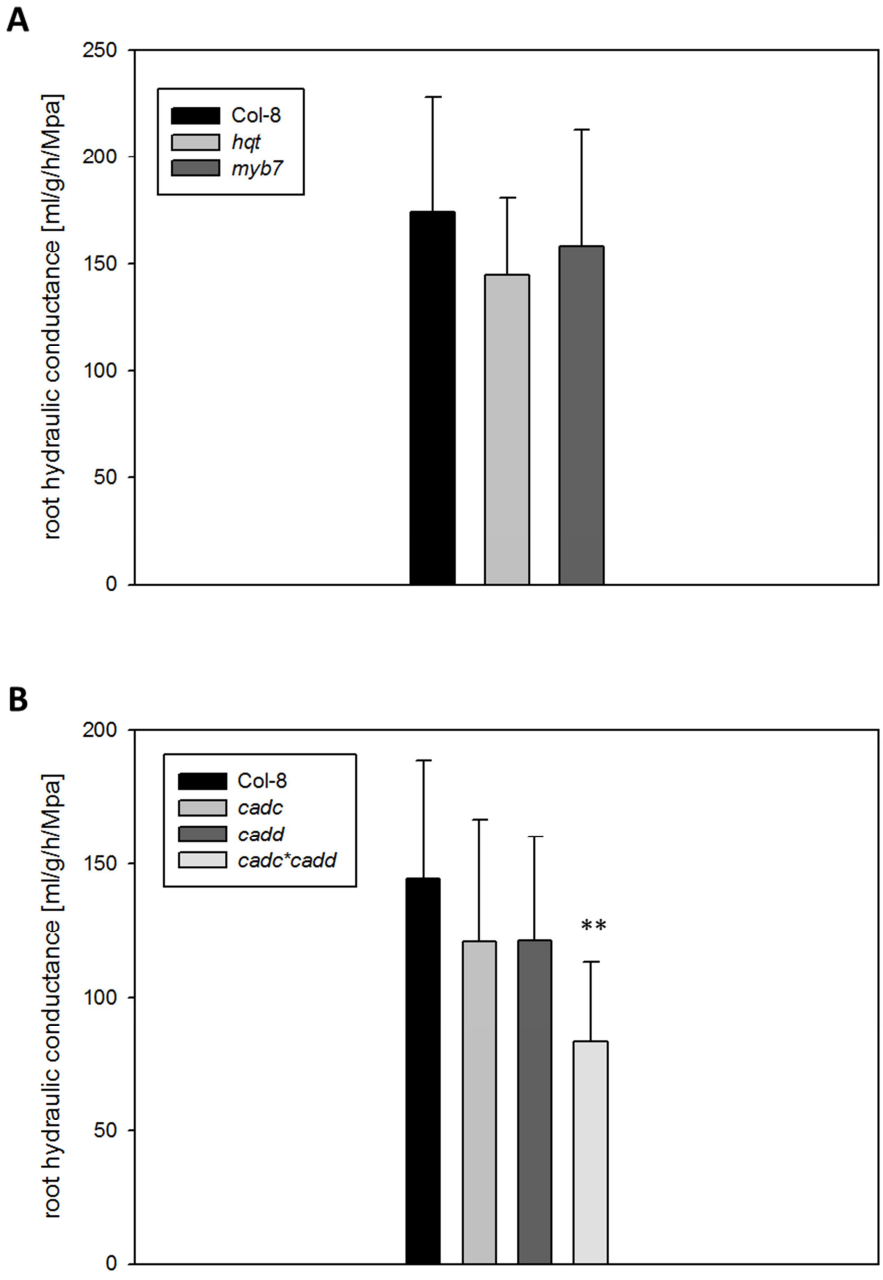

Fig. 147: Root hydraulic conductance of four weeks old roots

The root hydraulic conductance was measured in four weeks old roots of WT and mutant lines. **A**: Root hydraulic conductance of *hqt*, *myb7* and WT. Both mutants reveal a similar root hydraulic conductance to the WT. **B**: Root hydraulic conductance of *cadc*, *cadd*, *cadc*cadd* and WT. Only the double knockout mutant *cadc*cadd* has a significantly impaired root hydraulic conductance. The represented values are the arithmetic mean of the WT and mutant lines respectively and the calculated error bars of standard deviation. The sample amount corresponds to 10 roots for WT, 11 for *hqt* and 14 for *myb7* in the first set and 13 roots for WT and *cadc*, 12 for *cadd* and 14 for *cadc*cadd* in the second set. *: student's t-test, $p \leq 0.05$, **: student's t-test, $p \leq 0.01$.

9.12. Identification of supposed *HQT* and *VAN* gene in *Arabidopsis thaliana*

Fig. 148: Sequence alignment of *HCT* gene with *HQT* gene in *Solanum tuberosum*

Sequence alignment of both genes reveals an identity of 86.96 %. Sequence alignment was performed by using the website tool http://multalin.toulouse.inra.fr/multalin/ (Corpet, 1988).

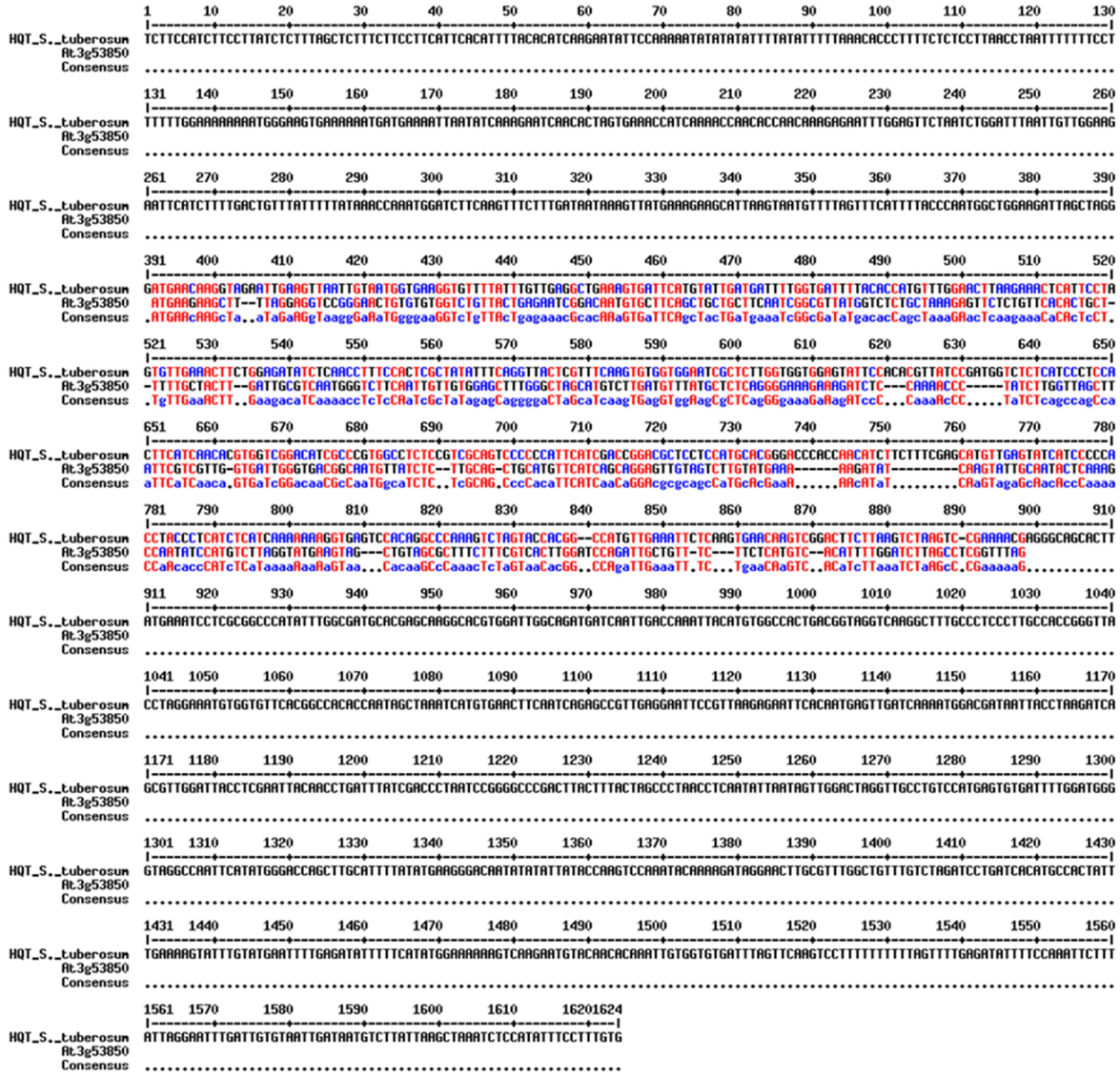

Fig. 149: Sequence alignment of *HQT* gene from *Solanum tuberosum* with supposed *HQT* orthologue in *Arabidopsis thaliana*

Sequence alignment of both genes reveals an identity of 46.23 %. Sequence alignment was performed by using the website tool http://multalin.toulouse.inra.fr/multalin/ (Corpet, 1988).

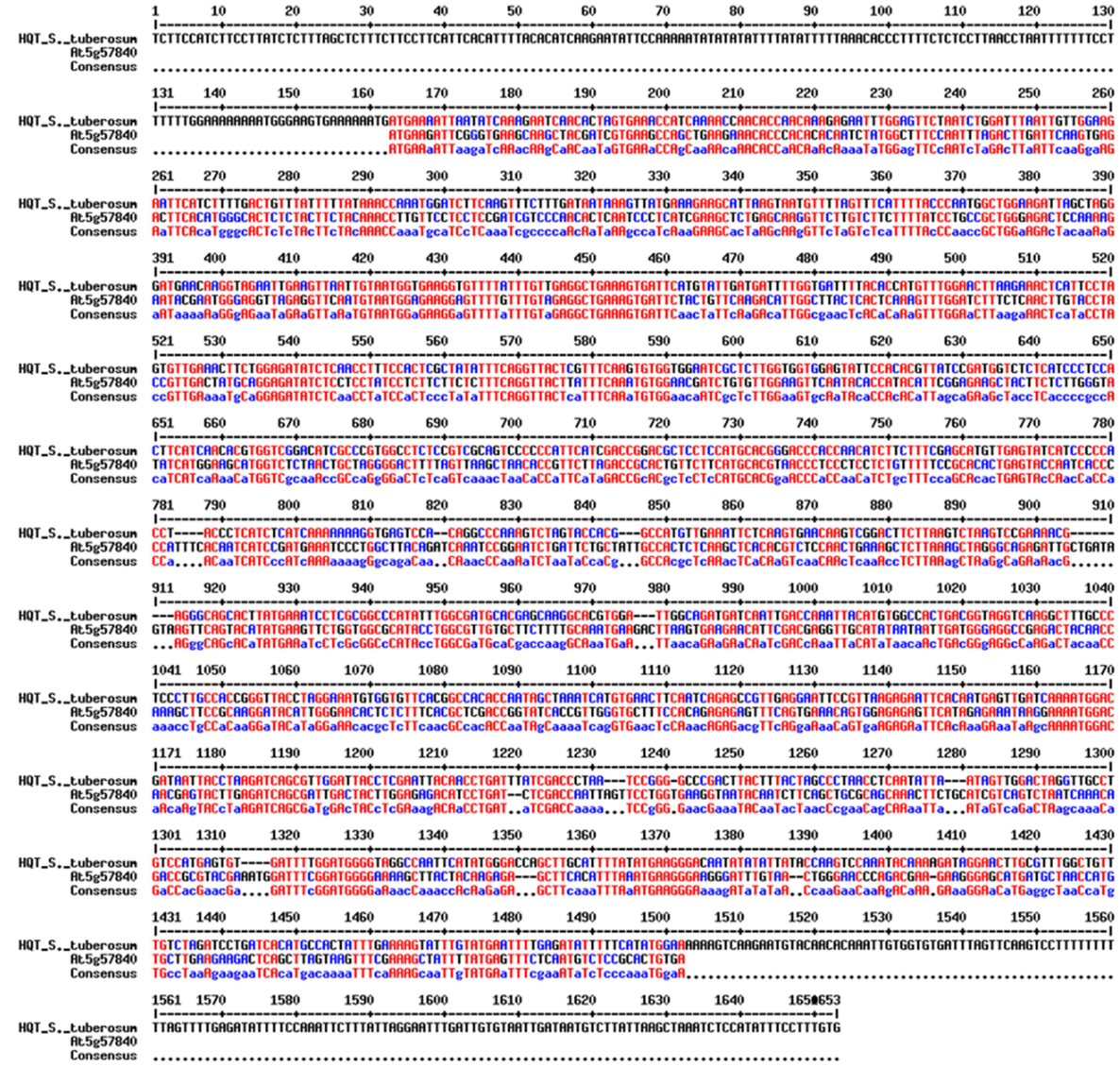

Fig. 150: Sequence alignment of *HQT* gene from *Solanum tuberosum* with supposed new *HQT* orthologue in *Arabidopsis thaliana*

Sequence alignment of both genes reveals an identity of 46.23 %. Sequence alignment was performed by using the website tool http://multalin.toulouse.inra.fr/multalin/ (Corpet, 1988).

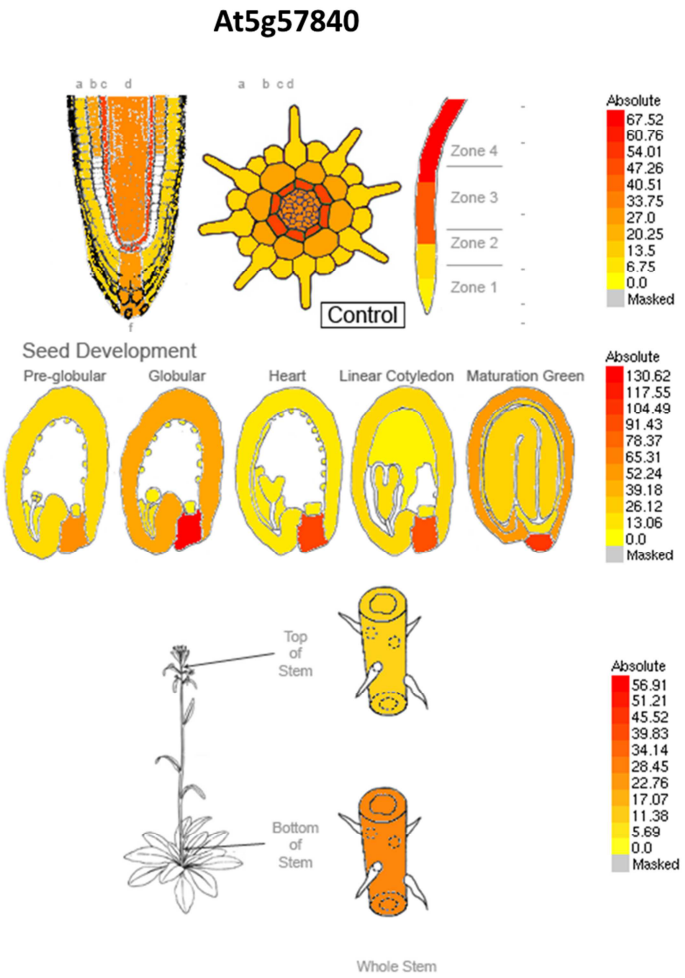

Fig. 151: Localisation of new supposed *HQT* gene (At5g57840) expression in the root, seed and stem tissue by using the *Arabidopsis eFP browser*

The Arabidopsis eFP browser graphics are based on expression analysis from microarray studies. Represented is the gene expression of longitudinal and cross sections of roots, longitudinal section of seeds and stem tissue. The intensity of the staining represents the intensity of the gene expression. Absolute values are shown in the adjacent scale. At5g57840 reveals an endodermal and chalazal endosperm tissue specific gene expression.

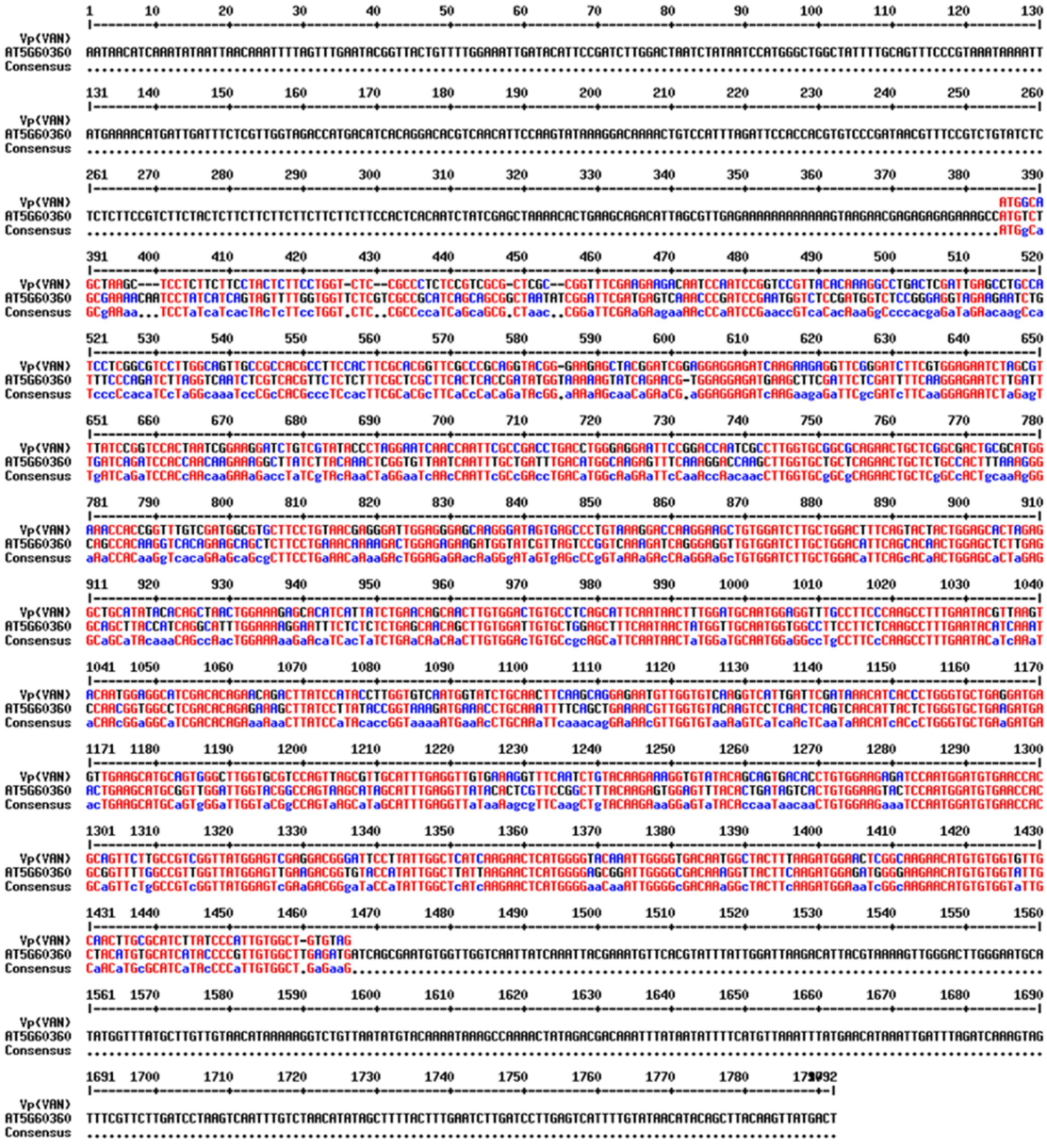

Fig. 152: Sequence alignment of *VAN* gene from *Vanilla planifolia* with supposed VAN orthologue in *Arabidopsis thaliana*

Sequence alignment of both genes reveals an identity of 80.9 %. Sequence alignment was performed by using the website tool http://multalin.toulouse.inra.fr/multalin/ (Corpet, 1988).

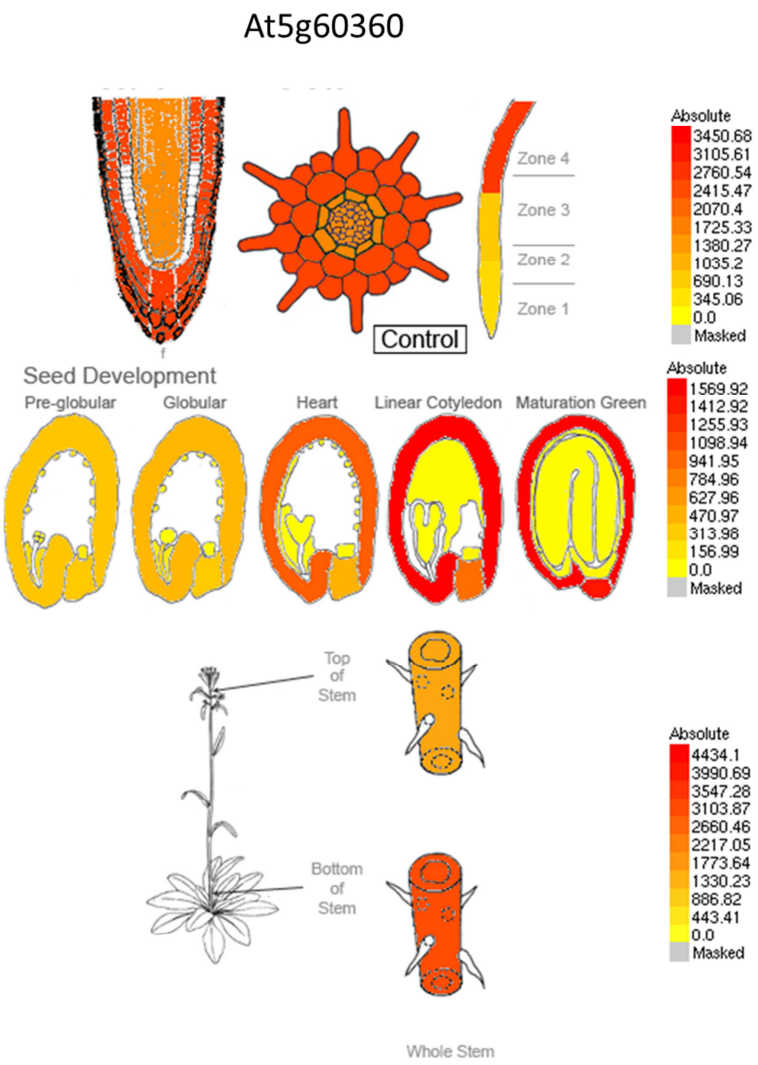

Fig. 153: Localisation of new supposed *VAN* gene (At5g60360) expression in the root, seed and stem tissue by using the *Arabidopsis eFP browser*

The Arabidopsis eFP browser graphics are based on expression analysis from microarray studies. Represented is the gene expression of longitudinal and cross sections of roots, longitudinal section of seeds and stem tissue. The intensity of the staining represents the intensity of the gene expression. Absolute values are shown in the adjacent scale. At5g60360 reveals an expression in epidermal, cortical, endodermal and central cylinder, seed coat and bottom stem tissue specific gene expression.

9.13. Vector maps of entry clone vector and expression clone vector

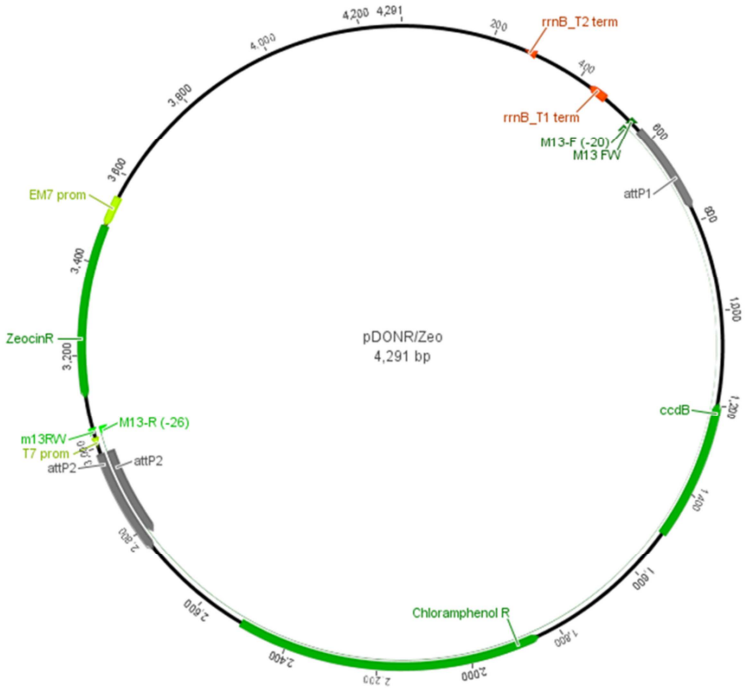

Fig. 154: Vector map of the pDONR/Zeo donor vector

attL1 and attL2: attachment sites; ChloramphenolR: chloramphenol resistance; EM7 promoter: bacterial promoter; M13-F and M13-R: forward and reverse primer for sequencing; rrnB T1 and rrnB T2: transcription terminators; ZeocinR: zeocin resistance

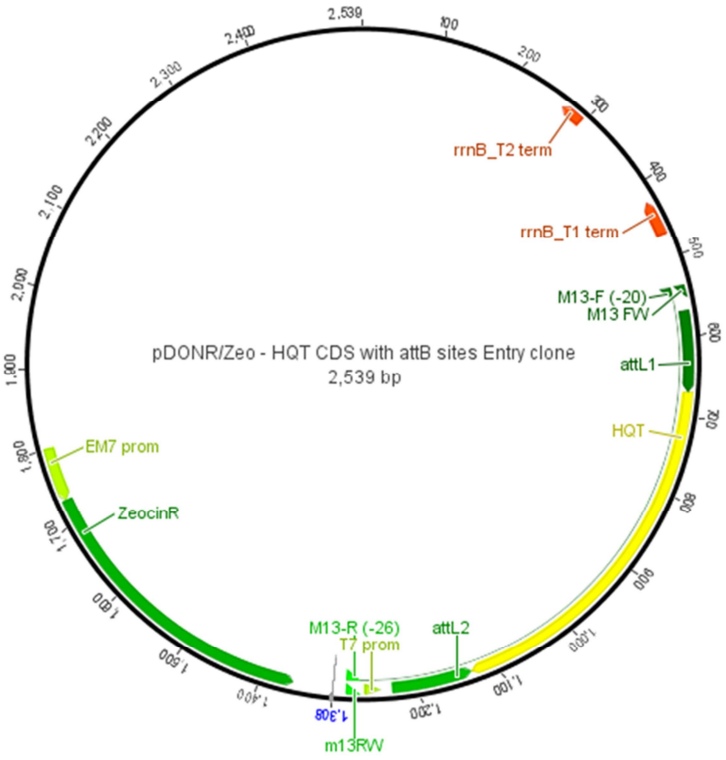

Fig. 155: Vector map of the pDONR/Zeo entry vector with *HQT*

attL1 and attL2: attachment sites; ChloramphenolR: chloramphenol resistance; EM7 promoter: bacterial promoter; HQT: *HQT* transcript sequence; M13-F and M13-R: forward and reverse primer for sequencing; rrnB T1 and rrnB T2: transcription terminators; ZeocinR: zeocin resistance

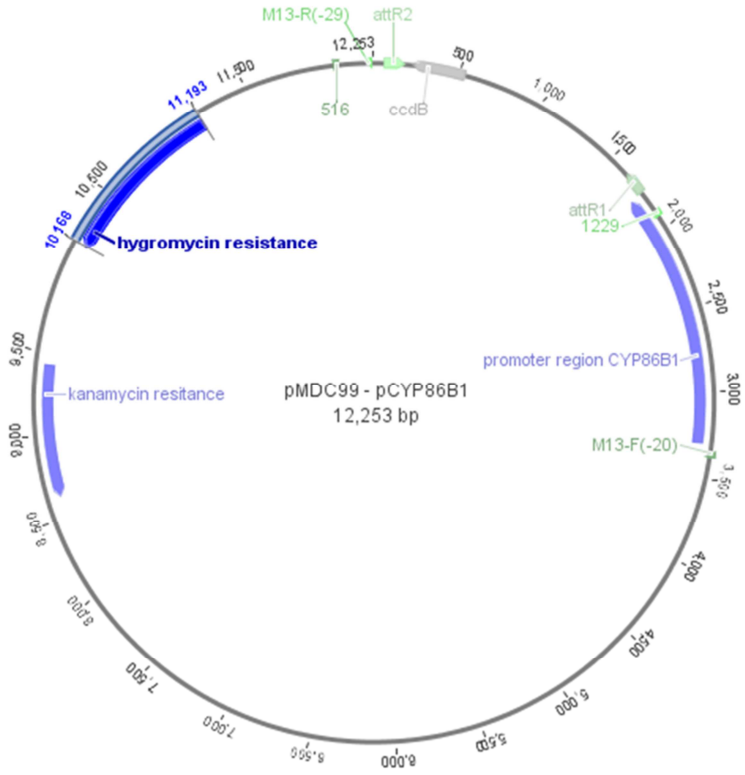

Fig. 156: Vector map of the pMDC99 – pCYP86B1 destination vector

attR1 and attR2: attachment sites; hygromycin resistance: antibiotic resistance against hygromycin; kanamycin resistance: antibiotic resistance against kanamycin; M13-F and M13-R: forward and reverse primer for sequencing; promoter region CYP86B1: promoter region of *RALPH* gene

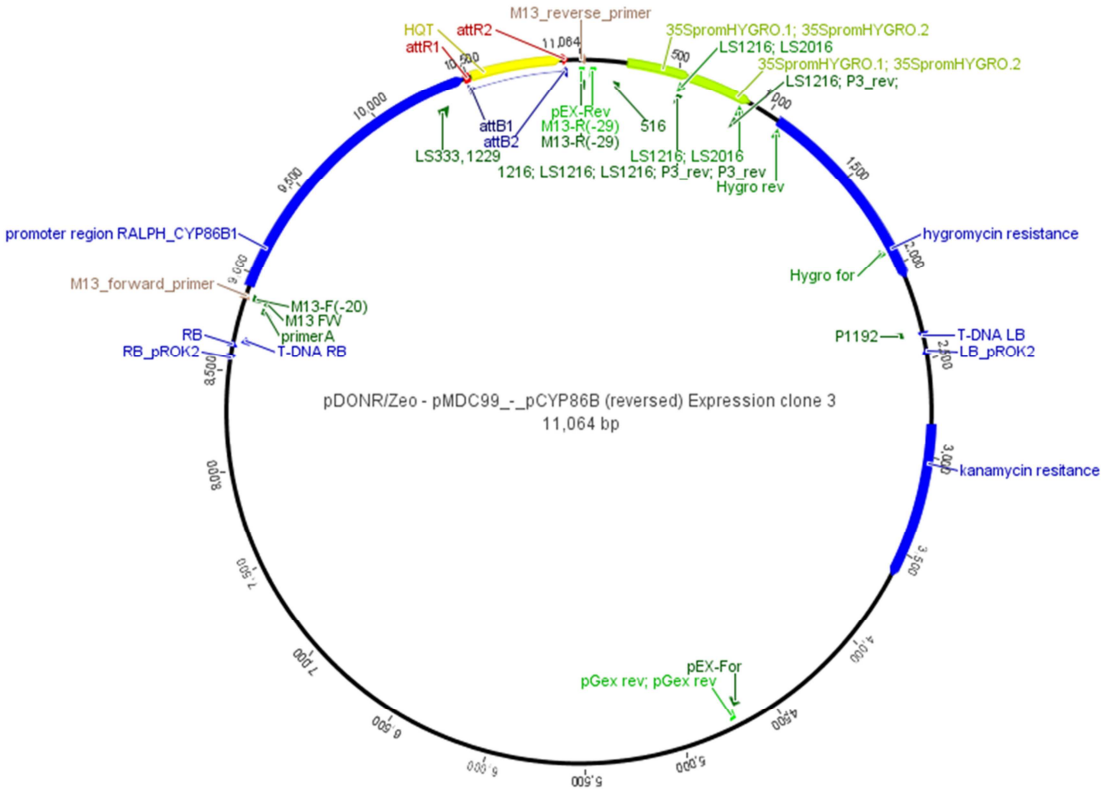

Fig. 157: Vector map of the pMDC99 – pCYP86B1 expression vector with *HQT*

attR1 and attR2: attachment sites; hygromycin resistance: antibiotic resistance against hygromycin; HQT: *HQT* gene; kanamycin resistance: antibiotic resistance against kanamycin; M13-F and M13-R: forward and reverse primer for sequencing; promoter region CYP86B1: promoter region of *RALPH* gene

9.14. Used buffers, media and solutions

Following buffers and solutions were used in this thesis.

Tab. 18: List of used buffer, media and solutions

Buffer/Media/Solution	Composition
Basic fuchsine staining solution	0.2 % (w/v) in ClearSee
ClearSee	10 % xylitol (w/v) 15 % sodium deoxycholate (w/v) 25 % urea (w/v) dissolved in distilled water
Enzyme solution	2 % cellulase 2 % pectinase 0.1 M citric acid monohydrate

	0.1 % NaN_3 pH = 3 dissolved in distilled water
5x ERL-media	29.5 g nonenyl succinic anhydride (NSA) 8.0 g D.E.R. 736 epoxy resin dow epoxy resin (DER) 20.5 g ERL-4221 epoxycyclohexanemethyl 3,4-epoxycyclohexane carbohydrate (ERL) 0.5 g 2-dimethylaminoethanol (DMAE)
Fluorol yellow 088 staining solution	0.01 % (w/v) fluorol yellow 088 in lactic acid heated at 70 °C for 30 min
Inoculation media	5.0 % sucrose (w/v) 0.05 % silwet L-7 (v/v) dissolved in tap water
LB agar	LB media 1 % agar (w/v) pH = 7.2 autoclaving
6x loading buffer	0.1 % bromine phenol blue (w/v) 40 % sucrose (w/v)
MS agar	4.4 g/l MS media (Duchefa) pH = 5.7 8 g/l agar
NCP	25 ml NCP (0.2 M) 5 ml glutaraldehyde (50 %) 0.025 g $CaCl_2$ 70 ml distilled water
Propidium iodide staining	10 µg/ml propidium iodide (15 µM) dissolved in distilled water
SOC-media	20.0 g/l tryptone 5.0 g/l yeast extract 0.5 g/l NaCl 0.5 mM KCl pH = 7.0

	autoclaving
	5.0 ml 2 M MgCl2 (sterile)
	20.0 ml 1 M glucose (sterile)
50x TAE buffer	242.28 g/l (2 M) TRIS
	60.05 g/l (1 M) acetic acid glacial
	18.61 g/l (0.05 M) EDTA

9.15. Used chemicals

The following table summarised the used chemicals of this thesis.

Tab. 19: List of used chemicals

Chemicals	Company
acetic acid glacial	100 %, Merck, Darmstadt, Germany
acetone	for analysis ≥ 99 %, Merck, Darmstadt, Germany
basic fuchsine	Merck, Darmstadt, Germany
boron trifluoride diethyl etherate	for analysis ≥ 99 %, Merck, Darmstadt, Germany
boron trifluoride-methanol	~ 10 % (~1.3 M), Merck, Darmstadt, Germany
bromine phenol blue	Fluka Feinchemikalien, GmbH, Neu-Ulm, Germany
BSFTA	Macherey-Nagel, Düren, Germany
calcium chloride	≥ 99 %, Roth, Karlsruhe, Germany
cellulase	0.8 U/mg, Merck, Darmstadt, Germany
chloroform	for analysis ≥ 99 %, Merck, Darmstadt, Germany
citric acid monohydrate	≥ 99 %, Roth, Karlsruhe, Germany
coniferyl alcohol	Merck, Darmstadt, Germany
dichlormethane	≥ 99.8 %, anhydrous, Merck, Darmstadt, Germany
dotriacontant	Analytical standard, Merck, Darmstadt, Germany
ethanethiol	for analysis ≥ 99 %, Merck, Darmstadt, Germany
ethanol	for analysis ≥ 99 %, Merck, Darmstadt, Germany
ethidium bromide	Merck, Darmstadt, Germany
formvar	Merck, Darmstadt, Germany

fluorol yellow 088	Merck, Darmstadt, Germany
glutaraldehyde	Dissolved in distilled water to 1.5 % Merck, Darmstadt, Germany
glycerol	≥ 99 %, Merck, Darmstadt, Germany
lactic acid	80 % (≥ 95 % L(+)-lactic acid), Roth, Karlsruhe, Germany
lead(II) citrate tribasic trihydrate	purum, for electron microscopy, Merck, Darmstadt, Germany
methanol	for analysis ≥ 99 %, VWR Chemicals, Fontenay-sous-Boise, France
osmium tetroxide	≥ 99.95 % for electron microscopy, Roth, Karlsruhe, Germany
pectinase	≥ 1 U/mg, Merck, Darmstadt, Germany
piperonylic acid	Merck, Darmstadt, Germany
propidium iodide	Merck, Darmstadt, Germany
pyridine	≥ 99 %, Merck, Darmstadt, Germany
silwet l-77	polyalkyleneoxide modified heptamethyl-trisiloxane (84 %) and allyloxypolyethyleneglycol methyl ether (16), Fisher Scientific, Schwerte, Germany
sodium chloride	≥ 99 %, Roth, Karlsruhe, Germany
sodium hydrogen carbonate	≥ 99 %, Roth, Karlsruhe, Germany
sodium hydroxide	≥ 98 %, Roth, Karlsruhe, Germany
sodium sulphate	≥ 99 %, water-free, Roth, Karlsruhe, Germany
TRIS	≥ 99 %, Roth, Karlsruhe, Germany
uranyl acetate	98 %, Polysciences, Inc., Hirschberg an der Bergstraße, Germany
vanillin	≥ 99 %, Merck, Darmstadt, Germany

9.16. Calculation of the hybridisation temperature of primers and the primer sequences

Formula 2: Calculation of the melting temperature of the used primers

$$T_M\,[°C] = 69.3 + 41\left(\frac{\sum G + \sum C}{\sum nucleotides}\right) - \left(\frac{650}{\sum nucleotides}\right)$$

T_M: Melting temperature, ∑G: number of guanine nucleotides in the primer sequence, ∑C: number of cytosine nucleotides in the primer sequence, ∑nucleotides: total number of nucleotides in the primer sequence.

Formula 3: Calculation of the annealing temperature of the used primers

$$T_A\,[°C] = T_M - 2$$

T_A: Annealing temperature, T_M: melting temperature.

Tab. 20: List of used primers

Target gene	Description	Sequence [5'→ 3']	T_M [°C]
At5g48930 (*HCT*)	LS1342 forward primer for genotyping SALK_061912 (At5g48930)	CCAAGAAACCATAGTGCAA	52.35
At5g48930 (*HCT*)	LS1343 reverse primer for genotyping SALK_061912 (At5g48930)	GGTCGTCCTATCTTTATG	51.41
At5g48930 (*HCT*)	LS1419 forward primer for genotyping SALK_063325 (At5g48930)	TTCATGACCTGAGGGTCA	53.69
At5g48930 (*HCT*)	LS1420 reverse primer for genotyping SALK_063325 (At5g48930)	TCTGGGTAAATGAGCGAAT	52.35
At3g53850 (*HQT*)	LS1234 forward primer for genotyping SALK_092459 (At3g53850)	TGATTTTGTCGGAATTTCTGG	53.97
At3g53850 (*HQT*)	LS1235 reverse primer for genotyping SALK_092459 (At3g53850)	TTATTTGCGAATATCCCGTTG	53.97
At4g34050 (CCoAOMT1)	LS1223 forward primer for genotyping SALK_151507 (At4g34050)	TTTTGTCGAACTTGGGAATTG	53.35
At4g34050	LS1224 reverse primer for	AATTTTCAAAGACCGGTGACC	55.92

(CCoAOMT1)	genotyping SALK_151507 (At4g34050)		
At5g54160 (COMT1)	LS1240 forward primer for genotyping SALK_020611 (At5g54160)	TCCGGTTTGCAAGTATTTGAC	55,92
At5g54160 (COMT1)	LS1241 reverse primer for genotyping SALK_020611 (At5g54160)	CTAGGGTCAGTCCCGTGGTAC	63,73
At5g54160 (COMT1)	LS1242 forward primer for genotyping SALK_135290 (At5g54160)	TTGAAACTAGCTTGGTCGGTG	57.87
At5g54160 (COMT1)	LS1243 reverse primer for genotyping SALK_135290 (At5g54160)	AATTCTTGATGGTGGGATTCC	55.92
At1g15950 (CCR1)	LS1294 forward primer for genotyping GABI_622C01 (At1g15950)	CAACACCTTTCTCCTTTGCT	55.25
At1g15950 (CCR1)	LS1295 reverse primer for genotyping GABI_622C01 (At1g15950)	ACCGTACGGAATCCAGGTA	56.67
At3g19450 (CADC)	LS1244 forward primer for genotyping SAIL_1265_A06 (At3g19450)	TAGGTGAGGTGTTGGAAGTGG	59.82
At3g19450 (CADC)	LS1307 reverse primer for genotyping SAIL_1265_A06 (At3g19450)	ACATTCGTTGGACAAACAAGCCC	60.65
At4g34230 (CADD)	LS1232 forward primer for genotyping SALK_019355 (At4g34230)	TCACCGCAATCAAATAAAACC	53.97
At4g34230 (CADD)	LS1233 reverse primer for genotyping SALK_019355 (At4g34230)	AGGTCAAGAATCAACACGTGG	57.87

At4g38620 (MYB4)	LS1227 forward primer for genotyping ET3967 (At4g38620)	CTTCAACCAAACCCAAAATCC	55.92
At4g38620 (MYB4)	LS1228 reverse primer for genotyping ET3967 (At4g38620)	ATCCATTGCTCATGTCACTCC	57.87
At2g16720 (MYB7)	LS1230 forward primer for genotyping SALK_020256 (At2g16720)	AAAATAATTGCAAAAGATGCCC	52.80
At2g16720 (MYB7)	LS1230 reverse primer for genotyping SALK_020256 (At2g16720)	TTTGCAAACTAACCCATTTCG	53.97
At5g48930 (*HCT*)	LS1477 forward primer for RT-PCR At5g48930	AACGGTGCTGGTGTTCTCTT	57.30
At5g48930 (*HCT*)	LS1477 reverse primer for RT-PCR At5g48930	GTGTTCAGATTGGAGGGCAA	57.30
At3g53850 (*HQT*)	LS1453 forward primer for RT-PCR At3g53850	ATGAAGAAGCTTTTAGGAGGTC	56.53
At3g53850 (*HQT*)	LS1454 reverse primer for RT-PCR At3g53850	CTAAACCGAGGCTAAGATCC	57.30
At4g34050 (CCoAOMT1)	LS1455 forward primer for RT-PCR At4g34050	ATGTGTGTGACTCACCAAGA	55.25
At4g34050 (CCoAOMT1)	LS1456 reverse primer for RT-PCR At4g34050	TCAACTGATCCGACGGCA	55.97
At5g54160 (COMT1)	LS1478 forward primer for RT-PCR At5g54160	CCTGCTCCAACCGTAAACTT	57.30
At5g54160 (COMT1)	LS1479 reverse primer for RT-PCR At5g54160	GAACGCGCTCATTCCATAAG	57.30
At1g15950 (CCR1)	LS1431 forward primer for RT-PCR At1g15950	TTGGTGCCGTCTACATGGAC	59.35
At1g15950 (CCR1)	LS1432 reverse primer for RT-PCR At1g15950	AGGAGGAGGAGGAGCAAGA	58.83
At3g19450 (CADC)	LS1425 forward primer for RT-PCR At3g19450	CTATGGTTCCTGGGCACGAG	61.40

At3g19450 (CADC)	LS1426 reverse primer for RT-PCR At3g19450	GGGGTCACGAACTGAAGAGG	61.40
At4g34230 (CADD)	LS1427 forward primer for RT-PCR At4g34230	GGAATCTGCCACACCGATCT	59.35
At4g34230 (CADD)	LS1428 reverse primer for RT-PCR At4g34230	ATGATGAACAGGCACCGTGTC	59.82
At4g38620 (MYB4)	LS1457 forward primer for RT-PCR At4g38620	ATGGGAAGGTCACCGTGC	58.24
At4g38620 (MYB4)	LS1458 reverse primer for RT-PCR At4g38620	TTATTTCATCTCCAAGCTTCGAAAG	58.06
At2g16720 (MYB7)	LS1480 forward primer for RT-PCR At2g16720	CGAGAAAGAACACATGAACA	53.20
At2g16720 (MYB7)	LS1460 reverse primer for RT-PCR At2g16720	TTATTTCATTTCCAAGCTTCGAAAATC	57.37
At3g53850 (*HQT*)	LS1443 forward primer for cloning GATEWAY of At3g53850	ggggacaagtttgtacaaaaaagcaggcttaAT GAAGAAGCTTTTAGGAGGTC	74.05
At3g53850 (*HQT*)	LS1444 reverse primer for cloning GATEWAY of At3g53850	ggggaccactttgtacaagaaagctgggtaCTA AACCGAGGCTAAGAT	75.40

9.17. List of figures

9.18. List of formulas

9.19. List of tables